TESIS DE LA UNIVERSIDAD
DE ZARAGOZA

2022

165

Juan Manuel Colom Díaz

Experimental and kinetic modeling study of hydrogen sulfide oxidation. Application to sour gas combustion.

Director/es
Millera Peralta, Ángela
Alzueta Ania, María Ujue

http://zaguan.unizar.es/collection/Tesis

ISSN 2254-7606

Prensas de la Universidad
Universidad Zaragoza

© Universidad de Zaragoza
Servicio de Publicaciones

ISSN 2254-7606

Tesis Doctoral

EXPERIMENTAL AND KINETIC MODELING STUDY OF HYDROGEN SULFIDE OXIDATION. APPLICATION TO SOUR GAS COMBUSTION.

Autor

Juan Manuel Colom Díaz

Director/es

Millera Peralta, Ángela
Alzueta Ania, María Ujue

UNIVERSIDAD DE ZARAGOZA
Escuela de Doctorado

Programa de Doctorado en Ingeniería Química y del Medio Ambiente

2021

Repositorio de la Universidad de Zaragoza – Zaguan   http://zaguan.unizar.es

Universidad Zaragoza

Experimental and kinetic modeling study of hydrogen sulfide oxidation. Application to sour gas combustion

This dissertation is submitted to the Department of Chemical Engineering and Environmental Technologies at the University of Zaragoza (Spain) in fulfillment of the requirements for the degree of Doctor

Juan Manuel Colom Díaz

Zaragoza, 2021

Departamento de Ingeniería Química y Tecnologías del Medio Ambiente
Universidad Zaragoza

Instituto Universitario de Investigación en Ingeniería de Aragón
Universidad Zaragoza

GPT Thermochemical Processes Group

Departamento de Ingeniería
Química y Tecnologías
del Medio Ambiente
Universidad Zaragoza

Dña. María Ujué Alzueta Anía, Catedrática de Universidad, y **Dña. Ángela Millera Peralta**, Profesora Titular, del Departamento de Ingeniería Química y Tecnologías del Medio Ambiente de la Universidad de Zaragoza,

INFORMAN

Que la presente memoria titulada:

Experimental and kinetic modeling study of hydrogen sulfide oxidation. Application to sour gas combustion

ha sido realizada bajo nuestra supervisión en el Grupo de Procesos Termoquímicos perteneciente al Instituto de Investigación en Ingeniería de Aragón (I3A) y en el Departamento de Ingeniería Química y Tecnologías del Medio Ambiente de la Universidad de Zaragoza, por **Don Juan Manuel Colom Díaz**, y AUTORIZAN su presentación como compendio de publicaciones y con la mención internacional en el título de Doctor, cumpliendo con las condiciones requeridas para que su autor pueda optar al grado de Doctor en el Programa de Doctorado de Ingeniería Química y del Medio Ambiente de la Universidad de Zaragoza.

Y para que así conste, lo firmamos en Zaragoza a 19 de mayo de 2021.

Dña. María Ujué Alzueta Anía **Dña. Ángela Millera Peralta**

Departamento de Ingeniería
Química y Tecnologías
del Medio Ambiente
Universidad Zaragoza

Professor María Ujué Alzueta Anía and Associate Professor Ángela Millera Peralta, both belonging to the Department of Chemical and Environmental Engineering of the University of Zaragoza,

REPORT that:

The Doctoral Thesis entitled:

Experimental and kinetic modeling study of hydrogen sulfide oxidation.
Application to sour gas combustion

has been carried out under our supervision in the Thermo-Chemical Processes Group belonging to the Aragón Institute of Engineering Research (I3A) and in the Department of Chemical and Environmental Engineering of the University of Zaragoza, by Mr. Juan Manuel Colom Díaz, and we AUTHORIZE and approve the presentation of this dissertation in the form of compendium of publications and with the international citation on the doctoral certificate, fulfilling the requirements for the degree of Doctor.

And for the record, we sign this document in Zaragoza on 19th May 2021.

Dña. María Ujué Alzueta Anía **Dña. Ángela Millera Peralta**

El presente trabajo ha sido publicado en los artículos que se mencionan a continuación, y que se adjuntan al final de esta memoria.

The present work has been published in the articles mentioned below and attached at the end of this dissertation.

I. **Colom-Díaz, J.M.**; Abián, M.; Ballester, M.Y.; Millera, Á.; Bilbao, R.; Alzueta, M.U. (2019). H_2S conversion in a tubular flow reactor: Experiments and kinetic modeling. *Proceedings of the Combustion Institute* 37, 727-734.

II. **Colom-Díaz, J.M.**; Millera, Á.; Bilbao, R.; Alzueta, M.U. (2019). High pressure study of H_2 oxidation and its interaction with NO. *International Journal of Hydrogen Energy* 44, 6325-6332.

III. **Colom-Díaz, J.M.**; Abián, M.; Millera, Á.; Bilbao, R.; Alzueta, M.U. (2019). Influence of pressure on H_2S oxidation. Experiments and kinetic modeling. *Fuel* 258, 116145.

IV. **Colom-Díaz, J.M.**; Leciñena, M.; Peláez, A.; Abián, M.; Millera, Á.; Bilbao, R.; Alzueta, M.U. (2020). Study of the conversion of H_2S/CH_4 mixtures at different pressures. *Fuel* 262, 116484.

V. **Colom-Díaz, J.M.**; Millera, Á.; Bilbao, R.; Alzueta, M.U. (2021). New results of H_2S oxidation at high pressures. Experiments and kinetic modeling. *Fuel* 285, 119261.

VI. **Colom-Díaz, J.M.**; Millera, Á.; Bilbao, R.; Alzueta, M.U. (2021). Conversion of $H_2S/O_2/NO$ mixtures at different pressures. Experiments and kinetic modeling. *Fuel* 290, 120060.

VII. **Colom-Díaz, J.M.**; Alzueta, M.U.; Zeng, Z.; Altarawneh, M.; Dlugogorski, B.Z. (2021). Oxidation of H_2S and CH_3SH oxidation in a jet-stirred reactor: Experiments and kinetic modeling. *Fuel* 283, 119258.

Las publicaciones numeradas del I-VII constituyen el compendio de artículos, modalidad por la que se presenta esta Tesis Doctoral. La numeración de las mismas corresponde al orden en que se mencionan en esta memoria. Al final de la misma, se pueden consultar las publicaciones completas.

The I-VII numbered publications constitute the compendium of publications, modality by which this Doctoral Thesis is presented. The numbering corresponds to the order in which they are mentioned in this memory, at the end of which, they can be consulted.

Por otro lado, el doctorando ha participado y presentado resultados parciales de la investigación en diferentes congresos nacionales e internacionales, relacionados con diferentes aspectos implicados en su trabajo.

On the other hand, the doctoral candidate has participated and presented partial results of this research in several national and international congresses, related to different aspects involved in his work.

Colom Díaz, J.M.; Conchello, J.; Millera, Á.; Bilbao, R.; Alzueta, M.U. Study of H_2S oxidation at atmopheric pressure and its interaction with NO. **VI Jornada de Jóvenes Investigadores del I3A**. Zaragoza (Spain), 2nd June 2017. *Poster presentation.*

Colom Díaz, J.M.; Conchello, J.; Millera, Á.; Bilbao, R.; Alzueta, M.U. Study of H_2S oxidation at atmospheric pressure and its interaction with NO. **13th International Conference on Energy for a Clean Environment**. Sao Miguel (Portugal), 3rd July 2017. *Oral presentation.*

Colom Díaz, J.M.; Millera, Á.; Bilbao, R.; Alzueta, M.U. Experimental and kinetic modelling study of H_2S oxidation. **10th World Congress of Chemical Engineering**. Barcelona (Spain), 1st October 2017. *Oral presentation.*

Colom Díaz, J.M.; Abián, M.; Millera, Á.; Bilbao, R.; Alzueta, M.U. Experimental and kinetic modeling study of H_2S oxidation at high pressures. **VII Jornada de Jóvenes Investigadores del I3A**. Zaragoza (Spain), 8th June 2018. *Poster presentation.*

Colom-Díaz, J.M.; Abián, M.; Millera, Á.; Bilbao, R.; Alzueta, M.U. H_2S conversion in a tubular flow reactor: Experiments and kinetic modeling. **37th International Symposium on Combustion**. Dublin (Ireland), 1st August 2018. *Oral presentation.*

Colom Díaz, J.M.; Abián, M.; Millera, Á.; Bilbao, R.; Alzueta, M.U. Estudio experimental y modelado cinético de la oxidación de H_2S a altas presiones. **8ª jornada de Jóvenes Investigadores (Física y Química) de Aragón.** Zaragoza (Spain), 22th November 2018. *Oral presentation.*

Colom-Díaz, J.M.; Abián, M.; Millera, Á.; Bilbao, R.; Alzueta, M.U. Experimental and kinetic modeling of CH_4/H_2S oxidation at high pressures. **1st International Conference on Smart Energy Carriers**. Napoli (Italy), 22th January 2019. *Oral Presentation.*

Colom Díaz, J.M.; Abián, M.; Millera, Á.; Bilbao, R.; Alzueta, M.U. Influence of pressure on H_2S conversion. **9th European Combustion Meeting**. Lisboa (Portugal), 14th April 2019. *Poster presentation.*

Colom Díaz, J.M.; Abián, M.; Millera, Á.; Bilbao, R.; Alzueta, M.U. Oxidación de H_2S a alta presión y su interacción con óxidos de nitrógeno (NO_x). **XXXVI Jornadas Nacionales de Ingeniería Química**. Zaragoza (Spain), 4th September 2019. *Poster presentation.*

Alzueta, M.U.; Millera, Á.; Bilbao, R.; **Colom-Díaz, J.M.**; Adánez-Rubio, I.; Abián, M. Study of the effect of hydrogen sulfide in combustion processes of different gas mixtures and its impact on the emission of pollutants. **XXXVI Jornadas Nacionales de Ingeniería Química**. Zaragoza (Spain), 4th September 2019. *Oral presentation.*

Colom Díaz, J.M.; Millera, Á.; Bilbao, R.; Alzueta, M.U. Progressing in the study of H_2S oxidation at high pressure: Experiments and kinetic modeling. **14th Mediterranean Congress of Chemical Engineering.** Barcelona (Spain), 18th November 2020. *Oral presentation.*

Acknowledgements. Agradecimientos

This Doctoral Thesis has been carried out in the Thermochemical Processes Group (GPT) that belongs to the Aragon Institute of Engineering Research (I3A), within the doctoral program of Chemical and Environmental Engineering (Department of Chemical Engineering and Environmental Technologies), under the direction and supervision of Professor Mª Ujué Alzueta Anía and Associate Professor Ángela Millera Peralta.

The research has been funded by the Government of Aragon (GPT Group, Ref. T22_20R), the European Social Fund and the Ministry of Economy and Competitiveness (MINECO) (Projects CTQ2015-65226 and RTI2018-098856-B-100). Likewise, MINECO awarded a pre-doctoral contract to the doctoral student (BES-2016-076610). Part of this research work was carried out at Murdoch University in Perth (Australia), under the supervision of Professor Bogdan Z. Dlugogorski, within the framework of a short research stay. I would like to say thanks to Prof. Dlugogorski and all the group in Perth for the help and assistance during my stay.

In the same way, I would like to thank all the people in the Department of Chemical and Environmental Engineering at the University of Zaragoza for all these years, whose advices, teachings and availability have made all the work much easier. This thesis would not have been possible either without the support, guidance and inspiration of friends and colleagues, especially coffee, office and lunch colleagues who have turned this experience into something more than an academic achievement, but also a process of personal development.

I would like to thank Dr. Rafael Bilbao for his insightful and kind supervision through this venture. His broad knowledge, accessibility and excellent advice have made working with him a consistently rewarding experience.

Particular thanks to my supervisors and mentors, Drs. Uxue Alzueta and Ángela Millera. Their dedication, professionalism and guidance have pressed huge footsteps that I aspire to follow. Thank you for giving me the opportunity of doing my PhD, believing in me and teaching me more than research.

Especial thanks to my family, who has been encouraging throughout the whole process. You know how important you are and immeasurable thanks for being an unfaltering source of understanding, guidance and love.

Abstract

Gases that contain impurities in significant quantities, such as hydrogen sulfide (H_2S), are defined as sour gas. Currently, most natural gas reserves, as well as waste gas streams from oil treatment or biogas generated by anaerobic digestion, include the presence of these impurities. When the concentration of H_2S is high, the common practice is to remove this compound (H_2S) from the gas with costly separation processes and use it for other applications, such as the production of sulfur using the Claus process. However, due to the increasing demand for energy, a more efficient use of natural resources is required. The use of this type of gas, containing H_2S, for small-scale energy use has recently emerged as a possible alternative that can contribute to this goal. The improvement and knowledge of sour gas combustion processes would be developed in parallel with the improvement of waste gas treatment, as well as the improvement of materials to resist the corrosive nature of this gas. The oxidation of H_2S produces mainly SO_2, and mechanisms describing its conversion are scarce in literature, particularly under fuel-rich conditions. At the same time, the knowledge of the interaction of H_2S with methane (CH_4) and possible polluting compounds, such as nitrogen oxides (NO_x), is of interest. To design and optimize combustion equipment, it is necessary to carry out experiments under well-controlled laboratory conditions, accompanied by chemical-kinetic studies that help to interpret and understand the reaction mechanisms by which the oxidation of the fuel takes place.

In this context, the objective of this work has been to analyze the H_2S oxidation under a wide range of conditions, studying the effect of temperature, pressure, the air-excess ratio and the interaction of H_2S with other compounds. To achieve this global objective, different experimental studies have been carried out, together with the continuous development of the chemical kinetic mechanism that can reproduce the H_2S oxidation under different conditions. First, the oxidation of H_2S at atmospheric pressure has been analyzed, from reducing to oxidizing conditions, compiling an initial kinetic model capable of simulating the conversion of H_2S at atmospheric pressure. For a better analysis of the oxidation of H_2S at high pressure, a preliminary study was carried out on the oxidation of H_2, in the presence of NO. As a result of this study, the reaction subsets of H_2/O_2 and NO_x were updated. Subsequently, the oxidation of H_2S was characterized at different pressures (0.65-40 bar of manometric pressure). The results have shown that H_2S oxidation occurs at lower temperatures as pressure increases, and the updated kinetic mechanism was able to predict the oxidation of H_2S fairly accurately at high pressures, except for the highest pressure studied (40 bar). Next, the oxidation of H_2S/CH_4 and

H_2S/NO mixtures has been analyzed at different pressures and stoichiometries from both experimental and kinetic modeling points of view. Both CH_4 and NO displace the oxidation of H_2S at atmospheric pressure to higher temperatures; while, at high pressure, they promote its oxidation, especially in the case of NO. In order to try to improve the kinetic mechanism of H_2S oxidation at high pressures, an additional study was carried out, conducting experiments with different excess air ratios and by introducing in the kinetic model reactions involving H_2O_2 molecules, which are important at high pressures. The resulting mechanism satisfactorily predicts the experimental results of the present work and from the literature.

During the development of this thesis, a research stay has been carried out at the University of Murdoch (Australia), with the objective of studying the oxidation of H_2S in a different reactor (jet-stirred reactor, JSR) compared to the one used to date in the University of Zaragoza (plug flow reactor, PFR). Oxidation experiments have been also carried out on a compound of sulfur and carbon, methyl mercaptan (CH_3SH), which may be an important component in sour gas composition. The mechanism compiled during the thesis allowed to satisfactorily predict the obtained experimental results of H_2S oxidation in the JSR, and was extended for analyzing CH_3SH conversion.

The wide range of experimental conditions used during the present study has allowed to know the behavior of H_2S in its oxidation under different conditions, as well as to validate a detailed chemical-kinetic mechanism capable of describing the process and analyzing the role of H_2S in the combustion of sour gas.

Resumen

Los gases que contienen impurezas en cantidades significativas, como sulfuro de hidrógeno (H_2S), se denominan comúnmente como gas ácido. Actualmente, la mayoría de las reservas de gas natural, así como las corrientes de gas residual del tratamiento de petróleo o el biogás generado por digestión anaeróbica, incluyen la presencia de estas impurezas. Cuando la concentración de H_2S es alta, la práctica común es eliminar este compuesto (H_2S) del gas con costosos procesos de separación y producir principalmente azufre mediante el proceso Claus. Sin embargo, debido a la creciente demanda de energía, se requiere un uso más eficiente de los recursos naturales. El uso de este tipo de gas ácido, que contiene H_2S, para uso energético a pequeña escala, ha surgido como una posible alternativa que puede contribuir a este objetivo. La mejora y el conocimiento del proceso de combustión de gases ácidos se desarrolla en paralelo con la mejora del tratamiento de los gases residuales y la mejora de los materiales para resistir la naturaleza corrosiva de este gas. La oxidación del H_2S produce principalmente SO_2 y los mecanismos que describen su conversión son escasos en bibliografía, particularmente en condiciones ricas en combustible. Al mismo tiempo, es de interés el conocimiento de la interacción del H_2S con el metano (CH_4) y posibles compuestos contaminantes, como los óxidos de nitrógeno (NO_x). Para diseñar y optimizar equipos de combustión, es necesario realizar experimentos en condiciones de laboratorio bien controladas, acompañados de estudios cinético-químicos que ayuden a interpretar y comprender los mecanismos de reacción a través de los cuales transcurre la oxidación del combustible.

En este contexto, el objetivo del presente trabajo es analizar la oxidación de H_2S bajo un amplio intervalo de condiciones, estudiando el efecto de la temperatura, la presión, la relación de exceso de aire, así como la interacción de H_2S con otros compuestos. Para lograr este objetivo global, se han llevado a cabo diferentes estudios experimentales, junto con el continuo desarrollo de un modelo cinético-químico que permite reproducir el proceso de oxidación de H_2S en diferentes condiciones. En primer lugar, se analizó la oxidación de H_2S a presión atmosférica, considerando desde condiciones reductoras hasta oxidantes, compilando un modelo cinético inicial capaz de simular la conversión de H_2S a presión atmosférica. Para un mejor análisis de la oxidación de H_2S a alta presión, se realizó un estudio preliminar sobre la oxidación de H_2, en presencia de NO. Como resultado de este estudio, se actualizaron los *subsets* de reacciones de H_2/O_2 y NO_x. Posteriormente, se estudió la oxidación de H_2S a distintas presiones (0.65-40 bar de presión manométrica). Los resultados han mostrado que la oxidación de H_2S ocurre a menores temperaturas conforme aumenta la presión. El mecanismo cinético

actualizado fue capaz de predecir la oxidación de H_2S a altas presiones, excepto para la presión más elevada estudiada (40 bar). Seguidamente, se analizó la oxidación de mezclas H_2S/CH_4 y H_2S/NO a diferentes presiones y estequiometrías, desde un punto de vista experimental y de modelado cinético. Tanto el CH_4 como el NO desplazan la oxidación de H_2S a presión atmosférica a mayores temperaturas, mientras que a alta presión promueven dicha oxidación, especialmente en el caso del NO. Para intentar mejorar el mecanismo cinético de oxidación de H_2S a altas presiones, se llevó a cabo un estudio adicional, realizando experimentos con distintas relaciones de exceso de aire e introduciendo en el modelo cinético reacciones que involucran la especie H_2O_2, que muestra un importante papel a altas presiones. Los resultados han sido satisfactorios en cuanto a la predicción teórica de los resultados experimentales del presente trabajo y de la bibliografía.

Durante el desarrollo de esta tesis doctoral, se realizó una estancia de investigación en la Universidad de Murdoch (Australia), donde el objetivo fue estudiar la oxidación de H_2S en un reactor distinto (*jet-stirred reactor*, JSR) al usado hasta la fecha en la Universidad de Zaragoza (reactor de flujo pistón, PFR). También se realizaron experimentos de oxidación de un compuesto de azufre y carbono, el metilmercaptano (CH_3SH), el cual puede ser un componente importante en el gas ácido. El mecanismo compilado durante esta tesis permitió predecir satisfactoriamente los resultados experimentales obtenidos de la oxidación de H_2S en el JSR, y fue extendido para analizar la conversión de CH_3SH.

El amplio intervalo de condiciones experimentales utilizadas durante el presente estudio ha permitido comprender al comportamiento de H_2S durante su oxidación en diferentes condiciones, así como validar un mecanismo cinético-químico detallado capaz de describir el proceso y analizar el papel del H_2S en la combustión de gas ácido.

Acronyms

CHEC	Combustion and Harmful Emission Control
CSTR	Continuous stirred tank reactor
DME	Dimethyl ether
DNV GL	Det Norske Veritas and Germanischer Lloyd
DTU	Technical University of Denmark
EOR	Enhanced oil recovery
FGR	Flue gas recirculation
GC	Gas-chromatograph
GPT	Thermo-Chemical Processes Group
HRSG	Heat recovery steam generator
I3A	Aragón Institute of Engineering Research
IEA	International Energy Agency
IR	Infra-red
ISC	Intersystem-crossing
JCR	Journal Citation Reports
JSR	Jet-stirred reactor
MF	Methyl formate
PFR	Plug flow reactor
ROP	Rate of production
SRU	Sulfur recovery unit
STP	Standard conditions for temperature and pressure
TCD	Thermal conductivity detector
UV	Ultra-violet

Index

1. INTRODUCTION AND OBJECTIVES 1

1.1 Introduction 1

1.2 Objectives 1

2. BACKGROUND 7

2.1 Sour gas 7

2.2 State of the art 13

3. EXPERIMENTAL METHODOLOGY 19

3.1 Atmospheric-pressure tubular flow reactor set-up 19

3.2 High-pressure tubular flow reactor set-up 23

3.3 Atmospheric-pressure jet-stirred reactor (JSR) set-up 26

4. MODELING. REACTION MECHANISM 31

4.1 H_2S oxidation at atmospheric pressure 33

4.2 H_2S oxidation at high pressure 34

4.2.1 H_2/NO mixtures oxidation 35

4.3 H_2S/CH_4 mixtures oxidation 37

4.4 H_2S/NO mixtures oxidation 38

5. RESULTS AND DISCUSSION 43

5.1 H_2S oxidation at atmospheric pressure 43

5.2 H_2 oxidation and its interaction with NO 51

5.3 H_2S oxidation at high pressure 59

5.3.1 Effect of residence time 68

5.3.2 Literature results simulations 70

5.4 H_2S/CH_4 mixtures oxidation 72

5.5 H_2S/NO mixtures oxidation 85

5.6 H_2S and CH_3SH oxidation in a jet-stirred reactor 94

5.7 Reaction pathways 101

6. SUMMARY AND CONCLUSIONS 105

6.1 H_2S oxidation at atmospheric pressure 105

6.2 H_2 oxidation and its interaction with NO 106

6.3 H_2S oxidation at high pressure 107

6.4 H_2S/CH_4 mixtures oxidation 108

6.5 H_2S/NO mixtures oxidation 108

6.6 H_2S and CH_3SH oxidation in a jet-stirred reactor 109

6.7 General conclusion 110

6. RESUMEN Y CONCLUSIONES 115

6.1 Oxidación de H_2S a presión atmosférica 115

6.2 Oxidación de H_2 y su interacción con NO 116

6.3 Oxidación de H_2S a alta presión 117

6.4 Oxidación de mezclas H_2S/CH_4 118

6.5 Oxidación de mezclas H_2S/NO 119

6.6 Oxidación de H_2S y CH_3SH en un reactor *jet-stirred* 120

6.7 Conclusión general 121

BIBLIOGRAPHY 123

Annexes

- Regulations required to submit a PhD Thesis by compendium of publications
- Article I
- Article II
- Article III
- Article IV
- Article V
- Article VI
- Article VII
- Final mechanism

List of figures

Figure 2.1 World primary energy supply by source (Hovem, 2020). 8

Figure 2.2 World final energy demand with and without covid-19. Historical data and future prediction (Hovem, 2020). 9

Figure 2.3 World natural gas production by field type vs. historical evolution and predictions into the future (Hovem, 2020). 10

Figure 2.4 Storing sulfur blocks produced from Claus plants (Harbaugh, 2011). 11

Figure 2.5 Representative diagram of the Claus process. Adopted from Speight (2007). ... 14

Figure 2.6 Generic gas turbine cycles based on the oxy-fuel combined cycle. Adopted from Bongartz et al. (2015). 15

Figure 3.1 Scheme of the experimental set-up 1 used to carry out the oxidation experiments at atmospheric pressure in a tubular flow reactor. Adapted from Marrodán (2018). 20

Figure 3.2 Scheme and dimensions (in mm) of the atmospheric-pressure tubular flow reactor. Adapted from Marrodán (2018). 21

Figure 3.3 Temperature profiles inside the reaction zone of the atmospheric-pressure tubular flow reactor as a function of distance, for different nominal temperatures. 21

Figure 3.4 Scheme of the experimental set-up 2 used to carry out the oxidation experiments at high pressure in a tubular flow reactor. 24

Figure 3.5 Longitudinal temperature profiles inside the reaction zone of the high-pressure tubular flow reactor, for different nominal temperatures and pressures, as a function of distance. 25

Figure 3.6 Scheme of the experimental set-up 3 used to carry out the oxidation experiments in the jet stirred reactor (JSR). Adapted from Zeng (2017)................................ 27

Figure 4.1 Progression in the development of the gas-phase kinetic mechanism for H_2S oxidation and its interaction with other species (CH_4 and NO). 31

Figure 5.1 Comparison between H_2S normalized concentrations vs. temperature from two experiments of H_2S oxidation by Zhou et al. (2013) (λ=1.2) and set 3 in Table 5.1 (λ=1.2). 45

Figure 5.2 Comparison results of set 5 (λ=5.1) and set 8 (1.2% H_2O, λ=5.0) in Table 5.1. Open symbols represent the experimental conditions without water and solid symbols with water vapor. 46

Figure 5.3 Experimental results from H_2S oxidation at atmospheric pressure. Symbols represent experimental data and lines model predictions (black lines denote the results from the final mechanism, while red lines represent the model initially presented in Paper I). 47

Figure 5.4 Sulfur mass balances as a function of temperature for sets 1-6 in Table 5.1. 48

Figure 5.5 Repeatability of experiments under reducing conditions (sets 1 and 1R in Table 5.1; λ=0.3) and almost stoichiometric conditions (sets 3 and 3R in Table 5.1; λ=1.2). 49

Figure 5.6 Results of H_2 oxidation, in the absence and presence of NO, obtained under oxidizing conditions at 10 bar, 20 bar and 40 bar. Solid symbols correspond to experimental results in the presence of NO, while open symbols represent concentrations in the experiments without NO. Lines denote simulations of the final model. Conditions of sets 9 to 14 in Table 5.2. 53

Figure 5.7 Results for the oxidation of NO, in the absence and presence of H_2, obtained under oxidizing conditions at 10 bar of pressure, 20 bar and 40 bar. Solid symbols correspond to experimental results in the presence of H_2, while open symbols represent concentrations in the experiments without H_2. Lines denote simulations of the final model. Conditions of sets 9-11 and sets 15-17 in Table 5.2. 55

Figure 5.8 Results obtained under stoichiometric conditions at 20 bar and 40 bar. Symbols represent experimental measurements and lines denote simulations of the final model. Conditions of sets 18 and 19 in Table 5.2. 56

Figure 5.9 Results obtained under reducing conditions at 20 bar and 40 bar. Symbols represent experimental measurements and lines denote simulations of the final model. Conditions of sets 20 and 21 in Table 5.2. 56

Figure 5.10 Comparison of different values for the kinetic constant logarithm of (R5.16) ($NO+NO+O_2=NO_2+NO_2$) vs. 1/T (K^{-1}), from the literature and the estimation of the present study. 59

Figure 5.11 Concentrations of H_2S, SO_2 and O_2 vs. temperature at 0.65 bar (sets 22, 23 and 24 in Table 5.3). Symbols represent experimental measurements and lines denote simulations of the final model (black lines) and model in Paper III (red line). 62

Figure 5.12 Concentrations of H_2S, SO_2 and O_2 vs. temperature at 10 bar (sets 25, 26 and 27 in Table 5.3). Symbols represent experimental measurements and lines denote simulations of the final model (black lines) and model in Paper III (red line). 63

Figure 5.13 Concentrations of H_2S, SO_2 and O_2 vs. temperature at 20 bar (sets 28, 29 and 30 in Table 5.3). Symbols represent experimental measurements and lines denote simulations of the final model (black lines) and model in Paper III (red line). 64

Figure 5.14 Concentrations of H_2S, SO_2 and O_2 vs. temperature at 40 bar (sets 31, 32 and 33 in Table 5.3). Symbols represent experimental measurements and lines denote simulations of the final model (black lines) and model in Paper III (red line). 65

Figure 5.15 Concentration of H_2S vs. temperature at 40 bar and λ=5.9 (set 33 in Table 5.3) using different mechanisms. Symbols represent experimental data and lines represent modeling predictions. 67

Figure 5.16 Concentrations of H_2S, SO_2 and O_2 vs. temperature at 10 and 20 bar using the same gas residence time (sets 30 and 34 in Table 5.3). Symbols represent experimental data and lines represent model predictions. 69

Figure 5.17 Concentrations of H_2S, SO_2 and O_2 vs. temperature at 10 bar using different gas residence times (sets 27 and 34 in Table 5.3). Symbols represent experimental data and lines represent model predictions. 69

Figure 5.18 Concentrations of H_2S, SO_2 and O_2 vs. temperature at 30 bar and λ=1.14 (data taken from set 1 in Table III of Song et al. (2017)). Symbols represent experimental data, while lines denote model predictions (final mechanism omitting reactions R5.31-5.34). 70

Figure 5.19 Concentrations of H_2S and SO_2 vs. temperature at 30 bar and λ=36 (data taken from set 3 in Table III of Song et al. (2017)). Symbols represent experimental data, while lines denote model predictions (final mechanism omitting reactions R5.31-5.34). 71

Figure 5.20 Concentrations of H_2S and SO_2 vs. temperature at 100 bar and λ=35 (data taken from set 4 in Table III of Song et al. (2017)). Symbols represent experimental data, while lines denote model predictions (final mechanism omitting reactions R5.31-5.34). 71

Figure 5.21 Ignition delay time measurements vs. temperature for different experimental conditions, using a mixture of 1% H_2/1% O_2, diluted in Ar and doped with H_2S. Experimental data are taken from the work of Mathieu et al. (2014). 72

Figure 5.22 Concentrations of H_2S, SO_2, CH_4 and CO vs. temperature under 0.65 bar at set-up 2, experimental conditions in Table 5.4: a) sets 35 (λ_{total}=1.2) and 24 (λ_{total}=5.7); b) sets 36 (λ_{total}=1.0) and 23 (λ_{total}=2.0); c) set 37 (λ_{total}=5.7); d) sets 38 (λ_{total}=3.9) and 24 (λ_{total}=5.7). The original model results (Paper IV) are represented with red lines, while those from the final version of the mechanism are represented with black lines. 74

Figure 5.23 Concentrations of H_2S, SO_2, CH_4 and CO vs. temperature at the experimental conditions in Table 5.4, under 10, 20 and 40 bar at set-up 2. Experiments are shown as follows: a) sets 39 (λ_{total}=1.0) and 26 (λ_{total}=2.1), 10 bar; b) sets 40 (λ_{total}=1.0), 43 (λ_{total}=1.6) and 29 (λ_{total}=2.0), 20 bar; c) sets 41 (λ_{total}=1.0), 44 (λ_{total}=1.6) and 32 (λ_{total}=2.1), 40 bar. The original model (Paper IV) is represented with red lines, while the final version of the mechanism is represented with black lines. 78

Figure 5.24 Concentrations of H_2S, SO_2, CH_4 and CO vs. temperature at the experimental conditions in Table 5.4, under atmospheric pressure at set-up 1: a) sets 45 (λ_{total}=0.3), 48 (λ_{total}=0.2) and 4 (λ_{total}=2.1); b) 46 (λ_{total}=1.0), 49 (λ_{total}=0.9) and 5 (λ_{total}=5.1); c) 47 (λ_{total}=2.0) and 50 (λ_{total}=1.7). The original model results (Paper IV) are represented with red lines, while those from the final version of the mechanism are represented with black lines. 81

Figure 5.25 Concentrations of H_2S, SO_2, CH_4, CO and O_2 vs. temperature from the experiments of Gersen et al. (2017) of H_2S/CH_4 oxidation in a flow reactor at 50 bar. Initial composition: 1.25% CH_4, 1110 ppm O_2, 200 ppm H_2S, and balance N_2 (λ_{total}=0.03). The mechanism results from the authors (Gersen et al., 2017) are represented with red lines, while those from the final version of the mechanism are represented with black lines. 83

Figure 5.26 Concentrations of H_2S, SO_2, CH_4, CO and O_2 vs. temperature from the experiments of Gersen et al. (2017) of H_2S/CH_4 oxidation in a flow reactor at 50 bar. Initial composition: 1500 ppm CH_4, 3010 ppm O_2, 200 ppm H_2S, and balance N_2

(λ_{total}=0.63). The mechanism results from the authors (Gersen et al., 2017) are represented with red lines, while those from the final version of the mechanism are represented with black lines. 84

Figure 5.27 Results from H_2S oxidation in conditions of set 51 in Table 5.5 (λ_{H2S}=0.3). Symbols represent experimental data and lines denote final model predictions. The results of H_2S oxidation without NO correspond to set 1 in Table 5.5 (λ_{H2S}=0.3). 86

Figure 5.28 Results from H_2S oxidation in conditions of set 52 in Table 5.5 (λ_{H2S}=1.3). Symbols represent experimental data and lines denote final model predictions. The results of H_2S oxidation without NO correspond to set 3 in Table 5.5 (λ_{H2S}=1.2). 87

Figure 5.29 Results from H_2S oxidation in conditions of set 53 in Table 5.5 (λ_{H2S}=2.1). Symbols represent experimental data and lines denote final model predictions. The results of H_2S oxidation without NO correspond to set 4 in Table 5.5 (λ_{H2S}=2.1). 87

Figure 5.30 Results from H_2S oxidation in conditions of set 54 in Table 5.5 (λ_{H2S}=2.0). The results of H_2S oxidation without NO (λ_{H2S}=2.0) correspond to set 29 in Table 5.5. Symbols represent experimental data and lines model predictions. The model results of the mechanism detailed in section 4.4 (H_2S/NO oxidation) are shown at the left, and at the right the simulations results include reaction (R5.65) (H_2S+NO_2= S+NO+H_2O). 90

Figure 5.31 Results from H_2S oxidation in conditions of set 55 in Table 5.5 (λ_{H2S}=6.0). The results of H_2S oxidation without NO (λ_{H2S}=6.0) correspond to set 30 in Table 5.5. Symbols represent experimental data and lines model predictions. The model results of the mechanism detailed in section 4.4 (H_2S/NO oxidation) are shown at the left, and at the right the simulations results include reaction (R5.65) (H_2S+NO_2= S+NO+H_2O). 90

Figure 5.32 Results from NO oxidation in the presence (sets 54 and 55 in Table 5.5) and absence (sets 56 and 57 in Table 5.5) of H_2S at 20 bar. The results for NO oxidation without H_2S at λ_{NO}=11.8 correspond to set 16 in Table 5.5. Symbols represent experimental data and lines denote model predictions. The model results of the mechanism detailed in section 4.4 (H_2S/NO oxidation) are shown in the upper graph, while at the bottom, the simulations include reaction R5.65 (H_2S+NO_2= S+NO+H_2O). 92

Figure 5.33 Concentration of H_2S and SO_2 as function of temperature for the experimental conditions of sets 58, 59 and 60 in Table 5.6. Symbols represent experimental concentrations, while lines denote final model predictions................................ 95

Figure 5.34 Concentrations of CH_3SH, CH_4, CO, H_2S, CO_2 and SO_2 vs. temperature for the experimental conditions of set 61 in Table 5.6 (λ=1.0). Symbols represent experimental concentrations, while lines denote final model predictions (continuous lines) and predictions using the model by Alzueta et al. (2019) (dashed lines)... 97

Figure 5.35 Concentrations of CH_3SH, CH_4, CO, H_2S, CO_2 and SO_2 vs. temperature at the experimental conditions of set 62 in Table 5.6 (λ=3.6). Symbols represent experimental concentrations, while lines denote final model predictions (continuous lines) and predictions using the model by Alzueta et al. (2019) (dashed lines)... 98

Figure 5.36 Comparison between experimental and modeling results for λ=5.08. Set 7 in Table 1 of the work by Alzueta et al. (2019). Symbols represent experimental concentrations, while lines denote final model predictions (continuous lines) and predictions using the model by Alzueta et al. (2019) (dashed lines).................. 99

Figure 5.37 Comparison between experimental and modeling results for λ = 0.99. Set 4 in Table 1 of the work by Alzueta et al. (2019). Symbols represent experimental concentrations, while lines denote final model predictions (continuous lines) and predictions using the model by Alzueta et al. (2019) (dashed lines)................ 100

Figure 5.38 Repeatability experiments for neat H_2S oxidation (sets 58 and 58R in Table 5.6) and CH_3SH oxidation (sets 62, $62R_1$ and $62R_2$ in Table 5.6) in the jet-stirred reactor at the Murdoch University.. 100

Figure 5.39 Reaction pathways for H_2S oxidation.. 101

List of tables

Table 2.1 Heat of combustion (ΔH_c) from different fuels. ... 12

Table 2.2 Experimental and kinetic modeling works on H_2S oxidation. ... 16

Table 4.1 Arrhenius parameters for the reactions proposed in this work according to the study by Bian et al. (2019). Arrhenius expression: $k = A\ T^{n}\ \exp[-E_a/(RT)]$. Units are cm^3, mol, s and cal. ... 38

Table 5.1 Experimental conditions for H_2S oxidation in the atmospheric-pressure set-up (set- up 1). N_2 as bath gas. $t_r(s)=194.6/T(K)$. ... 44

Table 5.2 Experimental conditions of H_2 oxidation in the high-pressure set-up 2. The total flow rate is balanced with N_2. Parameter λ_{H2} is calculated according to the reaction $H_2+1/2O_2 \rightleftharpoons H_2O$ and parameter λ_{NO} according to the reaction $NO+1/2O_2 \rightleftharpoons NO_2$. The gas residence time (t_r) is referred to the entire set-up, at one temperature in the reactor (875 K). ... 52

Table 5.3 Experimental conditions for H_2S oxidation in the high-pressure set-up 2. N_2 as bath gas. ... 60

Table 5.4 Experimental conditions for the H_2S/CH_4 mixtures oxidation. N_2 as bath gas..... 73

Table 5.5 Experimental conditions for H_2S/NO mixtures oxidation. N_2 as bath gas. The experiments repeated are denoted with the letter “R”. ... 85

Table 5.6 Experimental conditions for H_2S and CH_3SH oxidation in the JSR at atmospheric pressure. Residence time of 1 second. N_2 as bath gas. The experiments repeated are denoted with the letter “R”. ... 94

Chapter 1.

INTRODUCTION AND OBJETIVES

1. INTRODUCTION AND OBJECTIVES

1.1 INTRODUCTION

As the demand for energy increases worldwide, the necessity to use our natural resources more efficiently is intensified. Sour gas is referred as natural gas that contains a concentration of H_2S above 4 ppm. Natural gas reserves may contain up to 30% in volume of H_2S and it is estimated that from 1/5 to 1/3 of natural gas reserves can be classified as sour gas. Other sources of sour gas include: gases derived from shales and tar sands, refinery gas or biogas obtained by biodegradation of organic matter through anaerobic digestion, which mainly contain CH_4 and CO_2, and also H_2S. The significant amounts of H_2S in sour gas make difficult their application, both due to the environmental problems derived from the presence of H_2S and its corrosive nature.

Traditionally, it has been proposed that a refining of these gases and their adaptation to the formulations of the gases that are currently used would be necessary, and this is expensive. Currently, along with this strategy, it is also proposed not to refine the gases and dedicate the resources to the modification and improvement of combustion technologies and processes, and to the subsequent solution of pollutant problems. This is what is called the achievement of a “double revolution” (McIlroy et al., 2006). As fuel sources such as sour gas become more important, there will be a need to understand the combustion of natural gas and hydrogen sulfide mixtures. However, there are very few studies related to the behavior of the mentioned gaseous mixtures under combustion conditions. Specifically, the effect of the presence of sulfur compounds, mainly hydrogen sulfide, on the conversion of the hydrocarbons present in the fuel mixture is not very well known. Overall, there is a need for a greater number of experimental data to increase the knowledge on H_2S combustion and H_2S-containing mixtures and to validate the kinetic mechanisms that allow to describe the process, as well as a better determination of reaction rates involved in the oxidation of H_2S.

1.2 OBJECTIVES

This work has been developed in the framework of the “Fuel conversion and minimization of pollutants” research line of the Thermo-Chemical Processes Group (GPT) of the Aragón Institute of Engineering Research (I3A) of the University of Zaragoza.

The global objective of this doctoral thesis is to contribute to the knowledge, both from an experimental point of view, under well-controlled laboratory conditions, and from a kinetic modeling point of view, of the conversion of gaseous mixtures of CH_4 and hydrogen sulfide (representative of acid gas) under different operating conditions. The influence of H_2S concentration, temperature, stoichiometry (excess air ratio), as well as pressure, on the reaction products obtained is analyzed. Furthermore, the possible interaction with other typical pollutants in combustion, such as nitrogen oxides (NO_x), is also considered.

This global objective can be divided into the following specific objectives:

- To analyze the conversion of hydrogen sulfide under different operating conditions, at atmospheric pressure (as first step), analyzing variables such as the temperature and the excess air ratio (reducing, stoichiometric and oxidizing conditions) (Paper I).
- To analyze the influence of pressure on H_2S oxidation, evaluating the oxidation of H_2S under different conditions, such as temperature, pressure and gas residence time in the reactor (Paper III and V). Prior to this study, to perform a preliminary study about H_2 oxidation and its interaction with NO at high pressures, with the aim of updating the kinetic model with important subsets of reactions, such as H_2/O_2 and NO_x subsets (Paper II).
- To analyze the oxidation of H_2S/CH_4 mixtures, representative of acid gas, under a wide range of conditions, varying the pressure, temperature, air excess ratio and H_2S and CH_4 concentrations (Paper IV).
- To study the impact of NO addition, a well-known contaminant, on H_2S oxidation under different conditions, such as different pressures, temperatures and stoichiometries (Paper VI).
- To carry out a study of the oxidation of H_2S and CH_3SH (sulfur compound that might be present in sour gas) in different types of reactors (PFR and JSR), in order to compare results, at atmospheric pressure and under different air excess ratios (Paper VII).
- To develop a chemical kinetic mechanism, based on literature mechanisms, updated and improved, to describe the oxidation of H_2S and the different mixtures considered, under the different experimental conditions tested. Rate of production (ROP) analyses are performed to investigate the most important pathways for the consumption of the reactants and the formation of the products. Sensitivity

analyses have been conducted in order to determine the most sensitive reactions in the reaction mechanism.

To achieve these objectives, and in order to perform the experiments, two different experimental facilities with tubular flow reactors have been used, one for the experiments at atmospheric pressure and the other one for the experiments at high pressures. An additional experimental facility, which includes a jet-stirred reactor (JSR) at atmospheric pressure, has been used for specific experiments. The calculations and resolution of the detailed reaction mechanisms have been performed using the CHEMKIN chemical kinetics software (ANSYS Chemkin-Pro, 2016).

Chapter 2.

BACKGROUND

2. BACKGROUND

As stated in the Introduction chapter (Chapter 1), H_2S oxidation is of interest in different combustion processes. Therefore, in this chapter, the properties and characteristics of sour gas, where H_2S is present, and the state of the art regarding H_2S oxidation, are presented.

2.1 SOUR GAS

Sour gas is considered a type of natural gas or any gas that contains significant amounts of H_2S, typically over 4 ppm. H_2S can be formed through the processing of raw materials that contain sulfur or directly be present in the material sources. Coal, oil and natural gas all may contain sulfur in different concentrations and in different forms, for example as H_2S or as organic sulfur (e.g. CH_3SH) in the case of natural gas. When the natural gas is extracted from its source, the gas is treated in gas treating plants before its use in industries or households. When H_2S and other organic sulfur in the gas are removed from the raw material it is called sweetening of the gas. The main processes for the removal of H_2S from natural gas are the amine treating units and Claus sulfur recovery units (SRU) (Kidnay et al., 2019). Removing the sulfur from energy sources is considered important due to the toxic, corrosive and polluting nature of such element. H_2S toxicity is comparable to cyanide, it is smelly and colorless, it can affect severely the human health, blocking O_2 in mitochondria and stopping cellular respiration. Small levels of H_2S can be tolerated, it can be smelled at 5 ppb, it irritates the eyes at 10 ppm, and above 200 ppm it is dangerous to smell because it paralyzes the olfactory nerve. Brief exposures to high levels of H_2S (above 500 ppm) or long exposures to H_2S above 25 ppm are considered to be mortal (Parker, 2010).

Besides the dangerous characteristics of H_2S, usually it has been economically a disadvantage to deal with highly H_2S-contaminanted wells, due to the need for energy intensive separation equipment, that scale poorly with contaminant concentration. For example, H_2S absorption with amines is not economically favorable for feeds containing greater than 3.5 bar of partial pressure of H_2S due to high capital and operating costs (Harrigan et al., 2020). A lot of today's natural gas production comes from large, easily accessible fields. But, as new reserves are exploited, more gas will be produced from smaller fields in remote or off-shore locations, which results in an increasing need for technology able to treat small-scale gas streams.

According to the International Energy Agency (IEA, 2008), the abundance worldwide of reservoirs containing high concentrations of H_2S are estimated in more than 40% of the world's gas reserves, increasing to 60% for Middle Eastern gas reserves. Since natural gas production is expected to peak near 2035 (Maggio and Cacciola, 2012), the abundance of natural gas reserves can facilitate the transition from fossil fuels to renewable sources (Taifan and Baltrusaitis, 2017; Mac Kinnon et al., 2018).

The DNV GL company, that provides independent expert advisory services to the maritime, oil and gas, power and renewables industries, foresees that fossil fuels will account for around 54% of the primary energy supply in 2050, compared to around 80% today. Much of this supply will come from natural gas, as it becomes the world's largest energy source from the middle 2020s (Hovem, 2020). A comparative figure between the world primary energy supplies by source can be seen in Figure 2.1, where the historical data and future predictions are shown (Hovem, 2020).

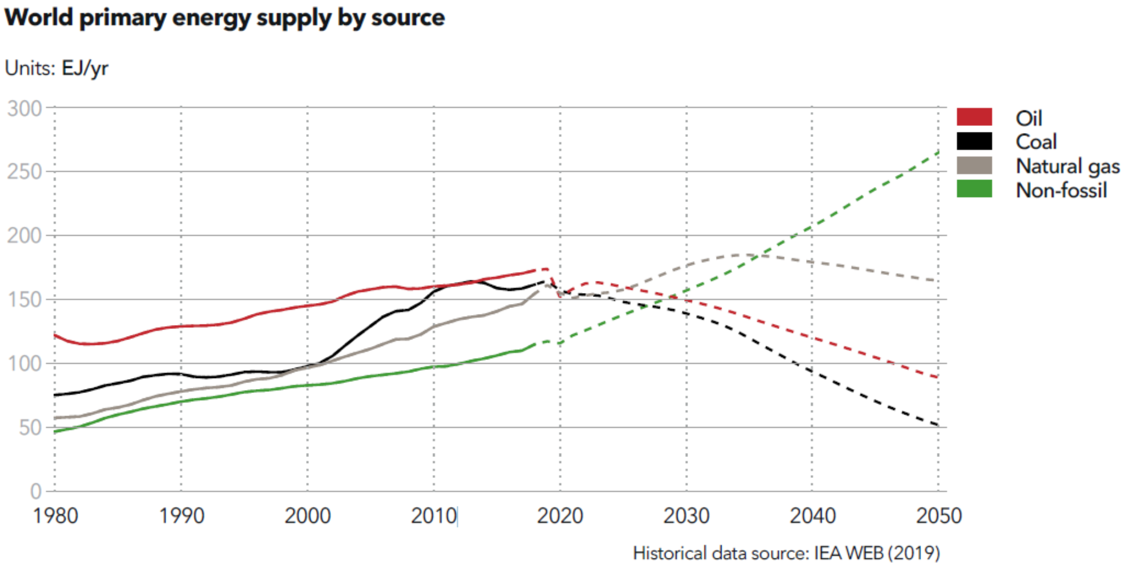

Figure 2.1 World primary energy supply by source (Hovem, 2020).

Natural gas currently represents a smaller portion of the global energy mix than oil and coal, but it will grow to become the largest energy source around 2026 (according to the predictions in Figure 2.1). The observed energy peak in natural gas around 2035 and posterior decline is related to a slower growth in productivity and global population, and the expected continuous increases in energy efficiency, particularly in transport, that will account for much of the decline in energy demand towards 2050. The total world energy demand also presents this forecasted peak, as observed in Figure 2.2, where the final energy demand worldwide is compared before and after covid-19. While the world energy demand has been rising by 30% in the last 15 years, it will not return to previous levels until 2025 and will peak around 2035. Prior to the shock caused by covid-19, energy demand was still set to peak in the mid-2030s, but the peak will now be lower.

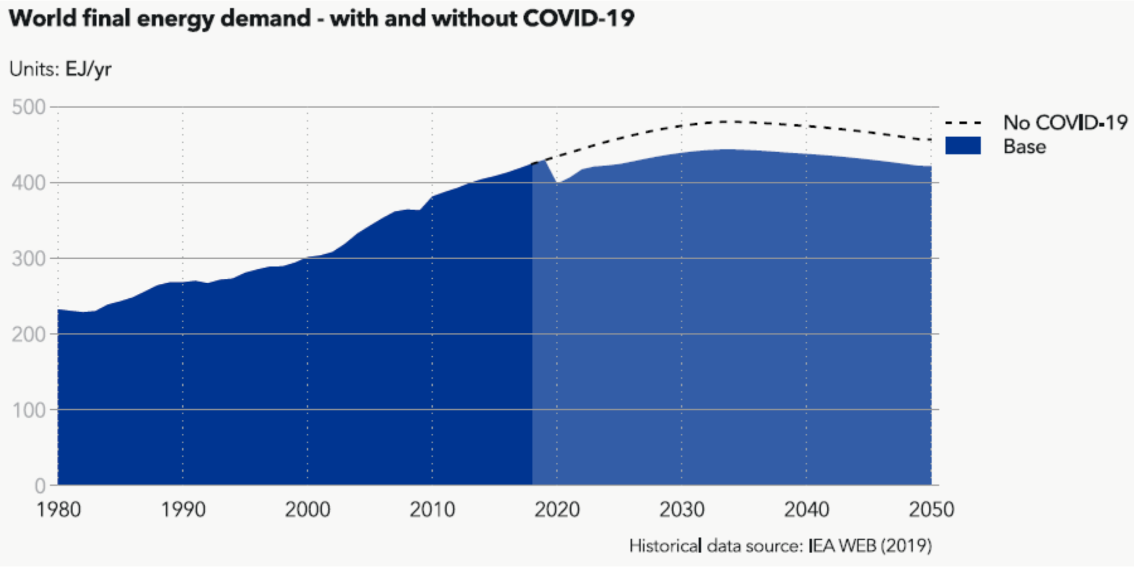

Figure 2.2 World final energy demand with and without covid-19. Historical data and future prediction (Hovem, 2020).

It was already around the year 2000 when the U.S. Department of Energy of the United States recognized that the exploitation of smaller, more sub-quality resources would be necessary to meet the demand as the large gas fields in the U.S. were depleted (Amo et al., 1998). An illustrative image can be seen in Figure 2.3, where the world natural gas production by field type (Tm^3/year) is plotted during the last decades and their future predictions. The production of natural gas from unconventional onshore reserves, depicted in the figure as dark blue, shows an explosion after the year 2000 and represents the natural gas resources where H_2S is more present, and it is expected to become more important in this current decade. In order to be self-sufficient in this important energy resource (natural gas), new fields and formations will be tapped. However, a significant portion of existing reserves are low-quality due to presence of hydrogen sulfide, carbon dioxide, and nitrogen. New gas fields are expected to be more remote and smaller than those currently used.

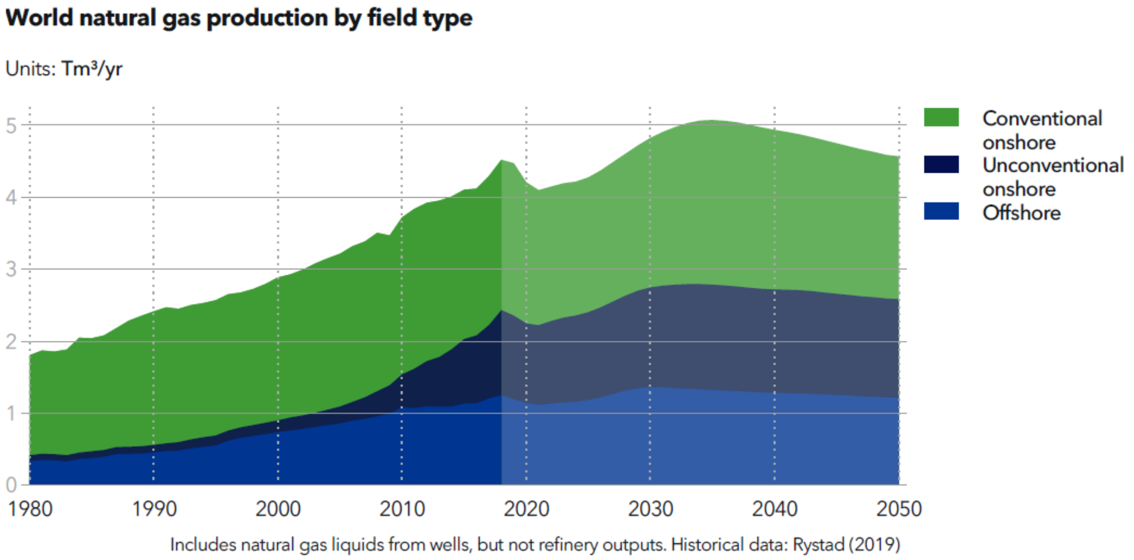

Figure 2.3 World natural gas production by field type vs. historical evolution and predictions into the future (Hovem, 2020).

In order to exploit gas fields, the usual procedure is to remove the H_2S to the pipeline specification of 4 ppm. One of the technologies used to achieve this specification is amine absorption, or a similar chemical or physical solvent process. Although this technology is mature and widely used in the gas industry, absorption processes are capital and energy-intensive. This makes these processes unsuitable for treating gas at low yields, in remote locations, or with a high concentration of acid gases (Amo et al., 1998).

Membrane technology is another option for removing hydrogen sulfide from natural gas. Economic analyses indicate that these processes provide 20-40% cost savings over absorption technologies. Membrane technology is more energy efficient with low capital cost, simple operation, and low maintenance, as well as minimal environmental impact. Despite these advantages, current membrane processes require the improvement of membrane materials in order to obtain high productivity and high selectivity to minimize capital and operating cost (Baker and Lokhandwala, 2008; Yi et al., 2015).

Another solution to deal with gas streams containing H_2S, known as the most significant one, is to convert H_2S to sulfur, through the Claus process in sulfur recovery units. Gases with a H_2S content over 25% can be treated by the Claus process (Fahim et al., 2010). Typically, industries have an amine scrubbing system, to concentrate the H_2S, and a sulfur recovery unit to convert it into sulfur. While this combination of amine scrubber with Claus plant is effective at large scale, it is too expensive on a small scale and requires very large plants to be economical

(Parker, 2010). Small sour natural gas sources must be connected to a central desulfurization facility through H_2S corrosion resistant stainless steel pipelines, or their H_2S removed at source by smaller amine plants and then transported by truck to the central facility. Both of these options are expensive, hindering the development of sour natural gas resources.

The fact that Claus plants at small scale are not economical are also related to the low sulfur price. Oil, gas, tar sand and metal smelters have replaced the production of sulfur from mining and pyrites worldwide over the last decades (U.S. Geological Survey, 2019). This has reached to the point that sulfur, as a by-product from these industries, has surpassed the demand for this commodity (Rappold and Lackner, 2010). As can be seen in Figure 2.4, piles of sulfur accumulate in the desulfurization facilities. When sulfur is not valuable enough to transport, it is poured into large blocks to solidify for long term storage. Later, when prices rise, it is shipped to market and burned where needed to produce the more useful sulfuric acid. Around 75 Mt of elemental sulfur are globally produced per year from oil and gas processing units, which contributes to a large economic area (Duong-Viet et al., 2020).

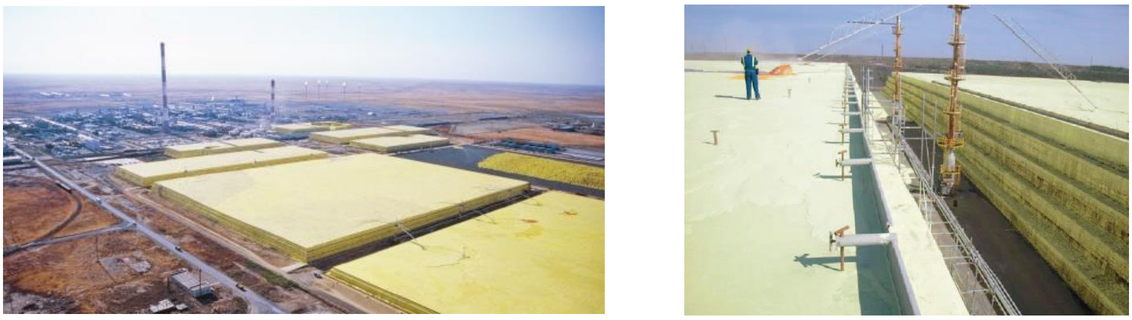

Figure 2.4 Storing sulfur blocks produced from Claus plants (Harbaugh, 2011).

Overall, more reserves containing high levels of H_2S need to enter production as natural gas demand rises and high-quality reserves become rare. This has led to think about alternative solutions to deal with sour gas and H_2S. For example, obtaining revenue of sour gas processing integrated with ethylene production (He and You, 2014), or producing hydrogen and syngas together with sulfur in the Claus process (Salisu and Abhijeet, 2016; Barba et al., 2017) or different catalytic processes which convert sour gas to valuable products such as: H_2, CS_2 and fertilizers (Taifan and Baltrusaitis, 2017), and also H_2S combustion, which if compared with coal combustion releases similar energy, around 100 kcal/mol (Rappold and Lackner, 2010) (according to $H_2S+1.5O_2=SO_2+H_2O+124$ kcal/mol). A comparison between the energy released during the combustion process using different fuel sources can be seen in Table 2.1. Hydrogen sulfide has similar ΔH_c (kcal/g) value to other alternative fuels such as ammonia, methanol, wood and some types of coal.

Table 2.1 Heat of combustion (ΔH_c) from different fuels.

Compound	ΔH_c (kcal/mol)	ΔH_c (kcal/g)
Ammonia (NH_3)	67	4
Butane (C_4H_{10})	623	11
Carbon (C)	94	8
Coal (Anthracite)	-	8
Coal (lignite-USA)	-	4
Wood fuel	-	5
Gasoline	-	11
Glucose ($C_6H_{12}O_6$)	592	3
Hydrogen (H_2)	55	28
Hydrogen sulfide (H_2S)	124	4
Methane (CH_4)	183	11
Methanol (CH_4O)	157	5
Sulfur (S)	71	2

Regarding H_2S combustion, economic and performance analyses of power generation systems have been published for un-treated sour gas as fuel (Chakroun and Ghoniem, 2015a, 2015b; Lu et al., 2018), showing estimations 30% cheaper than the natural gas combined cycle. In the same manner, sulfur as a fuel source has also been considered for power generation in combined power cycles (Hajar et al., 2016). The sulfur compounds are expected to be oxidized in a combustion chamber (10-50 bar) to produce work in a gas turbine. Rough estimations indicate that an existing sulfur surplus of 10 Mt per year implies an energy potential of 0.01-0.1% of the world's total primary energy supply of 15 Tera-Watts (Hajar et al., 2016). Additionally, Clark and Stevens (2005), with the idea that fossil fuel development requires long-term sulfur strategies, have proposed a way of using the energy liberated from acid gas combustion and returning the sulfur to the gas reservoir. In this way, SO_2 is compressed and liquefied into the sour gas or sour-oil reservoir. Once SO_2 is in the well, it is thought to react instantaneously with the residual H_2S, in an underground Claus reaction. Such reaction would produce sulfur and water, which are safer to store in the reservoir (Davis et al., 2008).

Apart from sour gas reserves, H_2S is also present together with CH_4 in biogas, in a range of 100 to 10000 ppm (Awe et al., 2017). Raw biogas consists mainly of: 40-75% of CH_4, 15-60% of CO_2 and minor constituents such as H_2S and NH_3 (Tilahun et al., 2017). Since renewable energies are going to constitute an important supply to the world energy demand and reduce greenhouse gas emissions, the energy from biomass has the potential to provide power to the grid on demand, for example, using biogas combustion in gas turbines (Valera-Medina et al., 2018), which can tolerate a H_2S content up to 10000 ppm (Awe et al., 2017). However, this needs to be further investigated (Jerzak et al., 2016).

As seen, ammonia (NH_3) might be present in biogas together with H_2S, but it may also be present in sour gas (Gupta et al., 2016). The presence of NH_3 could produce fuel NO_x emissions in the combustion process. In oxy-combustion, the flue gas recirculation (FGR) process could promote the interaction between H_2S/NO_x, since impurities in the flue gas are brought back to the combustion zone. FGR is a strategy to reduce NO_x emissions by decreasing the combustion temperature used in different combustion processes (Abián et al., 2012), such as oxy-combustion (De Diego et al., 2013). Also, in sulfur recovery units (Claus process), the formation of NO_x from NH_3 (up to 40% presence in the feed of sour gas, as it is a common by-product in fossil/bio-refineries, gas fields and petrochemical processes) might occur (Salisu et al., 2020). NO_x has been found to promote the oxidation of SO_2 to SO_3 (Fleig et al., 2013) and cause catalyst sulfation (deactivation) in the catalytic step of the Claus process (Li et al., 2016), as well as other operational problems like the interaction of NH_3 with SO_3 to form ammonium salts. The interaction between H_2S and NO_x might occur as well, since only 1/3 of all H_2S is converted to SO_2 in the previous step to the catalytic one (thermal step).

2.2 STATE OF THE ART

Regarding H_2S oxidation, studies from the literature are scarce. In the past, most of the studies were focused on atmospheric chemistry. However, the chemistry in the oxidation of H_2S remains unknown in many aspects, while the available experimental data are limited. In the last decades, significant progress in the kinetics and mechanisms of the atmospheric oxidation chemistry of sulfur has been done, although less effort has been placed on developing and understanding sulfur combustion kinetics (Gardiner, 2000; Gupta et al., 2016). The most studied combustion conditions are the ones related to the Claus process, which is the main chemical industrial process that deals with H_2S.

The Claus process is divided in two steps and a schematic figure of it can be seen in Figure 2.5. First, in the thermal step, a partial oxidation (1/3 of H_2S) with air at high temperature (1300-1700 K) occurs. The main reaction occurring is (R2.1):

$$2H_2S + 3O_2 \rightleftharpoons 2SO_2 + 2H_2O \qquad \text{(R2.1)}$$

In the next section, the catalytic step, the remaining H_2S reacts with SO_2 at low temperatures (500-600 K) over a catalyst (based on alumina and/or titanium) to form sulfur (R2.2).

$$2H_2S + SO_2 \rightleftharpoons 3S + 2H_2O \qquad \text{(R2.2)}$$

H_2S conversion typically reaches 96-98%, depending on the feed composition and the thermodynamic limitations of the process. About half of the H_2S handling costs in the Claus process are related to the tail gas treatment (De Crisci et al., 2019). To increase the efficiency of the system, some improvements have been developed over the last decades (Elsner et al., 2003). For example, CH_4 might be added to the process to increase furnace temperature and preventing flame extinction caused by the presence of CO_2 (main component of sour gas together with H_2S) (Salisu et al., 2017), or the use of oxygen enrichment, that manages to raise the flame temperature by eliminating the diluent effect of air nitrogen (Rameshni, 2002).

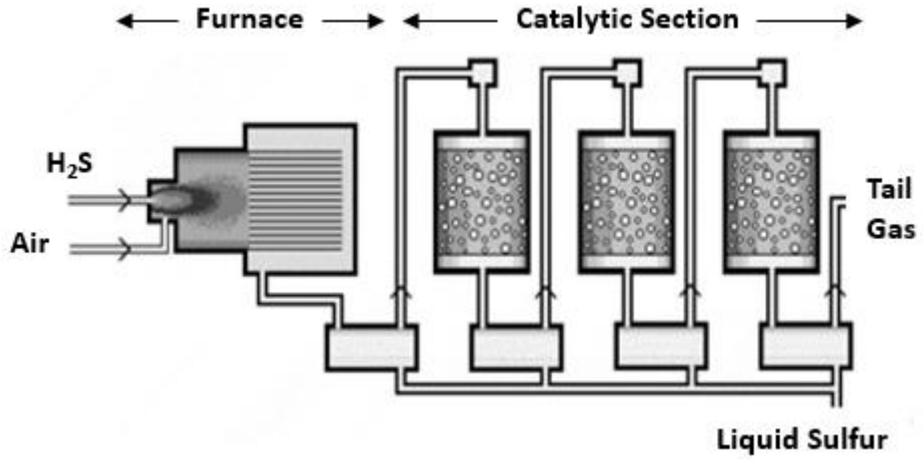

Figure 2.5 Representative diagram of the Claus process. Adopted from Speight (2007).

A detailed reaction mechanism would enable to predict with precision gas temperatures and species composition in the furnace (thermal step), which would help to conduct SRU optimization studies, for example, for the co-combustion of NH_3 with Claus feed components, like H_2S. However, reactions involving NH_3 (NO_x formation included) that occur in the Claus furnace are complex and not fully understood. As stated by Gupta et al. (2016), the destruction of NH_3 is governed by kinetics rather than equilibrium, hence, more studies are needed in this regard. In the same way, no reactions involving H_2S/NO_x interactions are contemplated yet or have been taken into account previously in the literature.

More recently, several scientific works have focused on H_2S theoretical studies of combustion chemistry. For example, Cong et al. (2016) developed a mechanism to assess the production of hydrogen through H_2S thermolysis and oxidation for the Claus process. Bongartz et al. (2015) and Bongartz and Ghoniem (2015a, 2015b) developed an optimized mechanism to make predictions on the combustion behavior of sour gas under oxy-fuel conditions. They designed power cycles to study the combustion of sour gas with enhanced oil recovery (EOR) and an example of a generic cycle by Bongartz et al. (2015) is shown in Figure 2.6. EOR is a technique to increase the extraction from a gas or oil reserves by injecting carbon dioxide and water (and potentially SO_2), which would be the products of the sour gas oxidation. According to these authors, there is still a need for more accurate direct determination of several important rate constants as well as more validation data.

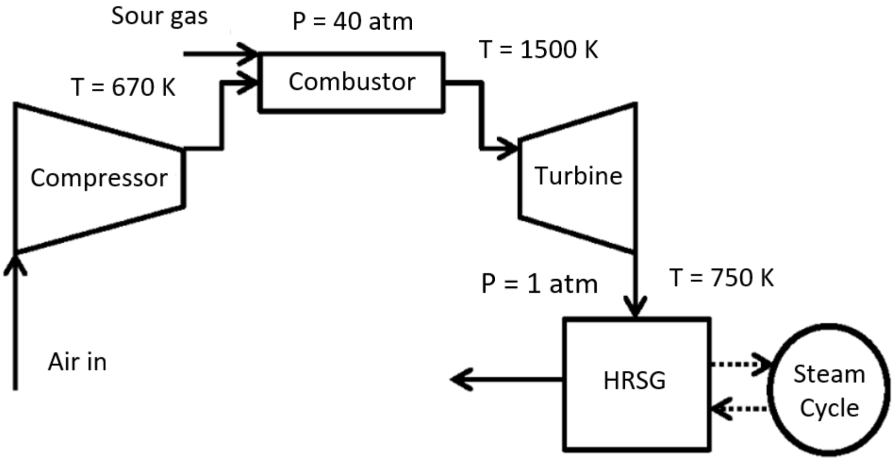

Figure 2.6 Generic gas turbine cycles based on the oxy-fuel combined cycle. Adopted from Bongartz et al. (2015).

Experimental and modeling works of H_2S conversion, more related to the ones performed in the present thesis, are not abundant. The last studies about H_2S oxidation under controlled laboratory conditions and providing new data in terms of kinetic modeling are detailed in Table 2.2, together with the corresponding experimental conditions, that include different air excess ratios (from stoichiometric to oxidizing conditions). These works include: the experiments about ignition delay times by Mathieu et al. (2014); the study at atmospheric pressure in a plug flow reactor by Zhou et al. (2013), who mentioned the possibility of catalytic reactions promoted by the quartz reactor walls on H_2S oxidation; the study at high pressures about H_2S oxidation in a plug flow reactor, which was entitled as “exploratory” by Song et al. (2017); and the work by Gersen et al. (2017) about H_2S/CH_4 mixtures oxidation in a flow reactor at 50 bar. However, the kinetic modeling carried out in those studies show gaps between experimental results and model predictions, as well as discrepancies from one work to the other, pointing to the necessity of a better characterization of certain reactions. At the same time, more experiments are desired in order to validate the kinetic mechanisms. This task is very important because the experimental results obtained might be useful for other studies. For example, for those based on kinetic mechanisms that perform computer simulations of sour gas oxy-combustion, similar to the ones by Bongartz et al. (2015).

Table 2.2 Experimental and kinetic modeling works on H_2S oxidation.

Reference	Type of experiment	Experimental conditions
Zhou et al. (2013)	Plug-flow reactor	T 950-1150 K; P=1 bar; λ_{H2S}=1.2-6.7
Mathieu et al. (2014)	Shock tube	T 1045-1860 K; P=1.6-33 bar; λ_{H2S}=4.2-66.7
Gersen et al. (2017)	Plug-flow reactor	T 500-900 K; P=50 bar; λ_{H2S}=3.7-10.0
Song et al. (2017)	Plug-flow reactor	T 500-900 K; P=30-100 bar; λ_{H2S}=1.1-35.7

*λ_{H2S}: the air excess ratio (λ) is defined as inlet oxygen divided by stoichiometric oxygen (calculated according to the reaction $H_2S+3/2O_2=SO_2+H_2O$).

In this context, there is a clear need to study the H_2S oxidation, as well as its mixtures with other sour gas components, both from an experimental and kinetic modeling point of view. This study aims to extend the results available in the literature related to H_2S conversion as well as to develop a kinetic model capable of reproducing such conversion under a wide variety of conditions.

Chapter 3.

EXPERIMENTAL METHODOLOGY

3. EXPERIMENTAL METHODOLOGY

The oxidation experiments have been performed in three different experimental set-ups, with different types of reactors: two tubular flow reactors operating at atmospheric and high pressure, located in the facilities of the Thermo-Chemical Processes Group (GPT group), in the framework of the Aragón Institute of Engineering Research (I3A) of the University of Zaragoza; and a perfectly stirred reactor (also known as jet-stirred reactor, JSR) available at the University of Murdoch, in the city of Perth (Australia), where a research stay was performed during the development of the present thesis.

A brief description with the more relevant features of the different experimental set-ups is included in this chapter, while a more complete description of them and of the experimental methodology followed can be consulted in previous works, such as those of Esarte (2011), Abián (2013), Zeng (2017) and Marrodán (2018).

The conditions of the different experiments performed are detailed in tables in Chapter 5, while analyzing the main results obtained in the corresponding study.

3.1 ATMOSPHERIC-PRESSURE TUBULAR FLOW REACTOR SET-UP

The oxidation experiments of H_2S, H_2S/CH_4 and H_2S/NO mixtures have been carried out in the experimental set-up shown in Figure 3.1, which has been successfully used in a number of previous works by our research group, addressing the study of homogeneous gas-phase reactions (set-up 1) (e.g. Alzueta et al., 2001a; Alzueta et al., 2008; Alexandrino, 2018; Marrodán, 2018).

In this set-up, the reactions take place in a quartz tubular flow reactor (Figure 3.2), which has been built according to the design proposed by the CHEC (Combustion and Harmful Emission Control) Group of the Technical University of Denmark (DTU) (Kristensen et al., 1996). The reactor presents a reaction zone of 8.7 mm internal diameter and 200 mm in length. It is placed in a three-zone electrically heated furnace, ensuring a uniform temperature profile throughout the reaction zone within ±5 K. An example of the longitudinal temperature profiles along the reaction zone, for different nominal temperatures, is shown in Figure 3.3. Temperature has been measured with a K-type thermocouple for a total N_2 flow rate of 1 L (STP)/min. The experiments were run from 700 to 1400 K.

The different gases are led to the reactor through mass flow controllers (Bronkhorst High-Tech), in four separate streams: a main flow containing nitrogen, which can, in some cases, have water vapor, and three injector tubes for the different reactants (H_2S, O_2, CH_4 and NO). Nitrogen is used to balance up to obtain a total flow rate of 1 L (STP)/min. Reactants are highly diluted in N_2, minimizing reaction thermal effects. Reactants and nitrogen are fed from gas cylinders, while water vapor is injected by saturating a N_2 stream through a water bubbler at the adequate temperature to get the desired H_2O concentration in the reaction zone. The function of water is to minimize the impact of radical recombination in the reactor walls, the quenching effect. Moreover, water is a representative species of the mixture generated under combustion conditions.

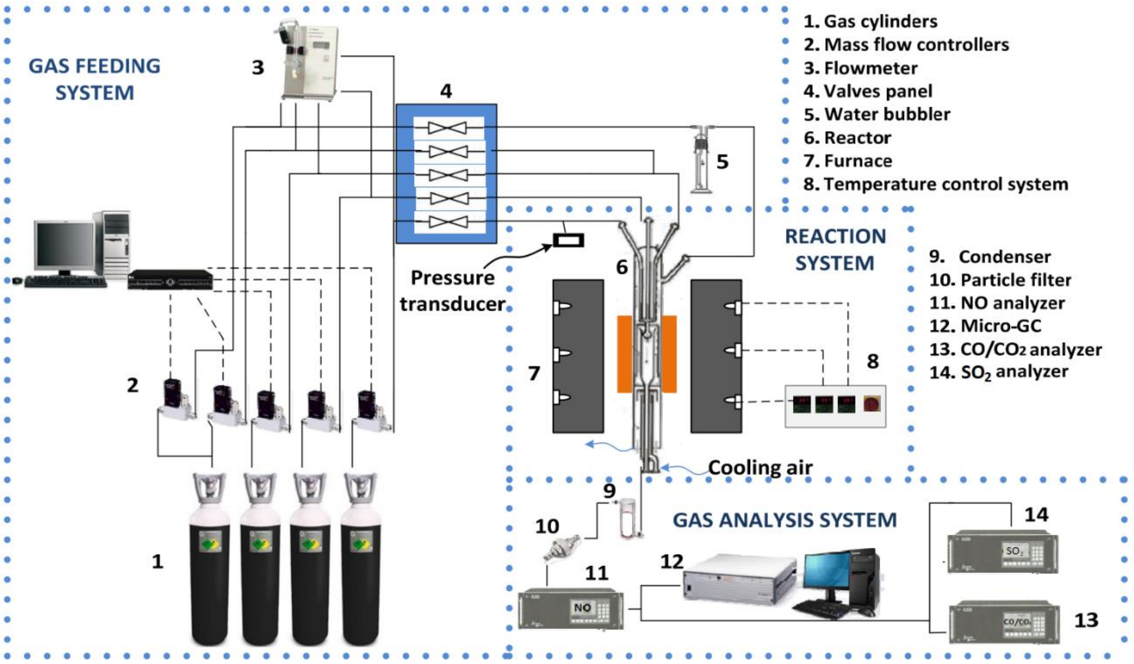
GAS FEEDING SYSTEM
REACTION SYSTEM
GAS ANALYSIS SYSTEM
1. Gas cylinders
2. Mass flow controllers
3. Flowmeter
4. Valves panel
5. Water bubbler
6. Reactor
7. Furnace
8. Temperature control system
9. Condenser
10. Particle filter
11. NO analyzer
12. Micro-GC
13. CO/CO2 analyzer
14. SO2 analyzer
Pressure transducer
Cooling air
1
2
3
4
5
6
7
8
9
10
11
12
13
14
NO
SO2
CO/CO2

Figure 3.1 Scheme of the experimental set-up 1 used to carry out the oxidation experiments at atmospheric pressure in a tubular flow reactor. Adapted from Marrodán (2018).

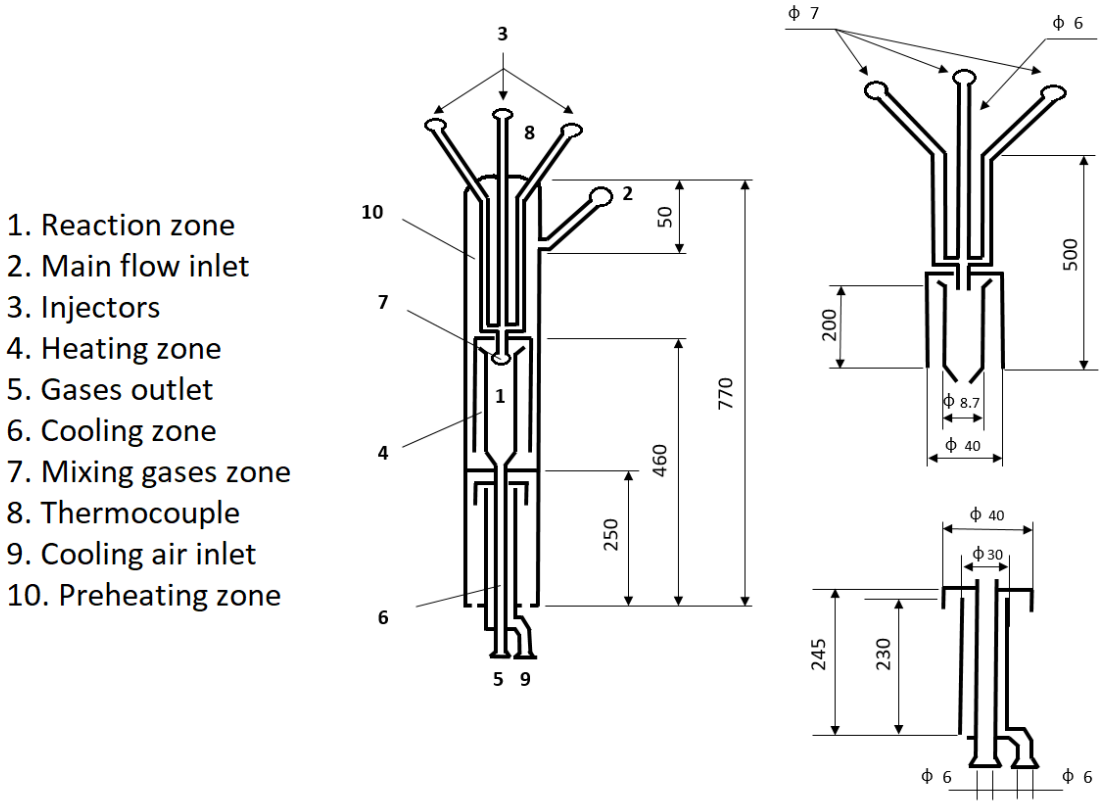
1. Reaction zone
2. Main flow inlet
3. Injectors
4. Heating zone
5. Gases outlet
6. Cooling zone
7. Mixing gases zone
8. Thermocouple
9. Cooling air inlet
10. Preheating zone
3
8
10
2
50
7
1
4
770
460
250
6
5
9
ϕ 7
ϕ 6
500
200
ϕ 8.7
ϕ 40
ϕ 40
ϕ 30
245
230
ϕ 6
ϕ 6

Figure 3.2 Scheme and dimensions (in mm) of the atmospheric-pressure tubular flow reactor. Adapted from Marrodán (2018).

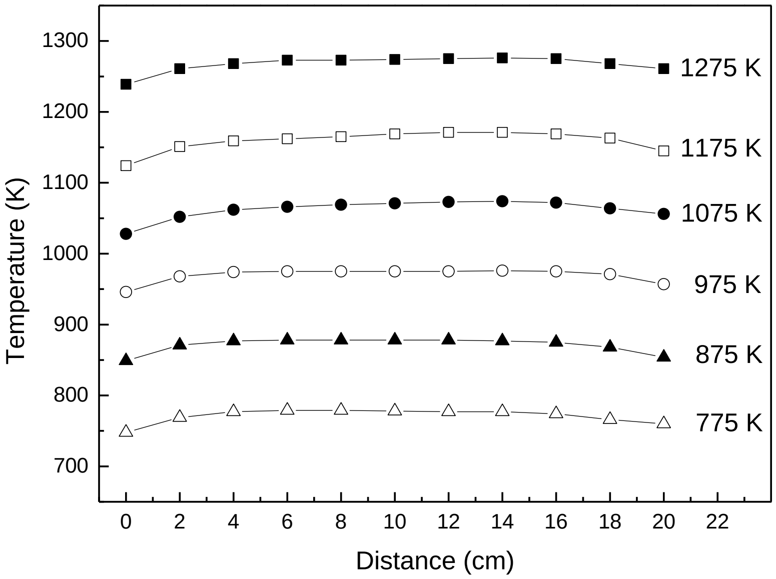

Figure 3.3 Temperature profiles inside the reaction zone of the atmospheric-pressure tubular flow reactor as a function of distance, for different nominal temperatures.

Under these conditions, the gas residence time (t_r) in the reaction zone depends on the temperature in this zone as follows:

$$t_r\,[\mathrm{s}] = \frac{194.6}{T\ [\mathrm{K}]} \qquad \text{(Eq. 3.1)}$$

The oxygen inlet concentration is determined by the air excess ratio (λ), which is defined as the real oxygen fed to the reactor ($O_{2,fed}$) divided by the stoichiometric oxygen ($O_{2,st}$), given the complete oxidation of the reactant (R3.1), which might be H_2S, H_2, CH_4, CH_3SH or NO:

$$\text{Reactant} + aO_2 \rightarrow wSO_2 + xCO_2 + yH_2O + zNO_2 \qquad \text{(R3.1)}$$

Thus, the amount of oxygen to be fed to the reactor is calculated by (Eq. 3.2) as a function of the air excess ratio analyzed,

$$\lambda = \frac{O_{2,fed}}{O_{2,st}} = \frac{O_{2,fed}}{a \cdot [reactant]_{inlet}} \qquad \text{(Eq. 3.2)}$$

being $[reactant]_{inlet}$ the inlet concentration of the reactant. Therefore:

$\lambda > 1 \rightarrow$ fuel-lean or oxidizing conditions

$\lambda = 1 \rightarrow$ stoichiometric conditions

$\lambda < 1 \rightarrow$ fuel-rich or reducing conditions

In the case of the mixtures, a total value of lambda has been calculated considering the oxygen required for the stoichiometric conversion of all the mixture components, according to the complete oxidation reaction (R3.1).

The same procedure to calculate the air excess ratio values (R3.1 and Eq. 3.2) has been followed in the experiments performed in the other reactors used in the present work: in the high-pressure set-up (set-up 2), where the oxidation of H_2S, H_2 and the mixtures H_2S/CH_4, H_2S/NO and H_2/NO has been studied; and the jet-stirred reactor (set-up 3), considering the oxidation of H_2S and CH_3SH.

At the outlet of the reaction zone, the gas product is quenched by means of an external cooling air flow, and before analysis, it passes through a condenser and a particle filter to ensure gas cleaning. The outlet gas composition is analyzed by an Agilent 3000A micro gas-chromatograph (micro-GC) equipped with thermal conductivity detectors (TCD), an Emerson continuous analyzer with ultraviolet (UV) detector for SO_2, and ABB continuous infrared (IR) analyzers for CO, CO_2 and UV analyzer for NO. The uncertainty of the measurements is estimated as ±5%. The error has been calculated according to the standard pooled deviation (the square root of the sum of the squares of the error), where the error does not depend on the temperature in the interval considered and it is an estimator of the experimental error associated with the oxidation of H_2S. The pooled standard deviation has been calculated as ±16 ppm. For each set, results at different temperatures (increasing the temperature by 25-50 K in the corresponding temperature range) are obtained.

3.2 HIGH-PRESSURE TUBULAR FLOW REACTOR SET-UP

The high-pressure oxidation experiments of H_2S, H_2 and the mixtures H_2S/CH_4, H_2S/NO and H_2/NO have been carried out in a laboratory-scale high-pressure tubular flow reactor designed to approximate plug flow (Rasmussen et al., 2008a), which has been successfully used in previous works by our research group addressing the study of homogeneous high-pressure reactions (e.g. Marrodán et al., 2014; Marrodán, 2018).

A scheme of the experimental set-up is shown in Figure 3.4 (set-up 2). In this set-up, the oxidation takes place in a tubular quartz tube (inner diameter of 6 mm and length of 1500 mm). The reactor is enclosed in an AISI 316L stainless steel tube, which acts as a pressure shell. Nitrogen is delivered to the shell side of the reactor by a pressure control system, to obtain a pressure similar to that inside the reactor, avoiding in this way the stress in the reactor. The pressure inside the reactor is monitored by a differential pressure transducer (EL-PRESS Bronkhorst High-Tech), located at the reactor entrance and controlled by a pneumatic pressure valve (RCV-RC200) situated after the reactor. The pressure values given throughout this thesis, referred to this high-pressure set-up, indicate manometric pressures. The reactor-pressure shell system is placed inside a three-zone electrically heated furnace with individual temperature control, which allows a maximum temperature over the whole pressure range up to 1300 K.

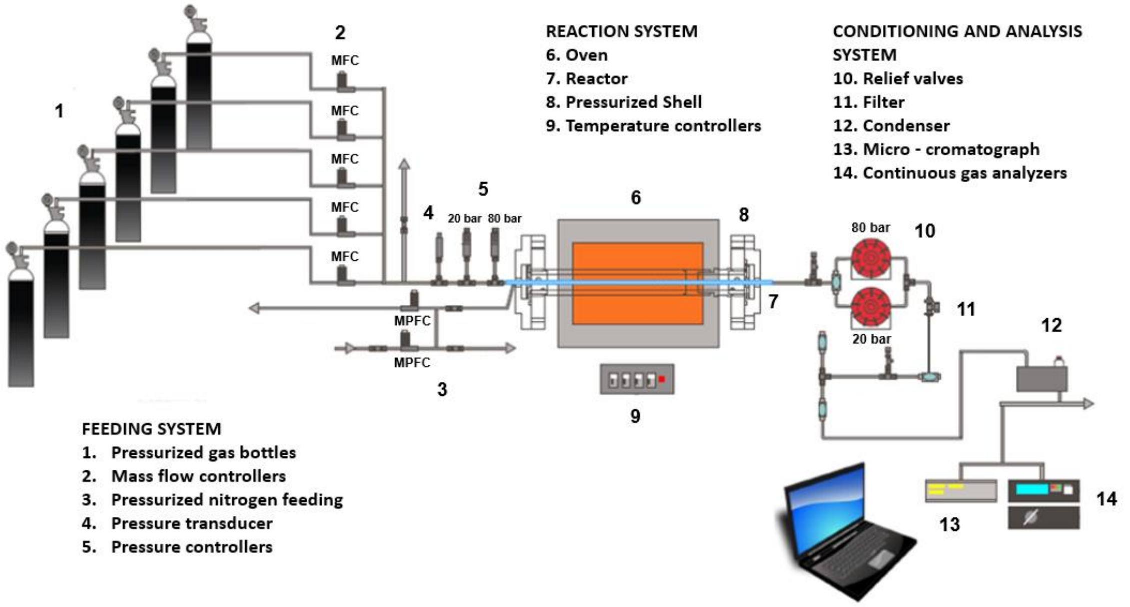
1
2
MFC
MFC
MFC
MFC
MFC
3
MPFC
MPFC
4
5
20 bar
80 bar
6
7
8
9
10
80 bar
20 bar
11
12
13
14
REACTION SYSTEM
6. Oven
7. Reactor
8. Pressurized Shell
9. Temperature controllers
CONDITIONING AND ANALYSIS SYSTEM
10. Relief valves
11. Filter
12. Condenser
13. Micro - cromatograph
14. Continuous gas analyzers
FEEDING SYSTEM
1. Pressurized gas bottles
2. Mass flow controllers
3. Pressurized nitrogen feeding
4. Pressure transducer
5. Pressure controllers

Figure 3.4 Scheme of the experimental set-up 2 used to carry out the oxidation experiments at high pressure in a tubular flow reactor.

Type K thermocouples, positioned in the void between the quartz reactor and the steel shell, were used to measure the longitudinal temperature profiles, obtaining an isothermal reaction zone (±5 K) of 50 cm. An example of the longitudinal temperature profiles along the reaction zone for different nominal temperatures and pressures is shown in Figure 3.5.

The gases (H_2S, CH_4, NO, H_2, O_2 and N_2) are fed into the reaction system from gas cylinders through mass flow controllers (Bronkhorst High-Tech). N_2 is used to balance up to obtain a total flow rate of 1 L (STP)/min. The gas residence time (t_r) in the reaction zone is a function of both temperature and manometric pressure in this zone and is given by (Eq. 3.3):

$$t_r\,[\mathrm{s}] = \frac{232 \cdot P\ [\mathrm{bar}]}{T\ [\mathrm{K}]} \qquad \text{(Eq. 3.3)}$$

Downstream the reactor, the pressure of the system is reduced to atmospheric level before the outlet gases analysis, which is performed using a gas micro gas-chromatograph (Agilent 3000A) equipped with thermal conductivity detectors (TCD), and the same continuous analyzers previously mentioned in the set-up at atmospheric pressure. The uncertainty of the measurements is estimated as ±5%. The error has been calculated according to the standard pooled deviation (the square root of the sum of the squares of the error), where the error does not depend on the temperature in the interval considered and it is an estimator of the experimental error associated with the oxidation of H_2S. The pooled standard deviation has been calculated as ±10 ppm. For each set, results at different temperatures (increasing the temperature by 25-50 K in the corresponding temperature range) are obtained.

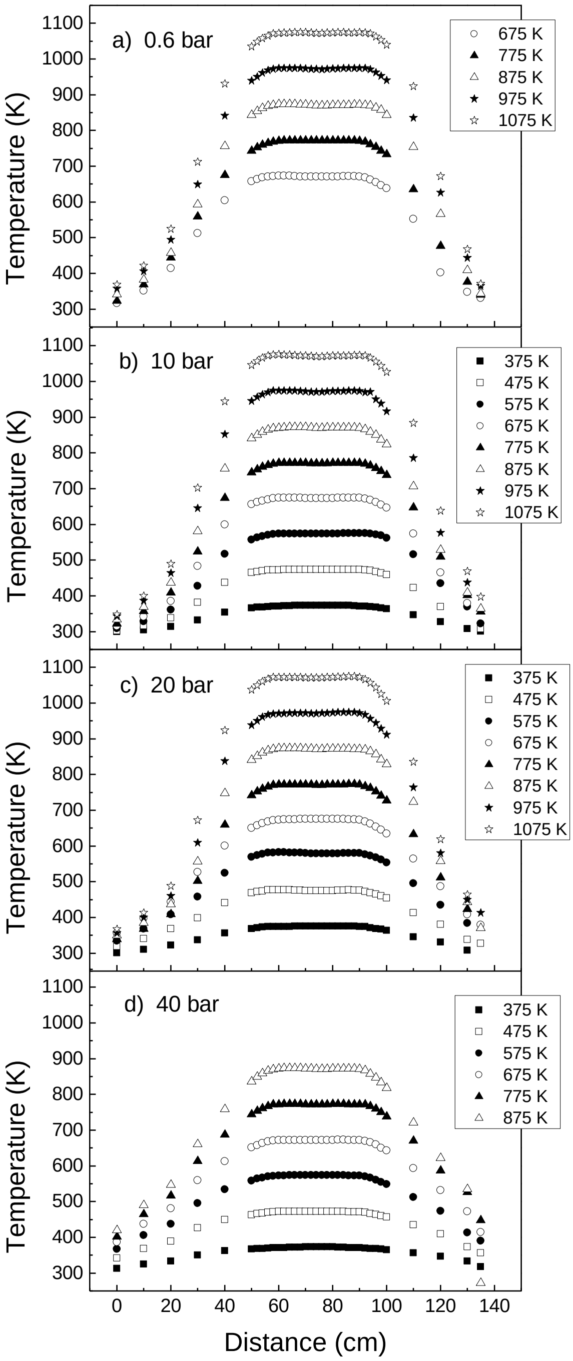

Figure 3.5 Longitudinal temperature profiles inside the reaction zone of the high-pressure tubular flow reactor, for different nominal temperatures and pressures, as a function of distance.

3.3 ATMOSPHERIC-PRESSURE JET-STIRRED REACTOR (JSR) SET-UP

The oxidation experiments of neat H_2S and neat CH_3SH, in a jet-stirred reactor (JSR) at atmospheric pressure, have been carried out in the experimental set-up shown in Figure 3.6 (set-up 3) and available at the University of Murdoch, Australia. This experimental set-up has been used with success in a number of previous works (e.g. Zeng et al., 2019a, 2019b), and it is similar to other experimental set-ups reported in the literature that also count with a JSR (Rodríguez et al., 2017; Song et al., 2019).

The JSR used in this work is based on the design of Herbinet and Dayma (2013) from the Laboratoire des Réactions et Génie des Procédés in Nancy (France) that came from the work of Matras and Villermaux (1973). The JSR sphere (59 mm of internal diameter (i.d.) and 107.5 cm^3 of volume) and access lines are made of quartz. The annular space of entrance tube affords the channel for inlet gas, forcing the reactants to flow rapidly into the sphere reactor. The injector part of the reactor has four nozzles of 0.3 mm i.d. each one, generating the jet flows into the sphere space, for the delivery of the reacting gas mixture. This arrangement minimizes temperature and concentration gradients in the reactor, representing the so-called continuous stirred-tank reactor (CSTR) (Herbinet and Dayma, 2013). The reactor rests along the center line of an electrically heated single-zone furnace (Brother Furnace), which goes from 600 K to 1200 K. The gases (air, H_2S and CH_3SH diluted in N_2) are fed into the reaction system from gas cylinders through two mass flow controllers (Brooks), that adjust the flow rate of reactants (H_2S or CH_3SH, and air) to maintain a fixed gas residence time of 1 second in the reactor.

The oxidation products are measured online at the reactor outlet with a micro gas-chromatograph (Agilent micro-GC 490) equipped with thermal conductivity detectors (TCD). A Fourier Transform InfraRed (FTIR) spectrometer monitors the SO_2 concentration exiting the JSR (Perkin Elmer Frontier 100 Fourier transform infrared spectroscope). Consistent SO_2 concentration data between FTIR and micro-GC measurements are obtained. The uncertainty of the measurements is estimated within 5%.

Literature presents no works on the application of jest-stirred reactors (JSR) to study the oxidation of H_2S and CH_3SH and, therefore, the present experimental results are of interest, since they increase the experimental database with experiments in a different type of reactor. The error has been calculated according to the standard pooled deviation (the square root of the sum of the squares of the error), where the error does not depend on the temperature in the interval considered and it is an estimator of the experimental error associated with the oxidation of H_2S and CH_3SH. The pooled standard deviation has been calculated as ±39 ppm. For each set, results at different temperatures (increasing the temperature by 25-50 K in the corresponding temperature range) are obtained.

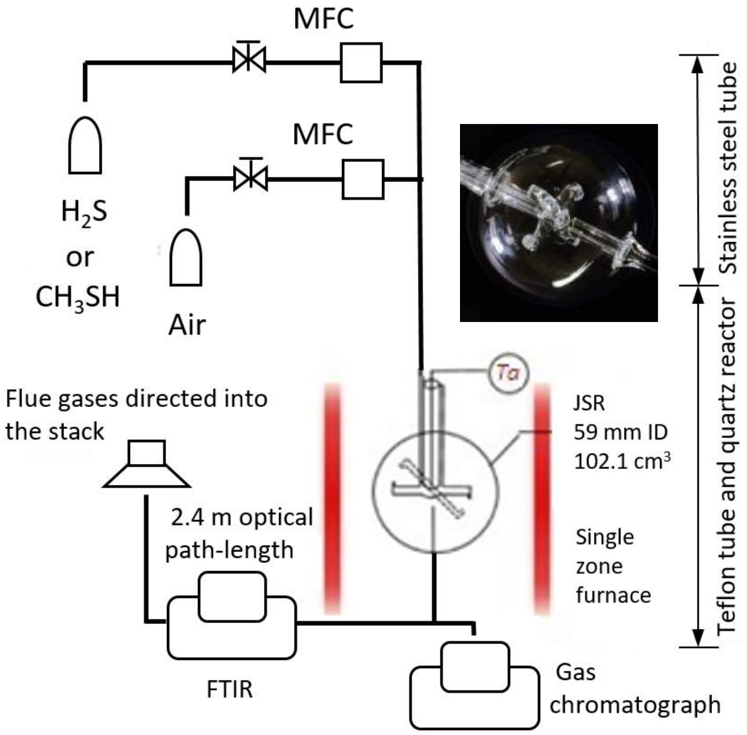
MFC
MFC
H2S
or
CH3SH
Air
Stainless steel tube
Teflon tube and quartz reactor
Ta
Flue gases directed into
the stack
JSR
59 mm ID
102.1 cm3
2.4 m optical
path-length
Single
zone
furnace
FTIR
Gas
chromatograph

Figure 3.6 Scheme of the experimental set-up 3 used to carry out the oxidation experiments in the jet stirred reactor (JSR). Adapted from Zeng (2017).

Chapter 4.

MODELING. REACTION MECHANISM

4. MODELING. REACTION MECHANISM

In order to predict ignition, extinction, fuel consumption and pollutant formation during combustion processes, detailed chemical kinetic models are required. To develop a mechanism systematically, it is necessary to build it hierarchically by adopting or developing reaction subsets of the simpler molecules and then, step by step, to add species and reactions relevant for more complex molecules.

In this manner, a detailed gas-phase chemical kinetic mechanism has been constructed progressively throughout the development of this thesis to describe the oxidation of H_2S, in laboratory reactors, under different experimental conditions, and its interaction with relevant species of the sour gas (CH_4) and potential contaminants, such as NO (which might be formed from N_2 or NH_3 present in the sour gas). The mechanism construction progress will be described below and is schematically represented in Figure 4.1.

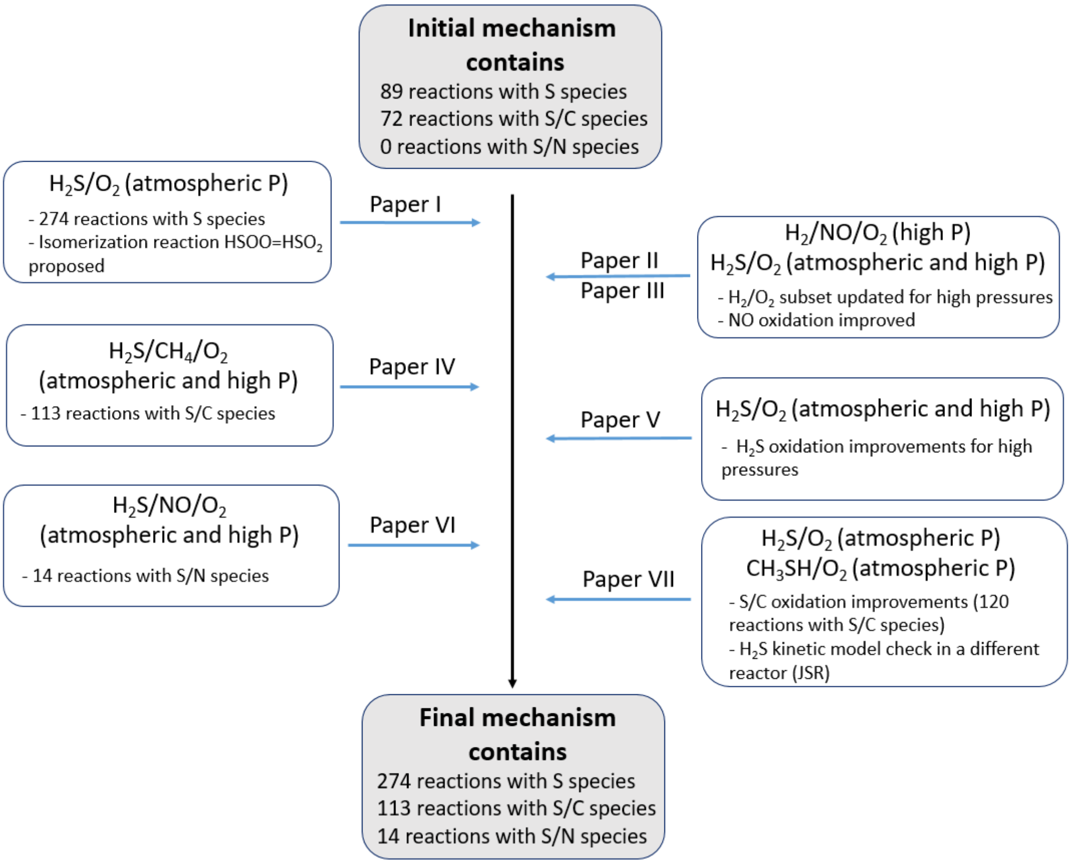
Initial mechanism contains
89 reactions with S species
72 reactions with S/C species
0 reactions with S/N species
H2S/O2 (atmospheric P)
- 274 reactions with S species
- Isomerization reaction HSOO=HSO2 proposed
Paper I
Paper II
Paper III
H2/NO/O2 (high P)
H2S/O2 (atmospheric and high P)
- H2/O2 subset updated for high pressures
- NO oxidation improved
H2S/CH4/O2 (atmospheric and high P)
- 113 reactions with S/C species
Paper IV
Paper V
H2S/O2 (atmospheric and high P)
- H2S oxidation improvements for high pressures
H2S/NO/O2 (atmospheric and high P)
- 14 reactions with S/N species
Paper VI
Paper VII
H2S/O2 (atmospheric P)
CH3SH/O2 (atmospheric P)
- S/C oxidation improvements (120 reactions with S/C species)
- H2S kinetic model check in a different reactor (JSR)
Final mechanism contains
274 reactions with S species
113 reactions with S/C species
14 reactions with S/N species

Figure 4.1 Progression in the development of the gas-phase kinetic mechanism for H_2S oxidation and its interaction with other species (CH_4 and NO).

The basis or initial mechanism of the present gas-phase kinetic model consists of different reactions subsets that belong to previous works by the research group at the University of Zaragoza. The initial mechanism takes as starting point the work of Alzueta et al. (2001b), where a study of fuel oxidation (CO) in the presence of SO_2 was performed, and whose mechanism is considered in the present work as the basis for SO_2 conversion under combustion conditions. The Alzueta's mechanism included as well a reaction subset describing the oxidation of C1-C2 hydrocarbons and their interactions with NO, the so-called GADM mechanism (Glarborg et al., 1998), together with further refinements of the chemistry involved (Glarborg et al., 1999). Later, this mechanism was updated and modified by Abián et al. (2015a, 2015b) in order to account for the conversion of SO_2 under reducing conditions and the conversion of important species for the sulfur chemistry, such as COS and CS_2. From this point, the mechanism was updated in the present thesis, as indicated in the following sections.

A successful way of developing kinetic models, which has been used previously by our research group (e.g. Alexandrino, 2018; Marrodán, 2018), consists of testing and validating the reaction subsets for the species of interest first under atmospheric-pressure conditions and, subsequently, under high-pressure conditions, which are of interest for different combustion processes. The following sections describe, in more detail, what specifically refers to the reaction subsets of the different compounds of interest. Special emphasis will be put in the modifications and updates made to the different reactions to obtain the final mechanism. The impact of the different modifications made is discussed in the corresponding publication of the compendium, as well as in Chapter 5 (Results and Discussion).

Model calculations have been performed using the Chemkin Pro software package (ANSYS Chemkin-Pro, 2016). The simulations have been conducted with the plug-flow reactor module and the fixed gas temperature assumption or, in specific cases, the temperature profiles of the entire high-pressure set-up (Paper II and Paper VI). The thermodynamic data have been taken from the same sources as the original mechanisms. Rate of production (ROP) and sensitivity analyses have been performed to identify the main reaction pathways occurring during reactant consumption and product formation under the different experimental conditions analyzed.

4.1 H_2S OXIDATION AT ATMOSPHERIC PRESSURE

Previous studies about H_2S oxidation, detailed below, have been used to update our initial mechanism. The initial mechanism counted with 89 reactions involving sulfur species and just a few related with H_2S, specifically about its pyrolysis process. In the last decades, the sulfur subsets of reactions have been more focused on atmospheric chemistry, mainly involving SO_x species, whose reactions were of a major concern due to its strong relation with acid rain (Gardiner, 2000). The understanding and kinetic mechanisms of reduced sulfur species (e.g. H_2S and CH_3SH) combustion were not really developed until recently, when some efforts were done regarding H_2S oxidation under combustion conditions, mainly due to the sour gas use and the Claus process. The work by Zhou et al. (2013) established several kinetic parameters for different reactions involved in the process of H_2S oxidation at atmospheric pressure. Later, Song et al. (2017), in their exploratory work on H_2S oxidation under high pressures (30-100 bar), adopted the kinetic model by Zhou et al. (2013) and presented a full description of the H/S/O reaction system at high pressures. The kinetic model by Song et al. (2017) was used to update the sulfur reaction subsets of the present mechanism, which counted with subsets of reactions for species such as: H_2S, HS_2, SH, S_2, HSO and SO_x, among others. The reactions of sulfur species increased from the 89 initial reactions to 274. Some of the initial reactions were updated with more recent kinetic parameters and the rest were simply added to the mechanism.

The updated mechanism was not capable of reproducing the experimental results of the present thesis. For this reason, an additional new reaction was proposed in the present thesis framework, which changes the reaction pathways of H_2S oxidation. As proposed by Garrido et al. (2011), in a high level ab initio study of the HSO_2 system, the evolution of the $SH+O_2$ reaction (key reaction step in H_2S oxidation) presents, a faster reaction path of SH oxidation leading to the final product SO_2, through isomerization from HSOO to HSO_2. For this isomerization (reaction R4.1), the energy barrier by Freitas et al. (2012), who determined an activation energy of 21.3 kcal/mol, has been used together with a pre-exponential factor of 10^{17} (s^{-1}).

$$HSOO \rightleftharpoons HSO_2 \qquad \text{(R4.1)}$$

Besides, calculations carried out in the work of H_2S oxidation at atmospheric pressure (Paper I) were very sensitive to reaction (R4.2).

$$H_2S + HO_2 \rightleftharpoons SH + H_2O_2 \qquad \text{(R4.2)}$$

The uncertainty of the kinetic parameters for this reaction and its high sensitivity have been previously mentioned, especially in high-pressure works, where HO_2 radicals are expected to play a major role (Mathieu et al., 2014; Gersen et al., 2017; Song et al., 2017). Only an upper limit to the rate constant at room temperature is available of $2\cdot10^{9}$ $cm^{3}\cdot mol^{-1}\cdot s^{-1}$ (Mellouki and Ravishankara, 1994). Available theoretical calculations include the ones by Zhou et al. (2013) for the reverse reaction (-R4.2) ($5.6\cdot10^{4}\cdot T^{2.8}\cdot e^{(-8668/RT)}$; cm^{3}, mol, s, cal), whose kinetic parameters were lowered by a factor of 2 by Mathieu et al. (2014), and calculations performed by Batiha et al. (2011) indicated a rate constant value of $3.2\cdot10^{12}\cdot e^{(-16889/RT)}$ (cm^{3}, mol, s, cal) for the direct reaction (R4.2). Within the uncertainty of the determinations, the rate constant has been estimated as 10^{12} $cm^{3}\cdot mol^{-1}\cdot s^{-1}$ in the present thesis for the reverse reaction (-R4.2), which agrees with the present experimental results. This estimation agrees well with the high temperature data of Zhou et al. (2013) and Mathieu et al. (2014).

This mechanism (Paper I) has been also tested against experimental results obtained in a different reactor, a jet-stirred reactor (Paper VII). The mechanism was able to reproduce the experimental results with accuracy under different air excess ratios.

4.2 H_2S OXIDATION AT HIGH PRESSURE

In order to simulate the experimental results obtained at high-pressure, the kinetic mechanism developed during the work of H_2S oxidation at atmospheric pressure was updated. In order to do so, a preliminary study was performed about H_2 oxidation and its interaction with NO (Paper II). This is described in detail in section 4.2.1. Briefly, the H_2/O_2 subset was updated for high pressures and added to the H_2S oxidation mechanism. The simulations showed slight improvements in the predictions of H_2S oxidation at high pressures (Paper III). Overall, the outcome of the kinetic model simulations matched the experimental trends, with the best results for pressure near atmospheric (0.65 bar of manometric pressure) and needing to improve results at the highest pressure studied (40 bar), where a gap between experimental and simulation results of 50 K was observed (Paper III). The model was also tested satisfactorily against experimental results from the literature in a flow reactor at high-pressure (Song et al., 2017) and ignition delay times of H_2S addition on H_2 oxidation (Mathieu et al., 2014).

The oxidation of H_2S at high pressures was re-evaluated in a posterior work (Paper V), studying additional air excess ratios, the influence of gas residence time and improving the model predictions at high pressures. Such improvements were related to H_2O_2 species, which are of importance at high pressures in the kinetic model developed, and pointed out as well in previous studies (e.g. Giménez-López et al., 2016; Marrodán et al., 2018a). In the present work, two reactions were proposed (R4.3 and R4.4):

$$SH + H_2O_2 \rightleftharpoons HSO + H_2O \qquad (R4.3)$$

$$HSO + H_2O_2 \rightleftharpoons HSO_2 + H_2O \qquad (R4.4)$$

A previous similar study with H_2O_2 species, that analyzed the reaction between HNO and H_2O_2 molecules, showed that it is possible to abstract an O radical from the H-O-O-H molecule (Beckett et al., 2017). This reaction pathway would be similar to one ocurring in the reactions proposed: (R4.3) and (R4.4).

Besides, some reactions are recognized to slow down the oxidation process and their kinetic parameters might not be characterized properly in the model, such as the reactions of S_2O (R4.5 and R4.6) and H_2S with O_3 (R4.7 and R4.8). These reactions have been pointed in a previous work of H_2S oxidation at high pressures in a flow reactor (Song et al., 2017), and are evaluated in the "Results and Discussion" section, Chapter 5.

$$S_2O + OH \rightleftharpoons S_2 + HO_2 \qquad (R4.5)$$

$$S_2O + S_2 \rightleftharpoons S_3 + SO \qquad (R4.6)$$

$$H_2S + O_3 \rightleftharpoons SO_2 + H_2O \qquad (R4.7)$$

$$H_2S + O_3 \rightleftharpoons HOSO + OH \qquad (R4.8)$$

4.2.1 H_2/NO MIXTURES OXIDATION

The study about H_2 oxidation in the presence and absence of NO (Paper II) served as a milestone for the further work about H_2S oxidation at high pressures in the presence and absence of NO (Paper VI). In this manner, the H_2/O_2 reaction subset was updated with reactions from the work by Hashemi et al. (2015), who also studied the oxidation of H_2 at high pressures in a flow reactor, and whose mechanism is mainly based on the work by Burke et al. (2012) about kinetic modeling for high-pressure combustion of H_2. The H_2 subset is relevant due to its importance in the radical pool composition (e.g. OH, H, O and HO_2 radicals) governing combustion chemistry.

H_2 is a well-known fuel and its chemistry is particularly well characterized in comparison with other species. Thus, the knowledge of the H_2 oxidation kinetics involving NO at high pressures would allow more complex systems to be addressed, such as H_2S/O_2/NO.

At high pressure, and in the presence of O_2, the interconversion NO/NO_2 is favored as pressure increases and temperature decreases, according to reaction (R4.9).

$$NO + NO + O_2 \rightleftharpoons NO_2 + NO_2 \qquad \text{(R4.9)}$$

Due to the configuration of the experimental set-up for high pressures (set-up 2), shown in section 3.2., there are zones prior and posterior to the reactor where the gas mixture might react, according to reaction (R4.9). This was observed experimentally during the NO oxidation study, forming NO_2, at room temperature (290 K) (Paper II). This implies that there will be a mixture of NO/NO_2 entering the reaction zone, which should be taken into account for the simulations. Such behavior has been pointed in previous works about fuels oxidation in the presence of NO at high pressures (e.g. Rasmussen et al., 2008a, 2008b; Marrodán et al., 2014). In order to predict accurately the amount of NO and NO_2 entering the reactor, the study above mentioned was conducted in the high-pressure reactor (Paper II), prior to perform the experiments of H_2S and its interaction with NO. The mechanism developed for NO oxidation is a revised and updated version of the work of Giménez-López et al. (2011), who performed experiments of oxidation of C_2H_4/NO mixtures in a flow reactor at high pressure (60 bar of absolute pressure), and under different stoichiometries. The kinetic parameters of reaction (R4.9) were revised in the present thesis (Paper II). This is due to the uncertainty of (R4.9), which most reliable value of the apparent activation energy determined up to date is -1052 [±789] cal/mol (Atkinson et al., 2004). The pre-exponential factor recommended by Atkinson et al. (2004) ($1.2 \cdot 10^9$ $cm^6 \cdot mol^{-2} \cdot s^{-1}$) was taken and the activation energy was varied between the uncertainty limits, taking the inferior limit, what makes an apparent activation energy of -1850 cal/mol, and which seemed to be adequate in all the experimental conditions of this work to reproduce properly the NO/NO_2 concentrations (Paper II). The experimental trends were captured precisely by using temperature profiles, describing the entire experimental set-up 2: from the mixing point of the reactants to the entrance of the reactor, the reactor itself, and from the reactor outlet to the pressure reduction valve (at atmospheric pressure).

4.3 H_2S/CH_4 MIXTURES OXIDATION

The mechanism used in the study about H_2S oxidation in the presence of CH_4 (Paper IV) includes the work of H_2S oxidation at high pressures (Paper III), which counted with the H_2/O_2 reaction subset updated for high pressures (Paper II). In relation to carbon species, it is based on previous works from the research group. Initially, it counted with reactions related to the interaction of carbon and sulfur species from the work of Alzueta et al. (2001b), about the inhibition and sensitization of fuel (CO) oxidation by SO_2, the study about CS_2 and COS conversion under different combustion conditions (Abián et al., 2015a), and the work from Abián et al. (2015b), where the impact of the presence of SO_2 on the formation of soot from ethylene pyrolysis was evaluated.

Besides, the mechanism was updated with some reactions from recent studies. New subsets were added from the study of Gersen et al. (2017), about H_2S/CH_4 oxidation at high pressures, where the CH_3OO and CH_3OOH peroxides chemistry was found to be important at high pressures and low temperatures. This study was based on previous studies from the same group about CH_4 oxidation at high pressures (Rasmussen et al., 2008c; Hashemi et al., 2016). Thus, CH_3OO and CH_3OOH reaction subsets have been added to the current mechanism (Gersen et al., 2017). The formation and consumption of organosulfur compounds, like CH_3SH, were also found important in the work by Gersen et al. (2017), and a subset describing CH_3SH conversion was taken from the work of Alzueta et al. (2019), which was based on the works of Zheng et al. (2011) and Van de Vijver et al. (2015).

Other important reactions were updated with more recent kinetic parameters, like (R4.10), whose kinetic constant was revised by Zeng et al. (2016), using the CBS-QB3 level of theory, seeing improvements in CH_4 oxidation at all conditions (Paper IV). Another important reaction for CH_4 oxidation at low temperatures (R4.11) was also updated, using the kinetic parameters by Srinivasan et al. (2007).

$$CH_3 + H_2S \rightleftharpoons CH_4 + SH \qquad \text{(R4.10)}$$

$$CH_3 + O_2 \rightleftharpoons CH_2O + OH \qquad \text{(R4.11)}$$

In the research stay at the University of Murdoch (Australia), the reaction pathways of CH_3SH conversion were re-evaluated (Paper VII). Bian et al. (2019), in a recent theoretical work, investigated the reaction mechanism of CH_3SH with O_2 using quantum chemical methods at the CCSD(T)//M06-2x level of theory. They discovered new reaction pathways, both on the ground-state triplet and excited state singlet surfaces to produce CH_2SO, H_2O, CH_3OH, SO, CH_4 and SO_2.

Accordingly, some of the reactions missing in the mechanism were proposed, as well as their corresponding kinetic parameters, i.e., the formation of CH_2SO and CH_3OH, and the consumption of CH_2SO. The rate constants for these reactions (R4.12-R4.18) were estimated and are summarized in Table 4.1. Bian et al. (2019) studied the reaction CH_3SH+O_2 both on the triplet and singlet surfaces. An examination of the Bian et al. (2019) reaction pathways led to suggest the appearance of the intersystem-crossing (ISC) process in our system, similarly to the oxidation of other reduced sulfur species (H_2S and CS_2) (Montoya et al., 2005; Zhou et al., 2008; Zeng et al., 2017; Zeng et al., 2019b). With respect to the results of Bian et al. (2019), the ISC comes to pass between the triplet (44.9 kcal/mol) and singlet (31.3 kcal/mol) transition states. The activation energy of reaction (R4.12) was estimated as 42 kcal/mol (Paper VII). We have proceeded in the same way by allowing the ISC to arise in the generation of CH_3OH from the oxidation of CH_3SH (R4.13), assigning the activation energy of 40 kcal/mol to this process.

Table 4.1 Arrhenius parameters for the reactions proposed in this work according to the study by Bian et al. (2019). Arrhenius expression: $k = A\,T^{n} \exp[-E_a/(RT)]$. Units are cm^3, mol, s and cal.

Reaction	***A***	***n***	E_a
(R4.12) $^1CH_3SH + {}^3O_2 = {}^1CH_2SO + {}^1H_2O$	10^{14}	1.4	42 000
(R4.13) $^1CH_3SH + {}^3O_2 = {}^1CH_3OH + {}^1SO$	10^{14}	0.0	40 000
(R4.14) $^1CH_2SO = {}^1CO + {}^1H_2S$	10^{11}	0.0	0
(R4.15) $^1CH_2SO + {}^2H = {}^1CH_3SO$	10^{11}	0.0	0
(R4.16) $^1CH_2SO = {}^1COS + {}^1H_2$	10^{11}	0.0	0
(R4.17) $^1CH_2SO = {}^1CS + {}^1H_2O$	10^{11}	0.0	0
(R4.18) $^1CH_3SO = {}^2CH_3 + {}^1SO$	10^{11}	0.0	0

4.4 H_2S/NO MIXTURES OXIDATION

The mechanism for H_2S oxidation in the presence of NO consists of three parts. First, the reactions subsets about sulfur chemistry (Paper V), described in section 4.2. Then, the subsets of reactions involving nitrogen species, which come from the preliminary study of H_2 oxidation and its interaction with NO (Paper II), as described previously in detail in section 4.2. Lastly, since so far the mechanism did not count with reactions involving nitrogen and sulfur species; some reactions involving S/N species were added to the model from the work of Glarborg (2007). In that study, the author mentions that the kinetic parameters proposed were rough estimations, pointing to the lack of understanding and research regarding S/N interactions in the literature. However, after adding these reactions, the final mechanism is capable of reproducing accurately the oxidation of H_2S in the presence of NO at atmospheric pressure. The relevance of some added reactions for S/N interactions is described later in the “Results and Discussion” section, Chapter 5.

At high pressure, the NO/NO_2 interconversion is favored in the presence of oxygen as pressure increases and temperature decreases. As above mentioned, in order to predict accurately the amount of NO and NO_2 entering the reactor, which might influence H_2S oxidation, a preliminary study was conducted in the high-pressure reactor, studying the oxidation of H_2 in the presence and absence of NO (section 4.2.1) (Paper II). The interaction between NO and H_2S at high pressures (20 bar) shown an unexpected conversion of H_2S in the experiments at low temperatures (475 K). This behavior was thought to be related with the reaction between H_2S and NO_2. An attempt to model such interaction was done by including in the model the reaction (R.4.19), according to the suggestion of Russel (2009). No kinetic parameters for (R4.19) are reported in the literature. Other studies from the literature just mention the formation of sulfur as a result of the reaction between H_2S and NO_2 at atmospheric pressure (Pierce, 1929; Cadle and Ledford, 1966; Hales et al., 1974; Frost and Thomas, 1975; Blackwood, 1980; Kim, 2003; Russel, 2009). Thus, in this thesis and in Paper VI, the kinetic constant value for the temperature range studied (475-1000 K) has been derived as 10^8 ($cm^3 \cdot mol^{-1} \cdot s^{-1}$).

$$H_2S + NO_2 \rightleftharpoons S + NO + H_2O \qquad \text{(R4.19)}$$

Chapter 5.

RESULTS AND DISCUSSION

5. RESULTS AND DISCUSSION

The results obtained throughout this thesis are shown below. The following sections are organized according to the objectives set forth in Chapter 1. The results presented encompass both the experimental and kinetic modeling results, and are shown together with a brief explanation, which summarizes what is stated in articles I-VII. First, the results of the oxidation of H_2S at atmospheric pressure are presented. Next, a preliminary study at high pressures on the oxidation of H_2 and its interaction with NO is shown. The results of H_2S oxidation at different pressures are shown afterwards. Subsequently, the study of the oxidation of H_2S/CH_4 and H_2S/NO mixtures, both at atmospheric pressure and high pressure, are presented. Finally, the study about the oxidation of H_2S and CH_3SH carried out during the research stay in Murdoch University (Australia) is shown.

Figures show the simulation results obtained with the final version of the mechanism. Since the mechanism has evolved throughout the whole thesis research, in those cases where significant differences are found, the results of the mechanism version that was used at the time of publishing the corresponding paper are also presented. Modifications in the kinetic mechanism entail the updating or modification of the kinetic parameters of certain reactions, the inclusion of new reactions from the bibliography and the proposal of new reactions. This process is described in detail in Chapter 4 (Modeling. Reaction Mechanism). Besides, the reaction pathways and the more relevant reactions are also discussed below together with the experimental results.

5.1 H_2S OXIDATION AT ATMOSPHERIC PRESSURE

The oxidation of H_2S at atmospheric pressure has been carried out in the experimental set-up described in section 3.1 (atmospheric-pressure tubular flow reactor set-up, set-up 1). This study served as the basis for the rest of the work, regarding the oxidation of H_2S under different operating conditions, such as different pressures, the presence of CH_4 or NO, and the use of different reactors (tubular flow reactors and a jet-stirred reactor). The experimental installation mentioned has previously been also used with success for more than 20 years in studies on the oxidation of other compounds at atmospheric pressure, such as dimethyl ether (DME) and methyl formate (MF) (Alexandrino, 2018; Marrodán, 2018). The usual strategy to analyze the H_2S oxidation at atmospheric pressure and to develop a kinetic model capable of reproducing the experimental results at atmospheric pressure, prior to carry out experiments with higher pressures.

In the case of H_2S oxidation at atmospheric pressure, there is almost no literature regarding this issue. One could think that the Claus process, as mentioned in the Introduction section, being the main industrial process to deal with H_2S and convert it to elemental sulfur, should provide a strong background in terms of knowledge and kinetics of the process. However, the scientific research is more related to the operational details, catalysts and emissions in the industrial Claus process. Another area where H_2S oxidation and its kinetics could be relevant is in atmospheric chemistry, but these conditions are quite different to the combustion conditions. There are just a few recent papers that deal with H_2S under combustion conditions in the laboratory. The most important one would be the experimental and kinetic modeling study of H_2S oxidation by Zhou et al. (2013), as already mentioned in the Introduction section. According to this work, it was proposed the possibility of catalytic reactions promoted by the silica reactor surface, and they intended to minimize them by using a B_2O_3 coated reactor. However, they could not conclude if the coating had an effect or not on H_2S oxidation. The experiments performed in the atmospheric-pressure set-up 1, are shown in Table 5.1, from reducing to oxidizing conditions. Repeated experiments are also shown. The temperature range studied goes from 700 to 1400 K.

Table 5.1 Experimental conditions for H_2S oxidation in the atmospheric-pressure set-up (set- up 1). N_2 as bath gas. t_r(s)=194.6/T(K).

Set	H_2S (ppm)	O_2 (ppm)	H_2O (%)	λ
1	476	225	-	0.3
1R	478	229	-	0.3
2	509	750	-	1.0
3	485	900	-	1.2
3R	485	896	-	1.2
4	482	1500	-	2.1
5	492	3750	-	5.1
6	514	15000	-	19.5
7	490	230	1.2	0.3
8	505	3750	1.2	5.0

In Figure 5.1, a comparison between the H_2S normalized concentration results from two experiments performed by Zhou et al. (2013), in two different reactors (one with bare silica and other coated with B_2O_3), can be seen. The corresponding results from set 3 (in Table 5.1) are also shown in Figure 5.1. All experiments were performed using a similar air-excess ratio and a gas residence time of the same order of magnitude. The experiments of Zhou et al. (2013) correspond to a gas residence time of 0.2 seconds in the isothermal zone of their reactors, while the gas residence time in set 3 (Table 5.1) goes from 0.14 to 0.24 seconds, depending on temperature. The major difference between the results would be related to the air-cooling used in the present experimental set-up at atmospheric pressure, in order to freeze de reaction at the reactor outlet to room temperature rapidly, and which is not present in the Zhou et al. (2013) experiments. In their case, they have a 0.3 seconds cooling zone without the use of air-cooling.

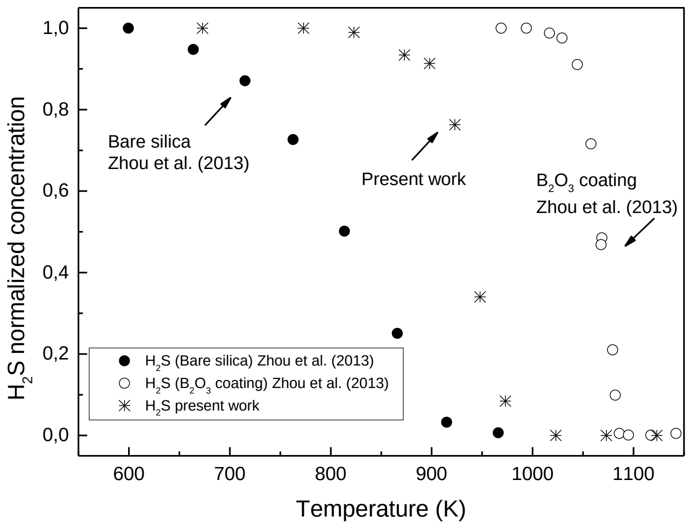

Figure 5.1 Comparison between H_2S normalized concentrations vs. temperature from two experiments of H_2S oxidation by Zhou et al. (2013) (λ=1.2) and set 3 in Table 5.1 (λ=1.2).

As can be observed in Figure 5.1, the conversion of H_2S from the present thesis lies between the results of the two experiments by Zhou et al. (2013). When bare silica reactor is used, H_2S is much more reactive than in the other cases. The H_2S oxidation presents a shift to higher temperatures in the B_2O_3 coated reactor, 400 K difference in comparison to the bare silica, and a shift of 200 K to the set 3 (in Table 5.1) of the present work. As mentioned, one of the possibilities of the differences observed between the results obtained in the two silica reactors (the one from Zhou et al. and the one from the present work) is related to the cooling process, as Zhou et al. do not freeze the reaction, the gas mixture might have more time to react. On the one hand, the present simulations show that H_2S has time to react in this cooling zone but, on the other hand, the authors used a probe in the reactor to gather information about the consumption of H_2S in the isothermal part of the reactor. They showed H_2S concentration vs. distance in the reactor at 1120 K in a graph, where H_2S was seen to be totally consumed in the isothermal part of the reactor, showing no influence of the cooling zone in H_2S oxidation.

At this point, it was decided to carry out experiments introducing water vapor and to evaluate its influence. The water vapor diminishes the effect of recombination of radicals on the reactor walls by enlarging the radical pool, which is called quenching effect. In this manner, the possible catalytic effect of the quartz reactor walls would be tested. The water vapor was introduced into the reactor in one of the streams of N_2, saturating this one by passing it through a bubbler at room temperature. Table 5.1 shows the experiments carried out in the installation at atmospheric pressure, both in the presence of water vapor and without it. In Figure 5.2, the differences between the results of two experiments for the same lambda value ($\lambda \sim 5$) with and without water vapor (sets 5 and 8 in Table 5.1) can be observed. The concentration results of different species (H_2S, SO_2 and H_2) are almost the same in both experiments. Therefore, it was concluded that radical recombination on the walls is not significant under the studied conditions.

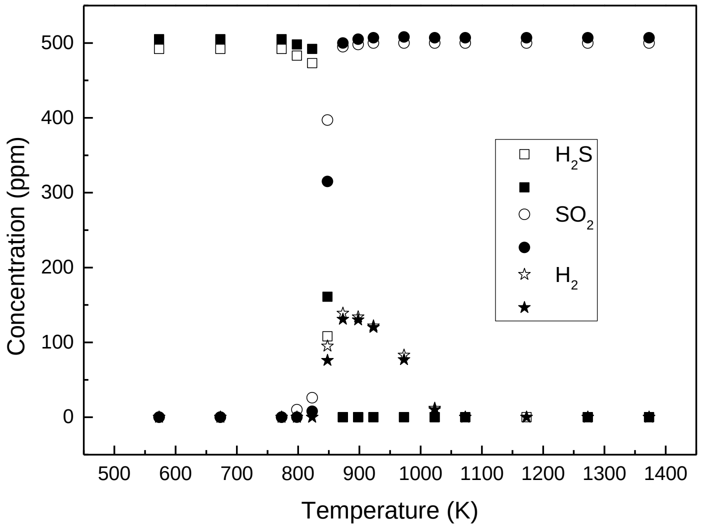

Figure 5.2 Comparison results of set 5 (λ=5.1) and set 8 (1.2% H_2O, λ=5.0) in Table 5.1. Open symbols represent the experimental conditions without water and solid symbols with water vapor.

In Figure 5.3, the results of the concentrations of H_2S, SO_2 and H_2 published in Paper I from reducing to oxidizing conditions are shown, which correspond to the sets of experiments 1-6 in Table 5.1. In the case of H_2S, its conversion is shifted to lower temperatures as the O_2 concentration is increased, as well as the conversion is sharper. The ignition occurs at 950 K in the case of reducing conditions (λ=0.3) and 700 K in the most oxidizing conditions considered (λ=19.5).

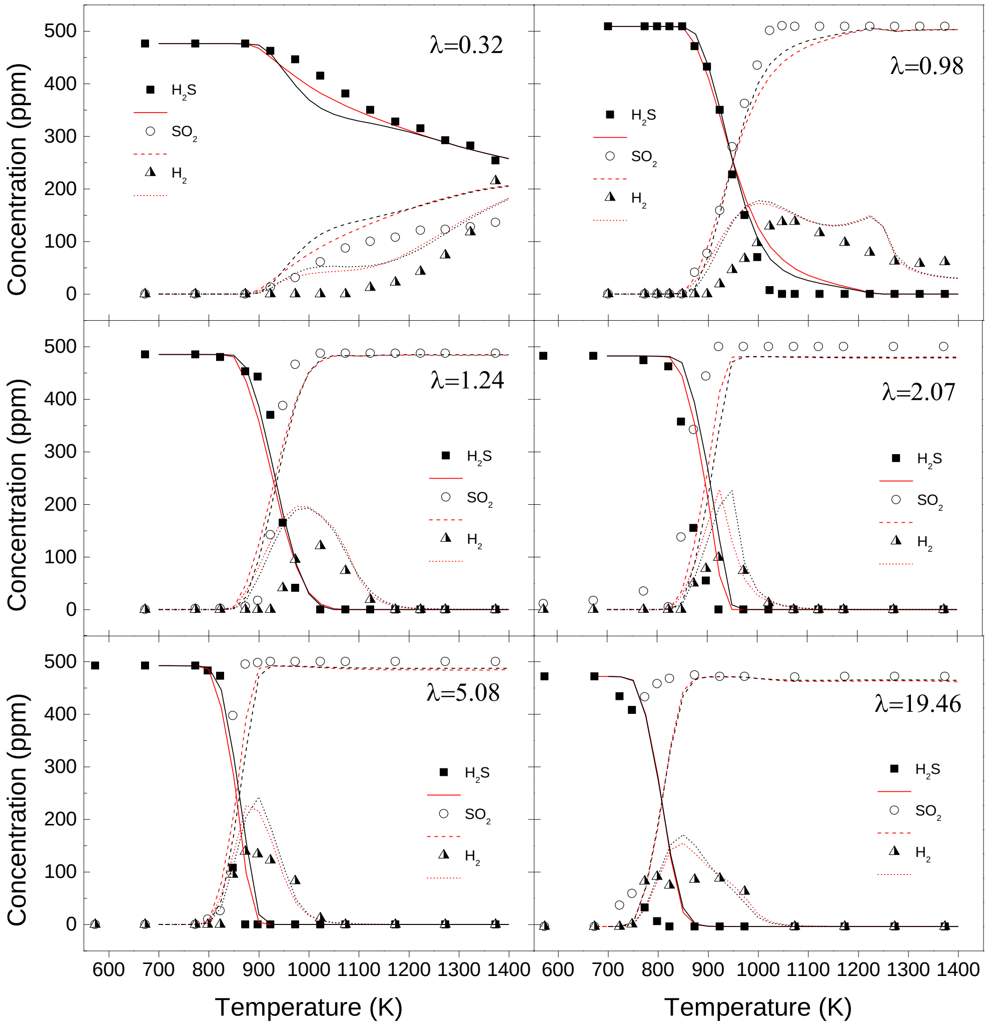

Figure 5.3 Experimental results from H_2S oxidation at atmospheric pressure. Symbols represent experimental data and lines model predictions (black lines denote the results from the final mechanism, while red lines represent the model initially presented in Paper I).

The main product of the oxidation of H_2S is SO_2. Figure 5.4 illustrates the sulfur balances vs. temperature from experiments 1-6 (Table 5.1). In almost all the experiments, the sulfur balance is kept around 100% ($H_2S + SO_2$), except in the case of reducing conditions (λ=0.3), where the conversion of H_2S is not complete and the sulfur balance is reduced down to 80% at the highest temperature (1400 K). In this case, under reducing conditions (λ=0.3), a yellowish color deposit was observed at the outlet of the reactor, which could be indicative of the formation of elemental sulfur. Such observation was also noted by Palma et al. (2015), who used experimental conditions in their work (O_2/H_2S=0.35, 1375 K, t_r=150 ms) similar to those of the present work (O_2/H_2S=0.47, 1375 K, t_r=140 ms), but using 10% H_2S instead of 0.05% H_2S. Palma et al. (2015) obtained 70% of H_2S conversion versus 52% of the present thesis. The presence of this yellowish deposit was also previously mentioned by Zhou et al. (2013) and was related to the formation of S_2 in the gas phase, which condenses when exhaust gases are cooled.

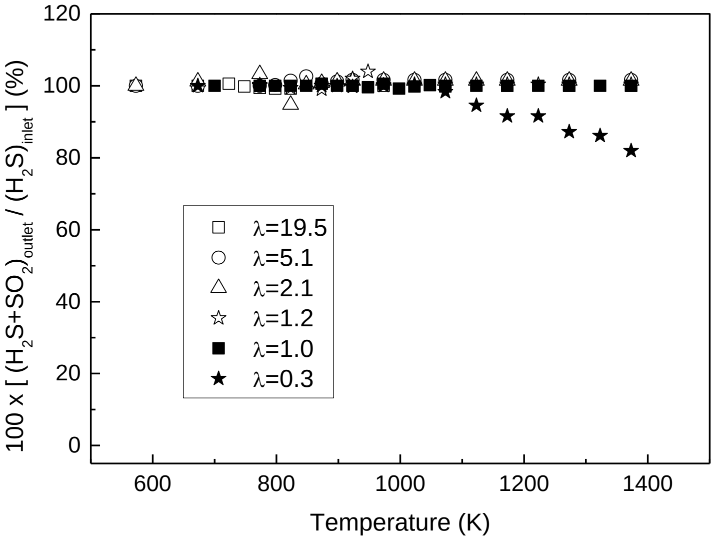

Figure 5.4 Sulfur mass balances as a function of temperature for sets 1-6 in Table 5.1.

The hydrogen formation occurs until the total consumption of H_2S (Figure 5.3). At this point, the available O_2 oxidizes the hydrogen and H_2 starts to vanish. This process is slow in the case of stoichiometric conditions and does not even occur under reducing conditions, where all the O_2 has reacted with H_2S. This was also observed by Zhou et al. (2013), who mentioned that H_2 selectivity presents a maximum with the last traces of H_2S.

The repetition experiments at atmospheric pressure (sets 1-1R and 3-3R in Table 5.1) can be seen together in Figure 5.5, under reducing conditions (λ=0.3) and almost stoichiometric conditions (λ=1.2). As can be seen, the experimental data show a fairly good repeatability.

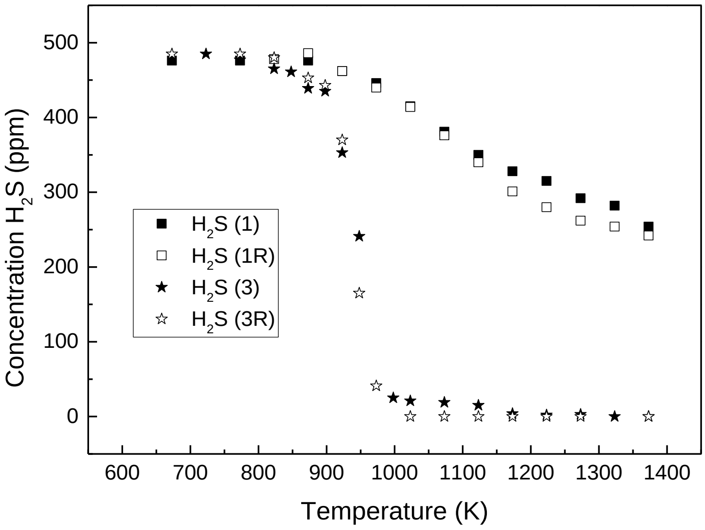

Figure 5.5 Repeatability of experiments under reducing conditions (sets 1 and 1R in Table 5.1; λ=0.3) and almost stoichiometric conditions (sets 3 and 3R in Table 5.1; λ=1.2).

Regarding the kinetic model, the one compiled during this first part of the work (Paper I) about H_2S oxidation at atmospheric pressure was mainly based on the study by Song et al. (2017), as mentioned earlier in section 4 (Modeling. Reaction mechanism) and, at the same time, the work by Song et al. was based on the work by Zhou et al. (2013). The latter introduced a lot of new reactions to the H_2S oxidation mechanism, and the authors were able to reproduce theoretically their flow reactor data by making changes, within a factor of 3, to the rate constants of two important reactions involving SH radicals. The factor required for this fitting was different for the different cases that they studied at atmospheric pressure (λ=1.23, 1.28 and 6.67).

In the present work, according to theoretical works of Freitas et al. (2012) and Garrido et al. (2011), the isomerization reaction of HSOO (R5.1), as a faster reaction path in H_2S oxidation to SO_2, has been included. This has led to good prediction results over all the conditions at atmospheric pressure, together with the proposed parameters for reaction (-R5.2). The modeling simulations can be observed in Figure 5.3 (black lines), which are satisfactory under all the air-excess ratios. These simulations do not change in comparison with the final mechanism (shown in red lines in Figure 5.3). This implies that the posterior changes that have been made in the mechanism regarding high pressure conditions do not have any influence under atmospheric pressure.

$HSOO \rightleftharpoons HSO_2$ (R5.1)

$H_2S + HO_2 \rightleftharpoons SH + H_2O_2$ (R5.2)

Calculations indicate that H_2S reacts with the radical pool (H, OH and HO_2), but mainly with H radicals, to rapidly form SH, independently of the stoichiometry. SH continues the reaction with O_2 to form mainly HSOO (R5.3), which isomerizes then to HSO_2 (R5.1).

$SH + O_2 (+M) \rightleftharpoons HSOO (+M)$ (R5.3)

Later, HSO_2 is consumed to HOSO (R5.4) or to the final product SO_2 through (R5.5) and (R5.6), this last one under highly oxidizing conditions. HOSO, as HSO_2, can dissociate or react with oxygen (R5.7, R5.8). The reaction paths with S, SO and HS_2 radicals are similar to the ones identified by Zhou et al. (2013), but comparatively less important in the present mechanism, due to the addition of (R5.1).

$HSO_2 (+M) \rightleftharpoons HOSO (+M)$ (R5.4)

$HSO_2 (+M) \rightleftharpoons SO_2 + H$ (R5.5)

$HSO_2 + O_2 \rightleftharpoons SO_2 + HO_2$ (R5.6)

$HOSO (+M) \rightleftharpoons SO_2 + H (+M)$ (R5.7)

$HOSO + O_2 \rightleftharpoons SO_2 + HO_2$ (R5.8)

The oxidation is maintained due to the release of H radicals in the final steps (R5.5) and (R5.7). H radicals consume H_2S through (R5.9), as well as HO_2 radicals, formed mainly in (R5.6) and (R5.8), react with H_2S through (R5.2). This latter step becomes more important as the oxygen concentration increases, due to the major occurrence of (R5.6) and (R5.8) and the increase in HO_2 concentration as a result. The H_2O_2 radicals formed in (R5.2) decompose to OH radicals through (R5.10), promoting the H_2S consumption through (R5.11).

$H_2S + H \rightleftharpoons SH + H_2$ (R5.9)

$H_2O_2 (+M) \rightleftharpoons OH + OH (+M)$ (R5.10)

$H_2S + OH \rightleftharpoons SH + H_2O$ (R5.11)

The modeling results are very sensitive to reaction (R5.2), additionally to the $HSOO \rightleftharpoons HSO_2$ isomerization reaction (R5.1). Therefore, a good characterization of the kinetic parameters of these reactions for an accurate modeling description is necessary.

Under reducing conditions, the consumption of H_2S follows the main reaction paths discussed above. However, other important species, such as H_2S_2, HS_2 and S_2, can be formed due to the minor presence of oxygen. S_2 can be produced through the sequence of reactions R5.12-R5.15, where SH, HS_2 and H_2S_2 interact with each other leading to the final product S_2 through reaction (R5.15). This pathway for H_2S consumption was also mentioned by Song et al. (2017) and was also considered in the work of Zhou et al. (2013).

$$SH + SH \rightleftharpoons HS_2 + H \qquad (R5.12)$$

$$SH + H_2S_2 \rightleftharpoons HS_2 + H_2S \qquad (R5.13)$$

$$HS_2 + HO_2 \rightleftharpoons H_2S_2 + O_2 \qquad (R5.14)$$

$$HS_2 + SH \rightleftharpoons S_2 + H_2S \qquad (R5.15)$$

5.2 H_2 OXIDATION AND ITS INTERACTION WITH NO

The analysis of the system ($H_2/O_2/NO$) was seen as a preliminary step before studying the H_2S/O_2 and $H_2S/O_2/NO$ systems at high pressures, since previous studies about H_2S oxidation at high pressures, in a tubular flow reactor, had shown deficiencies and one of them was referred as exploratory by their authors (Gersen et al., 2017; Song et al. 2017). Additionally, the study about H_2 oxidation and its interaction with NO was carried out to acquire experience and knowledge about the behavior of NO at high pressures, together with a well-known fuel like H_2. The experiments were performed at the high-pressure tubular flow-reactor set-up 2 described in section 3.2. The influence of different variables on the process, like temperature (450-1100 K), pressure (10, 20 and 40 bar) and air-excess ratio (λ=0.5-6.4), was tested. The kinetic analysis of the results of experiments performed was helpful to update the mechanism, regarding the H_2/O_2 subset of reactions, a key subset in combustion chemistry. The main results are reported in Paper II.

Different reaction systems were tested to analyze the influence of NO over H_2 oxidation at high pressures. The different experimental conditions are detailed in Table 5.2. First, under oxidizing conditions, the H_2/O_2 and $H_2/O_2/NO$ systems were studied (sets 9 to 14 in Table 5.2). The results of species concentration corresponding to the conversion of the H_2/O_2 system, with and without the NO presence, are shown in Figure 5.6, at 10, 20 and 40 bar under oxidizing conditions. As can be observed, pressure has a little effect on the conversion onset of H_2 in the absence of NO, showing approximately 50 K difference in the reaction onset between the three pressures, and shifting the conversion to lower temperatures as the pressure increases. When NO is present in the system, the H_2 conversion is promoted to lower temperatures as pressure rises, and is comparatively greater than in the experiments without NO. In the case of 40 bar, there is a difference of 125 K between the reaction onsets of H_2 without and with NO, and only 25 K between the experiments at 10 bar.

Table 5.2 Experimental conditions of H_2 oxidation in the high-pressure set-up 2. The total flow rate is balanced with N_2. Parameter λ_{H2} is calculated according to the reaction $H_2+1/2O_2 \rightleftharpoons H_2O$ and parameter λ_{NO} according to the reaction $NO+1/2O_2 \rightleftharpoons NO_2$. The gas residence time (t_r) is referred to the entire set-up, at one temperature in the reactor (875 K).

Set	Manometric pressure (bar)	H_2 (ppm)	NO (ppm)	O_2 (ppm)	λ_{H2}	λ_{NO}	t_r (s)
9	40	937	530	3000	6.4	11.3	107
10	20	935	517	3000	6.4	11.6	56
11	10	920	524	3000	6.5	11.5	29
12	40	1029	-	3000	5.8	-	107
13	20	930	-	3000	6.4	-	56
14	10	910	-	3000	6.6	-	29
15	40	-	521	3000	-	11.5	107
16	20	-	508	3000	-	11.8	56
17	10	-	514	3000	-	11.7	29
18	40	1022	485	500	1.0	2.1	107
19	20	1050	525	675	1.3	2.6	56
20	40	1024	535	250	0.5	0.9	107
21	20	1000	520	250	0.5	1	56

Regarding NO_x concentrations, both NO and NO_2 species were measured. Pressure has an important influence on the NO/NO_2 ratio, since the formation of NO_2 is favored as pressure increases, described by reaction (R5.16). A small concentration from NO_2 backs to NO as the temperature increases, as is also shown in Figure 5.6, since NO is favored thermodynamically at high temperatures. The balance of NO_x ($NO+NO_2$) closes fairly well (near 100%) in all the cases, except at 40 bar, where at high temperatures there is a NO_x decrease of approximately 20%.

$$NO + NO + O_2 \rightleftharpoons NO_2 + NO_2 \qquad \text{(R5.16)}$$

The results of the kinetic modeling are shown in the figures of this section as black lines. In these cases, the final version of the mechanism and the one that was published from this work

(Paper II) present the same modeling results, as no modifications were done posteriorly in NO_x reaction subset or in the H_2/O_2 reaction subset.

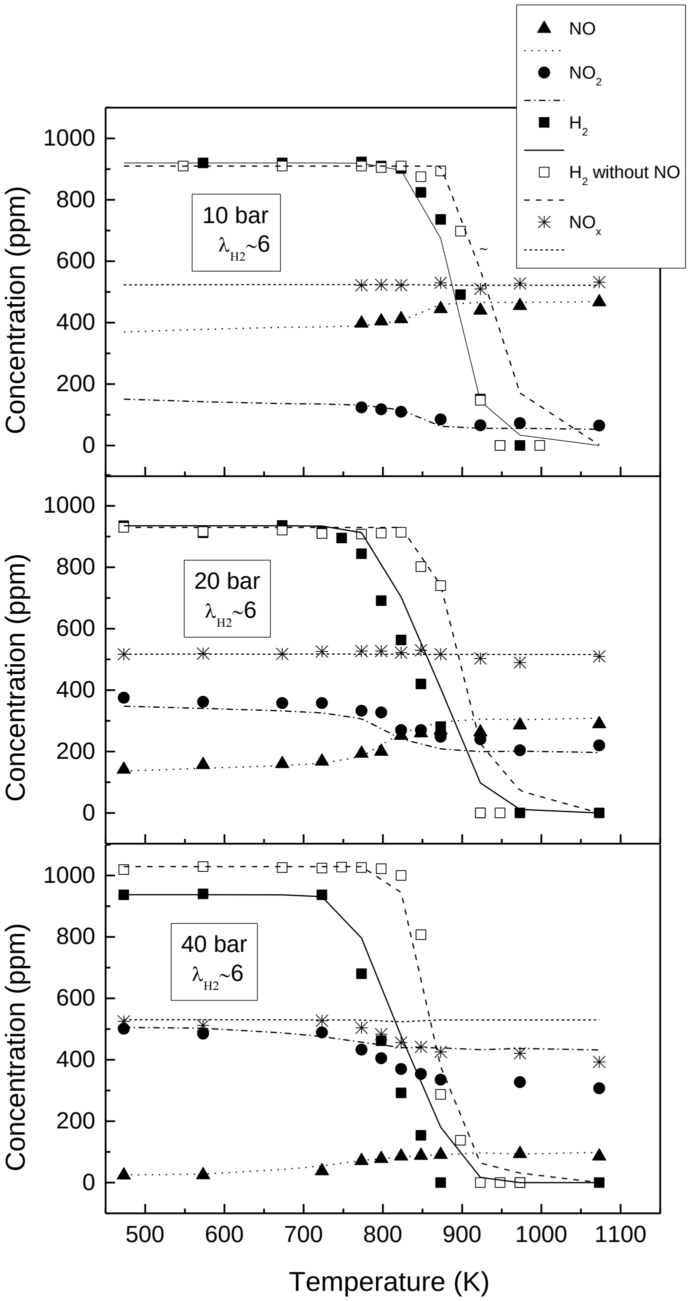

Figure 5.6 Results of H_2 oxidation, in the absence and presence of NO, obtained under oxidizing conditions at 10 bar, 20 bar and 40 bar. Solid symbols correspond to experimental results in the presence of NO, while open symbols represent concentrations in the experiments without NO. Lines denote simulations of the final model. Conditions of sets 9 to 14 in Table 5.2.

In order to further study the oxidation of H_2 in the presence of NO, some experiments were carried out just using NO under the same oxidizing conditions (sets 15-17 in Table 5.2). In Figure 5.7, the results of the NO/O_2 system are plotted, together with the results of NO oxidation in the presence of H_2 previously seen (sets 9-11 in Table 5.2), in order to compare results. The results show a similar behavior of NO and NO_2 concentrations, in general trends, when H_2 is present or not. However, minor differences are appreciated at 10 and 20 bar at high temperatures, which are related to the interaction of NO/NO_2 with the radical pool when H_2 is present, promoting its oxidation, as seen in Figure 5.6. A major difference can be observed at 40 bar between NO_2 concentrations in the absence and presence of H_2. As mentioned earlier, for the H_2/O_2/NO system at 40 bar, a decrease in the NO_x balance is found, which is not seen in the NO/O_2 system. Since the concentrations of NO are really similar at 40 bar compared to NO_2 concentrations, we might conclude that some interaction NO_2/H_2 is occurring in the experimental conditions at 40 bar and high temperatures. A study of the CO/H_2/O_2/NO_x system (Rasmussen et al., 2008a), in a high-pressure flow reactor, did not show a loss of NO_x when working at 50 bar and high oxidizing conditions (λ_{H2}=68). However, their lambda value was 10 times higher than in the present study, possibly preventing the NO_2/H_2 interaction to occur. A possible explanation for the NO_x decrease observed at 40 bar could be related with the formation of nitric acid. As said by Ajdari et al. (2015), if water vapor is present in pressurized flue gas systems, the formation of gaseous nitric acid and nitrous acid is promoted. While this could explain the loss of NO_x, this has not been proven.

The results of H_2 concentration in the presence of NO for stoichiometric conditions and different pressures (20 and 40 bar) are shown in Figure 5.8 (sets 18 and 19 in Table 5.2). As mentioned above, the NO/NO_2 ratio is lower as the pressure increases, which is also seen under stoichiometric conditions. The onset temperature for H_2 conversion remains the same at 40 bar as for oxidizing conditions (∼775 K), but the H_2 conversion finishes at higher temperatures due to the lack of oxygen. At 20 bar, the reaction starts at higher temperatures in comparison to the case of 40 bar, around ∼825 K. The results of experiments performed under reducing conditions (sets 20 and 21 in Table 5.2) are shown in Figure 5.9. The onset temperature for the conversion of H_2 at 40 bar remains the same as for other stoichiometries (∼775 K). H_2 is not fully consumed and the ratio NO/NO_2 is the highest obtained among all the stoichiometries, due to the lack of oxygen. The decrease of NO_x concentration seen at 40 bar and oxidizing conditions, probably due to some NO_2/H_2 interaction, is not observed under stoichiometric conditions, where the NO_2 formation is lower. For reducing conditions, the NO_x decrease happens again, which is captured by the model and explained below.

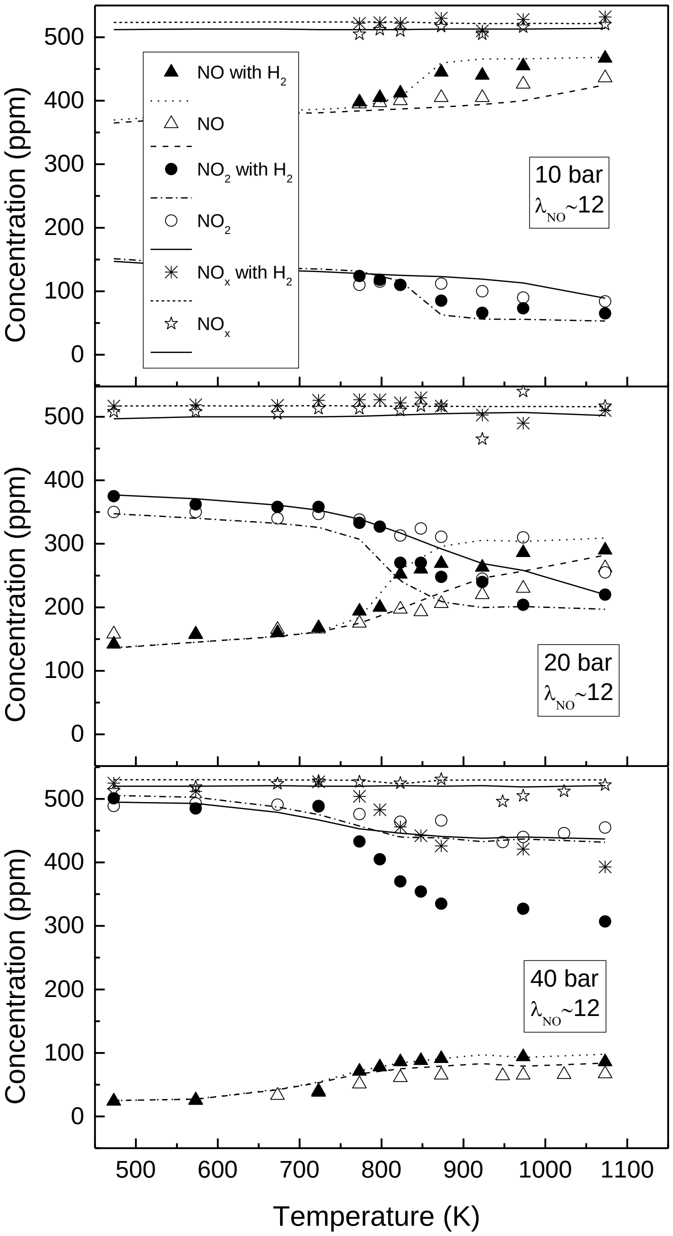

Figure 5.7 Results for the oxidation of NO, in the absence and presence of H_2, obtained under oxidizing conditions at 10 bar of pressure, 20 bar and 40 bar. Solid symbols correspond to experimental results in the presence of H_2, while open symbols represent concentrations in the experiments without H_2. Lines denote simulations of the final model. Conditions of sets 9-11 and sets 15-17 in Table 5.2.

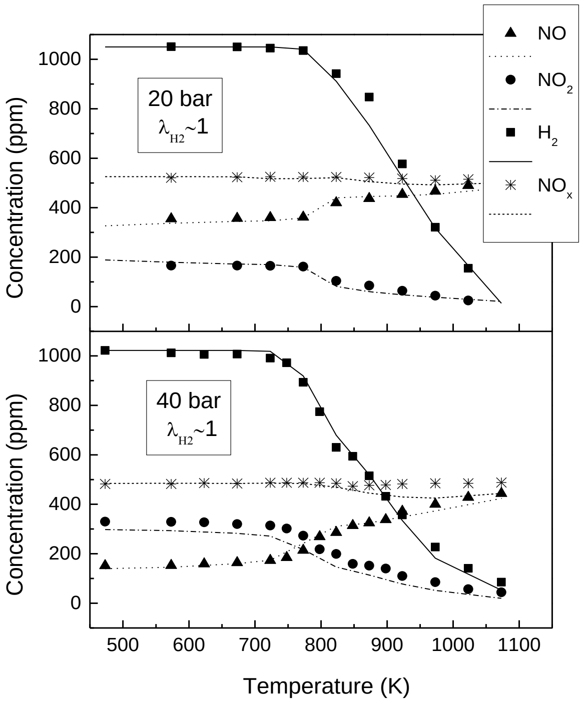

Figure 5.8 Results obtained under stoichiometric conditions at 20 bar and 40 bar. Symbols represent experimental measurements and lines denote simulations of the final model. Conditions of sets 18 and 19 in Table 5.2.

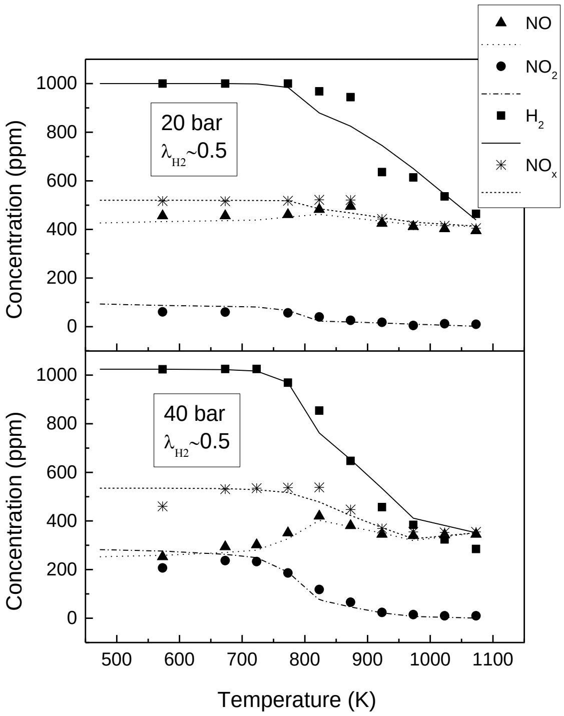

Figure 5.9 Results obtained under reducing conditions at 20 bar and 40 bar. Symbols represent experimental measurements and lines denote simulations of the final model. Conditions of sets 20 and 21 in Table 5.2.

Regarding the kinetic model, the present study about H_2 oxidation in the presence of NO helped to update the H_2/O_2 reaction subset under high pressure conditions, mainly taken from Burke et al. (2012) and Hashemi et al. (2015). Thermodynamic data were taken from the same sources as the sub-mechanisms. In general, the theoretical predictions shown in the previous figures match the consumption of H_2 with good precision in most cases. According to the calculations, the consumption of hydrogen can be described as a chain of reactions (R5.10, R5.17-R5.21), being (R5.17) the main step in the H_2 oxidation. Radicals HO_2 are formed due to the reaction of atomic H with O_2 through (R5.18), then, they are recombined to form H_2O_2 in reaction (R5.19). In the last step (R5.10), H_2O_2 thermal decomposition provides OH radicals for the consumption step (R5.17). At the same time, reaction (R.20) competes for H radicals with (R5.18), but this process is more relevant at low pressures. At high pressure, reaction (R5.18) is the main consumption pathway of H radicals. Reaction (R5.21) is considered to be important for H_2 conversion initiation at all stoichiometries and found to be one of the most sensitive (Hashemi et al., 2015). Kinetic parameters for this reaction were taken from Giménez-López et al. (2011), because they are more updated values and provide a better modeling behavior.

$$H_2 + OH \rightleftharpoons H_2O + H \qquad (R5.17)$$

$$H + O_2 (+M) \rightleftharpoons HO_2 (+M) \qquad (R5.18)$$

$$HO_2 + HO_2 \rightleftharpoons H_2O_2 + O_2 \qquad (R5.19)$$

$$H_2O_2(+M) \rightleftharpoons OH + OH (+M) \qquad (R5.10)$$

$$H + O_2 \rightleftharpoons OH + O \qquad (R5.20)$$

$$H_2O_2 + H \rightleftharpoons HO_2 + H_2 \qquad (R5.21)$$

Summing up, the oxidation of H_2 is explained at high pressures by reactions involving HO_2 and H_2O_2 species. When NO is added to the system, the role of HO_2 as a chain terminator changes and a new branching step, in which OH radicals are formed from HO_2, is activated. In particular, the cycle between NO and NO_2 consumes HO_2 radicals through (R5.22) and forms OH radicals through (R5.23), which promotes the oxidation of H_2. These reactions are part of a well-known catalytic cycle (Slack and Grillo, 1977; Bromly et al. 1995; Mueller et al., 1998), with $HO_2+H \rightleftharpoons OH+OH$ as net reaction.

$$NO + HO_2 \rightleftharpoons NO_2 + OH \qquad (R5.22)$$

$$NO_2 + H \rightleftharpoons NO + OH \qquad (R5.23)$$

In the work of Glarborg et al. (2000), where the ability of H_2 to reduce nitric oxide under conditions relevant for the reburning process was studied, the importance of species like HNO to react with H_2 was remarked, finding that the only kinetic parameters available for (R5.24), by Röhrig and Wagner (1994), gave a H_2 conversion too fast compared to their experimental data and finally not including this reaction in their model.

$$HNO + H_2 \rightleftharpoons NH + H_2O \qquad (R5.24)$$

In the present work, those kinetic parameters (Röhrig and Wagner, 1994) were also found to overpredict the consumption of H_2 under reducing conditions and the kinetic constant for reaction (R5.24) was estimated in the present study to be $7\cdot10^8$ ($cm^3\cdot mol^{-1}\cdot s^{-1}$), obtaining good agreement between experimental results and model predictions, both for H_2 as for NO_x concentrations at high temperatures, as can be seen in Figure 5.9. This reaction (R5.24) was found to be important only under reducing conditions, while no impact was observed for other stoichiometries. An accurate determination of the rate constant for (R5.24) would be desirable. The decrease in NO_x observed at 40 bar and reducing conditions might be explained thanks to this reaction. NO reacts with H radicals to form HNO (R5.25), then reaction (R5.24) occurs and NH is formed, which ends up reacting with NO to form N_2 and OH through (R5.26). Hence, NO_x decrease can be due to the formation of N_2, which is not quantified.

$$NO + H (+M) \rightleftharpoons HNO (+M) \qquad (R5.25)$$

$$NH + NO \rightleftharpoons N_2 + OH \qquad (R5.26)$$

The model matches well the experimental data under all the experimental conditions, except for the system $H_2/O_2/NO$ at 40 bar and oxidizing conditions. This good fit is achieved, in part, by the proposed kinetic parameters of reaction (R5.16), which is important for predicting the amount of NO and NO_2 that enters the reaction zone, influencing H_2 ignition as well as the NO oxidation process at high temperatures. A comparative plot of the kinetic constants for reaction (R5.16), proposed in this work and from the literature, is shown in Figure 5.10. As seen, scatter of the different reaction constants is high. The present kinetic constant chosen is in reasonable agreement with experimental data reported in the past (Ashmore et al., 1962; Greig and Hall, 1967; Hisatsune and Zafonte, 1969; England and Corcoran, 1975) more than with the latest review of this reaction (Atkinson et al., 2004), which is mainly based on the work of Olbregts (1985).

$$NO + NO + O_2 \rightleftharpoons NO_2 + NO_2 \qquad (R5.16)$$

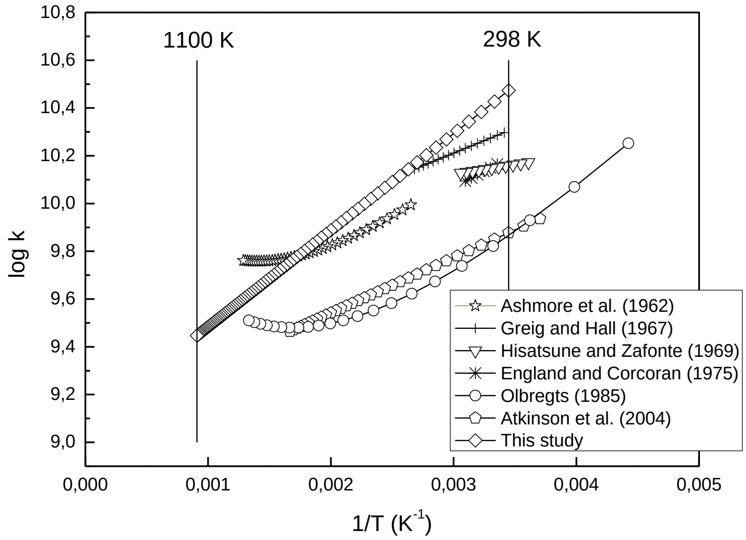

Figure 5.10 Comparison of different values for the kinetic constant logarithm of (R5.16) ($NO+NO+O_2=NO_2+NO_2$) vs. 1/T (K^{-1}), from the literature and the estimation of the present study.

5.3 H_2S OXIDATION AT HIGH PRESSURE

The study about H_2S oxidation at high pressures has been published in two different works (Papers III and V). All the experiments were carried out in the high-pressure facility described in section 3.2 (high-pressure tubular flow reactor set-up 2) from 450 to 1000 K. The experimental conditions are described in detail in Table 5.3.

Paper III reported the analysis of H_2S oxidation at high pressures (0.65, 10, 20 and 40 bar), where only one stoichiometric ratio was used ($\lambda \sim 2$). The kinetic model developed till that moment at atmospheric pressure (Paper I), together with the updated H_2/O_2 subset and validated under high pressure conditions (Paper II), were tested under those conditions. At the same time, the mechanism was tested against experiments from the literature. Previous studies about this topic are scarce in the literature. The group of Glarborg at DTU (Technical University of Denmark) published two papers about H_2S oxidation in a similar experimental set-up with a tubular flow reactor. In the first one, about neat H_2S oxidation (30-100 bar) (Song et al., 2017), they claimed for more research in this field and more experiments, as well as a better kinetic characterization of the oxidation process, since they had doubts about certain reactions (e.g. reactions involving O_3, which were pointed in the present work (Paper III) to have no relevance), and dispersion in their experimental data. The second one (Gersen et al., 2017), related to H_2S/CH_4 oxidation at high pressure, presented experiments in a tubular flow reactor and claimed as well for more experimental data and better kinetic parameter characterization, since the kinetic mechanism did not reproduce fairly well the experimental data. Another example would be the work by Mathieu et al. (2014), about H_2S addition on H_2 ignition delay times, where they summarized that the data in flow reactors, when H_2S is a reactant (referring to the work by Zhou et al. (2013)), were poorly reproduced by all the H_2S oxidation models available. At the same time, Mathieu et al. (2014) managed to simulate their data by modifying some important reactions within their reported error factor.

Table 5.3 Experimental conditions for H_2S oxidation in the high-pressure set-up 2. N_2 as bath gas.

Set	Manometric pressure (bar)	H_2S (ppm)	O_2 (ppm)	λ	t_r (s)	Flow rate (L (STP)/min)	Paper
22	0.65	520	750	1.0	371/T	1	V
23	0.65	505	1509	2.1	371/T	1	III
24	0.65	525	4510	5.7	371/T	1	V
24R	0.65	525	4450	5.7	371/T	1	V
25	10	500	792	1.1	2552/T	1	V
25R	10	500	822	1.1	2552/T	1	V
26	10	485	1510	2.1	2552/T	1	III
27	10	498	4380	5.5	2552/T	1	V
28	20	465	760	1.1	4872/T	1	V
29	20	497	1520	2.0	4872/T	1	III
30	20	500	4485	6.0	4872/T	1	V
31	40	500	753	1.0	9280/T	1	V
32	40	500	1545	2.1	9280/T	1	III
33	40	485	4296	5.9	9280/T	1	V
34	10	504	4485	5.9	4872/T	0.5	V

Overall, in Paper III, the results were satisfactory. New valuable experimental data were provided, as well as a kinetic model capable of reproducing the oxidation of H_2S at different pressures (0.65-40 bar), especially at low pressures (0.65 bar), confirming the good prediction at atmospheric pressure observed in Paper I in a different tubular flow reactor (atmospheric pressure set-up 1). The reaction pathways of H_2S oxidation obtained at high pressure were similar to the ones at atmospheric pressure. The differences were found in the species that are involved in the oxidation process at the different pressures, as H_2O_2 and H_2S_2, which become more important as pressure rises. At the same time, the mechanism was capable of reproducing the data from Song et al. (2017) with certain accuracy, as well as the ignition delay times by

Mathieu et al. (2014). Despite the good results, there was still room for improvement at the highest pressure tested (40 bar), where the model showed more deficiencies. This is one of the reasons why the study reported in Paper V was carried out.

The work about H_2S oxidation at high pressures, Paper V, presented new experimental data (two different stoichiometries; $\lambda\sim1$ and $\lambda\sim6$) together with an updated and improved kinetic mechanism for high pressures. The experimental and modeling results of the concentrations of H_2S, SO_2 and O_2 as a function of temperature from Paper V are shown together with the ones from Paper III in Figures 5.11-5.14. The graphs are ordered from 0.65 bar to 40 bar of pressure, showing the three different lambda values in each of the figures. The simulation results are plotted as lines, the black ones represent the final mechanism, published in Paper V, and which include the omission of some reactions which will be discussed later. The red lines are only present in the figures for conditions of $\lambda\sim2$, which represent the model published in Paper III. The sulfur balance closes in all cases within ±5%. As can be observed in the figures, the conversion of H_2S is shifted to lower temperatures, and the oxidation is more abrupt, as the pressure and the oxygen concentration increase (higher lambda value). Thus, the onset temperature for H_2S conversion is 725 K in the case of 10 bar and stoichiometric conditions ($\lambda=1.1$, set 25 in Table 5.3), while it is 575 K at 40 bar and oxidizing conditions ($\lambda=5.9$, set 33 in Table 5.3). The consumption of O_2 follows the same trend as hydrogen sulfide.

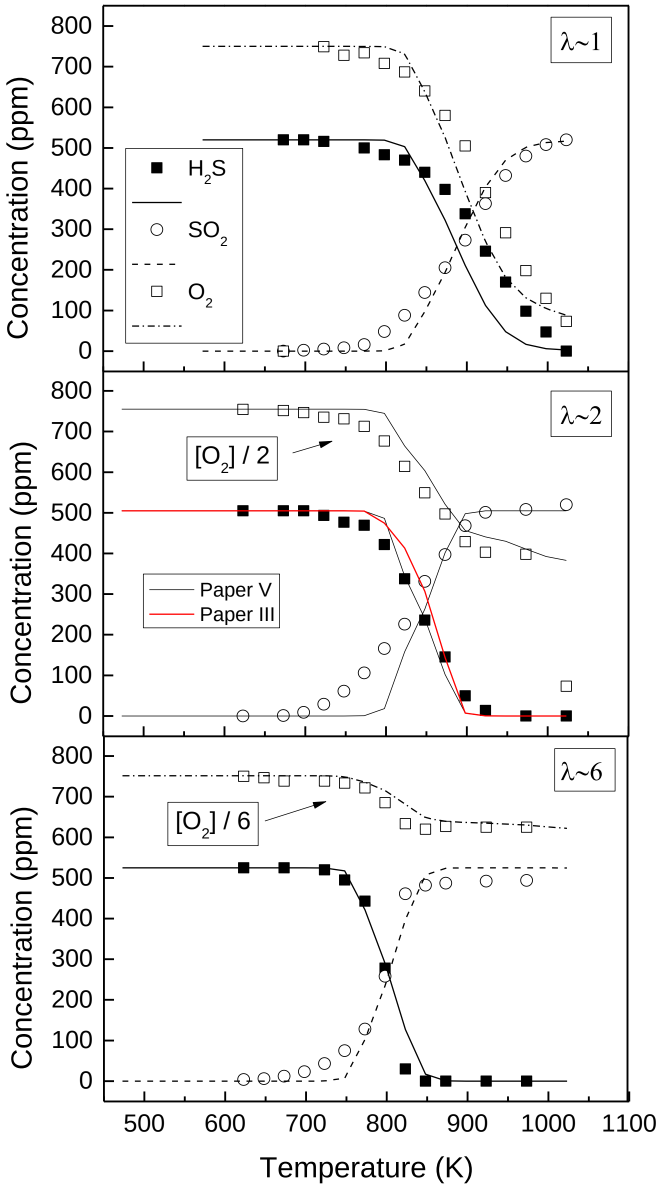

Figure 5.11 Concentrations of H_2S, SO_2 and O_2 vs. temperature at 0.65 bar (sets 22, 23 and 24 in Table 5.3). Symbols represent experimental measurements and lines denote simulations of the final model (black lines) and model in Paper III (red line).

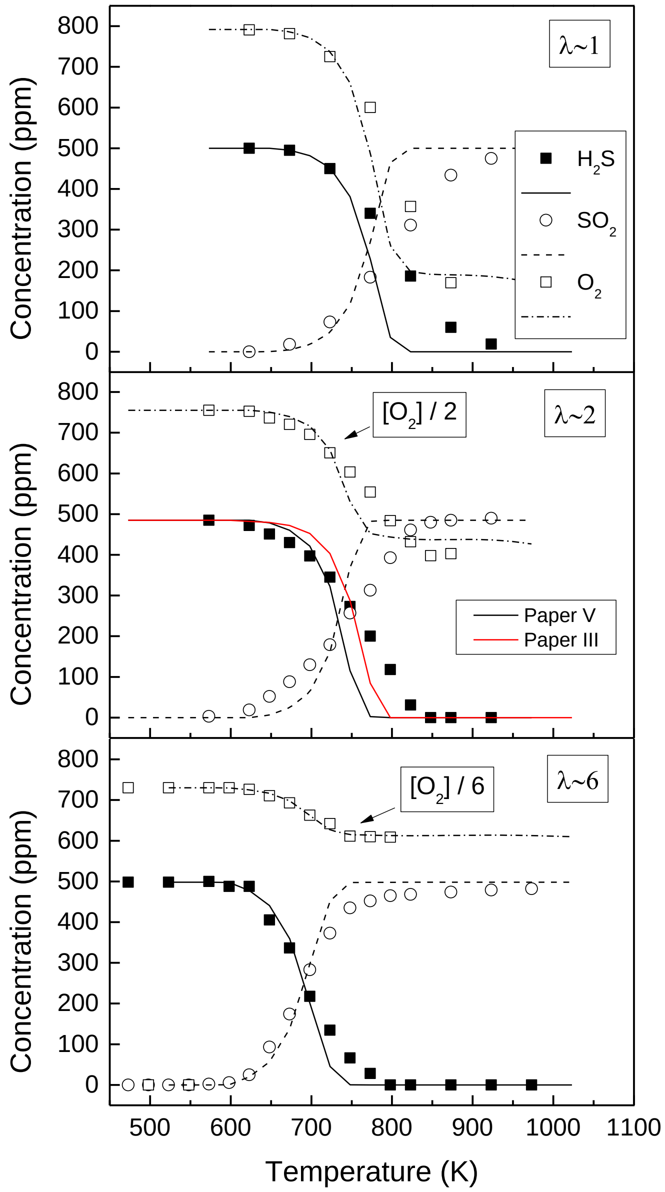

Figure 5.12 Concentrations of H_2S, SO_2 and O_2 vs. temperature at 10 bar (sets 25, 26 and 27 in Table 5.3). Symbols represent experimental measurements and lines denote simulations of the final model (black lines) and model in Paper III (red line).

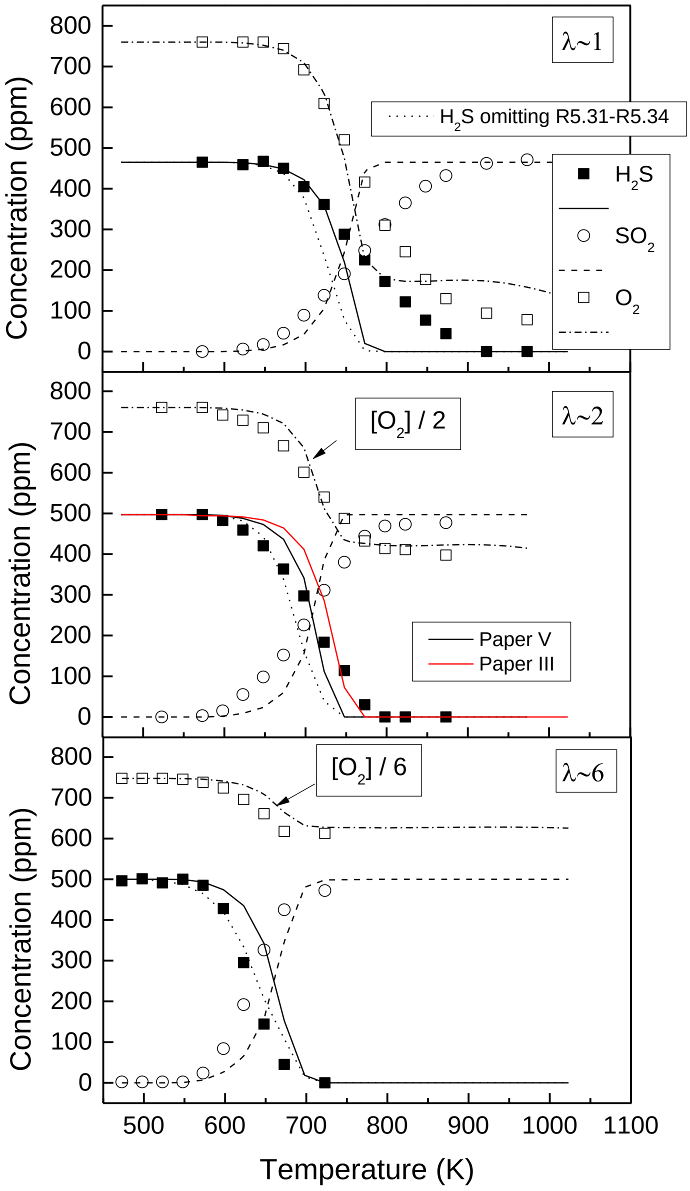

Figure 5.13 Concentrations of H_2S, SO_2 and O_2 vs. temperature at 20 bar (sets 28, 29 and 30 in Table 5.3). Symbols represent experimental measurements and lines denote simulations of the final model (black lines) and model in Paper III (red line).

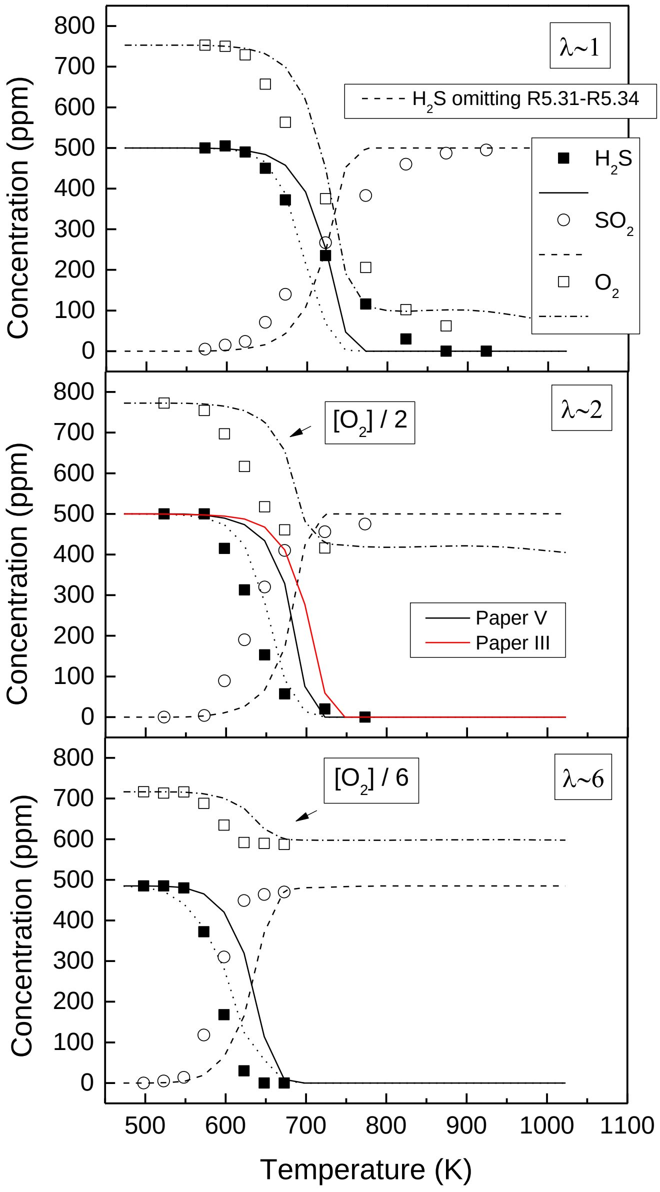

Figure 5.14 Concentrations of H_2S, SO_2 and O_2 vs. temperature at 40 bar (sets 31, 32 and 33 in Table 5.3). Symbols represent experimental measurements and lines denote simulations of the final model (black lines) and model in Paper III (red line).

Reactions involving H_2O_2 species were found as the most sensitive in the kinetic model analysis of H_2S oxidation at high pressures, as well as in the works by Song et al. (2017) and Mathieu at al. (2014). Hence, in Paper V, other possible reactions involving this peroxide, H_2O_2, were evaluated. For example, the reaction of H_2O_2 with SH radicals, for which only an upper limit for the rate constant at room temperature is available (Friedl et al., 1985). Three different possible reaction channels were evaluated for the SH+H_2O_2 reaction (R5.27-R5.29).

$SH + H_2O_2 \rightleftharpoons H_2S + HO_2$ (R5.27)

$SH + H_2O_2 \rightleftharpoons HSOH + OH$ (R5.28)

$SH + H_2O_2 \rightleftharpoons HSO + H_2O$ (R5.29)

Two of them (R5.27 and R5.28) were already present in earlier versions of the mechanism (Paper I). On the other hand, no kinetic parameters are available in the literature for the third reaction channel (R5.29). According to Friedl et al. (1985), the formation of HSO+H_2O is not relevant at room temperature. However, it was observed a higher reactivity of H_2S at high pressures (40 bar) if (R5.29), and also the possible reaction of HSO with H_2O_2 (R5.30), are included in the mechanism for the simulations of H_2S oxidation.

$HSO + H_2O_2 \rightleftharpoons HSO_2 + H_2O$ (R5.30)

There are no kinetic parameters for (R5.30) in the literature either. In this work, both reaction kinetic constants have been estimated as 10^{12} ($cm^3 \cdot mol^{-1} \cdot s^{-1}$), in the temperature range studied (450-1100 K). These reactions have no effect on the simulations at the other pressures studied.

Another important point about the reactivity of H_2S is related to the work by Song et al. (2017), who increased the reactivity of H_2S by skipping at high pressure and oxidizing conditions some reactions, such as H_2S reactions with O_3 (R5.31 and R5.32), and under stoichiometric and oxidizing conditions, a couple of reactions of the S_2O subset (R5.33 and R5.34). Following a similar procedure, i.e. removing the reactions mentioned above in our mechanism, no changes occur in the simulations presented in Paper I or Paper III. Only if (R5.29) and (R5.30) are included in our mechanism, the same behavior observed by Song et al. (2017) eliminating those reactions (R5.31-R5.34) happens. The reactivity of the system is increased at high pressures (40 bar and 20 bar), while it remains unaltered at other pressures.

$H_2S + O_3 \rightleftharpoons SO_2 + H_2O$ (R5.31)

$H_2S + O_3 \rightleftharpoons HOSO + OH$ (R5.32)

$S_2O + OH \rightleftharpoons S_2 + HO_2$ (R5.33)

$S_2O + S_2 \rightleftharpoons S_3 + SO$ (R5.34)

As an example, Figure 5.15 shows the H_2S concentration vs. temperature at 40 bar and oxidizing conditions (λ=5.9), by comparing the results of different mechanisms together with the corresponding experimental data. The simulations are improved compared to the mechanism in Paper III by adding reactions (R5.29) and (R5.30) in the model (PaperIII+R5.29+R5.30). Besides, apart from adding reactions (R5.29) and (R5.30), reactions (R5.31-R5.34) can also been omitted, as in the work by Song et al. (2017), managing to improve the model predictions (PaperIII+R5.29+R5.30-(R5.31-R5.34). The mechanism published by Song et al. (2017) is also presented in Figure 5.15 with the reactions that they omitted (R5.31-R5.34) in their original model (Song et al. (2017)+(R5.31-R5.34)), showing a big difference in the predictions (around 200 K difference) between their models.

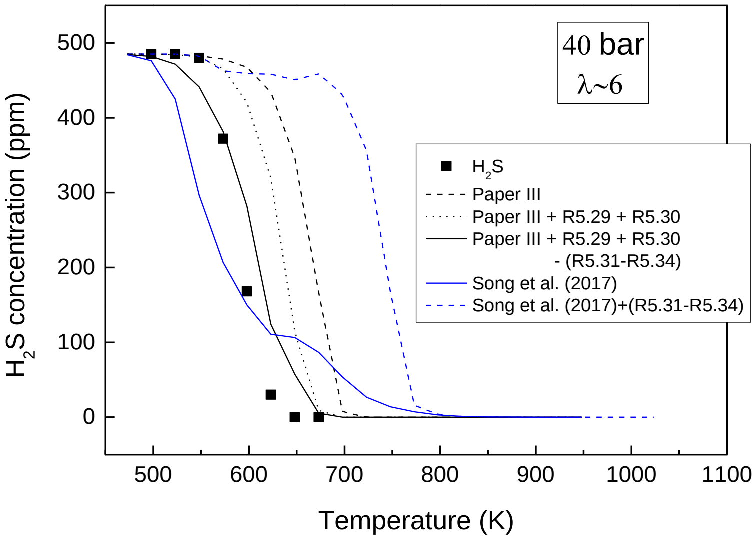

Figure 5.15 Concentration of H_2S vs. temperature at 40 bar and λ=5.9 (set 33 in Table 5.3) using different mechanisms. Symbols represent experimental data and lines represent modeling predictions.

When reactions (R5.31-R5.34) are present in the mechanism, they slow down the oxidation process of H_2S. Reaction of H_2S with O_3 (R5.31) is the most important one, but it is a chain-terminating step. As mentioned by Song et al. (2017), their kinetic parameters are currently not well established. The most reliable measurement for H_2S + O_3 is believed to be the room temperature upper limit by Becker et al. (1975). The kinetic parameters used here are taken from the theoretical work by Mousavipour et al. (2013), whose suggestion of (R5.31) as the dominant channel seems to be inconsistent with the experimental observations. In the case of the reactions with S_2O species, (R5.33) and (R5.34), they also slow down the reactivity of the

H_2S/O_2 system. Reaction (R5.33) converts OH radicals to less active HO_2 radicals. Once S_2O species are formed via (R5.35), they are mainly consumed via (R5.36) to form S_3, and, if (R5.34) is present in the model, it forms back S_2O from S_3, slowing down the oxidation process of H_2S. Reaction (R5.34) proceeds in the backward direction due to its high reverse kinetic constant, which is 10^{14} ($cm^3 \cdot mol^{-1} \cdot s^{-1}$) in all the temperature range, which kinetic parameters were determined theoretically by Zhou et al. (2013). According to the simulations, if its pre-exponential factor is reduced by two orders of magnitude, the reaction (R5.34) stops having any influence.

$$HSO + S_2 \rightleftharpoons S_2O + SH \qquad \text{(R5.35)}$$

$$S_2O + S_2O \rightleftharpoons S_3 + SO_2 \qquad \text{(R5.36)}$$

Overall, the mechanism shown in Figure 5.15 as Paper III+R5.29+R5.30-(R5.31-R5.34) simulates properly the experimental results. This is, adding new reactions involving H_2O_2 species and omitting (R5.31-R5.34) reactions. However, the final mechanism includes such reactions, since omitting reactions can be seen as just an exploratory analysis.

5.3.1 EFFECT OF RESIDENCE TIME

In order to evaluate independently the effect of gas residence time and pressure, an additional experiment has been performed at 10 bar and oxidizing conditions using a flow rate approximately of 0.5 L (STP)/min (set 34 in Table 5.3) instead of 1 L(STP)/min. This means that this set presents the same gas residence time as in the experiment at 20 bar and oxidizing conditions (set 30 in Table 5.3). Thus, we can observe in Figure 5.16 how pressure affects the oxidation of H_2S using the same residence time. As it is observed, the experimental results differ by a maximum of 25 K. Additionally, in Figure 5.17, it can be observed how the gas residence time affects H_2S oxidation, by comparing the experiment at 10 bar and 0.5 L (STP)/min (set 34 in Table 5.3) and the experiment at 10 bar and 1 L (STP)/min (set 27 in Table 5.3). As can be seen, the difference between experiments is around 50 K by doubling the flow rate, which means the gas residence time is the half. The larger the residence time, the earlier the oxidation of H_2S starts. The effect of gas residence time is, then, stronger than the effect of pressure under the conditions studied. All in all, the model seems capable of predicting H_2S oxidation well under the different conditions studied.

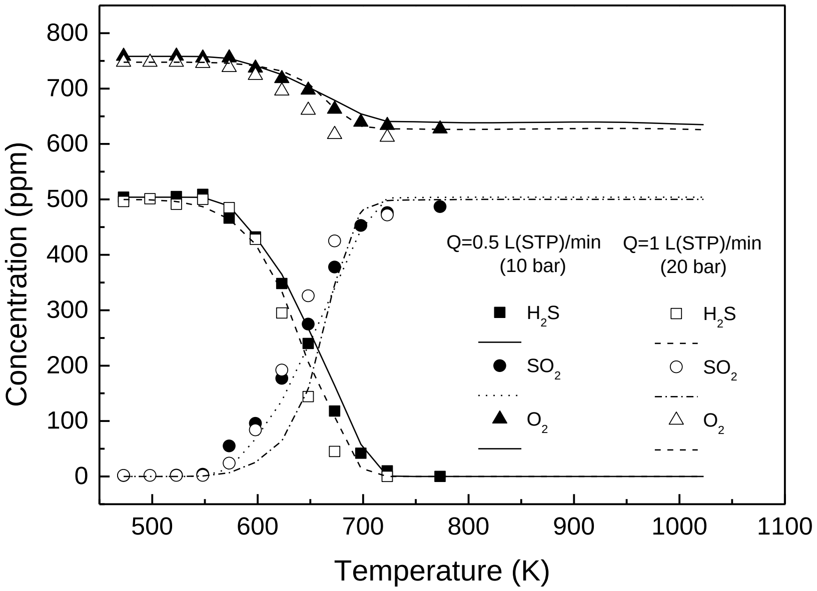

Figure 5.16 Concentrations of H2S, SO2 and O2 vs. temperature at 10 and 20 bar using the same gas residence time (sets 30 and 34 in Table 5.3). Symbols represent experimental data and lines represent model predictions.

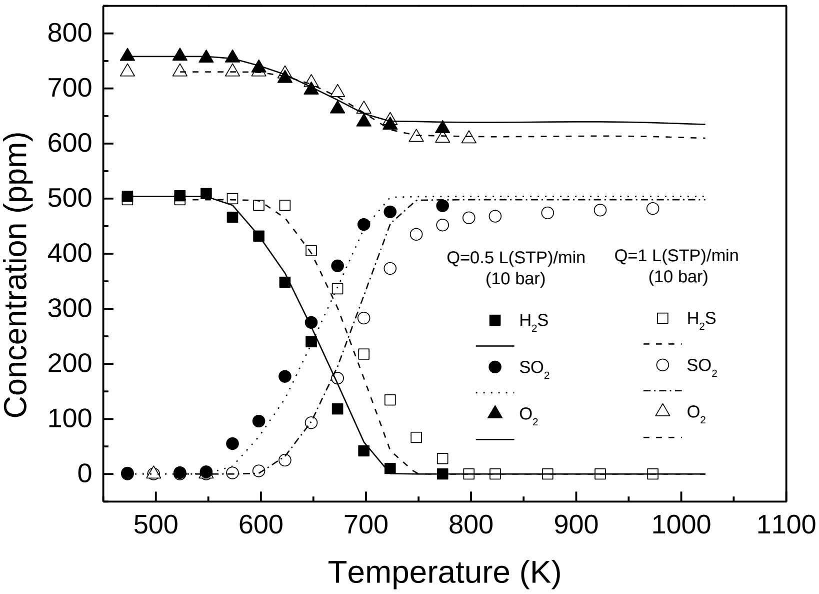

Figure 5.17 Concentrations of H2S, SO2 and O2 vs. temperature at 10 bar using different gas residence times (sets 27 and 34 in Table 5.3). Symbols represent experimental data and lines represent model predictions.

5.3.2 LITERATURE RESULTS SIMULATIONS

Results from the literature have also been simulated. The experimental results obtained by Song et al. (2017), about H_2S oxidation in a flow reactor at 30 bar and 100 bar (under stoichiometric and oxidizing conditions λ≈35), are shown in Figures 5.18-5.20, along with simulations using the final mechanism, but omitting reactions (R5.31-R5.34) as the authors did. A good match between experimental data and model calculations is obtained at all conditions.

The final mechanism has also been used to simulate the experiments from the work of Mathieu et al. (2014), about the effect of H_2S addition on hydrogen ignition delay times. The results obtained can be seen in Figure 5.21. The ignition delay times were measured experimentally behind reflected shock waves for mixtures of 1% H_2/1% O_2, diluted in Ar and doped with various concentrations of H_2S (100, 400 and 1600 ppm) at different pressures (1.6, 13 and 33 atm). The model predictions are reasonably close to the experimental results under almost all the conditions, except for two experiments, those corresponding to the highest H_2S concentration (1600 ppm) and pressures of 13 and 33 atm.

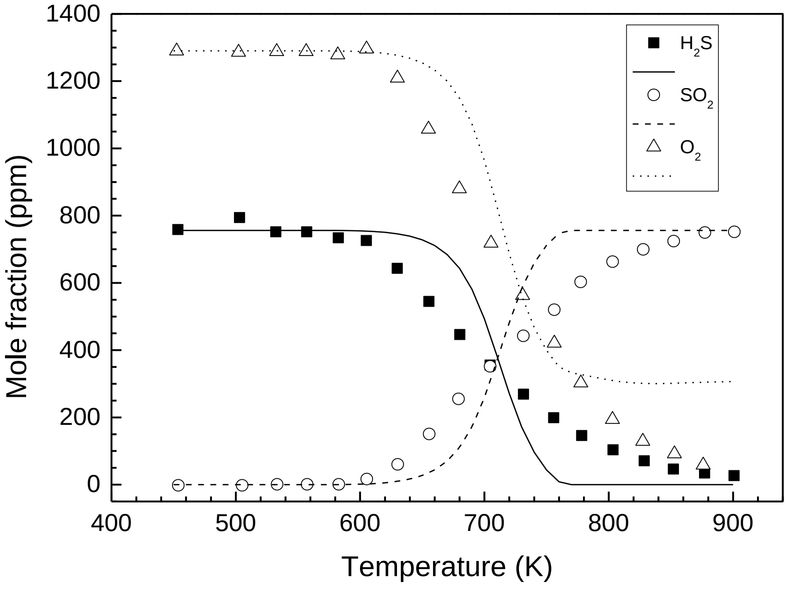

Figure 5.18 Concentrations of H_2S, SO_2 and O_2 vs. temperature at 30 bar and λ=1.14 (data taken from set 1 in Table III of Song et al. (2017)). Symbols represent experimental data, while lines denote model predictions (final mechanism omitting reactions R5.31-5.34).

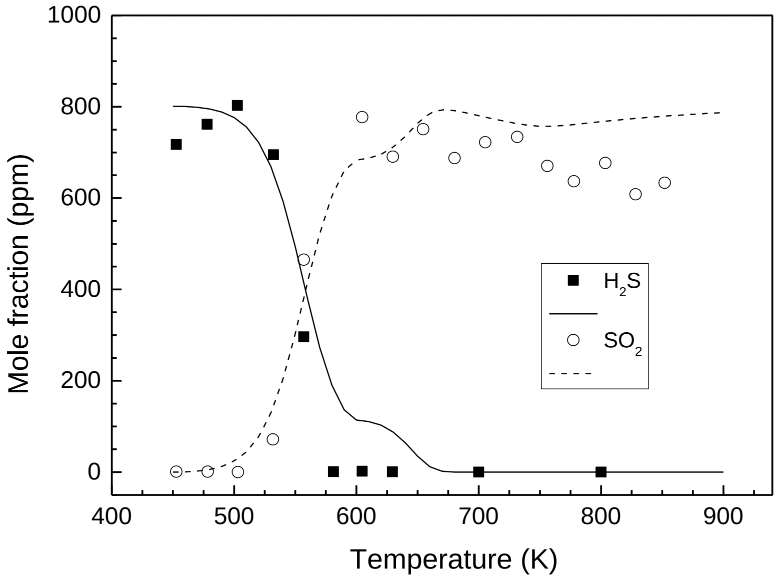

Figure 5.19 Concentrations of H_2S and SO_2 vs. temperature at 30 bar and λ=36 (data taken from set 3 in Table III of Song et al. (2017)). Symbols represent experimental data, while lines denote model predictions (final mechanism omitting reactions R5.31-5.34).

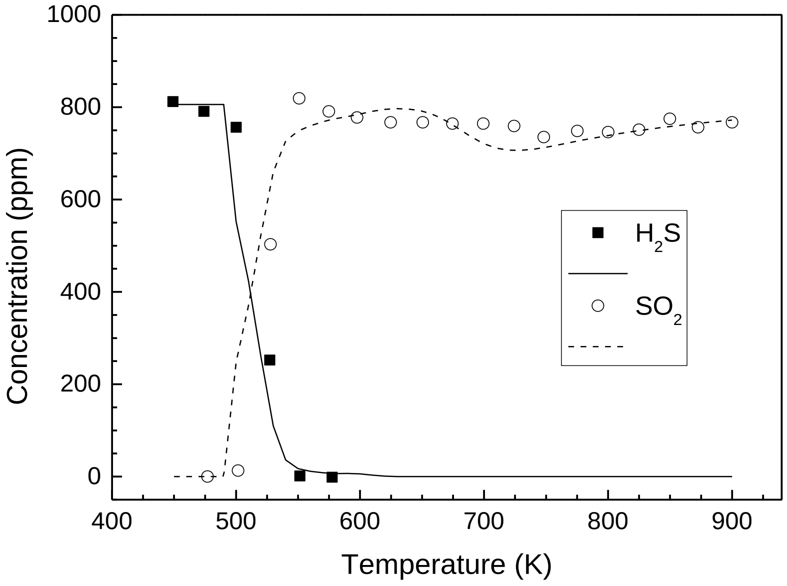

Figure 5.20 Concentrations of H_2S and SO_2 vs. temperature at 100 bar and λ=35 (data taken from set 4 in Table III of Song et al. (2017)). Symbols represent experimental data, while lines denote model predictions (final mechanism omitting reactions R5.31-5.34).

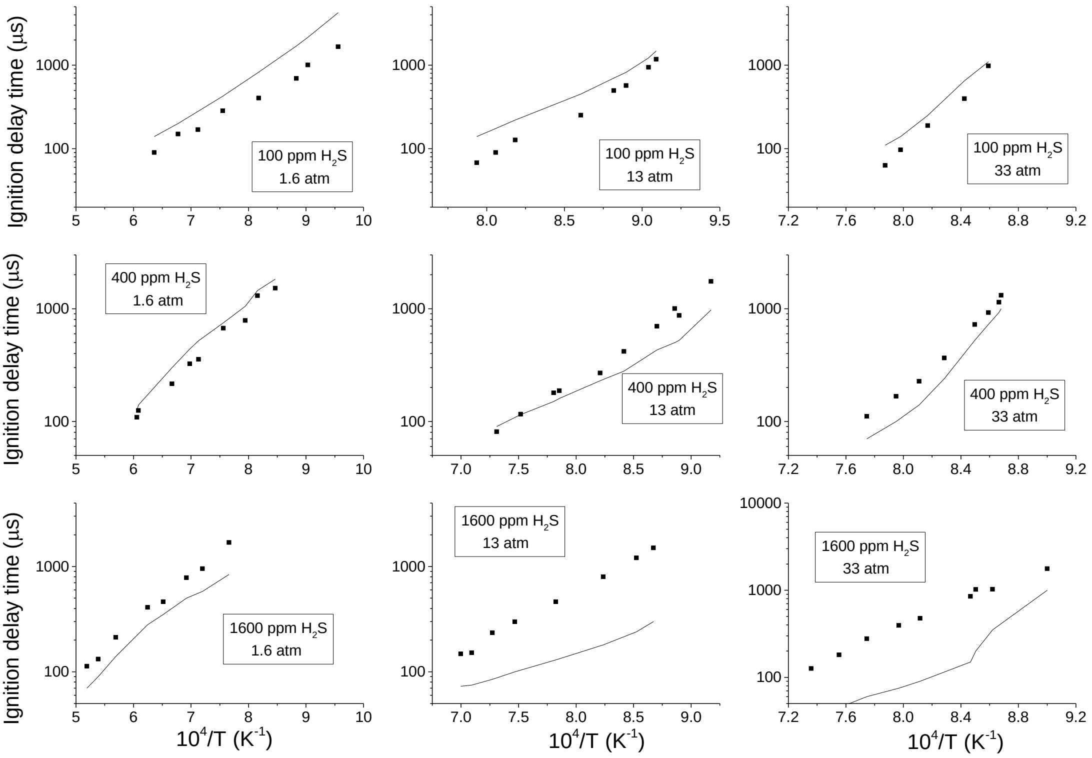

Figure 5.21 Ignition delay time measurements vs. temperature for different experimental conditions, using a mixture of 1% H_2/1% O_2, diluted in Ar and doped with H_2S. Experimental data are taken from the work of Mathieu et al. (2014).

5.4 H_2S/CH_4 MIXTURES OXIDATION

After studying the oxidation of H_2S under different experimental conditions, both at atmospheric pressure and at high pressures in 2 different facilities, as well as having developed a kinetic model capable of reproducing the oxidation of H_2S (Papers I, II and III), the next step has consisted of studying the oxidation behavior with methane, the main component of natural gas. This study covers different experimental conditions to study the H_2S/CH_4 interaction. The experiments have been conducted in 2 different facilities with tubular flow reactors, at atmospheric pressure (set-up 1) and at high pressure (set-up 2). Variables such as pressure (from atmospheric pressure to 40 bar), the air excess ratio, temperature (450-1400 K), as well as the influence of the initial H_2S/CH_4 ratio have been studied. The details of all the experimental conditions considered are described in Table 5.4. Nitrogen has been used as the inert atmosphere in the experiments. The results of this work were published in Paper IV.

Table 5.4 Experimental conditions for the H_2S/CH_4 mixtures oxidation. N_2 as bath gas.

Set	Manometric Pressure (bar)	CH_4 (ppm)	H_2S (ppm)	O_2 (ppm)	λ_{CH4}	λ_{H2S}	λ_{total}	t_r (s)	Set-up	Paper
35	0.65	1569	480	4500	1.4	6.3	1.2	$\frac{383}{T(K)}$	2	IV
24	0.65	-	525	4510	-	5.7	5.7	$\frac{383}{T(K)}$	2	V
36	0.65	1350	1250	4590	1.7	2.5	1.0	$\frac{383}{T(K)}$	2	IV
37	0.65	1307	1255	25500	9.8	13.5	5.7	$\frac{383}{T(K)}$	2	IV
38	0.65	480	1270	11300	11.8	5.9	3.9	$\frac{383}{T(K)}$	2	IV
39	10	1282	1243	4550	1.8	2.4	1.0	$\frac{2552}{T(K)}$	2	IV
40	20	1303	1224	4503	1.7	2.5	1.0	$\frac{4872}{T(K)}$	2	IV
41	40	1320	1230	4600	1.7	2.5	1.0	$\frac{9280}{T(K)}$	2	IV
42	20	1315	1295	1804	0.7	0.9	0.4	$\frac{4872}{T(K)}$	2	IV
43	20	1348	-	4286	1.6	-	1.6	$\frac{4872}{T(K)}$	2	IV
44	40	1400	-	4500	1.6	-	1.6	$\frac{9280}{T(K)}$	2	IV
23	0.65	-	505	1509	-	2.0	2.0	$\frac{383}{T(K)}$	2	III
26	10	-	485	1510	-	2.1	2.1	$\frac{2552}{T(K)}$	2	III
29	20	-	497	1520	-	2.0	2.0	$\frac{4872}{T(K)}$	2	III
32	40	-	500	1545	-	2.1	2.1	$\frac{9280}{T(K)}$	2	III
45	Atmospheric	1517	-	750	0.3	-	0.3	$\frac{194.6}{T(K)}$	1	IV
46	Atmospheric	1517	-	3000	1.0	-	1.0	$\frac{194.6}{T(K)}$	1	IV
47	Atmospheric	1508	-	6000	2.0	-	2.0	$\frac{194.6}{T(K)}$	1	IV
48	Atmospheric	1510	279	750	0.3	1.8	0.2	$\frac{194.6}{T(K)}$	1	IV
49	Atmospheric	1513	285	3000	1.0	7.0	0.9	$\frac{194.6}{T(K)}$	1	IV
50	Atmospheric	1508	298	6000	2.0	13.4	1.7	$\frac{194.6}{T(K)}$	1	IV
4	Atmospheric	-	482	1500	-	2.1	2.1	$\frac{194.6}{T(K)}$	1	I
5	Atmospheric	-	492	3750	-	5.1	5.1	$\frac{194.6}{T(K)}$	1	I

The experimental results of H_2S, SO_2, CH_4 and CO concentrations corresponding to the experiments near atmospheric pressure (set-up 2), sets 24 and 35-38 from Table 5.4, are presented in Figure 5.22 as symbols. Model predictions are also presented in the figure as lines, where the red ones correspond to the model published in Paper IV and the black ones represent the final mechanism. This pattern of line colors is followed in the rest of the figures of this section. The species CO_2, C_2H_4, C_2H_6, CH_3SH and CS_2 were detected in small concentrations and, therefore, they are not shown in the figures.

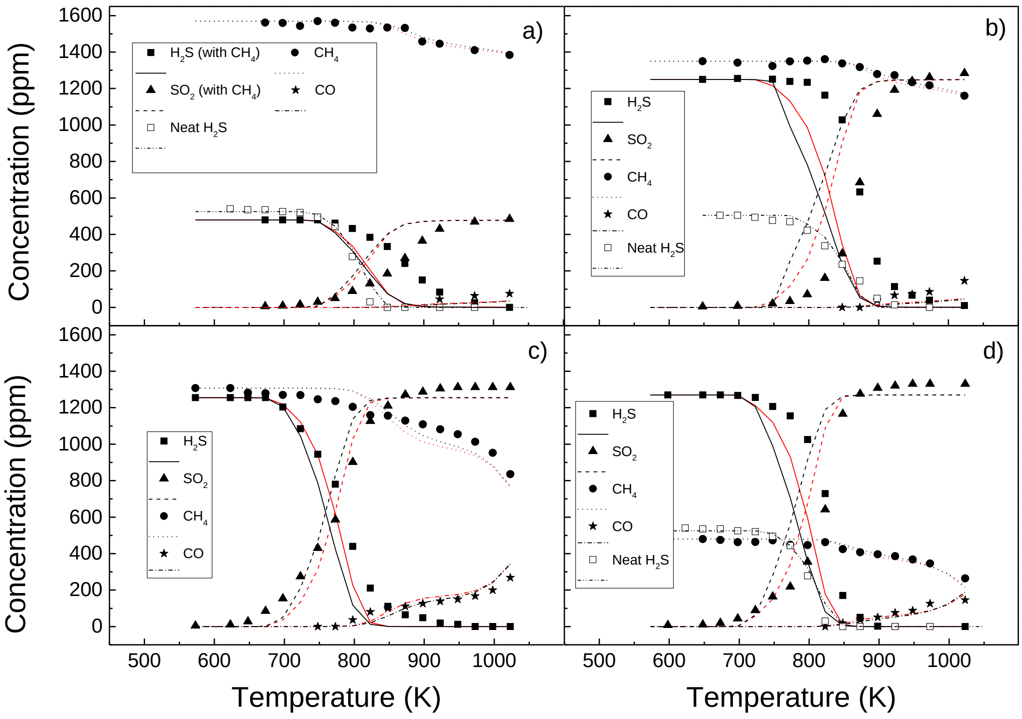

Figure 5.22 Concentrations of H_2S, SO_2, CH_4 and CO vs. temperature under 0.65 bar at set-up 2, experimental conditions in Table 5.4: a) sets 35 (λ_{total}=1.2) and 24 (λ_{total}=5.7); b) sets 36 (λ_{total}=1.0) and 23 (λ_{total}=2.0); c) set 37 (λ_{total}=5.7); d) sets 38 (λ_{total}=3.9) and 24 (λ_{total}=5.7). The original model results (Paper IV) are represented with red lines, while those from the final version of the mechanism are represented with black lines.

As can be observed in Figure 5.22, different stoichiometry values and H_2S/CH_4 ratios have been used to study the oxidation behavior of the H_2S/CH_4 mixture oxidation near atmospheric pressure. In all the cases, H_2S oxidation happens at temperatures lower than the ones at which CH_4 oxidation occurs, being H_2S completely converted into SO_2 at temperatures above approximately 900 K. Some tests were run with neat CH_4 and no reaction was observed, hence, CH_4 oxidation is promoted by H_2S. A higher concentration of O_2 shifts the oxidation of both H_2S and CH_4 to lower temperatures, as can be compared in cases a) and c) (λ_{total}=1.0 and λ_{total}=5.7, respectively). It can be observed that when H_2S is fully consumed, CH_4 conversion increases coinciding with a higher formation of CO. This is observed in all the cases and it is more noticeable at oxidizing conditions, cases c) λ_{total}=5.7 and d) λ_{total}=3.9.

In the case a), the experimental results from set 35 in Table 5.4 (λ_{total}=1.2, λ_{CH4}=1.4, λ_{H2S}=6.3), together with neat H_2S oxidation (set 24 in Table 5.4; λ_{total}=5.7, λ_{H2S}=5.7) are plotted, both with similar λ_{H2S} value. As can be observed, the consumption of H_2S is shifted to higher temperatures (by 75 K) compared to the neat oxidation of H_2S, indicating therefore the delay in H_2S oxidation by CH_4. A similar case can be observed in the study of Zeng et al. (2019b), about the co-oxidation of CH_4 and CS_2 in a flow reactor, where they also saw experimentally a delay in the oxidation of CS_2 by CH_4, and that trace amounts of CS_2 reduce the ignition temperature of CH_4. The authors indicated that the C-H-O-S combustion chemistry was complex and consequently their mechanism could not include all potential reactions. In our case, the kinetic model cannot predict the inhibition of H_2S conversion by CH_4 to higher temperatures either, despite the inclusion in the present mechanism of the CH_3SH, CS_2 and COS reaction subsets.

In the case b), the results obtained with the ones in the case a) can be compared, which have similar λ_{CH4} and λ_{total} values, but different H_2S inlet concentrations (1250 and 480 ppm, respectively) and H_2S/CH_4 ratio ratios (0.9 and 0.3, respectively). It can be observed that the onset of H_2S conversion in the case a) occurs at lower temperature than that obtained in the case b), due to the higher λ_{H2S} in the case a), but only by 25 K. In the case b), H_2S oxidation is also shifted to higher temperatures in comparison with neat H_2S oxidation, due to the presence of CH_4, but in a minor extent as in the case a), due to the major ratio H_2S/CH_4 (0.9), where less CH_4 molecules interfere in H_2S oxidation.

If the H_2S/CH_4 ratio is augmented, case d), using the same λ_{H2S} as in the case a) $\lambda_{H2S}\sim 6$, we can evaluate if a comparatively lower concentration of methane will decrease the inhibition process. As it is shown, the H_2S oxidation finishes at lower temperatures in comparison with the results shown in the case a), where a higher concentration of CH_4 was used, hence, competing with H_2S for the consumption of radicals. However, we cannot assure if the delay in the ignition temperature of H_2S, in comparison with neat H_2S oxidation, is due to the consumption of radicals of the radical pool by CH_4, or due to the formation of some carbon-sulfur intermediate species, not detected in the micro-GC analysis. It is worth to mention that, except in the case of oxidizing conditions (case c), in each of the other cases, a weak minimum in CH_4 concentration during the oxidation of H_2S can be observed at low temperatures. This could indicate some interaction somehow during the conversion of the mixtures, which might be responsible for the shift to high temperatures of H_2S oxidation in the presence of CH_4.

The experimental trends are fairly well captured by the mechanism, except for the observed delay in H_2S oxidation. The final mechanism barely changes the simulations respect to the ones published in Paper IV, which is a good indication and shows that the posterior changes at high pressures do not alter the simulations near atmospheric pressure. The consumption of H_2S follows the same reaction pathways as shown in section 5.1 (H_2S oxidation at atmospheric pressure). The oxidation of methane in the H_2S/CH_4 mixture occurs at lower temperatures compared to the oxidation of neat methane, due to the radicals coming from H_2S oxidation. Regarding neat CH_4, it did not show any reactivity in the simulation run under these conditions. Methane reacts with OH radicals to form CH_3 (R5.37), which, depending on the temperature, will form different products.

$$CH_4 + OH \rightleftharpoons CH_3 + H_2O \qquad \text{(R5.37)}$$

At low temperatures (850 K), CH_3 forms mainly CH_3O (R5.38) and C_2H_6 (R5.39), while at higher temperatures the reaction with O_2 to form CH_2O is predominant (R5.40). CH_3 also reacts with HO_2 to regenerate CH_4 via (R5.41), being less important as the temperature increases.

$$CH_3 + HO_2 \rightleftharpoons CH_3O + OH \qquad \text{(R5.38)}$$

$$CH_3 + CH_3\ (+M) \rightleftharpoons C_2H_6\ (+M) \qquad \text{(R5.39)}$$

$$CH_3 + O_2 \rightleftharpoons CH_2O + OH \qquad \text{(R5.40)}$$

$$CH_3 + HO_2 \rightleftharpoons CH_4 + O_2 \qquad \text{(R5.41)}$$

The oxidation continues with CH_3O species decomposing to CH_2O+H (5.42) and proceeding to CO via (R5.43) and (R5.44). The pathway leading to C_2H_6 might continue with its reaction to C_2H_5 (R5.45) and C_2H_4 (R5.46) later on. The oxidation behavior of methane is similar to that presented in the work of Giménez-López et al. (2015) about oxy-fuel oxidation of methane.

$$CH_3O\ (+M) \rightleftharpoons CH_2O + H\ (+M) \qquad \text{(R5.42)}$$

$$CH_2O + OH \rightleftharpoons HCO + H_2O \qquad \text{(R5.43)}$$

$$HCO + O_2 \rightleftharpoons CO + HO_2 \qquad \text{(R5.44)}$$

$$C_2H_6 + OH \rightleftharpoons C_2H_5 + H_2O \qquad \text{(R5.45)}$$

$$C_2H_5 + O_2 \rightleftharpoons C_2H_4 + HO_2 \qquad \text{(R5.46)}$$

With the purpose of improving the model predictions, regarding the delay in H_2S oxidation by CH_4, reaction (R5.47) was updated with the value for its kinetic constant recommended by Zeng et al. (2016), who revised this reaction using the CBS-QB3 level of theory, mentioning that it was overestimated before at lower temperatures.

$$CH_3 + H_2S \rightleftharpoons CH_4 + SH \qquad \text{(R5.47)}$$

This change managed to improve model predictions for the CH_4 oxidation under all conditions studied in the system $H_2S/CH_4/O_2$. However, the improvements are not enough and a gap between experimental data and model predictions is still observed, approximately of 75 K at stoichiometric conditions. Also, new reactions (R5.48) and (R5.49) from the work of Zeng et al. (2016) were added, but they are not important under the experimental conditions considered.

$$CH_4 + S_2 \rightleftharpoons CH_3 + HS_2 \qquad \text{(R5.48)}$$

$$CH_4 + SO \rightleftharpoons CH_3 + HSO \qquad \text{(R5.49)}$$

For the experiments of H_2S/CH_4 mixtures oxidation at high pressures (10, 20 and 40 bar), the concentrations of H_2S, SO_2, CH_4 and CO, as a function of temperature, using stoichiometric conditions ($\lambda_{total}\sim1$ and $\lambda_{H2S}\sim2.5$) are shown in Figure 5.23. The results obtained for the oxidation of neat H_2S ($\lambda_{total}\sim2$) are also shown for comparison. In the case of 20 and 40 bar, the oxidation of neat CH_4 ($\lambda_{total}\sim1.6$) is also included, since these are the only cases in which neat methane was found to be reactive, in the temperature range studied.

The conversions of both CH_4 and H_2S are shifted to lower temperatures as the pressure increases. In the case of 10 bar, the oxidation of H_2S is almost the same with and without CH_4, while at 20 and 40 bar the oxidation of H_2S is slightly promoted to lower temperatures. The oxidation trend of CH_4 is fairly well captured by the model, both in the case of the neat CH_4 and co-oxidation. The biggest differences between modeling results and experimental data are found in H_2S conversion at 40 bar, which are the same differences for neat H_2S oxidation as in the presence of CH_4. Thus, this gap could be attributed to the present description of the H_2S chemistry at high pressure (Paper III).

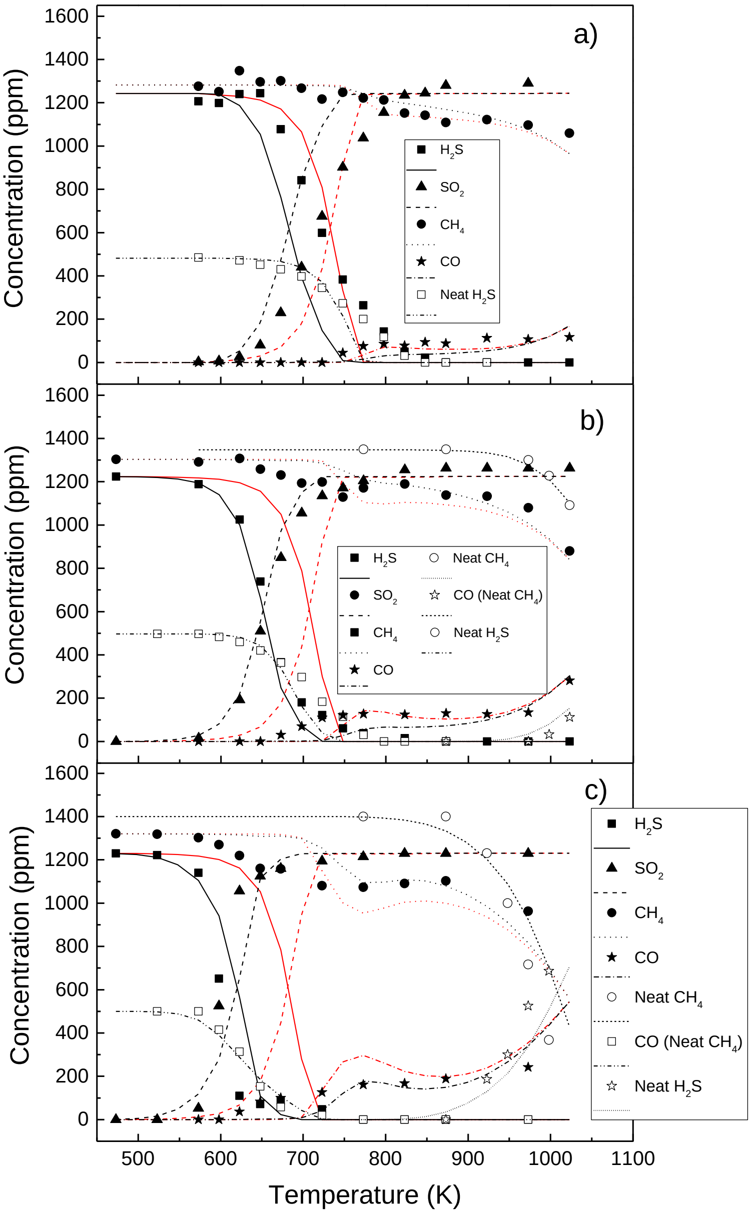

Figure 5.23 Concentrations of H_2S, SO_2, CH_4 and CO vs. temperature at the experimental conditions in Table 5.4, under 10, 20 and 40 bar at set-up 2. Experiments are shown as follows: a) sets 39 (λ_{total}=1.0) and 26 (λ_{total}=2.1), 10 bar; b) sets 40 (λ_{total}=1.0), 43 (λ_{total}=1.6) and 29 (λ_{total}=2.0), 20 bar; c) sets 41 (λ_{total}=1.0), 44 (λ_{total}=1.6) and 32 (λ_{total}=2.1), 40 bar. The original model (Paper IV) is represented with red lines, while the final version of the mechanism is represented with black lines.

According to the model calculations, H_2S conversion starts via (R5.50), as was also mentioned by Gersen et al. (2017). In the same way, Zhou et al. (2013) mentioned the high sensitivity to (R5.50) in their mechanism due to its role to determine the ignition temperature of H_2S.

$$H_2S + O_2 \rightleftharpoons SH + HO_2 \qquad \text{(R5.50)}$$

As mentioned before, in section 5.3 about H_2S oxidation at high pressure, the consumption of H_2S is mainly maintained through reaction of H_2S with HO_2 radicals, radicals which formation is enhanced at high pressures (Mathieu et al., 2014; Gersen et al., 2017; Song et al., 2017). At the same time, H_2O_2 formation (R5.2), also favored at high pressures, promotes the oxidation of the system $H_2S/CH_4/O_2$ via the branching reaction (R5.10).

$$H_2S + HO_2 \rightleftharpoons SH + H_2O_2 \qquad \text{(R5.2)}$$

$$H_2O_2\ (+M) \rightleftharpoons OH + OH\ (+M) \qquad \text{(R5.10)}$$

As well as near atmospheric pressure, the conversion of CH_4 in the mixture is influenced by H_2S oxidation, being the influence more noticeable as pressure increases, reaching 20% of conversion between 700 and 900 K at 40 bar. H_2S oxidation provides radicals to the radical pool and, at the same time, higher pressures involve a major role of peroxides like CH_3OO and HO_2 in the oxidation process of CH_4. At high pressures, other pathways become important in comparison with the previous ones mentioned near atmospheric pressure. Depending on temperature, the model predicts that CH_4 consumption is dependent on the reactions of CH_3 to form different products. At intermediate temperatures and high pressures, formation of peroxyl radicals may be significant (Hashemi et al., 2016; Marrodán et al., 2018a, 2018b). At low temperatures and high pressures (e.g. 725 K at 40 bar), the formation of the CH_3OO peroxide is the preferred channel (R5.51),

$$CH_3 + O_2 \rightleftharpoons CH_3OO \qquad \text{(R5.51)}$$

which will continue reacting through (R5.52), (R5.53), (R5.42), (R5.43) and (R5.44), and finally decomposing to CO (R5.54).

$$CH_3OO + HO_2 \rightleftharpoons CH_3OOH + O_2 \qquad \text{(R5.52)}$$

$$CH_3OOH\ (+M) \rightleftharpoons CH_3O + OH\ (+M) \qquad \text{(R5.53)}$$

$$HCO + M \rightleftharpoons H + CO + M \qquad \text{(R5.54)}$$

As temperature rises, other pathways become important. At 800 K and 40 bar, CH_3 radicals react with HO_2 radicals to give CH_3O (R5.38), instead of producing only CH_3OO, which also ends up as CH_3O, being the net result of the CH_3OO pathway similar to reaction (R5.38). CH_3O decomposes thermally to CH_2O, as mentioned before via (R5.42), and ends as CO through (R5.43), (R5.44) and (R5.54). From 900 K and above, the branching ratio shifts toward the production of CH_2O (R5.40) from CH_3, which is the main pathway for neat CH_4 oxidation as well. CH_2O can react with HO_2 radicals too (R5.55), as well as with CH_3 to regenerate CH_4 (R5.56), like reaction (R5.57), but mainly CH_2O reacts with OH radicals (R5.43).

$$CH_2O + HO_2 \rightleftharpoons HCO + H_2O_2 \qquad \text{(R5.55)}$$

$$CH_2O + CH_3 \rightleftharpoons HCO + CH_4 \qquad \text{(R5.56)}$$

$$CH_3 + H_2 \rightleftharpoons CH_4 + H \qquad \text{(R5.57)}$$

Regarding reaction (R5.40) ($CH_3 + O_2 \rightleftharpoons CH_2O + OH$), large discrepancies in the modeling results using different kinetic parameters from the literature were found. This reaction has been broadly discussed over the years, as it is important for the combustion of hydrocarbons, since a competition with reaction (R5.58) exists at high temperatures and with (R5.51) at low temperatures at roughly stoichiometric conditions. The more recent kinetic parameters by Srinivasan et al. (2007) were used for reaction (R5.40).

$$CH_3 + O_2 \rightleftharpoons CH_3O + O \qquad \text{(R5.58)}$$

Finally, the results obtained in the experiments of the H_2S/CH_4 co-oxidation in the atmospheric pressure set-up (set-up 1) are shown in Figure 5.24. The trends are similar to the ones found in the high-pressure reactor (set-up 2) under near atmospheric pressure conditions. CH_4 oxidation is shifted to lower temperatures due to the presence of H_2S at all conditions considered. In the case of H_2S oxidation, its conversion is shifted to higher temperatures in the presence of CH_4. The CH_4 conversion onset temperature is different from one reactor to another. If the experiments at stoichiometric conditions are compared, there is a difference of 200 K (900 K at the set-up 2 and 1100 K at the set-up 1). This might be attributed to the difference in gas residence times, as the gas residence time in the high pressure reactor (set-up 2) working near atmospheric pressure doubles the one in the reactor at atmospheric pressure (set-up 1). The kinetic model captures fairly well the oxidation trends. However, it overpredicts the oxidation of H_2S and CH_4 by a small margin, except at reducing conditions, where CH_4 oxidation is not captured at high temperatures. The simulations with the final mechanism do not differ of those from the original mechanism published in Paper IV. This can be considered good, since the changes made in the mechanism after Paper IV were focused on H_2S at high pressures, showing here no influence at atmospheric pressure.

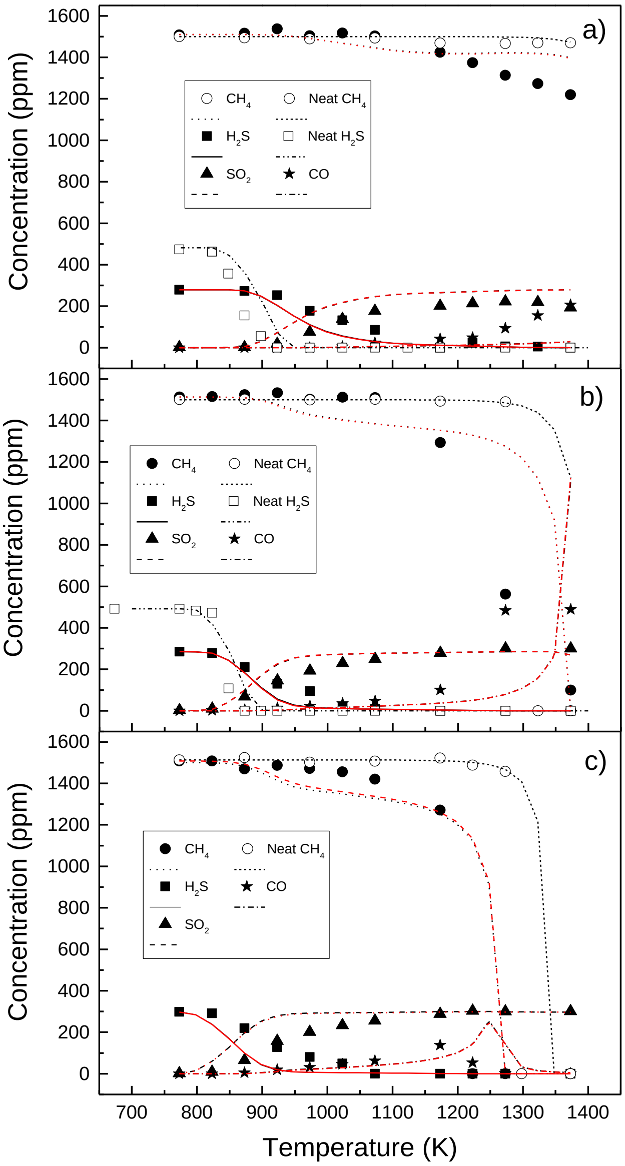

Figure 5.24 Concentrations of H_2S, SO_2, CH_4 and CO vs. temperature at the experimental conditions in Table 5.4, under atmospheric pressure at set-up 1: a) sets 45 (λ_{total}=0.3), 48 (λ_{total}=0.2) and 4 (λ_{total}=2.1); b) 46 (λ_{total}=1.0), 49 (λ_{total}=0.9) and 5 (λ_{total}=5.1); c) 47 (λ_{total}=2.0) and 50 (λ_{total}=1.7). The original model results (Paper IV) are represented with red lines, while those from the final version of the mechanism are represented with black lines.

In addition, some simulations have been run with experimental data from the literature. The results of the experiments by Gersen et al. (2017), in a flow reactor at 50 bar of pressure, are shown in Figures 5.25 and 5.26, together with the simulations running the mechanism from their authors (red lines) and the final mechanism form this thesis (black lines). As can be observed, two different experiments are shown under reducing conditions. First, in Figure 5.25, the ratio H_2S/CH_4 is 1/60 and the air-excess ratio is $\lambda_{total}=0.03$. H_2S concentration is consumed totally under these oxidizing conditions for H_2S ($\lambda_{H2S}=3.7$). The final mechanism improves the previous predictions by the authors and is only shifted 50 K from the experimental data. It is worth to mention that, experimentally, the partial conversion of CH_4 occurs at the same temperatures as H_2S, while the mechanism predicts the conversion of CH_4 when H_2S oxidation finishes, as seen in the experiments of this thesis at stoichiometric conditions. In Figure 5.26, the H_2S/CH_4 ratio is 1/15 and the air-excess ratio is $\lambda_{total}=0.6$. The oxidation of H_2S occurs prior to CH_4 oxidation and is shifted to lower temperatures, in comparison with the previous case in Figure 5.25, due to the higher availability of O_2 ($\lambda_{H2S}=10$). In this case, the conversion of CH_4 is shifted to higher temperatures, which is contradictory to what has been observed at more reducing conditions (Figure 5.25). Under oxidizing conditions, the mechanism is able to reproduce CH_4 oxidation. As mentioned by the authors, CH_4 oxidation is promoted by H_2S in comparison with neat CH_4 oxidation tests, as it has also been said earlier in this section. The final mechanism improves slightly the model predictions from the original paper. Overall, the final mechanism is able to model with certain accuracy the results obtained in different high-pressure flow reactors when H_2S/CH_4 oxidation is studied.

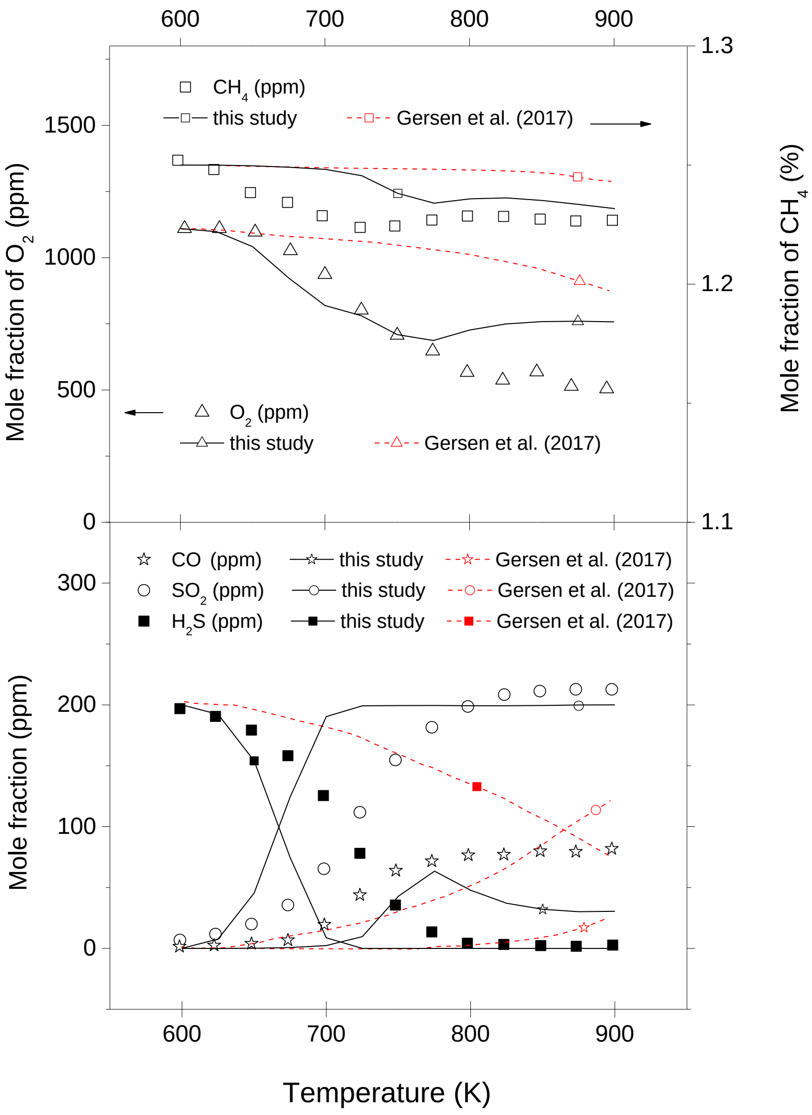

Figure 5.25 Concentrations of H_2S, SO_2, CH_4, CO and O_2 vs. temperature from the experiments of Gersen et al. (2017) of H_2S/CH_4 oxidation in a flow reactor at 50 bar. Initial composition: 1.25% CH_4, 1110 ppm O_2, 200 ppm H_2S, and balance N_2 (λ_{total}=0.03). The mechanism results from the authors (Gersen et al., 2017) are represented with red lines, while those from the final version of the mechanism are represented with black lines.

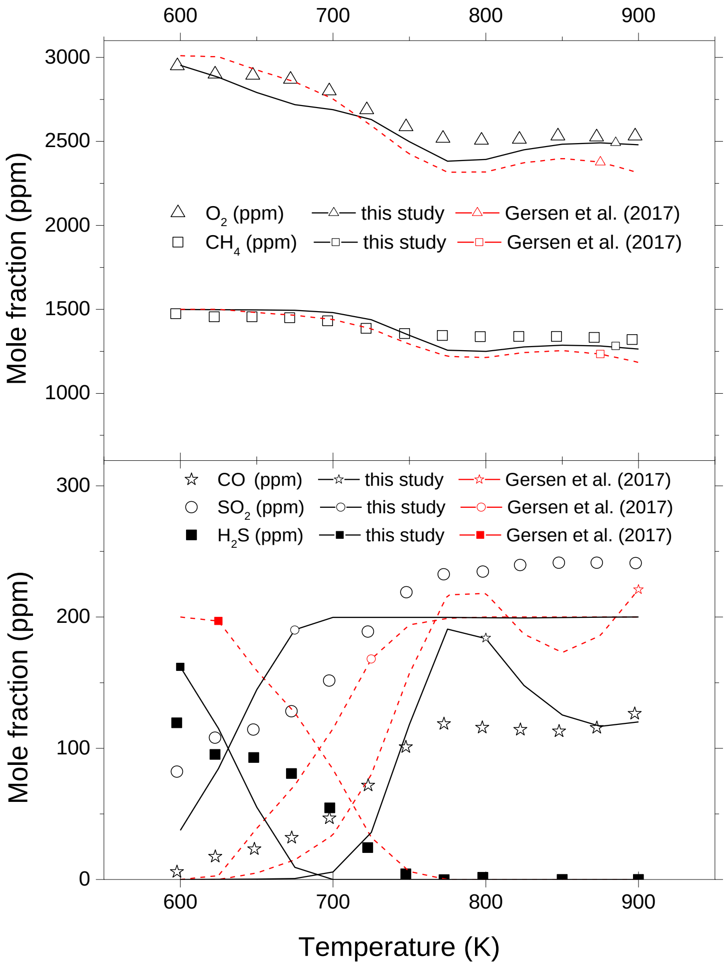

Figure 5.26 Concentrations of H_2S, SO_2, CH_4, CO and O_2 vs. temperature from the experiments of Gersen et al. (2017) of H_2S/CH_4 oxidation in a flow reactor at 50 bar. Initial composition: 1500 ppm CH_4, 3010 ppm O_2, 200 ppm H_2S, and balance N_2 (λ_{total}=0.63). The mechanism results from the authors (Gersen et al., 2017) are represented with red lines, while those from the final version of the mechanism are represented with black lines.

5.5 H_2S/NO MIXTURES OXIDATION

The work about the oxidation of H_2S/NO mixtures was carried out in two different facilities at the University of Zaragoza. The goal was to study first the oxidation behavior at atmospheric pressure (set-up 1, described in section 3.1) and, then, to move on to high pressures (set-up 2, described in section 3.2). Besides pressure, other variables such as temperature (450-1400 K) and air-excess ratio were also considered. All the experimental conditions are collected in Table 5.5. Two repeated experiments are also included, denoted with the letter "R". Additionally, the system NO/O_2 was tested at high pressures, since there were uncertainties in the influence of NO on H_2S oxidation under high pressure (20 bar).

Table 5.5 Experimental conditions for H_2S/NO mixtures oxidation. N_2 as bath gas. The experiments repeated are denoted with the letter "R".

Set	Manometric pressure (bar)	H_2S (ppm)	O_2 (ppm)	NO (ppm)	λ_{H2S}	λ_{NO}	t_r (s)	Set-up	Paper
51	Atmospheric	487	225	500	0.3	0.9	194.6/T	1	VI
51R	Atmospheric	493	225	500	0.3	0.9	194.6/T	1	VI
52	Atmospheric	474	900	500	1.3	3.6	194.6/T	1	VI
52R	Atmospheric	488	900	500	1.2	3.6	194.6/T	1	VI
53	Atmospheric	470	1500	500	2.1	6	194.6/T	1	VI
1	Atmospheric	476	225	-	0.3	-	194.6/T	1	I
3	Atmospheric	485	900	-	1.2	-	194.6/T	1	I
4	Atmospheric	482	1500	-	2.1	-	194.6/T	1	I
54	20	493	1644	489	2.0	6.7	4872/T	2	VI
55	20	484	4542	490	6.0	18.5	4872/T	2	VI
29	20	497	1520	-	2.0	-	4872/T	2	III
30	20	500	4485	-	6.0	-	4872/T	2	V
56	20	-	1500	500	-	6	4872/T	2	VI
57	20	-	4500	500	-	18	4872/T	2	VI
16	20	-	3000	508	-	11.8	4872/T	2	II

The experiments performed at atmospheric pressure using the experimental set-up 1, from reducing (λ_{H2S}=0.3) to oxidizing conditions (λ_{H2S}=2.1), are shown from Figure 5.27 to Figure 5.29 (sets 51-53 in Table 5.5). The concentrations of H_2S, SO_2 and NO concentrations are plotted as a function of temperature (700-1400 K). The results of the oxidation of neat H_2S oxidation are also included in the figures, corresponding to sets 1, 3 and 4 in Table 5.5.

The results show that H_2S oxidation onset occurs similarly for all lambda values (λ_{H2S}=0.3-2.1), in the absence and presence of NO. The NO presence has a little effect shifting H_2S conversion to higher temperatures, a 25 K difference is observed under oxidizing and near stoichiometric conditions. Under reducing conditions, Figure 5.27, H_2S conversion starts at the same temperature, but it is oxidized in a greater extent, above 1200 K, in the presence of NO. The concentration of NO remains unaltered for all experimental conditions at the initial value of 500 ppm. This was also observed in some tests analyzing the NO/O_2 system, where nothing occurred in the same temperature range (700-1400 K). The oxidation of H_2S produces mainly SO_2 and the sulfur balance is maintained within 100 ±5% under oxidizing and near stoichiometric conditions. Under reducing conditions, the sulfur balance goes down to 67% for the highest temperature considered (1375 K), in the presence of NO, and 80% in the case of neat H_2S oxidation (Paper I). As it was also observed in the case of neat H_2S oxidation, in the experiment carried out under reducing conditions (set 51 in Table 5.5, λ_{H2S}=0.3), a yellow deposit was seen at the outlet of the reactor, which can be the explanation for the poor balance closure.

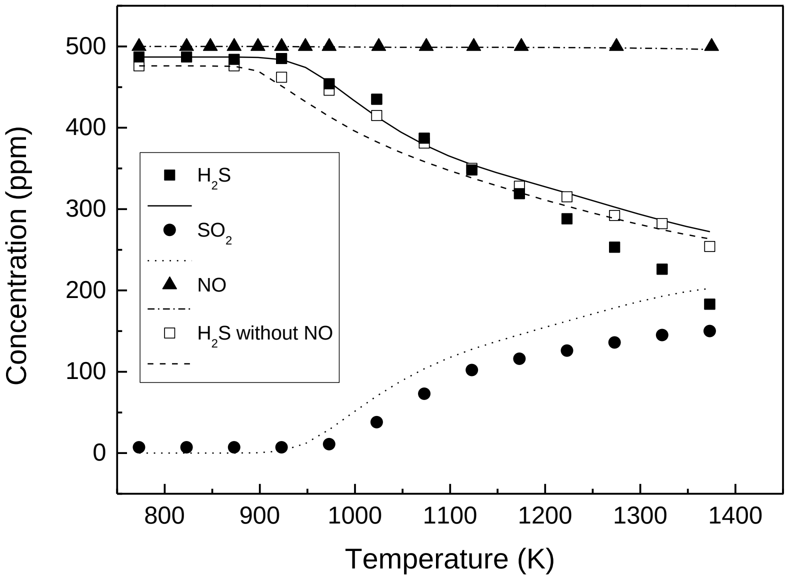

Figure 5.27 Results from H_2S oxidation in conditions of set 51 in Table 5.5 (λ_{H2S}=0.3). Symbols represent experimental data and lines denote final model predictions. The results of H_2S oxidation without NO correspond to set 1 in Table 5.5 (λ_{H2S}=0.3).

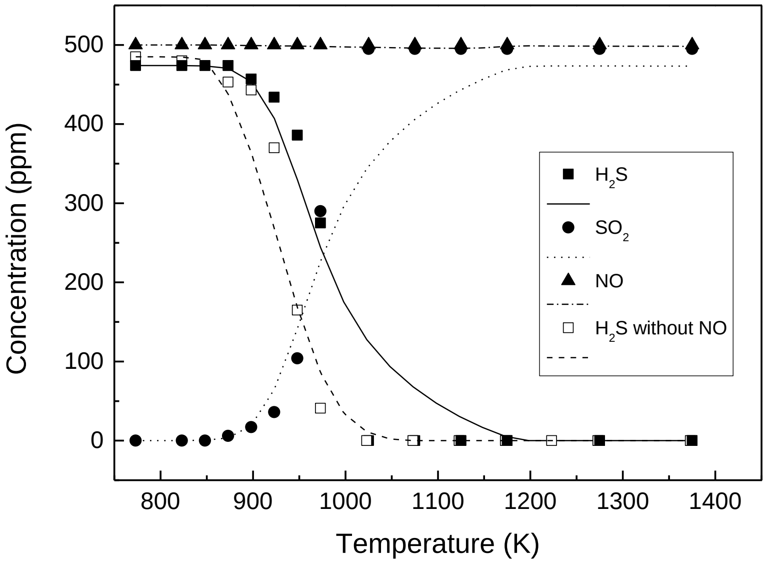

Figure 5.28 Results from H_2S oxidation in conditions of set 52 in Table 5.5 (λ_{H2S}=1.3). Symbols represent experimental data and lines denote final model predictions. The results of H_2S oxidation without NO correspond to set 3 in Table 5.5 (λ_{H2S}=1.2).

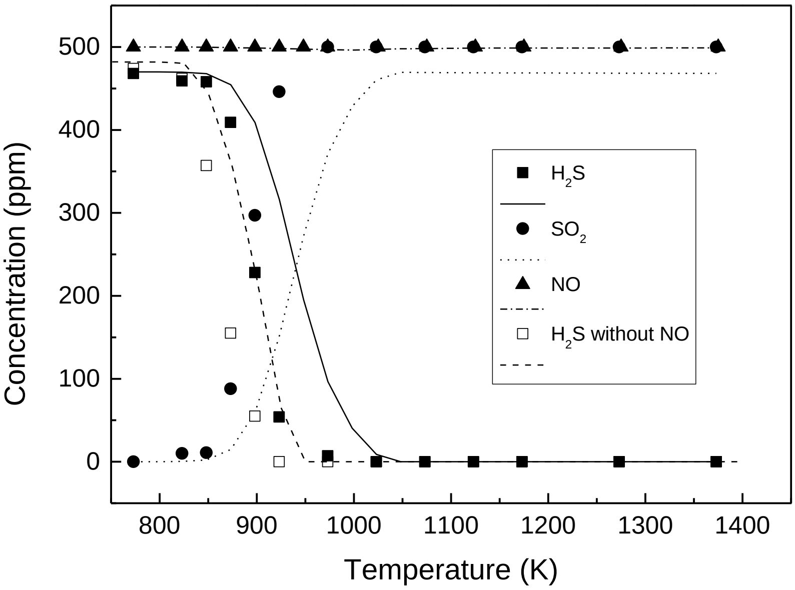

Figure 5.29 Results from H_2S oxidation in conditions of set 53 in Table 5.5 (λ_{H2S}=2.1). Symbols represent experimental data and lines denote final model predictions. The results of H_2S oxidation without NO correspond to set 4 in Table 5.5 (λ_{H2S}=2.1).

The kinetic model developed manages to simulate well the experimental data under all conditions at atmospheric pressure. Despite the constant concentration of NO observed experimentally, according to the calculations, the shift to higher temperatures in H_2S oxidation, when NO is present, is due to reactions involving NO. The following cycle is responsible for NO consumption and recycle to NO:

$$NO + HO_2 \rightleftharpoons NO_2 + OH \qquad (R5.22)$$

$$NO_2 + SH \rightleftharpoons HSO + NO \qquad (R5.59)$$

The following overall reaction (R5.60) would be the result of combining both (5.22) and (5.59):

$$SH + HO_2 \rightleftharpoons HSO + OH \qquad (R5.60)$$

which converts the unreactive HO_2 radicals into more reactive OH radicals. The HSO species would react in reaction (R5.61) to form SO and HSOH.

$$HSO + HSO \rightleftharpoons SO + HSOH \qquad (R5.61)$$

HSOH further reacts with the radical pool, but mainly through (R5.62) to give back H_2S:

$$HSOH + SH \rightleftharpoons H_2S + HSO \qquad (R5.62)$$

In a lesser extent, NO_2 species react with SO to form SO_2 and NO (R5.63), while SO radicals form SO_2 as well in reaction (R5.64).

$$NO_2 + SO \rightleftharpoons SO_2 + NO \qquad (R5.63)$$

$$SO + O_2 \rightleftharpoons SO_2 + O \qquad (R5.64)$$

Summing up, the presence of NO in H_2S oxidation at atmospheric pressure shifts the process to higher temperatures, by both competing for HO_2 radicals under oxidizing and near stoichiometric conditions. The conversion of HO_2 to more active radicals, like OH, enhances the process via (R5.22), as it is seen in other works using CO or CH_4 in the presence of NO (Glarborg et al., 1995; Roesler et al., 1995; Song et al., 2019). Under reducing conditions, where HO_2 radicals are not so important and other important species such as H_2S_2, HS_2 and S_2 might be formed, the simulations remain equal as for the neat H_2S oxidation. The model is not capable of predicting the major H_2S consumption at high temperatures when NO is present (1375 K), probably due to possible interactions between NO and disulfur species (e.g. H_2S_2, HS_2, S_2; more important at reducing conditions) that are not present in the model.

It is worth to mention that, under reducing conditions, a yellow deposit was seen at the outlet of the reaction zone, due to the condensation of the elemental sulfur formed, as also previously observed during the neat H_2S oxidation (Paper I). Hence, for the posterior experiments at high pressure (set-up 2), only oxidizing conditions were used for the experiments, to avoid the possible formation of sulfur in the experimental set-up, in case of using reducing conditions. However, during the experiments at high pressure, the sulfur balance did not close at 100% in any case, probably due to the formation of sulfur, as will be discussed later.

The results for the experiments of H_2S oxidation at 20 bar in the presence of NO are shown in Figures 5.30 and 5.31, for λ_{H2S}=2 and λ_{H2S}=6, respectively (sets 54 and 55 in Table 5.5) in the 475-1000 K temperature range. The results for neat H_2S oxidation are also plotted in the figures and are taken from previous works by the authors in the same experimental set-up, for λ_{H2S}=2.0 (Paper III) and for λ_{H2S}=6.0 (Paper V) (sets 29 and 30 in Table 5.5). In each figure, the results are plotted by duplicate in two separate graphs per figure. This has been done in order to show with clarity the results of two different kinetic models respect to the same experimental results. The graph at the left shows the poor performance of the kinetic model available at the beginning of this work, which is not able to simulate the unexpected conversion of the system $H_2S/NO/O_2$ at high pressure. The graph at the right shows an attempt to simulate such behavior, by proposing reaction (R5.74). This will be further discussed.

$$H_2S + NO_2 \rightleftharpoons S + NO + H_2O \qquad \text{(R5.65)}$$

Regarding the experimental results in the presence of NO, significant H_2S conversion is obtained over the entire temperature range studied. For example, at the lowest temperature considered (475 K), the conversion of H_2S reaches, at least, 50% for λ_{H2S}=2 and 90% for λ_{H2S}=6. At the same time, all the H_2S reacted is not quantified as SO_2. For λ_{H2S}=2, the sulfur balance is maintained around 86±5%, while for λ_{H2S}=6 the sulfur balance observed is maintained around 67±10%. These characteristics are not observed in the absence of NO (Paper III and Paper V). A possible explanation would be that NO and/or NO_2 are reacting with H_2S prior to the reactor inlet or at lower temperatures than 475 K in the reaction zone. The complete oxidation of H_2S at λ_{H2S}=2 is shifted to higher temperatures respect to neat H_2S oxidation (by 50 K).

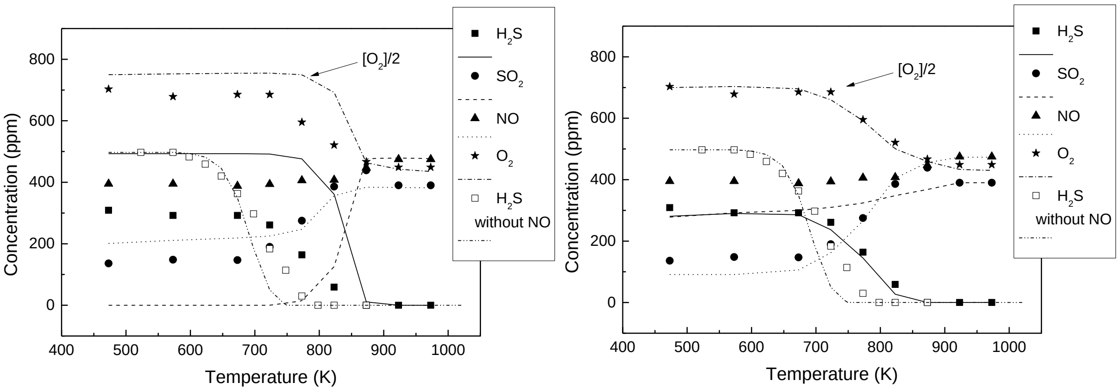

Figure 5.30 Results from H_2S oxidation in conditions of set 54 in Table 5.5 (λ_{H2S}=2.0). The results of H_2S oxidation without NO (λ_{H2S}=2.0) correspond to set 29 in Table 5.5. Symbols represent experimental data and lines model predictions. The model results of the mechanism detailed in section 4.4 (H_2S/NO oxidation) are shown at the left, and at the right the simulations results include reaction (R5.65) (H_2S+NO_2= $S+NO+H_2O$).

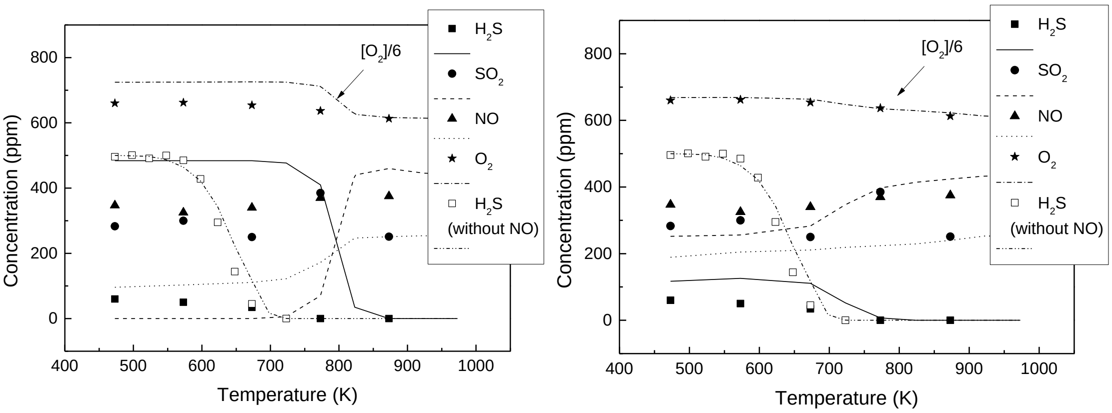

Figure 5.31 Results from H_2S oxidation in conditions of set 55 in Table 5.5 (λ_{H2S}=6.0). The results of H_2S oxidation without NO (λ_{H2S}=6.0) correspond to set 30 in Table 5.5. Symbols represent experimental data and lines model predictions. The model results of the mechanism detailed in section 4.4 (H_2S/NO oxidation) are shown at the left, and at the right the simulations results include reaction (R5.65) (H_2S+NO_2= $S+NO+H_2O$).

Additionally, in order to further evaluate the influence of NO in relation to the H_2S conversion at oxidizing conditions, experiments of neat NO oxidation under similar conditions (20 bar and same O_2 concentration; sets 54-57 in Table 5.5) were carried out. The evolution of NO concentration, with and without H_2S, versus temperature is plotted in Figure 5.32. Two different stoichiometries have been used (λ_{NO}=6 and 18). Two different graphs are shown in the figure in order to differentiate the kinetic mechanisms with and without reaction (R5.65). Results of neat NO oxidation with a different stoichiometry (λ_{NO}=11.8) (Paper II) have also been plotted in order to compare results (set 16 in Table 5.5). The experimental results for λ_{NO}=11.8 (Paper II) are placed between the ones done for λ_{NO}=6 and 18 (Paper VI), following a trend according to the lambda value. When the $H_2S/NO/O_2$ system is analyzed, the NO concentration at the exit is much higher than just in NO oxidation. The kinetic model is capable of reproducing accurately the experimental results of NO oxidation as in Paper II, but is far from reproducing the experimental data of the $H_2S/NO/O_2$ system.

The major conversion of NO in the absence of H_2S, higher when O_2 concentration increases, implies a major concentration of NO_2 molecules (Paper II). This is mainly due to reaction (R5.16, $NO+NO+O_2 \rightleftharpoons NO_2+NO_2$), which enhances the formation of NO_2 at high pressures and low temperatures. Since the concentration of NO is so high when H_2S is present, differing from the study of neat NO oxidation (Figure 5.32), this could mean that the NO_2 formed under high pressure conditions, prior to entering the reactor, is reacting with H_2S to form some elemental sulfur and NO (R5.65).

This behavior between H_2S and NO_2 has previously been reported in the literature. However, the studies are more qualitative than quantitative (Pierce, 1929; Cadle and Ledford, 1966; Hales et al., 1974; Frost and Thomas, 1975; Blackwood, 1980; Kim, 2003; Russel, 2009). The research carried out in the past between these species has been mainly focused on its implication for atmospheric chemistry. The measurements indicated that some mechanisms other than ozonation must be responsible for the atmospheric breakdown of reduced sulfur compounds in the atmosphere (Hales et al., 1974). Cadle and Ledford (1966) observed the formation of free sulfur upon exposing mixtures of nitrogen dioxide and hydrogen sulfide to light. However, Hales et al. (1974) indicated that this reaction may proceed to a limited extent even in a totally dark reactor. Blackwood (1980) studied the reaction of NO_2+H_2S in air and reported S and SO_2 as products, however, no mechanism was postulated. Frost and Thomas (1975) also studied this reaction over the 448-528 K temperature range in a Pyrex reaction vessel, saying that, when H_2S was in excess, sulfur was one of the reaction products. Thus, they performed the investigation using $P_{NO2} > 3P_{H2S}$. In the present work, the experiments are performed under H_2S excess, which could explain the formation of sulfur. More recently, Kim (2003) studied the atmospheric corrosion process of silver in environments containing 0.1 ppm H_2S and 1.2 ppm NO_2. He found sulfur formed in the silver, supposedly through (R5.66):

$$H_2S + 2NO_2 \rightleftharpoons S + 2HNO_2 \qquad \text{(R5.66)}$$

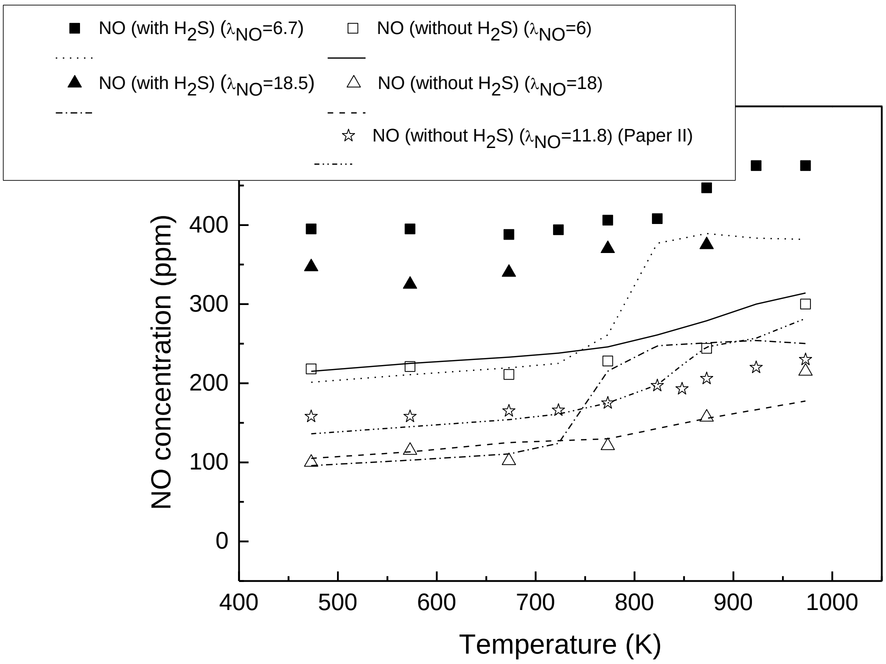

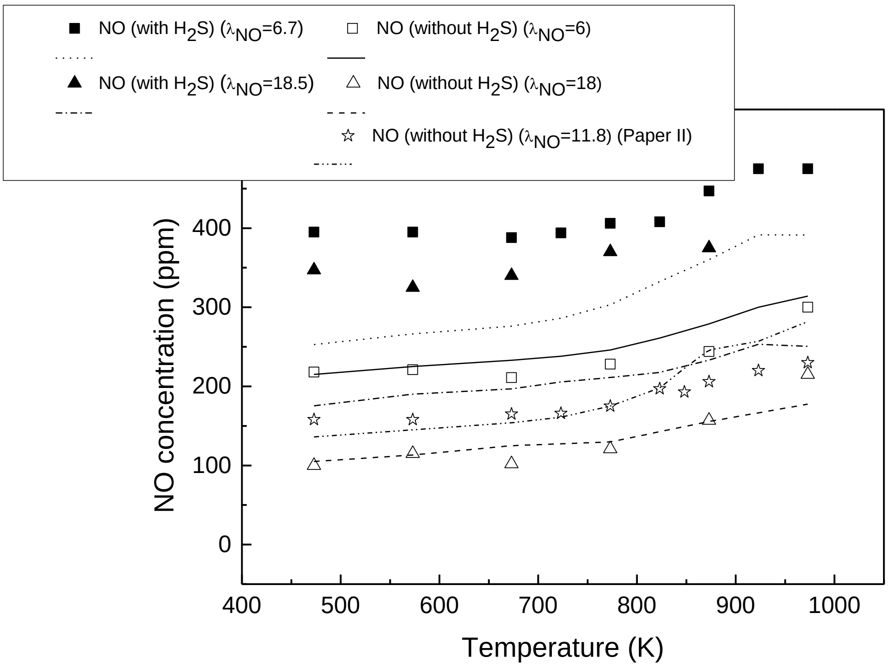

Figure 5.32 Results from NO oxidation in the presence (sets 54 and 55 in Table 5.5) and absence (sets 56 and 57 in Table 5.5) of H_2S at 20 bar. The results for NO oxidation without H_2S at λ_{NO}=11.8 correspond to set 16 in Table 5.5. Symbols represent experimental data and lines denote model predictions. The model results of the mechanism detailed in section 4.4 (H_2S/NO oxidation) are shown in the upper graph, while at the bottom, the simulations include reaction R5.65 (H_2S+NO_2= $S+NO+H_2O$).

It has also been mentioned, in studies dealing with fireworks, how H_2S and NO_2, which come respectively from the sulfur and the KNO_3 present in the black powder used, may react, and are supposed to produce and consume sulfur as follows (Russel, 2009) (R5.65 and R5.67):

$$H_2S + NO_2 \rightleftharpoons S + NO + H_2O \qquad \text{(R5.65)}$$

$$2NO_2 + 2S \rightleftharpoons 2SO_2 + N_2 \qquad \text{(R5.67)}$$

For the moment, no detailed kinetic models are available in the literature yet dealing with this issue. An attempt to simulate such behavior has been tried in this thesis by proposing the kinetic parameters of reaction (R5.65), using 10^8 ($cm^3 \cdot mol^{-1} \cdot s^{-1}$) as the kinetic constant value for the temperature range studied (475-1000 K), which provides good results. Reaction (R5.65) shows a high impact on the concentration trends of all the species (H_2S, SO_2, NO and O_2), as shown in the previous figures. According to the calculations, the reaction (R5.65) is important at room temperature, in the experimental set-up zones prior and posterior to the reactor. Reaction (R5.65) predicts the formation of sulfur, which is further oxidized to SO_2 via (R5.68), i.e.:

$$S + O_2 \rightleftharpoons SO + O \qquad \text{(R5.68)}$$

Observing the simulations, H_2S is totally consumed at lower temperatures in the case of the most oxidizing conditions studied, as observed in the experiments. This can be explained due to the major formation of NO_2 at oxidizing conditions, which reacts with H_2S (R5.65). In the case of λ_{H2S}=2, the oxidation of H_2S is also well predicted by the model. The model predictions of SO_2, NO and O_2 concentrations are close to the experimental data, although some differences are still noticeable. For example, NO_2 is supposed to react with H_2S to give back NO, but the amount of NO formed in the simulations is still low by 20%, in comparison with the experimental data. The important interaction between H_2S and NO_x at high pressure, presumably dominated by the NO_2 presence, has been pointed out both in the experiments and the simulations of the present work. A better characterization of this reaction (R.65) and other possible reactions involved in such interaction is desirable.

5.6 H_2S AND CH_3SH OXIDATION IN A JET-STIRRED REACTOR

The study about H_2S and CH_3SH oxidation in a jet-stirred reactor was performed during the research stay at Murdoch University (Perth, Australia), in Professor Bogdan Dlugogorski's group. The experimental set-up used is described in section 3.3 (atmospheric pressure jet-stirred reactor (JSR) set-up 3). The results from this work were published in Paper VII. In this section, the main results, together with a detailed explanation of them, are summarized. The experiments carried out are shown in Table 5.6, where they are separated in H_2S oxidation and CH_3SH oxidation experiments, both under stoichiometric conditions and oxidizing conditions, in the 600-1100 K temperature range. Repeatability of some experiments is also included in Table 5.6.

Table 5.6 Experimental conditions for H_2S and CH_3SH oxidation in the JSR at atmospheric pressure. Residence time of 1 second. N_2 as bath gas. The experiments repeated are denoted with the letter "R".

Set	H_2S (ppm)	CH_3SH (ppm)	λ
58	1975	-	1.1
58R	1996	-	1.0
59	1953	-	2.1
$59R_1$	1960	-	2.0
$59R_2$	1953	-	2.1
60	1885	-	5.0
61	-	1898	1.0
61R	-	1887	1.0
62	-	1782	3.6
$62R_1$	-	1774	3.6
$62R_2$	-	1757	3.6

The results of the experiments of H_2S oxidation at the jet-stirred reactor are shown in Figure 5.33. The H_2S and SO_2 concentrations are plotted, for three air excess ratios of $\lambda \sim 1$, 2 and 5, in the temperature range of 600-1100 K and for 1 s gas residence time. The lines denote the predictions from the model and points are referred to the experimental measurements. As observed, H_2S is fully converted to SO_2 for all stoichiometries, with the sulfur balance maintained within the range of 100 ± 5 %. The onset of H_2S oxidation occurs at 725 K in the case of $\lambda \sim 1$, which is shifted to lower temperatures as O_2 concentration increases, i.e. 675 K for $\lambda=5$. The kinetic model results match well the experimental data, as the final version of the mechanism shows a good behavior even at atmospheric pressure, as also seen in sections 5.1, 5.3 and 5.4, where the oxidation of H_2S in the atmospheric pressure tubular flow reactor facility (set-up 1) is shown, as well as the results at near atmospheric pressure (0.65 bar) in a high-pressure tubular flow reactor set-up (set-up 2). The reaction pathways remain the same as in section 5.1, about H_2S oxidation at atmospheric pressure. As mentioned earlier, the changes proposed in the mechanism to improve model predictions at high pressures have no influence on the results at atmospheric pressure. This satisfactory agreement between measurements and the kinetic model results, arising both for the tubular-flow reactor (modeled as PFR) and JSR (modeled as CSTR), indicates the reliability of the mechanism to simulate the oxidation of H_2S at atmospheric pressure in different reaction systems.

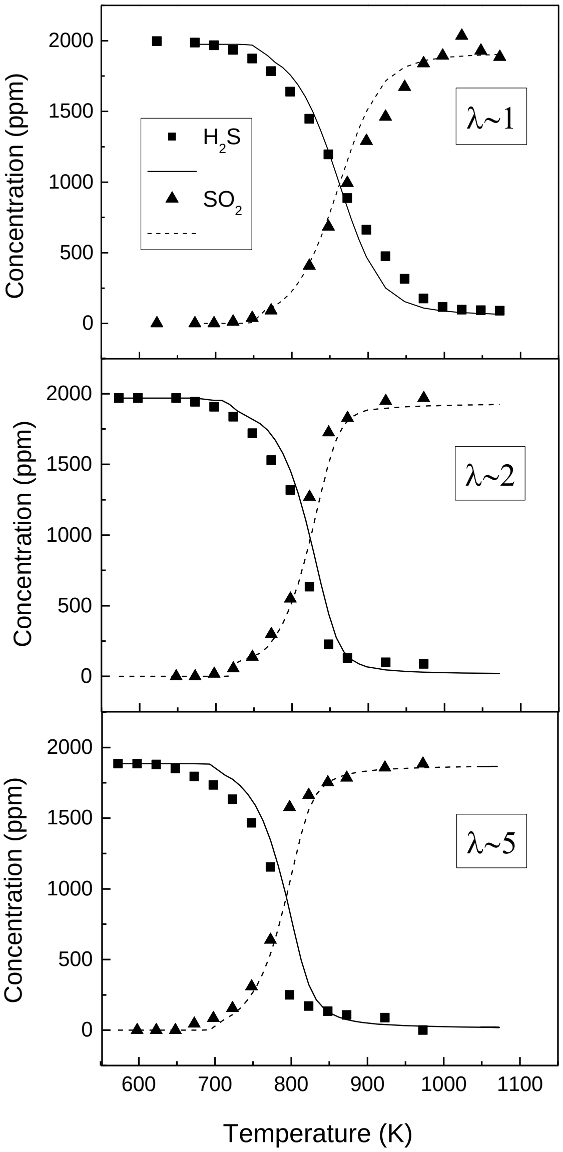

Figure 5.33 Concentration of H_2S and SO_2 as function of temperature for the experimental conditions of sets 58, 59 and 60 in Table 5.6. Symbols represent experimental concentrations, while lines denote final model predictions.

It is worth to mention that the surface/volume ratio of the tubular-flow reactor, from the experimental set-up in section 3.1 exceeds that of the JSR by a factor of 4.5. Thus, despite the difference in the surface/volume ratio, the model reproduces accurately the experimental results for both reactors. This seems to indicate a negligible catalytic effect of the quartz surface on the oxidation of H_2S.

The conversion of CH_3SH for the stoichiometries of $\lambda\sim1$ and 3.6, is plotted in Figures 5.34 and 5.35 respectively, showing the conversion of CH_3SH and the formation of reaction products as CO, CO_2, CH_4, H_2S and SO_2, as a function of temperature. In comparison to the stoichiometric oxidation, at fuel-lean conditions (λ=3.6), the onset of the reaction and the appearance of the oxidation products is found at lower temperatures. The sulfur contained in CH_3SH molecules is fully converted to SO_2 at high temperatures, while a maximum in the concentration of H_2S arises at intermediate temperatures in both air excess ratios. In the case of carbon species, under stoichiometric conditions (Figure 5.34), there is no formation of CO_2, with the main carbon species corresponding to those of CO and CH_4. Under fuel-lean conditions, as illustrated in Figure 5.35, CH_4 and CO start to disappear at high temperatures, forming CO_2, due to the complete combustion. The model predictions, plotted as lines, represent the mechanisms of Alzueta et al. (2019) (dashed lines) and the present work (solid lines); being the latter updated with reactions listed in Table 4.1. The updated mechanism exhibits minor improvements in CH_3SH conversion, in comparison with the one by Alzueta et al., while the prediction in the distribution of the reaction products is better now. In the present study, these improvements are related to the formation of sulfine (CH_2SO) through the intersystem crossing process described in the section 4.3 (Modeling. Reaction mechanism); through reaction (R5.69). Sulfine decomposes mainly to CO and H_2S (R5.70), and partly to COS and H_2 (R5.71).

$$CH_3SH + O_2 \rightleftharpoons CH_2SO + H_2O \qquad (R5.69)$$

$$CH_2SO \rightleftharpoons CO + H_2S \qquad (R5.70)$$

$$CH_2SO \rightleftharpoons COS + H_2 \qquad (R5.71)$$

There is no information in the literature regarding rate constants for the reactions of CH_2SO consumption. Therefore, in the present work, these rate constants are proposed based on an analogy with the decomposition of singlet formaldehyde oxide (CH_2OO). The work by Maricq et al. (1994) has served as a reference for such analogy. In their study on the reaction of chlorine atoms with methylperoxy and ethylperoxy radicals, they proposed that the decomposition of CH_2OO proceeds via three channels, with 61 ± 7 % of the reactant converted to CO and H_2O (which would be in accordance with the presently suggested CO + H_2S pathway), and the other two channels forming CO_2 + H_2 and CO_2 + 2H. Based on Maricq's et al. (1994) reactions for the decomposition of the Criegee intermediate, as an analogy to the unimolecular decomposition of CH_2SO, the kinetic parameters for reactions (R4.14, R4.16-R4.18) listed in Table 4.1 have been proposed, assuming a value of 10^{11} (s^{-1}) for the pre-exponential factor.

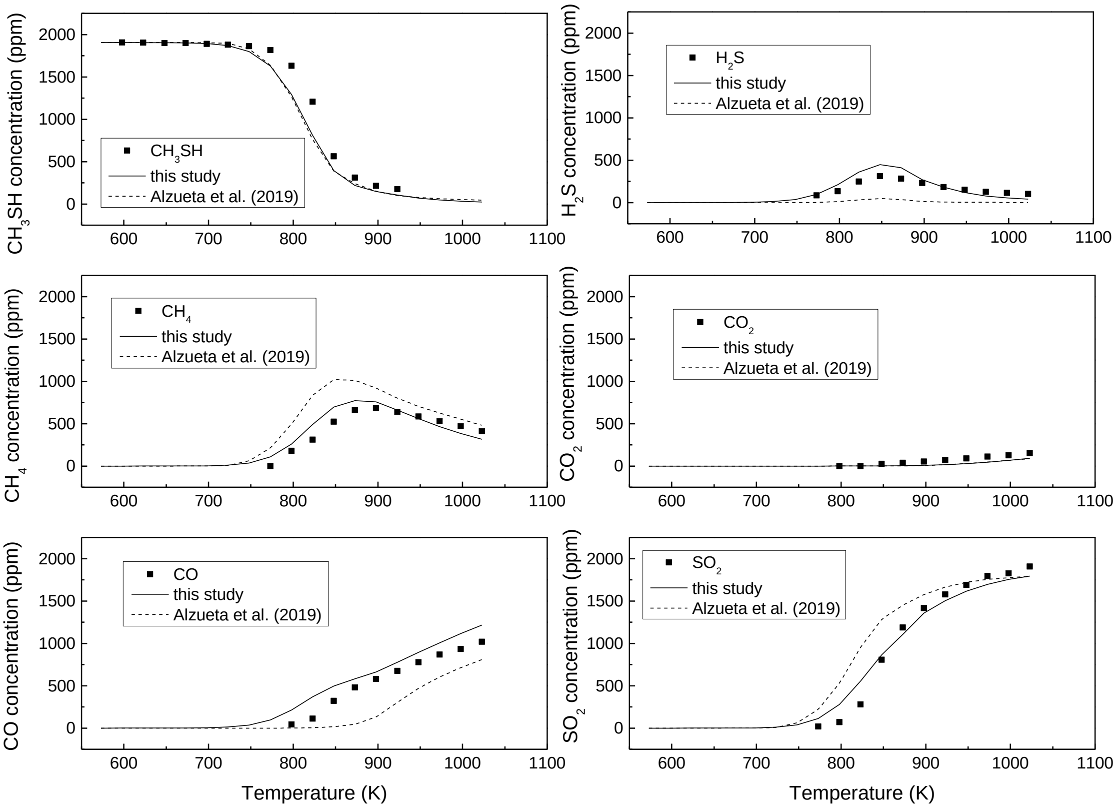

Figure 5.34 Concentrations of CH_3SH, CH_4, CO, H_2S, CO_2 and SO_2 vs. temperature for the experimental conditions of set 61 in Table 5.6 (λ=1.0). Symbols represent experimental concentrations, while lines denote final model predictions (continuous lines) and predictions using the model by Alzueta et al. (2019) (dashed lines).

Another possible product from CH_3SH oxidation is the methylthiol radical (CH_3S), illustrated in reaction (R5.72), where CH_3SH reacts with CH_3 to produce CH_4 in addition to CH_3S. The methylthiol radical reacts with O_2 to form SO_2 and CH_3 (R5.73), which results in the overall reaction of $CH_3SH + O_2 \rightleftharpoons SO_2 + CH_4$.

$$CH_3SH + CH_3 \rightleftharpoons CH_3S + CH_4 \qquad (R5.72)$$

$$CH_3S + O_2 \rightleftharpoons SO_2 + CH_3 \qquad (R5.73)$$

This radical (CH_3S) has been recognized previously as the most important intermediate in the oxidation of CH_3SH, together with CH_2SH (Alzueta et al., 2019). According to the calculations, CH_2SH is less abundant than CH_2SO or CH_3S.

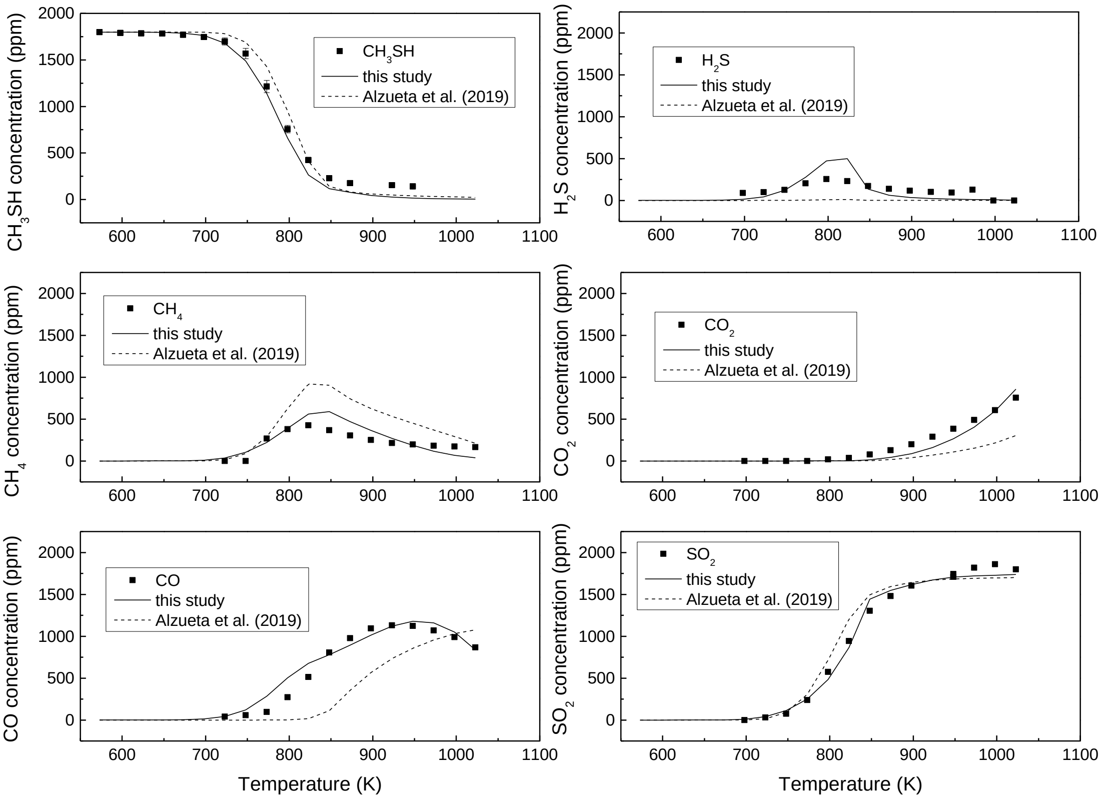

Figure 5.35 Concentrations of CH_3SH, CH_4, CO, H_2S, CO_2 and SO_2 vs. temperature at the experimental conditions of set 62 in Table 5.6 ($\lambda=3.6$). Symbols represent experimental concentrations, while lines denote final model predictions (continuous lines) and predictions using the model by Alzueta et al. (2019) (dashed lines).

The consumption pathway of neat H_2S in the jet-stirred reactor remains equal to that observed in the tubular-flow reactor (Paper I). Additionally, the same important reactions were found in the sensitivity analysis of neat H_2S oxidation from this work and the one in Paper I. However, the oxidation pathway of CH_3SH has changed from the one showed in the previous study about this topic (Alzueta et al., 2019), due to the formation of CH_2SO proposed. In the case of CH_3SH oxidation, where H_2S is found as a reaction product, the oxidation behavior that H_2S follows is different from the one observed of neat H_2S oxidation. SH radicals, instead of going through HSOO to the final product SO_2 (Paper I), continue the reaction pathway by reacting with CH_3SH to yield CH_3S and H_2S (R5.74), instead of producing HSOO. This is the reason of the H_2S

peak observed in Figures 5.34 and 5.35, together with the occurrence of reaction (R5.70), according to model calculations.

$$CH_3SH + SH \rightleftharpoons CH_3S + H_2S \qquad (R5.74)$$

Additionally, selected experiments (λ~1 and λ~5) from the previous work of Alzueta et al. (2019) on the oxidation of CH_3SH in a tubular-flow reactor have been simulated. Figures 5.36 and 5.37 compare the model predictions for the oxidation of CH_3SH and formation of the products from the present work (Paper VII) and Alzueta et al. reaction mechanism. The updated mechanism in this work improves the prediction in the formation of the reaction products, such as CO and H_2S, due mainly to the inclusion of the new reactions, while the mechanism underpredicts the generation of CH_4.

Some repeatability experiments from Table 5.6 can be seen in Figure 5.38. It can be concluded that the oxidation of neat H_2S and CH_3SH oxidation present a good repeatability in the jet-stirred reactor.

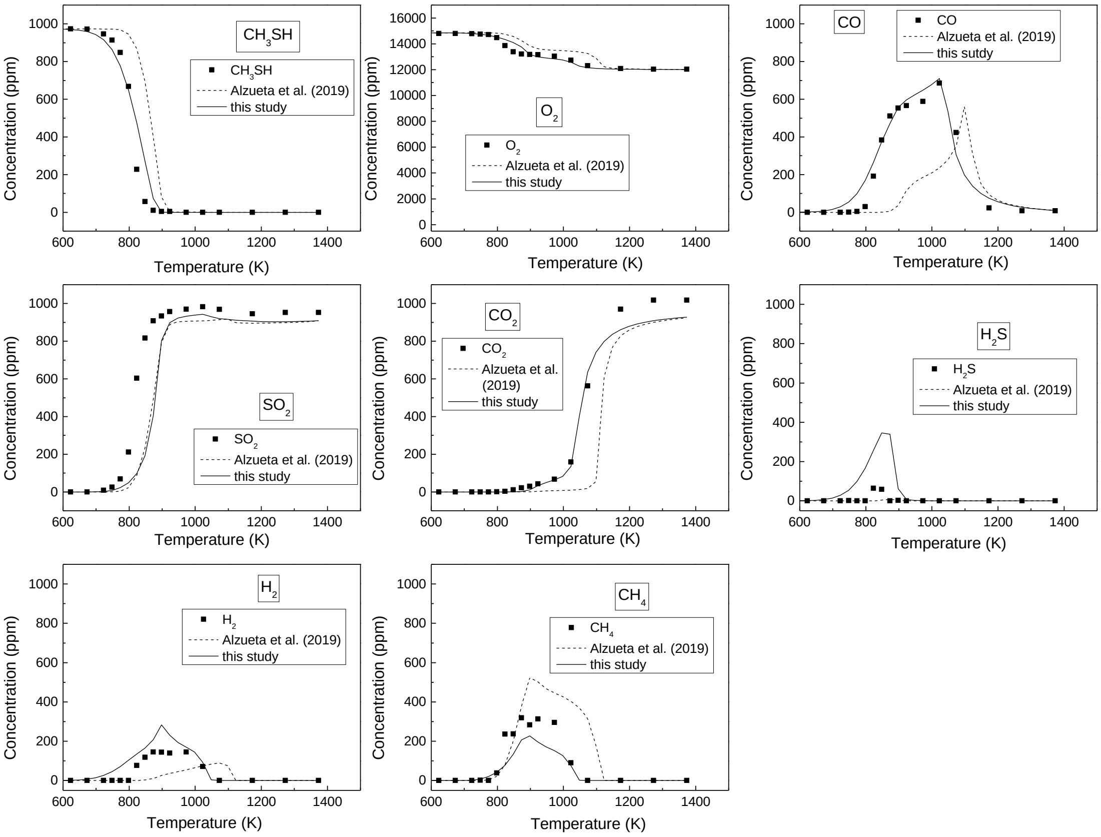

Figure 5.36 Comparison between experimental and modeling results for λ=5.08. Set 7 in Table 1 of the work by Alzueta et al. (2019). Symbols represent experimental concentrations, while lines denote final

model predictions (continuous lines) and predictions using the model by Alzueta et al. (2019) (dashed lines).

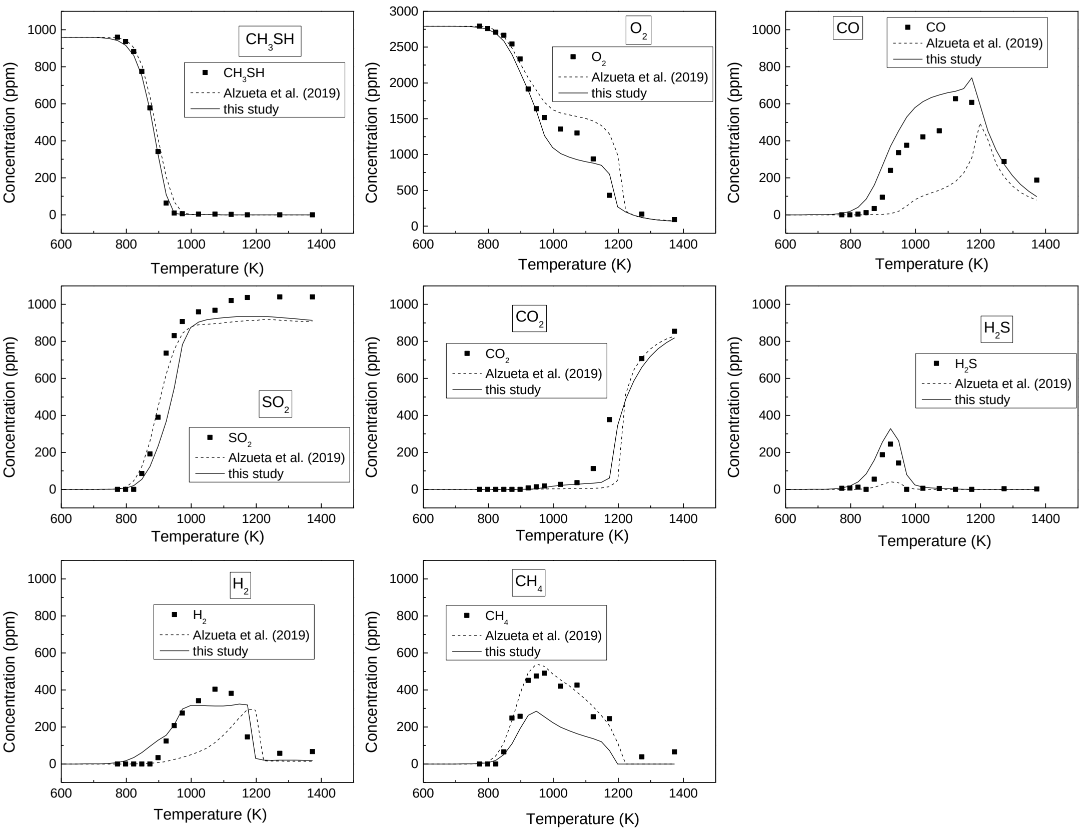

Figure 5.37 Comparison between experimental and modeling results for λ = 0.99. Set 4 in Table 1 of the work by Alzueta et al. (2019). Symbols represent experimental concentrations, while lines denote final model predictions (continuous lines) and predictions using the model by Alzueta et al. (2019) (dashed lines).

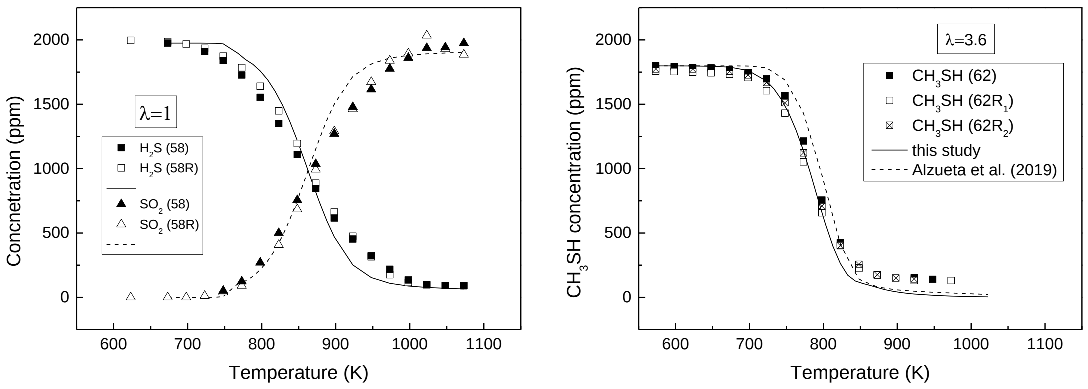

Figure 5.38 Repeatability experiments for neat H_2S oxidation (sets 58 and 58R in Table 5.6) and CH_3SH oxidation (sets 62, $62R_1$ and $62R_2$ in Table 5.6) in the jet-stirred reactor at the Murdoch University.

5.7 REACTION PATHWAYS

Finally, in order to summarize the oxidation behavior of H_2S under different conditions, a schematic diagram, showing the reaction pathways from H_2S to the final product SO_2, can be seen in Figure 5.39. The major and minor reaction pathways taking place in the H_2S oxidation process, together with important reactions occurring under reducing conditions, as well as the NO presence on H_2S oxidation under high pressure (right diagram), are presented.

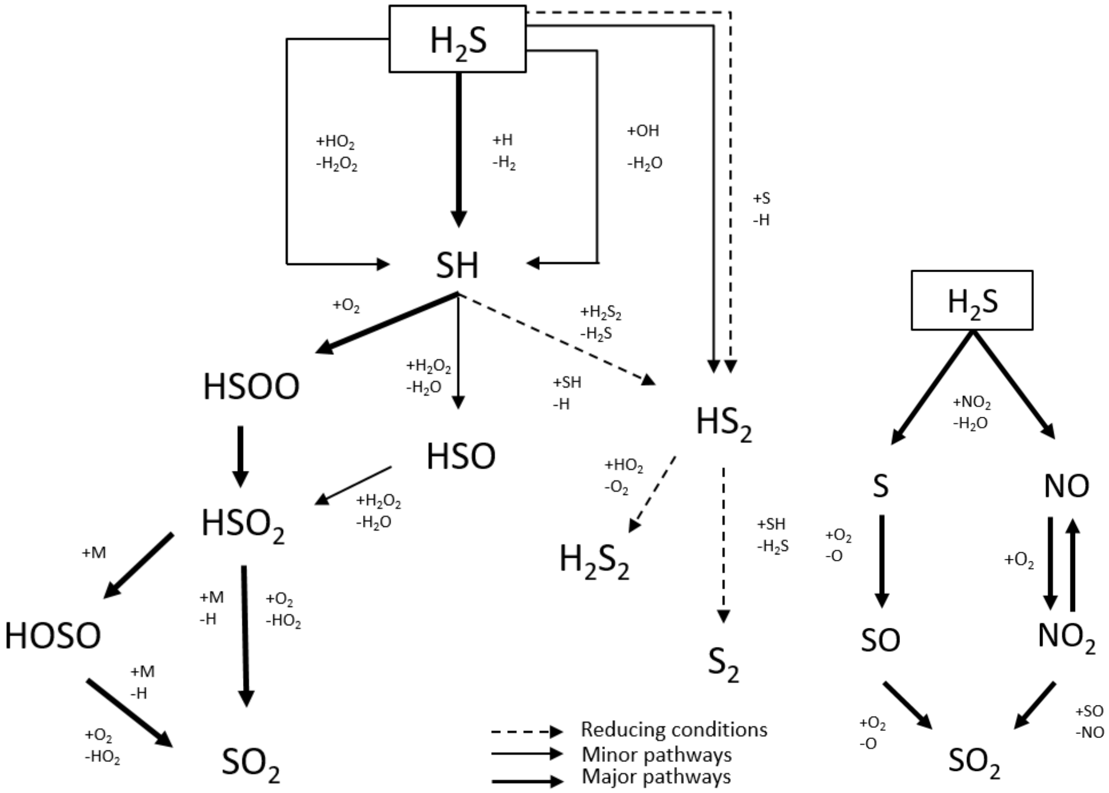
H₂S
+HO₂
-H₂O₂
+H
-H₂
+OH
-H₂O
+S
-H
SH
+O₂
+H₂S₂
-H₂S
+H₂O₂
-H₂O
+SH
-H
HSOO
HSO
HS₂
+HO₂
-O₂
HSO₂
+H₂O₂
-H₂O
+SH
-H₂S
H₂S₂
+M
HOSO
+M
-H
+O₂
-HO₂
+M
-H
+O₂
-HO₂
S₂
SO₂
Reducing conditions
Minor pathways
Major pathways
H₂S
+NO₂
-H₂O
S
NO
+O₂
-O
+O₂
SO
NO₂
+O₂
-O
+SO
-NO
SO₂

Figure 5.39 Reaction pathways for H_2S oxidation.

Chapter 6.

SUMMARY AND CONCLUSIONS

6. SUMMARY AND CONCLUSIONS

The oxidation of H_2S has been studied from both experimental and kinetic modeling points of view. The final goal is related to the application of sour gas combustion, where H_2S is present in significant amounts. Therefore, the study of H_2S oxidation, over a wide range of conditions, is important for the understanding and knowledge of sour gas combustion. This involves the H_2S oxidation study from atmospheric to high pressures, over a wide temperature range (300-1400 K) and under different stoichiometries. The H_2S interaction with other compounds, such as CH_4 (present in sour gas) and NO (a known contaminant) has been also contemplated. Additionally, the influence of the reactor type on H_2S oxidation and another important compound in sour gas (CH_3SH) has also been considered to be studied. The results have allowed to compile and validate a detailed chemical kinetic mechanism that is able to describe the oxidation behavior of H_2S, H_2S/CH_4 and H_2S/NO mixtures and the different species related in this work (e.g. CH_3SH), under different conditions, which might be useful for the practical application of sour gas oxidation.

6.1 H_2S OXIDATION AT ATMOSPHERIC PRESSURE

The oxidation of H_2S at atmospheric pressure has been studied as a first step. Although many combustion and industrial processes are carried out at high pressures, the study at atmospheric pressure is necessary for further understanding the H_2S oxidation process, together with the development of a kinetic modeling that might work under a wide range of conditions. The study has been performed in a quartz tubular flow reactor, in the 700-1400 K temperature range and the concentrations of H_2S, SO_2 and H_2 have been quantified. Different reaction atmospheres have been tested, varying the air excess ratio (λ) from reducing ($\lambda=0.3$) to oxidizing conditions ($\lambda=19.5$).

The H_2S oxidation is shifted to lower temperatures as the concentration of O_2 rises. The main product of the oxidation is SO_2 at all stoichiometries, but under reducing conditions, the sulfur balance does not close near 100% and a yellow deposit was detected during the experiments at the reactor outlet. This has been considered to be related to the formation of elemental sulfur. Apparently, catalytic reactions on wall surfaces are not significant. This has been tested by adding water vapour in H_2S oxidation experiments. In this manner, the radical pool is enlarged and the impact of radical recombination in the reactor walls is minimized. No significant differences have been observed in the H_2S oxidation experiments in the presence and absence of H_2O.

A detailed kinetic mechanism has been developed to predict the conversion of H_2S under such conditions. This mechanism has been used to simulate the experimental results obtained in the present work, together with data from the literature, obtaining a fairly good agreement under the different conditions. The changes in the initial mechanism included the addition of isomerization reaction ($HSOO \rightleftharpoons HSO_2$), supported by recent theoretical works as a key step in a faster reaction path of SH oxidation, and modification of the ($H_2S+HO_2 \rightleftharpoons SH+H_2O_2$) reaction kinetic parameters, which has a significant impact on the reaction pathways of H_2S oxidation. The most important reactions governing H_2S conversion have been identified. The modifications performed later in the model for high pressure conditions have no influence in the results under atmospheric pressure.

6.2 H_2 OXIDATION AND ITS INTERACTION WITH NO

As a preliminary step towards the study of H_2S oxidation at high pressures, the research about H_2 oxidation at high pressures and its interaction with NO has been carried out. The systems $H_2/NO/O_2$, H_2/O_2 and NO/O_2 have been analyzed in a tubular quartz flow reactor. Different variables have been studied, such as various manometric pressures (10, 20 and 40 bar), temperatures (450-1100 K) and air excess ratios (λ_{H2}=0.5-6.4). The results obtained have been useful to update the kinetic model with important reaction subsets (e.g. H_2/O_2) and to analyze the behavior of NO under high pressures.

The results have shown that the oxidation of H_2 is promoted by NO under oxidizing conditions, since NO reacts with the HO_2 radicals, important reaction at high pressure, to form the more active OH radical, enhancing the conversion of hydrogen. The onset for H_2 oxidation, when NO is present, for all stoichiometries at high pressures (40 bar), is shifted to higher temperatures as pressure decreases. The results have been successfully simulated using an updated mechanism from recent works and some of the kinetic parameters from specific reactions have been modified. One of them, reaction ($NO+NO+O_2 \rightleftharpoons NO_2+NO_2$), which is important under high pressures and low temperatures, has been modified according to the uncertainty of its activation energy. Another one is the ($HNO+H_2 \rightleftharpoons NH+H_2O$) reaction, which rate constant has been proposed as $7 \cdot 10^8$ ($cm^3 \cdot mol^{-1} \cdot s^{-1}$) to help reproduce the oxidation of H_2 under reducing conditions. The simulations have been run using the temperature profiles of the entire experimental set-up, due to the conversion of NO to NO_2 in the presence of O_2 at low temperatures and high pressures.

The kinetic model developed is able to predict the results about H_2 oxidation and its interaction with NO under a wide range of conditions, except for the case of 40 bar under oxidizing conditions, where a 20% drop of the NO_x balance has been found and can not be predicted by the model, presumably by some interaction between NO_2/H_2 or the possible formation of nitric acid. This issue would need a more detailed study.

6.3 H_2S OXIDATION AT HIGH PRESSURE

The study about H_2S oxidation at high pressures has been performed in a high-pressure facility with a quartz tubular flow reactor. The influence of pressure on H_2S oxidation has been analyzed at different manometric pressures (0.65, 10, 20 and 40 bar), under different stoichiometric ratios ($\lambda \sim 1$-6) and in the 450-1000 K temperature range. The kinetic model, which has been first developed at atmospheric pressure and updated with the H_2/O_2 subset for high pressures, has been tested using the above mentioned conditions and against experiments from the literature and from the present work.

The onset of H_2S oxidation is shifted to lower temperatures as the pressure and oxygen concentration rise. The influence of gas residence time has been found to be stronger than pressure under the conditions studied. The kinetic model has been able to predict H_2S oxidation under almost all the experimental conditions, specially near atmospheric pressure (0.65 bar). However, in the experiments at 40 bar, a gap of approximately 50 K between experimental concentrations and model predictions has been observed. The sensitivity analysis performed at 40 bar indicates that the H_2S conversion is mainly sensitive to the ($HSOO \rightleftharpoons HSO_2$) isomerization reaction, and to some branching reactions involving H_2S_2 and H_2O_2 species. Hence, the kinetic model has been updated with two new reactions involving H_2O_2 species ($SH+H_2O_2 \rightleftharpoons HSO+H_2O$ and $HSO+H_2O_2 \rightleftharpoons HSO_2+H_2O$), and has been successfully used to reproduce the experimental data from the present work and data from the literature. Their rate constants have been estimated as 10^{12} ($cm^3 \cdot mol^{-1} \cdot s^{-1}$), in the temperature range studied (450-1100 K). The reaction pathways of H_2S oxidation at high pressures are found to be similar to the ones at atmospheric pressure. The main differences are related to the relevance of H_2O_2 species and HO_2 radicals at higher pressures, which act to increase the H_2S oxidation reactivity. The simulations at atmospheric pressure remain essentially unaltered with the updated mechanism.

6.4 H_2S/CH_4 MIXTURES OXIDATION

In order to study the oxidation of H_2S under conditions more similar to sour gas oxidation, the work about H_2S/CH_4 mixtures oxidation has been carried out. The experiments have been performed in two different tubular flow reactor set-ups, at different pressures, in the temperature range of 450-1400 K and using different H_2S/CH_4 ratios and stoichiometries.

The concentrations of H_2S, SO_2, CH_4 and CO, as a function of temperature, have been quantified. The results have shown that, as the pressure increases, the conversion of both CH_4 and H_2S in the oxidation of H_2S/CH_4 mixtures is shifted to lower temperatures. H_2S oxidation has been found to occur prior to CH_4 oxidation at all conditions, which provides radicals to the system promoting CH_4 oxidation to lower temperatures (compared to neat CH_4 oxidation). The H_2S oxidation is inhibited by CH_4 at atmospheric pressure, being more noticeable when the H_2S/CH_4 ratio is lower. At high pressures, the conversion of H_2S occurs similarly in the absence and presence of CH_4. The carbon and sulfur balances remain near 100% at all temperatures and no C-S species were found in the gas chromatograph analysis (e.g. CS_2 or CH_3SH), even under reducing conditions.

In the work about H_2S/CH_4 oxidation mixtures, the mechanism has been updated with important subsets of reactions (CH_3SH and CH_3OO), and has managed to predict the experimental trends fairly well at all conditions. Later on, the final mechanism has been able to improve the simulations at high pressures of the published mechanism, while the simulations remain unaltered at atmospheric pressure, as it has been previously observed in the neat oxidation of H_2S as well. The influence of CH_4 on H_2S is more important as pressure rises, where CH_4 reaches a maximum conversion of 20% at 40 bar. At high pressures, peroxide species, like CH_3OO and HO_2, become important in the oxidation process of CH_4. The model predicts that CH_4 consumption is dependent on the reactions of CH_3 to form different products. The reaction ($CH_3+O_2 \rightleftharpoons CH_2O+OH$) kinetic parameters have been updated obtaining a better theoretical prediction of the experimental results.

6.5 H_2S/NO MIXTURES OXIDATION

The study about H_2S oxidation in the presence of NO, a well-known contaminant, has been carried out in two different facilities, under atmospheric pressure and high pressure conditions. Different air excess ratios and temperatures have been analyzed. First, the results obtained in the experimental set-up at atmospheric pressure, operating from 700 to 1400 K, have shown a slight shift of H_2S oxidation to higher temperatures (25 K) respect to neat H_2S when NO is present, for oxidizing (λ_{H2S}=2.1) and near stoichiometric conditions (λ_{H2S}=1.2). The kinetic model has been updated with S/N reactions that are capable of reproducing well the experimental data. Under reducing conditions (λ_{H2S}=0.3), the $H_2S/NO/O_2$ system presents a major reactivity above 1200 K, which can not be predicted by the model. The concentration of NO does not change in all the temperature range for all the stoichiometries, although an interconversion cycle between NO/NO_2 consuming HO_2 radicals is responsible for the oxidation shift, which is found both in the experimental data and model predictions.

The work about the oxidation of H_2S and its interaction with NO at high pressure has been performed only at 20 bar, for oxidizing conditions (λ_{H2S}=2 and λ_{H2S}=6), operating from 475 to 1000 K. The results have shown that, at the lowest temperature considered (475 K), it exists at least 50% of H_2S conversion for λ_{H2S}=2 and 90% for λ_{H2S}=6. The sulfur balance closes at 86±5% for λ_{H2S} =2, while for λ_{H2S}=6 the sulfur balance is maintained around 67±10%. In order to further study the influence of NO, neat oxidation experiments of NO have been performed using similar O_2 concentrations to those used in the H_2S oxidation in the presence of NO. The conversion of NO to NO_2 is favored at high pressures and low temperatures, and is higher as O_2 concentration increases. This is one of the reasons why two different oxidizing conditions were tested, in order to check how the formation of NO_2 could affect the H_2S oxidation. A reaction between NO_2 and H_2S is thought to be the responsible for the early conversion of H_2S and the decay in the sulfur balance. An attempt to simulate such behavior has been done by proposing reaction ($H_2S+NO_2 \rightleftharpoons S+NO+H_2O$), which forms sulfur and has allowed to reproduce well the experimental data at high pressure, while having no effect at atmospheric pressure. The kinetic constant has been estimated as 10^8 ($cm^3 \cdot mol^{-1} \cdot s^{-1}$).

6.6 H_2S AND CH_3SH OXIDATION IN A JET-STIRRED REACTOR

A different type of reactor has been chosen to perform the oxidation of H_2S (a jet-stirred reactor at atmospheric pressure), for comparison with the results obtained at atmospheric pressure in a quartz tubular flow reactor. The oxidation of another typical compound in sour gas has also been studied, the methyl mercaptan (CH_3SH) oxidation. This reactor works as a JSR (that can be modeled as a CSTR) and presents a surface/volume ratio 4.5 times lower than in the case of the tubular flow reactor at atmospheric pressure. Hence, the possible reactor surface interaction with H_2S oxidation has been tested again.

The study about H_2S and CH_3SH oxidation in a jet-stirred reactor has been carried out from both experimental and modeling points of view. Different air-excess ratios (λ~1-5) have been used in the temperature range of 600-1100 K, with a fixed residence time in the reactor of 1 second. Different compounds have been detected and quantified, such as O_2, CO_2, CH_4, H_2S, SO_2 and CH_3SH.

The results haven shown that the oxidation of both compounds (neat H_2S and neat CH_3SH) is shifted to lower temperatures as the oxygen concentration increases. The oxidation of H_2S forms SO_2. The sulfur contained in CH_3SH molecules is fully converted to SO_2 at high temperatures, while a maximum in the concentration of H_2S arises at intermediate temperatures of CH_3SH oxidation for both air excess ratios. In the case of carbon species, under the stoichiometric conditions, there is no formation of CO_2, and the main carbon species correspond to those of CO and CH_4. Under fuel-lean conditions, CH_4 and CO start to disappear at high temperatures forming CO_2, due to the major CH_3SH conversion, in comparison to stoichiometric conditions.

The model has been able to reproduce well the experimental trends under all conditions of this study and of investigations available in literature. Calculations indicate that the oxidation of CH_3SH involves the formation of the CH_2SO species that decompose mainly to CO and H_2S, improving the predictions with respect to the mechanisms described in the literature. The updated mechanism has shown minor improvements in CH_3SH conversion, while the prediction in the distribution of the reaction products is better now. In the present study, these improvements are related to the formation of sulfine (CH_2SO).

The reaction pathways of H_2S remain equal to the ones that have been shown earlier in the study performed in the tubular flow reactor at atmospheric pressure. This satisfactory agreement between measurements and the kinetic model results, both for the experiments in the tubular flow reactor and JSR, indicates the reliability of the mechanism to simulate the oxidation of H_2S at atmospheric pressure in different reaction systems.

6.7 GENERAL CONCLUSION

The results have shown that H_2S oxidation is shifted to lower temperatures as pressure increases. The residence time has an important influence on H_2S oxidation under the conditions studied. The results of experiments at atmospheric pressure show no significant differences in the presence and absence of water vapor. The possible catalytic reactions promoted by the quartz reactor walls at atmospheric pressure have been considered negligible. H_2S oxidation promotes the oxidation of CH_4 to lower temperatures under all the conditions studied. At the same time, CH_4 delays the oxidation of H_2S at atmospheric pressure, while, at higher pressures, the conversion of H_2S is slightly promoted to lower temperatures. The oxidation of H_2S is slightly delayed by NO at atmospheric pressure. At high pressure, NO_2 is thought to react considerably with H_2S at low temperatures forming sulfur. The kinetic mechanism developed is able to describe the oxidation behavior of H_2S, H_2S/CH_4 and H_2S/NO mixtures over a wide range of conditions, as well as to predict H_2S and CH_3SH oxidation in two different types of reactor at atmospheric pressure (JSR and PFR). Peroxide species like HSOO, H_2O_2 and HO_2 have been pointed out in this work to be key in H_2S oxidation.

Capítulo 6.

RESUMEN Y CONCLUSIONES

6. RESUMEN Y CONCLUSIONES

La oxidación de H_2S se ha estudiado tanto desde el punto de vista experimental como de modelado cinético. El objetivo final está relacionado con la aplicación de la combustión de gas ácido, donde el H_2S está presente en cantidades significativas. Por lo tanto, el estudio de la oxidación del H_2S, en un amplio intervalo de condiciones, es importante para la comprensión y el conocimiento de la combustión de gas ácido. Se han realizado estudios de oxidación de H_2S desde presión atmosférica hasta altas presiones (40 bar), en un amplio intervalo de temperaturas (300-1400 K) y bajo diferentes estequiometrías. También se ha contemplado la interacción de H_2S con otros compuestos, como el CH_4 (presente en el gas ácido) y el NO (un conocido contaminante). Además, también se ha considerado estudiar la influencia del tipo de reactor en la oxidación del H_2S y otro compuesto importante en el gas ácido (CH_3SH). Los resultados han permitido compilar y validar un mecanismo cinético químico detallado que es capaz de describir la oxidación de H_2S, mezclas de H_2S/CH_4 y H_2S/NO, así como otras especies relacionadas (CH_3SH), bajo diferentes condiciones, lo que podría ser útil para la aplicación práctica de la oxidación de gas ácido.

6.1 OXIDACIÓN DE H_2S A PRESIÓN ATMOSFÉRICA

La oxidación de H_2S a presión atmosférica se ha estudiado como primera etapa de este trabajo. Aunque muchos procesos de combustión e industriales se llevan a cabo a altas presiones, el estudio a presión atmosférica es necesario para comprender mejor el proceso de oxidación de H_2S, así como para el desarrollo de un modelo cinético que pueda describir el proceso bajo diferentes condiciones. El estudio se ha realizado en un reactor de flujo tubular de cuarzo, en el intervalo de temperatura de 700-1400 K y se han cuantificado las concentraciones de H_2S, SO_2 e H_2. Se han probado diferentes atmósferas de reacción, variando la relación de exceso de aire (λ) desde condiciones reductoras (λ=0.3) a oxidantes (λ=19.5).

La oxidación de H_2S se desplaza a temperaturas más bajas a medida que aumenta la concentración de O_2. El producto principal de la oxidación es SO_2 para todas las estequiometrías, salvo en condiciones reductoras, donde el balance de azufre no cierra al 100%. En estas condiciones se detectó un depósito amarillo a la salida del reactor durante los experimentos, que se ha considerado que está relacionado con la formación de azufre elemental. Aparentemente, las reacciones catalíticas en la superficie de las paredes del reactor no son significativas. Esto se ha probado añadiendo vapor de agua en experimentos de oxidación de

H_2S. De esta manera, la cantidad de radicales aumenta y se minimiza el impacto de la recombinación de radicales en las paredes del reactor. No se han observado diferencias significativas en los experimentos de oxidación de H_2S en presencia y ausencia de H_2O.

Se ha desarrollado un mecanismo cinético detallado para predecir la conversión de H_2S a presión atmosférica. Este mecanismo se ha utilizado para simular los resultados experimentales obtenidos en el presente trabajo, junto con datos de la bibliografía, obteniendo una concordancia bastante buena bajo las diferentes condiciones. Los cambios en el mecanismo inicial incluyeron la adición de la reacción de isomerización ($HSOO \rightleftharpoons HSO_2$), respaldada por trabajos teóricos recientes, como un paso clave en una ruta de reacción más rápida de oxidación de SH, y la modificación de los parámetros cinéticos de la reacción ($H_2S+HO_2 \rightleftharpoons SH+H_2O_2$), lo que tiene un impacto significativo en las vías de reacción de oxidación de H_2S. Se han identificado las reacciones más importantes que gobiernan la conversión de H_2S. Las modificaciones realizadas posteriormente en el modelo para condiciones de alta presión no influyen en los resultados a presión atmosférica.

6.2 OXIDACIÓN DE H_2 Y SU INTERACCIÓN CON NO

Como paso previo al estudio de la oxidación del H_2S a altas presiones, se ha llevado a cabo la investigación sobre la oxidación del H_2 a altas presiones y su interacción con el NO. Los sistemas $H_2/NO/O_2$, H_2/O_2 y NO/O_2 se han analizado en un reactor de flujo de cuarzo tubular. Se han estudiado diferentes variables, como diferentes presiones manométricas (10, 20 y 40 bar), temperaturas (450-1100 K) y relaciones de exceso de aire (λ_{H2}=0.5-6.4). Los resultados obtenidos han sido útiles para actualizar el modelo cinético con importantes *subsets* de reacciones (por ejemplo, H_2/O_2) y para analizar la oxidación de NO a altas presiones.

Los resultados han demostrado que la oxidación del H_2 es promovida por el NO en condiciones oxidantes, ya que el NO reacciona con los radicales HO_2, reacción importante a alta presión, para formar el radical OH más activo, favoreciendo la conversión de hidrógeno. El inicio de la oxidación de H_2, cuando NO está presente, para todas las estequiometrías y a altas presiones (40 bar), se desplaza a temperaturas más altas a medida que la presión disminuye. Los resultados se han simulado con éxito utilizando un mecanismo que se ha actualizado con resultados de recientes trabajos y en el que se han modificado algunos de los parámetros cinéticos de reacciones específicas. Una de ellas, la reacción ($NO+NO+O_2 \rightleftharpoons NO_2+NO_2$), que es importante a altas presiones y bajas temperaturas, se ha modificado en función de la incertidumbre de su energía de activación. Otra es la reacción ($HNO+H_2\rightleftharpoons NH+H_2O$), cuya constante de velocidad se ha propuesto como $7\cdot10^8$ ($cm^3\cdot mol^{-1}\cdot s^{-1}$) para ayudar a reproducir la oxidación de H_2 en condiciones reductoras. Las simulaciones se han realizado utilizando los perfiles de temperatura considerando todo el sistema experimental, debido a la conversión de NO a NO_2 en presencia de O_2 a bajas temperaturas y altas presiones.

El modelo cinético desarrollado es capaz de predecir los resultados sobre la oxidación del H_2 y su interacción con el NO en un amplio intervalo de condiciones, excepto en el caso de 40 bar en condiciones oxidantes, donde se ha encontrado una caída del 20% del balance de NO_x que no puede ser predicho por el modelo, presumiblemente por alguna interacción entre NO_2/H_2 o la posible formación de ácido nítrico. Este tema necesitaría un estudio más detallado.

6.3 OXIDACION DE H_2S A ALTA PRESIÓN

El estudio sobre la oxidación de H_2S a altas presiones se ha realizado en una instalación de alta presión con un reactor de flujo tubular de cuarzo. La influencia de la presión en la oxidación de H_2S se ha analizado a diferentes presiones manométricas (0.65, 10, 20 y 40 bar), bajo diferentes relaciones estequiométricas ($\lambda\sim$1-6) y en el intervalo de temperatura de 450-1000 K. El modelo cinético, que se desarrolló a presión atmosférica y se actualizó con el subconjunto H_2/O_2 para altas presiones, se ha utilizado tanto para simular los experimentos de esta tesis como experimentos de la bibliografía.

El inicio de la oxidación de H_2S se desplaza a temperaturas más bajas a medida que aumentan la presión y la concentración de oxígeno. Se ha encontrado que la influencia del tiempo de residencia del gas es mayor que la de la presión en las condiciones estudiadas. El modelo cinético ha sido capaz de predecir la oxidación de H_2S bajo casi todas las condiciones experimentales, especialmente a presiones cercanas a la presión atmosférica (0.65 bar). Sin embargo, en los experimentos a 40 bar, se ha observado un desplazamiento de aproximadamente 50 K entre las concentraciones experimentales y las predicciones del modelo. El análisis de sensibilidad realizado a 40 bar indica que la conversión de H_2S es principalmente sensible a la reacción de isomerización ($HSOO\rightleftharpoons HSO_2$) y a algunas reacciones de ramificación que involucran especies como H_2S_2 y H_2O_2. Por lo tanto, el modelo cinético se ha actualizado con dos nuevas reacciones que involucran especies de H_2O_2 ($SH+H_2O_2\rightleftharpoons HSO+H_2O$ y $HSO+H_2O_2\rightleftharpoons HSO_2+H_2O$), y se ha utilizado con éxito para reproducir los datos experimentales del presente trabajo y algunos datos de la bibliografía. Sus constantes de velocidad se han estimado como 10^{12} ($cm^3 \cdot mol^{-1} \cdot s^{-1}$), en el intervalo de temperatura estudiado (450-1100 K). Los caminos de reacción de la oxidación del H_2S a altas presiones son similares a los de presión atmosférica. Las principales diferencias están relacionadas con la relevancia de las especies de H_2O_2 y los radicales HO_2 a presiones más altas, que actúan para aumentar la reactividad del H_2S en su oxidación. Las simulaciones a presión atmosférica permanecen esencialmente inalteradas con el mecanismo actualizado.

6.4 OXIDACIÓN DE MEZCLAS H_2S/CH_4

Con el fin de estudiar la oxidación de H_2S en condiciones más similares a la oxidación de gas ácido, se ha realizado el estudio de la oxidación de mezclas de H_2S/CH_4. Los experimentos se han realizado en dos configuraciones diferentes de reactores de flujo tubular, a diferentes presiones, en el intervalo de temperatura de 450-1400 K y utilizando diferentes relaciones y estequiométricas H_2S/CH_4.

Se han cuantificado las concentraciones de H_2S, SO_2, CH_4 y CO, en función de la temperatura. Los resultados han demostrado que, a medida que aumenta la presión, la conversión de CH_4 y H_2S en la oxidación de mezclas de H_2S/CH_4 se desplaza a temperaturas más bajas. Se ha encontrado que la oxidación de H_2S ocurre antes que la oxidación de CH_4 en todas las condiciones, lo que proporciona radicales al sistema que promueven la oxidación del CH_4 a más bajas temperaturas (en comparación con la oxidación del CH_4 puro). La oxidación de H_2S es inhibida por el CH_4 a presión atmosférica, siendo este hecho más notorio cuando la relación H_2S/CH_4 es menor. A altas presiones, la conversión de H_2S ocurre de manera similar en ausencia y presencia de CH_4. Los balances de carbono y azufre permanecen cerca del 100% a todas las temperaturas y no se han encontrado especies C-S en el análisis cromatográfico realizado (por ejemplo, CS_2 o CH_3SH), incluso en condiciones reductoras.

En el estudio sobre la oxidación de mezclas H_2S/CH_4, se ha actualizado el mecanismo con importantes *subsets* de reacciones (CH_3SH y CH_3OO), lo que ha permitido predecir bastante bien las tendencias experimentales en todas las condiciones. Posteriormente, el mecanismo final ha sido capaz de mejorar las simulaciones a altas presiones, mientras que las simulaciones permanecen inalteradas a presión atmosférica, como se ha observado previamente también en la oxidación del H_2S puro. La influencia de la presencia de CH_4 en la oxidación de H_2S es más importante a altas presiones, donde el CH_4 alcanza una conversión máxima del 20% a 40 bar. A altas presiones, las especies de peróxido, como CH_3OO y HO_2, adquieren mayor importancia en el proceso de oxidación de CH_4. El modelo predice que el consumo de CH_4 depende de las reacciones de CH_3 para formar diferentes productos. Por tanto, se han actualizado los parámetros cinéticos de la reacción ($CH_3+O_2 \rightleftharpoons CH_2O+OH$) obteniendo una mejor predicción teórica de los resultados experimentales.

6.5 OXIDACION DE MEZCLAS H_2S/NO

El estudio de la oxidación de H_2S en presencia de NO, un conocido contaminante, se ha realizado en dos instalaciones diferentes, en condiciones de presión atmosférica y alta presión. Se han analizado diferentes relaciones de exceso de aire y temperaturas. Los resultados obtenidos en la configuración experimental a presión atmosférica, operando de 700 a 1400 K, han mostrado un ligero desfase (25 K) a las temperaturas más altas en la oxidación de H_2S cuando NO está presente con respecto a la oxidación de H_2S puro, para condiciones oxidantes (λ_{H2S}=2.1) y condiciones casi estequiométricas (λ_{H2S}=1.2). El modelo cinético se ha actualizado con reacciones que involucran especies S/N que son capaces de reproducir bien los datos experimentales. En condiciones reductoras (λ_{H2S}=0.3), el sistema $H_2S/NO/O_2$ presenta una reactividad mayor por encima de 1200 K, con respecto al sistema H_2S/O_2, que no puede predecirse con el modelo. La concentración inicial de NO no cambia en todo el intervalo de temperatura para todas las relaciones de exceso de aire, aunque el ciclo de interconversión NO/NO_2, que consume radicales HO_2, es responsable del desplazamiento de la oxidación de H_2S a altas temperaturas.

El trabajo sobre la oxidación de H_2S y su interacción con NO a alta presión se ha realizado solo a 20 bar, para condiciones oxidantes (λ_{H2S}=2 y λ_{H2S}=6), operando de 475 a 1000 K. Los resultados han demostrado que, a la temperatura más baja considerada (475 K), existe al menos 50% de conversión de H_2S para λ_{H2S}=2 y 90% para λ_{H2S}=6. El balance de azufre se cierra en 86±5% para λ_{H2S}=2, mientras que para λ_{H2S}=6 el balance de azufre se mantiene alrededor de 67±10%. Para estudiar más a fondo la influencia de NO, se han realizado experimentos puros de oxidación de NO puro utilizando concentraciones de O_2 similares a las utilizadas en la oxidación de H_2S en presencia de NO. La conversión de NO a NO_2 se favorece a altas presiones y bajas temperaturas, y es mayor a medida que aumenta la concentración de O_2. Esta es una de las razones por las que se probaron dos condiciones oxidantes diferentes, con el fin de comprobar cómo la formación de NO_2 podría afectar a la oxidación de H_2S. Se cree que una reacción entre NO_2 y H_2S es la responsable de la conversión a bajas temperaturas de H_2S y la caída del balance de azufre. Se ha intentado simular dicho comportamiento proponiendo la reacción ($H_2S+NO_2 \rightleftharpoons S+NO+H_2O$), que forma azufre, y que ha permitido reproducir bien los datos experimentales a alta presión, sin tener efecto a presión atmosférica. La constante cinética se ha estimado en 10^8 ($cm^3 \cdot mol^{-1} \cdot s^{-1}$).

6.6 OXIDACION DE H_2S Y CH_3SH EN UN REACTOR *JET-STIRRED*

Se ha elegido un tipo diferente de reactor para realizar la oxidación de H_2S (un reactor *jet-stirred* a presión atmosférica), para comparar los resultados con los obtenidos a presión atmosférica en un reactor de flujo tubular de cuarzo. También se ha estudiado la oxidación de otro compuesto presente en el gas ácido, el metilmercaptano (CH_3SH). Este reactor funciona como un JSR (que puede modelarse como un CSTR) y presenta una relación superficie/volumen 4.5 veces menor que en el caso del reactor de flujo tubular a presión atmosférica. Por tanto, se ha probado de nuevo la posible influencia de la superficie del reactor en la oxidación del H_2S.

El estudio de la oxidación de H_2S y CH_3SH en un reactor *jet-stirred* se ha realizado tanto desde el punto de vista experimental como de modelado cinético. Se han utilizado diferentes relaciones de exceso de aire ($\lambda \sim 1$-5), en el intervalo de temperatura de 600-1100 K, con un tiempo de residencia fijo en el reactor de 1 segundo. Se han detectado y cuantificado diferentes compuestos, como O_2, CO_2, CH_4, H_2S, SO_2 y CH_3SH.

Los resultados han demostrado que la oxidación de ambos compuestos (H_2S y CH_3SH), se desplaza a temperaturas más bajas a medida que aumenta la concentración de oxígeno. La oxidación de H_2S forma SO_2. El azufre contenido en las moléculas de CH_3SH se convierte completamente en SO_2 a altas temperaturas, apareciendo un máximo en la concentración de H_2S a temperaturas intermedias para relaciones de exceso de aire ($\lambda \sim 1$ y 3.6). En el caso de las especies de carbono, en condiciones estequiométricas, no hay formación de CO_2, y las principales especies de carbono corresponden a CO y CH_4. En condiciones oxidantes, el CH_4 y el CO comienzan a desaparecer a altas temperaturas formando CO_2, debido a la mayor conversión de CH_3SH, en comparación con condiciones estequiométricas.

El modelo ha sido capaz de reproducir bien las tendencias experimentales en todas las condiciones de este estudio y de diferentes investigaciones disponibles en la bibliografía. Los cálculos indican que la oxidación de CH_3SH implica la formación de especies CH_2SO, que se descomponen principalmente en CO y H_2S, mejorando las predicciones con respecto a los mecanismos descritos en la bibliografía. El mecanismo actualizado ha mostrado pequeñas mejoras menores en la conversión de CH_3SH, mientras que mejora de forma significativa la predicción de la distribución de los productos de reacción. En el presente estudio, estas mejoras se han relacionado con la formación de sulfina (CH_2SO).

Los caminos de reacción de la oxidación de H_2S permanecen igual a los que se han mostrado anteriormente en el estudio realizado en el reactor de flujo tubular a presión atmosférica. Esta satisfactoria concordancia entre los datos experimentales y los resultados del modelo cinético, tanto para los experimentos en el reactor de flujo tubular como en JSR, indica la fiabilidad del mecanismo para simular la oxidación de H_2S a presión atmosférica en diferentes sistemas de reacción.

6.7 CONCLUSIÓN GENERAL

Los resultados han demostrado que la oxidación de H_2S se desplaza a temperaturas más bajas a medida que aumenta la presión. El tiempo de residencia tiene una influencia importante en la oxidación de H_2S. Los resultados de los experimentos a presión atmosférica no muestran diferencias significativas en la presencia y ausencia de vapor de agua. Las posibles reacciones catalíticas promovidas por las paredes del reactor de cuarzo a presión atmosférica se han considerado insignificantes. La oxidación de H_2S promueve la oxidación de CH_4 a temperaturas más bajas en todas las condiciones estudiadas. Al mismo tiempo, el CH_4 retarda la oxidación de H_2S a presión atmosférica, mientras que, a presiones más altas, promueve ligeramente la conversión de H_2S a temperaturas más bajas. La oxidación de H_2S se retrasa ligeramente en presencia de NO a presión atmosférica. A alta presión, se cree que NO_2 reacciona considerablemente con H_2S a bajas temperaturas formando azufre. El mecanismo cinético desarrollado es capaz de describir el comportamiento de oxidación de H_2S, de mezclas de H_2S/CH_4 y H_2S/NO bajo diferentes condiciones, así como predecir la oxidación de H_2S y CH_3SH en dos tipos diferentes de reactores a presión atmosférica (JSR y PFR). En este trabajo, se ha puntualizado que especies peróxido como HSOO, H_2O_2 y HO_2 son clave en la oxidación del H_2S.

BIBLIOGRAPHY

Abián, M.; Millera, Á.; Bilbao, R.; Alzueta, M.U. (2012). Effect of recirculation gases on soot formed from ethylene pyrolysis. *Combustion Science and Technology* 184, 980-994.

Abián, M. (2013). Pollutant reduction in combustion systems through flue gas recirculation (FGR). PhD Thesis, Universidad de Zaragoza, Spain.

Abián, M.; Cebrián, M.; Millera, Á.; Bilbao, R.; Alzueta, M.U. (2015a). CS_2 and COS conversion under different combustion conditions. *Combustion and Flame* 162, 2119-2127.

Abián, M.; Millera, Á.; Bilbao, R.; Alzueta, M.U. (2015b). Impact of SO_2 on the formation of soot from ethylene pyrolysis. *Fuel* 159, 550-558.

Ajdari, S.; Normann, F.; Andersson, K.; Johnsson, F. (2015). Modeling the nitrogen and sulfur chemistry in pressurized flue gas systems. *Industrial and Engineering Chemistry Research* 54, 1216-1227.

Alzueta, M.U.; Bilbao, R.; Finestra, M. (2001a). Methanol oxidation and its interaction with nitric oxide. *Energy and Fuels* 15, 724-729.

Alzueta, M.U.; Bilbao, R.; Glarborg, P. (2001b). Inhibition and sensitization of fuel oxidation by SO_2. *Combustion and Flame* 127, 2234-2251.

Alzueta, M.U.; Borruey, M.; Callejas, A.; Millera, Á.; Bilbao, R. (2008). An experimental and modeling study of the oxidation of acetylene in a flow reactor. *Combustion and Flame* 152, 377-386.

Alzueta, M.U.; Pernía, R.; Abián, M.; Millera, Á.; Bilbao, R. (2019). CH_3SH conversion in a tubular flow reactor. Experiments and kinetic modelling. *Combustion and Flame* 203, 23-30.

Alexandrino, K. (2018). Study of the oxidation and pyrolysis of different oxygenated compounds proposed as alternative fuels. PhD Thesis, Universidad de Zaragoza, Spain.

Amo, K.; Baker, R.W.; Helm, V.D.; Hofmann, T.; Lokhandwala, K.A.; Pinnau, I.; Ringer, M.B.; Su, T.T.; Toy, L.; Wijmans, J.G. (1998). Low-quality natural gas sulfur removal/recovery system. Technical report, Department of Energy, United States.

ANSYS Chemkin-Pro 17.2 (2016). ANSYS Reaction Design: San Diego, USA.

Ashmore, P.G.; Burnett, M.G.; Tyler, B.J. (1962). Reaction of nitric oxide and oxygen. *Transactions of the Faraday Society* 58, 685-691.

Atkinson, R.; Baulch, D.L.; Cox, R.A.; Crowley, J.N.; Hampson, R.F.; Hynes, R.G.; Jenkin, M.E.; Rossi, M.J.; Troe, J. (2004). Evaluated kinetic and photochemical data for atmospheric chemistry: Volume I - gas phase reactions of O_x, HO_x, NO_x and SO_x species. *Atmospheric Chemistry and Physics* 4, 1461-1738.

Awe, O.; Zhao, Y.; Nzihou, A.; Minh, D.; Lyczko, N. (2017). A review of biogas utilization, purification and upgrading technologies. *Waste Biomass Valorization* 8, 267-283.

Baker, R.W.; Lokhandwala, K. (2008). Natural gas processing with membranes: An overview. *Industrial and Engineering Chemistry Research* 47, 2109-2121.

Barba, D.; Cammarota, F.; Vaiano, V.; Salzano, E.; Palma, V. (2017). Experimental and numerical analysis of the oxidative decomposition of H_2S. *Fuel* 198, 68-75.

Batiha, M.; Altarawneh, M.; Al-Harahsheh, M.; Altarawneh, I.; Rawadieh, S. (2011). Theoretical derivation for reaction rate constants of H abstraction from thiophenol by the H/O radical pool. *Computational and Theoretical Chemistry* 970, 1-5.

Becker, K.H.; Inocencio, M.A.; Schurath, U. (1975). Reaction of ozone with hydrogen-sulfide and its organic derivatives. *International Journal of Chemical Kinetics* 1, 205-220.

Beckett, D.; Edelmann, M.; Raff, J.D.; Raghavachari, K. (2017). Hidden complexities in the reaction of H_2O_2 and HNO revealed by ab initio quantum chemical investigations. *Physical Chemistry Chemical Physics* 19, 29549-29560.

Blackwood, T.R. (1980). A study of the reaction between hydrogen sulfide and nitrogen dioxide. Report. Department of Chemical Engineering, University of Michigan, Ann Arbor, Michigan.

Bian, H.; Xu, B.; Zhang, H.; Wang, Q.; Zhang, H.; Zhang, S.; Xia, D. (2019). Theoretical study on the atmospheric reaction of CH_3SH with O_2. *International Journal of Quantum Chemistry* 119, 25822.

Bongartz, D.; Shanbhogue, S.J.; Ghoniem, A.F. (2015). Formation and control of sulfur oxides in sour gas oxy-combustion: prediction using a reactor network model. *Energy and Fuels* 29, 7670-7680.

Bongartz, D.; Ghoniem, A.F. (2015a). Chemical kinetics mechanism for oxy-fuel combustion of mixtures of hydrogen sulfide and methane. *Combustion and Flame* 162, 544-553.

Bongartz, D.; Ghoniem, A.F. (2015b). Impact of sour gas composition on ignition delay and burning velocity in air and oxy-fuel combustion. *Combustion and Flame* 162, 2749-2757.

Bromly, J.; Barnes, F.; Nelson, P.; Haynes, B. (1995). Kinetics and modeling of the $H_2/O_2/NO_x$ system. *International Journal of Chemical Kinetics* 27, 1165-1178.

Burke, M.P.; Chaos, M.; Ju, Y; Dryer, F.L.; Klippenstein, S.J. (2012). Comprehensive H_2/O_2 kinetic model for high-pressure combustion. *International Journal of Chemical Kinetics* 44, 444-474.

Cadle, R.D.; Ledford M. (1966). Reaction of ozone with hydrogen sulfide. *International Journal of Air and Water Pollution* 10, 25-30.

Chakroun, N.W.; Ghoniem, A.F. (2015a). Techno-economic assessment of sour gas oxy-combustion water cycles for CO2 capture. *International Journal of Greenhouse Gas Control* 36, 1-12.

Chakroun N.W.; Ghoniem, A.F. (2015b). High-efficiency low LCOE combined cycles for sour gas oxy-combustion with CO_2 capture. *International Journal of Greenhouse Gas Control* 41, 163-173.

Clark, P.D.; Stevens, D.K. (2005). Method for energy recovery from hydrogen sulfide. U.S. Patent 7282193-B2.

Cong, T.Y.; Raj, A.; Chanaphet, J.; Mohammed, S.; Ibrahim, S.; Al Shoaibi, A. (2016). A detailed reaction mechanism for hydrogen production via hydrogen sulphide (H_2S) thermolysis and oxidation. *International Journal of Hydrogen Energy* 41, 6662-6675.

Davis, P.; Marriott, R. A.; Fitzpatrick, E.; Wan, H.; Bernard, F.; Clark, P.D. (2008). Fossil fuel development requires long-term sulfur strategies. *Oil and Gas Journal* 106, 45-46, 48, 50-53.

De Crisci, A.G.; Moniri, A.; Xu, Y. (2019). Hydrogen from hydrogen sulfide: towards a more sustainable hydrogen economy. *International Journal of Hydrogen Energy* 44, 1299-1327.

De Diego, L.F.; De las Obras-Loscertales, M.; Rufas, A.; García-Labiano, F.; Gayán, P.; Abad, A.; Adánez, J. (2013). Pollutant emissions in a bubbling fluidized bed combustor working in oxy-fuel operating conditions: Effect of flue gas recirculation. *Applied Energy* 102, 860-867.

Duong-Viet, C.; Nhut, J.-M.; Truong-Huu, T.; Tuci, G.; Nguyen-Dinh, L.; Liu, Y.; Pham, C.; Giambastiani, G.; Pham-Huu, C. (2020). A nitrogen-doped carbon-coated silicon carbide as a robust and highly efficient metal-free catalyst for sour gas desulfurization in the presence of aromatics as contaminants. *Catalysis Science and Technology* 10, 5487-5500.

Elsner, M.P.; Menge, M.; Müller, C.; Agar, D.W. (2003). The Claus process: teaching an old dog new tricks. *Catalysis Today* 79-80, 487-494.

England, C.; Corcoran, W.H. (1975). The rate and mechanism of the air oxidation of parts-per-million concentrations of nitric oxide in the presence of water vapor. *Industrial and Engineering Chemistry Fundamentals* 14, 55-63.

Esarte, C. (2011). Pyrolysis of acetylene with ethanol and other oxygenated compounds. Study of formation of soot and gaseous pollutants. PhD Thesis, Universidad de Zaragoza, Spain.

Fahim, M.A.; Alsahhaf, T.A.; Elkilani, A. (2010). Chapter 15 - Acid gas processing and mercaptans removal. Fundamentals of Petroleum Refining. Elsevier, Amsterdam.

Fleig, D.; Alzueta, M.U.; Normann, F.; Abián, M.; Andersson, K.; Johnsson, F. (2013). Measurement and modeling of sulfur trioxide formation in a flow reactor under post-flame conditions. *Combustion and Flame* 160, 1142-1151.

Freitas, G.N.; Garrido, J.D.; Ballester, M.Y.; Nascimiento, M.A.C. (2012). Connection between the upper and lower energy regions of the potential energy surface of the ground electronic state of the HSO_2 system. *Journal of Physical Chemistry A* 116, 7677-7685.

Friedl, R.R.; Brune, W.H.; Anderson, J.G. (1985). Kinetics of SH with NO_2, O_3, O_2, and H_2O_2. *Journal of Physical Chemistry* 89, 5505-5510.

Frost, P.; Thomas, J.H. (1975). Reaction between hydrogen-sulfide and nitrogen-dioxide. *Combustion and Flame* 25, 213-217.

Gardiner, W.C. (2000). Gas-phase combustion chemistry. Springer, New York.

Garrido, J.D.; Ballester, M.Y.; Orozco-González, Y.; Canuto, S. (2011). CASPT2 study of the potential energy surface of the HSO_2 system. *Journal of Physical Chemistry A* 115, 1453-1461.

Gersen, S.; Van Essen, M.; Darmeveil, H.; Hashemi, H.; Rasmussen, C.T.; Christensen, J.M.; Glarborg, P.; Levinsky, H. (2017). Experimental and modeling investigation of the effect of H_2S addition to methane on the ignition and oxidation at high pressures. *Energy and Fuels* 31, 2175-2182.

Giménez-López, J.; Alzueta, M.U.; Rasmussen, C.; Marshall, P.; Glarborg, P. (2011). High pressure oxidation of C_2H_4/NO mixtures. *Proceedings of the Combustion Institute* 33, 449-457.

Giménez-López, J.; Millera, Á.; Bilbao, R.; Alzueta, M.U. (2015). Experimental and kinetic modeling study of the oxy-fuel oxidation of natural gas, CH_4 and C_2H_6. *Fuel* 160, 404-412.

Giménez-López, J.; Rasmussen, C.T.; Hashemi, H.; Alzueta, M.U.; Gao, Y.; Marshall, P.; Goldsmith, C.F.; Glarborg, P. (2016) Experimental and kinetic modeling study of C_2H_2 oxidation at high pressure. *International Journal of Chemical Kinetics* 48, 724-738.

Glarborg, P.; Kristensen, P.G.; Kubel, D.; Hansen, J.; Dam-Johansen, K. (1995). Interactions of CO, NO_x and H_2O under post-flames conditions. *Combustion Science Technology* 110-111, 461-485.

Glarborg, P.; Alzueta, M.U.; Dam-Johansen, K.; Miller, J.A. (1998). Kinetic modeling of hydrocarbon/nitric oxide interactions in a flow reactor. *Combustion and Flame* 115, 1-27.

Glarborg, P.; Østberg, M.; Alzueta, M.U.; Dam-Johansen, K.; Miller, J.A. (1999). The recombination of hydrogen atoms with nitric oxide at high temperatures. *Proceedings of the Combustion Institute* 27, 219-227.

Glarborg, P.; Kristensen, P.G.; Dam-Johansen, K.; Alzueta, M.U.; Millera, Á.; Bilbao, R. (2000). Nitric oxide reduction by non-hydrocarbon fuels. Implications for reburning with gasification gases. *Energy and Fuels* 14, 828-838.

Glarborg, P. (2007). Hidden interactions-trace species governing combustion and emissions. *Proceedings of the Combustion Institute* 31, 77-98.

Greig, J.D.; Hall, P.G. (1967). Thermal oxidation of nitric oxide at low concentrations. *Transactions of the Faraday Society* 63, 655-661.

Gupta, A.K.; Ibrahim, S.; Al Shoaibi, A. (2016). Advances in sulfur chemistry for treatment of acid gases. *Progress in Energy and Combustion Science* 54, 65-92.

Hajar, Y.; McAuley, K.; Zeman, F. (2016). Sulfur as a fuel source in a combined power cycle equipped with dry flue gas desulfurization system. *Energy and Fuels* 30, 8511-8519.

Harbaugh, E. (2011). Building blocks. *Hydrocarbon Engineering* 16, 68-72.

Hales, J.M.; Wilkes, J.O.; York, J.L. (1974). Some recent measurements of H_2S oxidation rates and their implications to atmospheric chemistry. *Tellus* 26, 277-283.

Harrigan D.J.; Yang, J.; Sundell, B.J.; Lawrence III, J.A.; O'Brien, J.T.; Ostraat, M.L. (2020). Sour gas transport in poly(ether-b-amide) membranes for natural gas separations. *Journal of Membrane Science* 595, 117497.

Hashemi, H.; Christensen, J.M.; Gersen, S.; Glarborg, P. (2015). Hydrogen oxidation at high pressure and intermediate temperatures: experiments and kinetic modeling, *Proceedings of the Combustion Institute* 35, 553-560.

Hashemi, H.; Christensen, J.M.; Gersen, S.; Levinsky, H.B.; Klippenstein, S.J.; Glarborg, P. (2016). High pressure oxidation of methane. *Combustion and Flame* 172, 349-364.

He, C.; You, F. (2014). Shale gas processing integrated with ethylene production: novel process designs, exergy analysis, and techno-economic analysis. *Industrial and Engineering Chemical Research* 53, 11442-11459.

Herbinet, O.; Dayma, G. (2013). Jet-stirred Reactors. Battin-Leclerc, F.; Simmie, J.M.; Blurock, E. (eds) Cleaner Combustion. Green Energy and Technology. Springer, London.

Olivier Herbinet, Dayma Guillaume. Jet-Stirred Reactors. Frédérique Battin-Leclerc, John M. Simmie, Edward Blurock. Cleaner Combustion: Developing Detailed Chemical Kinetic Models, springer, pp.183-210, 2013, Green Energy and Technology, 978-1-4471-5306-1.

Hisatsune, I.C.; Zafonte, L. (1969). Kinetic study of some third-order reactions of nitric oxide. *The Journal of Physical Chemistry* 73, 2980-2989.

Hovem, L.A. (2020). Energy transition outlook, oil and gas. Technical report. Det Norske Veritas and Germanischer Lloyd (DNV GL).

International Energy Agency (IEA). (2008). Natural gas resources and production prospects. World Energy Outlook. Technical Report. OECD Publishing, Paris.

Jerzak, W.; Kuźnia, M.; Szajding, A. (2016). Experimental studies and the chemical kinetics modelling of oxidation of hydrogen sulfide contained in biogas. *Procedia Engineering* 157, 222-229.

Kidnay, A.J.; Parrish, W.R.; McCartney, D.G. (2019). Fundamentals of natural gas processing. CRC press, Boca Ratón.

Kim, H. (2003). Corrosion process of silver in environments containing 0.1 ppm H_2S and 1.2 ppm NO_2. *Materials and Corrosion* 54, 243-250.

Kristensen, P.G.; Glarborg, P.; Dam-Johansen, K. (1996). Nitrogen chemistry during burnout in fuel-staged combustion. *Combustion and Flame* 107, 211-222.

Li, D.; Dowling, N.; Marriott, R.; Clark, P. (2016). Kinetics and mechanisms for destruction of ammonia in the Claus furnace; Alberta Sulphur Research Ltd. Chalk Talk: Calgary AB, Canada.

Lu, X.; Palmer, M.; Forrest, B.; McGroddy, M. (2018). A novel power generation system utilizing un-treated sour gas fuel. Society of Petroleum Engineers. https://doi.org/10.2118/192823-MS (accessed 31/5/2020)

Mac Kinnon, M.A.; Brouwer, J.; Samuelsen, S. (2018). The role of natural gas and its infrastructure in mitigating greenhouse gas emissions, improving regional air quality, and renewable resource integration. *Progress in Energy and Combustion Science* 64, 62-92.

Maggio, G.; Cacciola, G. (2012). When will oil, natural gas, and coal peak?. *Fuel* 98, 111-123.

Maricq, M.M.; Szente, J.J.; Kaiser, E.W.; Shi, J. (1994). Reaction of chlorine atoms with methylperoxy and ethylperoxy radicals. *Journal of Physical Chemistry A* 98, 2083-2089.

Marrodán, L.; Millera, Á.; Bilbao, R.; Alzueta, M.U. (2014). High-pressure study of methylformate oxidation and its interaction with NO. *Energy and Fuels* 28, 6107-6115.

Marrodán, L. (2018). Oxidation of organic compounds present in fuels under conditions of interest for combustion processes. PhD Thesis, Universidad de Zaragoza, Spain.

Marrodán, L.; Fuster, M.; Millera, Á.; Bilbao, R.; Alzueta, M.U. (2018a). Ethanol as a fuel additive: High pressure oxidation of its mixtures with acetylene. *Energy and Fuels* 32, 10078-10087.

Marrodán, L.; Arnal, A.J.; Millera, Á.; Bilbao, R.; Alzueta, M.U. (2018b) The inhibiting effect of NO addition on dimethyl ether high-pressure oxidation. *Combustion and Flame* 197, 1-10.

Mathieu, O.; Deguillaume, F.; Petersen, E.L. (2014). Effects of H_2S addition on hydrogen ignition behind reflected shock waves: Experiments and modeling. *Combustion and Flame* 161, 23-36.

Matras, D.; Villermaux, J. (1973). Continuous reactor perfectly agitated by gas jets for kinetic study on rapid chemical reactions. *Chemical Engineering Science* 28, 129-137.

McIlroy, A.; McRae, G.; Sick, V.; Siebers, D.L.; Westbrook, C.K.; Smith, P.J.; Taatjes, C.; Trouve, A.; Wagner, A.F.; Rohlfing, E.; Manley, D.; Tully, F.; Hilderbrandt, R.; Green, W.; Marceau, D.; O'Neal, J.; Lyday, M.; Cebulski, F.; Garcia, T.R.; Strong, D. (2006). Basic research needs for clean and efficient combustion of 21st century transportation fuels. Technical report. US Department of Energy, United States.

Mellouki, A.; Ravishankara, A.R. (1994). Does the HO_2 radical react with H_2S, CH_3SH, and CH_3SCH_3?. *International Journal of Chemical Kinetics* 26, 355-365.

Montoya, A.; Sendt, K.; Haynes, B.S. (2005). Gas-phase interaction of H_2S with O_2: A kinetic and quantum chemistry study of the potential energy surface. *Journal of Physical Chemistry A* 109, 1057-1062.

Mousavipour, S.H.; Mortazavi, M.; Hematti, O. (2013). Multichannel RRKM-TST and direct-dynamics CVT study of the reaction of hydrogen sulfide with ozone. *Journal of Physical Chemistry A* 117, 6744-6756.

Mueller, M.A.; Yetter, R.A.; Dryer, F.L. (1998). Measurement of the rate constant for $H+O_2+M = HO_2+M(M=N_2;\ Ar)$ using kinetic modeling of the high-pressure $H_2/O_2/NO_x$ reaction. *Symposium (International) on Combustion* 27, 177-184.

Olbregts, J. (1985). Termolecular reaction of nitrogen monoxide and oxygen: A still unsolved problem. *International Journal of Chemical Kinetics* 17, 835-848.

Palma, V.; Vaiano, V.; Barba, D.; Colozzi, M.; Palo, E.; Barbato, L.; Cortese, S. (2015). H_2 production by thermal decomposition of H_2S in the presence of O_2. *International Journal of Hydrogen Energy* 40, 106-113.

Parker, M. (2010). Method for removing hydrogen sulfide from sour gas and converting it to hydrogen and sulfuric acid. PhD Thesis, Stanford University, United States.

Pierce, J.A. (1929). A study of the reaction between nitric oxide and hydrogen sulphide. *Journal of Physical Chemistry* 33, 22-36.

Rameshni M. (2002). Cost effective options to expand SRU capacity using oxygen. Sulfur Recovery Symposium Brimstone Engineering Services. Inc. Banlf. Alberta, Calgary.

Rappold, T.A.; Lackner, K.S. (2010). Large scale disposal of waste sulfur: From sulfide fuels to sulfate sequestration. *Energy* 35, 1368-1380.

Rasmussen, C.L.; Hansen, J.; Marshall, P.; Glarborg, P. (2008a). Experimental measurements and kinetic modeling of $CO/H_2/O_2/NO_x$ conversion at high pressure. *International Journal of Chemical Kinetics* 40, 454-480.

Rasmussen, C.L.; Rasmussen, A.E.; Glarborg, P. (2008b) Sensitizing effects of NO_x on CH_4 oxidation at high pressure. *Combustion and Flame* 154, 529-545.

Rasmussen, C.L.; Jakobsen, J.G.; Glarborg, P. (2008c). Experimental measurements and kinetic modeling of CH_4/O_2 and $CH_4/C_2H_6/O_2$ conversion at high pressure. *International Journal of Chemical Kinetics* 40, 778-807.

RodrÍguez, A.; Herbinet, O.; Wang, Z.; Qi, F.; Fittschen, C.; Westmoreland, P.R.; Battin-Leclerc, F. (2017). Measuring hydroperoxide chain-branching agents during n-pentane low-temperature oxidation. *Proceedings of the Combustion Institute* 36, 333-342.

Roesler, J.F.; Yetter, R.A.; Dryer, F.L. (1995). Kinetic interactions of CO, NO_x, and HCI emissions in postcombustion gases. *Combustion and Flame* 100, 495-504.

Röhrig, M.; Wagner, H.G. (1994). An investigation about the NH (X^3P^-) formation in the thermal decomposition of HN_3. *Berichte der Bunsengesellschaft für Physikalische Chemie* 98 1073-1076.

Russel, M.S. (2009). The chemistry of fireworks. Royal Society of Chemistry, Cambridge.

Salisu, I.; Abhijeet, R. (2016). Kinetic simulation of acid gas (H_2S and CO_2) destruction for simultaneous syngas and sulfur recovery. *Industrial and Engineering Chemical Research* 55, 6743-6752.

Salisu, I.; Ramees, K.R.; Abhijeet, R. (2017). Roles of hydrogen sulfide concentration and fuel gas injection on aromatics emission from Claus furnace. *Chemical Engineering Science* 172, 513-527.

Salisu, I.; Mohammad, A.H.; Abhijeet, R. (2020). Detailed reaction mechanism to predict ammonia destruction in the thermal section of sulfur recovery units. *Industrial and Engineering Chemical Research* 59, 74912-74923.

Slack, M.; Grillo, A. (1977). Investigation of hydrogen-air ignition sensitised by nitric oxide and by nitrogen dioxide. Technical report, NASA Report CR-2896.

Song, Y.; Hashemi, H.; Christensen, J.M.; Zou, C.; Haynes, B.S.; Marshall, P.; Glarborg, P. (2017). An exploratory flow reactor study of H_2S oxidation at 30-100 bar. *International Journal of Chemical Kinetics* 49, 37-52.

Song, Y.; Marrodán, L.; Vin, N.; Herbinet, O.; Assaf, E.; Fittschen, C.; Stagni, A.; Faravelli, T.; Alzueta, M.U.; Battin-Leclerc, F. (2019). The sensitizing effects of NO_2 and NO on methane low temperature oxidation in a jet stirred reactor. *Proceedings of the Combustion Institute* 37, 667-675.

Speight, J.G. (2007). Natural gas: A basic handbook. Gulf Publishing Company, Houston.

Srinivasan, N.K.; Su, M.C.; Michael, J.V. (2007). $CH_3+O_2=H_2CO+OH$ Revisited. *Journal of Physical Chemistry A* 11, 11589-11591.

Taifan, W.; Baltrusaitis, J. (2017). Minireview: direct catalytic conversion of sour natural gas (CH_4 + H_2S + CO_2) components to high value chemicals and fuels. *Catalysis Science and Technology* 7, 2919-2929.

Tilahun, E.; Bayrakdar, A.; Sahinkaya, E.; Çalli, B. (2017). Performance of polydimethylsiloxane membrane contactor process for selective hydrogen sulfide removal from biogas. *Waste Management* 61, 250-257.

U.S. Geological Survey (USGS). (2019). Mineral commodity summaries - sulfur. Technical report. USGS.

Valera-Medina, A.; Giles, A.; Pugh, D.; Morris, S.; Pohl, M.; Ortwein, A. (2018). Investigation of combustion of emulated biogas in a gas turbine test rig. *Journal of Thermal Science* 27, 331-340.

Van de Vijver, R.; Vandewiele, N.M.; Vandeputte, A.G.; Van Geem, K.M.; Reyniers, M.-F.; Green, W.H.; Marin, G.B. (2015). Rule-based ab initio kinetic model for alkyl sulfide pyrolysis. *Chemical Engineering Journal* 278, 385-393.

Yi, S.; Ma, X.; Pinnau, I.; Koros, W.J. (2015). A high-performance hydroxyl-functionalized polymer of intrinsic microporosity for an environmentally attractive membrane-based approach to decontamination of sour natural gas. *Journal of Physical Chemistry A* 3, 22794-22806.

Zeng, Z.; Altarawneh, M.; Oluwoye, I.; Glarborg, P.; Dlugogorski, B.Z. (2016). Inhibition and promotion of pyrolysis by hydrogen sulfide (H_2S) and sulfanyl radical (SH). *Journal of Physical Chemistry A* 120, 8941-8948.

Zeng, Z. (2017). Oxidation chemistry of carbon disulfide (CS_2) and its interaction with hydrocarbons in combustion processes. PhD Thesis, Murdoch University, Australia.

Zeng, Z.; Dlugogorski, B.Z.; Altarawneh, M. (2017). Flammability of CS_2 and other reduced sulfur species. *Fire Safety Journal* 91, 226-234.

Zeng, Z.; Dlugogorski, B.Z.; Oluwoye, I.; Altarawneh, M. (2019a). Combustion chemistry of carbon disulphide (CS_2). *Combustion and Flame* 210, 413-425.

Zeng, Z.; Dlugogorski, B.Z.; Oluwoye, I.; Altarawneh, M. (2019b). Co-oxidation of methane (CH_4) and carbon disulfide (CS_2). *Proceedings of the Combustion Institute* 37, 677-685.

Zheng, X.; Fisher, E.M.; Gouldin, F.C.; Bozzelli, J.W. (2011). Pyrolysis and oxidation of ethyl methyl sulfide in a flow reactor. *Combustion and Flame* 158, 1049-1058.

Zhou, C.R.; Sendt, K.; Haynes, B.S. (2008). Theoretical study of hydrogen abstraction and sulfur insertion in the reaction H_2S + S. *Journal of Physical Chemistry A* 112, 3239-3247.

Zhou, C.R.; Sendt, K.; Haynes, B.S. (2013). Experimental and kinetic modelling study of H_2S oxidation. *Proceedings of the Combustion Institute* 34, 625-632.

Annexes:

Regulations required to submit a PhD Thesis by compendium of publications

Annexes

Regulations required to submit a PhD Thesis by compendium of Publications

According to the specific regulations for the presentation of the PhD Thesis by a compendium of publications (Articles 19, 20 and 21 of the Regulation, of the Agreement of 20/12/2013 of the Governing Council of the University of Zaragoza), the following sections are presented below:

- Subject category and impact factor of the journals reported in this dissertation.
- PhD student's contributions.
- Resignation to claim authority rights by contributing authors, not holding a PhD degree, included in any of the publications of the present dissertation.

Según la normativa específica para la presentación de Tesis Doctoral como compendio de publicaciones (Artículos 19, 20 y 21 del Reglamento, del Acuerdo de 20/12/2013 del Consejo de Gobierno de la Universidad de Zaragoza), se presentan a continuación los siguientes apartados:

- Áreas temáticas y factor de impacto de las revistas en donde se ha publicado el trabajo realizado.
- Aportaciones del doctorando.
- Renuncia de los coautores no doctores participantes en los trabajos incluidos en esta Tesis Doctoral presentada por la modalidad de compendio de publicaciones.

Subject category and impact factor of the articles reported in this dissertation

The characteristics of the journals in which the articles that make up this dissertation have been published are shown below. Impact factor from the Journal of Citation Reports (JCR) corresponding to the year of publication, and the thematic areas, are also indicated. The numbering follows the same order as the indicated at the beginning of this dissertation.

I. **Colom-Díaz, J.M.**; Abián, M.; Ballester, M.Y.; Millera, Á.; Bilbao, R.; Alzueta, M.U. (2019). H_2S conversion in a tubular flow reactor: Experiments and kinetic modeling. *Proceedings of the Combustion Institute* 37, 727-734. Citations: 11

Journal: Proceedings of the Combustion Institute

Impact Factor 2019: 5.627

Thematic Areas 2019:

- Chemical Engineering 17/143
- Mechanical Engineering 8/130
- Energy & Fuels 22/112
- Thermodynamics 4/61

II. **Colom-Díaz, J.M.**; Millera, Á.; Bilbao, R.; Alzueta, M.U. (2019). High pressure study of H_2 oxidation and its interaction with NO. *International Journal of Hydrogen Energy* 44, 6325-6332. Citations: 5

Journal: International Journal of Hydrogen Energy

Impact Factor 2019: 4.939

Thematic Areas 2019:

- Energy & Fuels 30/112
- Electrochemistry 7/27
- Physical Chemistry 48/159

III. **Colom-Díaz, J.M.**; Abián, M.; Millera, Á.; Bilbao, R.; Alzueta, M.U. (2019). Influence of pressure on H_2S oxidation. Experiments and kinetic modeling. *Fuel* 258, 116145. Citations: 8

Journal: Fuel

Impact Factor 2019: 5.578

Thematic Areas 2019:
- Chemical Engineering 18/143
- Energy & Fuels 24/112

IV. **Colom-Díaz, J.M.**; Leciñena, M.; Peláez, A.; Abián, M.; Millera, Á.; Bilbao, R.; Alzueta, M.U. (2020). Study of the conversion of H_2S/CH_4 mixtures at different pressures. *Fuel* 262, 116484. Citations: 4

Journal: Fuel

Impact Factor 2019: 5.578

Thematic Areas 2019:
- Chemical Engineering 18/143
- Energy & Fuels 24/112

V. **Colom-Díaz, J.M.**; Millera, Á.; Bilbao, R.; Alzueta, M.U. (2021). New results of H_2S oxidation at high pressures. Experiments and kinetic modeling. *Fuel* 285, 119261. Citations: 1

Journal: Fuel

Impact Factor 2019: 5.578

Thematic Areas 2019:
- Chemical Engineering 18/143
- Energy & Fuels 24/112

VI. **Colom-Díaz, J.M.**; Alzueta, M.U.; Zeng, Z.; Altarawneh, M.; Dlugogorski, B.Z. (2021). Oxidation of H_2S and CH_3SH oxidation in a jet-stirred reactor: Experiments and kinetic modeling. *Fuel* 283, 119258. Citations: 1

Journal: Fuel

Impact Factor 2019: 5.578

Thematic Areas 2019:
- Chemical Engineering 18/143
- Energy & Fuels 24/112

VII. **Colom-Díaz, J.M.**; Millera, Á.; Bilbao, R.; Alzueta, M.U. (2021). Conversion of $H_2S/O_2/NO$ mixtures at different pressures. Experiments and kinetic modeling. *Fuel* 290, 120060.

Journal: Fuel

Impact Factor 2019: 5.578

Thematic Areas 2019:

1. Chemical Engineering 18/143
2. Energy & Fuels 24/112

Áreas temáticas y factor de impacto de las revistas en donde se ha publicado el trabajo realizado

Las características de las revistas en las que se han publicado los artículos que componen esta tesis se muestran a continuación. También se indica el factor de impacto según el *Journal of Citation Reports* (JCR) correspondiente al año de publicación, y las áreas temáticas. La numeración sigue el mismo orden que el indicado al comienzo de esta memoria.

I. **Colom-Díaz, J.M.**; Abián, M.; Ballester, M.Y.; Millera, Á.; Bilbao, R.; Alzueta, M.U. (2019). H_2S conversion in a tubular flow reactor: Experiments and kinetic modeling. *Proceedings of the Combustion Institute* 37, 727-734. Citations: 11

Revista: Proceedings of the Combustion Institute

Factor de impacto 2019: 5.627

Áreas temáticas 2019:

- Chemical Engineering 17/143
- Mechanical Engineering 8/130
- Energy & Fuels 22/112
- Thermodynamics 4/61

II. **Colom-Díaz, J.M.**; Millera, Á.; Bilbao, R.; Alzueta, M.U. (2019). High pressure study of H_2 oxidation and its interaction with NO. *International Journal of Hydrogen Energy* 44, 6325-6332. Citations: 5

Revista: International Journal of Hydrogen Energy

Factor de impacto 2019: 4.939

Áreas temáticas 2019:

- Energy & Fuels 30/112
- Electrochemistry 7/27
- Physical Chemistry 48/159

III. **Colom-Díaz, J.M.**; Abián, M.; Millera, Á.; Bilbao, R.; Alzueta, M.U. (2019). Influence of pressure on H_2S oxidation. Experiments and kinetic modeling. *Fuel* 258, 116145. Citations: 8

Revista: Fuel

Factor de impacto 2019: 5.578

Áreas temáticas 2019:
- Chemical Engineering 18/143
- Energy & Fuels 24/112

IV. **Colom-Díaz, J.M.**; Leciñena, M.; Peláez, A.; Abián, M.; Millera, Á.; Bilbao, R.; Alzueta, M.U. (2020). Study of the conversion of H_2S/CH_4 mixtures at different pressures. *Fuel* 262, 116484. Citations: 4

Revista: Fuel

Factor de impacto 2019: 5.578

Áreas temáticas 2019:
- Chemical Engineering 18/143
- Energy & Fuels 24/112

V. **Colom-Díaz, J.M.**; Millera, Á.; Bilbao, R.; Alzueta, M.U. (2021). New results of H_2S oxidation at high pressures. Experiments and kinetic modeling. *Fuel* 285, 119261. Citations: 1

Revista: Fuel

Factor de impacto 2019: 5.578

Áreas temáticas 2019:
- Chemical Engineering 18/143
- Energy & Fuels 24/112

VI. **Colom-Díaz, J.M.**; Alzueta, M.U.; Zeng, Z.; Altarawneh, M.; Dlugogorski, B.Z. (2021). Oxidation of H_2S and CH_3SH oxidation in a jet-stirred reactor: Experiments and kinetic modeling. *Fuel* 283, 119258. Citations: 1

Revista: Fuel

Factor de impacto 2019: 5.578

Áreas temáticas 2019:
- Chemical Engineering 18/143
- Energy & Fuels 24/11

VII. **Colom-Díaz, J.M.**; Millera, Á.; Bilbao, R.; Alzueta, M.U. (2021). Conversion of $H_2S/O_2/NO$ mixtures at different pressures. Experiments and kinetic modeling. *Fuel* 290, 120060.

Revista: Fuel

Factor de impacto 2019: 5.578

Áreas temáticas 2019:

- Chemical Engineering 18/143
- Energy & Fuels 24/112

PhD student contributions

The contribution of the author of this PhD Thesis, in the different publications included in this dissertation, has been the decision and realization of the different experiments in the laboratory and the analysis of the results, the update, modification and optimization of the chemical kinetic mechanisms used, and the performance of the modeling calculations. He has also had a very active participation in the writing of the different publications.

Aportaciones del doctorando

La contribución del autor de esta Tesis Doctoral, en las diferentes publicaciones incluidas en esta memoria, ha sido la decisión y ejecución de los diferentes experimentos en el laboratorio y el análisis de los resultados obtenidos, la actualización, modificación y optimización de los mecanismos cinéticos químicos utilizados, y la realización de los cálculos de modelado. También ha tenido una participación muy activa en la redacción de los diferentes artículos.

Resignation to claim authority rights by contributing authors not holding a PhD degree included in any of the publications of the present dissertation

The non-doctor co-authors of the articles included in this PhD Thesis submitted in the form of compendium of publications have signed the corresponding resignation documents, which have been delivered at the time of the deposit of the present dissertation.

Renuncia de los coautores no doctores de los trabajos incluidos en la presente Tesis Doctoral presentada en la modalidad de compendio de publicaciones

Los coautores no doctores de los trabajos incluidos en la presente Tesis Doctoral, presentada en la modalidad de compendio de publicaciones, han firmado los correspondientes documentos de renuncia, los cuales han sido entregados en el momento del depósito de la presente memoria.

Article I

Colom-Díaz, J.M.; Abián, M.; Ballester, M.Y.; Millera, Á.; Bilbao, R.; Alzueta, M.U. (2019). H_2S conversion in a tubular flow reactor: Experiments and kinetic modeling. *Proceedings of the Combustion Institute* 37, 727-734.

Available online at www.sciencedirect.com

ScienceDirect

Proceedings of the Combustion Institute 37 (2019) 727–734

Proceedings of the Combustion Institute

www.elsevier.com/locate/proci

H_2S conversion in a tubular flow reactor: Experiments and kinetic modeling

J.M. Colom-Díaz [a], M. Abián [a], M.Y. Ballester [b], Á. Millera [a], R. Bilbao [a], M.U. Alzueta [a,*]

[a] *Aragón Institute of Engineering Research (I3A). Department of Chemical and Environmental Engineering, University of Zaragoza, 50018 Zaragoza, Spain*

[b] *Physics Department, Federal University of Juiz de Fora, MG 36036-330, Brasil*

Received 30 November 2017; accepted 25 May 2018
Available online 19 June 2018

Abstract

Oxidation of H_2S at atmospheric pressure has been studied under different reaction atmospheres, varying the air excess ratio (λ) from reducing ($\lambda = 0.32$) to oxidizing conditions ($\lambda = 19.46$). The experiments have been carried out in a tubular flow reactor, in the 700-1400 K temperature range. The concentrations of H_2S, SO_2 and H_2 have been determined and the experimental results have been simulated with a detailed chemical mechanism compiled in the present work. The experimental results obtained indicate that H_2S consumption is shifted to lower temperatures as the stoichiometry increases, starting at 925 K for reducing conditions and at 700 K for the most oxidizing ones. The model reproduces well, in general, the experimental data from the present work, and those from the literature at high pressures. Supported by theoretical calculations, the isomerization of HSOO to HSO_2 has been determined as an alternative and possible pathway to the final product SO_2, from the key $SH + O_2$ reaction.

© 2018 The Combustion Institute. Published by Elsevier Inc. All rights reserved.

Keywords: H_2S; Oxidation; Sour gas; PFR; Kinetic modeling

---

1. Introduction

Conventional natural gas, as well as different non-conventional fuel mixtures or biogas generated in anaerobic digestion, may contain different amounts of hydrogen sulfide (H_2S) in their composition. Additionally, hydrogen sulfide can also be found as a by-product from the oil industry, released from the pyrolysis of fuels containing sulfur, natural gas cleaning or in synthesis gas produced from gasification of coal and biomass. Due to the corrosive and harmful nature of hydrogen sulfide, streams containing H_2S are led to cleaning treatments (e.g., amine absorption) and sulfur recovery units, which convert hydrogen sulfide into sulfur through the Claus process. This process is divided in two reaction steps: in the first one (thermal step), H_2S undergoes a partial oxidation in air, and then in the second one, it reacts with SO_2 to form sulfur in the presence of a catalyst (catalytic step) [1–3].

---

* Corresponding author.
E-mail address: uxue@unizar.es (M.U. Alzueta).

https://doi.org/10.1016/j.proci.2018.05.005

1540-7489 © 2018 The Combustion Institute. Published by Elsevier Inc. All rights reserved.

As the energy demand increases worldwide, an efficient utilization of available natural resources is needed. The increasing importance of fuel sources, such as sour and shale gas (up to 30% of hydrogen sulfide content in volume), brings interest to the direct use of these fuels without the use of expensive cleaning treatments and to devote the main effort to the development of technologies and combustion processes [4]. The different fuel compositions, together with the presence of different combustion atmospheres, may affect the conversion of H_2S. In this context, it is interesting to be able to predict the most appropriate conditions for stable combustion at the desired temperatures, with minor pollutant emissions.

However, the oxidation steps chemistry of H_2S remains unknown in many aspects, and the available experimental data are limited. In 2000, Gardiner et al. [5] reviewed the significant progress in the understanding of the kinetics and mechanisms of the atmospheric oxidation chemistry of sulfur in the last decades, indicating the less effort placed on developing and understanding sulfur combustion kinetics. More recent studies have faced different combustions chemistry studies. For example, Bongartz and Ghoniem [6] developed an optimized mechanism to make predictions on the combustion behavior of sour gas under oxy-fuel conditions. In the same way, Cong et al. [2] developed a mechanism to assess the production of hydrogen through H_2S thermolysis for the Claus process. Despite these efforts, there is still a need for more accurate direct determination of several important rate constants as well as more validation data [6].

Additionally, there are also experimental works involving H_2S oxidation. For example, earlier investigations at high temperatures [7], H_2S mixtures explosion limit determinations [8], induction time measurements in reflected shock waves [9] or premixed flames [10], have been performed. Besides, recent researches in flow reactors, more related to this study, include the work of Zhou et al. [11], who performed experiments of H_2S oxidation in a flow reactor at atmospheric pressure, under fuel-lean conditions and in the temperature range of 950–1150 K. In another study, Song et al. [12] conducted experiments at high pressures (30–100 bar), evaluating the oxidation of H_2S under oxidizing and stoichiometric conditions, concluding that the combustion behavior depends strongly on the stoichiometry and pressure.

In this context, the present study aims to extend the results available in the literature related to H_2S conversion, and addresses the oxidation of H_2S under different stoichiometries, ranging from fuel-rich to fuel lean conditions. Experimental work in a tubular flow reactor at atmospheric pressure has been performed, in the temperature range of 700–1400 K. A kinetic model developed by our group, updated for this work, has been used to simulate the experimental results.

2. Experimental methodology

The experiments have been carried out in a quartz tubular flow reactor at atmospheric pressure. Only a brief experimental setup description is given here and a more detailed description can be found elsewhere [13]. The reactor has a reaction zone of 20 cm in length and 0.87 cm of internal diameter. Total flow rate in all experiments was 1 L (STP)/min, resulting in a gas residence time as a function of temperature of 194.6/T(K), in seconds. The reactor is placed in a three-zone electrically heated oven, ensuring a uniform temperature profile (± 5 K) along the reaction zone. Besides, heat release from chemical reactions is minimized by performing the experiments under highly diluted conditions and using nitrogen to balance. Gases from gas cylinders are led to the reactor in up to four separate streams, which are heated separately and mixed in cross flow at the reactor inlet. At the outlet of the reaction zone, using an external cooling air, the product gas is quenched. The flue gases are led to the analysis system previous pass through a condenser and a filter, that remove any possible residual solid and moisture, therefore a constant supply of clean dry combustion gases is delivered to the analyzers. The analysis instrumentation consists of a UV continuous analyzer for sulfur dioxide (SO_2) concentration measurements and a gas micro-chromatograph for H_2S and H_2 quantification. The uncertainty of the measurements is estimated within 5%.

3. Kinetic model

The experimental results were interpreted in terms of kinetic modeling, using an updated kinetic model based on earlier works by our group [14–16]. This updated model counted with a sub-set of sulfur chemistry reactions, but it was focused on SO_2 reactions. Therefore, additional hydrogen sulfide reactions have been added, taken mainly from the kinetic model by Song et al. for H_2S oxidation at high pressures [12]. The final reaction mechanism listing is included as supplementary material and can be obtained directly from authors. Modifications made in the present work are denoted as "present work: pw". As for thermochemical data, same sources as for the corresponding reactions were used. Calculations were carried out in the frame of Chemkin Pro with the PFR model [17].

Hydrogen sulfide reacts primarily with radicals like H, OH or HO_2 to form mainly SH radicals. In general, the reactions of H_2S with the radical pool have been determined either experimental and/or theoretically, and are known with certain confidence. The exception is the $H_2S + HO_2$ reaction, for which only an upper limit for the rate constant at room temperature is available [18]. This reaction has two different product channels: $H_2S + HO_2 \rightleftharpoons SH + H_2O_2$ and $H_2S + HO_2 \rightleftharpoons HSO + H_2O$. The uncertainty of the reaction kinetic parameters for the first channel and its high sensitivity have been previously mentioned elsewhere, especially in high-pressure works, where HO_2 radicals are expected to play a major role [12,19,20]. Scarce data referred to this reaction are available in the literature. There is also an experimental determination at room temperature for the reverse channel producing $SH + H_2O_2$ [21]. Available theoretical calculations include those by Zhou et al. [11] for the reversible $H_2S + HO_2 \rightleftharpoons SH + H_2O_2$ reaction, which was then lowered by a factor of 2 by Mathieu et al. [20], and calculations by Batiha et al. [22], indicating a much lower rate constant value. The recent work of Gersen et al. [19] on the effect of H_2S addition to methane ignition and oxidation at high pressures also identified the $H_2S + HO_2$ reaction to be important and claimed for the need of an accurate determination of its rate constant. Calculations in the present work were very sensitive to this reaction, in particular to the $SH + H_2O_2$ channel, and thus their kinetic parameters were estimated in the present work as $5 \cdot 10^{12}$ cm^3/mol s for the reverse reaction, i.e., $SH + H_2O_2 \rightleftharpoons H_2S + HO_2$. This estimation agrees well with the high temperature data of Zhou et al. [11] and Mathieu et al. [20], while it is considerably higher than the value of Friedl et al. [21], experimentally characterized at 298 K. The impact of this important reaction is further discussed in the "Results and discussion" section.

H_2S conversion mainly produces SH radicals. Subsequently such a diatom reacts and intermediate species are formed. This is considered as a key reaction step in the bibliography for H_2S combustion. Particular attention has been devoted to the $SH + O_2$ reaction [11,12,19,23,24] and significant differences concerning the rate constants and product channels of the $SH + O_2$ reaction have been reported in the literature. Stachnik and Molina [25] provided an upper limit rate constant for this reaction at 298 K of $2 \cdot 10^5$ cm^3/mol s. This reaction has been largely studied theoretically [11,26–29] and several product channels have been proposed, i.e., $HSO + O$, $S + HO_2$, and $SO + OH$.

Zhou and coworkers [11], in their atmospheric pressure study, indicated that the production of $SO + OH$ predominates at temperatures below 1000 K, while the formation of $HSO + O$ is the main pathway above this temperature. As will be seen later, these reactions are not very important for the conditions of the present work. Garrido et al. [26], in a high level ab initio study of the HSO_2 system, identified a new reaction channel for the $SH + O_2$ reaction, which would produce the preferred $SO_2 + H$ channel, via the HSO_2 intermediate. Song et al. [12] determined the kinetic parameters for the $SH + O_2 \rightleftharpoons SO_2 + H$ reaction through ab initio calculations, obtaining a rate constant of $1.5 \cdot 10^5 \cdot T^{2.1} \cdot e^{(-11{,}020/RT)}$ (cal, mol, cm^3, s). The inclusion of this reaction and corresponding kinetic parameters in the mechanism does not have any effect in the calculations under the conditions of the present work. Freitas et al. [27] mentioned that the connection between the intermediate structures, HSOO and HSO_2, takes place via an HSOO* isomer in an electronic excited state. HSOO has been reported to be formed in the $SH + O_2(+M) \rightleftharpoons HSOO(+M)$ reaction [26–30], while in some of these works the formation of HSO_2 and HOSO was considered to be inaccessible directly from $SH + O_2$. The fate of HSOO may include dissociation to $HSO + O$, but this reaction has been reported to have a significant energy threshold [28], and thus is not competitive. Following the work of Ballester et al. [31], where they studied the $SH + O_2$ reaction through quasi-classical trajectory (QCT) methods, HSOO may be considered to isomerize to HSO_2. Taking into account the barrier for HSO_2 formation determined by Freitas et al. [27], we assume an activation energy of 21.3 kcal/mol for the HSOO to HSO_2 isomerization. In this work, a reaction rate of $10^{17} \cdot e^{(-21{,}300/RT)}$(cal, mol, cm^3, s) has been proposed for this reaction. The impact of this assumption will be discussed later.

Table 1
Experimental conditions.

Set	H_2S (ppm)	O_2 (ppm)	λ
1	476	225	0.32
2	509	750	0.98
3	485	900	1.24
4	482	1500	2.07
5	492	3750	5.08
6	514	15000	19.46

4. Results and discussion

The study of H_2S oxidation in a tubular flow reactor at atmospheric pressure from fuel-lean to fuel-rich conditions, in the temperature range of 700–1400 K, has been carried out. The experimental conditions are listed in Table 1. The influence of the amount of oxygen available on the process was studied for different values of λ, defined as O_2(real)/O_2(stoichiometric). For an inlet total flow rate of 1 L (STP)/min, the gas residence time in the reactor varies in the 0.14–0.24 s range.

For the conditions listed in Table 1, the concentrations of H_2S, SO_2 and H_2 obtained as a function of temperature are presented in Fig. 1. Symbols represent experimental data and lines model predictions using the mechanism compiled in this work. As seen, modeling predictions agree fairly well with the experimental data. Additionally, experimental sulfur mass balances

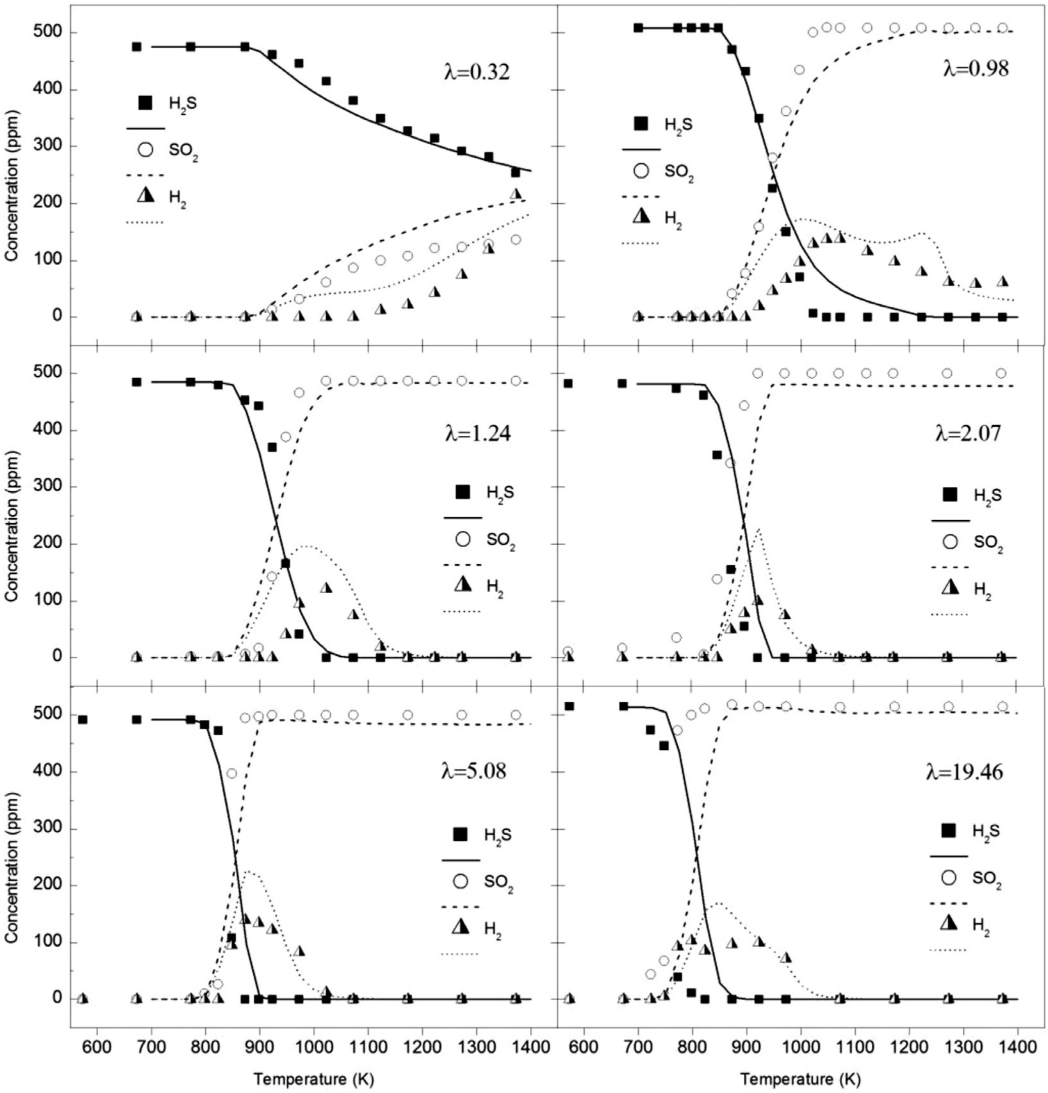

Fig. 1. Experimental results from H_2S oxidation in conditions of sets 1–6 in Table 1. Symbols represent experimental data and lines model predictions.

are shown in the supplementary material (Fig. S1), being close to 100% (±5 %) in most cases.

Hydrogen sulfide starts to react at 925 K under reducing conditions ($\lambda = 0.32$), with lower temperatures for the onset of H_2S consumption as the stoichiometry increases, dropping to 700 K for the highest oxygen concentration used ($\lambda = 19.46$). The onset of H_2S conversion is coincident with the onset for hydrogen and sulfur dioxide formation. H_2S is fully converted into SO_2 at high temperatures, except for the case of $\lambda = 0.32$, due to the lack of oxygen. Such a result was also observed in [32], where H_2S was neither consumed by the oxygen available nor by thermolysis. Under similar experimental conditions ($O_2/H_2S = 0.35$, 1375 K, $t_r = 150$ ms), but using 10% H_2S, Palma et al. [32] obtained 70% of H_2S conversion versus our 52% ($O_2/H_2S = 0.47$, 1375 K, $t_r = 140$ ms, 0.05% H_2S).

For $\lambda \geq 1$, when almost all H_2S is converted to SO_2, the H_2 formed starts to vanish. This was also observed by Zhou et al. [11], who mentioned that H_2 selectivity presents a maximum with the last traces of H_2S. The two maxima, observed for $\lambda = 0.98$ in H_2 predictions, are found to occur in the modeling by the concurrent formation and consumption of H_2. Hydrogen is formed mainly from H_2S and consumed by reaction with O/OH radicals. Once H_2S is fully consumed, the H_2 levels start to decrease at high temperatures.

A diagram showing the main reaction pathways is described in Fig. S2 of the supplementary material. Solid lines represent reaction paths at all stoichiometries, with the important species connected by thick arrows, and dashed lines correspond to additional reactions important only under reducing conditions. The most relevant pathways for H_2S oxidation show that the addition and modification of the reactions made in this work have a significant relevance in the oxidation behavior.

Calculations indicate that H_2S reacts with the radical pool (H, OH and HO_2), but primarily with H radicals, to rapidly form SH, independently of the stoichiometry. SH continues the reaction with O_2 to form mainly HSOO (R1), which isomerizes to HSO_2 (R2).

$$SH + O_2\ (+M) \rightleftharpoons HSOO\ (+M) \quad (R1)$$

$$HSOO \rightleftharpoons HSO_2 \quad (R2)$$

Then, HSO_2 is branched to HOSO (R3) or to the final product SO_2 through (R4) and (R5), this last one under highly oxidizing conditions. HOSO, as well as HSO_2, can dissociate or react with oxygen (R6, R7). The reaction paths with S, SO and HS_2 radicals are quite similar to the ones identified by Zhou et al. [11], but less important in the present mechanism.

$$HSO_2\ (+M) \rightleftharpoons HOSO\ (+M) \quad (R3)$$

$$HSO_2\ (+M) \rightleftharpoons H + SO_2 \quad (R4)$$

$$HSO_2 + O_2 \rightleftharpoons SO_2 + HO_2 \quad (R5)$$

$$HOSO\ (+M) \rightleftharpoons SO_2 + H\ (+M) \quad (R6)$$

$$HOSO + O_2 \rightleftharpoons SO_2 + HO_2 \quad (R7)$$

The reaction process is maintained primarily by cause of H radicals released in the final step (R4), which maintain the consumption of H_2S through (R8), together with HO_2 radicals formed in (R7), which react with H_2S through (R9). Reaction (R9) becomes more important as the oxygen concentration increases, due to the major occurrence of (R5) and the increase in HO_2 concentration. The H_2O_2 radicals formed in (R9) decompose to OH radicals through (R10), promoting H_2S consumption through (R11).

$$H_2S + H \rightleftharpoons SH + H_2 \quad (R8)$$

$$H_2S + HO_2 \rightleftharpoons SH + H_2O_2 \quad (R9)$$

$$H_2O_2\ (+M) \rightleftharpoons OH + OH\ (+M) \quad (R10)$$

$$H_2S + OH \rightleftharpoons SH + H_2O \quad (R11)$$

The production of HO_2 radicals through (R5) and (R7) makes reactions with this kind of radicals to become important, as for example (R9), which was found, together with (R2), to be the most sensitive under our experimental conditions at all stoichiometries. Figure S3 in the supplementary material shows, as an example, the sensitivity analysis for SO_2, obtained for $\lambda = 5.08$ at 823 K. Calculations indicate that the results are sensitive to the $SH + H_2O_2 \rightleftharpoons H_2S + HO_2$ reaction (-R9), which appears always as one of the top five most sensitive reactions. Therefore, we can confirm the necessity of having a good determination of the kinetic parameters of this reaction for an accurate modeling description. Results are also sensitive to the HSOO $\rightleftharpoons HSO_2$ reaction (R2), which has been proposed to occur and is included in the present mechanism. The impact of modifying the rate for (R2) is shown in Figs. S4 and S5 of the SM. Calculations indicate the necessity of including reaction (R2) in the model, even though the impact of varying the rate for (R2) is appreciable but not very significant.

Under reducing conditions, the consumption of H_2S follows the main reaction paths discussed in previous paragraphs. However, due to the lack of oxygen, other important species, such as H_2S_2, HS_2 and S_2, can be formed. S_2 can be produced through the sequence of reactions with SH (R12-R15), which self-reacts (R12) and forms HS_2, as well as with H_2S_2 (R13) formed by (R14). Finally, the HS_2 radical converts to S_2 through (R15). In the experiment carried out in the present work under reducing conditions, $\lambda = 0.32$, a yellow deposit was seen at the outlet of the reactor. In this experiment, for high temperatures, the mass balance for sulfur, which is calculated by adding the concentrations of H_2S and SO_2 measured at the reactor outlet, did not close, Fig. S1. Such unbalance can be explained by the presence of the yellow deposit, presumably S_2. The apparition of this deposit was also previously mentioned by Zhou et al. [11] and was attributed to the formation of S_2 in the gas phase, which condenses when exhaust gases are quenched.

$$SH + SH \rightleftharpoons HS_2 + H \quad (R12)$$

$$SH + H_2S_2 \rightleftharpoons HS_2 + H_2S \quad (R13)$$

$$HS_2 + HO_2 \rightleftharpoons H_2S_2 + O_2 \quad (R14)$$

$$HS_2 + SH \rightleftharpoons S_2 + H_2S \quad (R15)$$

In order to evaluate the model compiled in this work, we have performed simulations of literature results. In particular, we have simulated the flow reactor results from Song et al. [12] and Gersen et al. [19] of H_2S conversion at high pressures, where HO_2 radicals are important, and thus the impact of

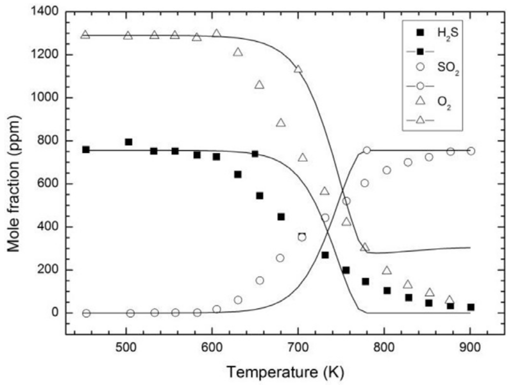

Fig. 2. Comparison of experimental data (symbols) of Song et al. [12] and simulations (lines) with the model developed in the present work. Stoichiometric conditions at 30 bar. Inlet composition: 756 ppm H_2S, 1290 ppm O_2, balance N_2 ($\lambda = 1.14$). The residence time in the isothermal zone is calculated from t_r (s) = 3520/T (K).

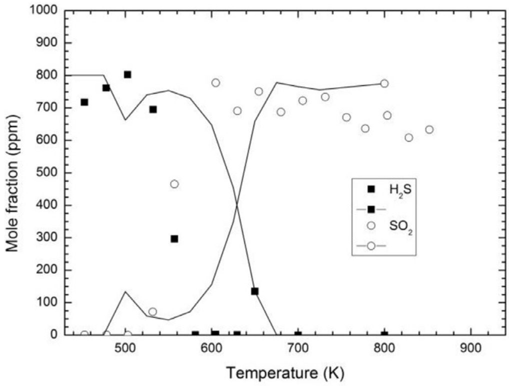

Fig. 3. Comparison of experimental data (symbols) of Song et al. [12] and simulations (lines) with the model developed in the present work. Oxidizing conditions at 30 bar. Inlet composition: 801 ppm H_2S, 4.4% O_2, balance N_2 ($\lambda = 36$). The residence time in the isothermal zone is calculated from t_r (s) = 3100/T (K).

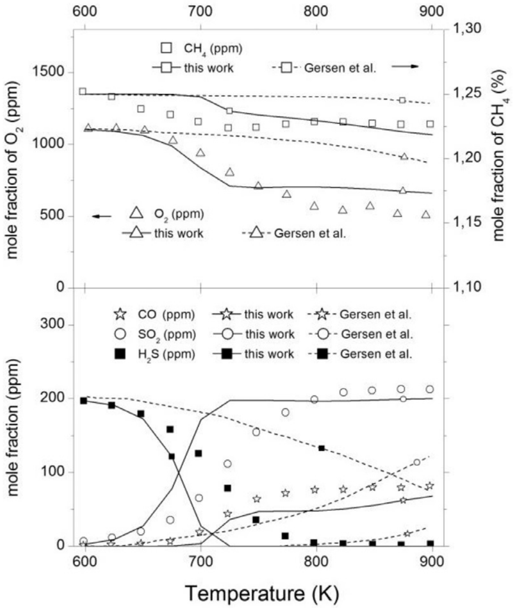

Fig. 4. Comparison between experimental data of Gersen et al. [19] (symbols) and model predictions (lines). Experiments with CH_4/H_2S in a flow reactor at 50 bar. Inlet composition: 1.25% CH_4, 1110 ppm of O_2, 200 ppm of H_2S, and balance N_2. The gas residence time is calculated as t_r(s) = 5990/T (K).

(-R9) and its rate estimation may potentially be important. The simulation results are shown in Figs. 2 and 3 for the experiments of Song et al. [12] (stoichiometric and oxidizing conditions at 30 bar), and in Fig. 4 for the experiment of Gersen et al. [19] of H_2S/CH_4 oxidation (reducing conditions at 50 bar). In general, the present model reproduces well the main trends, and actually improves the previous predictions of the experimental results. The present simulation results are very similar to those obtained by Song et al. [12] under stoichiometric conditions, meanwhile, under oxidizing conditions, the authors were able to approximate the simulation results to experimental ones by suppressing two reactions involving O_3 (R16 the most important one and R17), proposed by Mousavipour et al. [33]. The model in the present work keeps these reactions, which are found to be indeed important under the experimental conditions of Song et al. [12]. Reaction (R17) is a source of ozone and H_2S consumes it through (R16). Despite the scatter in the experimental SO_2 concentrations reported by Song et al. [12], the main trends in SO_2 evolution can be seen. Although, the simulation in Fig. 3 is 50 K shifted to higher temperatures compared to the experimental results, it is worthwhile to mention that the mechanism is able to reproduce the diminution in the observed H_2S mole fraction (ca. 480 K). Calculations indicate that the mentioned decrease between approximately 480 and 540 K occurs through the interaction between H_2S and O_3 (R16), which is the dominant consumption reaction of H_2S at these temperatures. Above 500 K, reaction (R16) becomes less important because of the decrease in the O_3 concentration, and H_2S conversion proceeds mainly through reaction (R9).

$$H_2S + O_3 \rightleftharpoons SO_2 + H_2O \qquad \text{(R16)}$$

$$SH + O_2 + O_2 \rightleftharpoons HSO + O_3 \qquad \text{(R17)}$$

Figure 4 includes the simulation results of both the model of Gersen et al. [19] and the present model at 50 bar. Simulation of the combustion behavior of CH_4/H_2S and formation of products is improved with the present mechanism, which predicts well the tendencies. Under these conditions, H_2S reacts to SO_2 through the SH reaction channel (R1 and R2). In the case of CH_4/H_2S oxidation, the model predicts that CO starts to be formed when H_2S is almost consumed, although experimentally this happens earlier. This might be due to the lack of reactions in the present mechanism describing the interaction between CH_4 and H_2S or to a non appropriate value for the kinetic parameters of the reaction of H_2S with the CH_3OO peroxide, which were estimated to be the same as in the reverse $H_2S + HO_2$ reaction (-R9) by Zhou et al. [11], and mentioned by the authors to be important [19].

5. Conclusions

Oxidation of H_2S at atmospheric pressure has been studied under different reaction atmospheres, varying the air excess ratio (λ) from reducing ($\lambda = 0.32$) to oxidizing conditions ($\lambda = 19.46$). The experiments were carried out in a tubular flow reactor, in the 700–1400 K temperature range and concentrations of H_2S, SO_2 and H_2 were determined. A detailed kinetic mechanism for the conversion of H_2S under the present conditions has been developed, evidencing the importance of given reactions, like the interaction of SH radicals with the radical pool and oxygenated species, such as O_2 and H_2O_2. This mechanism has been used to simulate the experimental results obtained in the present work, together with data from the literature, obtaining a fairly good agreement under the different conditions. The changes in the mechanism included the addition of reaction ($HSOO \rightleftharpoons HSO_2$), supported by recent theoretical works, as a key step in a faster reaction path of SH oxidation, and modification of ($SH + H_2O_2 = H_2S + HO_2$) kinetic parameters, which has a significant impact on the reaction pathways of H_2S oxidation. The main reactions governing the conversion of H_2S have been identified, together with the necessity for a better determination of the kinetic parameters of important reactions, including the isomerization of HSOO into HSO_2 and the interaction of H_2S with HO_2. This work supports the evolution of $SH + O_2$ reaction through HSOO to HSO_2 isomerization.

Acknowledgments

The authors express their gratitude to Aragón Government and European Social Fund (GPT group), and to MINECO and FEDER (Project CTQ2015-65226 and grant BES-2016-076610) for financial support.

Supplementary materials

Supplementary material associated with this article can be found, in the online version, at doi:10.1016/j.proci.2018.05.005.

REFERENCES

[1] M. Binoist, B. Labégorre, F. Monnet, et al., *Ind. Eng. Chem. Res.* 42 (2003) 3943–3951.

[2] T.Y. Cong, A. Raj, J. Chanaphet, S. Mohammed, S. Ibrahim, A. Al Shoaibi, *Int. J. Hydrogen Energy* 41 (2016) 6662–6675.

[3] W.D. Monnery, K.A. Hawboldt, A. Pollock, W.Y. Svrcek, *Chem. Eng. Sci.* 55 (2000) 5141–5148.

[4] US Department of Energy, *Report of Basic Research Needs for Clean and Efficient Combustion of 21st Century Transportation Fuels*, US Department of Energy, 2006.

[5] W.C. Gardiner, *Gas-phase Combustion Chemistry* (Ed.), Springer, New York, 2000.

[6] D. Bongartz, A.F. Ghoniem, *Combust. Flame* 162 (2015) 544–553.

[7] C.F. Cullis, M.F.R. Mulcahy, *Combust. Flame* 18 (1972) 225–292.

[8] R. Pahl, K. Holtappels, *Chem. Eng. Technol* 28 (2005) 746–749.

[9] M. Frenklach, J.H. Lee, J.N. White, W.C. Gardiner, *Combust. Flame* 41 (1981) 1–16.

[10] H. Selim, S. Ibrahim, A. Al Shoaibi, A.K. Gupta, *Appl. Energy* 113 (2014) 1134–1140.

[11] C.R. Zhou, K. Sendt, B.S. Haynes, *Proc. Combust. Inst.* 34 (2013) 625–632.

[12] Y. Song, H. Hashemi, J.M. Christensen, C. Zou, B.S. Haynes, P. Marshall, P. Glarborg, *Int. J. Chem. Kinet* 49 (2017) 37–52.

[13] M.U. Alzueta, R. Bilbao, M. Finestra, *Energy Fuels* 15 (2001) 724–729.

[14] M.U. Alzueta, R. Bilbao, P. Glarborg, *Combust. Flame* 127 (2001) 2234–2251.

[15] M. Abián, Á. Millera, R. Bilbao, M.U. Alzueta, *Fuel* 159 (2015) 550–558.

[16] M. Abián, M. Cebrián, Á. Millera, R. Bilbao, M.U. Alzueta, *Combust. Flame* 162 (2015) 2119–2127.

[17] CHEMKIN-PRO 15131, Reaction Design, 2013.

[18] A. Mellouki, A.R. Ravishankara, *Int. J. Chem. Kinet.* 26 (1994) 355–365.

[19] S. Gersen, M. van Essen, H. Darmeveil, et al., *Energy Fuels* 31 (2017) 2175–2182.

[20] O. Mathieu, F. Deguillaume, E.L. Petersen, *Comb. Flame* 161 (2014) 23–36.

[21] R.R. Friedl, W.H. Brune, J.G. Anderson, *J. Phys. Chem.* 89 (1985) 5505–5510.

[22] M. Batiha, M. Altarawneh, M. Al-Harahsheh, I. Altarawneh, S. Rawadieh., *Comput. Theor. Chem.* 970 (2011) 1–5.

[23] K. Tsuchiya, K. Kamiya, H. Matsui, *Int. J. Chem. Kinet.* 29 (1997) 57–66.

[24] F.G. Cerru, A. Kronenburg, R.P. Lindstedt, *Combust. Flame* 146 (2006) 437–455.

[25] R.A. Stachnik, M.J. Molina, *J. Phys. Chem.* 91 (1987) 4603–4606.

[26] J.D. Garrido, M.Y. Ballester, Y. Orozco-González, S. Canuto, *J. Phys. Chem. A* 115 (2011) 1453–1461.

[27] G.N. Freitas, J.D. Garrido, M.Y. Ballester, M.A.C. Nascimiento, *J. Phys. Chem. A* 116 (2012) 7677–7685.

[28] A. Goumri, J.-D.R. Rocha, D. Laakso, C.E. Smith, P. Marshall, *J. Phys. Chem. A* 103 (1999) 11328–11335.

[29] A. Goumri, D. Laakso, J.D.R Rocha, C.E. Smith, P. Marshall, *J. Chem. Phys.* 102 (1995) 161–169.

[30] C. Zhou, K. Sendt, B.S. Haynes, *J. Phys. Chem. A* 113 (2009) 2975–2981.

[31] M.Y. Ballester, Y.O. Guerrero, J.D. Garrido, *Int. J. Quantum Chem.* 108 (2008) 1705–1713.

[32] V. Palma, V. Vaiano, D. Barba, et al., *Int. J. Hydrog. Energy* 40 (2015) 106–113.

[33] S.H. Mousavipour, M. Mortazavi, O. Hematti, *J. Phys. Chem. A* 117 (2013) 6744–6756.

SUPPLEMENTARY MATERIAL

H_2S conversion in a tubular flow reactor. Experiments and kinetic modeling

J.M. Colom-Díaz, M. Abián, M.Y. Ballester, Á. Millera, R. Bilbao, M.U. Alzueta

Aragón Institute of Engineering Research (I3A). Department of Chemical and Environmental Engineering, University of Zaragoza, 50018 Zaragoza, Spain.

Table of contents:

1) **Sulfur mass balance of the experiments**

   Figure S1. Sulfur mass balances as a function of temperature for the set of experiments (1-6) in Table 1.

2) **Reaction pathways**

   Figure S2. Reaction pathways for H_2S oxidation under the conditions studied.

3) **Sensitivity analysis for SO_2**

   Figure S3. Sensitivity coefficients for SO_2 in conditions of set 5 in Table 1: λ=5.08, T = 823 K.

4) **Modeling calculations modifying R2 ($HSOO \rightleftharpoons HSO_2$)**

   Figure S4. Modeling calculations with the present model, multiplying the pre-exponential factor of R2 reaction by 2, and without R2 reaction, for stoichiometric conditions (λ=0.98). Solid lines show the original model results, dashed lines show predictions changing the R2 rate and dotted lines show predictions suppressing R2.

   Figure S5. Modeling calculations with the present model, multiplying the pre-exponential factor of R2 reaction by 2, and without R2 reaction, for oxidizing conditions (λ=5.08). Solid lines show the original model results, dashed lines show predictions changing R2 rate and dotted lines show predictions suppressing R2.

1) Sulfur mass balance of the experiments

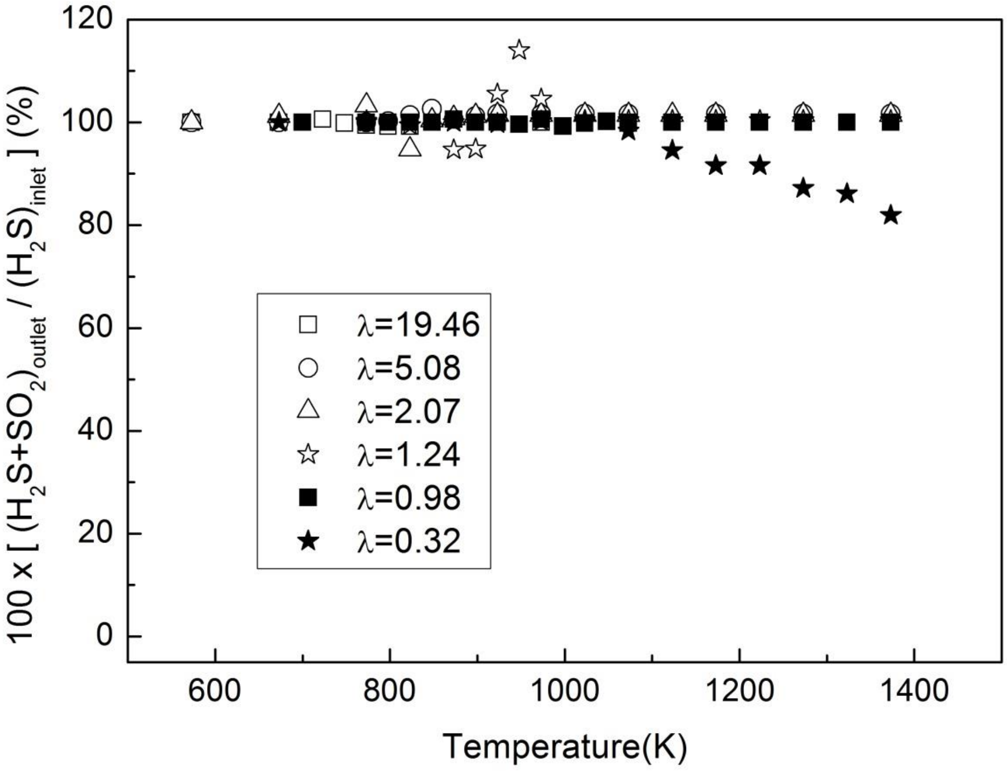

Figure S1. Sulfur mass balances as a function of temperature for the set of experiments (1-6) in Table 1.

2) Reaction pathways

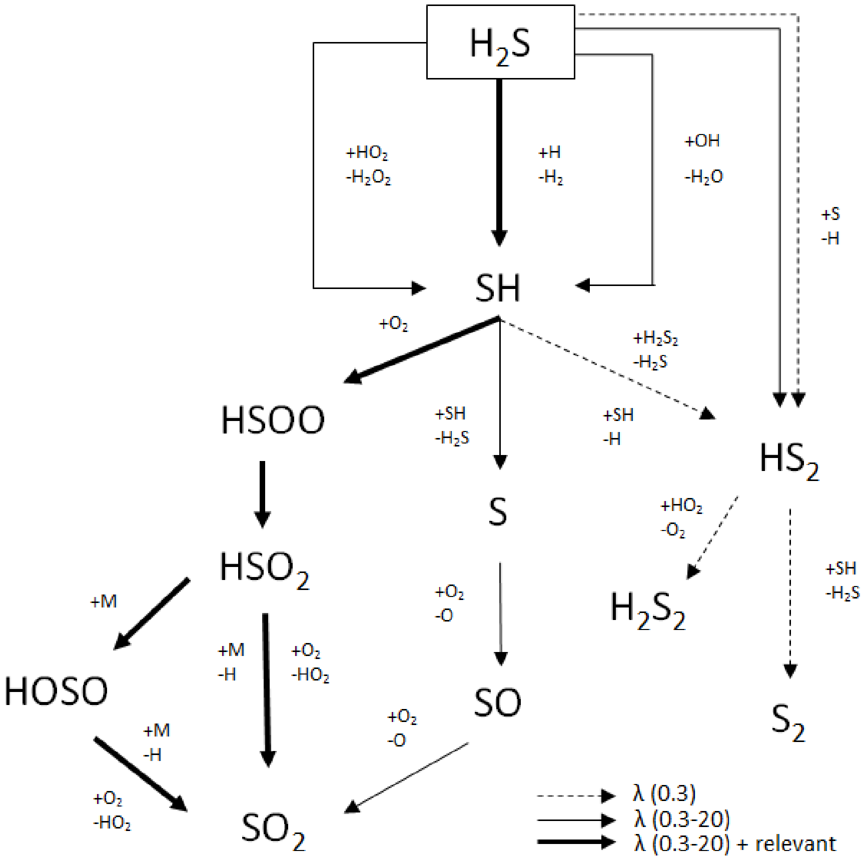
H₂S
+HO₂
-H₂O₂
+H
-H₂
+OH
-H₂O
+S
-H
SH
+O₂
+H₂S₂
-H₂S
HSOO
+SH
-H₂S
+SH
-H
HS₂
S
+HO₂
-O₂
HSO₂
+O₂
-O
+SH
-H₂S
H₂S₂
+M
+M
-H
+O₂
-HO₂
HOSO
SO
S₂
+M
-H
+O₂
-O
+O₂
-HO₂
SO₂
λ (0.3)
λ (0.3-20)
λ (0.3-20) + relevant

Figure S2. Reaction pathways for H_2S oxidation under the conditions studied.

3) Sensitivity analysis for SO_2

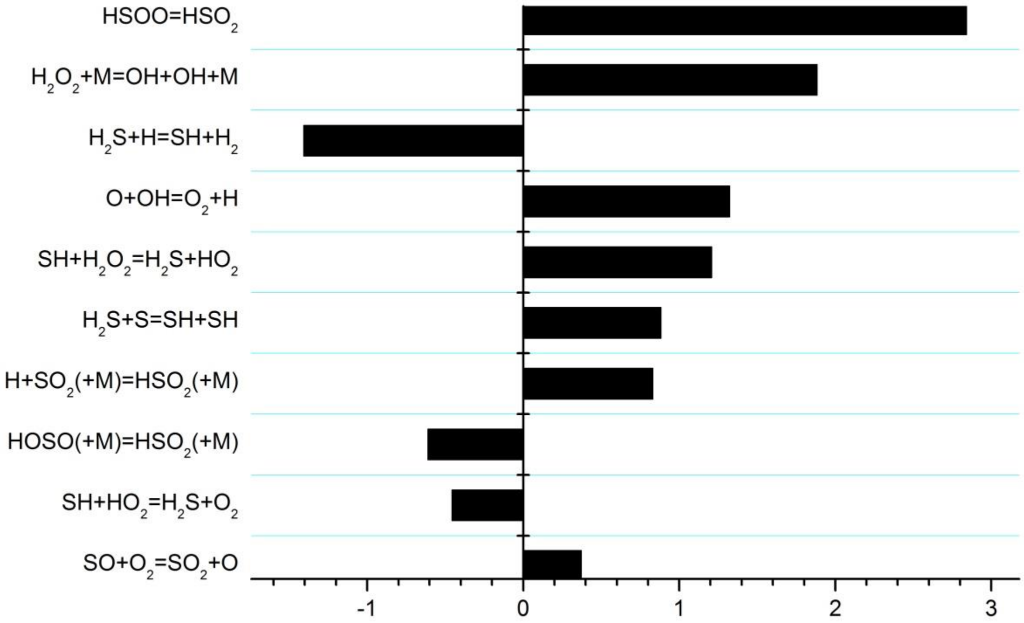

Figure S3. Sensitivity coefficients for SO_2 in conditions of set 5 in Table 1: λ=5.08, T = 823 K.

4) Modeling calculations modifying R2 (HSOO⇌HSO_2)

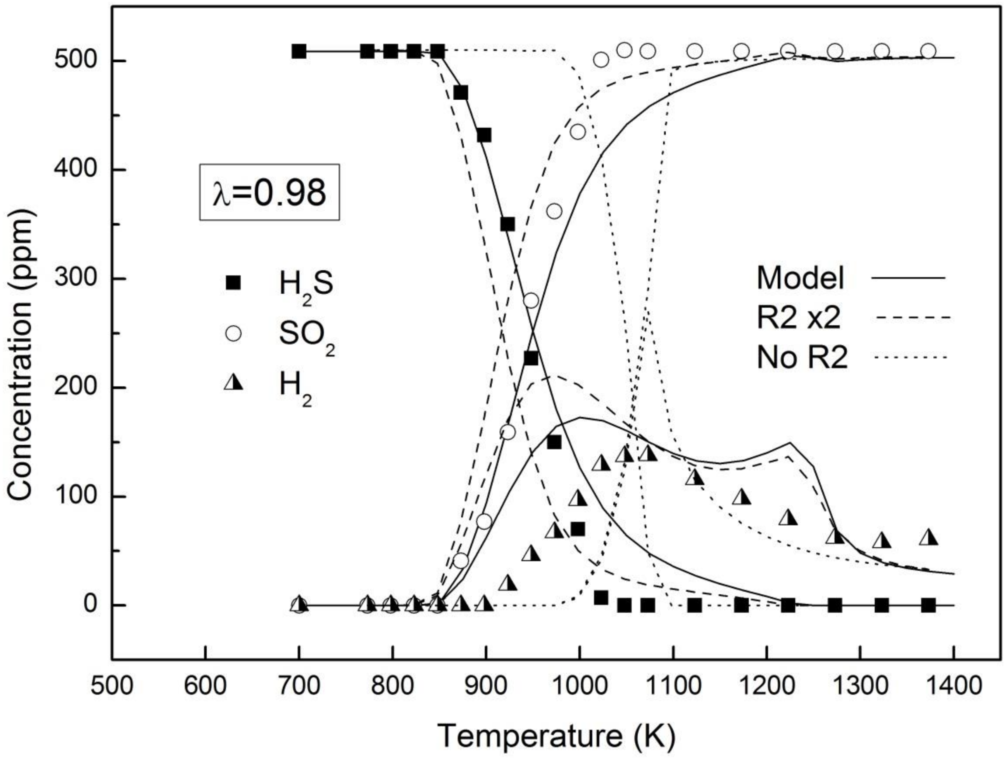

Figure S4. Modeling calculations with the present model, multiplying the pre-exponential factor of R2 reaction by 2, and without R2 reaction, for stoichiometric conditions (λ=0.98). Solid lines show the original model results, dashed lines show predictions changing the R2 rate and dotted lines show predictions suppressing R2.

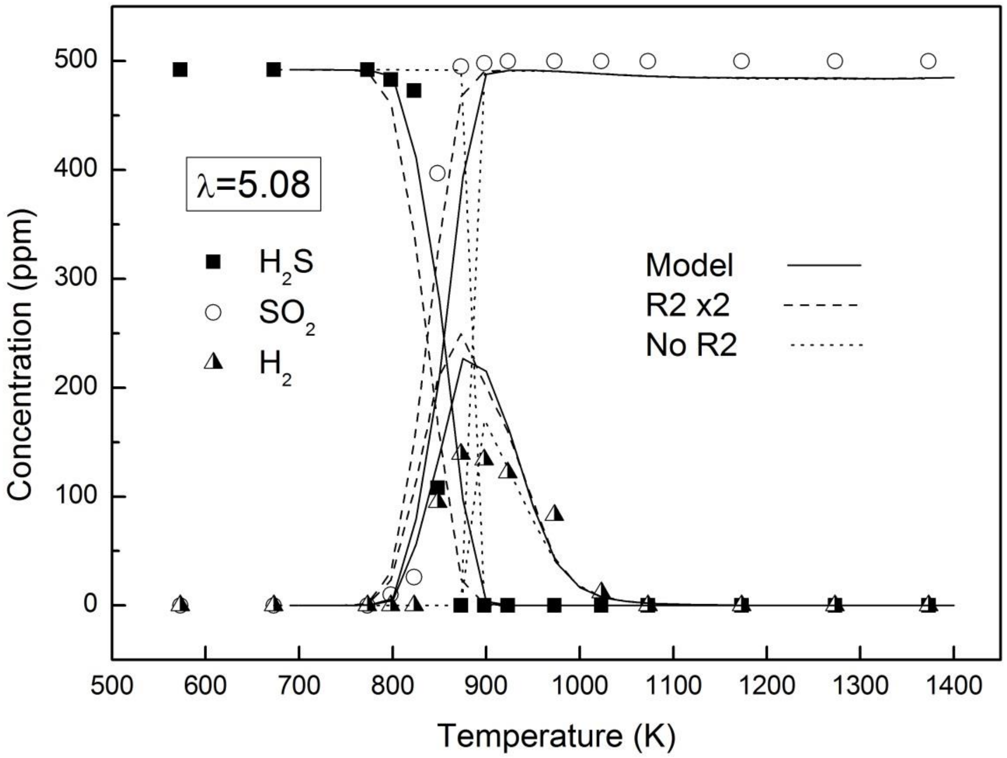

Figure S5. Modeling calculations with the present model, multiplying the pre-exponential factor of R2 reaction by 2, and without R2 reaction, for oxidizing conditions (λ=5.08). Solid lines show the original model results, dashed lines show predictions changing R2 rate and dotted lines show predictions suppressing R2.

Article II

Colom-Díaz, J.M.; Millera, Á.; Bilbao, R.; Alzueta, M.U. (2019). High pressure study of H_2 oxidation and its interaction with NO. *International Journal of Hydrogen Energy* 44, 6325-6332.

INTERNATIONAL JOURNAL OF HYDROGEN ENERGY 44 (2019) 6325–6332

Available online at www.sciencedirect.com

ScienceDirect

journal homepage: www.elsevier.com/locate/he

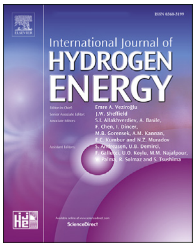

High pressure study of H_2 oxidation and its interaction with NO

J.M. Colom-Díaz, Á. Millera, R. Bilbao, M.U. Alzueta*

Aragón Institute of Engineering Research (I3A). Department of Chemical and Environmental Engineering, University of Zaragoza, C/Mariano Esquillor s/n, 50018 Zaragoza, Spain

A R T I C L E I N F O

Article history:
Received 5 December 2018
Received in revised form
8 January 2019
Accepted 13 January 2019
Available online 6 February 2019

Keywords:
Hydrogen oxidation
NO_x Interaction
Flow reactor
High pressure

A B S T R A C T

The present study deals with the oxidation of H_2 at high pressure and its interaction with NO. The high pressure behavior of the $H_2/NO_x/O_2$ system has been tested over a wide range of temperatures (500–1100 K) and different air excess ratios ($\lambda = 0.5$–6.4). The experiments have been carried out in a tubular flow reactor at 10, 20 and 40 bar NO has been found to promote H_2 oxidation under oxidizing conditions, reacting with HO_2 radicals to form the more active OH radical, which enhances the conversion of hydrogen. The onset temperature for hydrogen oxidation, when doped with NO, was approximately the same at all stoichiometries at high pressures (40 bar), and shifted to higher temperatures as the pressure decreases. The experimental results have been analyzed with an updated kinetic model. The reaction $NO + NO + O_2 \rightleftharpoons NO_2 + NO_2$ has been found to be important at all conditions studied and its kinetic parameters have been modified, according to its activation energy uncertainty. Furthermore, the kinetic parameters of reaction$HNO + H_2 \rightleftharpoons NH + H_2O$ have been estimated, in order to obtain a good prediction of the oxidation behavior of H_2 and NO conversion under reducing conditions. The kinetic model shows a good agreement between experimental results and model predictions over a wide range of conditions.

© 2019 Hydrogen Energy Publications LLC. Published by Elsevier Ltd. All rights reserved.

Introduction

Hydrogen has been taking attention in the last decades because of its potential as fuel. Due to its high energetic value per mass unit and its almost inexistent contribution to pollution, H_2 is seen as an attractive option [1], although the problem with its high transportation cost makes difficult hydrogen storage. Solutions like ammonia as a hydrogen carrier [2,3] or on-board reforming of hydrocarbon fuels [4] have emerged to deal with the hydrogen storage issue. Efforts are being undertaken on the development of high pressure combustion systems [5], what has created the need of kinetic models validated in these high pressure conditions and the target of increasing their efficiency. The H_2/O_2 sub-mechanism is the basis in the kinetic models of hydrocarbons oxidation and NO_x formation, being studied in the past years in some works [6–9], but despite being a reliable subset of reaction, uncertainty towards the determination of precise rate constants still exists. Miller et al. [10] mentioned that repeated direct measurements of the rate parameters of important reactions, even performed independently by several groups, did not decrease the uncertainty of the rate coefficients below a certain limit, as happens for reaction $H +$

---

* *Corresponding author.*
E-mail address: uxue@unizar.es (M.U. Alzueta).

https://doi.org/10.1016/j.ijhydene.2019.01.078
0360-3199/© 2019 Hydrogen Energy Publications LLC. Published by Elsevier Ltd. All rights reserved.

$O_2 \rightleftharpoons OH + O$ and reaction $H + O_2 + M \rightleftharpoons HO_2 + M$, where a 30% and 50% uncertainty in their kinetic parameters was estimated, respectively. Hence, new experimental data to validate kinetic models are valuable.

On the other hand, NO_x might be present in combustion processes, and they come from the conversion of the nitrogen in air atmospheres. Thermal NO is the most important source of NO_x in gas combustion and its formation is described by the Zeldovich mechanism [11,12]. While most of gas fuels (e.g. natural gas) don't have much nitrogen in their composition, in the case of the use of NH_3 as a new fuel, NO_x formation is feasible [13,14]. The advantages in transportation and storage versus H_2, together with the existing infrastructure to supply NH_3, and the fact that potentially can be fully turned into N_2 and H_2O, make ammonia a desirable option among other fuels for combustion purposes. However, apart from NO_x emissions, there are still issues related to this fuel that need a further research in terms of combustion characteristics, being its high ignition energy and its low flammability some of the drawbacks to tackle [15]. In this sense, some studies have proposed the use of other fuels like H_2 blended with NH_3 (till 50:50 ratios), to improve its oxidation behavior [14,16]. Besides, NH_3 combustion is not completely understood and some experimental issues are still barriers or unresolved. According to some sources [13,17], NH_3 has been reported to adsorb on stainless steel surfaces, as to decompose on given materials [18,19]. Thus, providing new experimental data for NH_3 conversion under different combustion conditions, and assuring a reliable kinetic model for the H_2/NO_x system seems important for addressing NH_3 oxidation.

Less conventional sources of NO_x in combustion processes might be the addition of alkyl-nitrates as cetane enhancers in diesel fuels [20] or the use of exhaust gas recirculation (EGR) [21], which recirculates NO_x back into the combustion chamber among other gases. EGR has been proved to reduce NO_x emissions in diesel engines due to a lower flame temperature but increasing CO and hydrocarbons (HC) emissions. On the other hand, the idea about the addition of H_2 into the intake mixture of a diesel engine with EGR has shown great potential in improving diesel engine performance and reducing NO_x and soot emissions [22,23]. However, determining the optimum amount of H_2 to add seems to be important to avoid concerns of pre-ignition, backfire, and other combustion problems such as the onset of knock.

Some studies have considered in the past the oxidation of H_2 doped with NO_x. Bromly et al. [24] studied it in a flow reactor at atmospheric pressure, finding that the presence of NO (0–400 ppm) promotes the oxidation of H_2 except for high concentrations of O_2 (22%). This work was extended by Mueller et al. [25], who perturbed the $H_2/O_2/N_2$ system with small amounts of NO at pressures and temperatures ranging from 10 to 14 atm and from 800 to 900 K, respectively, finding that the modeling results were highly sensitive to the $H+O_2+M \rightleftharpoons HO_2+M$ pressure-dependent reaction and recommending a kinetic expression for it. This reaction was also studied by Ashman and Haynes [26], who compared theoretical predictions and experimental concentration values of NO_2 in the H_2/O_2 system, allowing them to determine a rate constant and different third body efficiencies (N_2, H_2O, CO_2 and Ar). This reaction is considered to be important, due to the high number of reactions that become important at high pressures consuming HO_2 radicals.

Autoignition of H_2/air/NO_x mixtures has also been studied in some works. Slack and Grillo [27] tested the addition of both NO and NO_2 (0–4.5%) in a shock tube, in the pressure range of 0.27–2 atm, and temperature range of 800–1500 K, finding that the induction times were reduced up to more than an order of magnitude, compared to H_2 conversion in the absence of nitrogen oxides. Laster and Sojka [28] also studied this system, reaching the same conclusion as Slack and Grillo, i.e. the NO addition decreases ignition delay times until a concentration of about 0.5%, and above this concentration induction times are lengthened due to the scavenging of H atoms from NO. They concluded that the NO promoting effect is lessened as temperature rises and pressure decreases. More recently, Mathieu et al. [29] published ignition delay time measurements of $H_2/O_2/NO_2$ mixtures diluted in Ar using shock tube behind reflected shock waves, finding a strong dependency on pressure and NO_2 concentration, which needs thus to be carefully evaluated.

At high pressures, the NO/NO_2 interconversion becomes important, specially at low temperatures and high O_2 concentrations, where NO_2 presence is favoured. The presence of NO_x under engine-relevant conditions might influence notably the reactivity of the fuel, through a sequence of reactions in which NO and NO_2 convert less reactive peroxy radicals into more reactive OH and alkyloxy radicals [30]. Knowing accurately the amount of NO/NO_2 that interacts with the fuel seems to be an important task to approach. An important reaction determining the conversion of NO into NO_2 is $NO + NO + O_2 \rightleftharpoons NO_2 + NO_2$. In particular, in the case of premixed reactants feeding, this reaction may occur in the inlet section of the reactor, varying the initial concentration of NO_x chosen for the experiment, which needs thus to be carefully determined.

The present work addresses the oxidation of H_2 and its interaction with NO under high pressure conditions. For this purpose, different experiments of H_2 oxidation in the absence and presence of NO have been performed in a quartz tubular flow reactor at high pressure, studying the influence of temperature (500–1100 K) and manometric pressure (10, 20 and 40 bar), using different stoichiometries related to H_2 ($\lambda = 0.5$–6.4). The experimental conditions chosen are useful to validate a kinetic model for describing hydrogen oxidation, over a wide range of conditions that might occur in any high-pressure system where H_2 is oxidized and interacts with NO_x species.

Experimental

The experiments have been carried out in a high-pressure flow reactor set-up, which is described in detail elsewhere [31]. Testing different manometric pressures (10, 20 and 40 bar) and different stoichiometries in the temperature range of 500–1100 K, the oxidation of H_2 and its interaction with NO have been studied. Briefly, the set-up includes gas cylinders that supply the gases to the system, while mass flow controllers assure a total flow rate of 1 L (STP)/min. Gases used in this work (H_2, O_2 and NO) have been highly diluted in nitrogen

Table 1 – Experimental conditions. The total flow rate is balanced with N_2. Parameter λ_{H2} is calculated according to the reaction $H_2 + 1/2O_2 \rightleftharpoons H_2O$ and parameter λ_{NO} according to the reaction $NO + 1/2O_2 \rightleftharpoons NO_2$. The residence time is referred, as an example, to the entire set-up at one particular temperature in the isothermal zone of the reactor (875 K).

Set	P (bar)	H_2 (ppm)	NO (ppm)	λ_{H2}	λ_{NO}	t_r (s)	O_2 (ppm)
1	40	937	530	6.4	11.3	107	3000
2	20	935	517	6.4	11.6	56	3000
3	10	920	524	6.5	11.5	29	3000
4	40	1029	–	5.8	–	107	3000
5	20	930	–	6.4	–	56	3000
6	10	910	–	6.6	–	29	3000
7	40	–	521	–	11.5	107	3000
8	20	–	508	–	11.8	56	3000
9	10	–	514	–	11.7	29	3000
10	40	1022	485	0.98	2.1	107	500
11	20	1050	525	1.3	2.6	56	675
12	40	1024	535	0.5	0.9	107	250
13	20	1000	520	0.5	1	56	250

and different concentrations of oxygen have been tested. The experimental conditions are detailed in Table 1. The $H_2/NO/O_2$ system has been tested at different stoichiometries (oxidizing, stoichiometric and reducing atmospheres with respect to H_2, λ_{H2} in Table 1), while the comparison with the NO/O_2 and H_2/O_2 systems has been done only under oxidizing conditions. The reaction system included a quartz tubular reactor (inner diameter of 6 mm and 1500 mm in length) enclosed in a stainless-steel tube that acts as a pressure shell. The steel tube is placed horizontally in a tubular oven, with three individually controlled electrical heating elements that ensure an isothermal reaction zone of approximately 56 cm, with a uniform temperature profile (±10 K). The reactor temperature is monitored by type K thermocouples positioned between the quartz reactor and the steel shell. An example of the temperature profiles at 40 bar can be seen in Fig. 1. Gas residence time depends on pressure and temperature and it can be expressed as: $t_r[s] = 261.1$ P [bar]/T [K] in the isothermal zone of the reactor. The total gas residence time is calculated taking into account the temperature profiles in the experimental entire set-up. An example of the total gas residence time in the entire set-up is shown in Table 1, corresponding to a temperature of 875 K in the isothermal part of the reactor. Previously to the gas analysis systems, gases pass through a filter and a condenser to ensure gas cleaning and water-free content. Products are analyzed by a gas chromatograph equipped with thermal conductivity detector (TCD) to detect H_2 and a continuous chemiluminescence analyzer to detect NO and NO_2. The uncertainty of the measurements is estimated within 5%.

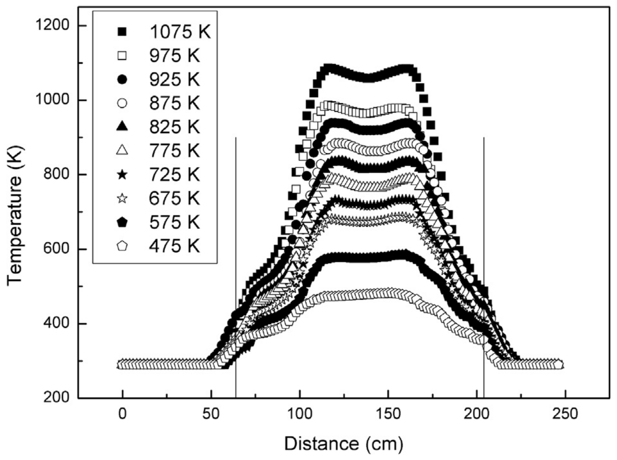

Fig. 1 – Temperature profiles in the entire experimental set-up at 40 bar, as a function of the set-up length. 0 cm corresponds to the point where the gases are premixed, while the reactor zone starts at 64 cm and ends at 204 cm.

Kinetic model

The experimental results have been interpreted in terms of kinetic modeling using Chemkin-PRO. The kinetic model used in this work is a revised and updated version of the work of Giménez-López et al. [32], who performed experiments of C_2H_4/NO mixtures at high pressure (60 bar) and different stoichiometries in a flow reactor. The subset for H_2/O_2 has been taken from the work of Hashemi et al. [8] on H_2 oxidation at high pressures in a flow reactor, which was based on the kinetic model developed by Burke et al. [6]. Thermodynamic data were taken from the same sources as the sub mechanisms.

Consumption of hydrogen can be described as a chain of reactions, being R1 the main step in the H_2 oxidation. Radicals HO_2 are formed due to the reaction of atomic H with oxygen through R2, then, are recombined to form H_2O_2 in R3. In the last step, R4, through H_2O_2 decomposition provides OH radicals for the consumption step R1 [8,25]. R5 is considered to be important for H_2 conversion initiation at all stoichiometries and found to be one of the most sensitive [8]. Kinetic parameters for this reaction were taken from Giménez-López et al. [32], because they are more updated values compared to the ones used in the H_2/O_2 sub-mechanism by Hashemi et al. [8] and provide a better modeling behavior in this work.

$$H_2 + OH \rightleftharpoons H_2O + H \tag{R1}$$

$$H + O_2(+M) \rightleftharpoons HO_2(+M) \tag{R2}$$

$$HO_2 + HO_2 \rightleftharpoons H_2O_2 + O_2 \tag{R3}$$

$$H_2O_2(+M) \rightleftharpoons OH + OH(+M) \tag{R4}$$

$$H_2O_2 + H \rightleftharpoons HO_2 + H_2 \tag{R5}$$

The competition between reactions R2 and R6 determines the generation of chain carriers in combustion of hydrogen, as well as of most hydrocarbons [33,34].

$$H + O_2 \rightleftharpoons O + OH \tag{R6}$$

In the present work, operating at high pressures, the H_2 oxidation behavior has been explained to happen under conditions dominated by reactions involving HO_2 and H_2O_2 (e.g. Ref. [8]). When NO is added to the system, the role of HO_2 as a chain terminator is changed, and HO_2 is consumed by NO in R7, forming NO_2 and OH. Then, NO_2 reacts with H radicals to give back NO and OH radicals (R8), forming a well known NO/NO_2 catalytic cycle, represented by R7 and R8 [24,25,27], with $HO_2 + H \rightleftharpoons OH + OH$ as net reaction.

$$NO + HO_2 \rightleftharpoons NO_2 + OH \tag{R7}$$

$$NO_2 + H \rightleftharpoons NO + OH \tag{R8}$$

In the work of Mathieu et al. [29] on ignition delay time measurements of $H_2/O_2/NO_2$ mixtures diluted with Ar, using shock tube behind reflected shock waves, a strong sensitivity of reaction R9 was found in their analysis. R9 is followed by the rapid decomposition of $HONO$ to NO and OH, promoting the overall oxidation of H_2. They used the kinetic parameters from Park et al. [35] for reaction R9.

$$NO_2 + H_2 \rightleftharpoons HONO + H \tag{R9}$$

Chai and Goldsmith [30] studied rate coefficients for fuel+NO_2, predicting the formation of HONO, and they distinguished 3 different isomers (*cis-HONO*, *trans-HONO* and HNO_2). As said by Zhang et al. [36], the total rate of the 3 isomers formation calculated by Chai and Goldsmith [30] is in excellent agreement with that reported in both the Park et al. [35] experimental measurement and Rasmussen et al. [9] calculation. In this work, we use the recent kinetic parameters for the three different isomers from Chai and Goldsmith [30]. Although modeling studies rarely distinguish the *HONO* isomers as the products of R9, a slight improvement in the onset temperature of H_2 conversion at all conditions was found in this work including the different isomers.

The work from Glarborg et al. [37], where the ability of H_2 to reduce nitric oxide under conditions relevant for the reburning process was studied, remarked the importance of species like *HNO* to react with H_2, finding that the only kinetic parameters available for R10, by Röhrig and Wagner [38], gave a H_2 conversion too fast compared to their experimental data and finally not using this reaction in their model.

$$HNO + H_2 \rightleftharpoons NH + H_2O \tag{R10}$$

We also found that the kinetic parameters [38] overpredict the consumption of H_2, and we estimated the kinetic constant to be 7E8 ($cm^3 \cdot mol^{-1} \cdot s^{-1}$), obtaining good agreement between experimental results and model predictions, as well as for H_2 as for NO_x concentrations at high temperatures, as can be seen in the next section. A comparison in the model predictions without R10 can be found in the supplementary material (Fig. S1), where the consumption of H_2 is not well captured if R10 does not occur and is overpredicted with the kinetic parameters from the bibliography [38]. R10 was found to be important only under reducing conditions, while no impact was observed at other stoichiometries. An accurate determination of the rate constant for R10 would be desirable.

The amount of NO and NO_2 that enters the reactor zone can affect the oxidation behavior of hydrogen. NO molecules can be converted to NO_2 through R11 before entering the reactor, since the gases are premixed at room temperature.

$$NO + NO + O_2 \rightleftharpoons NO_2 + NO_2 \tag{R11}$$

Due to high pressures and the presence of oxygen, there will have a mixture of NO/NO_2 at the reactor inlet. This was observed while the oven was still cool (290 K) and has been pointed in previous works experimenting with NO at high pressures [31,39,40]. For this reason, in the present work, the model was run with temperature profiles, an example shown in Fig. 1, that describe the entire experimental set-up: from the mixing point of the reactants to the entrance of the reactor, the reactor itself, and from the reactor outlet to the pressure reduction valve (1 atm).

In order to simulate the experimental data, the kinetic parameters of R11 were revised in the present work. Some uncertainty exists towards R11 [41], for which most reliable value of activation energy determined up to date is −4.41 [±3.33] kJ/mol [42]. We have taken the pre-exponential factor recommended by Atkinson et al. [42] and varied the activation energy in the uncertainty limits, taking the inferior limit, what makes an apparent activation energy of −7.74 kJ/mol (−1850 cal/mol), and which seems to be adequate in all the experimental conditions of this work to reproduce properly the NO/NO_2 concentrations. As can be seen in Fig. S2 from the supplementary material, the kinetic parameters chosen are in reasonable agreement with experimental data reported in the past at low temperatures [43–46], more than with the latest review of this reaction [42], which is mainly based on the work of Olbregts [47].

Results and discussion

Different systems have been tested under oxidizing conditions: $H_2/NO/O_2$, H_2/O_2 and NO/O_2 (sets 1 to 9 in Table 1), and their results have been plotted showing the comparisons between them. In Fig. 2, the results corresponding to the conversion of the system H_2/O_2 with and without NO addition are shown, at 10, 20 and 40 bar under oxidizing conditions. Pressure has a little effect on the conversion onset of H_2 when NO is not present, showing approximately 50 K difference in the reaction onset between the three pressures, and shifting the conversion to lower temperatures as the pressure increases. When NO is added to the system, the promotion of H_2 conversion to lower temperatures is increased as pressure rises, and comparatively greater than in the experiment without NO. In the case of 40 bar, there is a difference of 125 K in the reaction onset, and only 25 K in the case of 10 bar. With respect to NO_x, pressure has an important influence on the NO/NO_2 ratio, showing a major concentration of NO_2 as the pressure rises, due to R11, and a slight conversion back to NO as the temperature increases. The experimental trends of H_2 conversion and NO/NO_2 concentrations are well captured by the mechanism, confirming the behavior mentioned in the literature about NO_x promoting H_2 oxidation. This promotion can be explained through the interconversion of NO and NO_2 converting radicals HO_2 into more active radicals OH, as has been mentioned in the kinetic modeling section. The ability to capture this behavior (hydrogen promotion) is, in part, achieved by the proposed kinetic parameters of R11, which is important predicting the amount of NO and NO_2 that enters the reaction zone, influencing hydrogen ignition as well as the

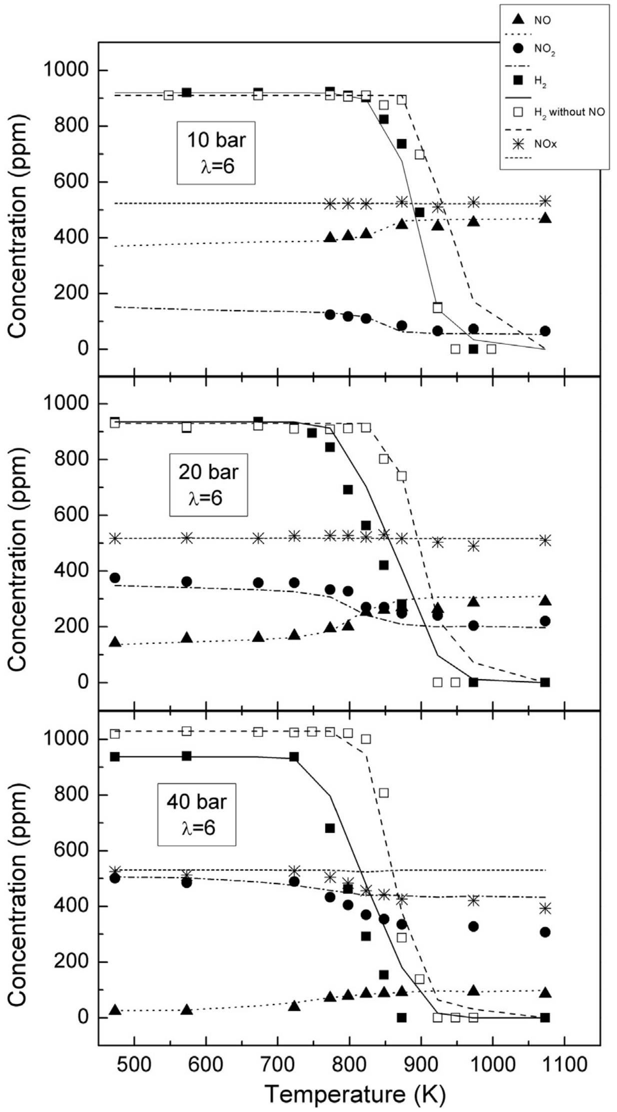

Fig. 2 – Results obtained under oxidizing conditions (λ referred to H_2) at 10 bar (up), 20 bar (centre) and 40 bar (down). Solid symbols correspond to experimental results in the presence of NO, while open symbols represent concentrations in the experiments without NO. Lines denote simulations of the model. Conditions of sets 1 to 6 in Table 1.

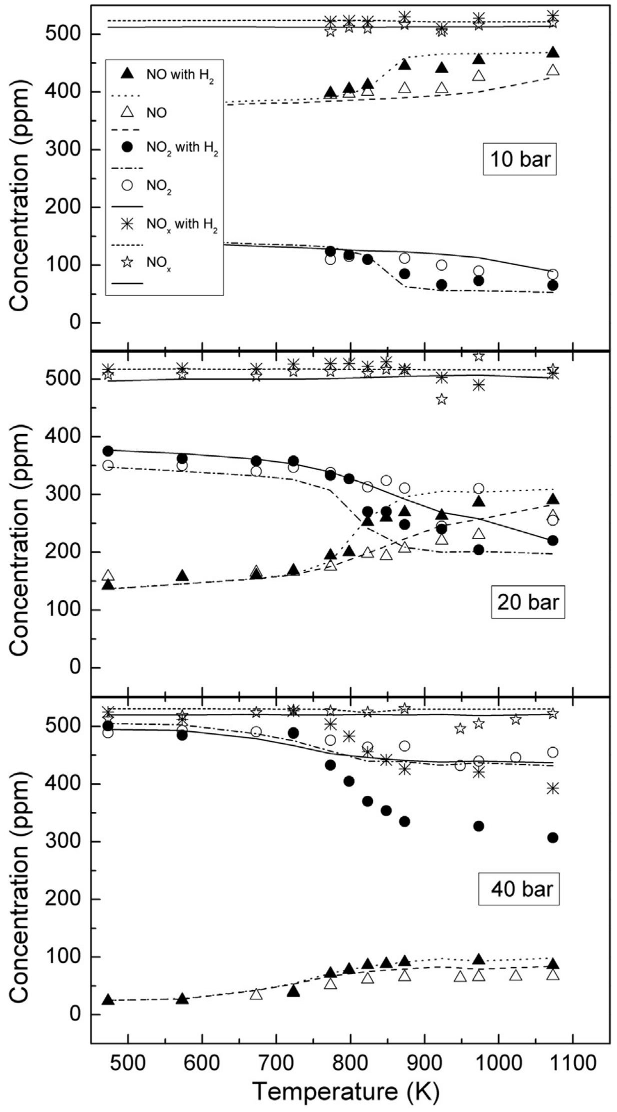

Fig. 3 – Results obtained under oxidizing conditions (λ_{NO} approximately 12) at 10 bar of pressure (up), 20 bar (centre) and 40 bar (down). Solid symbols correspond to experimental results in the presence of H_2, while open symbols represent concentrations in the experiments without H_2. Lines denote simulations of the model. Conditions of sets 1–3 and sets 7–9 in Table 1.

oxidation process at high pressures, and might be seen as an improvement in the predictions of the kinetic model.

It is worth to mention that the balance of NO_x closes fairly well (near 100%) in all the cases, except at 40 bar and under oxidizing conditions, where at high temperatures there is a NO_x decrease of approx. 20% (Fig. 2). This behavior of NO_x balance not closing at 100% was not seen in the experiment without hydrogen at 40 bar (set 7) (Fig. 3). A similar study of the $CO/H_2/O_2/NO_x$ system [9] in a flow reactor at high pressures did not show a loss of NO_x when working at 50 bar and high oxidizing conditions ($\lambda = 68$ for H_2). According to the present results, we might conclude that some interaction NO_2/H_2 not captured by the model is occurring in our experimental conditions at 40 bar and high temperatures. Another possible explanation could be related with the formation of nitric acid. As said by Ajdari et al. [40], if water vapor is present in pressurized flue gas systems, the formation of gaseous nitric acid and nitrous acid and the decomposition of nitrous acid may proceed as shown by reactions: $N_2O_4 + H_2O = HNO_2 + HNO_3$ and $2HNO_2 = NO + NO_2 + H_2O$, what could explain the loss of NO_x as nitric acid, but this has not been possible to prove.

In Fig. 3, the comparison of the results in the system NO/NO_2 with and without H_2, at 40, 20 and 10 bar under oxidizing conditions can be observed. Due to the major amount of radicals when hydrogen is present, NO and NO_2 react through R7 and R8, while in the system without hydrogen, the main reaction is the NO/NO_2 interconversion (R11), being favoured the NO presence at low pressures and high temperatures. In the current simulations, the concentration of NO_2 is the sum of NO_2 and N_2O_4, the latter only found to be important under 40 bar, with a maximum concentration of around 35 ppm in the reactor outlet section, according to the model. Due to the equilibrium between these two species, represented by R12, the existing N_2O_4 molecules are totally converted to NO_2 as the pressure is decreased to 1 bar in the relief valve of the set-up. The experimental trends are fairly well fitted by the model and the balance of NO_x does not close only at 40 bar.

$$NO_2 + NO_2(+M) \rightleftharpoons N_2O_4(+M) \tag{R12}$$

Fig. 4 shows the results of H_2 conversion in the presence of NO for stoichiometric conditions and different pressures. Under these conditions, the NO_2/NO ratio is higher as the pressure increases, as mentioned before, and the onset temperature for H_2 conversion remains the same at 40 bar as for oxidizing conditions (773 K), but finishes at higher temperatures due to the lack of oxygen. At 20 bar, the reaction starts at higher temperatures in comparison to the case of 40 bar, around 823 K. The kinetic model reproduces well the experimental data.

Similar results are plotted, in Fig. 5, for experiments performed under reducing conditions. The onset temperature for the reaction of hydrogen at 40 bar remains the same as for other stoichiometries (773 K), which is different to what was observed in the work of Hashemi et al. [8] of hydrogen oxidation at high pressures (50 bar) in a flow reactor, where they found that the onset of the reaction happened at lower temperatures under reducing conditions, compared to stoichiometric and oxidizing conditions, due to the competition between R2 and R6. In our case, when NO is added, R2 remains the main path in the oxidation of H_2, involving HO_2 radicals in the oxidation process. This oxidation process is more effective at higher pressures (40 bar) and R2 starts to compete with R6 as the pressure drops, shifting the onset of the reaction to higher temperatures, as seen in the results of Fig. 5. At 40 bar, the H_2 conversion onset is well captured by the model as well as its experimental trend. However, in the case of 20 bar, the experimental H_2 concentration suffers a sudden experimental decrease that is predicted smoothlier by the model. The general conversion trends are still well captured by the model, and the modification of the kinetic parameters of R10 clearly improves the prediction of H_2 concentration at 20 and 40 bar under reducing conditions, as well as the drop of NO_x at 40 bar (Fig. 5 down). This can be explained because NO reacts with H radicals to form HNO, through R13, then R10 occurs and NH is formed, which will end up reacting with NO to form N_2 and OH through R14.

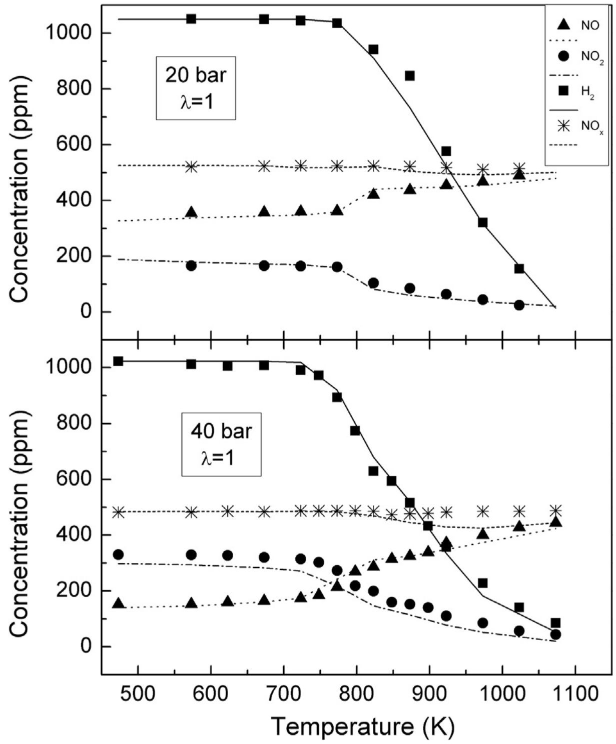

Fig. 4 – Results obtained under stoichiometric (λ referred to H_2) conditions at 20 bar (up) and 40 bar (down). Symbols represent experimental measurements and lines denote simulations of the model. Conditions of sets 10 and 11 in Table 1.

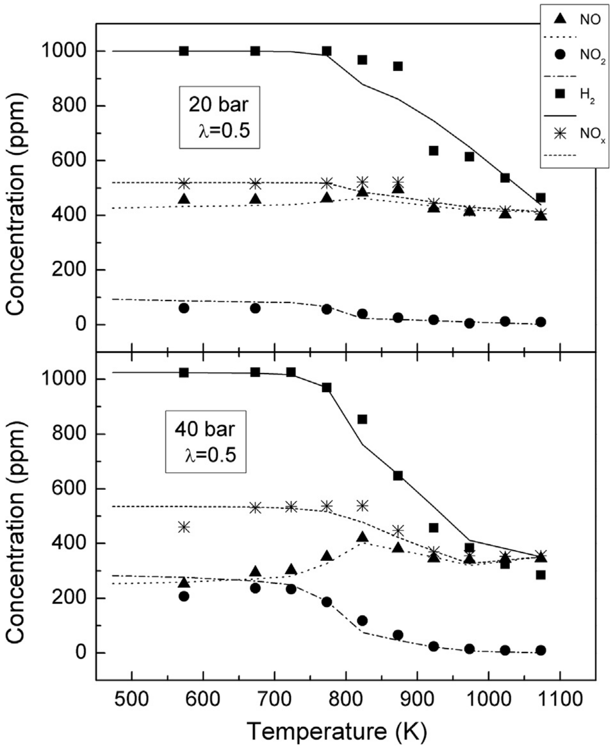

Fig. 5 – Results obtained under reducing conditions (λ referred to H_2) at 20 bar (up) and 40 bar (down). Symbols represent experimental measurements and lines denote simulations of the model. Conditions of sets 12 and 13 in Table 1.

$$NO + H(+M) \rightleftharpoons HNO(+M) \tag{R13}$$

$$HNO + H_2 \rightleftharpoons NH + H_2O \tag{R14}$$

$$NH + NO \rightleftharpoons N_2 + OH \tag{R15}$$

Conclusions

The system $H_2/NO/O_2$ has been studied in a tubular quartz flow reactor. Experiments under different controlled conditions, such as high manometric pressures (10, 20 and 40 bar), in the temperature range of 500–1100 K, testing different excess ratios for H_2 ($\lambda = 0.5–6.4$) have been carried out. The results obtained are useful for practical purposes where different technologies can be used. The results have been interpretated in terms of kinetic modeling, using an updated mechanism from recent works and modifying the kinetic parameters of the reactions: $2NO + O_2 \rightleftharpoons NO_2 + NO_2$, according to the uncertainty of its activation energy; and the $HNO + H_2 \rightleftharpoons NH + H_2O$ reaction, proposing a rate constant of 7E8 ($cm^3 \cdot mol^{-1} \cdot s^{-1}$), which reproduces fairly well the oxidation of H_2 under reducing conditions. This kinetic model allows us to predict results about the H_2 oxidation and its interaction with NO under a variety of operating conditions.

NO has been found to promote H_2 oxidation under oxidizing conditions, reacting with the HO_2 radical to form the more active OH radical, which enhances the conversion of hydrogen. The onset for hydrogen oxidation when doped with NO is the same at all stoichiometries at high pressures (40 bar), and is shifted to higher temperatures as the pressure decreases. The kinetic model matches fairly well the experimental data at all conditions, explaining the oxidation of H_2 and NO under oxidizing, stoichiometric and reducing conditions, except for the case of 40 bar under oxidizing conditions, where a 20% drop of the NO_x balance has been found and can not be predicted by the model, presumably by some interaction between NO_2/H_2 or the possible formation of nitric acid, which needs a more detailed study.

Acknowledgements

The authors express their gratitude to Aragón Government and European Social Fund (GPT group), and to MINECO and FEDER (Project CTQ2015-65226/PPQ and grant BES-2016-076610) for financial support.

Appendix A. Supplementary data

Supplementary data to this article can be found online at https://doi.org/10.1016/j.ijhydene.2019.01.078.

REFERENCES

[1] Unni JK, Govindappa P, Das LM. Development of hydrogen fuelled transport engine and field tests on vehicles. Int J Hydrogen Energy 2017;42:643–51.

[2] Plana C, Armenise S, Monzón A, García-Bordejé E. Ni on alumina-coated cordierite monoliths for in situ generation of CO-free $H_2$from ammonia. J Catal 2010;275:228–35.

[3] Wang W, Herreros JM, Tsolakis A, York AP. Ammonia as hydrogen carrier for transportation; investigation of the ammonia exhaust gas fuel reforming. Int J Hydrogen Energy 2013;38:9907–17.

[4] Martin S, Wörner A. On-board reforming of biodiesel and bioethanol for high temperature pem fuel cells: comparison of autothermal reforming and steam reforming. J Power Sources 2011;196:3163–71.

[5] Basic research needs for clean and efficient combustion of 21stcentury transportation fuels. In: Tech. Rep., Office of Science. U.S. Department of Energy; 2006.

[6] Burke MP, Chaos M, Ju Y, Dryer FL, Klippenstein SJ. Comprehensive H_2/O_2 kinetic model for high-pressure combustion. Int J Chem Kinet 2012;44:444–74.

[7] Hong Z, Davidson DF, Hanson RK. An improved H_2/O_2 mechanism based on recent shock tube/laser absorption measurements. Combust Flame 2011;158:633–44.

[8] Hashemi H, Christensen JM, Gersen S, Glarborg P. Hydrogen oxidation at high pressure and intermediate temperatures: experiments and kinetic modeling. Proc Combust Inst 2015;35:553–60.

[9] Rasmussen CL, Hansen J, Marshall P, Glarborg P. Experimental measurements and kinetic modeling of $CO/H_2/O_2/NO_x$ conversion at high pressure. Int J Chem Kinet 2008;40:454–80.

[10] Miller JA, Pilling MJ, Troe J. Unravelling combustion mechanisms through a quantitative understanding of elementary reactions. Proc Combust Inst 2005;30:43–88.

[11] Zeldovich YB. The oxidation of nitrogen in combustion and explosions. Acta Physicochem 1946;21:577628.

[12] Abián M, Alzueta MU, Glarborg P. Formation of NO from/N_2 O_2 mixtures in a flow reactor: toward an accurate prediction of thermal ,NO. Int J Chem Kinet 2015;47:518–32.

[13] Mathieu O, Petersen EL. Experimental and modeling study on the high-temperature oxidation of ammonia and related NO_x chemistry. Combust Flame 2015;162:554–70.

[14] Pugh D, Bowen P, Valera-Medina A, Giles A, Runyon J, Marsh R. Influence of steam addition and elevated ambient conditions on NO_x reduction in a staged premixed swirling NH_3/H_2 flame. Proc Combust Inst 2019;37:5401–9.

[15] Valera-Medina A, Pugh D, Marsh P, Bulat G, Bowen P. Preliminary study on lean premixed combustion of ammonia-hydrogen for swirling gas turbine combustors. Int J Hydrogen Energy 2017;42:24495–503.

[16] Nozari H, Karaca G, Tuncer O, Karabeyoglu A. Porous medium based burner for efficient and clean combustion of ammonia hydrogen air systems. Int J Hydrogen Energy 2017;42:14775–85.

[17] Salimian S, Hanson R, Kruger C. Ammonia oxidation in shock-heated $NH_3–N_2O–Ar$ mixtures. Combust Flame 1984;56:83–95.

[18] Cooper DA, Ljungstroem EB. Decomposition of ammonia over quartz sand at 840-960 °C. Energy Fuels 1988;2:716–9.

[19] Song Y, Hashemi H, Christensen JM, Zou C, Marshall P, Glarborg P. Ammonia oxidation at high pressure and intermediate temperatures. Fuel 2016;181:358–65.

[20] Hartmann M, Tian K, Hofrath C, Fikri M, Schubert A, Schießl R, Starke R, Atakan B, Schulz C, Maas U, Jäger FK, Kühling K. Experiments and modeling of ignition delay times, flame structure and intermediate species of EHN-doped stoichiometric n-heptane/air combustion. Proc Combust Inst 2009;32:197–204.

[21] Agarwal D, Singh SK, Agarwal AK. Effect of exhaust gas recirculation (EGR) on performance, emissions, deposits and durability of a constant speed compression ignition engine. Appl Energy 2011;88:2900–7.

[22] Wang L, Liu D, Yang Z, Li H, Wei L, Li Q. Effect of H_2 addition on combustion and exhaust emissions in a heavy-duty diesel engine with ,EGR. Int J Hydrogen Energy 2018;43:22658–68.

[23] Bose PK, Maji D. An experimental investigation on engine performance and emissions of a single cylinder diesel engine using hydrogen as inducted fuel and diesel as injected fuel with exhaust gas recirculation. Int J Hydrogen Energy 2009;34:4847–54.

[24] Bromly J, Barnes F, Nelson P, Haynes B. Kinetics and modeling of the $H_2/O_2/NO_x$ system. Int J Chem Kinet 1995;27(12):1165–78.

[25] Mueller MA, Yetter RA, Dryer FL. Measurement of the rate constant for $H+O_2+M=HO_2+M(M=N_2,Ar)$ using kinetic modeling of the high-pressure/$H_2/O_2/NO_x$ reaction. Symp (Int) on Combust 1998;27:177–84.

[26] Ashman PJ, Haynes BS. Rate coefficient of $H+O_2+M=HO_2+M(M=H_2O,N_2,Ar,CO_2)$. Symp (Int) on Combust 1998;27:185–91.

[27] Slack M, Grillo A. Investigation of hydrogen-air ignition sensitised by nitric oxide and by nitrogen dioxide. Tech. Rep., NASA report CR-2896. 1977.

[28] Laster WR, Sojka PE. Autoignition of H_2/air/NO_x mixtures - the effect of temperature and pressure. 4 J Propul Power 1989;5:510–2.

[29] Mathieu O, Levacque A, Petersen E. Effects of NO_2 addition on hydrogen ignition behind reflected shock waves. Proc Combust Inst 2013;34:633–40.

[30] Chai J, Goldsmith CF. Rate coefficients for fuel+NO_2: predictive kinetics for $HONO$ and HNO_2 formation. Proc Combust Inst 2017;36:617–26.

[31] Marrodan L, Millera Á, Bilbao R, Alzueta MU. High-pressure study of methyl formate oxidation and its interaction with NO. Energy Fuels 2014;28:6107–15.

[32] Giménez-López J, Alzueta M, Rasmussen C, Marshall P, Glarborg P. High pressure oxidation of C_2H_4/NO mixtures. Proc Combust Inst 2011;33:449–57.

[33] Zhang Y, Huang Z, Wei L, Zhang J, Law CK. Experimental and modeling study on ignition delays of lean mixtures of methane, hydrogen, oxygen, and argon at elevated pressures. Combust Flame 2012;159:918–31.

[34] Fotache C, Kreutz T, Law C. Ignition of counter flowing methane versus heated air under reduced and elevated pressures. Combust Flame 1997;108:442–70.

[35] Park J, Giles ND, Moore J, Lin MC. A comprehensive kinetic study of thermal reduction of NO_2 by ,H_2. J Phys Chem 1998;102:10099–105.

[36] Zhang Y, Mathieu O, Petersen EL, Bourque G, Curran HJ. Assessing the predictions of a NO_x kinetic mechanism on recent hydrogen and syngas experimental data. Combust Flame 2017;182:122–41.

[37] Glarborg P, Kristensen PG, Dam-Johansen K, Alzueta MU, Millera A, Bilbao R. Nitric oxide reduction by non-hydrocarbon fuels. implications for reburning with gasification gases. Energy Fuels 2000;14:828–38.

[38] Röhrig M, Wagner HG. An investigation about the $NH(X^3\Sigma^-)$ formation in the thermal decomposition of, HN_3. Berichte der Bunsengesellschaft fr Physikalische Chemie 1994;98:1073–6.

[39] Rasmussen CL, Rasmussen AE, Glarborg P. Sensitizing effects of NO_x on CH_4 oxidation at high pressure. Combust Flame 2008;154:529–45.

[40] Ajdari S, Normann F, Andersson K, Johnsson F. Modeling the nitrogen and sulfur chemistry in pressurized flue gas systems. Ind Eng Chem Res 2015;54:1216–27.

[41] Gadzhiev OB, Ignatov SK, Gangopadhyay S, Masunov AE, Petrov AI. Mechanism of nitric oxide oxidation reaction ($2NO + O_2= 2NO_2$) revisited. J Chem Theor Comput 2011;7:2021–4.

[42] Atkinson R, Baulch DL, Cox RA, Crowley JN, Hampson RF, Hynes RG, Jenkin ME, Rossi MJ, Troe J. Evaluated kinetic and photochemical data for atmospheric chemistry: volume I - gas phase reactions of O_x, HO_x, NO_x and SO_x species. Atmos Chem Phys 2004;4:1461–738.

[43] England C, Corcoran WH. The rate and mechanism of the air oxidation of parts-per-million concentrations of nitric oxide in the presence of water vapor. Ind Eng Chem Fundam 1975;14:55–63.

[44] Hisatsune IC, Zafonte L. Kinetic study of some third-order reactions of nitric oxide. J Phys Chem 1969;73:2980–9.

[45] Greig JD, Hall PG. Thermal oxidation of nitric oxide at low concentrations. Trans Faraday Soc 1967;63:655–61.

[46] Ashmore PG, Burnett MG, Tyler BJ. Reaction of nitric oxide and oxygen. Trans Faraday Soc 1962;58:685–91.

[47] Olbregts J. Termolecular reaction of nitrogen monoxide and oxygen: a still unsolved problem. Int J Chem Kinet 1985;17:835–48.

SUPPLEMENTARY MATERIAL

High pressure study of H_2 oxidation and its interaction with NO

J.M. Colom-Díaz, Á. Millera, R. Bilbao, M.U. Alzueta

Aragón Institute of Engineering Research (I3A). Department of Chemical and Environmental Engineering, University of Zaragoza, 50018 Zaragoza, Spain.

Table of contents:

1) **Modeling calculations modifying reaction R10 ($HNO+H_2=NH+H_2O$) under reducing conditions and 40 bar of pressure**

   Figure S1. Set 12 from Table 1. Results under reducing conditions at 40 bar of pressure. Symbols represent experimental measurements and lines denote simulations of the model. Solid lines indicate the simulation without R10 in the model, dotted lines the simulation with our estimation for rate constant of R10: 7E8 ($cm^3\ mol^{-1}\ s^{-1}$), and dashed line shows the simulation of H_2 concentration using the kinetic parameters of R10 from Röhrig and Wagner [38].

2) **Comparison of different values for the kinetic constant logarithm of R11 ($2NO+O_2=NO_2+NO_2$)**

   Figure S2. Comparison of different values for the kinetic constant logarithm of R11 ($2NO+O2=NO_2+NO_2$) vs. 1/T(K), from the literature [42-47] and the estimation of this study.

1) Modeling calculations modifying reaction R10 ($HNO+H_2=NH+H_2O$) under reducing conditions and 40 bar of pressure

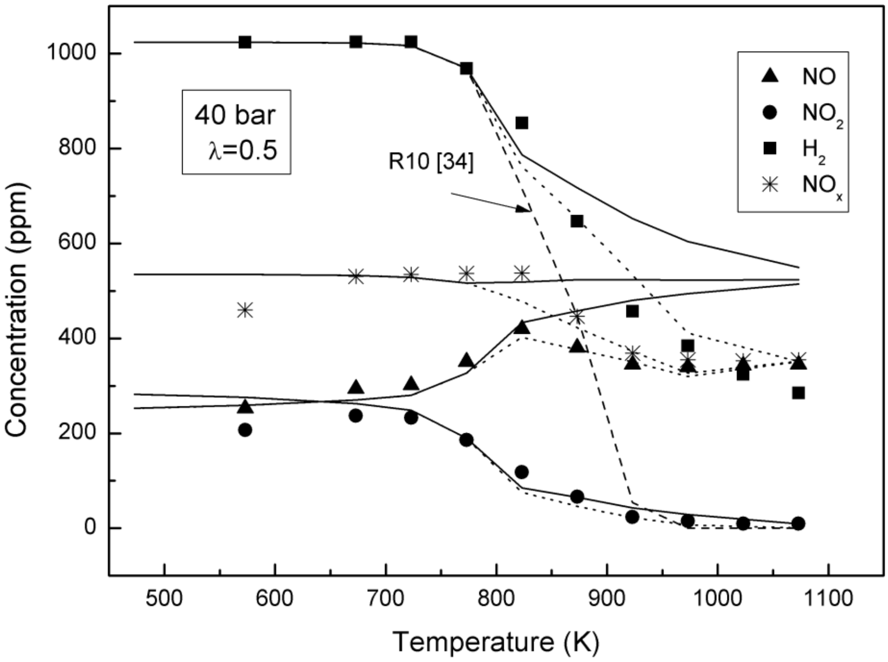

Figure S1. Set 12 from Table 1. Results under reducing conditions at 40 bar of pressure. Symbols represent experimental measurements and lines denote simulations of the model. Solid lines indicate the simulation without R10 in the model, dotted lines the simulation with our estimation for rate constant of R10: 7E8 (cm^3 mol^{-1} s^{-1}), and dashed line shows the simulation of H_2 concentration using the kinetic parameters of R10 from Röhrig and Wagner [38].

2) Comparison of different values for the kinetic constant logarithm of R11 ($2NO+O_2=NO_2+NO_2$)

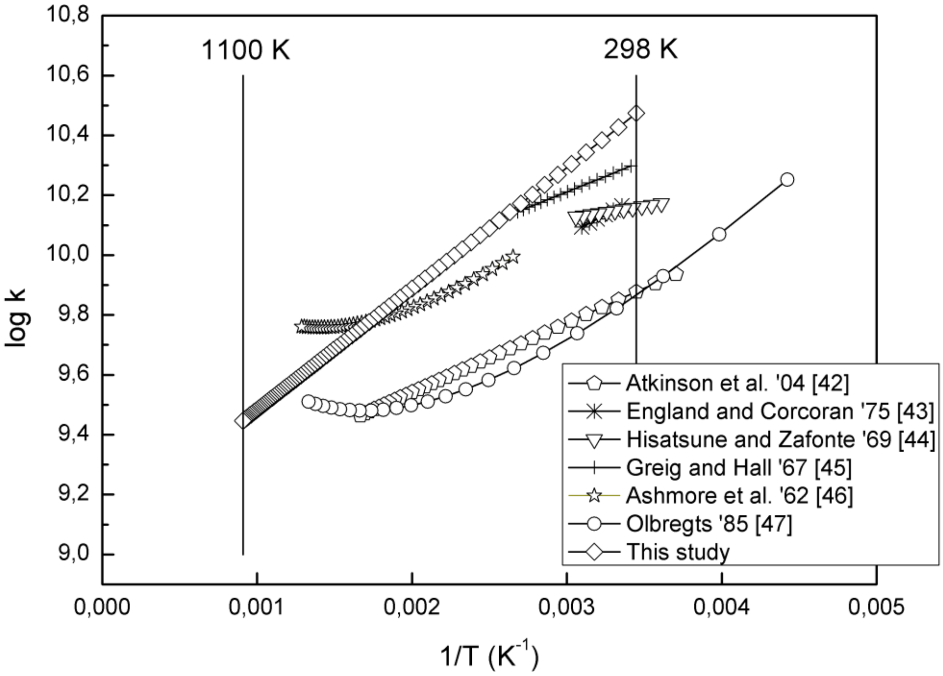

Figure S2. Comparison of different values for the kinetic constant logarithm of R11 ($2NO+O2=NO_2+NO_2$) vs. 1/T(K), from the literature [42-47] and the estimation of this study.

References:

[38] Röhrig, M.; Wagner, H.G. (1994). An investigation about the NH (X^3P^-) formation in the thermal decomposition of HN_3. *Berichte der Bunsengesellschaft für Physikalische Chemie* 98 1073-1076.

[42] Atkinson, R.; Baulch, D.L.; Cox, R.A.; Crowley, J.N.; Hampson, R.F.; Hynes, R.G.; Jenkin, M.E.; Rossi, M.J.; Troe, J. (2004). Evaluated kinetic and photochemical data for atmospheric chemistry: Volume I - gas phase reactions of O_x, HO_x, NO_x and SO_x species. *Atmospheric Chemistry and Physics* 4, 1461-1738.

[43] England, C.; Corcoran, W.H. (1975). The rate and mechanism of the air oxidation of parts-per-million concentrations of nitric oxide in the presence of water vapor. *Industrial & Engineering Chemistry Fundamentals* 14, 55-63.

[44] Hisatsune, I.C.; Zafonte, L. (1969). Kinetic study of some third-order reactions of nitric oxide. *The Journal of Physical Chemistry* 73, 2980-2989.

[45] Greig, J.D.; Hall, P.G. (1967). Thermal oxidation of nitric oxide at low concentrations. *Transactions of the Faraday Society* 63, 655-661.

[46] Ashmore, P.G.; Burnett, M.G.; Tyler, B.J. (1962). Reaction of nitric oxide and oxygen. *Transactions of the Faraday Society* 58, 685-691.

[47] Olbregts, J. (1985). Termolecular reaction of nitrogen monoxide and oxygen: A still unsolved problem. *International Journal of Chemical Kinetics* 17, 835-848.

Article III

Colom-Díaz, J.M.; Abián, M.; Millera, Á.; Bilbao, R.; Alzueta, M.U. (2019). Influence of pressure on H_2S oxidation. Experiments and kinetic modeling. *Fuel* 258, 116145.

Fuel 258 (2019) 116145

Contents lists available at ScienceDirect

Fuel

journal homepage: www.elsevier.com/locate/fuel

Full Length Article

Influence of pressure on H_2S oxidation. Experiments and kinetic modeling

J.M. Colom-Díaz, M. Abián, Á. Millera, R. Bilbao, M.U. Alzueta*

Aragón Institute of Engineering Research (I3A), Department of Chemical and Environmental Engineering, University of Zaragoza, 50018 Zaragoza, Spain

ARTICLE INFO

Keywords:
H_2S, oxidation
High pressure
Sour gas
Kinetic modeling

ABSTRACT

The oxidation of H_2S at different manometric pressures (0.6–40 bar), in the temperature range of 500–1000 K and under slightly oxidizing conditions ($\lambda = 2$), has been studied. Experiments have been performed in a quartz tubular flow reactor. The results have shown that H_2S conversion shifts to lower temperatures as the pressure increases. The kinetic model used in this work is based on a previous one proposed by the authors to describe H_2S oxidation at atmospheric pressure, which has been updated with a H_2/O_2 reaction subset for high pressures. Model results match fairly well the experimental ones both from the present work and from the literature. The reaction pathways of H_2S oxidation analyzed are similar to the ones at atmospheric pressure. The differences are found in the radicals that are involved in the oxidation process at the different pressures. For a given temperature it is shown that, under the operating conditions of this work, pressure will have a major role than the gas residence time in the oxidation rate.

1. Introduction

As the energy demand increases worldwide, an efficient utilization of available natural resources is needed. Natural gas production is expected to peak near 2035, taking into consideration a scenario of cumulative production, plus remaining reserves, plus undiscovered resources [1]. The abundance of natural gas reserves can facilitate the transition from fossil derived to fully renewable fuels and chemical generation [2,3]. The total long-term recoverable conventional gas resource base is more than 400 trillion cubic metres (tcm), and another 400 tcm are estimated for unconventional sources (sour gas) [4]. The increasing importance of unconventional fuel sources, such as sour and shale gas (natural gas with significant amounts of H_2S and CO_2, up to 30% content in volume each one [5]), brings interest to the direct use of these fuels, developing technologies and combustion processes focused on their knowledge and understanding under high pressure conditions [6]. The technology most used for the treatment of H_2S is the Claus process, by producing sulfur from it [7,8]. However, due to the large offer of sulfur worldwide [9] and the variable feedstock of H_2S in natural gas reserves, different processes for treating sour gas and H_2S streams are emerging [2,10–13]. Thus, Langè et al. [14] proposed a detailed description of the phase behavior of the $CH_4 + H_2S$ system, in a wide range of temperatures and pressures, with the goal of performing the correct process design of new gas purification technologies. Another interesting process for exploitation of sour gas reserves is the direct gas combustion, for example, through oxy-combustion [15], which has been studied at high pressures to increase efficiency in power plants [16,17].

Some studies about mixtures of sulfur species and carbon species oxidation have been performed, with the final goal of knowing more about sour gas conversion. For example, Gersen et al. [18] experimentally studied the autoignition and oxidation of CH_4/H_2S mixtures in a rapid compression machine (RCM) and a flow reactor at high pressure. They showed prediction results with their model that agree well with the measured autoignition delay times. On the other hand, they also indicated that the H_2S oxidation chemistry and the interaction of CH_4 and H_2S at high pressure are not well understood. Zeng et al. [19], in their work on the co-oxidation of CH_4 and CS_2 (a known impurity of the Claus process) in a flow reactor, experimentally observed an inhibiting effect by CS_2 in the oxidation of methane at atmospheric pressure. They became aware of the complexity of the C–H–O–S combustion chemistry and claimed that their current model could not reflect all potentially significant reactions. Other recent studies have been devoted to validate their kinetic mechanisms on sulfur compounds oxidation with experiments from the literature. Bongartz et al. [15] and Bongartz and Ghoniem [20,21] developed an optimized mechanism to make qualitative and even quantitative predictions on the combustion behavior of sour gas under oxy-fuel conditions. Salisu and Abhijeet [22] carried out kinetic simulations of acid gas (H_2S and CO_2) pyrolysis and oxidation for simultaneous syngas ($H_2 + CO$) and sulfur recovery, which results will assist in the design and optimization of acid gas conversion reactors. Despite these efforts, there is still a need for more

---

* Corresponding author.
E-mail address: uxue@unizar.es (M.U. Alzueta).

https://doi.org/10.1016/j.fuel.2019.116145
Received 4 June 2019; Received in revised form 22 August 2019; Accepted 3 September 2019
Available online 13 September 2019
0016-2361/ © 2019 Elsevier Ltd. All rights reserved.

accurate direct determination of several important rate constants as well as more validation data in order to improve modeling predictions of sour gas conversion [15].

The reaction steps in the H_2S oxidation process remain unknown in many aspects and the available experimental data are limited. Some works have been carried out in the last years trying to understand H_2S kinetic behavior under combustion conditions. The experimental and theoretical work of Zhou et al. [23] about H_2S oxidation at atmospheric pressure established several kinetic parameters for different reactions involved in the process. Later, the exploratory work from Song et al. [24] on H_2S oxidation under high pressures showed that, under oxidizing and stoichiometric conditions, the H_2S oxidation depends strongly on the stoichiometry and pressure, claiming that experimental results for H_2S oxidation at elevated pressures are scarce.

As H_2S conversion can be affected by the operating conditions, such as temperature, pressure and combustion atmosphere, the present work addresses the oxidation of H_2S at high pressures, with the basis of the work from the authors at atmospheric pressure [25], where H_2S oxidation was studied in a flow reactor from reducing to oxidizing conditions and different temperatures (700–1400 K). In that study, H_2S conversion was predicted reasonably well by the kinetic model proposed, which included the addition of $HSOO \rightleftharpoons HSO_2$ isomerization reaction, supported by recent theoretical works, as a key step in a faster reaction path of SH oxidation.

In this context, the present work studies the influence of manometric pressure (0.6–40 bar) at different temperatures (500–1000 K) and at slightly oxidizing conditions (approximately $\lambda = 2$), on the conversion of hydrogen sulfide, performing flow reactor experiments, under laboratory controlled conditions. Moreover, a kinetic model capable of describing the oxidation process of H_2S at high pressures has been used to interpret the experimental results. The results obtained in this work can be also useful for different industrial processes, such as the Claus process [26] or oxy-combustion of the sour gas [15,20,21,27].

2. Experimental methodology

The experimental set-up used to perform the high-pressure H_2S oxidation experiments has been previously described in detail elsewhere [28]. Therefore, only a brief description of the main features is provided here. 1 L (STP)/min of gas reactants: H_2S (approximately 500 ppm), O_2 (approximately 1500 ppm) and N_2 as carrier gas, were supplied from gas cylinders through mass flow controllers with an uncertainty in the flow rate measurements of approximately 0.5%. The oxygen required to carry out each oxidation experiment is determined by the air excess ratio (λ, defined as inlet oxygen divided by stoichiometric oxygen). Slightly oxidizing conditions ($\lambda = 2$) were selected to study the oxidation of hydrogen sulfide at different manometric pressures. Table 1 contains the conditions for the different experiments performed. The moderate concentration of oxygen used in this work was chosen to avoid deposition of sulfur in the experimental set-up, if reducing conditions were used, and to minimize SO_3 formation, which is enhanced at high pressures and very oxidizing conditions and could lead to corrosion problems. The reactant gases were premixed before entering the reactor, which consists of a quartz tube (inner diameter of 6 mm and 1500 mm in length) designed to approximate plug flow conditions [29]. The reactor is enclosed in a stainless-steel tube that acts as a pressure shell. The steel tube is placed horizontally in a tubular oven, with three individually controlled electrical heating elements that ensure an isothermal reaction zone of approximately 500 mm, with a uniform temperature profile (± 5 K). Gas residence time depends on pressure and temperature and it can be expressed as $t_r(s) = 232^*P(bar)/T(K)$ in the isothermal part of the reactor. Previously to the gas analysis systems, gases pass through a filter and a condenser to ensure gas cleaning. Products are analyzed by a gas chromatograph equipped with a thermal conductivity detector (TCD) to quantify H_2S and O_2, and a continuous UV analyzer to quantify SO_2. The uncertainty of the measurements is estimated within 5%.

Table 1
Experimental conditions. N_2 as bath gas. $t_r(s) = 232^*P(bar)/T(K)$.

Set	λ	Manometric pressure (bar)	H_2S (ppm)	O_2 (ppm)
1	1.99	0.6	505	1509
2	2.1	5	480	1520
3	2.06	10	485	1510
4	2.04	20	497	1520
5	2.06	40	500	1545

3. Kinetic model

The kinetic model used in this work has been taken from a recent work by the authors, where H_2S oxidation at atmospheric pressure was studied in a flow reactor, from reducing to oxidizing conditions [25]. The simulations have been carried out with the software Chemkin-Pro and the plug flow reactor code [30]. The oxidation mechanism proposed in [25] supported the evolution of the $SH + O_2$ reaction (key reaction step in H_2S oxidation) through isomerization from HSOO to HSO_2, leading to the final product SO_2, as proposed by Garrido et al. [31], in a high level ab initio study of the HSO_2 system. The main reactions for H_2S oxidation belong to the work from Zhou et al. [23] and Alzueta et al. [32]. The H_2/O_2 subset was updated for high pressures [33] and has been included in the present study with no modifications. However, no big differences have been observed in the simulations in this work using the updated H_2/O_2 subset.

The oxidation of H_2S under high pressure conditions might be a source of O_3, as mentioned by Song et al. [24], according to the $SH + O_2 + O_2 \rightleftharpoons HSO + O_3$ reaction, and ozone may promote H_2S conversion, as it is a much more reactive molecule than molecular oxygen. Thus, a subset for O_3 reactions has been added from their work [24], which is mainly based on the work from Atkinson et al. [34]. Reactions involving O_3 have not been found to be important under the present conditions.

4. Results and discussion

The experimental (symbols) and simulated (lines) results of the concentrations of H_2S, SO_2 and O_2 as a function of temperature are plotted from Figs. 1–5. All the experiments were carried out at slightly oxidizing conditions ($\lambda = 2$), being SO_2 the main product from the oxidation of H_2S. The sulfur balance closes in all cases within ± 5%. The conversion of H_2S is shifted to lower temperatures as the pressure

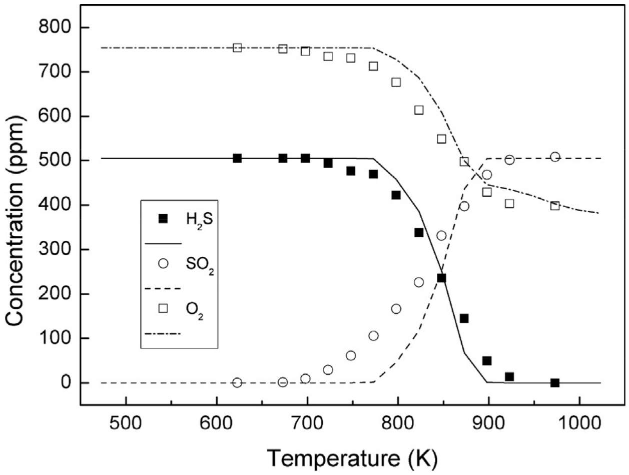

Fig. 1. Experimental results of H_2S oxidation at 0.6 bar (Set 1 of Table 1). Initial conditions: O_2 = 1509 ppm, H_2S = 505 ppm; λ = 1.99.

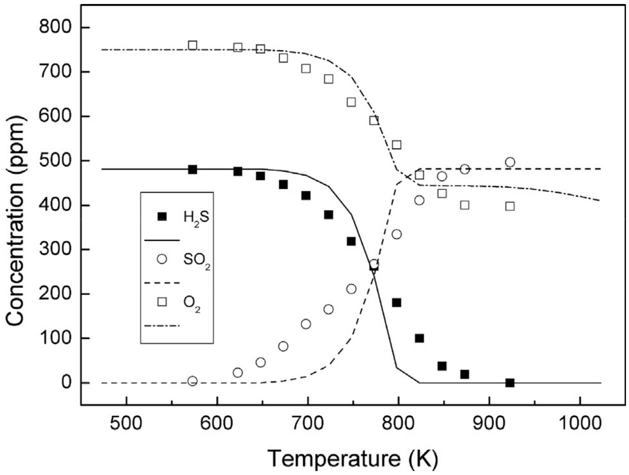

Fig. 2. Experimental results of H_2S oxidation at 5 bar (Set 2 of Table 1). Initial conditions: O_2 = 1520 ppm, H_2S = 480 ppm; λ = 2.1.

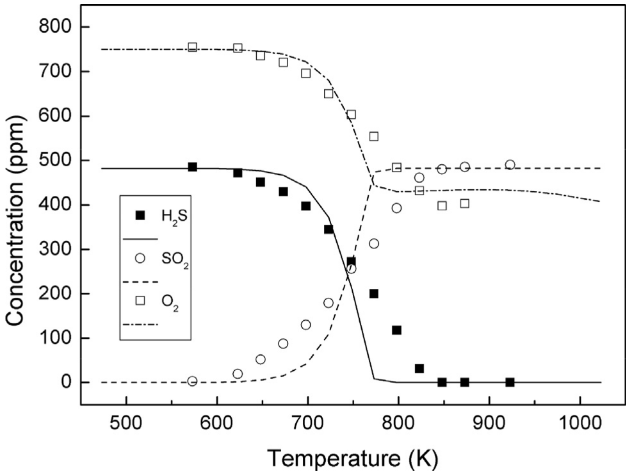

Fig. 3. Experimental results of H_2S oxidation at 10 bar (Set 3 of Table 1). Initial conditions: O_2 = 1510 ppm, H_2S = 485 ppm; λ = 2.06.

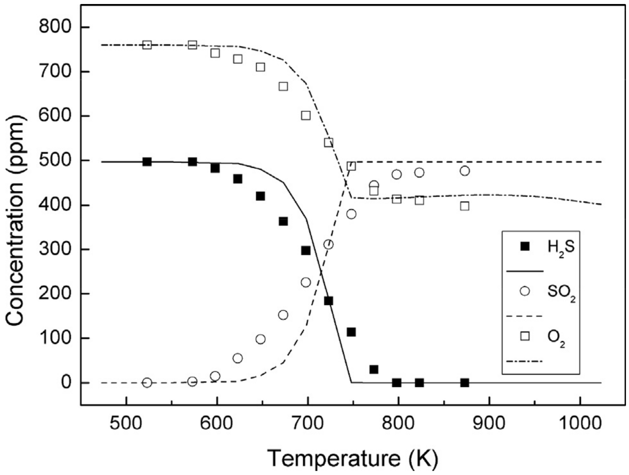

Fig. 4. Experimental results of H_2S oxidation at 20 bar (Set 4 of Table 1). Initial conditions: O_2 = 1520 ppm, H_2S = 497 ppm; λ = 2.04.

increases. Thus, the onset temperature for H_2S conversion is 775 K in the case of 0.6 bar and 600 K at the highest pressure studied (40 bar). The consumption of O_2 follows the same trend as hydrogen sulfide.

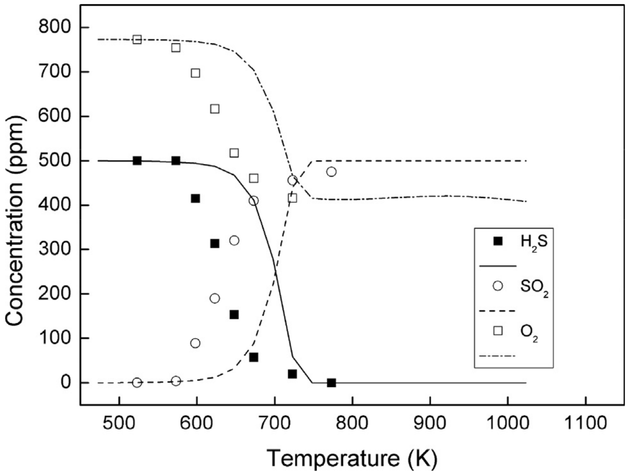

Fig. 5. Experimental results of H_2S oxidation at 40 bar (Set 5 of Table 1). Initial conditions: O_2 = 1545 ppm, H_2S = 500 ppm; λ = 2.06.

The simulated results obtained with the kinetic model used in this work reproduce well the experimental data, mainly those obtained at near atmospheric pressure (0.6 bar manometric pressure). This fact confirms that the kinetic model is capable of predicting H_2S conversion at near atmospheric pressure. For the rest of the pressures studied, the kinetic model underpredicts slightly the oxidation of H_2S at the beginning of the reaction and overpredicts to some extent the H_2S conversion at the end of the conversion. The exception would be the case at the highest pressure (40 bar), where a shift of 50 K between experimental H_2S concentrations and model predictions is seen.

The results near atmospheric pressure of this work (0.6 bar manometric pressure) are compared with the ones obtained by the authors in their study of H_2S oxidation at atmospheric pressure in other flow reactor [25]. This reactor has 8.7 mm inner diameter. The results are shown in Fig. 6. It can be observed that the results are quite similar, although a difference in the conversion onset temperature of 50 K exists, which might be due to the pressure difference (0.6 bar) or the residence time, as both experiments are carried out in different experimental installations. Previously, these set-ups operating at atmospheric pressure have already shown a similar behavior for CH_3SH oxidation under stoichiometric conditions [35].

It is worth to mention that the gas residence time in the reactor increases with the pressure. An additional analysis, through modeling results, of the effect of the residence time at two different pressures (1

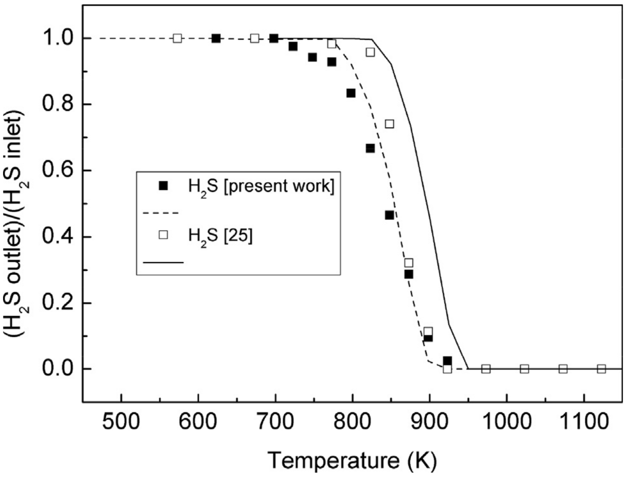

Fig. 6. Concentrations of H_2S vs. temperature at λ = 2 and atmospheric pressure. Open symbols from [25] (H_2S = 482 ppm, O_2 = 1500 ppm; λ = 2.07) and solid symbols from the present work (Set 1 of Table 1, O_2 = 1509 ppm, H_2S = 505 ppm; λ = 1.99).

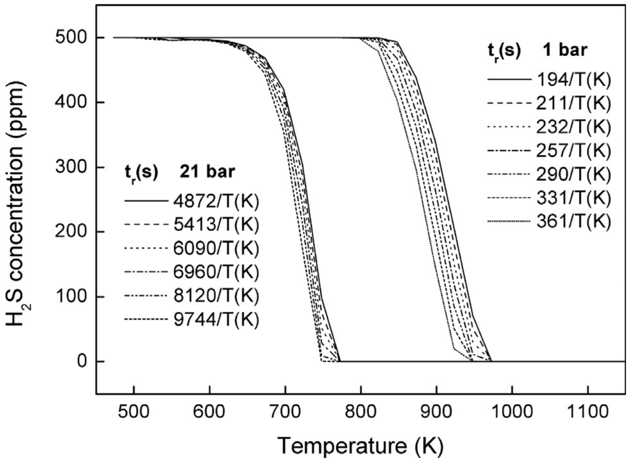

Fig. 7. Simulations of the concentration of H_2S vs. temperature at two pressures (1 and 21 bar absolute pressure) and different residence times. Initial conditions: H_2S = 500 ppm, O_2 = 1500 ppm; λ = 2.

and 21 bar absolute pressure) on H_2S conversion can be seen in Fig. 7. In this figure, at 1 bar and 21 bar, the solid lines on the right correspond, respectively, to the gas residence time of the atmospheric pressure set-up used in [25] (t_r = 194/T(K)) and the gas residence time of the present work high-pressure set-up (t_r = 4872/T(K)), which are used as the reference cases. For both pressures, their reference residence time values are subsequently increased up to being approximately doubled. As it can be observed, at 1 bar a 50 K temperature difference in H_2S concentration profiles exists when the residence time is doubled. At high pressure (21 bar), under the operating conditions of this work, the effect of the residence time is less important; in this case, the solid line represents the residence time of set 4 in Table 1. Thus, under these conditions, the influence of gas residence time is less significant as the pressure increases. However, it is worth to highlight that the specific effect of the gas residence time depends on the given process studied. For example, Marrodán et al. [36], in their study about DME oxidation at high pressure, observed an important effect of the residence time at pressures even higher than those presented in Fig. 7 on DME conversion when doubling the residence time at stoichiometric conditions.

Hydrogen sulfide oxidation proceeds via its reaction with the O/H radical pool to form SH, as can be seen in the reaction pathways shown in Fig. 8. Under slightly oxidizing conditions, SH radicals react mainly with O_2 to form the HSOO peroxide, which isomerizes to HSO_2 and forms by decomposition the SO_2 + H final products, feeding the radical pool with H radicals. The HSO_2 radicals can also react with oxygen, if it is available, or isomerize again to the radical HOSO, which will react in the same way as HSO_2, decomposing or reacting with O_2 to form SO_2. The changes in reactivity during the H_2S conversion process at different pressures are attributed to different radicals that participate depending on pressure. In the case of relatively low pressures (0.6, 5 and 10 bar manometric pressure), H_2S will react mainly with radicals H (R1).

$$H_2S + H \rightleftharpoons SH + H_2 \quad \text{(R1)}$$

However, as the pressure increases (20 and 40 bar), other pathways become also important, involving HO_2 and OH radicals (R2 and R3).

$$H_2S + HO_2 \rightleftharpoons SH + H_2O_2 \quad \text{(R2)}$$

$$H_2S + OH \rightleftharpoons SH + H_2O \quad \text{(R3)}$$

Formation of HO_2 radicals is favored at high pressures (R4) [e.g. 18,24,37]. These radicals react with H_2S to form SH and H_2O_2 (R2), and promote the oxidation via the branching reaction of H_2O_2 to give OH radicals (R5), which then interact again with H_2S (R3).

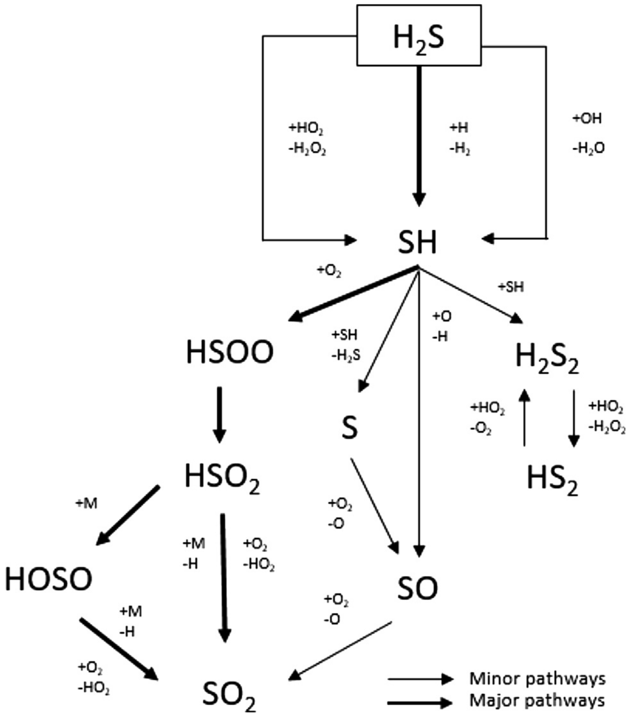

Fig. 8. Reaction pathways for the oxidation of H_2S.

$$O_2 + H\ (+M) \rightleftharpoons HO_2\ (+M) \quad \text{(R4)}$$

$$H_2O_2\ (+M) \rightleftharpoons OH + OH\ (+M) \quad \text{(R5)}$$

A sensitivity analysis of model calculations has been performed for the highest pressure studied (40 bar), at the temperature when H_2S is starting to react (675 K). In Fig. 9, the sensitivity analysis for H_2S shows the isomerization reaction (R6) as the most sensitive one:

$$HSOO \rightleftharpoons HSO_2 \quad \text{(R6)}$$

followed by the branching reaction of H_2O_2 (R5), which is comparatively a well stablished reaction. The next most important reaction is (R7):

$$SH + SH\ (+M) \rightleftharpoons H_2S_2\ (+M) \quad \text{(R7)}$$

which has also been seen in the top 3 most sensitive reactions in works about H_2S oxidation [24,37]. In this work, the observed sensitivity has been related to the capability of H_2S_2 to convert HO_2 radicals into H_2O_2, which would enhance the oxidation process and reaction (R8) is found as the fourth most sensitive reaction.

$$H_2S_2 + HO_2 \rightleftharpoons HS_2 + H_2O_2 \quad \text{(R8)}$$

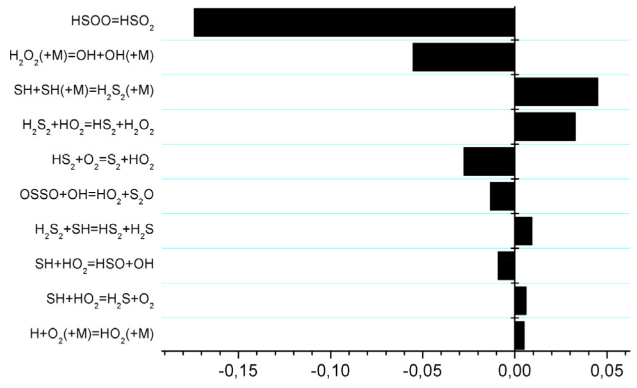

Fig. 9. Sensitivity analysis for H_2S conversion, at λ = 2, 40 bar and 675 K.

The formation of these species (H_2S_2 and HS_2) is usually more important at reducing conditions. As mentioned by Zhou et al. [23], disulfur interactions as (R9) are important in the ignition and propagation reactions during H_2S oxidation even under fuel lean conditions, being (R7) chain terminating reaction, while (R9) is chain propagating reaction, due to the subsequent reaction of S with oxygen to form SO and then SO_2.

$$SH + SH \rightleftharpoons H_2S + S \tag{R9}$$

The same kinetic parameters for (R9) as in the work from Gao et al. [38] have been used. However, these authors mention that care should be taken in applying (R9) above 1 bar. Gao et al. also mention that H_2S_2 is more stable at high pressures and low temperatures than SH. Discrepancies in the model results compared to experimental ones might be related to the chemistry of disulfur species and claim for a better characterization of these reactions at high pressures.

With the purpose of evaluating the performance of the kinetic model used in the present work, it has been tested against literature ignition delay time measurements at different pressures. Some cases from the work of Mathieu et al. [37], about the effects of H_2S addition on hydrogen ignition behind reflected shock waves, have been taken, and the results are shown in Fig. 10. In that study, ignition delay times were measured behind reflected shock waves for mixtures of 1% H_2/1% O_2, diluted in Ar and doped with various concentrations of H_2S (100, 400, and 1600 ppm), over large pressure (around 1.6, 13, and 33 atm) and temperature (1045–1860 K) ranges. Their results showed a significant increase in the ignition delay time due to the addition of H_2S, in some cases by a factor of 4 or more, over the baseline mixtures without H_2S. This behavior was explained because H_2S initially reacts before the H_2 fuel does, mainly through the reaction $H_2S + H \rightleftharpoons SH + H_2$ (R1), thus taking H atoms away from the main branching reaction (R10), which would produce OH radicals, and thus inhibit the ignition process.

$$H + O_2 \rightleftharpoons OH + O \tag{R10}$$

However, an increase in the reactivity was observed at the highest pressure investigated (33 atm) and at the temperature of 1100 K, using the highest H_2S concentration investigated (1600 ppm). This fact would be in accordance with the discrepancy found in this work at high pressure (40 bar), where a higher experimental reactivity is observed. The present kinetic model fits well the ignition delay time measurements under different conditions of pressure and H_2S concentration. The results from the present work and the previous study at atmospheric pressure in a flow reactor [25] suggest that the update in the kinetic model, adding the isomerization of HSOO to HSO_2 as a possible step in H_2S oxidation until the final product SO_2, should be taken into consideration for future works on the oxidation of H_2S.

5. Conclusions

The present work addresses the oxidation of H_2S at different manometric pressures (0.6–40 bar), in the temperature range of 500–1000 K, using a quartz tubular flow reactor. The experiments were performed at slightly oxidizing conditions ($\lambda = 2$). The results show that the oxidation of H_2S is shifted to lower temperatures as the pressure increases. The onset for H_2S conversion starts at 775 K in the case of 0.6 bar and 600 K at the highest pressure studied (40 bar). For a given temperature, and under the operating conditions of this work, pressure will have a major role than gas residence time in the oxidation rate. The kinetic model about H_2S oxidation at atmospheric pressure developed by the group in a previous work, together with an updated H_2/O_2 subset for high pressures, seems to work fairly well at different pressures. The kinetic model matches the experimental trends, except for the experiment at 40 bar, where a gap of 50 K in temperature between experimental concentrations and model predictions is observed. The sensitivity analysis performed at 40 bar indicates that the H_2S conversion is mainly sensitive to the $HSOO \rightleftharpoons HSO_2$ isomerization reaction, and to some branching reactions involving H_2S_2 and H_2O_2.

Acknowledgements

The authors express their gratitude to the Aragón Government (Ref. T22_17R), co-funded by FEDER 2014-2020 "Construyendo Europa desde Aragón", and to MINECO and FEDER (Project CTQ2015-65226)

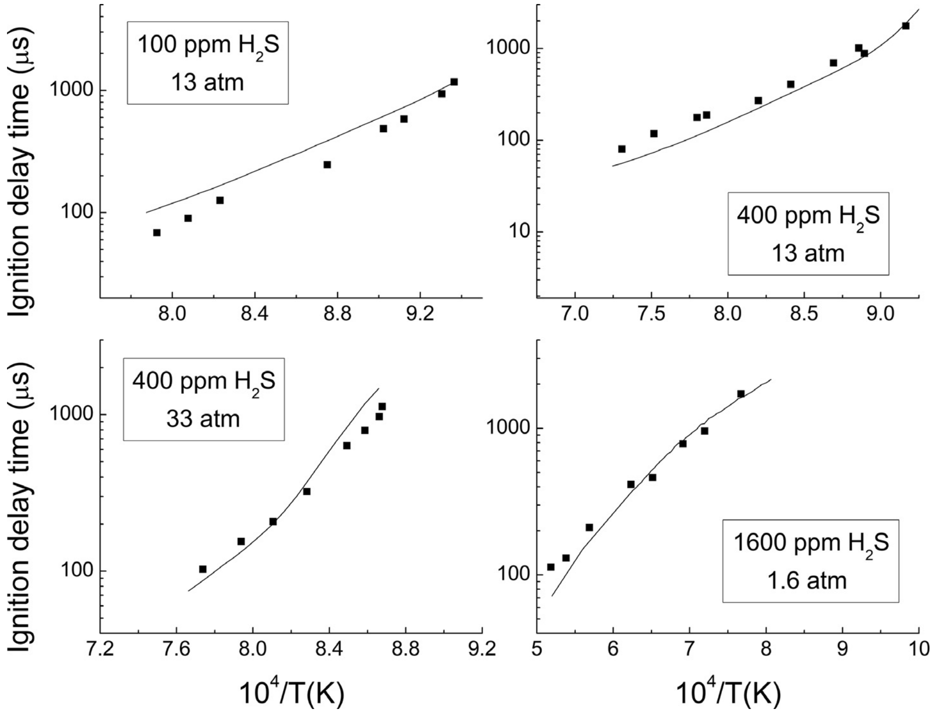

Fig. 10. Ignition delay time measurements vs. temperature for different experimental conditions, using a mixture of 1% H_2/1% O_2, diluted in Ar and doped with H_2S. Experimental data are taken from the work of Mathieu et al. [37].

for financial support. J.M. Colom acknowledges to MINECO for the predoctoral grant awarded (BES-2016-076610).

References

[1] Maggio G, Cacciola G. When will oil, natural gas, and coal peak? Fuel 2012;98:111–23.

[2] Taifan W, Baltrusaitis J. Minireview: direct catalytic conversion of sour natural gas (CH_4 + H_2S + CO_2) components to high value chemicals and fuels. Catal Sci Technol 2017;7:2919–29.

[3] Mac Kinnon MA, Brouwer J, Samuelsen S. The role of natural gas and its infrastructure in mitigating greenhouse gas emissions, improving regional air quality, and renewable resource integration. Prog Energy Combust Sci 2018;64:62–92.

[4] IEA International Energy Agency, Are we entering a golden age of gas?, World Energy Outlook. https://www.iea.org/publications/freepublications/publication/WEO2011_GoldenAgeofGasReport.pdf; 2011 [accessed 1 April 2019].

[5] Hammer G, Lübcke T, Kettner R, Pillarella MR, Recknagel H, Commichau A, Neumann H-J, Paczynska-Lahme B. Ullmann's Encyclopedia of Industrial Chemistry. Wiley-VCH: Weinheim, Germany, vol. 23; 2012. Chapter Natural Gas, p. 739–92.

[6] US Department of Energy. Report of basic research needs for clean and efficient combustion of 21st century transportation fuels. https://www.osti.gov/servlets/purl/935428-bbBji1/; 2006 [accessed 1 April 2019].

[7] Zarei S, Ganji H, Sadi M, Rashidzadeh M. Thermo-kinetic modeling and optimization of the sulfur recovery unit thermal stage. Appl Therm Eng 2016;103:1095–104.

[8] Nabikandi NJ, Fatemi S. Kinetic modelling of a commercial sulfur recovery unit based on Claus straight through process: comparison with equilibrium model. J Ind Eng Chem 2015;30:50–63.

[9] Rappold TA, Lackner KS. Large scale disposal of waste sulfur: from sulfide fuels to sulfate sequestration. Energy 2010;35:1368–80.

[10] AuYeung N, Yokochi AFT. Steam reformation of hydrogen sulfide. Int J Hydrogen Energy 2013;38:6304–13.

[11] Villasmil W, Steinfeld A. Hydrogen production by hydrogen sulfide splitting using concentrated solar energy – thermodynamics and economic evaluation. Energy Convers. Manag. 2010;51:2353–61.

[12] Kappauf T, Fletcher EA. Hydrogen and sulfur from hydrogen sulfide-VI. Solar thermolysis. Energy 1989;14:443–9.

[13] Salman OA, Bishara A, Marafi A. An alternative to the claus process for treating hydrogen sulfide. Energy 1987;12:1227–32.

[14] Langè S, Campestrini M, Stringari P. Phase behavior of system methane + hydrogen sulfide. AIChE J 2016;62:4090–108.

[15] Bongartz D, Shanbhogue SJ, Ghoniem AF. Formation and control of sulfur oxides in sour gas oxy-combustion: prediction using a reactor network model. Energy Fuels 2015;29:7670–80.

[16] Gopan A, Kumfer BM, Axelbaum RL. Effect of operating pressure and fuel moisture on net plant efficiency of a staged pressurized oxy-combustion power plant. Int J Greenh Gas Control 2015;39:390–6.

[17] Wang X, Adeosun A, Yablonsky G, Gopan A, Du P, Axelbaum RL. Synergistic SO_x/NO_x chemistry leading to enhanced SO_3 and NO_2 formation during pressurized oxy-combustion. React Kinet Mech Catal 2018;123:313–22.

[18] Gersen S, van Essen M, Darmeveil H, Hashemi H, Rasmussen CT, Christensen JM, et al. Experimental and modeling investigation of the effect of H_2S addition to methane on the ignition and oxidation at high pressures. Energy Fuels 2017;31:2175–82.

[19] Zeng Z, Dlugogorski BZ, Oluwoye I, Altarawneh M. Co-oxidation of methane (CH_4) and carbon disulfide (CS_2). Proc Combust Inst 2019;27:677–85.

[20] Bongartz D, Ghoniem AF. Impact of sour gas composition on ignition delay and burning velocity in air and oxy-fuel combustion. Combust Flame 2015;162:2749–57.

[21] Bongartz D, Ghoniem AF. Chemical kinetics mechanism for oxy-fuel combustion of mixtures of hydrogen sulfide and methane. Combust Flame 2015;162:544–53.

[22] Salisu I, Abhijeet R. Kinetic simulation of acid gas (H_2S and CO_2) destruction for simultaneous syngas and sulfur recovery. Ind Eng Chem Res 2016;55:6743–52.

[23] Zhou CR, Sendt K, Haynes BS. Experimental and kinetic modelling study of H_2S oxidation. Proc Combust Inst 2013;34:625–32.

[24] Song Y, Hashemi H, Christensen JM, Zou C, Haynes BS, Marshall P, et al. An exploratory flow reactor study of H_2S oxidation at 30–100 bar. Int J Chem Kinet 2017;49:37–52.

[25] Colom-Díaz JM, Abián M, Ballester MY, Millera Á, Bilbao R, Alzueta MU. H_2S conversion in a tubular flow reactor: experiments and kinetic modeling. Proc Combust Inst 2019;37:727–34.

[26] Haynes BS. Combustion research for chemical processing. Proc Combust Inst 2019;37:1–32.

[27] Toftegaard MB, Brix J, Jensen PA, Glarborg P, Jensen AD. Oxy fuel combustion of solid fuels. Prog Energy Combust Sci 2010;36:581–625.

[28] Marrodán L, Millera Á, Bilbao R, Alzueta MU. High-pressure study of methylformate oxidation and its interaction with NO. Energy Fuels 2014;28:6107–15.

[29] Rasmussen CL, Hansen J, Marshall P, Glarborg P. Experimental measurements and kinetic modeling of $CO/H_2/O_2/NO_x$ conversion at high pressure. Int J Chem Kinet 2008;40:454–580.

[30] CHEMKIN-PRO 15151. Reaction Design, San Diego; 2013.

[31] Garrido JD, Ballester MY, Orozco-González Y, Canuto S. CASPT2 study of the potential energy surface of the HSO_2 system. J Phys Chem A 2011;115:1453–61.

[32] Alzueta MU, Bilbao R, Glarborg P. Inhibition and sensitization of fuel oxidation by SO_2. Combust Flame 2001;127:2234–51.

[33] Colom-Díaz JM, Millera Á, Bilbao R, Alzueta MU. High pressure study of H_2 oxidation and its interaction with NO. Int. J. Hydrogen Energy 2019;44:6325–32.

[34] Atkinson R, Baulch DL, Cox RA, Crowley JN, Hampson RF, Hynes RG, et al. Evaluated kinetic and photochemical data for atmospheric chemistry: Volume I – gas phase reactions of O_x, HO_x, NO_x and SO_x species. Atmos Chem Phys 2004;4:1461–738.

[35] Alzueta MU, Pernía R, Abián M, Millera Á, Bilbao R. CH_3SH conversion in a tubular flow reactor. Experiments and kinetic modelling. Combust. Flame 2019;203:23–30.

[36] Marrodán L, Arnal AJ, Millera Á, Bilbao R, Alzueta MU. The inhibiting effect of NO addition on dimethyl ether high-pressure oxidation. Combust Flame 2018;197:1–10.

[37] Mathieu O, Deguillaume F, Petersen EL. Effects of H_2S addition on hydrogen ignition behind reflected shock waves: experiments and modeling. Combust Flame 2014;161:23–36.

[38] Gao Y, Zhou CR, Sendt K, Haynes BS, Marshall P. Kinetic and modeling studies of the reaction $S + H_2S$. Proc Combust Inst 2011;33:459–65.

Article IV

Colom-Díaz, J.M.; Leciñena, M.; Peláez, A.; Abián, M.; Millera, Á.; Bilbao, R.; Alzueta, M.U. (2020). Study of the conversion of H_2S/CH_4 mixtures at different pressures. *Fuel* 262, 116484.

Fuel 262 (2020) 116484

Contents lists available at ScienceDirect

Fuel

journal homepage: www.elsevier.com/locate/fuel

Full Length Article

Study of the conversion of CH_4/H_2S mixtures at different pressures

J.M. Colom-Díaz, M. Leciñena, A. Peláez, M. Abián, Á. Millera, R. Bilbao, M.U. Alzueta*

Aragón Institute of Engineering Research (I3A), Department of Chemical and Environmental Engineering, University of Zaragoza, 50018 Zaragoza, Spain

ARTICLE INFO

Keywords:
H_2S
Sour gas
Oxidation
High pressure
PFR
Kinetic modeling

ABSTRACT

Due to the different scenarios where sour gas is present, its composition can be different and, therefore, it can be exploited through different processes, being combustion one of them. In this context, this work deals with the oxidation of CH_4 and H_2S at different pressures and under a wide variety of conditions. The oxidation has been evaluated experimentally in two different flow reactor set-ups, one working at atmospheric pressure and another one operating from atmospheric to high pressures (40 bar). Different CH_4/H_2S mixtures have been tested, together with different oxygen concentrations and in the temperature range of 500–1400 K. The experimental results obtained show that the oxidation of the CH_4/H_2S mixtures is shifted to lower temperatures as pressure increases, obtaining the same trends at atmospheric pressure in both experimental set-ups. H_2S oxidation occurs prior to CH_4 oxidation at all conditions, providing radicals to the system that promote CH_4 oxidation to lower temperatures (compared to neat CH_4 oxidation). This effect is more relevant as pressure increases. H_2S oxidation is inhibited by CH_4 at atmospheric pressure, being more noticeable when the CH_4/H_2S ratio is higher. At higher pressures, the H_2S conversion occurs similarly in the absence or presence of CH_4. The experimental results have been modeled with an updated kinetic model from previous works from the literature, which, in general, matches well the experimental trends, while some discrepancies between experimental and modeling results at atmospheric pressure and 40 bar are found in the conversion of H_2S and CH_4.

1. Introduction

Recently, the International Energy Agency has paid special attention to natural gas, exploring how the rise of shale gas and natural gas reserves is changing the global gas market, as well as the opportunities and risks for gas use in the transition to cleaner energy systems [1]. The abundance of natural gas reserves can facilitate the transition from fossil derived to fully renewable fuels [2,3]. Unconventional sources, such as sour and shale gas (natural gas with significant amounts of H_2S and CO_2, up to 30% content in volume each [4]), are becoming more important and bring interest to the direct use of these fuels, with the consequent development of proper combustion processes and technologies for their utilization, including the necessity of an increase of the knowledge and understanding of their conversion under high pressure conditions [5].

The high CO_2 content, as well as the presence of hydrogen sulfide (H_2S), limit the economic and environmental viability of sour gas resources. So far, the main solution has relied upon the production of sulfur through sulfur recovery units (SRU) using acid gas, that includes both CO_2 and H_2S [6], based on the Claus process [7], performing thus a prior cost effective separation process from the fuel. In these units, the H_2S is partially oxidized, producing both SO_2 and S that further react in the Claus reactor in the presence of a catalyst. CH_4 might be added to the process to increase furnace temperature and preventing flame extinction [8]. Improvements of the Claus process include: the use of oxygen enrichment, as it raises the flame temperature by eliminating the diluent effect of nitrogen in air [9], production of hydrogen or syngas together with sulfur in the Claus process [10,11], or sulfur production from SO_2 containing streams, by reaction of SO_2 with methane to produce CS_2 and H_2S, and later on sulfur [12].

Another possibility for natural gas utilization, particularly shale gas containing significant amounts of H_2S, is its direct combustion. Not many studies on that are available in the literature. Actually, to our knowledge, only oxy-combustion of sour gas has been addressed in the literature [13–15], including the development of this process at high pressures to increase efficiency in power plants [16,17]. The high-pressure conditions may allow the direct use of sour gas in a gas turbine process [13].

Apart from sour gas reserves, H_2S is also present together with CH_4 in biogas obtained from the anaerobic biochemical conversion of biomass, in a range of 100–10000 ppm [18]. As increasing the share of renewable energy is considered to be one of the main options to reduce

---

* Corresponding author.
E-mail address: uxue@unizar.es (M.U. Alzueta).

https://doi.org/10.1016/j.fuel.2019.116484
Received 21 June 2019; Received in revised form 2 October 2019; Accepted 22 October 2019
Available online 31 October 2019
0016-2361/ © 2019 Elsevier Ltd. All rights reserved.

Table 1
Experimental conditions. N_2 as bath gas.

Set	Set-up	Residence time, t_r (s)	Manometric Pressure (bar)	$[CH_4]$ (ppm)	$[H_2S]$ (ppm)	$[O_2]$ (ppm)	λ CH_4	λ H_2S	λ_{total}	Ref.
1	1	$232 \cdot \frac{P(bar)}{T(K)}$	0.65	1569	480	4500	1.43	6.25	1.17	p.w.
2	1	$232 \cdot \frac{P(bar)}{T(K)}$	0.65	–	525	4510	–	5.73	5.73	p.w.
3	1	$232 \cdot \frac{P(bar)}{T(K)}$	0.65	1350	1250	4590	1.70	2.45	1.00	p.w.
4	1	$232 \cdot \frac{P(bar)}{T(K)}$	0.65	1307	1255	25,500	9.76	13.5	5.67	p.w.
5	1	$232 \cdot \frac{P(bar)}{T(K)}$	0.65	480	1270	11,300	11.77	5.93	3.94	p.w.
6	1	$232 \cdot \frac{P(bar)}{T(K)}$	10	1282	1243	4550	1.77	2.44	1.03	p.w.
7	1	$232 \cdot \frac{P(bar)}{T(K)}$	20	1303	1224	4503	1.73	2.45	1.01	p.w.
8	1	$232 \cdot \frac{P(bar)}{T(K)}$	40	1320	1230	4600	1.74	2.49	1.03	p.w.
9	1	$232 \cdot \frac{P(bar)}{T(K)}$	20	1315	1295	1804	0.68	0.93	0.39	p.w.
10	1	$232 \cdot \frac{P(bar)}{T(K)}$	20	1348	–	4286	1.59	–	1.59	p.w.
11	1	$232 \cdot \frac{P(bar)}{T(K)}$	40	1400	–	4500	1.61	–	1.61	p.w.
12	1	$232 \cdot \frac{P(bar)}{T(K)}$	0.65	–	505	1509	–	1.99	1.99	[40]
13	1	$232 \cdot \frac{P(bar)}{T(K)}$	10	–	485	1510	–	2.06	2.06	[40]
14	1	$232 \cdot \frac{P(bar)}{T(K)}$	20	–	497	1520	–	2.04	2.04	[40]
15	1	$232 \cdot \frac{P(bar)}{T(K)}$	40	–	500	1545	–	2.06	2.06	[40]
16	2	$\frac{194.6}{T(K)}$	Atmospheric	1517	–	750	0.25	–	0.25	p.w.
17	2	$\frac{194.6}{T(K)}$	Atmospheric	1517	–	3000	0.99	–	0.99	p.w.
18	2	$\frac{194.6}{T(K)}$	Atmospheric	1508	–	6000	1.99	–	1.99	p.w.
19	2	$\frac{194.6}{T(K)}$	Atmospheric	1510	279	750	0.25	1.79	0.22	p.w.
20	2	$\frac{194.6}{T(K)}$	Atmospheric	1513	285	3000	0.99	7.02	0.87	p.w.
21	2	$\frac{194.6}{T(K)}$	Atmospheric	1508	298	6000	1.99	13.4	1.73	p.w.
22	2	$\frac{194.6}{T(K)}$	Atmospheric	–	482	1500	–	2.07	2.07	[29]
23	2	$\frac{194.6}{T(K)}$	Atmospheric	–	492	3750	–	5.08	5.08	[29]

p.w. denotes present work.

greenhouse gas emissions, energy from biomass has the potential to provide power to the grid on demand, for example, using biogas combustion in gas turbines [19], which can tolerate a H_2S content up to 10000 ppm [18]. However, this issue has not been deeply investigated yet [20].

It is clear that conversion of CH_4/H_2S mixtures under combustion conditions is an important research topic. In particular, studies carried out under high pressure conditions are necessary because of turbine combustion applications. In this context, both experimental studies and kinetic modeling development to describe the conversion of CH_4/H_2S mixtures can be of great interest and usefulness.

All in all, to go further into the knowledge of the combustion behavior of H_2S under different conditions, it exists a need for the development of comprehensive kinetic models that can capture the combustion chemistry of H_2S, as well as the co-oxidation of CH_4 and H_2S, which remain unknown in many aspects, while the available experimental data are limited. Previous studies of co-oxidation of CH_4/H_2S mixtures have considered mainly Claus process conditions (this is, 1–1.5 bar, 1075–1350 K) [21,22]. The only study at high pressures is the recent work from Gersen et al. [23], where they studied experimentally the autoignition and oxidation of CH_4/H_2S mixtures in a rapid compression machine (RCM) and a flow reactor. They showed prediction results with their model that agree well with the measured autoignition delay times. On the other hand, the authors indicated that the H_2S oxidation chemistry and the interaction of CH_4 and H_2S at high pressure are not well understood, emphasizing that more work is desirable on the reactions of H_2S and SH with peroxides (HO_2 and CH_3OO) and the formation and consumption of organosulfur compounds. The kinetic mechanism used in the work of Gersen et al. [23] is based on the works from Hashemi et al. [24] for CH_4 oxidation and Song et al. [25] about H_2S oxidation at high pressures.

While the conversion of methane is known with a certain confidence, more work is desirable regarding the H_2S oxidation. The current mechanisms used for H_2S oxidation [e.g. 13–15,26] are mainly based on the work from Zhou et al. [27], which has been used for describing H_2S oxidation in recent works, addressing ignition delay times and laminar flame speed measurements [26,28] and flow reactors studies [23,25,29]. However, despite these efforts, there is still necessity of both, more accurate direct experimental determination of important rate constants and more experimental data to be used for validation and further improvement of modeling predictions [13,15].

In this context, this work addresses the conversion of CH_4/H_2S mixtures at different pressures, from atmospheric to 41 bar, analyzing the influence of temperature (500–1050 K) and for different oxygen concentrations, which results in different stoichiometry conditions, both global and/or individual for either CH_4 and H_2S. The study includes both experiments performed in two different tubular flow reactors, which have been used in different works [29–34], and a kinetic modeling study for analyzing the conversion of the CH_4/H_2S mixtures considered. These results would be useful for analyzing the conventional combustion of natural sour gas, but also for the combustion of biogas [19], the Claus process [35] or oxy-combustion of the sour gas

[13–15,36].

2. Experimental methodology

The co-oxidation of CH_4 and H_2S was studied performing experiments in two different experimental set-ups. The experimental set-up 1 was used to perform the high-pressure CH_4/H_2S mixtures oxidation experiments and it has been previously described in detail elsewhere [e.g. 30]. Therefore, only a brief description of the main features is provided here. Reactants: H_2S, CH_4, O_2 and N_2 as carrier gas, were supplied from gas cylinders through mass flow controllers with an uncertainty in the flow rate measurements of approximately 0.5%. The reactant gases were premixed before entering the reactor, which consists of a quartz tube (inner diameter of 6 mm and 1500 mm in length) designed to approximate plug flow conditions [37]. The reactor is enclosed in a stainless-steel tube that acts as a pressure shell. The steel tube is placed horizontally in a tubular oven, with three individually controlled electrical heating elements that ensure an isothermal reaction zone of approximately 500 mm, with a uniform temperature profile (± 5 K). The total flow rate in all experiments has been 1 L (STP)/min. Gas residence time in the isothermal part of the reactor depends on pressure and temperature and it can be expressed as $t_r(s) = 232*P$ (bar)/T(K). Previously to the gas analysis systems, gases pass through a filter and a condenser to ensure gas cleaning. Products are analyzed by a gas micro-chromatograph (μGC) equipped with a thermal conductivity detector (TCD) calibrated to quantify H_2S, CH_4, O_2, CO, CO_2, C_2H_4, C_2H_6, CH_3SH and CS_2. A continuous UV analyzer was used to quantify SO_2. The uncertainty of the measurements is estimated within 5%.

The experiments carried out in this work using the set-up 1 correspond to sets 1–11 in Table 1. The experimental conditions for each set of experiments: manometric pressure, concentrations of reactants and corresponding air excess ratios used (λ, defined as inlet oxygen divided by stoichiometric oxygen) are specified. In order to calculate λ, the oxygen required for the complete oxidation of H_2S has been used (λ_{H2S}, according to reaction $H_2S + 1.5O_2 = SO_2 + H_2O$), for CH_4 (λ_{CH4}, according to reaction $CH_4 + 2O_2 = CO_2 + 2H_2O$) and for both together (λ_{total}). Stoichiometric and slightly fuel lean conditions ($\lambda_{total} \approx 1$) were selected to study the oxidation of CH_4/H_2S mixtures at high pressures, while stoichiometric and oxidizing conditions were used under near atmospheric pressures. Only an experiment for a $\lambda_{total} < 1$, set 9, was also done for the pressure of 20 bar, due to the potential deposition of sulfur species in the high-pressure experimental set-up under reducing conditions. The moderate concentration of oxygen used in this work was chosen to minimize SO_3 formation, which is enhanced at oxidizing conditions and high pressures and could lead to corrosion problems [38,39]. Stoichiometric and more oxidizing conditions were used under near atmospheric pressures (0.65 bar manometric pressure). Also different ratios between CH_4 and H_2S inlet concentrations were chosen for this pressure.

Additionally to the mixtures, selected experiments using only CH_4 (sets 10 and 11 in Table 1) or H_2S were performed for comparison. Experimental data for neat H_2S oxidation experiments (sets 12–15 in Table 1) were taken from another work of the authors carried out in the same high-pressure installation (set-up 1) [40].

A different set-up (set-up 2 in Table 1) was used in order to evaluate the oxidation of CH_4 and H_2S at atmospheric pressure. A detailed description of this set-up can be found in a recent work [41]. It consists of a tubular flow reactor in an electrically heated oven, with an isothermal reaction zone of 200 mm and 8.7 mm of internal diameter. The total flow rate in all experiments was 1 L (STP)/min, resulting in a gas residence time as a function of temperature of 194.6/T(K), in seconds. The oxidation experiments, sets 16–21 in Table 1, were performed at three different stoichiometries (reducing, stoichiometric and oxidizing conditions) in the temperature range of 700–1400 K, using a concentration of water vapour of 1%. In the process, the water vapour was used to minimize the effect, if any, of radical termination reactions on the walls of the reactor, which can be more important operating at atmospheric pressure. However, in this case, water vapour presence is not expected to have an influence on the present results, as reported in the work by Alzueta et al. [41] about CH_3SH oxidation in one of the reactors used here (set-up 2 in Table 1), where the effect of H_2O (0.5%) was evaluated. Additionally, an example of the results obtained in experiments for H_2S oxidation at atmospheric pressure, with and without water, in the set-up 2, is shown in Fig. S1 of the supplementary material. Since the differences between the results were negligible, we inferred that no significant effects of radical recombination on surface were occurring. The results obtained in the neat H_2S oxidation experiments, sets 22 and 23 in Table 1, have been taken from another work of the authors [29].

3. Kinetic model

The kinetic model used in the present study is based on previous works from the authors, and it counts with reactions related to the interaction of carbon and sulfur species from the work of Alzueta et al. [42], about the inhibition and sensitization of fuel (CO) oxidation by SO_2. It also considers another study about CS_2 and COS conversion under different combustion conditions [43], and the work from Abián et al. [44] where the impact of the presence of SO_2 on the formation of soot from ethylene pyrolysis was evaluated. The description of H_2S conversion is taken from the work by Colom-Díaz et al. [29], counting with an updated subset of H_2S reactions, mainly based on the work from Zhou et al. [27] and Song et al. [25].

Besides, the present mechanism has been updated with some reactions from recent studies. For example, the H_2/O_2 reaction subset, which is important for the radical pool composition, has been taken from the examination at high pressures of H_2 oxidation and its interaction with NO [34]. New subsets have been added from the study of Gersen et al. [23], about CH_4/H_2S oxidation at high pressures, where the peroxides CH_3OO and CH_3OOH chemistry was found to be important at high pressures and low temperatures, based on previous studies from the same group about CH_4 oxidation at high pressures [24,45]. Thus, CH_3OO and CH_3OOH reaction subsets have been added. The formation and consumption of organosulfur compounds like CH_3SH were also found important in [23], and a subset describing CH_3SH conversion taken from the work of Alzueta et al. [41], which was based on the works of Zheng et al. [46] and Van de Vijver et al. [47], has been included. As for thermochemical data, same sources as for the corresponding reactions were used. Kinetic calculations were carried out in the frame of Chemkin Pro with the PFR model [48]. Ultimately, some key reactions have been updated, which are described in detail in the next section. The mechanism listing can be found as supplementary material.

4. Results and discussion

The experimental results of H_2S, SO_2, CH_4 and CO concentrations corresponding to the experiments near atmospheric pressure (set-up 1), sets 1–5 and 12 from Table 1, are presented from Figs. 1–4 together with the kinetic modelling predictions (lines). The species CO_2, C_2H_4, C_2H_6, CH_3SH and CS_2 were detected in small concentrations and, therefore, they are not shown in the figures. In all figures, symbols represent experimental concentrations, while lines denote model predictions. Additional graphics with normalized H_2S and CH_4 concentrations have been included in the supplementary material to facilitate the posterior discussion (Figs. S2 and S3) on the effect of λ and pressure in the results. Different stoichiometry values and CH_4/H_2S ratios have been used to study the oxidation behaviour of the CH_4/H_2S mixtures near atmospheric pressure. The experimental results using oxidizing conditions (set 4, $\lambda_{total} = 5.67$) are shown in Fig. 1. H_2S oxidation occurs at temperatures lower than the ones at which CH_4

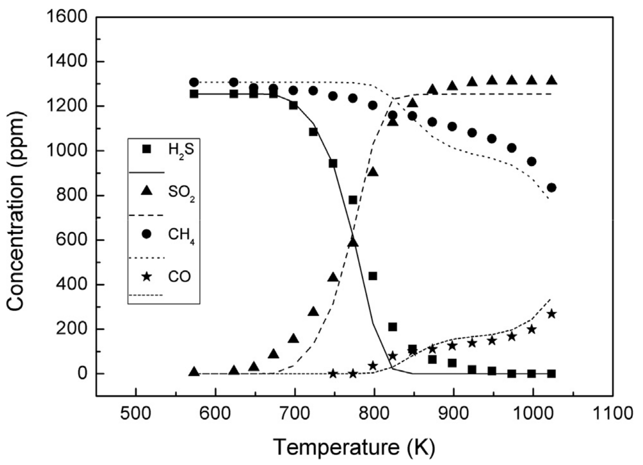

Fig. 1. Concentrations of H_2S, SO_2, CH_4 and CO vs. temperature at the experimental conditions of set 4 in Table 1 (λ_{total} = 5.67), 0.65 bar.

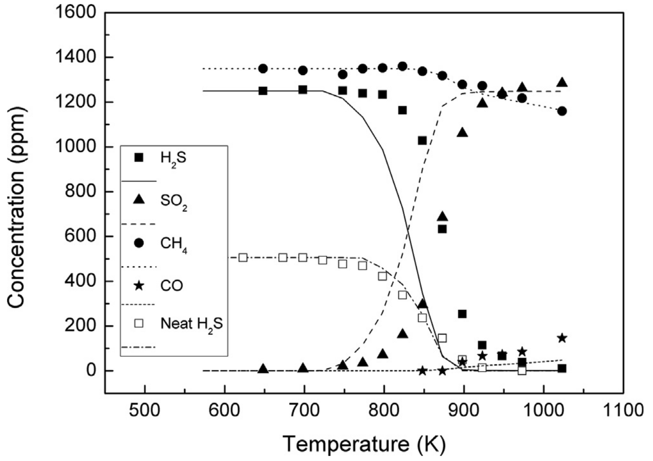

Fig. 2. Concentrations of H_2S, SO_2, CH_4 and CO vs. temperature at the experimental conditions of sets 3 (λ_{total} = 1.00) and 12 (λ_{total} = 1.99) in Table 1, 0.65 bar.

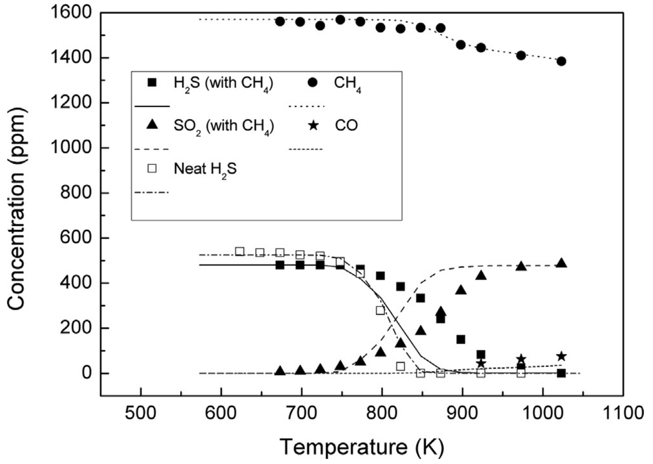

Fig. 3. Concentrations of H_2S, SO_2, CH_4 and CO vs. temperature at the experimental conditions of set 1 (λ_{total} = 1.17) and 2 (λ_{total} = 5.73) in Table 1, 0.65 bar.

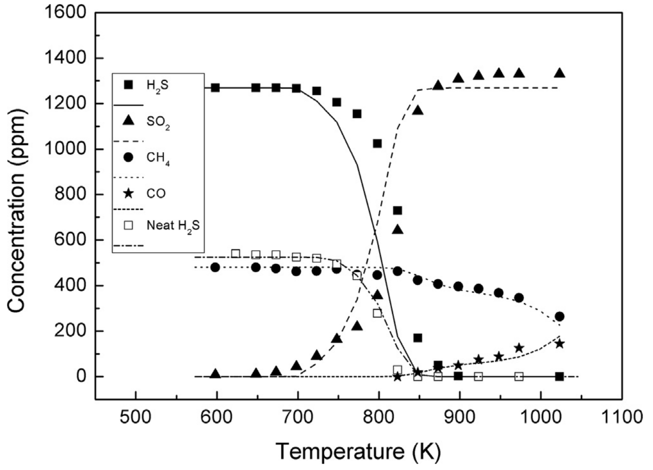

Fig. 4. Concentrations of H_2S, SO_2, CH_4 and CO vs. temperature at the experimental conditions of sets 5 (λ_{total} = 3.94) and 2 (λ_{total} = 5.73) in Table 1, 0.65 bar.

oxidation occurs, being H_2S completely converted into SO_2 at temperatures above approximately 900 K. The experimental trends are fairly well captured by the mechanism. It is remarkable that the oxidation of hydrogen sulfide occurs similarly to the results obtained in a work at atmospheric pressure in a different flow reactor (set-up 2) when studying the conversion of neat H_2S at atmospheric pressure [29]. The consumption of H_2S is due to its reactions with H and HO_2 radicals (R1 and R2). The radical SH formed further reacts with oxygen to form the peroxide HSOO (R3), which isomerizes to HSO_2 (R4) and, then, forms SO_2 + H via (R5) or reacts with O_2, due to the high concentration available, to form SO_2 + HO_2 (R6).

$$H_2S + H \rightleftharpoons SH + H_2 \tag{R1}$$

$$H_2S + HO_2 \rightleftharpoons SH + H_2O_2 \tag{R2}$$

$$SH + O_2(+M) \rightleftharpoons HSOO(+M) \tag{R3}$$

$$HSOO \rightleftharpoons HSO_2 \tag{R4}$$

$$HSO_2(+M) \rightleftharpoons SO_2 + H(+M) \tag{R5}$$

$$HSO_2 + O_2 \rightleftharpoons SO_2 + HO_2 \tag{R6}$$

The oxidation of methane in the CH_4/H_2S mixture occurs at lower temperatures compared to the oxidation of neat methane, due to the radicals coming from H_2S oxidation. Regarding neat CH_4, it did not show any reactivity in the simulation runs in these conditions. Methane reacts with OH radicals to form CH_3 (R7), which, depending on the temperature, will form different products.

$$CH_4 + OH \rightleftharpoons CH_3 + H_2O \tag{R7}$$

At low temperatures (850 K), CH_3 forms mainly CH_3O (R8) and C_2H_6 (R9), while at higher temperatures the reaction with O_2 to form CH_2O is predominant (R10). CH_3 also reacts with HO_2 to regenerate CH_4 via (R11), being less important as the temperature increases.

$$CH_3 + HO_2 \rightleftharpoons CH_3O + OH \tag{R8}$$

$$CH_3 + CH_3(+M) \rightleftharpoons C_2H_6(+M) \tag{R9}$$

$$CH_3 + O_2 \rightleftharpoons CH_2O + OH \tag{R10}$$

$$CH_3 + HO_2 \rightleftharpoons CH_4 + O_2 \tag{R11}$$

The oxidation continues with CH_3O species decomposing to CH_2O + H (R12) and proceeding to CO via (R13) and (R14). The pathway leading to C_2H_6 might continue with its reaction to C_2H_5 (R15) and C_2H_4 (R16) later on. The oxidation behavior of methane is similar to that presented in the work of Giménez-López et al. [49] about oxy-fuel oxidation of methane.

$$CH_3O(+M) \rightleftharpoons CH_2O + H(+M) \tag{R12}$$

$$CH_2O + OH \rightleftharpoons HCO + H_2O \tag{R13}$$

$$HCO + O_2 \rightleftharpoons CO + HO_2 \tag{R14}$$

$$C_2H_6 + OH \rightleftharpoons C_2H_5 + H_2O \tag{R15}$$

$$C_2H_5 + O_2 \rightleftharpoons C_2H_4 + HO_2 \tag{R16}$$

The oxidation of both species (CH_4 and H_2S) occurs separately at a high concentration of O_2; i.e. when H_2S is fully consumed, CH_4 conversion increases coinciding with a higher formation of CO, and no presence of C-S species is detected. However, if the oxygen concentration is reduced, the oxidation behavior changes. The experimental trends of the oxidation of CH_4/H_2S mixtures at stoichiometric conditions ($\lambda_{total} = 1.00$, $\lambda_{CH4} = 1.70$, $\lambda_{H2S} = 2.45$) (set 3 in Table 1) are presented in Fig. 2, together with its comparison with neat H_2S oxidation (set 12 in Table 1), using around the same λ_{H2S} value. It is shown that methane oxidation is still promoted to lower temperatures, but to a lower extent compared to the case of oxidizing conditions. In the case of H_2S, its consumption is shifted to higher temperatures (by 75 K) compared to the neat oxidation of H_2S, indicating therefore the different behavior of H_2S conversion when studying neat oxidation of H_2S or in the CH_4/H_2S mixture. A similar case can be observed in the study of Zeng et al. [50], about the co-oxidation of CH_4 and CS_2 in a flow reactor, where they also saw experimentally a delay in the oxidation of CS_2 by CH_4 and that trace amounts of CS_2 reduce the ignition temperature of CH_4. The authors indicated that the C-H-O-S combustion chemistry was complex and consequently their mechanism could not include all potential reactions. In our case, the kinetic model cannot predict the inhibition of H_2S conversion by CH_4 to higher temperatures either, despite the inclusion in the present mechanism of the CH_3SH, CS_2 and COS conversion subsets.

With the aim of improving this situation, reaction (R17) has been also updated with the value for its kinetic constant recommended by Zeng et al. [51], who revised this reaction using the CBS-QB3 level of theory, mentioning that it was overestimated before at lower temperatures.

$$CH_3 + H_2S \rightleftharpoons CH_4 + SH \tag{R17}$$

This change has produced improvements in model predictions for the CH_4 oxidation at all conditions studied. Also new reactions (R18) and (R19) from the work of Zeng et al. [51] have been added, but they are not important under the experimental conditions considered.

$$CH_4 + S_2 \rightleftharpoons CH_3 + HS_2 \tag{R18}$$

$$CH_4 + SO \rightleftharpoons CH_3 + HSO \tag{R19}$$

Fig. 3 shows the results of the conversion of the CH_4/H_2S mixture (set 1 in Table 1) and neat H_2S (set 2 in Table 1) for similar inlet concentrations of H_2S and O_2, i.e. similar values of λ_{H2S}. In this manner, we can analyze if for $\lambda_{H2S} \approx 6$, CH_4 still has the potential to inhibit the oxidation of H_2S or the O_2 will oxidize completely the H_2S, as in the case of Fig. 1. As can be observed in Fig. 3, there is still a shift of the H_2S conversion to higher temperatures in the presence of CH_4 in comparison with the case of neat H_2S. While the conversion of neat H_2S and the neat CH_4 oxidation are well captured by the model, simulations are shifted at lower temperatures for H_2S in the mixture oxidation.

It is also interesting to compare the results obtained in set 3 (Fig. 2) and set 1 (Fig. 3) corresponding to similar λ_{CH4} and λ_{total}, but different H_2S inlet concentrations (1250 and 480 ppm, respectively) and CH_4/H_2S ratios (1.1 and 3.2, respectively). It can be observed that the onset of H_2S conversion in set 1 (Fig. 3) occurs at lower temperature than that obtained in set 3 (Fig. 2), due to the higher λ_{H2S} in set 1. On the other hand, by comparison with set 3, the conversion of H_2S in set 1 finishes at higher temperatures, which might be due to the higher CH_4/H_2S ratio in set 1 (i.e. more CH_4 consuming necessary radicals for H_2S oxidation). This can also be clearly observed in Fig. S2 of the supplementary material.

If the CH_4/H_2S ratio is reduced, Fig. 4, using the same λ_{H2S} as in Fig. 3 ($\lambda_{H2S} \approx 6$), we can evaluate if a comparatively lower concentration of methane will decrease the inhibition process. As it is shown, the H_2S oxidation finishes at lower temperatures in comparison with the results shown in Fig. 3 (see also Fig. S2 of the supplementary material), where a higher concentration of CH_4 was used, hence, consuming more radicals needed for the conversion of H_2S. However, we cannot assure if the delay in the ignition temperature of H_2S, in comparison with neat H_2S, is due to the consumption of radicals from the radical pool by CH_4, or due to the formation of some carbon-sulfur intermediate species, even though they were not detected in the μGC analysis. It is worth to mention that, except in the case of oxidizing conditions (Fig. 1), in each of the Figs. 2–4 a weak minimum in CH_4 concentration during the oxidation of H_2S can be observed at low temperatures, which could indicate some interaction somehow during the conversion of the mixtures. Additionally, as mentioned by Mulvihill et al. [28] about the importance of C-S species in process modeling, Gersen et al. [23] included C-S species in their mechanism, while Bongartz and Ghoniem [14] excluded them, obtaining both of them predictions with their models nearly similar for all shock-tube experiments. It is suggested, then, that this similarity in predictions between the two mechanisms could indicate that these C-S species are unimportant at shock-tube conditions, while the work from Mulvihill et al. [28] about flame speeds showed 4 reactions involving C-S species within the most sensitive ones. Thus, depending on the experimental conditions, C-S species might take a significant role in the oxidation process.

As the pressure increases, the conversion of both CH_4 and H_2S in the oxidation of CH_4/H_2S mixtures is shifted to lower temperatures. The concentrations of H_2S, SO_2, CH_4 and CO, as a function of temperature, at 10, 20 and 40 bar, using stoichiometric conditions (λ_{total} near 1) for CH_4/H_2S mixtures, are plotted in Figs. 5–7. Results obtained for oxidation of neat H_2S ($\lambda_{total} \approx 2$) are also shown. In the case of 20 and 40 bar, the oxidation of neat CH_4 ($\lambda_{total} \approx 1.6$) is also included, since these are the only cases in which neat methane was found to be reactive, in the temperature range studied.

The conversion of CH_4 is seen to occur and, as the conversion of H_2S, it is shifted to lower temperatures as the pressure increases. The effect of the pressure at stoichiometric conditions for CH_4/H_2S oxidation ($\lambda \approx 1$, sets 3, 6, 7 and 8 in Table 1) can be observed in Fig. S3 of the supplementary material. In the case of 10 bar, the oxidation of H_2S is almost the same with and without CH_4, whereas at 20 and 40 bar, H_2S is even slightly promoted. The oxidation trend of CH_4 is still fairly well

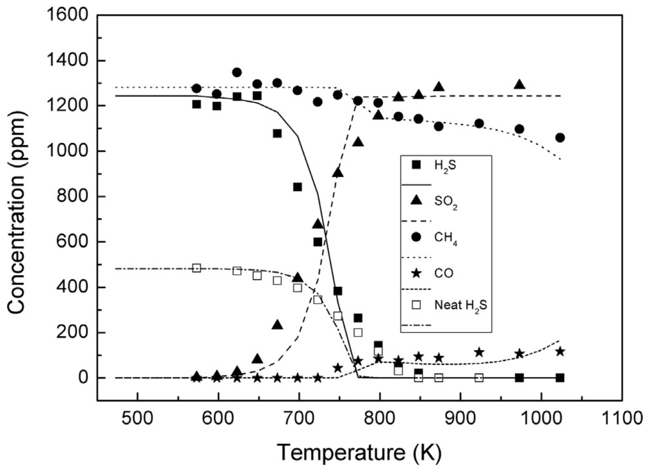

Fig. 5. Concentrations of H_2S, SO_2, CH_4 and CO vs. temperature at the experimental conditions of sets 6 ($\lambda_{total} = 1.03$) and 13 ($\lambda_{total} = 2.06$) in Table 1, 10 bar.

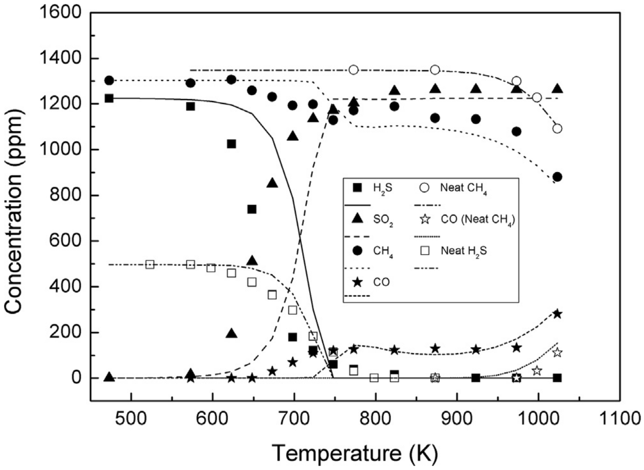

Fig. 6. Concentrations of H_2S, SO_2, CH_4 and CO vs. temperature at the experimental conditions of sets 7 (λ_{total} = 1.01), 10 (λ_{total} = 1.59) and 14 (λ_{total} = 2.04) in Table 1, 20 bar.

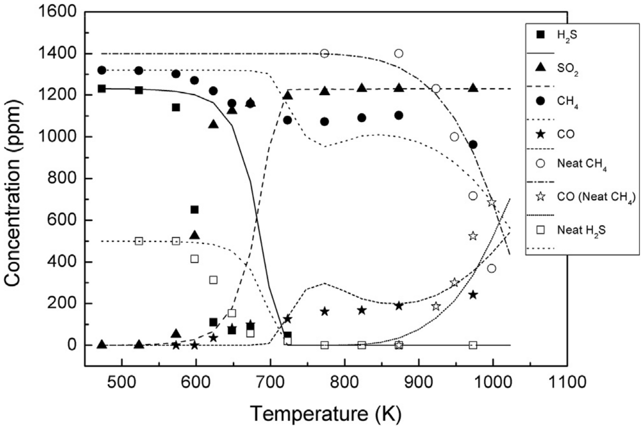

Fig. 7. Concentrations of H_2S, SO_2, CH_4 and CO vs. temperature at the experimental conditions of sets 8 (λ_{total} = 1.03), 11 (λ_{total} = 1.61) and 15 (λ_{total} = 2.06) in Table 1, 40 bar.

captured by the model, in the case of the neat CH_4 and co-oxidation. The biggest differences between modeling results and experimental concentrations are found in H_2S conversion at 40 bar, which are the same differences for neat H_2S as in the presence of CH_4. Thus, this could be attributed to the present description of the H_2S chemistry at high pressure [40].

According to the model calculations, H_2S conversion starts via (R20), as was also mentioned by Gersen et al. [23]. In the same way, Zhou et al. [27] mentioned the sensitivity of (R20) in their model due to the role to determine the ignition temperature of H_2S.

$$H_2S + O_2 \rightleftharpoons SH + HO_2 \qquad (R20)$$

Once conversion is started, the consumption of H_2S is mainly maintained through reaction of H_2S with HO_2 radicals (R2), radicals which formation is enhanced at high pressures [e.g. 23,25,26]. At the same time, H_2O_2 formation (R2), also favored at high pressures, promotes the reaction via the branching reaction (R21). The conversion of H_2S follows, as mentioned before, with (R3) and (R4), with (R6) as the main final step.

$$H_2O_2(+M) \rightleftharpoons OH + OH(+M) \qquad (R21)$$

The conversion of CH_4 in the mixture is influenced by H_2S oxidation, being the influence more noticeable as pressure increases, reaching 20% of conversion between 700 and 900 K at 40 bar. H_2S oxidation provides radicals to the radical pool and, at the same time, higher pressures involve a major role of peroxides like CH_3OO and HO_2 in the oxidation process of CH_4. At high pressures, other pathways become important in comparison with the previous ones mentioned near atmospheric pressure. Depending on temperature, the model predicts that CH_4 consumption is dependent on the reactions of CH_3 to form different products. At intermediate temperatures and high pressures, formation of peroxyl radicals may be significant [e.g. 24,32,33]. Actually, at low temperatures and high pressures (e.g. 725 K at 40 bar), the formation of the peroxide CH_3OO is the preferred channel (R22),

$$CH_3 + O_2 \rightleftharpoons CH_3OO \qquad (R22)$$

which will continue reacting through (R23), (R24), (R12), (R13) and (R14), and finally decomposed to CO in the final step (R25).

$$CH_3OO + HO_2 \rightleftharpoons CH_3OOH + O_2 \qquad (R23)$$

$$CH_3OOH(+M) \rightleftharpoons CH_3O + OH(+M) \qquad (R24)$$

$$HCO + M \rightleftharpoons H + CO + M \qquad (R25)$$

As temperature rises, other pathways become important. At 800 K and 40 bar, radical CH_3 reacts with HO_2 radicals to give CH_3O (R8), instead of producing only CH_3OO, which also ends up as CH_3O, being the net result of the CH_3OO pathway similar to reaction (R8). CH_3O decomposes thermally to CH_2O, as mentioned before via (R12), and ends as CO through (R13), (R14) and (R25). The pathway to produce C_2H_6 also becomes important at this temperature (R9). From 900 K and above, the branching ratio shifts toward the production of CH_2O (R10) from CH_3, which is the main pathway for neat CH_4 oxidation as well. CH_2O can react with HO_2 radicals too (R26), as well as with CH_3 to regenerate CH_4 (R27), like reaction (R28), but mainly CH_2O reacts with OH radicals (R13).

$$CH_2O + HO_2 \rightleftharpoons HCO + H_2O_2 \qquad (R26)$$

$$CH_2O + CH_3 \rightleftharpoons HCO + CH_4 \qquad (R27)$$

$$CH_3 + H_2 \rightleftharpoons CH_4 + H \qquad (R28)$$

Regarding reaction R10 ($CH_3 + O_2 \rightleftharpoons CH_2O + OH$), we found large discrepancies in our modeling results using different kinetic parameters from the literature. This reaction has been broadly discussed over the years, as it is important for the combustion of hydrocarbons, since it exists a competition with reaction (R29) at high temperatures and with (R22) at low temperatures.

$$CH_3 + O_2 \rightleftharpoons CH_3O + O \qquad (R29)$$

It is difficult to determine the product branching ratios quantitatively for the two high temperature competitive reaction channels (R10 and R29), because the reactions are slow and only high-temperature measurements, above approximately 1300 K, behind shock waves could produce some meaningful data [52]. A large scatter in the rate coefficients determined over the years for the $CH_3 + O_2$ reaction system exists. In the case of the works of Glarborǵs group involving CH_4 oxidation at high pressures [23,24,45,53], they use the kinetic parameters from Srinivasan et al. [54], who combined their own measurements with literature data [55–57] across the temperature range 1237–2430 K. In our simulations, these kinetic parameters are too fast for neat CH_4 conversion, which are out of the temperature range considered in the present work. Although, as mentioned by Fernandes et al. [58], this problem seemed to have been settled by Herbon et al. [57] and Srinivasan et al. [54], whose determinations for these reactions were in near agreement with the theoretical modelling results from Zhu et al. [52]. Srinivasan et al. reviewed this reaction (R10) in 2007 providing new experiments in a shock tube over the temperature range of 1224–1502 K, and yielding an updated kinetic expression [59].

Other recent studies including subsets for CH_4 conversion in their mechanisms, such as the works of Alzueta et al. [41] and Marrodán

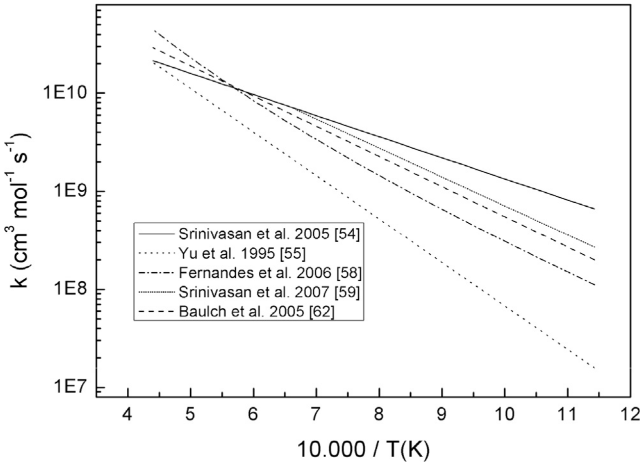

Fig. 8. Kinetic constant for reaction $CH_3 + O_2 = CH_2O + OH$ (R10) using kinetic parameters from the literature as a function of temperature, $1{\cdot}10^4/T(K)$.

et al. [32,33], used the expression of Yu et al. [55], but these values appear to be too slow to describe the neat oxidation of CH_4 under the current experimental conditions. Also, the parameters proposed by Fernandes et al. [58] have been used in different woks [e.g. 15,60,61], but those appear to be too low to reproduce our experimental results.

Hence, the authors have decided to use for (R10) the revisited parameters proposed from Srinivasan et al. [59]. As seen in Fig. 8, the kinetic constant values chosen fall just between the kinetic parameters lastly used in the literature in high pressures studies [54] and [58], and it is near the recommendation from Baulch et al. [62]. We think that this might be a reasonable estimation for the temperature range studied in this work, which falls out of the ones usually used to determine it (R10).

The experimental results for the experiment at reducing conditions ($\lambda_{total} = 0.39$) at 20 bar (set 9 in Table 1) are shown in Fig. 9. The carbon and sulphur balances remain near 100% at all temperatures (around 5%) and no C-S species were found in the analysis. H_2S conversion is more gradual than in the case near stoichiometric conditions at 20 bar, which cannot be predicted by the model. Methane concentration presents two slight minimums and is almost unreactive all across the temperature range considered.

In addition, the results obtained in the experiments of the CH_4/H_2S co-oxidation in the atmospheric pressure set-up (set-up 2) are shown in Figs. 10–12. As it can be observed, the trends are similar to the ones found in the high-pressure reactor (set-up 1) under near atmospheric pressure conditions. CH_4 oxidation is shifted to lower temperatures due

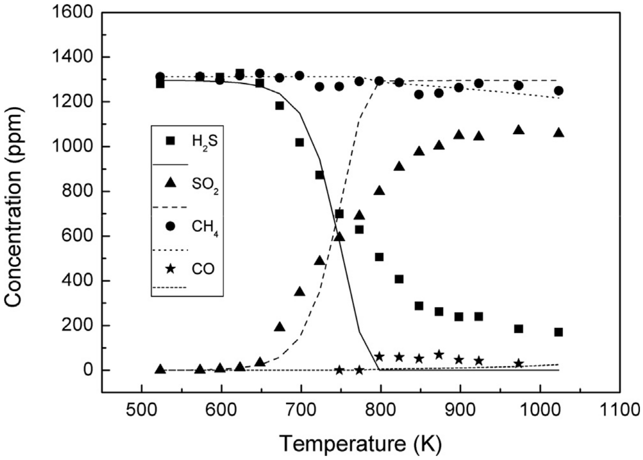

Fig. 9. Concentrations of H_2S, SO_2, CH_4 and CO vs. temperature at the experimental conditions of set 9 ($\lambda_{total} = 0.39$) in Table 1, 20 bar.

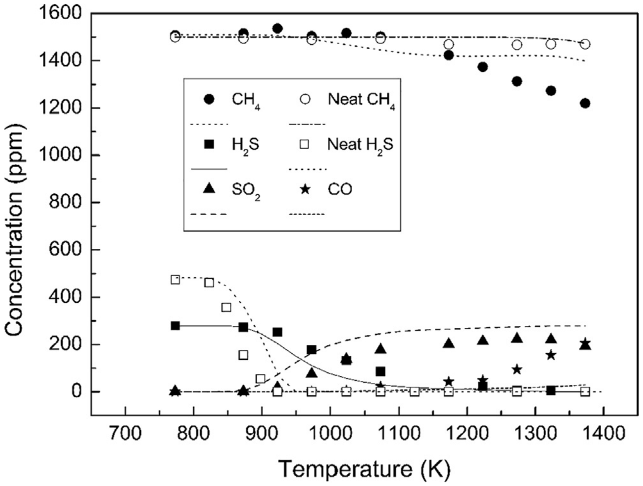

Fig. 10. Concentrations of H_2S, SO_2, CH_4 and CO vs. temperature at the experimental conditions of sets 16 ($\lambda_{total} = 0.25$), 19 ($\lambda_{total} = 0.22$) and 22 ($\lambda_{total} = 2.07$) in Table 1, atmospheric pressure.

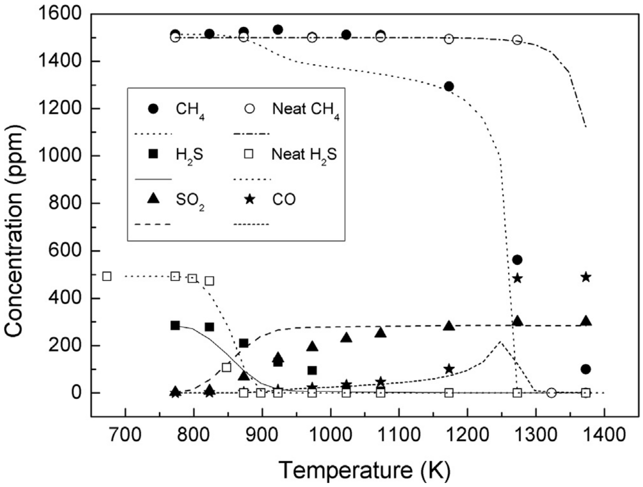

Fig. 11. Concentrations of H_2S, SO_2, CH_4 and CO vs. temperature at the experimental conditions of sets 17 ($\lambda_{total} = 0.99$), 20 ($\lambda_{total} = 0.87$) and 23 ($\lambda_{total} = 5.08$) in Table 1, atmospheric pressure.

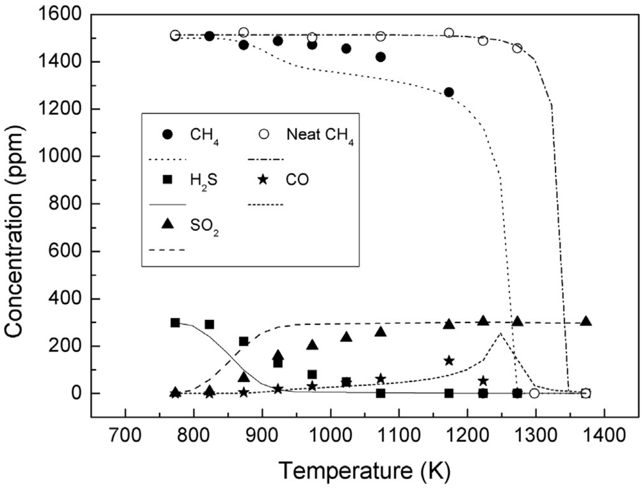

Fig. 12. Concentrations of H_2S, SO_2, CH_4 and CO vs. temperature at the experimental conditions of sets 18 ($\lambda_{total} = 1.99$) and 21 ($\lambda_{total} = 1.73$) in Table 1, atmospheric pressure.

to the presence of H_2S at all conditions considered. In the case of H_2S oxidation, its conversion is shifted to higher temperatures in the presence of CH_4, and a more gradual behaviour is seen at all conditions. The CH_4 onset temperature is different from one reactor to another. If the experiments at stoichiometric conditions are compared, there is a difference of 200 K (900 K at the set-up 1 and 1100 K at the set-up 2). This is attributed to the difference in gas residence times, as the gas residence time in the high pressure reactor (set-up 1) working near atmospheric pressure doubles the one in the reactor at atmospheric pressure (set-up 2). The kinetic model captures fairly well the oxidation trends. However, it overpredicts the oxidation of H_2S and CH_4 by a small margin, except at reducing conditions, where CH_4 oxidation is not captured at high temperatures.

5. Conclusions

The oxidation of CH_4/H_2S mixtures in two different flow reactor set-ups, at different pressures, CH_4/H_2S ratios and stoichiometries, in the temperature range of 500–1400 K, has been studied. The oxidation of both CH_4 and H_2S in the mixtures is shifted to lower temperatures as pressure increases. H_2S promotes CH_4 oxidation to lower temperatures. The presence of CH_4 inhibits the oxidation of H_2S under near atmospheric pressure, being this inhibition less important at higher pressures. A kinetic model based on published literature mechanisms has been further updated in order to reproduce the experimental results over a wide range of conditions. The kinetic model here used seems to predict fairly well the trend of CH_4 and H_2S evolution at almost all conditions considered. However, in the case of H_2S, the model does not capture accurately the experimental results under near atmospheric pressure and 40 bar, which might be related to H_2S conversion chemistry. The results obtained in this work, as well as the kinetic model used, might be useful for practical purposes dealing with both combustion or chemical processes, such as the Claus process.

Acknowledgements

The authors express their gratitude to the Aragón Government (Ref. T22_17R), co-funded by FEDER 2014-2020 “Construyendo Europa desde Aragón“, and to MINECO and FEDER (Project CTQ2015-65226) for financial support. J.M. Colom acknowledges to MINECO for the predoctoral grant awarded (BES-2016-076610).

Declaration of Competing Interest

The authors declare that they have no known competing financial interests or personal relationships that could have appeared to influence the work reported in this paper.

Appendix A. Supplementary data

Supplementary data to this article can be found online at https://doi.org/10.1016/j.fuel.2019.116484.

References

[1] IEA International Energy Agency, World Energy Outlook, 2017.
[2] Taifan W, Baltrusaitis J. Minireview: direct catalytic conversion of sour natural gas (CH_4 + H_2S + CO_2) components to high value chemicals and fuels. Catal Sci Technol 2017;7:2919–29.
[3] Mac Kinnon MA, Brouwer J, Samuelsen S. The role of natural gas and its infrastructure in mitigating greenhouse gas emissions, improving regional air quality, and renewable resource integration. Prog Energy Combust Sci 2018;64:62–92.
[4] Hammer G, Lübcke T, Kettner R, Pillarella MR, Recknagel H, Commichau A, Neumann H-J, Paczynska-Lahme B. Ullmann’s Encyclopedia of Industrial Chemistry, Wiley-VCH: Weinheim, Germany, 2012, Vol. 23; Chapter Natural Gas, 739–92.
[5] US Department of Energy, Report of basic research needs for clean and efficient combustion of 21st century transportation fuels, 2006.
[6] Salisu I, Ramees KR, Abhijeet R. Dual-stage acid gas combustion to increase sulfur recovery and decrease the number of catalytic units in sulfur recovery units. Appl Therm Eng 2019;156:576–86.
[7] Zarei S, Ganji H, Sadi M, Rashidzadeh M. Thermo-kinetic modeling and optimization of the sulfur recovery unit thermal stage. Appl Therm Eng 2016;103:1095–104.
[8] Salisu I, Ramees KR, Abhijeet R. Roles of hydrogen sulfide concentration and fuel gas injection on aromatics emission from Claus furnace. Chem Eng Sci 2017;172:513–27.
[9] Rameshni M. Cost effective options to expand SRU capacity using oxygen, Sulfur Recovery Symposium Brimstone Engineering Services, Inc Banlf, Alberta, Calgary Alberta, Calgary, May 2002.
[10] Barba D, Cammarota F, Vaiano V, Salzano E, Palma V. Experimental and numerical analysis of the oxidative decomposition of H_2S. Fuel 2017;198:68–75.
[11] Salisu I, Abhijeet R. Kinetic simulation of acid gas (H_2S and CO_2) destruction for simultaneous syngas and sulfur recovery. Ind Eng Chem Res 2016;55:6743–52.
[12] Rameshni M, Santo S. Production of elemental sulphur from SO2 (RSR). 2006 TMS Fall Extraction and Processing Division: Sohn International Symposium. 8. 469–488.
[13] Bongartz D, Shanbhogue SJ, Ghoniem AF. Formation and control of sulfur oxides in sour gas oxy-combustion: prediction using a reactor network model. Energy Fuels 2015;29:7670–80.
[14] Bongartz D, Ghoniem AF. Impact of sour gas composition on ignition delay and burning velocity in air and oxy-fuel combustion. Combust Flame 2015;162:2749–57.
[15] Bongartz D, Ghoniem AF. Chemical kinetics mechanism for oxy-fuel combustion of mixtures of hydrogen sulfide and methane. Combust Flame 2015;162:544–53.
[16] Gopan A, Kumfer BM, Axelbaum RL. Effect of operating pressure and fuel moisture on net plant efficiency of a staged, pressurized oxy-combustion power plant. Int J Greenhouse Gas Control 2015;39:390–6.
[17] Wang X, Adeosun A, Yablonsky G, Gopan A, Du P, Axelbaum RL. Synergistic SO_x/NO_x chemistry leading to enhanced SO_3 and NO_2 formation during pressurized oxy-combustion. React Kinet Mech Catal 2018;123:313–22.
[18] Awe O, Zhao Y, Nzihou A, Minh D, Lyczko N. A review of biogas utilisation, purification and upgrading technologies. Waste Biomass Valor 2017;8:267–83.
[19] Valera-Medina A, Giles A, Pugh D, Morris S, Pohl M, Ortwein A. Investigation of combustion of emulated biogas in a gas turbine test rig. J Therm Sci 2018;27:331–40.
[20] Jerzak W, Kuźnia M, Szajding A. Experimental studies and the chemical kinetics modelling of oxidation of hydrogen sulfide contained in biogas. Procedia Eng 2016;157:222–9.
[21] Chin HSF, Karan K, Mehrotra AK, Behie LA. The fate of methane in a Claus plant reaction furnace. Can J Chem Eng 2001;79:482–90.
[22] Karan K, Behie LA. CS_2 formation in the Claus reaction furnace: a kinetic study of methane-sulfur and methane-hydrogen sulfide reactions. Ind Eng Chem Res 2004;43:3304–13.
[23] Gersen S, Van Essen M, Darmeveil H, Hashemi H, Rasmussen CT, Christensen JM, et al. Experimental and modeling investigation of the effect of H_2S addition to methane on the ignition and oxidation at high pressures. Energy Fuels 2017;31:2175–82.
[24] Hashemi H, Christensen JM, Gersen S, Levinsky HB, Klippenstein SJ, Glarborg P. High pressure oxidation of methane. Combust Flame 2016;172:349–64.
[25] Song Y, Hashemi H, Christensen JM, Zou C, Haynes BS, Marshall P, et al. An exploratory flow reactor study of H_2S oxidation at 30–100 bar. Int J Chem Kinet 2017;49:37–52.
[26] Mathieu O, Deguillaume F, Petersen EL. Effects of H_2S addition on hydrogen ignition behind reflected shock waves: experiments and modeling. Combust Flame 2014;161:23–36.
[27] Zhou CR, Sendt K, Haynes BS. Experimental and kinetic modelling study of H_2S oxidation. Proc Combust Inst 2013;34:625–32.
[28] Mulvihill CR, Keesee CL, Sikes T, Teixeira RS, Mathieu O, Petersen EL. Ignition delay times, laminar flame speeds, and species time-histories in the H_2S/CH_4 system at atmospheric pressure. Proc Combust Inst 2019;37:735–42.
[29] Colom-Díaz JM, Abián M, Ballester MY, Millera Á, Bilbao R, Alzueta MU. H_2S conversion in a tubular flow reactor: Experiments and kinetic modeling. Proc Combust Inst 2019;37:727–34.
[30] Marrodán L, Millera Á, Bilbao R, Alzueta MU. High-pressure study of methylformate oxidation and its interaction with NO. Energy Fuels 2014;28:6107–15.
[31] Marrodán L, Royo E, Millera Á, Bilbao R, Alzueta MU. High-pressure oxidation of dimethoxymethane. Energy Fuels 2015;29:3507–17.
[32] Marrodán L, Arnal AJ, Millera Á, Bilbao R, Alzueta MU. The inhibiting effect of NO addition on dimethyl ether high-pressure oxidation. Combust Flame 2018;197:1–10.
[33] Marrodán L, Fuster M, Millera Á, Bilbao R, Alzueta MU. Ethanol as a fuel additive: high-pressure oxidation of its mixtures with acetylene. Energy Fuels 2018;32:10078–87.
[34] Colom-Díaz JM, Millera Á, Bilbao R, Alzueta MU. High pressure study of H_2 oxidation and its interaction with NO. Int J Hydrog Energy 2019;44:6325–32.
[35] Haynes BS. Combustion research for chemical processing. Proc Combust Inst 2019;37:1–32.
[36] Toftegaard MB, Brix J, Jensen PA, Glarborg P, Jensen AD. Oxy fuel combustion of solid fuels. Prog Energy Combust Sci 2010;36:581–625.
[37] Rasmussen CL, Hansen J, Marshall P, Glarborg P. Experimental measurements and kinetic modeling of $CO/H_2/O_2/NO_x$ conversion at high pressure. Int J Chem Kinet 2008;40:454–580.
[38] Colom JM, Alzueta MU, Christensen JM, Glarborg P, Cordtz R, Schramm J. Importance of vanadium-catalyzed oxidation of SO_2 to SO_3 in two-stroke marine diesel engines. Energy Fuels 2016;30:6098–102.

[39] Fleig D, Alzueta MU, Normann F, Abián M, Andersson K, Johnsson F. Combust Flame 2013;160:1142–51.

[40] Colom-Díaz JM, Abián M, Millera Á, Bilbao R, Alzueta MU. Influence of pressure on H_2S oxidation. Experiments and kinetic modeling. Fuel 2019;258:116145.

[41] Alzueta MU, Pernía R, Abián M, Millera Á, Bilbao R. CH_3SH conversion in a tubular flow reactor. Experiments and kinetic modelling. Flame 2019;203:23–30.

[42] Alzueta MU, Bilbao R, Glarborg P. Inhibition and sensitization of fuel oxidation by SO_2. Combust Flame 2001;127:2234–51.

[43] Abián M, Cebrián M, Millera Á, Bilbao R, Alzueta MU. CS_2 and COS conversion under different combustion conditions. Combust Flame 2015;162:2119–27.

[44] Abián M, Millera Á, Bilbao R, Alzueta MU. Impact of SO_2 on the formation of soot from ethylene pyrolysis. Fuel 2015;159:550–8.

[45] Rasmussen CL, Jakobsen JG, Glarborg P. Experimental measurements and kinetic modeling of CH_4/O_2 and $CH_4/C_2H_6/O_2$ conversion at high pressure. Int J Chem Kinet 2008;40:778–807.

[46] Zheng X, Fisher EM, Gouldin FC, Bozzelli JW. Pyrolysis and oxidation of ethyl methyl sulfide in a flow reactor. Combust Flame 2011;158:1049–58.

[47] Van de Vijver R, Vandewiele NM, Vandeputte AG, Van Geem KM, Reyniers M-F, Green WH, et al. Rule-based ab initio kinetic model for alkyl sulfide pyrolysis. Chem Eng J 2015;278:385–93.

[48] CHEMKIN-PRO 15151, Reaction Design, San Diego, (2013).

[49] Giménez-López J, Millera Á, Bilbao R, Alzueta MU. Experimental and kinetic modeling study of the oxy-fuel oxidation of natural gas, CH_4 and C_2H_6. Fuel 2015;160:404–12.

[50] Zeng Z, Dlugogorski BZ, Oluwoye I, Altarawneh M. Co-oxidation of methane (CH_4) and carbon disulfide (CS_2). Proc Combust Inst 2019;27:677–85.

[51] Zeng Z, Altarawneh M, Oluwoye I, Glarborg P, Dlugogorski BZ. Inhibition and Promotion of Pyrolysis by Hydrogen Sulfide (H_2S) and Sulfanyl Radical (SH). J Phys Chem A 2016;120:8941–8.

[52] Zhu R, Hsu C-C, Lin MC. Ab initio study of the $CH_3 + O_2$ reaction: kinetics, mechanism and product branching probabilities. J Chem Phys 2001;115:195–203.

[53] Rasmussen CL, Rasmussen AE, Glarborg P. Sensitizing effects of NO_x on CH_4 oxidation at high pressure. Combust Flame 2008;154:529–45.

[54] Srinivasan NK, Su MC, Sutherland JW, Michael JV. Reflected shock tube studies of high-temperature rate constants for $CH_3 + O_2$, $H_2CO + O_2$, and $OH + O_2$. J Phys Chem A 2005;109:7902–14.

[55] Yu C-L, Wang C, Frenklach M. Chemical kinetics of methyl oxidation by molecular oxygen. J Phys Chem 1995;99:14377–87.

[56] Hwang SM, Ryu S-O, De Witt KJ, Rabinowitz MJ. Rate coefficient measurements of the reaction $CH_3 + O_2 = CH_3O + O$. J Phys Chem A 1999;103:5949–58.

[57] Herbon JT, Hanson RK, Bowman CT, Golden DM. The reaction of $CH_3 + O_2$: experimental determination of the rate coefficients for the product channels at high temperatures. Proc Combust Inst 2005;30:955–63.

[58] Fernandes RX, Luther K, Troe J. Falloff curves for the reaction $CH_3 + O_2(+M) = CH_3O_2(+M)$ in the pressure range 2–1000 bar and the temperature range 300–700 K. J Phys Chem A 2006;110:4442–9.

[59] Srinivasan NK, Su MC, Michael JV. $CH_3 + O_2 = H_2CO + OH$ Revisited. J Phys Chem A 2007;11:11589–91.

[60] Song Y, Marrodán L, Vin N, Herbinet O, Assaf E, Fittschen C, et al. The sensitizing effects of NO_2 and NO on methane low temperature oxidation in a jet stirred reactor. Proc Combust Inst 2019;37:667–75.

[61] Metcalfe WK, Burke SM, Ahmed SS, Curran HJ. A hierarchical and comparative kinetic modeling study of C1–C2 hydrocarbon and oxygenated fuels. Int J Chem Kinet 2013;45:638–75.

[62] Baulch DL, Bowman CT, Cobos CJ, Cox RA, Just Th, Kerr JA, et al. Phys Chem Ref Data 2005;34:1244.

SUPPLEMENTARY MATERIAL

Study of the conversion of CH_4/H_2S mixtures at different pressures

J. M. Colom-Díaz, M. Leciñena, A. Peláez, M. Abián, Á. Millera, R. Bilbao, M. U. Alzueta*

Aragón Institute of Engineering Research (I3A). Department of Chemical and Environmental Engineering, University of Zaragoza, 50018 Zaragoza, Spain.

Table of contents:

1) **Comparison of H_2S concentration at atmospheric pressure in the presence and absence of water vapor**

   Figure S1. Comparison of concentration results vs. temperature of H_2S oxidation ($\lambda \approx 5$). Open symbols correspond to the experimental conditions without water vapour (inlet concentrations: H_2S=492 ppm, O_2=3750 ppm) and solid symbols with water vapour (1%) (inlet concentrations: H_2S=508 ppm, O_2=3750 ppm).

2) **Comparison of the concentrations of CH_4 and H_2S vs. temperature at the different pressures and lambda values presented in Table 1.**

   Figure S2. Concentration of H_2S and CH_4 vs. temperature for experiments at the same pressure (manometric pressure = 0.65 bar) and different air excess ratios. Experimental conditions of sets 1, 3, 4 and 5 in Table 1.

   Figure S3. Concentration of H_2S and CH_4 vs. temperature for experiments with similar air excess ratio ($\lambda_{total} \approx 1$) and different manometric pressures. Experimental conditions of sets 3, 6, 7 and 8 in Table 1.

1) Comparison of H_2S concentration at atmospheric pressure in the presence and absence of water vapor

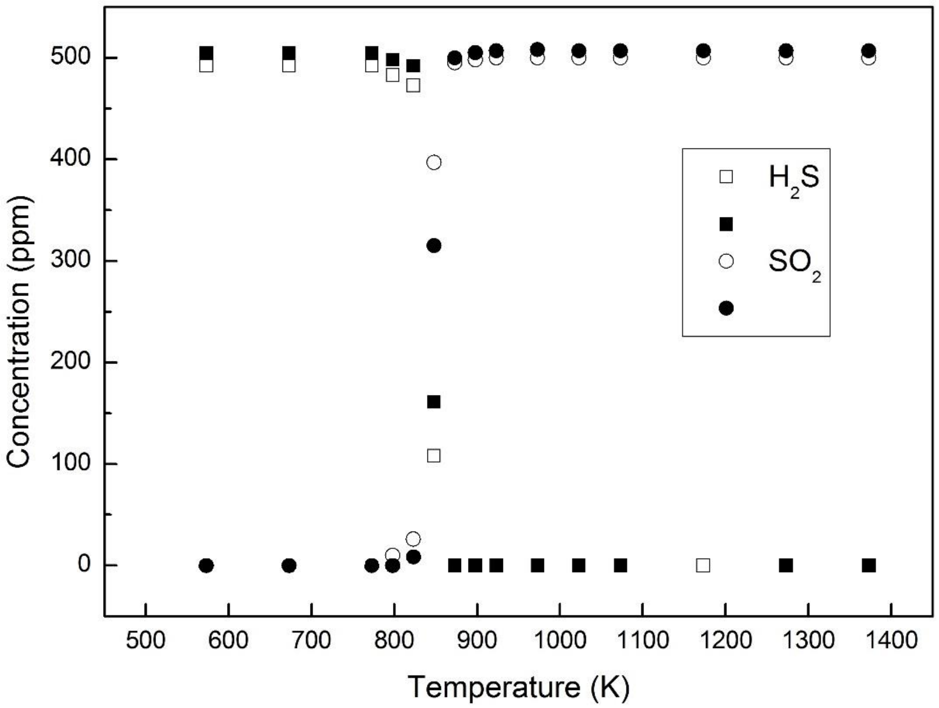

Figure S1. Comparison of concentration results vs. temperature of H_2S oxidation (λ≈5). Open symbols correspond to the experimental conditions without water vapour (inlet concentrations: H_2S=492 ppm, O_2=3750 ppm) and solid symbols with water vapour (1%) (inlet concentrations: H_2S=508 ppm, O_2=3750 ppm).

2) Comparison of the concentrations of CH_4 and H_2S vs. temperature at the different pressures and lambda values presented in Table 1.

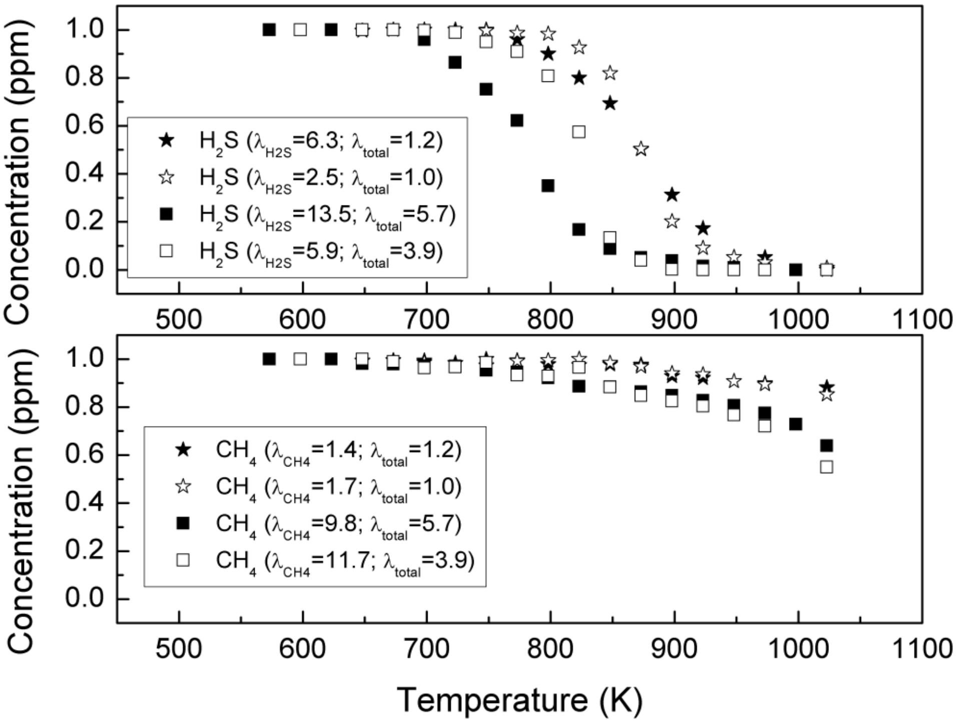

Figure S2. Concentration of H_2S and CH_4 vs. temperature for experiments at the same pressure (manometric pressure = 0.65 bar) and different air excess ratios. Experimental conditions of sets 1, 3, 4 and 5 in Table 1.

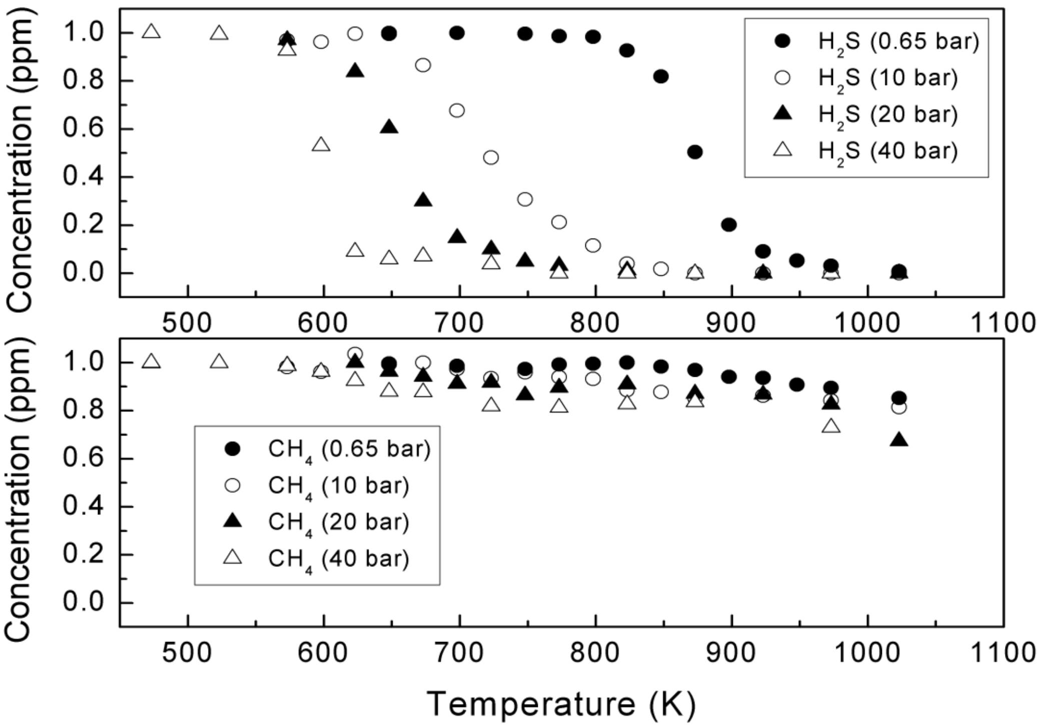

Figure S3. Concentration of H_2S and CH_4 vs. temperature for experiments with similar air excess ratio (λ_{total}≈1) and different manometric pressures. Experimental conditions of sets 3, 6, 7 and 8 in Table 1.

Article V

Colom-Díaz, J.M.; Millera, Á.; Bilbao, R.; Alzueta, M.U. (2021). New results of H_2S oxidation at high pressures. Experiments and kinetic modeling. *Fuel* 285, 119261.

Fuel 285 (2021) 119261

Contents lists available at ScienceDirect

Fuel

journal homepage: www.elsevier.com/locate/fuel

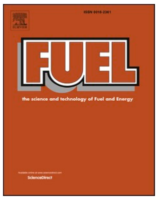

Full Length Article

New results of H_2S oxidation at high pressures. Experiments and kinetic modeling

J.M. Colom-Díaz, Á. Millera, R. Bilbao, M.U. Alzueta *

Aragón Institute of Engineering Research (I3A), Department of Chemical and Environmental Engineering, University of Zaragoza, 50018 Zaragoza, Spain

ARTICLE INFO

Keywords:
H_2S
Oxidation
High pressure
Sour gas
Kinetic modeling

ABSTRACT

The present study deals with the oxidation of H_2S at high pressures. In some local scenarios, combustion is seen as an alternative possibility for the use of sour gas mixtures containing H_2S. Therefore, further research is needed in terms of H_2S oxidation characteristics and kinetics, which might be useful for existing processes like the Claus process. Experiments have been performed in the present work in a flow reactor under diluted conditions at different manometric pressures (0.6, 10, 20 and 40 bar). The influence of oxygen concentration ($\lambda = 1$ and $\lambda = 6$), temperature (450–1100 K) and gas residence time (371/T(K)-9280/T(K), in seconds) have been studied. At a given pressure, increasing oxygen concentration shifts the onset of H_2S conversion to lower temperatures and makes the H_2S consumption more abrupt. Gas residence time has an important influence on the H_2S oxidation behavior under the experimental conditions studied. A recent kinetic model by the authors has been updated with two new reactions, obtaining a good prediction of H_2S oxidation over a wide variety of experimental conditions, both from this work and the literature. The formation of H_2O_2 species, favored at high pressures, is responsible for the importance of the two new reactions here proposed, improving the model predictions at high pressures. At atmospheric pressure, the reaction pathways obtained using the current mechanism, remain essentially unaltered in comparison with previous studies.

1. Introduction

Natural gas reserves that contain significant concentrations of H_2S and CO_2 (up to 30% content in volume each one) are referred as sour gas [1]. According to the International Energy Agency [2], the abundance of these reserves worldwide is estimated in more than 40% of the world's gas reserves, increasing to 60% for Middle East. The natural gas production is expected to peak near 2035 [3].

Gas reserves with high H_2S contents might have problems with their exploitation, due to economic or practical limitations [4]. The most extended way of treating gas streams with high H_2S gas contents is to produce sulfur, through the well-known Claus process or sulfur recovery units [5,6]. About half of the H_2S handling costs in the Claus process are related to the tail gas treatment of H_2S (recovery yield of sulfur up to 97%) [7], which increases the price of sulfur as raw material. Additional solutions to deal with sour gas and H_2S have been proposed. For example, obtaining revenue of shale gas processing integrated with ethylene production [8], producing hydrogen and syngas together with sulfur in the Claus process [9,10], or different catalytic processes which convert sour gas to valuable products such as: H_2, CS_2 and fertilizers [11].

Another possible alternative is the direct combustion of the sour gas. Usually, this kind of gas is treated prior to its use in order to remove sulfur compounds, although recently the direct combustion of these fuels, without the use of expensive cleaning treatments, has received a significant interest [12]. This also causes the H_2S combustion, which releases around 500 kJ/mol H_2S [13] (according to the $H_2S + 1.5O_2 = SO_2 + H_2O$ reaction). Apart from sour gas reserves, H_2S is also present, in a range of 0.01–1 % in volume [14], together with CH_4, in biogas obtained from the anaerobic biochemical conversion of biomass. Increasing the share of renewable energy is considered to be one of the main options to reduce greenhouse gas emissions. Therefore, energy from biomass has the potential to provide power to the grid on demand, for example, using biogas combustion in gas turbines [15], which can tolerate a H_2S content up to 1% [14]. The combustion of biogas containing H_2S has not been deeply investigated yet [16]. On the other hand, studies about power generation systems have been published for un-treated sour gas as fuel [17–19].

---

* Corresponding author.
E-mail address: uxue@unizar.es (M.U. Alzueta).

https://doi.org/10.1016/j.fuel.2020.119261
Received 1 June 2020; Received in revised form 3 September 2020; Accepted 13 September 2020
Available online 5 October 2020
0016-2361/© 2020 Elsevier Ltd. All rights reserved.

Despite the importance of the sour gas combustion performed under pressure, the research in the literature about H_2S oxidation at high pressures is scarce. Apart from the initial study by Frenklach et al. [20] about high-pressure shock-tube ignition delay time measurements in air, in the last years just some experimental studies have been reported about ignition delay times [21], or using flow reactors, analyzing neat H_2S oxidation [22,23], as well as CH_4/H_2S mixtures oxidation [24,25]. However, the kinetic modeling used in those studies shows gaps between experimental results and model predictions, just as discrepancies from one work to the other. This points to the necessity of a better characterization of certain reactions [22,23], specially, those involving the self-combination of SH ($SH + SH = H_2S + S$ and $SH + SH = H_2S_2$), which have been pointed as important in sensitivity analyses in works about ignition delay times [21] and flow reactors [23,24]. Discrepancies between experimental data and modeling predictions are attributed to uncertainties in the S_2 chemistry [22,23]. At the same time, more experiments are desired in order to increase the knowledge related to H_2S chemistry and validate kinetic mechanisms. This task is important because the results obtained might be useful for other studies, like the ones by Bongartz et al. [26–28], that rely on kinetic mechanisms to perform computer simulations of sour gas oxy-combustion, as well as in the understanding of sulfur chemistry in the industry, like in Claus process plants [29–32].

In a previous work, we performed a study about H_2S oxidation at different manometric pressures (0.6–40 bar), in a tubular flow reactor and under slightly oxidizing conditions ($\lambda = 2$) [22]. In that work, a kinetic model based on previous studies of H_2S oxidation atmospheric pressure was proposed [33,34] and an overall good match between the simulations and experimental trends was obtained. However, it failed to predict H_2S oxidation at the highest pressure studied (40 bar), what happened again in the study of CH_4/H_2S mixtures oxidation at high pressures [25]. In this context, the study of the conversion of H_2S at different pressures, from 0.6 to 40 bar, is extended in the present work and new results are presented. The influence of temperature (450–1100 K), oxygen concentrations ($\lambda = 1$ and $\lambda = 6$), and gas residence time is analyzed. A kinetic model by the authors [22] is slightly modified and used to analyze the conversion of H_2S from this work and from the literature.

2. Experimental methodology

The experimental set-up used to perform the high-pressure H_2S oxidation experiments has been described in detail elsewhere [e.g. 35]. Therefore, only a brief description of the main features is provided here. A flow rate of 1 L (STP)/min of gas reactants: H_2S (approximately 500 ppm), O_2 and N_2 as carrier gas, is supplied from gas cylinders through mass flow controllers, with an uncertainty in the flow rate measurements of approximately 0.5%. The oxygen required to carry out each oxidation experiment is determined by the air excess ratio: λ, defined as inlet oxygen divided by stoichiometric oxygen, according to reaction $H_2S + 1.5O_2 = SO_2 + H_2O$. In the present work, the effect of oxygen concentration on H_2S oxidation at different pressures has been studied. Two different air excess ratios have been selected ($\lambda = 6$ and $\lambda = 1$) at different manometric pressures (0.6, 10, 20 and 40 bar). Table 1 contains the conditions for the different experiments performed, as well as some experiments taken from the previous work by the authors, about H_2S oxidation at high pressures (0.6–40 bar) and slightly oxidizing conditions ($\lambda = 2$) [22]. The reactant gases are premixed before entering the reactor, which consists of a quartz tube (inner diameter of 6 mm and 1500 mm in length) designed to approximate plug flow conditions [36]. The reactor is enclosed in a stainless-steel tube that acts as a pressure shell. The steel tube is placed horizontally in a tubular oven, with three individually controlled electrical heating elements that ensure an isothermal reaction zone of approximately 500 mm, with a uniform temperature profile (±5 K). Gas residence time depends on flow rate, pressure and temperature. For most of the experiments, with a flow rate of 1 L(STP)/min (sets 1–12 in Table 1), it can be expressed as $t_r(s) = 232 * P(bar)/T(K)$ in the isothermal zone of the reactor. One additional experiment has been performed at 10 bar with a flow rate of 0.5 L (STP)/min (set 13 in Table 1), in order to have approximately the same residence time as using 1 L (STP)/min at 20 bar (set 9 in Table 1). Both experiments have been carried out at oxidizing conditions $\lambda \approx 6$. Previously to the gas analysis systems, gases pass through a filter and a condenser to ensure gas cleaning. The products are analyzed by a gas micro-chromatograph equipped with a thermal conductivity detector (TCD) to quantify H_2S and O_2, and a continuous UV analyzer to quantify SO_2. The uncertainty of the measurements is estimated within 5%.

3. Kinetic model

The kinetic model used in this work is taken from a recent study by the authors, where H_2S oxidation was studied at high pressures in a flow reactor under slightly oxidizing conditions ($\lambda = 2$) [22]. That model has been updated in the present study. The simulations have been carried out with the software Chemkin-Pro and the plug flow reactor code [37]. The main reactions for H_2S oxidation belong to the work from Zhou et al. [33] and Alzueta et al. [38].

The mechanism was initially proposed and used in a study about H_2S oxidation at atmospheric pressure in a flow reactor, and the experimental trends were predicted with accuracy [34] at different stoichiometries ($\lambda = 0.3$–20). After that, in a high pressure study of H_2S oxidation in other flow reactor [22], using the same mechanism (but with the H_2/O_2 subset updated for high pressures), the experimental trends were generally well captured from 0.6 to 40 bar. Some discrepancies between experimental results and model predictions were found at the highest pressure (40 bar), with a gap of 50 K between them. All the experiments were performed at slightly oxidizing conditions ($\lambda = 2$). Hence, the present study shows additional updates and features of the model in order to improve the simulation performance. Besides, the model has been used to simulate the new experiments of H_2S oxidation

Table 1
Experimental conditions. N_2 as bath gas. p.w. denotes “present work”.

Set	λ	Manometric pressure (bar)	H_2S (ppm)	O_2 (ppm)	Flow rate(L (STP)/min)	Residence time (s)	Ref.
1	0.96	0.6	520	750	1	371/T (K)	p.w.
2	2.06	0.6	505	1509	1	371/T (K)	[22]
3	5.73	0.6	525	4510	1	371/T (K)	p.w.
4	1.06	10	500	792	1	2552/T (K)	p.w.
5	2.06	10	485	1510	1	2552/T (K)	[22]
6	5.48	10	498	4380	1	2552/T (K)	p.w.
7	1.09	20	465	760	1	4872/T (K)	p.w.
8	2.04	20	497	1520	1	4872/T (K)	[22]
9	5.98	20	500	4485	1	4872/T (K)	p.w.
10	1.00	40	500	753	1	9280/T (K)	p.w.
11	2.06	40	500	1545	1	9280/T (K)	[22]
12	5.90	40	485	4296	1	9280/T (K)	p.w.
13	5.93	10	504	4485	0.5	4872/T (K)	p.w.

at different pressures and lambda values, evaluating the effect of O_2 concentration, pressure and gas residence time on the conversion of H_2S and formation of main reaction products.

The H_2S oxidation mechanism, described in the previous studies [22,34], supported the evolution of the $SH + O_2$ reaction through isomerization from HSOO to HSO_2, leading to the final product SO_2, as proposed by Garrido et al. [39] in a high level ab initio study of the HSO_2 system. The reaction pathways of H_2S oxidation are similar at atmospheric and high pressure. The difference found between the results obtained at different pressures, in terms of kinetic modeling, is related to the formation of HO_2 radicals, which is favored at high pressures [e.g. 21,22,24,25]. The HO_2 radicals react with H_2S to form SH and H_2O_2 (R1) and promote the oxidation via the branching reaction of H_2O_2 to give OH radicals (R2), which then interact again with H_2S (R3).

$$H_2S + HO_2 \rightleftharpoons SH + H_2O_2 \quad (R1)$$

$$H_2O_2\ (+M) \rightleftharpoons OH + OH\ (+M) \quad (R2)$$

$$H_2S + OH \rightleftharpoons SH + H_2O \quad (R3)$$

At the highest pressure (40 bar), where more discrepancies were found between experimental and simulation results [22], reaction (R2) (involving H_2O_2 species) was one of the most sensitive reactions. This indicates that the relevance of OH liberation from H_2O_2 is more important as pressure increases. At the same time, reaction (R1) was identified as one of the most sensitive reactions in the work by Mathieu et al. [21], about H_2S addition to H_2 oxidation when determining ignition delay times, and in the work by Song et al. [23], who studied H_2S oxidation at high pressures (30 and 100 bar) in a flow reactor. Hence, in the present study, we have evaluated other possible reactions involving this peroxide: H_2O_2.

For example, we have considered the reaction of H_2O_2 with SH radicals, for which only an upper limit for the rate constant at room temperature is available [40]. In that work [40], three different possible reaction channels were evaluated for the $SH + H_2O_2$ reaction (R4a-R4c).

$$SH + H_2O_2 \rightleftharpoons H_2S + HO_2 \quad (R4a)$$

$$SH + H_2O_2 \rightleftharpoons HSOH + OH \quad (R4b)$$

$$SH + H_2O_2 \rightleftharpoons HSO + H_2O \quad (R4c)$$

Two of them (R4a and R4b) were already present in our previous mechanism, with kinetic parameters previously proposed in the literature [33,34]. On the other hand, to our knowledge, no kinetic parameters are available in the literature for the third reaction channel (R4c, giving as products $HSO + H_2O$). According to Friedl et al. [40], the formation of $HSO + H_2O$ is not relevant at room temperature. However, it is worthwhile to mention that we have observed a higher reactivity of H_2S at high pressures (40 bar) if (R4c) and the possible reaction of HSO with H_2O_2 (R5) are included in our mechanism for the simulations of H_2S oxidation.

$$HSO + H_2O_2 \rightleftharpoons HSO_2 + H_2O \quad (R5)$$

There are no kinetic parameters for (R5) in the literature either. In this work, both reaction kinetic constants have been here estimated as 10^{12} (mol, s, cm^3), in the temperature range studied (450–1100 K). These reactions have no effect on the simulations at the other pressures studied. A good determination of the reaction parameters for these reactions would be desirable, in order to confirm their inclusion in mechanisms describing H_2S chemistry. These chemical reactions are supposed to occur with the addition of an oxygen atom from H_2O_2 species to SH in R4c, and to HSO in R5, and the formation of a water molecule. This is similarly proposed in the recent study by Beckett et al. [41] about the reaction $HNO + H_2O_2 \rightleftharpoons HNO_2 + H_2O$. In that work, according to B3LYP calculations, in the transition state that leads to HNO_2, the reaction follows by the breaking of the peroxide bond and a short proton transfer to the opposite peroxide oxygen. Additionally, the authors also studied the posterior isomerization of HNO_2 to HONO, which they concluded that is more feasible if water molecules are included in the quantum simulation.

Song et al. [23] increased the reactivity of H_2S in their work about H_2S oxidation at high pressures, by skipping, at high pressure and oxidizing conditions, some reactions such as H_2S reactions with O_3 (R6 and R7) and, at stoichiometric and oxidizing conditions, a couple of reactions of the S_2O subset (R8 and R9). Following a similar procedure, i.e. removing the reactions mentioned above in our previous mechanism, no changes occur in the simulations presented in [22,25,34]. Only if (R4c) and (R5) are included in our mechanism, the same behavior observed by Song et al. [23] eliminating those reactions (R6-R9) happens. The reactivity of the system is increased at high pressures (40 bar and 20 bar), while it remains unaltered at other pressures. This will be further discussed in the next section.

$$H_2S + O_3 \rightleftharpoons SO_2 + H_2O \quad (R6)$$

$$H_2S + O_3 \rightleftharpoons HOSO + OH \quad (R7)$$

$$S_2O + OH \rightleftharpoons S_2 + HO_2 \quad (R8)$$

$$S_2O + S_2 \rightleftharpoons S_3 + SO \quad (R9)$$

As an example, Fig. 1 shows the H_2S concentration vs. temperature at 40 bar and oxidizing conditions ($\lambda = 5.9$), by comparing the results of different mechanisms together with the corresponding experimental data. The simulations are improved compared to the original mechanism (Colom-Díaz et al. [22]) by adding reactions (R4c) and (R5) in the model (Colom-Díaz et al. [22] + R4c + R5). Besides, apart from adding reactions R4c and R5, reactions R6-R9 can also been omitted, as in the work by Song et al. [23], managing to improve the model predictions (Colom-Díaz et al. [22] + R4c + R5-(R6-R9). The mechanism published by Song et al. [23] is also presented in Fig. 1 with the reactions that they omitted (R6-R9) in their original model (Song et al. [23]+(R6-R9)), showing a big difference in the predictions (around 200 K difference).

When reactions (R6-R9) are present in the mechanism, they slow down the oxidation process of H_2S. Reaction of H_2S with O_3 (R6) is the most important one, but it is a chain-terminating step. As mentioned by Song et al. [23], their kinetic parameters are currently not well established. The most reliable measurement for $H_2S + O_3$ is believed to be the room temperature upper limit by Becker et al. [42]. The kinetic parameters used here are from the theoretical work by Mousavipour et al. [43], whose suggestion of R6 as the dominant channel seems to be inconsistent with the experimental observations. In the case of the reactions with S_2O species, R8 and R9, they also slow down the reactivity

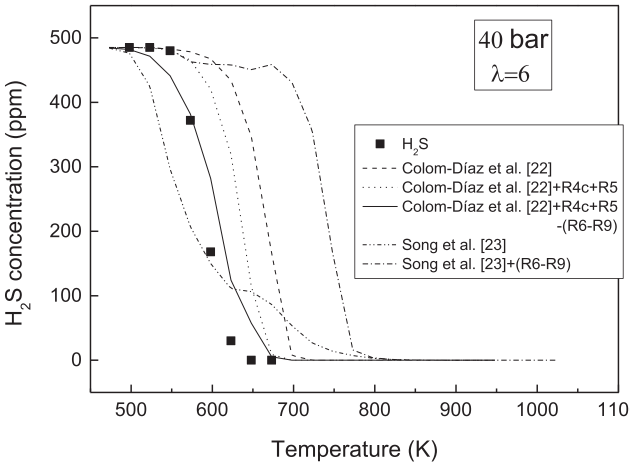

Fig. 1. Concentration of H_2S vs. temperature at 40 bar and $\lambda = 5.9$ (set 12 in Table 1) using different mechanisms.

of the H_2S/O_2 system. Reaction R(8) converts OH radicals to less active HO_2 radicals. Once S_2O species are formed via R10, they are mainly consumed via R11 to form S_3, and, if R9 is present in the model, it forms back S_2O from S_3, slowing down the oxidation process of H_2S. Reaction R(9) is reacting inversely due to its high reverse kinetic constant, which is 10^{14} in all the temperature range. According to the simulations, if its pre-exponential factor is reduced by two orders of magnitude, the reaction R(9) stops having any influence.

$$HSO + S_2 \rightleftharpoons S_2O + SH(R \qquad 10)$$

$$S_2O + S_2O \rightleftharpoons S_3 + SO_2(R \qquad 11)$$

Overall, the mechanism shown in Fig. 1 as Colom-Díaz et al. [22] + R4c + R5-(R6-R9) presents the best case scenario to simulate the experimental results. This is, adding new reactions involving H_2O_2 species and omitting R6-R9 reactions.

4. Results and discussion

The experimental (symbols) and simulated (lines) results of the concentrations of H_2S, SO_2 and O_2 as a function of temperature are plotted from Figs. 2–5, for each individual manometric pressure considered, i.e. 0.6, 10, 20 and 40 bar. The experiments carried out at slightly oxidizing conditions ($\lambda = 2$) were taken from the previous work from the authors [22] in order to compare results. SO_2 is the main product from the oxidation of H_2S. The sulfur balance closes in all cases within ± 5%. As can be observed in the figures, the conversion of H_2S is shifted to lower temperatures, and the oxidation trend is more abrupt, as the pressure increases and the oxygen concentration rises (higher lambda value). Thus, the onset temperature for H_2S conversion is 725 K in the case of 10 bar and stoichiometric conditions ($\lambda = 1.06$, set 4 in Table 1), while it is 575 K at 40 bar and oxidizing conditions ($\lambda = 5.90$, set 12 in Table 1). The consumption of O_2 follows the same trend as hydrogen sulfide.

The kinetic model matches fairly well the experimental trends at all conditions, especially at oxidizing conditions. In Figs. 2 and 3, at 0.6 and 10 bar, the simulations using the mechanism with the addition of reactions R4c and R5, and without omitting reactions R6-R9, are shown. No differences were observed in the simulations if reactions R6-R9 were omitted. At 20 and 40 bar, (Figs. 4 and 5), the simulation of H_2S oxidation when R6-R9 are omitted (dashed lines) is shown, and slight improvements in the simulations can be observed. The simulations for SO_2 and O_2 concentration profiles, in each figure, are done using the same mechanism as for H_2S, without omitting reactions R6-R9. As it is observed, the changes are not significant, but simulations match closer to the H_2S experimental data if reactions R6-R9 are omitted at high pressures. Song et al. [23] did this in order to increase the reactivity of the H_2S/O_2 system at high pressures, as explained before in the kinetic model section, these reactions slow down the H_2S oxidation. The simulations carried out in the following figures at high pressure are done in the same way. The major differences can be found at stoichiometric conditions, where the mechanism is able to predict the H_2S reaction onset, but falls too rapidly. The major outcome is related to the previous differences found at high pressures (40 bar) in the last study [22]. With the addition of R4c and R5, the gap between experimental data and model predictions is reduced, and even more if reactions R6-R9 are omitted.

The reaction pathways have slightly changed from our previous study at high pressure [22] due to the addition of (R4c) and (R5) in the model. The first steps governing H_2S oxidation remain the same. H_2S starts reacting mainly with HO_2 radicals (R1), which are important at high pressures [21–25], and forms SH radicals, which react with O_2 to form the peroxide HSOO and, in this work, with H_2O_2 species as well, to give HSO.

At atmospheric pressure, the reaction of SH with O_2 to form HSOO radicals is the dominant one, isomerizing to HSO_2 and then to HOSO, which are the previous steps to SO_2 as the final product [34]. In order to evaluate the impact of the modifications made to the mechanism of the present work on already published results, we have used the presently modified mechanism to simulate results of the hydrogen sulfide conversion of our previous work at atmospheric pressure in a flow reactor [34]. The results, shown in Fig. S1 of the supplementary material, are compared with predictions using the original mechanism [34] and the outcome of the simulations is really similar.

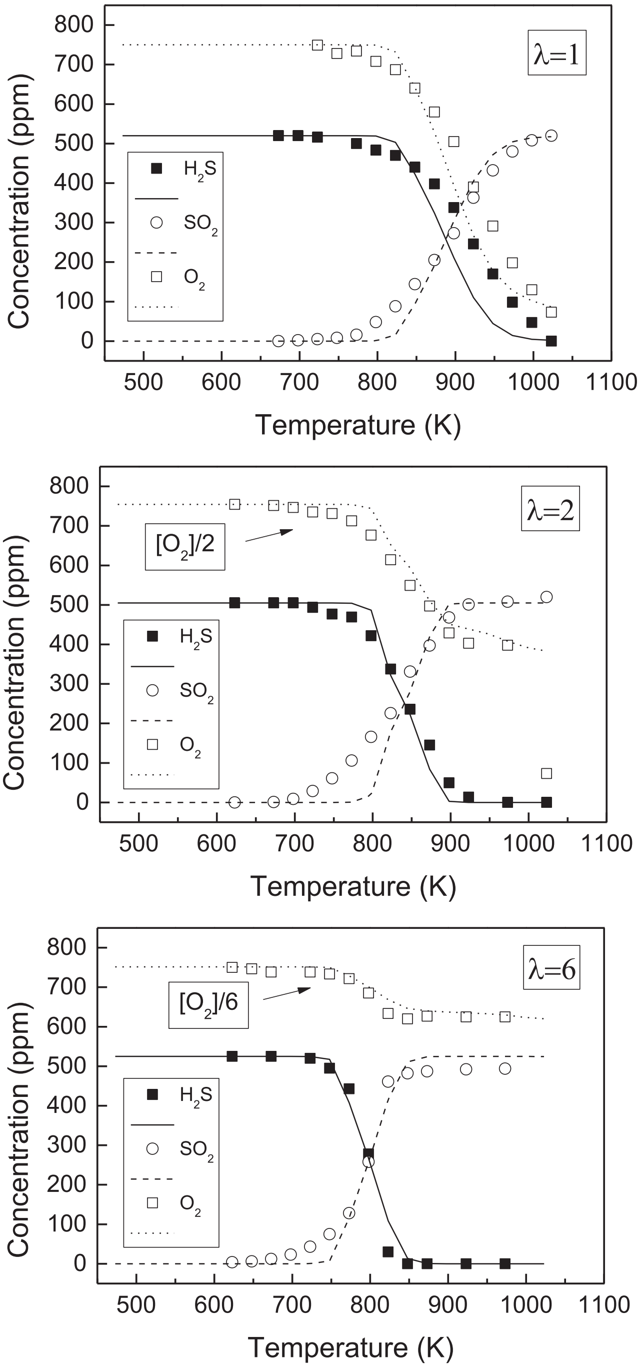

Fig. 2. Concentrations of H_2S, SO_2 and O_2 vs. temperature at 0.6 bar of manometric pressure (sets 1, 2 and 3 in Table 1).

In the same manner, the experimental results obtained by Song et al. [23], about H_2S oxidation in a flow reactor at 30 bar and 100 bar (under stoichiometric and oxidizing conditions λ≈35), are shown in Figs. 6–8, along with simulations using the mechanism omitting R6-R9, as the authors did. A good match between experimental data and model

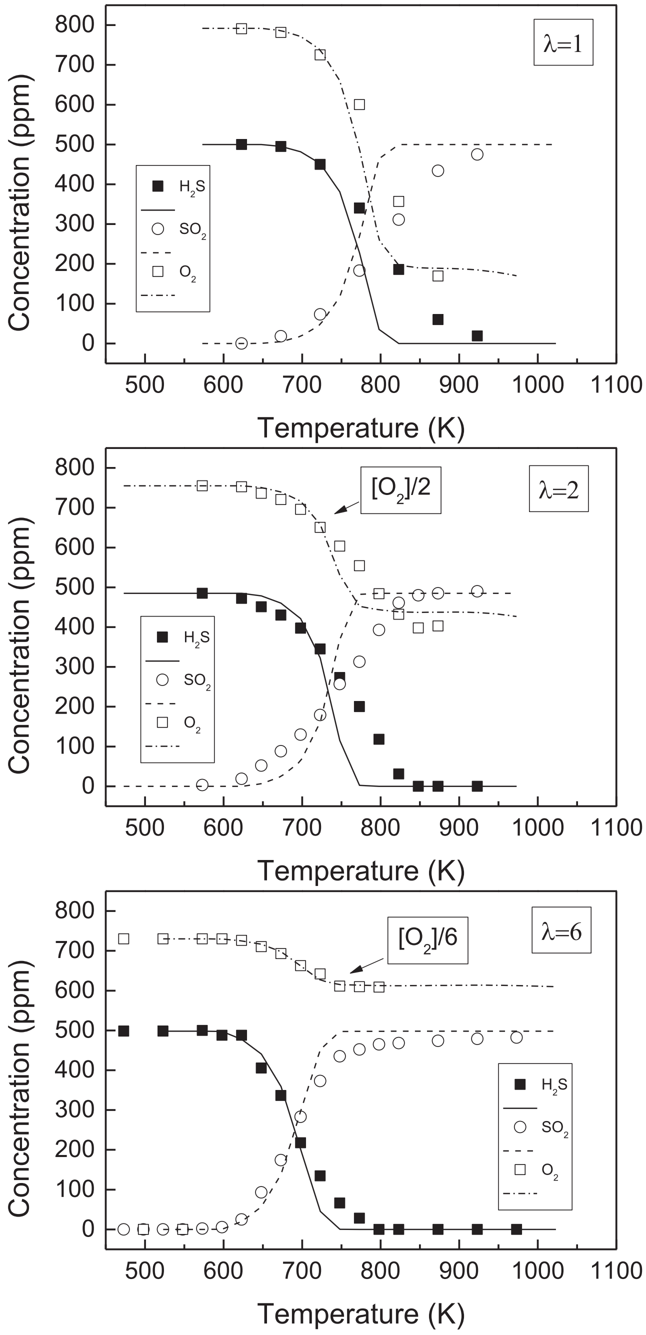

Fig. 3. Concentrations of H_2S, SO_2 and O_2 vs. temperature at 10 bar of manometric pressure (sets 4, 5 and 6 in Table 1).

calculations is obtained at all conditions. Song et al. [23] attributed the discrepancy between their experimental results and modeling predictions at high pressures mostly to uncertainties in the S_2 chemistry. As it has been seen here before, following their procedure of omitting some S_2O reactions (R8 and R9) improves the simulations at high pressures. However, it could also be that other important reactions of S_2O species or other S_2 species might not be present in the model yet, like the interaction of S_2O with O_2.

If we compare the results obtained under different experimental conditions, for example, those obtained under stoichiometric conditions at 20 and 40 bar in the present work, along with the results by Song et al. [23] at 30 bar, we could expect to find the data ordered by pressure, what means that the H_2S oxidation at 30 bar should be located between the experiments at 20 and 40 bar. The comparison between them can be

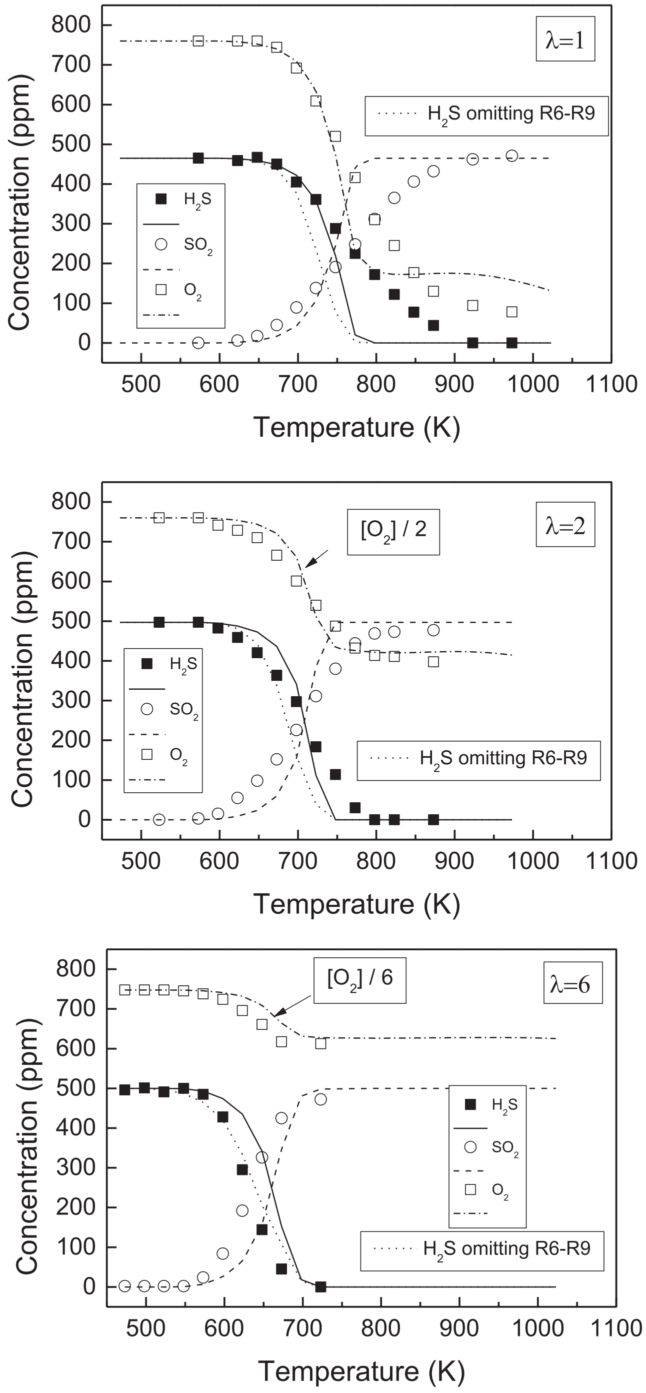

Fig. 4. Concentrations of H_2S, SO_2 and O_2 vs. temperature at 20 bar of manometric pressure (sets 7, 8 and 9 in Table 1).

seen in the supplementary material (Fig. S2). The experiment at 30 bar from the literature is shifted to higher temperatures in comparison with the other two at 20 and 40 bar. This can be due to the different gas residence time values. The experiment at 20 bar presents a residence time of 4872/T (K) seconds, while the experiment at 30 bar in the experimental set-up used by Song et al. has a residence time of 3520/T (K) seconds, which is 25% less than the residence time in our experiment at 20 bar.

To evaluate independently the effect of residence time and pressure, an additional experiment has been performed at 10 bar and oxidizing conditions using a flow rate approximately of 0.5 L (STP)/min (set 13 in Table 1) instead of 1 L(STP)/min. Firstly, this set presents the same

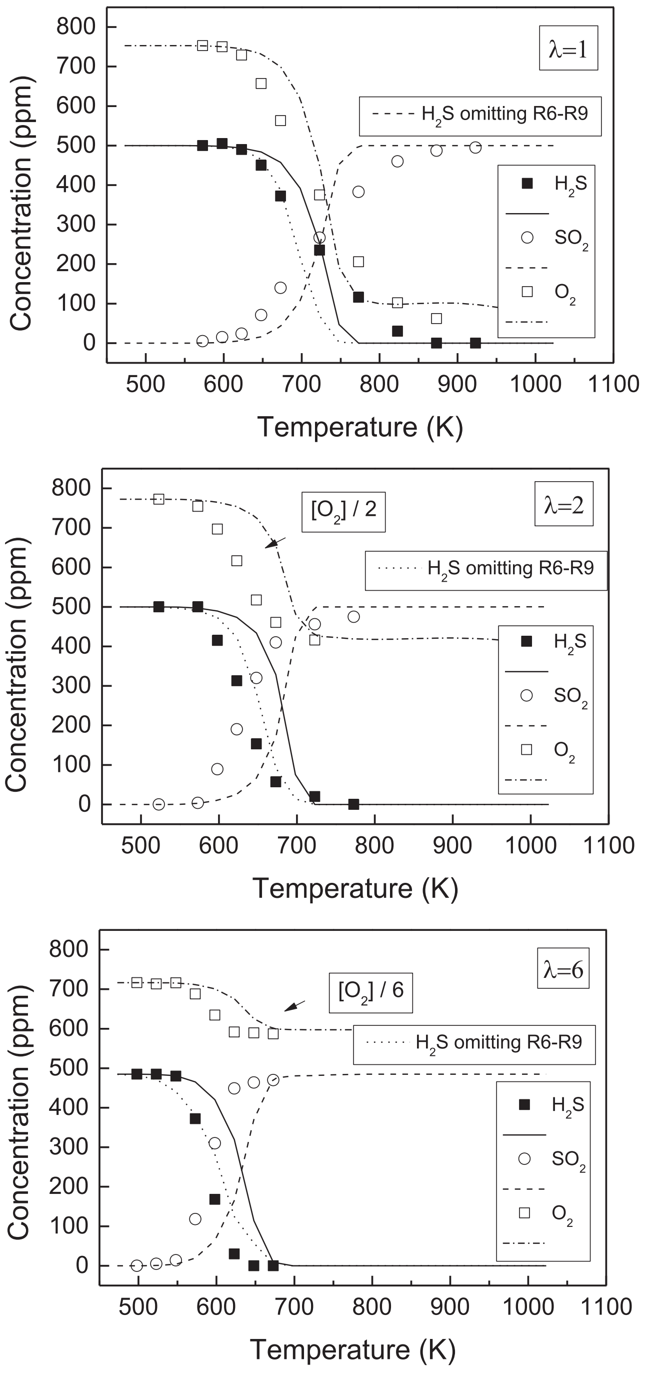

Fig. 5. Concentrations of H_2S, SO_2 and O_2 vs. temperature at 40 bar of manometric pressure (sets 10, 11 and 12 in Table 1).

residence time as in the experiment at 20 bar and oxidizing conditions (set 9 in Table 1). Thus, we can observe in Fig. 9 how pressure affects the oxidation of H_2S using the same residence time. As it is seen, the experimental results differ by a maximum of 25 K. Later, in Fig. 10, it can be observed how the residence time affects H_2S oxidation, by comparing the experiment at 10 bar and 0.5 L (STP)/min (set 13 in Table 1) and the experiment at 10 bar and 1 L (STP)/min (set 6 in Table 1). As can be seen, the difference between experiments is around 50 K by doubling the flow rate, which means the residence time is the half. The larger the residence time, the earlier starts the oxidation of H_2S. The effect of residence time is, then, stronger than the effect of pressure in the ranges studied. All in all, the model seems capable of predicting H_2S oxidation fairly well under the different conditions studied.

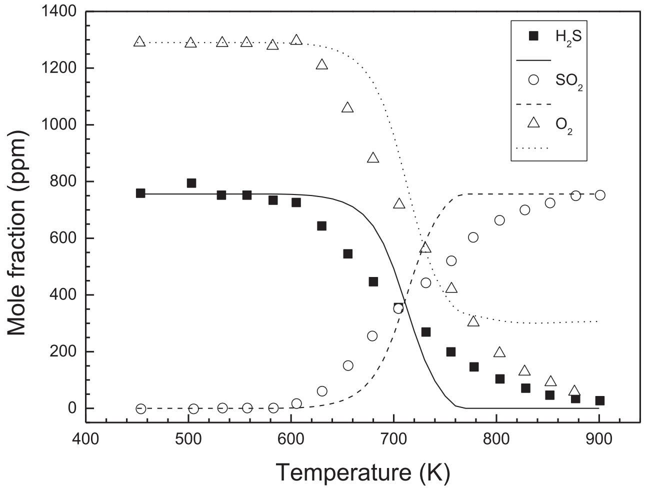

Fig. 6. Concentrations of H_2S, SO_2 and O_2 vs. temperature at 30 bar and λ = 1.14 (data taken from set 1 in Table III of [23]).

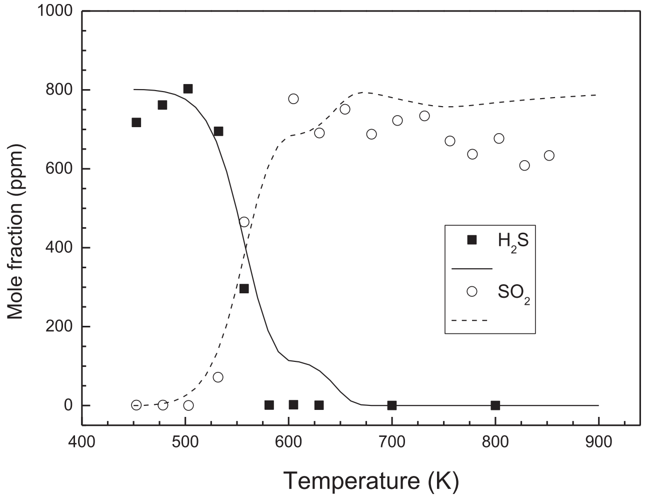

Fig. 7. Concentrations of H_2S and SO_2 vs. temperature at 30 bar and λ = 36 (data taken from set 3 in Table III of [23]).

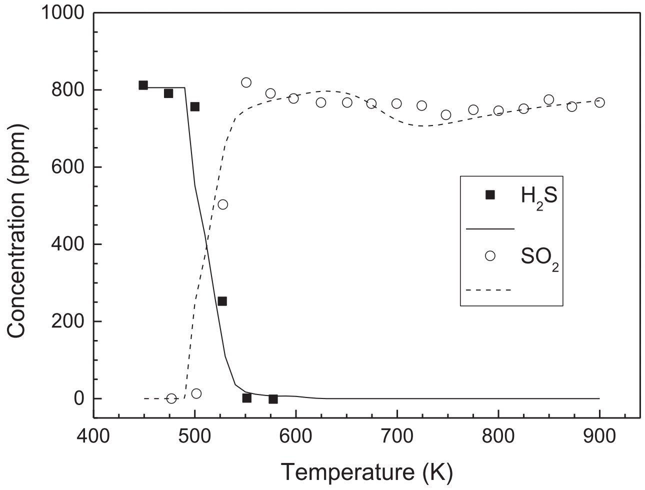

Fig. 8. Concentrations of H_2S and SO_2 vs. temperature at 100 bar and λ = 35 (data taken from set 4 in Table III of [23]).

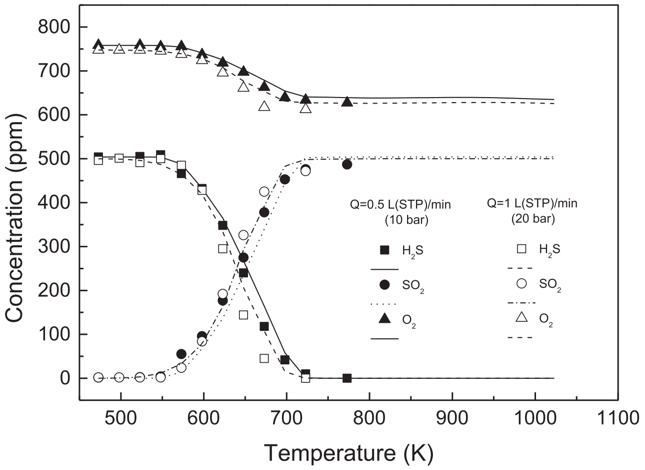

Fig. 9. Concentrations of H_2S, SO_2 and O_2 vs. temperature at 10 and 20 bar using the same residence time (sets 9 and 13 in Table 1).

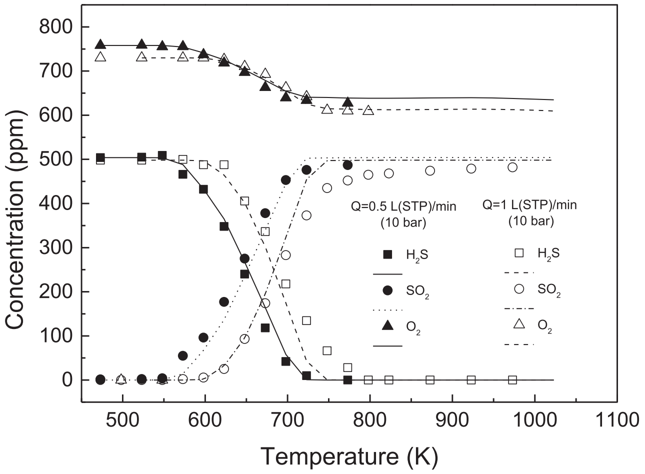

Fig. 10. Concentrations of H_2S, SO_2 and O_2 vs. temperature at 10 bar using different residence times (sets 6 and 13 in Table 1).

Additionally, the current mechanism has been used to simulate the experiments from the work of Mathieu et al. [21], about the effect of H_2S addition on hydrogen ignition delay times. The results can be seen in Fig. S3 of the supplementary material. The ignition delay times were measured experimentally behind reflected shock waves for mixtures of 1% H_2/1% O_2, diluted in Ar and doped with various concentrations of H_2S (100, 400 and 1600 ppm) at different pressures (1.6, 13 and 33 atm). The model predictions are close to the experimental results under almost all the conditions, except for two experiments, those corresponding to the highest H_2S concentration (1600 ppm) and pressures of 13 and 33 atm. These results agree with the work by Mathieu et al. [21], where they simulate their experiments using different mechanisms from the literature and found a major dispersion of modeling results for these two experimental conditions.

Lastly, simulations of some experimental results about the oxidation of CH_4/H_2S mixtures at different pressures have been performed [25]. This study presents three experiments under stoichiometric conditions at 10, 20 and 40 bar of CH_4/H_2S mixtures oxidation in a flow reactor. For simulations, we have used the mechanism updated in the present work with the new two reactions (R4c) and (R5) and omitting the same reactions as Song et al. [23]. The results obtained are shown in Fig. S4–S6 of the supplementary material. As was reported by the authors [25], H_2S conversion occurs experimentally similarly in the absence or presence of CH_4, which can be well captured now with the current mechanism at 10, 20 and 40 bar, improving the previous simulations of H_2S and SO_2. No interaction between CH_4 and H_2S during oxidation is found according to the model, as they just share radicals such as HO_2 or OH. Nevertheless, CH_4 is still under-predicted at the highest pressure (40 bar) by 100 K, where a 10% conversion occurs.

Overall, the simulations of different data from the literature have been improved and constitute an additional step forward in the mechanism. The kinetic parameters for reactions (R4c) and (R5), estimated in the present work, have provided a good performance across for the different experimental conditions tested, but definitely deserve a proper determination, since here are presented as rough estimations at high temperatures. Considering the work by Beckett et al. [41], a possible pathway for the reactions proposed, R4c and R5, is shown by abstracting an O radical from the H-O-O-H molecule, as well as an analogy of HNO with HSO in the reaction with H_2O_2 species. At the same time, we enlighten the importance of reactions involving the H_2O_2 peroxide in H_2S oxidation at high pressures, as has been demonstrated in other reaction systems [44,45]. Besides, the results for stoichiometric conditions are not fully captured by the model in the present study. A sensitivity analysis has been run for H_2S at the highest pressure (40 bar) and $\lambda = 1$, as can be seen in Fig. S7 of the supplementary material. This plot shows as the most sensitive reactions those involving the self-combination of SH (R12 and -R13), despite being a very little reactive radical, and the isomerization reaction (R14). Reactions R12 and R13 were also shown as the most sensitive ones in the work by Song et al. [23] and claimed more work in these reactions together with the S_2 subset improvement in the mechanism.

$SH + SH (+M) \rightleftharpoons H_2S_2 (+M)$(R 12)

$H_2S + S \rightleftharpoons SH + SH$(R 13)

$HSOO \rightleftharpoons HSO_2$(R 14)

The mechanisms used in the present work, together with the present experimental results, may be of interest for analyzing the conventional combustion of natural sour gas, the Claus process [10], the combustion of biogas [14] or oxy-combustion of the sour gas [26–28].

5. Conclusions

The present study deals with the oxidation of H_2S at high pressures, presenting new experiments in a flow reactor at different manometric pressures (0.6, 10, 20 and 40 bar) and under different oxygen atmospheres ($\lambda = 1$ and $\lambda = 6$), as well as an updated kinetic mechanism. Experimentally, SO_2 has been observed to be the main product from the oxidation of H_2S. The oxidation onset of H_2S oxidation is shifted to lower temperatures as the pressure and oxygen concentration rise. The influence of gas residence time has been found to be stronger than pressure under the conditions studied. A kinetic mechanism from the authors has been updated with two new reactions ($SH + H_2O_2 = HSO + H_2O$ and $HSO + H_2O_2 = HSO_2 + H_2O$), and has been successfully used to reproduce the experimental data from the present work and data from the literature. The reaction pathways of H_2S oxidation at high pressures are similar to the ones at atmospheric pressure, with difference found in the abundance and importance of H_2O_2 species and HO_2 radicals at higher pressures, which act to increase the H_2S reactivity. The simulations at atmospheric pressure remain essentially unaltered with the updated mechanism.

CRediT authorship contribution statement

J.M. Colom-Díaz: Methodology, Validation, Investigation, Data curation, Writing - original draft, Visualization. **Á. Millera:** Conceptualization, Writing - review & editing, Supervision, Funding acquisition. **R. Bilbao:** Conceptualization, Writing - review & editing, Supervision, Funding acquisition, Project administration. **M.U. Alzueta:**

Conceptualization, Methodology, Writing - review & editing, Supervision, Funding acquisition, Project administration.

Declaration of Competing Interest

The authors declare that they have no known competing financial interests or personal relationships that could have appeared to influence the work reported in this paper.

Acknowledgements

The authors express their gratitude to the Aragón Government (Ref. T22_20R), co-funded by FEDER 2014-2020 “Construyendo Europa desde Aragón“, and to MINECO, MCIU and FEDER (Projects CTQ2015-65226 and RTI2018-098856-B-100) for financial support. J.M. Colom acknowledges to MINECO for the predoctoral grant awarded (BES-2016-076610).

Appendix A. Supplementary data

Supplementary data to this article can be found online at https://doi.org/10.1016/j.fuel.2020.119261.

References

[1] Hammer G, Lübcke T, Kettner R, Pillarella MR, Recknagel H, Commichau A, Neumann H-J, Paczynska-Lahme B. Ullmann’s Encyclopedia of Industrial Chemistry. Wiley-VCH: Weinheim, Germany, 2012, Vol. 23; Chapter Natural Gas.
[2] International Energy Agency “Natural gas resources and production prospects”, in World Energy Outlook 2008 Organisation for economic co-operation and development Paris.
[3] Maggio G, Cacciola G. When will oil, natural gas, and coal peak? Fuel 2012;98: 111–23.
[4] Burgers WFJ, Northrop PS, Kheshgi HS, Valencia JA. Worldwide development potential for sour gas. 10th International Conference on Greenhouse Gas Control Technologies. Energy Procedia 2011;4:2178–84.
[5] Zarei S, Ganji H, Sadi M, Rashidzadeh M. Thermo-kinetic modeling and optimization of the sulfur recovery unit thermal stage. Appl Therm Eng 2016;103: 1095–104.
[6] Nabikandi NJ, Fatemi S. Kinetic modelling of a commercial sulfur recovery unit based on Claus straight through process: Comparison with equilibrium model. J Ind Eng Chem 2015;30:50–63.
[7] De Crisci AG, Moniri A, Xu Y. Hydrogen from hydrogen sulfide: towards a more sustainable hydrogen economy. Int. J. Hydrog. Energy 2019;44:1299–327.
[8] He C, You F. Shale gas processing integrated with ethylene production: novel process designs, exergy analysis, and techno-economic analysis. Ind Eng Chem Res 2014;53:11442–59.
[9] Barba D, Cammarota F, Vaiano V, Salzano E, Palma V. Experimental and numerical analysis of the oxidative decomposition of H_2S. Fuel 2017;198:68–75.
[10] Salisu I, Abhijeet R. Kinetic simulation of acid gas (H_2S and CO_2) destruction for simultaneous syngas and sulfur recovery. Ind Eng Chem Res 2016;55:6743–52.
[11] Taifan W, Baltrusaitis J. Minireview: direct catalytic conversion of sour natural gas ($CH_4 + H_2S + CO_2$) components to high value chemicals and fuels. Catal Sci Technol 2017;7:2919–29.
[12] US Department of Energy. Report of basic research needs for clean and efficient combustion of 21st century transportation fuels. https://www.osti.gov/servlets/purl/935428-bbBji1/; 2006 [accesed 1 April 2020].
[13] Rappold TA, Lackner KS. Large scale disposal of waste sulfur: From sulfide fuels to sulfate sequestration. Energy 2010;35(3):1368–80.
[14] Awe O, Zhao Y, Nzihou A, Minh D, Lyczko N. A review of biogas utilization, purification and upgrading technologies. Waste Biomass Valor 2017;8:267–83.
[15] Valera-Medina A, Giles A, Pugh D, Morris S, Pohl M, Ortwein A. Investigation of combustion of emulated biogas in a gas turbine test rig. J Therm Sci 2018;27: 331–40.
[16] Jerzak W, Kuźnia M, Szajding A. Experimental Studies and the Chemical Kinetics Modelling of Oxidation of Hydrogen Sulfide Contained in Biogas. Procedia Eng 2016;157:222–9.
[17] Lu X, Palmer M, Forrest B, McGroddy M. A novel power generation system utilizing un-treated sour gas fuel. Soc Pet Eng 2018.
[18] Chakroun NW, Ghoniem AF. Techno-economic assessment of sour gas oxy-combustion water cycles for CO_2 capture. Int J Greenhouse Gas Control 2015;36: 1–12.
[19] Chakroun NW, Ghoniem AF. High-efficiency low LCOE combined cycles for sour gas oxy-combustion with CO_2 capture. Int J Greenhouse Gas Control 2015;41: 163–73.
[20] Frenklach M, Lee JH, White JN, Gardiner Jr WC. Oxidation of hydrogen sulfide. Combust Flame 1981;41:1–16.
[21] Mathieu O, Deguillaume F, Petersen EL. Effects of H_2S addition on hydrogen ignition behind reflected shock waves: Experiments and modeling. Combust Flame 2014;161(1):23–36.
[22] Colom-Díaz JM, Abián M, Millera Á, Bilbao R, Alzueta MU. Influence of pressure on H_2S oxidation. Experiments and kinetic modeling. Fuel 2019;258:116145. https://doi.org/10.1016/j.fuel.2019.116145.
[23] Song Y, Hashemi H, Christensen JM, Zou C, Haynes BS, Marshall P, Glarborg P. An exploratory flow reactor study of H2S oxidation at 30-100 bar. Int. J. Chem. Kinet. 2017;49:37-52.
[24] Gersen S, van Essen M, Darmeveil H, Hashemi H, Rasmussen CT, Christensen JM, Glarborg P, Levinsky H. Experimental and modeling investigation of the effect of H2S addition to methane on the ignition and oxidation at high pressures. Energy Fuels 2017;31:2175-82.
[25] Colom-Díaz JM, Leciñena M, Peláez A, Abián M, Millera Á, Bilbao R, Alzueta MU. Study of the conversion of CH_4/H_2S mixtures at different pressures. Fuel 2020;262: 116484. https://doi.org/10.1016/j.fuel.2019.116484.
[26] Bongartz D, Shanbhogue SJ, Ghoniem AF. Formation and Control of Sulfur Oxides in Sour Gas Oxy-Combustion: Prediction Using a Reactor Network Model. Energy Fuels 2015;29(11):7670–80.
[27] Bongartz D, Ghoniem AF. Impact of sour gas composition on ignition delay and burning velocity in air and oxy-fuel combustion. Combust Flame 2015;162(7): 2749–57.
[28] Bongartz D, Ghoniem AF. Chemical kinetics mechanism for oxy-fuel combustion of mixtures of hydrogen sulfide and methane. Combust Flame 2015;162(3):544–53.
[29] Raj A, Ibrahim S, Jagannath A. Combustion kinetics of H_2S and other sulfurous species with relevance to industrial processes. Prog Energy Combust Sci 2020;80: 100848.
[30] Rahman RK, Raj A. A reaction kinetics study and model development to predict the formation and destruction of organosulfur species (carbonyl sulfide and mercaptans) in Claus furnace. Int J Chem Kinet 2018;50:880–96.
[31] Ibrahim S, Raj A. Kinetic simulation of acid gas (H_2S and CO_2) destruction for simultaneous syngas and sulfur recovery. Ind Eng Chem Res 2016;55:6743–52.
[32] Mehmood A, Alhasani H, Alamoodi N, Alwahedi YF, Ibrahim S, Raj A. An evaluation of kinetic models for the simulation of Claus reaction furnaces in sulfur recovery units under different feed conditions. J Nat Gas Sci Eng 2020;74:103106.
[33] Zhou CR, Sendt K, Haynes BS. Experimental and kinetic modelling study of H_2S oxidation. Proc Combust Inst 2013;34:625–32.
[34] Colom-Díaz JM, Abián M, Ballester MY, Millera Á, Bilbao R, Alzueta MU. H_2S conversion in a tubular flow reactor: Experiments and kinetic modeling. Proc Combust Inst 2019;37:727–34.
[35] Marrodán L, Millera Á, Bilbao R, Alzueta MU. High-Pressure Study of Methyl Formate Oxidation and Its Interaction with NO. Energy Fuels 2014;28(9):6107–15.
[36] Rasmussen CL, Hansen J, Marshall P, Glarborg P. Experimental measurements and kinetic modeling of CO/H 2 /O 2 /NO x conversion at high pressure. Int J Chem Kinet 2008;40(8):454–80.
[37] CHEMKIN-PRO 15151. Reaction Design, San Diego. 2013.
[38] Alzueta MU, Bilbao R, Glarborg P. Inhibition and sensitization of fuel oxidation by SO_2. Combust Flame 2001;127(4):2234–51.
[39] Garrido JD, Ballester MY, Orozco-González Y, Canuto S. CASPT2 study of the potential energy surface of the HSO_2 system. J Phys Chem A 2011;115:1453–61.
[40] Friedl RR, Brune WH, Anderson JG. Kinetics of SH with NO_2, O_3, O_2, and H_2O_2. J Phys Chem 1985;89:5505–10.
[41] Beckett D, Edelmann M, Raff JD, Raghavachari K. Hidden complexities in the reaction of H_2O_2 and HNO revealed by ab initio quantum chemical investigations. PCCP 2017;19:29549–60.
[42] Becker KH, Inocencio MA, Schurath U. Reaction of ozone with hydrogen-sulfide and its organic derivatives. Int J Chem Kinet 1975;1:205–20.
[43] Mousavipour SH, Mortazavi M, Hematti O. Multichannel RRKM-TST and direct-dynamics CVT study of the reaction of hydrogen sulfide with ozone. J Phys Chem A 2013;117:6744–56.
[44] Marrodán L, Fuster M, Millera Ángela, Bilbao R, Alzueta MaríaU. Ethanol as a Fuel Additive: High-Pressure Oxidation of Its Mixtures with Acetylene. Energy Fuels 2018;32(10):10078–87.
[45] Giménez-López J, Rasmussen CT, Hashemi H, Alzueta MU, Gao Y, Marshall P, et al. Experimental and kinetic modeling study of C_2H_2 oxidation at high pressure. Int J Chem Kinet 2016;48:724–38.

SUPPLEMENTARY MATERIAL

New results of H_2S oxidation at high pressures. Experiments and kinetic modeling

J. M. Colom-Díaz, Á. Millera, R. Bilbao, M. U. Alzueta

Aragón Institute of Engineering Research (I3A). Department of Chemical and Environmental Engineering, University of Zaragoza, 50018 Zaragoza, Spain.

Table of contents:

1) **Comparison between the present model and the original model in the experiments at atmospheric pressure from a previous work [34]**

   Figure S1. Experimental results from H_2S oxidation at atmospheric pressure taken from Colom-Díaz et al. [34]. Symbols represent experimental data and lines model predictions (red lines denote the mechanism from the present work, while black lines represent the model presented in [34]).

2) **Comparison of H_2S concentrations at different pressures and same lambda value**

   Figure S2. Comparison of H_2S concentrations vs. temperature under stoichiometric conditions at 20 bar and 40 bar from this work (sets 7 and 10 in Table 1) and 30 bar from the work by Song et al. [23].

3) **Model predictions of experiments from the literature**

   Figure S3. Ignition delay time measurements vs. temperature for different experimental conditions, using a mixture of 1% H_2/1% O_2, diluted in Ar and doped with H_2S. Experimental data are taken from the work of Mathieu et al. [21].

   Figure S4. Concentrations of H_2S, SO_2, CH_4 and CO vs. temperature for conditions of set 6 in Table 1 of [25] (manometric pressure = 10 bar, $\lambda=1.03$). Symbols represent experimental data and lines model predictions.

   Figure S5. Concentrations of H_2S, SO_2, CH_4 and CO vs. temperature for conditions of set 7 in Table 1 of [25] (manometric pressure = 20 bar, $\lambda=1.01$). Symbols represent experimental data and lines model predictions.

   Figure S6. Concentrations of H_2S, SO_2, CH_4 and CO vs. temperature for conditions of set 8 in Table 1 of [25] (manometric pressure = 40 bar, $\lambda=1.03$). Symbols represent experimental data and lines model predictions.

4) **Sensitivity analysis of H_2S at 40 bar**

   Figure S7. Sensitivity analysis for H_2S conversion, at $\lambda=1$, 40 bar and 650 K.

1) Comparison between the present model and the original model in the experiments at atmospheric pressure from a previous work [34]

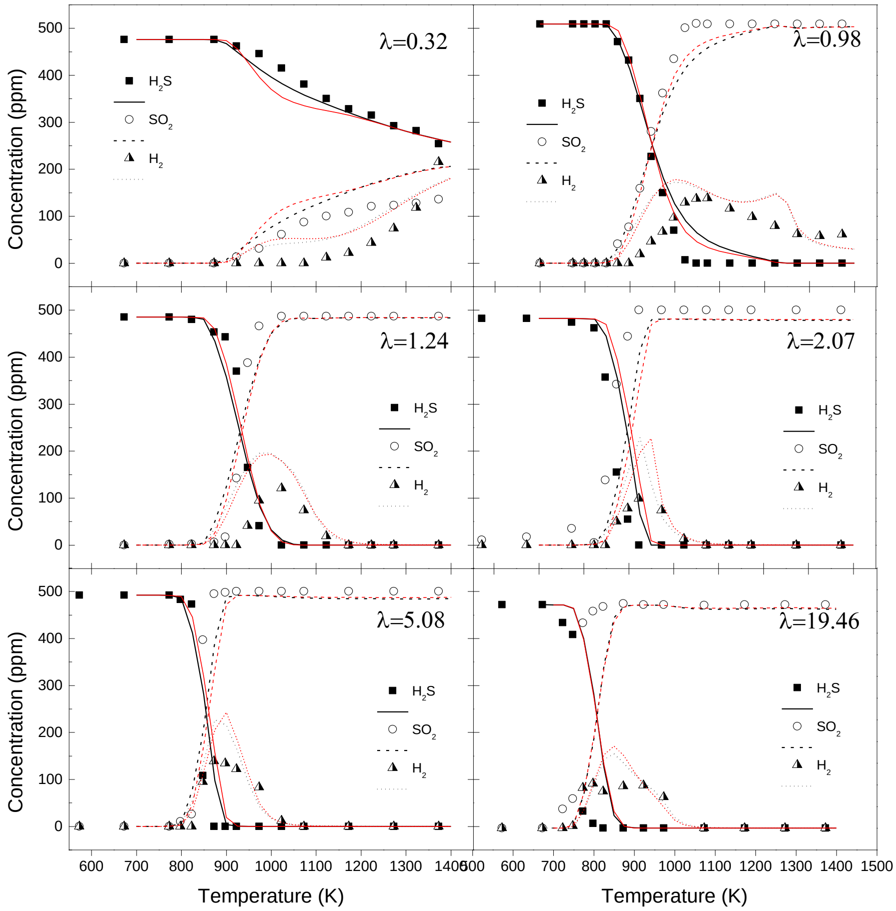

Figure S1: Experimental results from H2S oxidation at atmospheric pressure taken from Colom-Díaz et al. [34]. Symbols represent experimental data and lines model predictions (red lines denote the mechanism from the present work, while black lines represent the model presented in [34]).

2) Comparison of H_2S concentration at different pressures and same lambda value

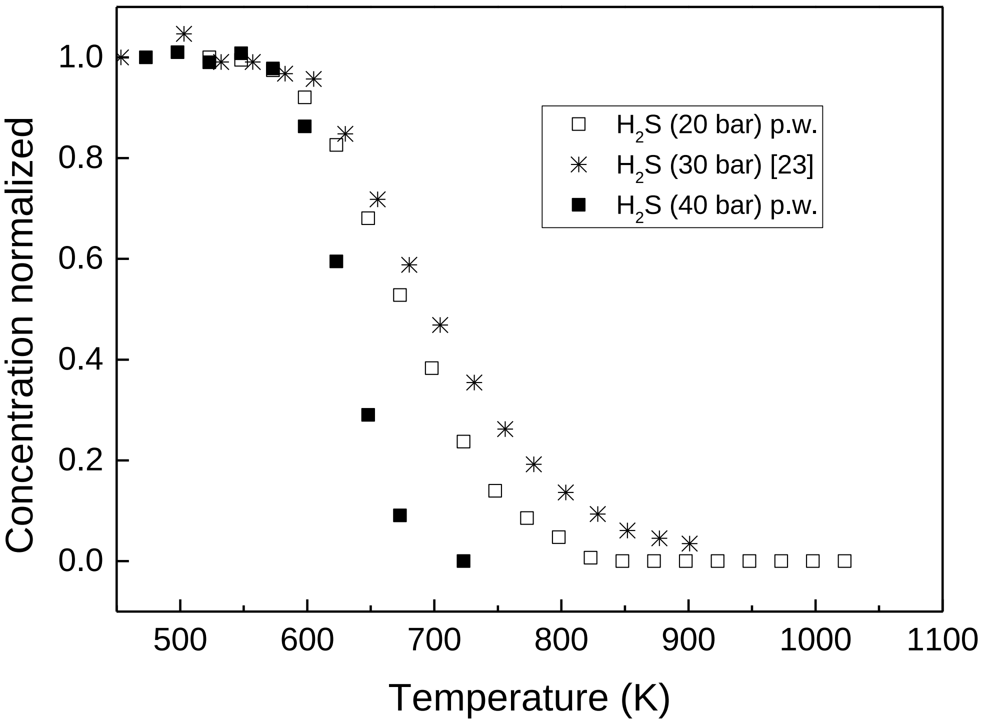

Figure S2: Comparison of H_2S concentrations vs. temperature under stoichiometric conditions at 20 bar and 40 bar from this work (sets 7 and 10 in Table 1) and 30 bar from the work by Song et al. [23].

3) Model predictions of experiments from the literature

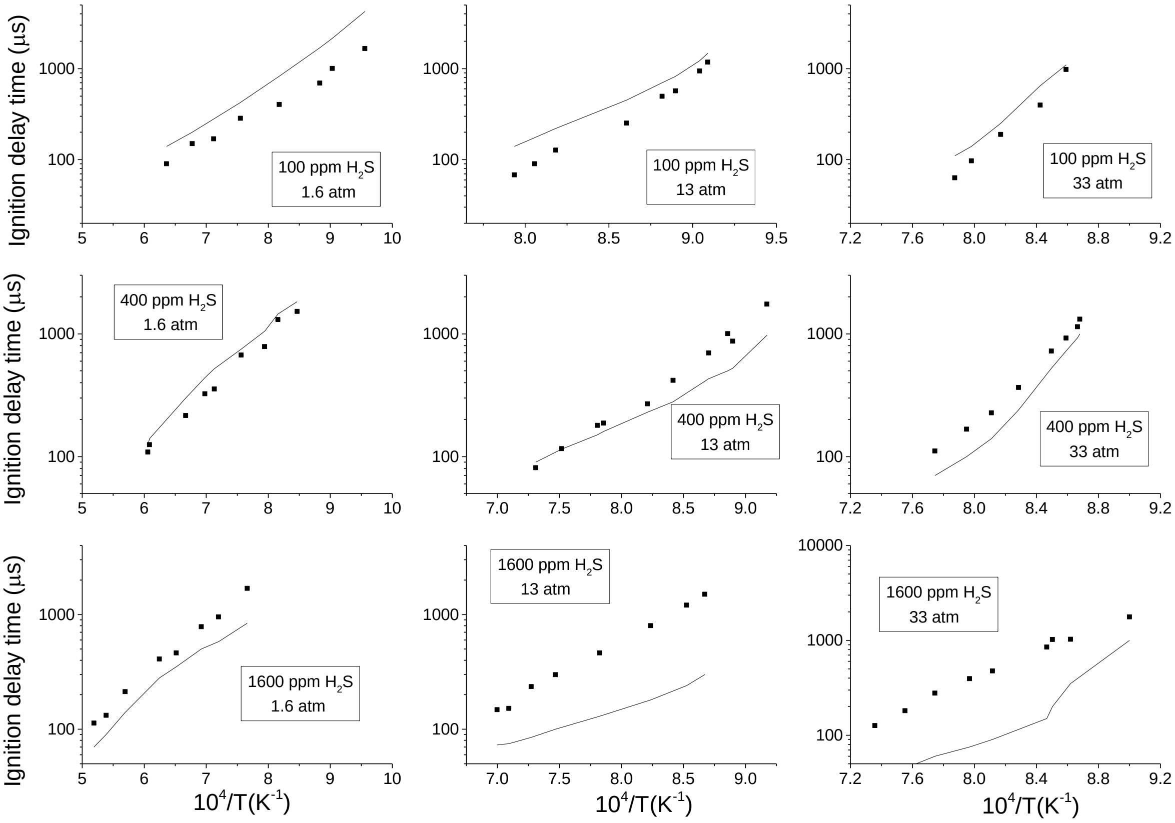

Figure S3. Ignition delay time measurements vs. temperature for different experimental conditions, using a mixture of 1% H_2/1% O_2, diluted in Ar and doped with H_2S. Experimental data are taken from the work of Mathieu et al. [21].

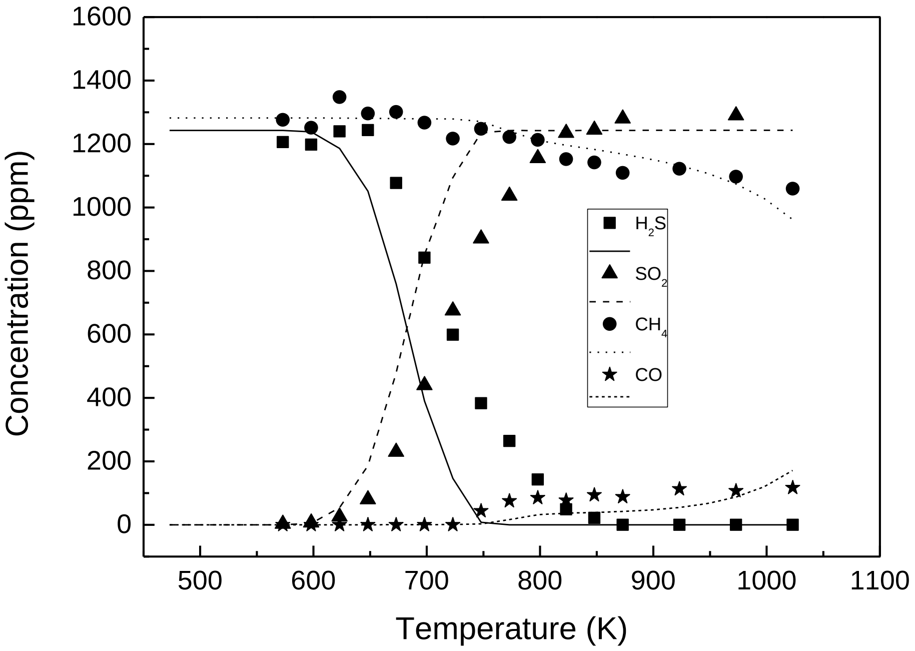

Figure S4. Concentrations of H_2S, SO_2, CH_4 and CO vs. temperature for conditions of set 6 in Table 1 of [25] (manometric pressure = 10 bar, λ=1.03). Symbols represent experimental data and lines model predictions.

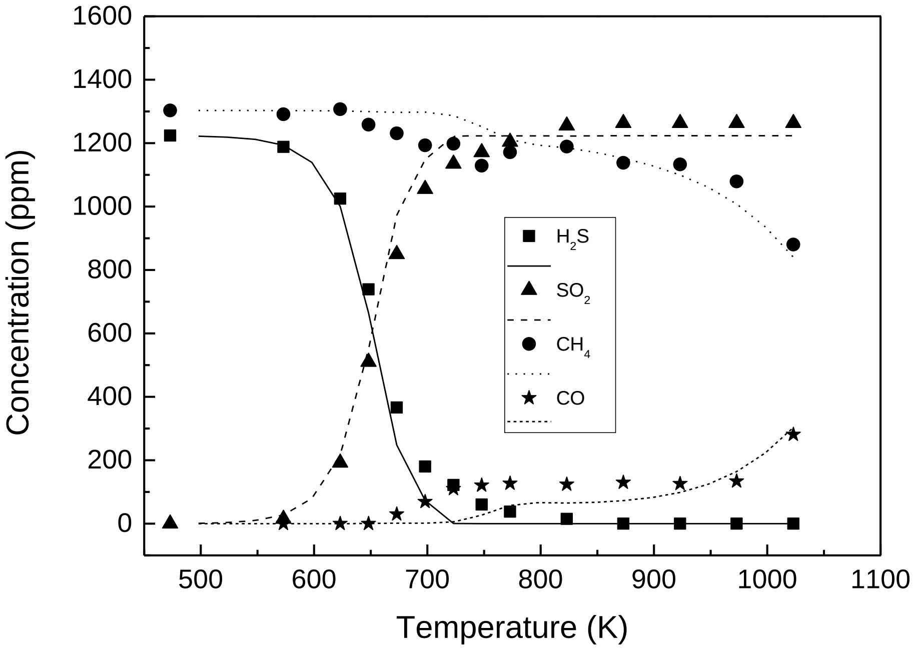

Figure S5. Concentrations of H_2S, SO_2, CH_4 and CO vs. temperature for conditions of set 7 in Table 1 of [25] (manometric pressure = 20 bar, λ=1.01). Symbols represent experimental data and lines model predictions.

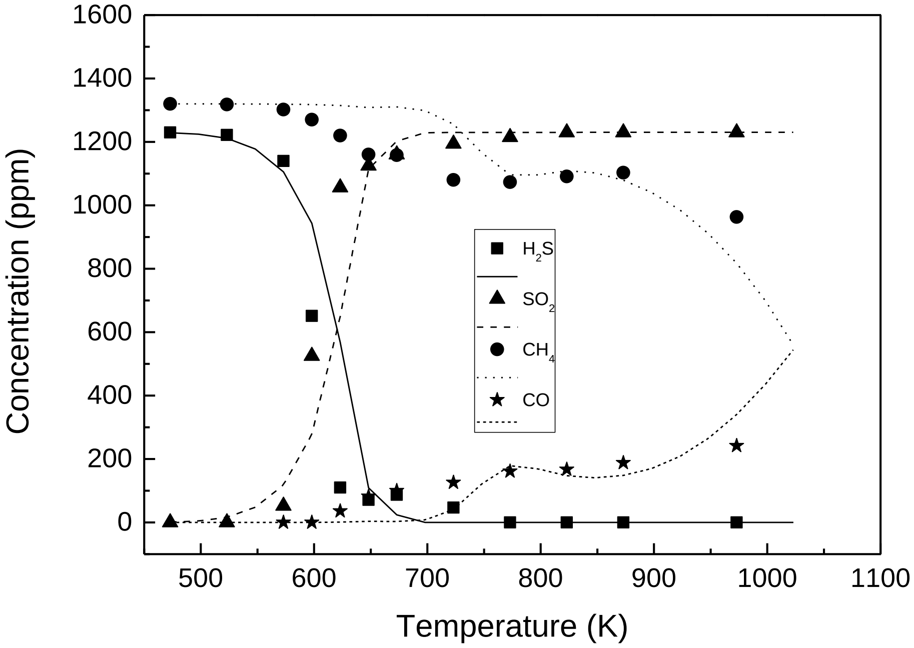

Figure S6. Concentrations of H_2S, SO_2, CH_4 and CO vs. temperature for conditions of set 8 in Table 1 of [25] (manometric pressure = 40 bar, λ=1.03). Symbols represent experimental data and lines model predictions.

4) Sensitivity analysis of H_2S at 40 bar

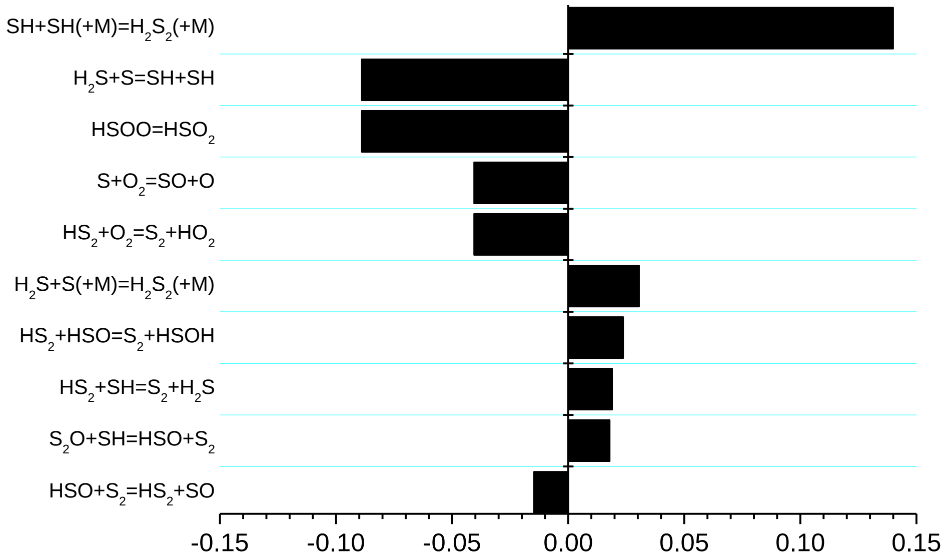

Figure S7. Sensitivity analysis for H_2S conversion, at λ=1, 40 bar and 650 K.

References:

[21] Mathieu, O.; Deguillaume, F.; Petersen, E.L. (2014). Effects of H_2S addition on hydrogen ignition behind reflected shock waves: Experiments and modeling. *Combustion and Flame* 161, 23-36.

[23] Song, Y.; Hashemi, H.; Christensen, J.M.; Zou, C.; Haynes, B.S.; Marshall, P.; Glarborg, P. (2017). An exploratory flow reactor study of H_2S oxidation at 30-100 bar. *International Journal of Chemical Kinetics* 49, 37-52.

[25] Colom-Díaz, J.M.; Leciñena, M.; Peláez, A.; Abián, M.; Millera, Á.; Bilbao, R.; Alzueta, M.U. (2020). Study of the conversion of H_2S/CH_4 mixtures at different pressures. *Fuel* 262, 116484.

[34] Colom-Díaz, J.M.; Abián, M.; Ballester, M.Y.; Millera, Á.; Bilbao, R.; Alzueta, M.U. (2019). H_2S conversion in a tubular flow reactor: Experiments and kinetic modeling. *Proceedings of the Combustion Institute* 37 727-734.

Article VI

Colom-Díaz, J.M.; Millera, Á.; Bilbao, R.; Alzueta, M.U. (2021). Conversion of $H_2S/O_2/NO$ mixtures at different pressures. Experiments and kinetic modeling. *Fuel* 290, 120060.

Fuel 290 (2021) 120060

Contents lists available at ScienceDirect

Fuel

journal homepage: www.elsevier.com/locate/fuel

Full Length Article

Conversion of $H_2S/O_2/NO$ mixtures at different pressures. Experiments and kinetic modeling

J.M. Colom-Díaz, Á. Millera, R. Bilbao, M.U. Alzueta *

Aragón Institute of Engineering Research (I3A), Department of Chemical and Environmental Engineering, University of Zaragoza, 50018 Zaragoza, Spain

A R T I C L E I N F O

Keywords:
H_2S
Oxidation
High pressure
NO_x
Kinetic modeling

A B S T R A C T

The present study deals with the oxidation of H_2S/NO mixtures, in the temperature range of 475–1400 K, at atmospheric pressure and 20 bar of manometric pressure. The experiments have been performed in two different set-ups, using tubular flow reactors, for different air excess ratios (λ_{H2S} = 0.3–6). A kinetic model has been updated with recent reactions from the literature. When NO is present, the oxidation of H_2S at atmospheric pressure proceeds at slightly higher temperatures (25 K) with respect to neat H_2S oxidation. At high pressure (20 bar), the experiments of the oxidation of H_2S in the absence and presence of NO have been performed only at oxidizing conditions ($\lambda_{H2S} = 2$ and $\lambda_{H2S} = 6$), in order to avoid sulfur formation under reducing conditions. The outcomes of these experiments show that, in presence of NO, at the lowest temperature considered (475 K), at least 50% of H_2S conversion for $\lambda_{H2S} = 2$ and 90% for $\lambda_{H2S} = 6$ is obtained. In order to further evaluate the influence of the presence of NO in H_2S oxidation, additional experiments of neat NO oxidation have been performed. As NO_2 formation is favored at high pressures and high O_2 concentrations, the NO_2-H_2S interaction is thought to be responsible for the consumption of H_2S, even at low temperatures (475 K). While the kinetic mechanism is able to reproduce the experimental results at atmospheric pressure, discrepancies are more relevant at high pressure (20 bar).

1. Introduction

Due to the importance of alternative energy sources, such as sour gas and biogas [1,2], an efficient utilization of these resources is needed [3]. Hydrogen sulfide (H_2S) is present in both sources. Usually, this compound is previously removed from the gas streams in order to avoid corrosion and emission problems (SO_x), using cost-effective equipment and having to deal only with the residual H_2S [4,5].

Another possible alternative of sour gas use is its direct combustion [6–8], together with the improvement of technologies and combustion processes [3]. For example, oxy-combustion of sour gas has been recently investigated as a potential alternative to treat this gas [9–11], including the development of this process at high pressures to increase efficiency in power plants [12,13]. Basically, oxy-combustion consists of fuel combustion in pure O_2 and, in this way, the formation of thermal NO_x species is not expected [9–11].

Ammonia (NH_3) may also be present in sour gas [14] and it might be seen as an energy vector as well [15], which may increase the interest of using such gas. However, the presence of NH_3 could produce fuel NO_x emissions in the combustion process. NO_x emission (mg/MJ) during oxy-fuel combustion from fuels containing N can be estimated as 34% of the NO_x emission (mg/MJ) during air firing [16]. Some technologies have been developed to mitigate these emissions. For example, integrated SO_x/NO_x removal technology is considered as a promising approach for flue gas purification by using liquid phase absorbing processes [12,17], where is important to know the amount of SO_2 and NO_2 that will be absorbed due to possible reactions forming acids in the liquid phase. Another aspect to take into account during oxy-combustion would be the flue gas recirculation (FGR), that is a strategy to reduce NO_x emissions by decreasing the combustion temperature used in different combustion processes, such as oxy-combustion [18–20]. This would promote the interaction between H_2S/NO_x, since impurities in the flue gas are brought back to the combustion zone.

In sulfur recovery units (based on the Claus process), where H_2S is oxidized to produce sulfur [21], NO_x formation from NH_3 (up to 40% presence in the feed) might take place [22], which promotes the oxidation of SO_2 to SO_3 and causes catalyst sulfation (deactivation) in the catalytic step [23], as well as other operational problems like the

---

* Corresponding author.
E-mail address: uxue@unizar.es (M.U. Alzueta).

https://doi.org/10.1016/j.fuel.2020.120060
Received 8 October 2020; Received in revised form 14 December 2020; Accepted 18 December 2020
Available online 2 January 2021
0016-2361/© 2020 Published by Elsevier Ltd.

interaction of NH_3 with SO_3 to form ammonium salts [22]. The interaction between H_2S and NO_x might occur as well, since only 1/3 of all H_2S is converted to SO_2 in the previous step to the catalytic one (thermal step). Reactions involving ammonia that occur in the Claus furnace are complex and not fully understood, and the destruction of NH_3 is governed by kinetics rather than equilibrium [14].

Besides sour gas, biogas is considered to be one important alternative energy source. Its use diminishes the dependence on fossil fuels and has the potential to provide power to the grid on demand. For example, biogas can be combusted in gas turbines [2], which can tolerate a H_2S content up to 10,000 ppm [5]. Biogas also contains H_2S and NH_3. The common practice of using biogas containing H_2S is to remove it, while few works have addressed so far the issue of H_2S in biogas combustion [24,25].

Regarding combustion characteristics and kinetics of the sulfur chemistry, the literature is mainly focused on the study of the influence of the presence of SO_2 under combustion conditions [26–30]. Recent works about H_2S oxidation have presented experimental results as well as kinetic mechanisms to understand the chemical behavior of neat H_2S oxidation and its interaction with CH_4 in combustion environments [25,31–37]. However, even though nitrogen (NO_x) may be present in sour gas and biogas combustion, to our knowledge, no study about H_2S/NO_x interactions is available in the literature. Hence, the present work focuses on the experimental study of H_2S/NO oxidation in two tubular flow reactors, under different operational conditions such as temperatures (475–1400 K), pressures (atmospheric and 20 bar) and air excess ratios (λ_{H2S} = 0.3–6). Additionally, it is also intended to develop a kinetic mechanism capable of reproducing the oxidation of H_2S in the presence of NO_x, which might be useful for industrial purposes, such as oxy-combustion of sour gas or the Claus process.

2. Experimental methodology

The oxidation of H_2S and NO was studied by performing experiments in two different experimental set-ups. The experimental conditions for each set of experiments: manometric pressure, concentration of reactants, experimental set-up and corresponding air excess ratios used (λ, defined as inlet oxygen divided by stoichiometric oxygen) are specified in Table 1. In order to calculate λ, the oxygen required for the complete oxidation of H_2S or NO (λ_{H2S} according to reaction $H_2S + 3/2O_2 = SO_2 + H_2O$, and λ_{NO} according to reaction $NO + 1/2O_2 = NO_2$) has been used. The experiments corresponding to sets 1 and 2 have been carried out in duplicated, denoted with the letter "R" in Table 1. In this manner, two results are obtained for each temperature studied within the temperature range considered. The error has been calculated according to the standard pooled deviation (the square root of the sum of the squares of the error), where the error does not depend on the temperature in the interval considered and it is an estimator of the experimental error associated with the oxidation of H_2S. The pooled standard deviation has been calculated as ±9 ppm. For each set, results at different temperatures (increasing the temperature by 25–50 K in the corresponding temperature range) are obtained.

The first experimental set-up (set-up 1 in Table 1) was used in order to evaluate the oxidation of H_2S and NO at atmospheric pressure, at three different stoichiometries with respect to H_2S (reducing, near stoichiometric and oxidizing conditions) and in the temperature range of 700–1400 K, sets 1–3 in Table 1. A detailed description of this set-up can be found in a recent work of neat H_2S oxidation at atmospheric pressure [31]. It consists of a tubular flow reactor within an electrically heated oven, with an isothermal reaction zone of 200 mm and 8.7 mm of internal diameter. The total gas flow rate in all experiments was 1 L (STP)/min, resulting in a gas residence time as a function of temperature of 194.6/T(K), in seconds. The results of H_2S oxidation obtained in other work [31] under similar conditions in absence of NO, sets 4–6 in Table 1, will be used for comparison.

The second set-up (set-up 2 in Table 1), including a high-pressure reactor, was used in order to evaluate the oxidation of H_2S and its interaction with NO at high pressure, at 20 bar of manometric pressure, and in the temperature range of 475–1000 K (sets 7 and 8 in Table 1). Results obtained in experiments of neat H_2S oxidation under similar conditions [32,37] have been used for comparison (sets 9 and 10 in Table 1). Due to the conversion of NO to NO_2 at high pressures in the presence of O_2 [17,38–40], experiments under similar conditions as with H_2S but using just NO were also performed, in order to quantify the NO/NO_2 interconversion (sets 11–13 in Table 1). A detailed description of the set-up 2 can be seen in [32] and only a brief description of the main features is provided here. Reactants: H_2S, NO, O_2 and N_2 as carrier gas, were supplied from gas cylinders through mass flow controllers with an uncertainty in the flow rate measurements of 0.5%. The reactant gases were premixed before entering the reactor, which consists of a quartz tube (inner diameter of 6 mm and 1500 mm in length) designed to approximate plug flow conditions [41]. The reactor is enclosed in a stainless-steel tube that acts as a pressure shell. The steel tube is placed horizontally in a tubular oven, with three individually controlled electrical heating elements that ensure an isothermal reaction zone of approximately 500 mm, with a uniform temperature profile (±5 K). The total gas flow rate in all experiments has been 1 L (STP)/min. Gas residence time in the isothermal zone of the reactor depends on pressure and temperature and it can be expressed as $t_r(s) = 232*P(bar)/T(K)$, where P is absolute pressure.

In both cases, atmospheric and high pressure, previously to the gas analysis systems, gases pass through a filter and a condenser to ensure gas cleaning. Products are analyzed by a gas micro-chromatograph (μGC) equipped with a thermal conductivity detector (TCD) calibrated to quantify H_2S and O_2. Continuous UV analyzers were used to quantify SO_2 and NO. The uncertainty of the measurements is estimated within

Table 1
Experimental conditions. N_2 as bath gas, p.w. denotes "present work". The set of experiments repeated are denoted with the letter "R".

Set	λ_{H2S}	λ_{NO}	Manometric pressure (bar)	H_2S (ppm)	O_2 (ppm)	NO (ppm)	Exp. set-up	Gas residence time (s)	Ref.
1	0.3	0.9	0	487	225	500	1	194.6/T (K)	p.w.
1R	0.3	0.9	0	493	225	500	1	194.6/T (K)	p.w.
2	1.3	3.6	0	474	900	500	1	194.6/T (K)	p.w.
2R	1.2	3.6	0	488	900	500	1	194.6/T (K)	p.w.
3	2.1	6	0	470	1500	500	1	194.6/T (K)	p.w.
4	0.3	–	0	476	225	–	1	194.6/T (K)	[31]
5	1.2	–	0	485	900	–	1	194.6/T (K)	[31]
6	2.1	–	0	482	1500	–	1	194.6/T (K)	[31]
7	2.0	6.7	20	493	1644	489	2	4872/T (K)	p.w.
8	6.0	18.5	20	484	4542	490	2	4872/T (K)	p.w.
9	2.0	–	20	497	1520	–	2	4872/T (K)	[32]
10	6.0	–	20	500	4485	–	2	4872/T (K)	[37]
11	–	6	20	–	1500	500	2	4872/T (K)	p.w.
12	–	18	20	–	4500	500	2	4872/T (K)	p.w.
13	–	11.8	20	–	3000	508	2	4872/T (K)	[38]

5%. In the case of atmospheric pressure, the experimental set-up counts with external air-cooling at the end of the reactor, which freezes the reaction. In the high-pressure reactor, air-cooling does not exist, and temperature profiles of the experimental set-up were used for the simulations.

3. Kinetic model

A kinetic model has been compiled in the present work to simulate the oxidation of H_2S in the presence of NO. The updates of the different parts of the mechanism are detailed below. In the case of H_2S chemistry, the reactions used in this work have been taken from a recent work by the authors about H_2S oxidation at high pressures [37]. These reactions are based on previous works about H_2S oxidation at different pressures [25,31,32] and other works from the group about SO_2 under combustion conditions [26,27,42]. Specifically, the modifications that were evaluated in [37] include two reactions involving H_2O_2, which allowed to improve model predictions at high pressures, while maintaining a good prediction at atmospheric pressure.

For the chemistry involving NO_x species, the reaction subsets used in the present study have been taken from the work by Colom-Díaz et al. [38], where the oxidation of H_2 and its interaction with NO was studied at high-pressures (10, 20 and 40 bar), in a tubular flow reactor. These subsets are mainly based on the work by Giménez-López et al. [43], who performed experiments of the oxidation of C_2H_4/NO mixtures at high pressure (60 bar) and different stoichiometries. Some of the reactions have been updated with the kinetic parameters published in the work by Abián et al. [44], about the formation of NO in N_2/O_2 mixtures in a flow reactor.

Besides, in the work by Colom-Díaz et al. [38], the reaction kinetic parameters of NO with O_2 to form NO_2 (R1) were revised, due to the importance of this reaction at high pressures. The apparent activation energy was varied between the uncertainty limits (-1.05 ± 0.79 kcal/mol [45], and a good agreement between experimental results and model predictions was observed over a wide range of conditions, using a final activation energy value of -1.84 kcal/mol.

$NO + NO + O_2 \rightleftharpoons NO_2 + NO_2$ (R1)

Due to the high pressure conditions and the presence of oxygen, there is a mixture of NO/NO_2 at the reactor inlet. This was observed while the oven was still cool (290 K) [38] and has already been reported in previous works experimenting with NO at high pressures (e.g. [17,38–41,43]). For this reason, in the present work, the model was run with temperature profiles in the high-pressure set-up, in order to know at each position of the reactor the concentration of NO and NO_2 due to the oxidation of NO at high pressures occurring at low temperatures.

Regarding S/N species interactions, their kinetics seem to be a field of great uncertainty [46,47]. Selected reactions have been added to the mechanism, which can be seen in Table 2. Such reactions have been taken from the work of Glarborg [46], where he stablished a preliminary subset of reactions for S/N interactions. As the author mentioned, the rate constants of the S/N subset are no more than rough guesses. He stated in his work [46] that determinations were qualitative at best. Nevertheless, the simulations carried out in the present work with these reactions seem to be in accordance with the experimental results, as seen in the next section.

4. Results and discussion

The results of H_2S, SO_2 and NO concentrations obtained as a function of temperature corresponding to sets 1–3 in Table 1 are presented in Figs. 1–3. The experiments have been performed at atmospheric pressure using the set-up 1, from reducing to oxidizing conditions with respect to H_2S. The results of the oxidation of neat H_2S corresponding to sets 4–6 in Table 1 are also shown. The experimental results for the neat H_2S oxidation have been taken from a previous work by the authors [31], where the same experimental set-up and similar lambda values

Table 2
Arrhenius parameters for the reactions proposed in this work taken from the study by Glarborg [46]. Arrhenius expression: $k = AT^n \exp[-E_a/(RT)]$. Units are mol, cm, s and cal.

Reaction		A	n	Ea
R2	$NO_2 + SO \rightleftharpoons SO_2 + NO$	8.43E12	0.00	0
R3	$NO_2 + SO_2 \rightleftharpoons SO_3 + NO$	6.31E12	0.00	27,000
R4	$NO_2 + SH \rightleftharpoons HSO + NO$	1.75E13	0.00	−477
R5	$NH + SO \rightleftharpoons NO + SH$	3.3E13	0.00	0
R6	$SH + NH \rightleftharpoons SN + H_2$	1.0E13	0.00	0
R7	$SN + OH \rightleftharpoons SH + NO$	1.0E13	0.00	0
R8	$SO + N \rightleftharpoons S + NO$	7.0E12	0.00	0
R9	$SO_2 + N \rightleftharpoons SO + NO$	6.4E9	1.00	6280
R10	$SO_2 + NH \rightleftharpoons SO + HNO$	5.0E12	0.00	20,000
R11	$S + NO(+M) \rightleftharpoons SNO(+M)$	3.4E13	0.24	0
	LOW			
	TROE/0.22 7445 1E30 −1E30/	2.2E15	0.00	−1870
R12	$SH + NO(+M) \rightleftharpoons HSNO(+M)$	1.6E13	0.00	0
	LOW			
	TROE/0.5 1E30 −1E30/	1.4E23	−2.50	0
R13	$SN + O \rightleftharpoons S + NO$	3.0E12	0.00	0
R14	$SNO + H \rightleftharpoons SH + NO$	1.0E13	0.00	0
R15	$S + HNO \rightleftharpoons SH + NO$	1.0E13	0.00	0

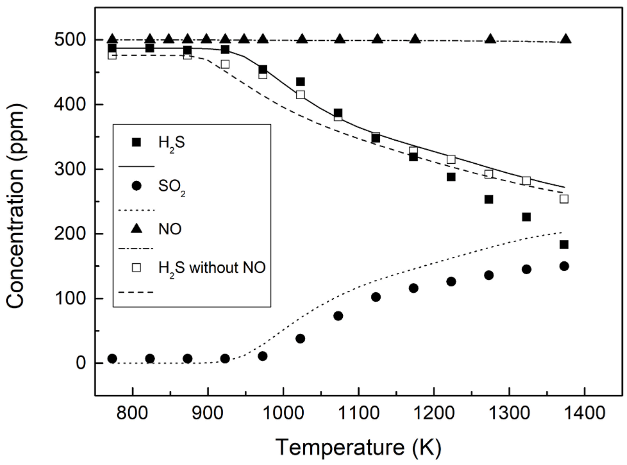

Fig. 1. Results from H_2S oxidation in conditions of set 1 in Table 1 ($\lambda_{H2S} = 0.3$). Symbols represent experimental data and lines model predictions. The results of H_2S oxidation without NO ($\lambda_{H2S} = 0.3$) have been taken from [31] (set 4 in Table 1).

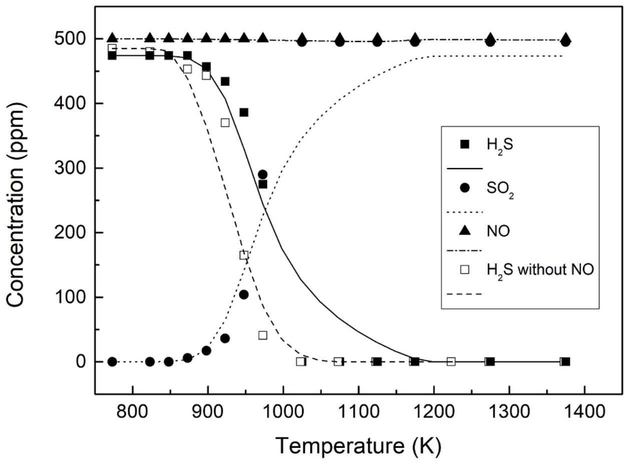

Fig. 2. Results from H_2S oxidation in conditions of set 2 in Table 1 ($\lambda_{H2S} = 1.3$). Symbols represent experimental data and lines model predictions. The results of H_2S oxidation without NO ($\lambda_{H2S} = 1.2$) have been taken from [31] (set 5 in Table 1).

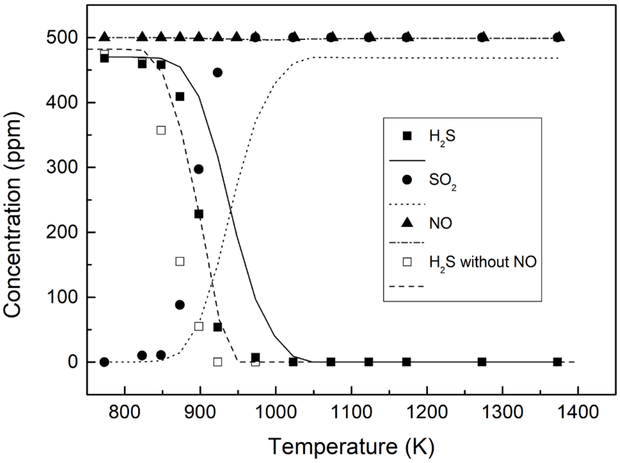

Fig. 3. Results from H_2S oxidation in conditions of set 3 in Table 1 ($\lambda_{H2S} = 2.1$). Symbols represent experimental data and lines model predictions. The results of H_2S oxidation without NO ($\lambda_{H2S} = 2.1$) have been taken from [31] (set 6 in Table 1).

were used.

H_2S oxidation onset occurs similarly for all lambda values ($\lambda_{H2S} = 0.3–2.1$), in the absence and presence of NO. H_2S conversion in the presence of NO is shifted 25 K to higher temperatures under oxidizing and near stoichiometric conditions. Under reducing conditions, Fig. 1, H_2S conversion starts at the same temperature, but it is oxidized in a greater extent above 1200 K in the presence of NO. The concentration of NO remains unaltered for all experimental conditions at the initial value of 500 ppm. The main oxidation product is SO_2 and the sulfur balance is maintained within 100 ± 5% under oxidizing and near stoichiometric conditions. Under reducing conditions, the sulfur balance goes down to 67% for the highest temperature considered (1375 K), in the presence of NO, and 80% in the case of neat H_2S oxidation [28]. It is worthwhile to mention that, in the experiment carried out under reducing conditions (set 1 in Table 1, $\lambda_{H2S} = 0.3$), a yellow deposit was seen at the outlet of the reactor, as it was also observed in the case of neat H_2S oxidation [31], and this can be the explanation for the poor balance closure.

Overall, simulations match well the experimental data under all conditions at atmospheric pressure, including the differences observed in the experimental H_2S oxidation data, in the absence and presence of NO. The shift to higher temperatures in H_2S oxidation, when NO is present, is due to reactions involving NO, despite the constant concentration of NO observed. According to the model, the following cycle is responsible for NO consumption and recycle to NO:

$NO + HO_2 \rightleftharpoons NO_2 + OH$ (R16)

$NO_2 + SH \rightleftharpoons HSO + NO$ (R4)

The following overall reaction (R17) would be the result of combining both R16 and R4:

$SH + HO_2 \rightleftharpoons HSO + OH$ (R17)

which converts the unreactive HO_2 radicals into more reactive OH radicals. The HSO species would react in reaction (R18) to form SO and HSOH.

$HSO + HSO \rightleftharpoons SO + HSOH$ (R18)

HSOH further reacts with the radical pool, but mainly through (R19) to give back H_2S:

$HSOH + SH \rightleftharpoons H_2S + HSO$ (R19)

In a lesser extent, NO_2 species react with SO to form SO_2 and NO (R2), while SO radicals form SO_2 as well in reaction (R20).

$NO_2 + SO \rightleftharpoons SO_2 + NO$ (R2)

$SO + O_2 \rightleftharpoons SO_2 + O$ (R20)

All in all, the NO presence in H_2S oxidation at atmospheric pressure shifts to higher temperatures the process by consuming and competing for HO_2 radicals under oxidizing and near stoichiometric conditions. The conversion of HO_2 to more active radicals, like OH, enhances the process via (R16), as it is seen in other works using CO or CH_4 in the presence of NO (e.g. [48–50]). However, when SH radicals react with NO_2 (R4), forming HSO, it leads to a slower reaction pathway to produce the final product SO_2 (R4, R18, R20). This can also be observed in the sensitivity analysis presented in Fig. 4, where reaction (R16, $NO + HO_2 \rightleftharpoons NO_2 + OH$) is shown as the most sensitive one at $\lambda = 2.1$ and 923 K (set 3 in Table 1). The positive coefficient indicates that an increase of the pre-exponential factor of (R16) would result in a slower consumption of H_2S. The main reaction pathway for H_2S oxidation would be the one by which SH radicals react mainly with O_2 to form HSOO, which previously isomerizes to HSO_2 to form SO_2 [31]. Under reducing conditions, where HO_2 radicals are not so important and other important species such as H_2S_2, HS_2 and S_2 might be formed, the simulations remain equal as for the neat H_2S oxidation. The model is not capable of predicting the major H_2S consumption at high temperatures when NO is present (1375 K), probably due to possible interactions between NO and disulfur species (more important at reducing conditions) that are not present in the model.

As mentioned, the H_2S oxidation in the presence of NO at atmospheric pressure has been studied for different air excess ratios ($\lambda_{H2S} = 0.3–2.1$). Under reducing conditions, a yellow deposit was seen outside the reaction zone, due to the condensation of the sulfur formed, as previously observed during the neat H_2S oxidation [31]. In the high-pressure reactor (set-up 2), only oxidizing conditions are used for the experiments, to avoid the possible formation of sulfur in the experimental set-up, in case of using reducing conditions. However, during the experiments at high pressure, the sulfur balance did not close at 100% in any case, probably due to the formation of sulfur, as will be discussed later.

The results for the experiments of H_2S oxidation at 20 bar in the presence of NO are shown in Figs. 5 and 6, for $\lambda_{H2S} = 2$ and $\lambda_{H2S} = 6$, respectively (sets 7 and 8 in Table 1). The results for neat H_2S oxidation are also plotted in the figures and are taken from previous works by the authors in the same experimental set-up, for $\lambda_{H2S} = 2.0$ [32] and for $\lambda_{H2S} = 6.0$ [37] (sets 9 and 10 in Table 1).

As it can be observed, in the presence of NO, significant H_2S conversion is obtained over the entire temperature range studied. For example, at the lowest temperature considered (475 K), the conversion of H_2S reaches, at least, 50% for $\lambda_{H2S} = 2$ and 90% for $\lambda_{H2S} = 6$. At the same time, all the H_2S reacted is not quantified as SO_2. For $\lambda_{H2S} = 2$, the sulfur balance is maintained around 86 ± 5%, while for $\lambda_{H2S} = 6$ the sulfur balance observed is maintained around 67 ± 10%. These characteristics are not observed in the absence of NO. A possible explanation would be that NO and/or NO_2 are reacting with H_2S prior to the reactor inlet or at lower temperatures than 475 K in the reaction zone. The complete oxidation of H_2S at $\lambda_{H2S} = 2$ is shifted to higher temperatures respect to neat H_2S oxidation (by 50 K).

In order to evaluate the influence of NO in relation to the high H_2S conversion shown at relatively low temperatures, experiments of neat

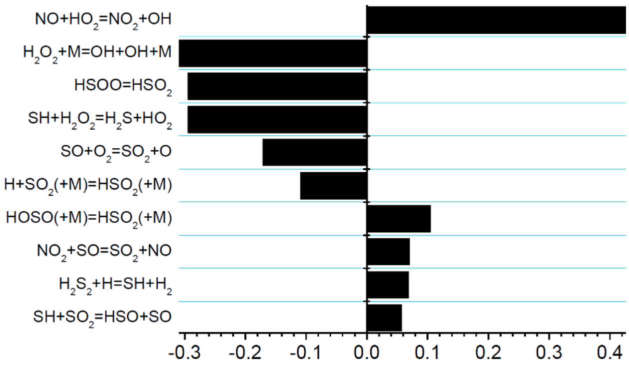

Fig. 4. Normalized sensitivity analysis for H_2S. Set 3 in Table 1, $\lambda = 2.1$, 923 K.

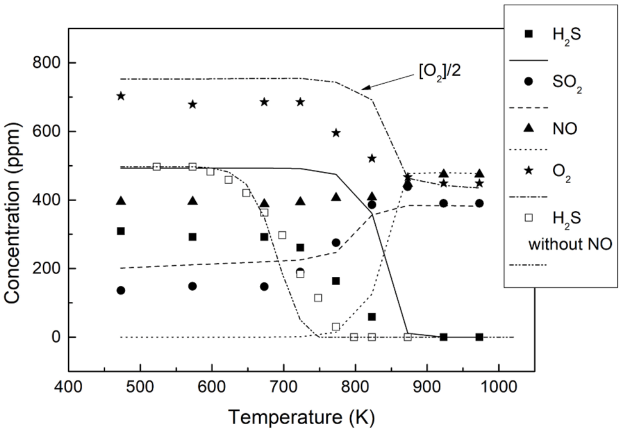

Fig. 5. Results from H_2S oxidation in conditions of set 7 in Table 1 ($\lambda_{H2S} = 2.0$). Symbols represent experimental data and lines model predictions. The results of H_2S oxidation without NO ($\lambda_{H2S} = 2.0$) have been taken from [32] (set 9 in Table 1).

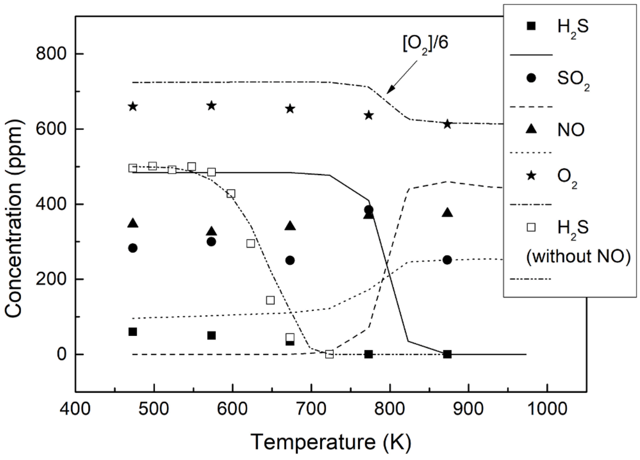

Fig. 6. Results from H_2S oxidation in conditions of set 8 in Table 1 ($\lambda_{H2S} = 6.0$). Symbols represent experimental data and lines model predictions. The results of H_2S oxidation without NO ($\lambda_{H2S} = 6.0$) have been taken from [37] (set 10 in Table 1).

NO oxidation under similar conditions (20 bar and O_2 concentration) were carried out. The evolution of NO concentration, with and without H_2S, versus temperature is plotted in Fig. 7. Two different lambda values have been used (λ_{NO}6 and 18) (sets 7, 8, 11 and 12 in Table 1). Results of neat NO oxidation [38] with a different stoichiometry ($\lambda_{NO} = 11.8$) have also been plotted in order to compare results (set 13 in Table 1). The experimental results of the experiment for $\lambda_{NO} = 11.8$ [38] are placed between the ones done in the present work, following a trend according to the lambda value. When H_2S is present in the experiments, the NO concentration at the exit is much higher than just using NO. The kinetic model is capable of reproducing accurately the experimental results just using NO as in [38], but is far from reproducing the experimental data when H_2S is present.

The major conversion of NO in the absence of H_2S, higher when O_2 increases, implies a major concentration of NO_2 molecules, as seen in [38]. This is mainly due to reaction (R1, $NO + NO + O_2 \rightleftharpoons NO_2 + NO_2$), which enhances the formation of NO_2 at high pressures and low temperatures. Since the concentration of NO is so high when H_2S is present, differing from the study of neat NO oxidation, this could mean that the NO_2 formed under high pressure conditions, prior to entering the reactor, is reacting with H_2S to form some elemental sulfur and NO.

In the literature, the reaction between H_2S and NO_2 has been previously studied, more qualitatively than quantitatively [51–55]. The study of the interaction between these species has been mainly focused on its implication for atmospheric chemistry. The measurements indicated that some mechanisms other than ozonation must be responsible for the atmospheric breakdown of reduced sulfur compounds in the atmosphere [53]. Cadle and Ledford [55] observed the formation of free sulfur upon exposing mixtures of nitrogen dioxide and hydrogen sulfide to light. However, Hales et al. [53] indicate that this reaction may proceed to a limited extent even in a totally dark reactor. Blackwood [54] studied the reaction of $NO_2 + H_2S$ in air and reported S and SO_2 as products; however, no mechanism was postulated. Frost and Thomas [51] also studied this reaction over the 448–528 K temperature range in a Pyrex reaction vessel, saying that, when H_2S was in excess, sulfur was one of the reaction products. Thus, they performed the investigation using $P_{NO2} > 3P_{H2S}$. In the present work, the experiments are performed under H_2S excess, which could explain the formation of sulfur. More recently, Kim [56] studied the atmospheric corrosion process of silver in environments containing 0.1 ppm H_2S and 1.2 ppm NO_2. He found sulfur formed in the silver, supposedly through (R21):

$H_2S + 2NO_2 \rightleftharpoons S + 2HNO_2$ (R21)

It has also been mentioned, in studies dealing with fireworks, how H_2S and NO_2, which come from the sulfur and the KNO_3 present in the black powder used, may react, and are supposed to produce and consume sulfur as follows [57] (R22 and R23):

$H_2S + NO_2 \rightleftharpoons S + NO + H_2O$ (R22)

$2NO_2 + 2S \rightleftharpoons 2SO_2 + N_2$ (R23)

Despite the literature observations of sulfur formation from H_2S and NO_2 at atmospheric pressure, no detailed kinetic models are available in the literature yet dealing with this issue. In the present work, we point to the necessity for a better characterization of this process, since both species are important not only at atmospheric pressure but at high pressures as well.

An attempt to simulate such behavior has been done in this work by proposing the kinetic parameters of reaction (R22), using 10^8 (mol, s, cm^3) as the kinetic constant value for the temperature range studied (475–1000 K), which provides good results. The simulation results corresponding to the high-pressure experiments, sets 7–13 in Table 1, are shown in Figs. S1–S3 of the supplementary material. Reaction (R22) has a high impact on the concentration trends of all the species (H_2S, SO_2, NO and O_2), in comparison with the simulation results shown in Figs. 5 and 6. The reaction (R22) is important at room temperature, in

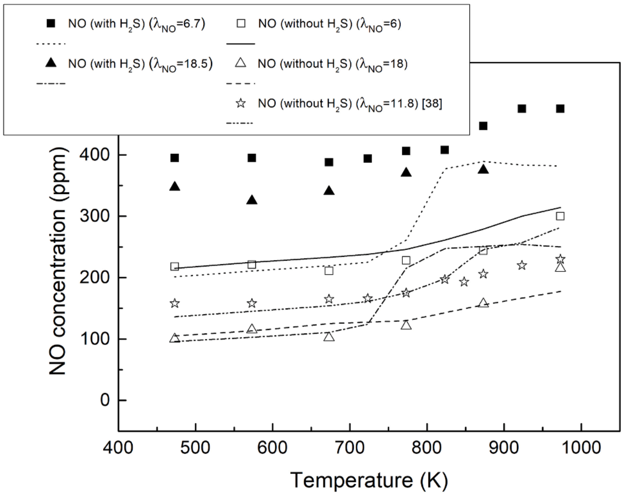

Fig. 7. Experimental results from NO oxidation in the presence (sets 7 and 8 in Table 1) and absence (sets 11 and 12 in Table 1) of H_2S at 20 bar. Symbols represent experimental data and lines model predictions. The results for NO oxidation without H_2S at $\lambda_{NO} = 11.8$ have been taken from [38] (set 13 in Table 1).

the experimental set-up zones prior and posterior to the reactor, according to Chemkin rate of production. With reaction (R22) in the mechanism, the formation of sulfur is predicted, with the sulfur balance ($SO_2 + H_2S$) closing around 95 ± 4% in the experimental simulations. This is due to the oxidation of the sulfur formed in (R22) to SO_2 via (R24) and (R19), according to the model.

$S + O_2 \rightleftharpoons SO + O$ (R24)

In simulations, H_2S is totally consumed at lower temperatures in the case of more oxidizing conditions, as observed in the experiments, due to the major formation of NO_2 (R1), which reacts with H_2S. In the case of $\lambda_{H2S} = 2$, the oxidation of H_2S is also well predicted by the model. The model predictions of SO_2, NO and O_2 are close to the experimental data, although some differences are still noticeable. For example, NO_2 is supposed to react with H_2S to give back NO, but the amount of NO formed in the simulations is still low by 20%, in comparison with the experimental data. The important interaction between H_2S and NO_x at high pressure, presumably dominated by the NO_2 presence, has been pointed out both in the experiments and the simulations of the present work. The authors recommend a better characterization of this reaction and other possible reactions involved in such interaction.

Another possible explanation for not matching the sulfur balance at high pressures, which is found even working at oxidizing conditions, could be related to the SO_x/NO_x interaction. Since the conversion rates of SO_2 to SO_3 and of NO to NO_2 are strong at elevated pressures and low temperatures [12], reaction (R25) could be partly responsible for the unbalance of sulfur, producing SO_3, which is not measured in the present work and might form H_2SO_4 in contact with H_2O, which may condensate:

$SO_2 + NO_2 \rightleftharpoons SO_3 + NO$ (R25)

However, in a study of the reaction of SO_2 with NO_2 in the absence and presence of water vapour [58] in a stainless steel vessel, it was found that, under dry conditions, oxidation of SO_2 by NO_2 does not take place significantly at conditions similar to the ones here studied (5–15 bar and 375–675 K). In other works, the impact of nitrogen oxides on SO_2 oxidation during cooling is believed to be small in the burnout region of stationary combustion systems [29,46]. The inclusion of reaction (R25), which kinetic parameters have been taken from the work by Glarborg [46], does not imply any influence on the model simulations under the conditions of the present work.

5. Conclusions

The study carried out in the present work shows experimental and kinetic modeling results of H_2S oxidation in the presence of NO. The results have been obtained in two different experimental set-ups, for different air excess ratios, pressures and temperatures. The results obtained in the first experimental set-up, an atmospheric tubular flow reactor operating from 700 to 1400 K, have shown a slight shift to higher temperatures (25 K) of H_2S oxidation respect to neat H_2S when NO is present, for oxidizing ($\lambda_{H2S} = 2.1$) and near stoichiometric conditions ($\lambda_{H2S} = 1.2$). A kinetic model updated with S/N reactions has been able to reproduce well such experimental data. Under reducing conditions ($\lambda_{H2S} = 0.3$), the H_2S oxidation in the presence of NO presents a major reactivity above 1200 K, which can not be predicted by the model. While the concentration of NO does not vary in all the temperature range for all the stoichiometries, an interconversion cycle between NO/NO_2 consuming HO_2 radicals is responsible for the oxidation shift, which is found both in the experimental data and model predictions.

The oxidation of H_2S at 20 bar, in the absence and presence of NO, has been performed only for oxidizing conditions ($\lambda_{H2S} = 2$ and $\lambda_{H2S} = 6$) in the second experimental set-up that corresponds to a high pressure flow reactor, operating from 475 to 1000 K. The results have shown that, at the lowest temperature considered (475 K), it exists at least 50% of H_2S conversion for $\lambda_{H2S} = 2$ and 90% for $\lambda_{H2S} = 6$. The sulfur balance closes at 86 ± 5% for $\lambda_{H2S} = 2$, while for $\lambda_{H2S} = 6$ the sulfur balance is maintained around 67 ± 10%. In order to evaluate the influence of NO, neat oxidation experiments of NO have been performed using similar O_2 concentrations to those used in the H_2S oxidation in the presence of NO. The conversion of NO to NO_2 is favored at high pressures and low temperatures, and is higher as O_2 concentration increases. A reaction between NO_2 and H_2S may be the responsible for the early conversion of H_2S and the decay in the sulfur balance. An attempt to simulate such behavior has been done by proposing reaction $H_2S + NO_2 \rightleftharpoons S + NO + H_2O$, which forms sulfur and allows to reproduce well the experimental data. We point for a better understanding and characterization of the reactions involved in the S/N chemistry, which might be of importance for industrial processes.

CRediT authorship contribution statement

J.M. Colom-Díaz: Conceptualization, Investigation, Writing - original draft, Data curation, Visualization, Methodology. **Á. Millera:** Conceptualization, Writing - review & editing, Supervision, Funding acquisition, Project administration. **R. Bilbao:** Conceptualization, Writing - review & editing, Supervision, Funding acquisition, Project administration. **M.U. Alzueta:** Conceptualization, Writing - review & editing, Supervision, Funding acquisition, Project administration.

Declaration of Competing Interest

The authors declare that they have no known competing financial interests or personal relationships that could have appeared to influence the work reported in this paper.

Acknowledgements

The authors express their gratitude to the Aragón Government (Ref. T22_20R), co-funded by FEDER 2014-2020 “Construyendo Europa desde Aragón”, and to MINECO and FEDER (Project CTQ2015-65226 and RTI2018-098856-B-100) for financial support. J.M. Colom acknowledges to MINECO for the predoctoral grant awarded (BES-2016-076610).

Appendix A. Supplementary data

Supplementary data to this article can be found online at https://doi.org/10.1016/j.fuel.2020.120060.

References

[1] International Energy Agency. Natural gas resources and production prospects. In: World Energy Outlook, Paris, Organisation for economic co-operation and development; 2008.

[2] Valera-Medina A, Giles A, Pugh D, Morris S, Pohl M, Ortwein A. Investigation of combustion of emulated biogas in a gas turbine test rig. J Therm Sci 2018;27(4): 331–40. https://doi.org/10.1007/s11630-018-1024-1.

[3] Department of Energy. Report of basic research needs for clean and efficient combustion of 21st century transportation fuels. https://www.osti.gov/servlets/purl/935428-bbBji1/; 2006.

[4] Baccanelli M, Langé S, Rocco MV, Pellegrini LA, Colombo E. Low temperature techniques for natural gas purification and LNG production: an energy and exergy analysis. Appl Energy 2016;180:546–59. https://doi.org/10.1016/j.apenergy.2016.07.119.

[5] Awe OW, Zhao Y, Nzihou A, Minh DP, Lyczko N. A Review of Biogas Utilisation, Purification and Upgrading Technologies. Waste Biomass Valor 2017;8(2):267–83. https://doi.org/10.1007/s12649-016-9826-4.

[6] Lu X, Palmer M, Forrest B, McGroddy M. A novel power generation system utilizing un-treated sour gas fuel. Society of Petroleum Engineers. Abu Dhabi International Petroleum Exhibition & Conference. Abu Dhabi, UAE, 2018.

[7] Chakroun NW, Ghoniem AF. Techno-economic assessment of sour gas oxy-combustion water cycles for CO_2 capture. Int J Greenhouse Gas Control 2015;36: 1–12. https://doi.org/10.1016/j.ijggc.2015.02.004.

[8] Chakroun NW, Ghoniem AF. High-efficiency low LCOE combined cycles for sour gas oxy-combustion with CO_2 capture. Int J Greenhouse Gas Control 2015;41: 163–73. https://doi.org/10.1016/j.ijggc.2015.06.025.

[9] Bongartz D, Shanbhogue SJ, Ghoniem AF. Formation and control of sulfur oxides in sour gas oxy-combustion: prediction using a reactor network model. Energy Fuels 2015;29(11):7670–80. https://doi.org/10.1021/acs.energyfuels.5b01709.

[10] Bongartz D, Ghoniem AF. Impact of sour gas composition on ignition delay and burning velocity in air and oxy-fuel combustion. Combust Flame 2015;162(7): 2749–57. https://doi.org/10.1016/j.combustflame.2015.04.014.

[11] Bongartz D, Ghoniem AF. Chemical kinetics mechanism for oxy-fuel combustion of mixtures of hydrogen sulfide and methane. Combust Flame 2015;162(3):544–53. https://doi.org/10.1016/j.combustflame.2014.08.019.

[12] Wang X, Adeosun A, Yablonsky G, Gopan A, Du P, Azelbaum RL. Synergistic SO_x/NO_x chemistry leading to enhanced SO_3 and NO_2 formation during pressurized oxy-combustion. Reac Kinet Mech Cat 2018;123:313–22.

[13] Gopan A, Kumfer BM, Axelbaum RL. Effect of operating pressure and fuel moisture on net plant efficiency of a staged, pressurized oxy-combustion power plant. Int J Greenhouse Gas Control 2015;39:390–6. https://doi.org/10.1016/j.ijggc.2015.05.014.

[14] Gupta AK, Ibrahim S, Al Shoaibi A. Advances in sulfur chemistry for treatment of acid gases. Prog Energy Combust Sci 2016;54:65–92. https://doi.org/10.1016/j.pecs.2015.11.001.

[15] Wang W, Herreros JM, Tsolakis A, York APE. Ammonia as hydrogen carrier for transportation; investigation of the ammonia exhaust gas fuel reforming. Int J Hydrogen Energy 2013;38(23):9907–17. https://doi.org/10.1016/j.ijhydene.2013.05.144.

[16] Normann F, Andersson K, Leckner Bo, Johnsson F. Emission control of nitrogen oxides in the oxy-fuel process. Prog Energy Combust Sci 2009;35(5):385–97. https://doi.org/10.1016/j.pecs.2009.04.002.

[17] Ajdari S, Normann F, Andersson K, Johnsson F. Modeling the nitrogen and sulfur chemistry in pressurized flue gas systems. Ind Eng Chem Res 2015;54(4):1216–27. https://doi.org/10.1021/ie504038s.

[18] Jafari H, Yang W, Ryu C. Evaluation of a distributed combustion concept using 1-D modeling for pressurized oxy-combustion system with low flue gas recirculation. Fuel 2020;263:116723. https://doi.org/10.1016/j.fuel.2019.116723.

[19] de Diego LF, de las Obras-Loscertales M, Rufas A, García-Labiano F, Gayán P, Abad A, Adánez J. Pollutant emissions in a bubbling fluidized bed combustor working in oxy-fuel operating conditions: Effect of flue gas recirculation. Appl Energy 2013;102:860–7. https://doi.org/10.1016/j.apenergy.2012.08.053.

[20] Abián M, Millera A, Bilbao R, Alzueta MU. Effect of Recirculation Gases on Soot Formed from Ethylene Pyrolysis. Combust Sci Technol 2012;184(7-8):980–94. https://doi.org/10.1080/00102202.2012.663990.

[21] Salisu I, Abhijeet R. Kinetic simulation of acid gas (H2S and CO2) destruction for simultaneous syngas and sulfur recovery. Ind Eng Chem Res 2016;55:6743–52.

[22] Salisu I, Mohammad Al H, Abhijeet R. Detailed reaction mechanism to predict ammonia destruction in the thermal section of sulfur recovery units. Ind Eng Chem Res 2020;59:74912–23.

[23] Li D, Dowling N, Marriott R, Clark P. Kinetics and mechanisms for destruction of ammonia in the Claus furnace. Chalk Talk: Calgary AB, Canada: Alberta Sulphur Research Ltd.; 2016.

[24] Jerzak W, Kuźnia M, Szajding A. Experimental Studies and the Chemical Kinetics Modelling of Oxidation of Hydrogen Sulfide Contained in Biogas. Procedia Eng 2016;157:222–9. https://doi.org/10.1016/j.proeng.2016.08.360.

[25] Colom-Díaz JM, Leciñena M, Peláez A, Abián M, Millera Á, Bilbao R, Alzueta MU. Study of the conversion of CH_4/H_2S mixtures at different pressures. Fuel 2020;262: 116484. https://doi.org/10.1016/j.fuel.2019.116484.

[26] Giménez-López J, Martínez M, Millera A, Bilbao R, Alzueta MU. SO_2 effects on CO oxidation in a CO_2 atmosphere, characteristic of oxy-fuel conditions. Combust Flame 2011;158(1):48–56. https://doi.org/10.1016/j.combustflame.2010.07.017.

[27] Alzueta MU, Bilbao R, Glarborg P. Inhibition and sensitization of fuel oxidation by SO_2. Combust Flame 2001;127(4):2234–51. https://doi.org/10.1016/S0010-2180(01)00325-X.

[28] Rasmussen CL, Glarborg P, Marshall P. Mechanisms of radical removal by SO_2. Proc Combust Inst 2007;31(1):339–47. https://doi.org/10.1016/j.proci.2006.07.249.

[29] Miccio F, Löffler G, Wargadalam VJ, Winter F. The influence of SO_2 level and operating conditions on NO_x and N_2O emissions during fluidised bed combustion of coals. Fuel 2001;80(11):1555–66. https://doi.org/10.1016/S0016-2361(01)00029-1.

[30] Wendt JOL, Sternling CV. Catalysis of SO_2 oxidation by nitrogen oxides. Combust Flame 1973;21(3):387–90. https://doi.org/10.1016/S0010-2180(73)80062-8.

[31] Colom-Díaz JM, Abián M, Ballester MY, Millera Á, Bilbao R, Alzueta MU. H_2S conversion in a tubular flow reactor: experiments and kinetic modeling. Proc Combust Inst 2019;37(1):727–34. https://doi.org/10.1016/j.proci.2018.05.005.

[32] Colom-Díaz JM, Abián M, Millera Á, Bilbao R, Alzueta MU. Influence of pressure on H_2S oxidation. Experiments and kinetic modeling. Fuel 2019;258:116145. https://doi.org/10.1016/j.fuel.2019.116145.

[33] Gersen S, Van Essen M, Darmeveil H, Hashemi H, Rasmussen CT, Christensen JM, Glarborg P, Levinsky H. Experimental and modeling investigation of the effect of H2S addition to methane on the ignition and oxidation at high pressures. Energy Fuels 2017;31:2175-82.

[34] Song Y, Hashemi H, Christensen JM, Zou C, Haynes BS, Marshall P, Glarborg P. An exploratory flow reactor study of H2S oxidation at 30-100 bar. Int J Chem Kinet 2017;49:37-52.

[35] Mathieu O, Deguillaume F, Petersen EL. Effects of H_2S addition on hydrogen ignition behind reflected shock waves: experiments and modeling. Combust Flame 2014;161(1):23–36. https://doi.org/10.1016/j.combustflame.2013.07.011.

[36] Zhou C(, Sendt K, Haynes BS. Experimental and kinetic modelling study of H_2S oxidation. Proc Combust Inst 2013;34(1):625–32. https://doi.org/10.1016/j.proci.2012.05.083.

[37] Colom-Díaz JM, Millera Á, Bilbao R, Alzueta MU. New results of H_2S oxidation at high pressures. Experiments and kinetic modeling. Fuel 2021;285:119261. https://doi.org/10.1016/j.fuel.2020.119261.

[38] Colom-Díaz JM, Millera Á, Bilbao R, Alzueta MU. High pressure study of H_2 oxidation and its interaction with NO. Int J Hydrogen Energy 2019;44:6325–32.

[39] Marrodán L, Millera Á, Bilbao R, Alzueta MU. High-Pressure Study of Methyl Formate Oxidation and Its Interaction with NO. Energy Fuels 2014;28(9):6107–15. https://doi.org/10.1021/ef501313x.

[40] Rasmussen CL, Rasmussen AE, Glarborg P. Sensitizing effects of NO_x on CH_4 oxidation at high pressure. Combust Flame 2008;154(3):529–45. https://doi.org/10.1016/j.combustflame.2008.01.012.

[41] Rasmussen CL, Hansen J, Marshall P, Glarborg P. Experimental measurements and kinetic modeling of CO/H2/O2/NOx conversion at high pressure. Int J Chem Kinet 2008;40:454-80.

[42] Abián M, Millera Á, Bilbao R, Alzueta MU. Interaction of soot-SO2: Experimental and kinetic analysis. Combust Sci Technol 2016;188:482-491.

[43] Giménez-López J, Alzueta MU, Rasmussen CT, Marshall P, Glarborg P. High pressure oxidation of C_2H_4/NO mixtures. Proc Combust Inst 2011;33(1):449–57. https://doi.org/10.1016/j.proci.2010.05.098.

[44] Abián M, Alzueta MU, Glarborg P. Formation of NO from N_2/O_2 mixtures in a flow reactor: toward an accurate prediction of thermal NO. Int J Chem Kinet 2015;47: 518–32.

[45] Atkinson R, Baulch DL, Cox RA, Crowley JN, Hampson RF, Hynes RG, et al. Evaluated kinetic and photochemical data for atmospheric chemistry: Volume I – gas phase reactions of O_x, HO_x, NO_x and SO_x species. Atmos Chem Phys 2004;4: 1461–738.

[46] Glarborg P. Hidden interactions—trace species governing combustion and emissions. Proc Combust Inst 2007;31(1):77–98. https://doi.org/10.1016/j.proci.2006.08.119.

[47] Schofield K. The kinetic nature of sulfur's chemistry in flames. Combust Flame 2001;124(1-2):137–55. https://doi.org/10.1016/S0010-2180(00)00189-9.

[48] Roesler JF, Yetter RA, Dryer FL. Kinetic interactions of CO, NO_x, and HCI emissions in postcombustion gases. Combust Flame 1995;100:495–504.

[49] Song Y, Marrodán L, Vin N, Herbinet O, Assaf E, Fittschen C, Stagni A, Faravelli T, Alzueta MU, Battin-Leclerc F. The sensitizing effects of NO_2 and NO on methane low temperature oxidation in a jet stirred reactor. Proc Combust Inst 2019;37(1): 667–75. https://doi.org/10.1016/j.proci.2018.06.115.

[50] Glarborg P, Kristensen PG, Kubel D, Hansen J, Dam-Johansen K. Interactions of CO, NO_x and H_2O under post-flames conditions. Combust Sci Technol 1995;110–111: 461–85.

[51] Frost P, Thomas JH. Reaction between hydrogen-sulfide and nitrogen-dioxide. Combust Flame 1975;25:213–7.

[52] Pierce JA. A study of the reaction between nitric oxide and hydrogen sulphide. J Phys Chem 1929;33(1):22–36. https://doi.org/10.1021/j150295a003.

[53] Hales JM, Wilkes JO, York JL. Some recent measurements of H_2S oxidation rates and their implications to atmospheric chemistry. Tellus 1974;26(1-2):277–83. https://doi.org/10.3402/tellusa.v26i1-2.9795.

[54] Blackwood TR. A study of the reaction between hydrogen sulfide and nitrogen dioxide. 1980. Report. Department of Chemical Engineering, University of Michigan, Ann Arbor, Michigan.

[55] Cadle RD, Ledford M. Reaction of ozone with hydrogen sulfide. Int J Air Water Pollut 1966;10:25–30.

[56] Kim H. Corrosion process of silver in environments containing 0.1 ppm H2S and 1.2 ppm NO2. Mater Corros 2003;54:243-50.

[57] Russel MS. The chemistry of fireworks. 2nd ed. Cambridge: Royal Society of Chemistry; 2009.

[58] Murciano LT, White V, Petrocelli F, Chadwick D. Sour compression process for the removal of SO_x and NO_x from oxyfuel-derived CO_2. Energy Procedia 2011;4: 908–16. https://doi.org/10.1016/j.egypro.2011.01.136.

SUPPLEMENTARY MATERIAL

Conversion of $H_2S/O_2/NO$ mixtures at different pressures. Experiments and kinetic modeling

J. M. Colom-Díaz, Á. Millera, R. Bilbao, M. U. Alzueta*

Aragón Institute of Engineering Research (I3A). Department of Chemical and Environmental Engineering, University of Zaragoza, 50018 Zaragoza, Spain.

Table of contents:

1) **Calculation results of the system $H_2S/NO/O_2$ including reaction (R22) in the model ($H_2S+NO_2=S+NO+H_2O$)**

   Figure S1. Results from H_2S oxidation in conditions of set 7 in Table 1 (λ_{H2S}=2.0). Symbols represent experimental data and lines model predictions. The results of H_2S oxidation without NO (λ_{H2S}=2.0) have been taken from [32]. The simulations results include reaction (R22) ($H_2S+NO_2=S+NO+H_2O$).

   Figure S2. Results from H_2S oxidation in conditions of set 8 in Table 1 (λ_{H2S}=6.0). Symbols represent experimental data and lines model predictions. The results of H_2S oxidation without NO (λ_{H2S}=6.0) have been taken from [37]. The simulations results include reaction (R22) ($H_2S+NO_2= S+NO+H_2O$).

   Figure S3. Results from NO oxidation in the presence (sets 7 and 8 in Table 1) and absence (sets 11 and 12 in Table 1) of H_2S at 20 bar. Symbols represent experimental data and lines model predictions. The results for NO oxidation without H_2S at λ_{NO}=11.8 have been taken from ref. [38] (set 13 in Table 1). The simulations results of NO in the presence of H_2S include reaction (R22) ($H_2S+NO_2= S+NO+H_2O$).

1) **Calculation results of the system $H_2S/NO/O_2$ including reaction (R22) in the model ($H_2S+NO_2=S+NO+H_2O$)**

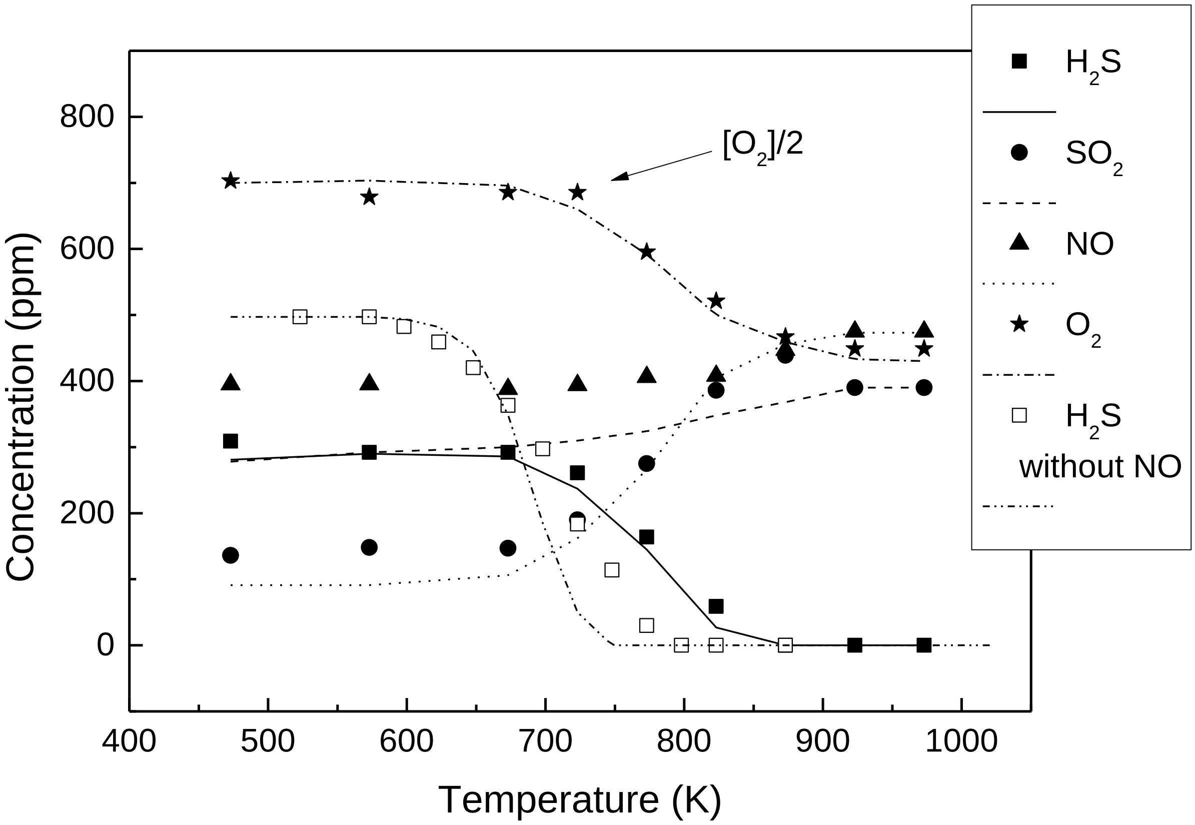

Figure S1. Results from H_2S oxidation in conditions of set 7 in Table 1 ($λ_{H2S}$=2.0). Symbols represent experimental data and lines model predictions. The results of H_2S oxidation without NO ($λ_{H2S}$=2.0) have been taken from [32]. The simulations results include reaction (R22) ($H_2S+NO_2=S+NO+H_2O$).

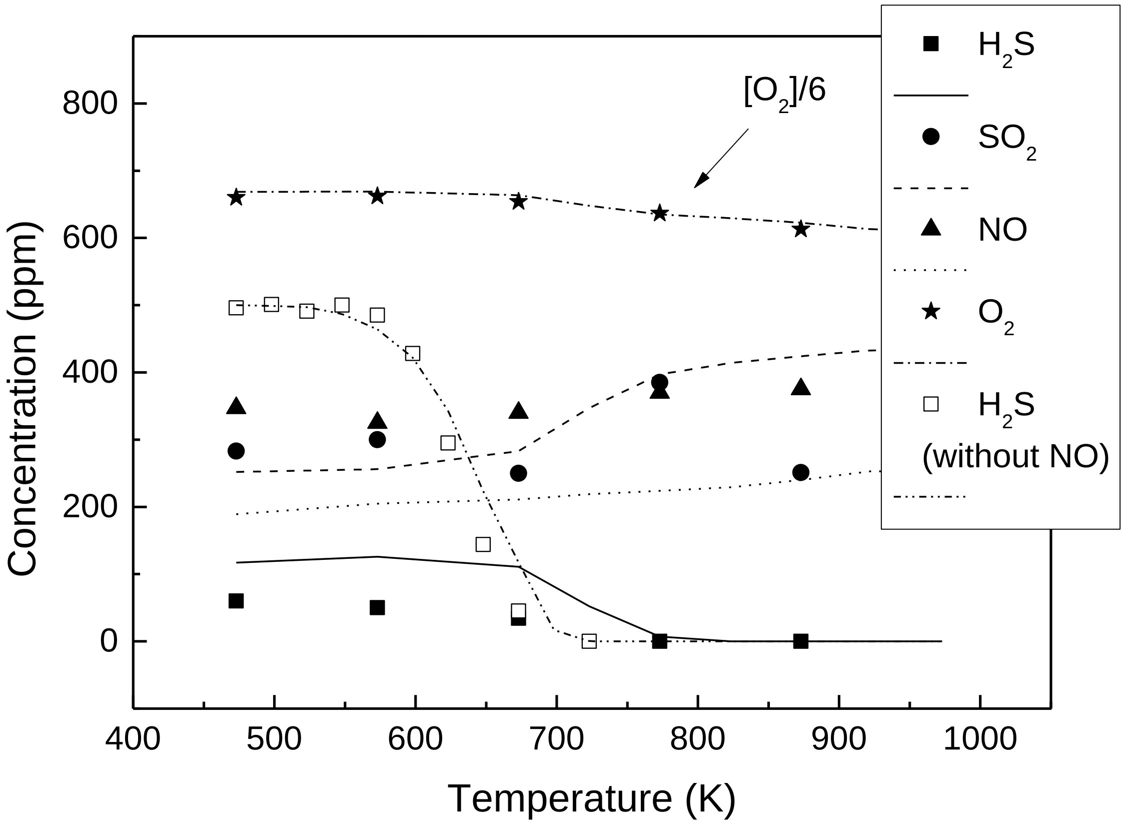

Figure S2. Results from H_2S oxidation in conditions of set 8 in Table 1 (λ_{H2S}=6.0). Symbols represent experimental data and lines model predictions. The results of H_2S oxidation without NO (λ_{H2S}=6.0) have been taken from [37]. The simulations results include reaction (R22) ($H_2S+NO_2= S+NO+H_2O$).

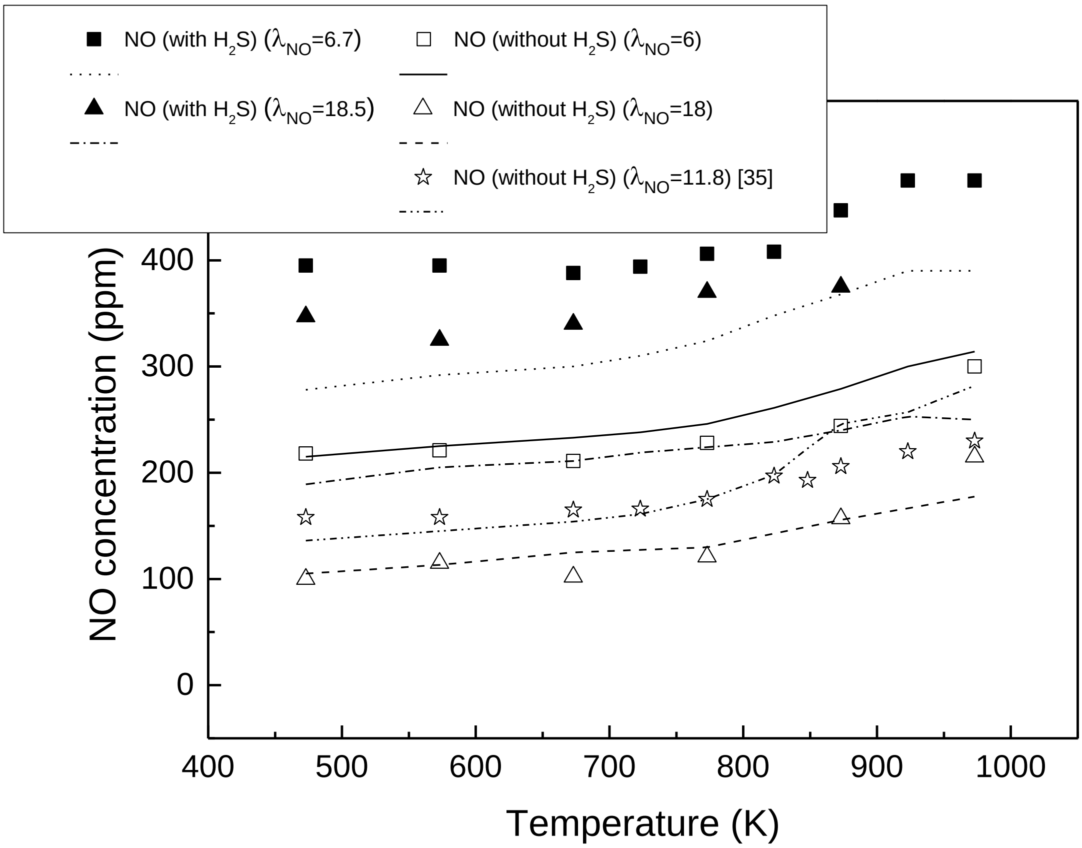

Figure S3. Results from NO oxidation in the presence (sets 7 and 8 in Table 1) and absence (sets 11 and 12 in Table 1) of H_2S at 20 bar. Symbols represent experimental data and lines model predictions. The results for NO oxidation without H_2S at λ_{NO}=11.8 have been taken from ref. [38] (set 13 in Table 1). The simulations results of NO in the presence of H_2S include reaction (R22) ($H_2S+NO_2= S+NO+H_2O$).

References:

[32] Colom-Díaz, J.M.; Abián, M.; Millera, Á.; Bilbao, R.; Alzueta, M.U. (2019). Influence of pressure on H_2S oxidation. Experiments and kinetic modeling. *Fuel* 258, 116145.

[37] Colom-Díaz, J.M.; Millera, Á.; Bilbao, R.; Alzueta, M.U. (2021). New results of H_2S oxidation at high pressures. Experiments and kinetic modeling. *Fuel* 285, 119261.

[38] Colom-Díaz, J.M.; Millera, Á.; Bilbao, R.; Alzueta, M.U. (2019). High pressure study of H_2 oxidation and its interaction with NO. *International Journal of Hydrogen Energy* 44 6325-6332.

Article VII

Colom-Díaz, J.M.; Alzueta, M.U.; Zeng, Z.; Altarawneh, M.; Dlugogorski, B.Z. (2021). Oxidation of H_2S and CH_3SH oxidation in a jet-stirred reactor: Experiments and kinetic modeling. *Fuel* 283, 119258.

Fuel 283 (2021) 119258

Contents lists available at ScienceDirect

Fuel

journal homepage: www.elsevier.com/locate/fuel

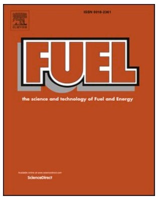

Full Length Article

Oxidation of H_2S and CH_3SH in a jet-stirred reactor: Experiments and kinetic modeling

J.M. Colom-Díaz [a,b,*], M.U. Alzueta [a], Z. Zeng [b], M. Altarawneh [c], B.Z. Dlugogorski [d]

[a] *Aragón Institute of Engineering Research (I3A), Department of Chemical and Environmental Engineering, University of Zaragoza, 50018 Zaragoza, Spain*
[b] *Murdoch University, College of Science, Health, Engineering and Education, 90 South Street, WA 6150, Australia*
[c] *United Arab Emirates University, Department of Chemical and Petroleum Engineering, Al-Ain 15551, United Arab Emirates*
[d] *Charles Darwin University, Energy and Resources Institute, Darwin, NT 0909, Australia*

ARTICLE INFO

Keywords:
H_2S
CH_3SH
Oxidation
JSR
Kinetic modeling

ABSTRACT

This contribution reports experimental measurements of the oxidation of H_2S and CH_3SH, under atmospheric pressure in a jet-stirred reactor (JSR), in the temperature range of 600–1100 K and for stoichiometric and oxidizing conditions. We update a recent kinetic model, originally developed based on the measurements of oxidation of H_2S and CH_3SH in a tubular flow-reactor and apply it to simulate the experimental data. The CH_3SH subset of the kinetic model features new reactions based on a recent theoretical work and the rate parameters proposed in the present investigation. The oxidation of CH_3SH proceeds mainly through an intersystem crossing process that leads to the formation of sulfine (CH_2SO). The unimolecular decomposition of CH_2SO in two competing reactions produces CO + H_2S and COS + H_2. The results from the model concur well with the experimental measurements, both from the present work and from the literature. We demonstrate that, both H_2S and CH_3S exhibit a similar ignition temperature, due to the initiation step that involves the abstraction of H initially bonded to sulfur. It is expected that, the results from the present investigation find application in processing of sour gas, including shale gas, especially in the direct combustion of the gas (i.e., without purification) for energy production.

1. Introduction

The exploitation of reserves of shale gas is changing the global gas market, engendering new opportunities and risks for gas use in the transition to cleaner energy systems, according to the International Energy Agency [1]. The reserves of shale gas are rich in natural gas liquids (C_2H_6, C_3H_8, C_4H_{10}, C_5) that display potential as feedstocks to petrochemical plants, making shale gas more affordable to extract [2,3]. Streams from unconventional fuel sources, such as sour shale gas, may comprise significant amounts of H_2S and CO_2, up to 30 vol% content of each of the two contaminants [4], requiring pre-treatment to separate H_2S and CO_2. The separation technologies include the energy intensive desulfurization, also known as the Claus process, to remove H_2S and convert it to sulfur powder, a valuable precursor for several chemicals [5,6]. Different process modifications have been proposed to overcome severe operating problems due to the variable content of H_2S in natural gas and the presence of contaminants, such as aromatics and mercaptans (CH_3SH), which reduce the efficiency of sulfur recovery and increase the operating costs. For example, the application of oxygen enrichment in the Claus process [7,8] raises the flame temperature by eliminating the diluent effect of nitrogen in air, favoring contaminant destruction and reducing costs [9].

Combustion represents an alternative to deal with the sour gas. Recently, the direct combustion of this fuel without the use of expensive cleaning treatments has received a significant interest [10–12], with published studies involving the economic and performance analyses of power generation systems operating on untreated sour gas [13,14]. In the same manner, literature reports other oxidation options, different to combustion, of gases containing H_2S. For example, Meusinger et al. [15] presented a novel air cleaning technology based on ozone to remove reduced sulfur compounds, such as H_2S and CH_3SH, emitted from farms.

Biogas contains mainly CH_4 and CO_2 and traces of H_2S (in a range of 0.01–2 %) and CH_3SH (20–100 ppm) [16], requiring the removal of these contaminants to upgrade biogas to a standard of renewable natural

---

[*] Corresponding author at: Aragón Institute of Engineering Research (I3A), Department of Chemical and Environmental Engineering, University of Zaragoza, 50018 Zaragoza, Spain.

E-mail address: juanmcd@unizar.es (J.M. Colom-Díaz).

https://doi.org/10.1016/j.fuel.2020.119258
Received 29 May 2020; Received in revised form 16 August 2020; Accepted 11 September 2020
Available online 5 October 2020
0016-2361/© 2020 Elsevier Ltd. All rights reserved.

gas [16–19]. This is because, biogas serves as a replacement for natural gas derived from fossil sources, in the transportation and electric-power sectors. However, gas turbines that provide power to the grid can tolerate a H_2S content of up to 1% [20–22] allowing direct combustion of biogas without desulfurization.

In addition, the reduced sulfur species, such as H_2S and CS_2, exhibit extremely low ignition temperature and flash point making them most hazardous materials that arise in the processing of hydrocarbon fuels. For example, the autoignition temperature of CS_2 (365 K) and H_2S (505 K) falls significantly below that of hydrogen (775 K). The reason is that, the key oxidation steps of the reduced sulfur species involve the intersystem-crossing (ISC) reactions that lead to considerable decrease in the activation energies for the crucial mechanistic steps [23–26]. Even as minor impurities in natural gas, H_2S and CS_2 depress the ignition point of methane, elevating fire hazards of fuel processing [27–29].

In the case of mercaptans, the research efforts have focused on gaining insights into the atmospheric sulfur cycle [30], with little attention paid to the behavior of these species under the combustion conditions. Alzueta et al. [31] published what appears to be the only study that investigated the oxidation of CH_3SH in a tubular-flow reactor under atmospheric pressure. In the case of H_2S and CS_2, the recent works dealt with the oxidation of these gases in flow reactors under different pressures [27,32–35], improving the understanding of the intersystem crossing reaction that decreases the activation energy by switching the combustion pathways from triplet to singlet corridors [25,26,36], and producing improved reaction mechanisms for modeling studies [10–12,37]. Literature presents no reports on the application of continuous stirred-tank reactors (CSTR, also known as perfectly-stirred reactor, PSR, in combustion literature) to study the oxidation of H_2S and CH_3SH, although CSTR minimize surface effects, are simple to model and straightforward to implement in practice, as jet-stirred reactors (JSR).

Hence, in the present work, we investigate the oxidation of H_2S and CH_3SH in a jet-stirred reactor in the temperature range of 600–1100 K, under stoichiometric and fuel-lean conditions and at the residence time of 1 s. The kinetic modeling affords the interpretation of the experimental results. This work is thus valuable for the novelty of the reactor employed and the contribution to the chemistry of oxidation of reduced sulfur species, greatly expanding the available set of experimental measurements. The results will find practical use in designing combustor systems that operate on untreated natural gas as fuel.

2. Experimental methodology

The experimental set-up used to perform the experiments on the oxidation of H_2S and CH_3SH has been previously described in detail elsewhere [28], with an illustrative diagram presented in Fig. 1. The set-up consisted of two mass flow controllers (MFC) that adjusted the flow rate of H_2S (2000 ± 40 ppm) or CH_3SH (2000 ± 40 ppm) in N_2 and zero grade synthetic air, with the composition of 20.5% oxygen in nitrogen, to maintain a fixed reaction residence time of 1 s in the jet-stirred reactor (JSR). BOC Australia supplied all gases deployed in the investigation (HiQ Certificate). Previous studies on the oxidation of reduced sulfur species employed the JSR to determine the details of the oxidation kinetics of CS_2 and CH_4 [26,28,36], yielding new and valuable measurements for germane sulfur systems. The JSR, with its design developed and extensively tested in previous works [38,39], rested along the centerline of an electrically-heated single-zone furnace (T_l). The furnace functioned from 600 to 1100 K with an error of ± 5 K. A thermocouple monitored the reaction temperature T_a in the center of the JSR sphere. The turbulent mixing induced by the four nozzles at the inlet of the JSR maintained a uniform temperature profile in the reactor as indicated by the equal temperature reading of T_l (single zone furnace) and T_a (central position in the JSR sphere).

The oxidation products are measured online at the reactor outlet with a Fourier transform infrared (FTIR) spectrometer that monitors the SO_2 concentration exiting the JSR. The Perkin Elmer Frontier 100 FTIR spectrometer, equipped with a gas cell that exhibits an optical path of 0.1 m (Pike Scientific, USA), facilitated online monitoring and quantitating of SO_2. We maintained the gas cell at 110 °C to avoid potential condensation of species, acquired spectra at a resolution of 1.0 cm^{-1} and accumulated four spectra for each condition. The QASoft software (Infrared Analysis Inc., USA) served to quantitate the species concentration with the limit of detection (LOD) at 5 ppm for SO_2 (based on background noise for the baseline). The FTIR spectrometer recorded a lower peak of CO than for SO_2 making the quantitation of CO less accurate. For this reason, we employed an Agilent micro-GC 490 fitted with a 10 m Porapak Q (PPQ) column, a 20 m molecular sieve 5A (MS5A) column, a 5 CB column and thermal conductivity detectors (TCD), to quantitate CO_2 (PPQ), CO and CH_4 (MS5A), and H_2S, CH_3SH and SO_2 (5CB). For the three columns, the injections to micro-GC lasted 80 ms, using He a carrier gas, with the injection ports heated to 110 °C. The Porapak Q column operated at 80 °C, molecular sieve at 110 °C and 5 CB at 50 °C, with the static pressures set to 150 kPa, 200 kPa and 150 kPa, respectively. Run times varied from 120 s for the Porapak Q and 5 CB columns to 150 s for the molecular sieve 5A column.

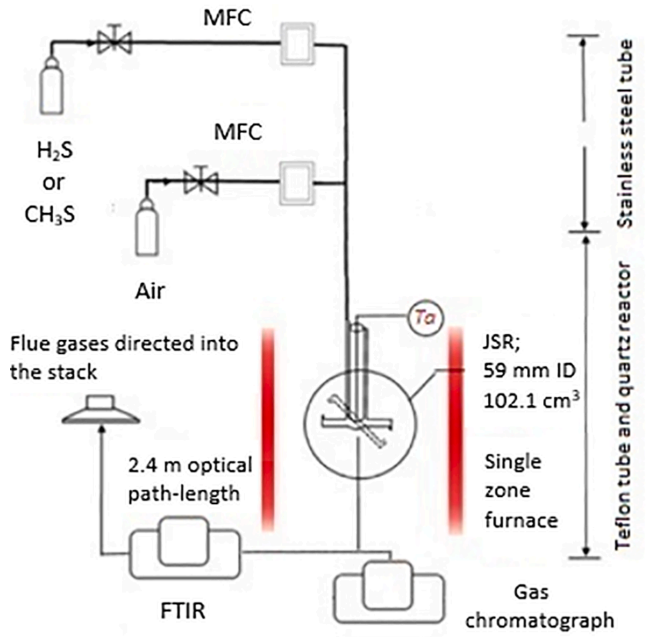
MFC
MFC
H_2S or CH_3S
Air
Flue gases directed into the stack
2.4 m optical path-length
FTIR
Ta
JSR; 59 mm ID 102.1 cm^3
Single zone furnace
Gas chromatograph
Stainless steel tube
Teflon tube and quartz reactor

Fig. 1. Schematic diagram of the experimental set-up.

For calibrating the micro-GC we used the reaction gases for H_2S and CH_3SH (2000 ± 40 ppm; BOC, HiQ certificate) and 500 ± 10 ppm calibration gas for CH_4 (BOC, HiQ Certificate). The remaining gases were calibrated with a calibration mixture, purchased from BOC Australia (HiQ certificate), based on the integral peak area. The calibration curves involved at least two calibration points, and the instrument achieved the limit of detection of 1 ppm for each species. Unfortunately, our experiment set-up prevented us from quantitating nitrogen and oxygen; the former because of a large peak that saturated the TCD detector (as N_2 was the make-up gas for H_2S and CH_3SH) and the latter because of a leak that occurred between the reactor and the micro-GC. We did not observe the formation of H_2, but one should bear in mind low sensitivity of TCD detectors to H_2 when using He as the carrier gas. It is possible that, at the temperatures of the present study, hydrogen was consumed as soon as it was produced. The two diagnostic instruments, FTIR and micro-GC, provided consistent measurements of the concentration of SO_2; see Fig. S1. Table 1 lists the conditions of the experimental program. The pre-set air excess ratio (λ, defined as inlet oxygen divided by stoichiometric amount of oxygen) allowed computing of the desired oxygen flow for each experiment. The stoichiometric

Table 1
Experimental conditions. N_2 as bath gas.

Set	H_2S (ppm)	CH_3SH	λ
1	1975	–	1.01
2	1953	–	2.05
3	1885	–	4.98
4	–	1898	1.01
5	–	1782	3.55

amount of oxygen followed from the complete oxidation reactions: $H_2S + 3/2O_2 = SO_2 + H_2O$ and $CH_3SH + 3O_2 = CO_2 + 2H_2O + SO_2$. The experiments were reproducible to within 5% based on three repeated measurements.

3. Kinetic model

The kinetic model deployed in this work to describe the oxidation of H_2S and CH_3SH is based on the previous investigations of the present authors and the literature. In the case of the oxidation of H_2S, we use the model of Colom-Díaz et al. [33] developed to describe the combustion behavior of H_2S under atmospheric pressure in a tubular-flow reactor, modeled as a plug-flow reactor (PFR). The tubular-flow reactor operated in the temperature window of 700–1400 K and for a range of oxygen concentration corresponding to $\lambda = 0.3$–20 [33]. The kinetic model proposed by Colom-Díaz et al. [33] displayed a good match between its predictions and the experimental results. The mechanism itself was based on the works of Zhou et al. [34] and Song et al. [35] on the oxidation of H_2S, included the isomerization reaction (R1) $HSOO \rightleftharpoons HSO_2$, and was supported by recent theoretical studies that had proposed the isomerization as a fast reaction pathway for the oxidation of SH [40,41]. Colom-Díaz et al. [33] suggested new kinetic parameters for reaction (R2) $SH + H_2O_2 \rightleftharpoons H_2S + HO_2$, which governs the oxidation of H_2S, according to the authors. This H_2S model has been recently tested in a high-pressure set-up, to evaluate the oxidation of H_2S under manometric pressures ranging from 0.65 to 40 bar [32]. The model yielded predictions matching well the experimental results for near atmospheric pressure, leaving room for improvement at higher pressure.

In the case of the oxidation kinetics of CH_3SH, the mechanism comprises a subset of mercaptan reactions. The CH_3SH reactions and related thermochemistry follow the work of Alzueta et al. [31], which was based on the published mechanisms of Zheng et al. [42] and Van de Vijver et al. [43], who studied, respectively, the oxidation of diethyl sulfide and the pyrolysis of alkyl sulfides. Colom-Díaz et al. [44] and Gersen et al. [27] have recently applied the subset of mercaptan reactions to model the oxidation of mixtures of CH_4 and H_2S under different pressures in their research on the effect of doping CH_4 flames with H_2S on the high-pressure ignition and oxidation.

In a recent theoretical work, Bian et al. [45] investigated the reaction mechanism of CH_3SH with O_2 using quantum chemical methods at the CCSD(T)//M06-2x level of theory and discovered new reaction pathways, both on the ground-state triplet and excited state singlet surfaces to produce CH_2SO, H_2O, CH_3OH, SO, CH_4 and SO_2. Accordingly, we have included these reactions, and their corresponding kinetic parameters that were missing in our previous mechanism, i.e., the formation of CH_2SO and CH_3OH, and the consumption of CH_2SO, as indicated by reactions (R3) to (R9). In the present work, we estimate the rate constants for these reactions and summarize the findings in Table 2. Bian et al. [45] studied the reaction of $CH_3SH + O_2$ both on the triplet and singlet surfaces. An examination of the Bian et al. reaction pathways and an apparent low activation barrier that we observed in the experiments has prompted us to suggest the appearance of the intersystem-crossing (ISC) process in our system, similarly to the oxidation of other reduced sulfur species (H_2S and CS_2) [23–26]. With respect to the results of Bian et al., the ISC comes to pass between the triplet (44.9 kcal/mol) and singlet (31.3 kcal/mol) transition states. Accordingly, we estimate the activation energy of reaction (R3) as 42 kcal/mol. We have proceeded in the same fashion by allowing the ISC to arise in the generation of CH_3OH from the incomplete oxidation of CH_3SH (R4), assigning the activation energy of 40.0 kcal/mol to this process; see Bian et al. [45] for the modeling of the separate triplet and singlet pathways.

Table 2
Arrhenius parameters for the reactions proposed in this work according to the study by Bian et al. [45]. Arrhenius expression: $k = AT^n \exp[-E_a/(RT)]$. Units are mol, cm, s and cal.

Reaction	A	n	E_a
(R3) $^1CH_3SH + {}^3O_2 = {}^1CH_2SO + {}^1H_2O$	10^{14}	1.4	42 000
(R4) $^1CH_3SH + {}^3O_2 = {}^1CH_3OH + {}^1SO$	10^{14}	0.0	40 000
(R5) $^1CH_2SO = {}^1CO + {}^1H_2S$	10^{11}	0.0	0
(R6) $^1CH_2SO + {}^2H = {}^1CH_3SO$	10^{11}	0.0	0
(R7) $^1CH_2SO = {}^1COS + {}^1H_2$	10^{11}	0.0	0
(R8) $^1CH_2SO = {}^1CS + {}^1H_2O$	10^{11}	0.0	0
(R9) $^1CH_3SO = {}^2CH_3 + {}^1SO$	10^{11}	0.0	0

Finally, the Chemkin software [46], executed with the input files that comprised the thermo-kinetic data for the two mechanisms, served to model the ideal PSR and PFR, which approximated the jet-stirred and tubular-flow reactors, respectively.

4. Results

Fig. 2 plots the results of the experiments involving the oxidation of H_2S in the JSR, in terms of concentration of H_2S and SO_2, for three air excess ratios of $\lambda = 1$, 2 and 5, in the temperature range of 600–1100 K and for 1 s residence time. The lines signify the predictions from the model and points denote the experimental measurements. As depicted in the figure, H_2S converts totally to SO_2 for all stoichiometries and at high temperatures, with the sulfur balance maintained within the range of 100 ± 5%. The diagnostics for SO_2 provided consistent data between FTIR and micro-GC measurements, as seen in Fig. S1 of the supplementary material. The onset of oxidation occurs at 725 K in the case of $\lambda = 1$, shifting to lower temperatures at elevated concentration of oxygen; i.e., 675 K for $\lambda = 5$. The kinetic model validated for the atmospheric pressure, within the context of a plug-flow reactor simulated under the atmospheric pressure [33], matches well the experimental results obtained from the tubular-flow reactor. This agreement between measurements and the models, arising both for the tubular-flow reactor (modeled as PFR) and JSR (modeled as CSTR/PSR), indicates the reliability of the mechanism to simulate the oxidation of H_2S under atmospheric pressure.

Note that, the surface/volume ratio of the tubular-flow reactor [33] exceeds that of the JSR by a factor of 4.5. Thus, despite the difference in the surface/volume ratio, the model reproduces accurately the experimental results for both reactors. This indicates a negligible catalytic effect of the ultra-pure quartz surface on the oxidation of CH_3SH and H_2S [31, 33, present work].

Figs. 3 and 4 illustrate the oxidation of CH_3SH for the air excess ratio of $\lambda = 1$ and 3.55, respectively, in terms of the consumption of CH_3SH and the formation of reaction products of CO, CO_2, CH_4, H_2S and SO_2, as function of temperature. In comparison to the stoichiometric oxidation, fuel-lean conditions ($\lambda = 3.55$) engender the onset of the reaction and the appearance of the oxidation products at lower temperatures. All sulfur initially present in CH_3SH is converted to SO_2 at high temperatures, while a maximum in the concentration of H_2S arises at intermediate temperatures. In the case of carbon species, under the stoichiometric condition, there is negligible formation of CO_2, with the main carbon species corresponding to those of CO and CH_4.

Under the fuel-lean conditions, as illustrated in Fig. 4, CH_4 and CO commence to disappear at high temperatures, forming CO_2. The model predictions, plotted as lines, represent the mechanisms of Alzueta et al. [31] (dashed lines) and the present work (solid lines); the latter comprises the new reactions listed in Table 2. The updated mechanism

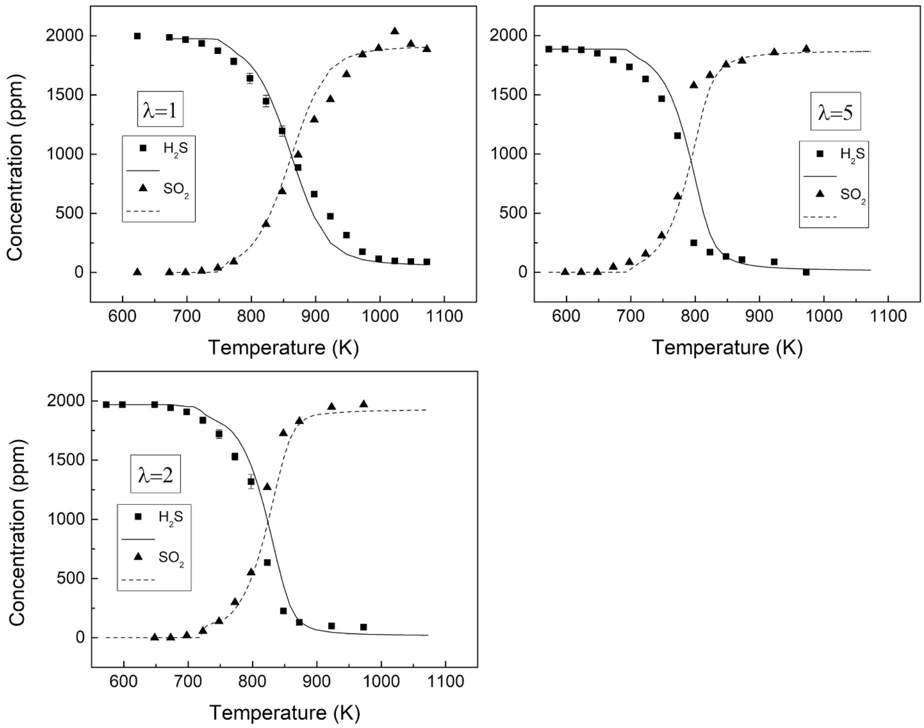

Fig. 2. Concentration of H_2S and SO_2 as function of temperature for the experimental conditions of sets 1, 2 and 3 in Table 1. Symbols represent experimental concentration, while lines denote model predictions.

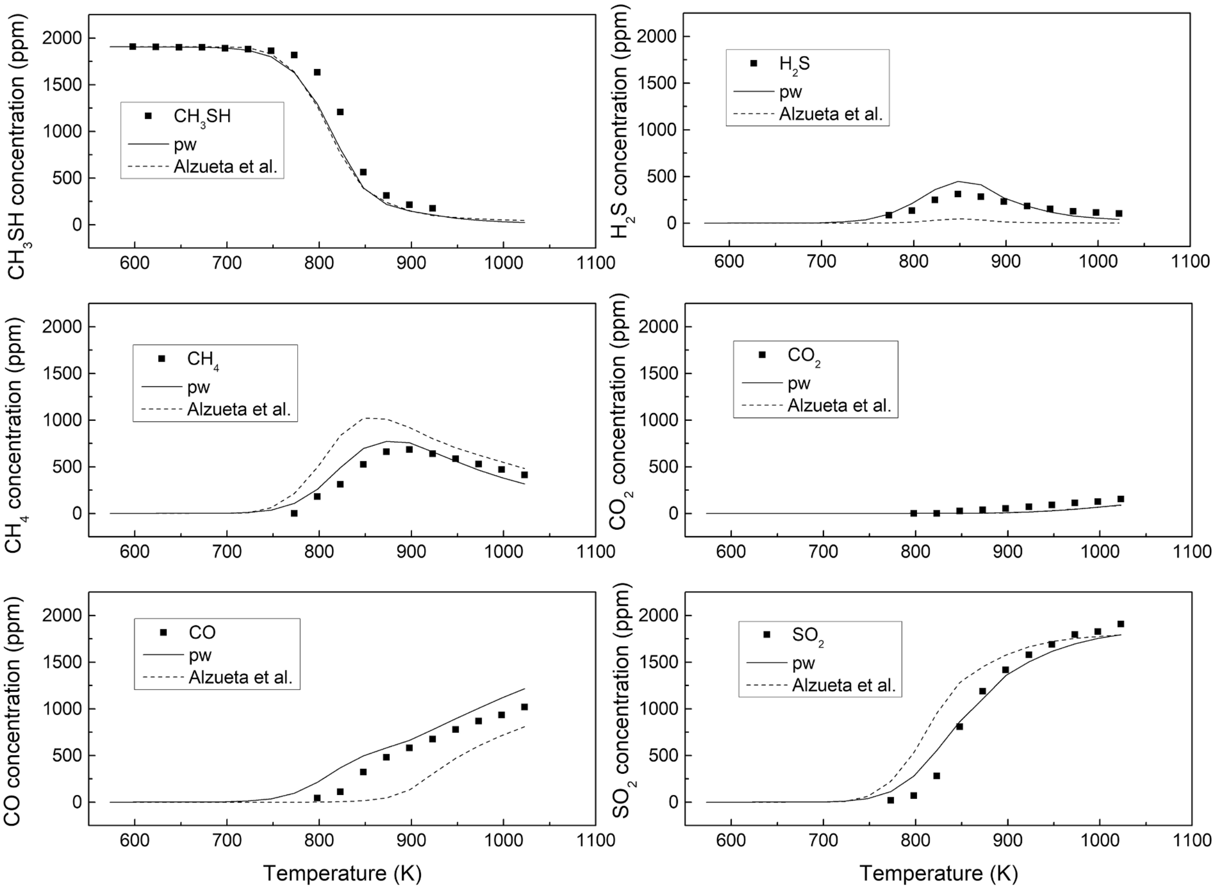

Fig. 3. Concentrations of CH_3SH, CH_4, CO, H_2S, CO_2 and SO_2 vs. temperature for the experimental conditions of set 4 in Table 1 ($\lambda = 1.01$). Symbols represent experimental concentrations, while lines denote model predictions.

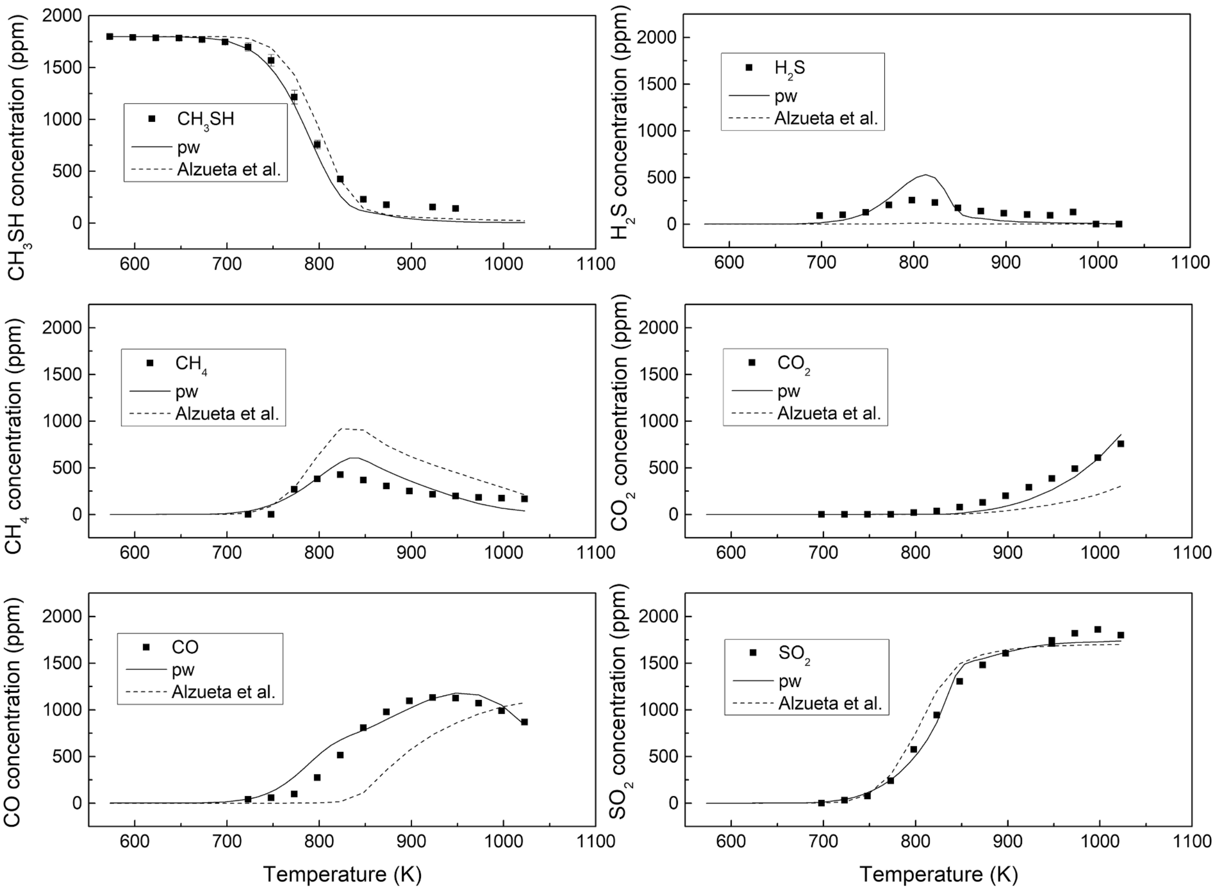

Fig. 4. Concentrations of CH_3SH, CH_4, CO, H_2S, CO_2 and SO_2 vs. temperature at the experimental conditions of set 5 in Table 1 ($\lambda = 3.55$). Symbols represent experimental concentrations, while lines denote model predictions.

features an improved agreement between the results from the experiments and from the modeling, especially for distribution of the reaction products. In the present study, the oxidation of CH_3SH prompts the formation of sulfine (CH_2SO) through the intersystem crossing process between the triplet and singlet surfaces; i.e., with the $CH_3SH + {}^3O_2$ reactants residing on the former, and the reaction products of ${}^1CH_2SO$ and H_2O on the latter; see reaction (R3). Bian et al. [45] studied the singlet and triplet pathways for the oxidation of CH_3SH, but without connecting them by an intersystem-crossing process that decreases the kinetic barrier. Sulfine decomposes mainly to CO and H_2S (R5), and partly to COS and H_2 (R7).

$$CH_3SH + O_2 \rightleftharpoons CH_2SO + H_2O \tag{R3}$$

$$CH_2SO \rightleftharpoons CO + H_2S \tag{R5}$$

$$CH_2SO \rightleftharpoons COS + H_2 \tag{R7}$$

Literature provides no rate constants for the reactions of CH_2SO consumption. Therefore, in the present work, we estimate these rate constants based on an analogy with the decomposition of singlet formaldehyde oxide (CH_2OO, aka Criegee intermediate). It is now well known that, the ground states of CH_2SO and CH_2OO are, respectively, thioformaldehyde oxide (aka, sulfine or thiocarbonyl S-oxide) and formaldehyde oxide (aka, carbonyl oxide or Criegee intermediate). Both species have higher energy isomers, such as, for the case of the Criegee intermediate, dioxirane, formic acid and methylenebis(oxy), but these isomers do not appear in combustion. The dominant ground-state electronic configurations of both species are singlet zwitterions of formaldehyde oxide ($CH_2{=}O^{+}$-O^{-}) and thioformaldehyde oxide ($CH_2{=}S^{+}$-O^{-}). While the C-S and S-O bonds in CH_2SO are slightly longer than those of C-O and O-O in CH_2OO, i.e., 1.610 Å and 1.469 Å vs 1.272 Å and 1.345 Å, respectively, the CSO and COO angles are similar, that is 114.8° vs 118.0°, in that order [47–49]. Thus, CH_2OO represent a good analogue to CH_2SO.

Maricq et al. [50], in their study on the reaction of chlorine atoms with methylperoxy and ethylperoxy radicals, proposed that, the decomposition of CH_2OO proceeds via three channels, with 61 ± 7% of the reactant converting to CO and H_2O (which would be in accordance with the presently suggested CO + H_2S pathway), with the remainder forming $CO_2 + H_2$ and $CO_2 + 2H$. Based on Maricq's et al. [50] reactions for the decomposition of the Criegee intermediate, as an analogy to the unimolecular decomposition of CH_2SO, we propose the kinetic parameters for reactions (R5, R7-R9) listed in Table 2, assuming a value of 10^{11} (s^{-1}) for the pre-exponential factor.

Another possible product is the methylthio radical (CH_3S) illustrated in reaction (R10), which arises from the contact of CH_3SH with CH_3 to produce CH_4, in addition to CH_3S (R10). The methylthio radical reacts with O_2 to form SO_2 and CH_3 (R11), which results in the overall reaction of $CH_3SH + O_2 \rightleftharpoons SO_2 + CH_4$.

$$CH_3SH + CH_3 \rightleftharpoons CH_3S + CH_4 \tag{R10}$$

$$CH_3S + O_2 \rightleftharpoons SO_2 + CH_3 \tag{R11}$$

Alzueta et al. [31] have recognized the methylthio radical (CH_3S) as the most important intermediate in the oxidation of CH_3SH, together with CH_2SH. They mentioned that, the conversion to SO_2 proceeds through CS_2 as the stoichiometry becomes fuel rich. The lack of appearance of CS_2 could probably be the result of relatively high reaction temperature of at 800 K – 1100 K, for which CS_2 oxidizes to COS, CO and SO_2. While CH_2SH forms in the present work, it is rather less abundant than CH_2SO or CH_3S, transforming to C_2H_4. Carbon dioxide appears mainly via reactions (R12) and (R13) due to the interaction between CO and OH. We remark that, Zeng et al. reported no formation of CO_2 in the absence of hydrogen-bearing radicals [26].

$$COS + O \rightleftharpoons CO_2 + S \tag{R12}$$

$$CO + OH \rightleftharpoons CO_2 + H \tag{R13}$$

Figure S2, in the supplementary material, explicates the reactions pathways for the oxidation of CH_3SH. While the mechanistic description of the oxidation behavior of CH_3SH has changed from that introduced in the previous study [31], the consumption of neat H_2S remains equal to that observed in the tubular-flow reactor [33]. Figure S3 depicts a sensitivity analysis for the oxidation of H_2S (at $\lambda = 2.05$ and 800 K), showing the same important reactions as in reference [34]. Figure S2 also illustrates the main consumption path of neat H_2S, demonstrating the conversion of SH through HSOO to the final product SO_2. In the oxidation of CH_3SH, the preferred channel for SH radicals constitutes the reaction with CH_3SH to yield CH_3S and H_2S (R14), instead of producing HSOO.

$$CH_3SH + SH \rightleftharpoons CH_3S + H_2S \tag{R14}$$

If we compare the oxidation of H_2S with the oxidation of CH_3SH under the stoichiometric condition, both species commence to react at similar temperature; i.e., 750 K for H_2S and 800 K for CH_3SH. In both cases, the starting reaction involves the abstraction of hydrogen from the sulfur. In the case of H_2S, equation (R15) represents the initiation process, while the decomposition of CH_3SH proceeds via the reaction pathways proposed by Bian et al. [45]; i.e., through reaction (R3) that entails the initial formation of CH_2SO. However, despite the decomposition of H_2S beginning at lower temperatures than that of CH_3SH, its full conversion is reached at the temperature that exceeds that for CH_3SH by 100 K. This probably occurs due to the formation of less reactive HO_2 radicals in the oxidation of H_2S [33].

$$H_2S + O_2 \rightleftharpoons HO_2 + SH \tag{R15}$$

Additionally, as part of the supplementary material, we simulated selected experiments ($\lambda = 1$ and $\lambda = 5$) from the previous work of Alzueta et al. [31] on the oxidation of CH_3SH in a tubular-flow reactor. Figures S4 and S5 compare the model predictions for the oxidation of CH_3SH and formation of the products from our present and prior reaction mechanisms. The updated mechanism can improve the prediction in the formation of the reaction products, such as CO and H_2S, due mainly to the inclusion of reactions R(3), R5 and R7 in this work, while the mechanism underpredicts the generation of CH_4. Specifically, the sensitivity analysis recognizes the profound effect of the rate constants of reaction R(3) on the oxidation of CH_3SH (Fig. S6 of the supplementary material). Thus, we have studied the influence of the activation energy and the pre-exponential factor of reaction (R3) on the simulated conversion of CH_3SH in the JSR, modeled as a CSTR/PSR and plotted the results in Figs. S7-S10 in the supplementary material; with the experiments summarized in sets 4 and 5 in Table 1. Varying the Arrhenius parameters impacts the conversion of CH_3SH and the formation of the oxidation products. Overall, the results paint an overwhelming case for the inclusion of the reactions mapped by Bian et al. [45], with the triplet and singlet pathways joined by the intersystem crossings as proposed in the present work, for describing the conversion of CH_3SH in the oxidation processes.

5. Conclusions

This study dealt with the oxidation of both H_2S and CH_3SH, in a jet-stirred reactor in the temperature range of 600–1100 K and the residence time of 1 s. The oxidation experiments, which involved the stoichiometric and fuel-lean conditions, demonstrated the conversion of both sulfur compounds shifting to lower temperatures as the oxygen concentration increases. The updated kinetic model, including recent progress on the conversion of CH_3SH reported in the literature, reproduces well the measurements collected under all conditions in this study and in the prior investigations available in literature. The oxidation of CH_3SH involves the formation of the transitional species of CH_2SO that decomposes mainly to CO and H_2S, improving the predictions with respect to the mechanisms described in the literature. Nevertheless, future studies should embark on better characterization of the consumption reactions of CH_2SO. The species of H_2S and CH_3SH commence to react at a comparable temperature due to the initiation reactions that involve the abstraction of hydrogen from the sulfur. The oxidation of H_2S completes at a higher temperature than that of CH_3SH, due to the appearance of unreactive HO_2 radicals.

CRediT authorship contribution statement

J.M. Colom-Díaz: Conceptualization, Investigation, Data curation, Writing - original draft, Visualization, Methodology, Validation. **M.U. Alzueta:** Conceptualization, Writing - review & editing, Funding acquisition, Supervision, Project administration. **Z. Zeng:** Conceptualization, Methodology, Writing - review & editing, Supervision. **M. Altarawneh:** Conceptualization, Writing - review & editing, Funding acquisition, Supervision, Project administration. **B.Z. Dlugogorski:** Conceptualization, Writing - review & editing, Funding acquisition, Supervision, Project administration, Resources.

Declaration of Competing Interest

The authors declare that they have no known competing financial interests or personal relationships that could have appeared to influence the work reported in this paper.

Acknowledgement

The authors express their gratitude to the Aragón Government (Ref. T22_17R), FEDER 2014-2020 “Construyendo Europa desde Aragón“, MINECO and FEDER (Project CTQ2015-65226) for co-funding this investigation. J. M. Colom acknowledges MINECO for the pre-doctoral grant awarded (BES-2016-076610). The Australian and UAE authors appreciate the funding from the Australian Research Council and grants of computing time from the National Computational Infrastructure (NCI), Canberra, Australia and the Pawsey Supercomputing Centre, Perth, Australia. M. Altarawneh acknowledges a start-up grant from College of Engineering at The United Arab Emirates University, UAEU (grant number: 31N421)

Appendix A. Supplementary data

Supplementary data to this article can be found online at https://doi.org/10.1016/j.fuel.2020.119258.

References

[1] International Energy Agency (IEA), World Energy Outlook 2017, Paris.
[2] He C, You F. Deciphering the true life cycle environmental impacts and costs of the mega-scale shale gas-to-olefins projects in the United States. Energy Environ Sci 2016;9:820–40.
[3] He C, You F. Toward more cost-effective and greener chemicals production from shale gas by integrating with bioethanol dehydration: Novel process design and simulation-based optimization. AIChE J 2015;61(4):1209–32.
[4] Hamme G, Lübcke T, Kettner R, Pillarella MR, Recknagel H, Commichau A, Neumann HJ, Paczynska-Lahme B. Ullmann's Encyclopedia of Industrial Chemistry, Wiley-VCH: Weinheim, Germany, 2012, Vol. 23; Chapter Natural Gas, p. 739-792.
[5] Zarei S, Ganji H, Sadi M, Rashidzadeh M. Thermo-kinetic modeling and optimization of the sulfur recovery unit thermal stage. Appl. Therm Eng 2016;103:1095–104.

[6] Nabikandi NJ, Fatemi S. Kinetic modelling of a commercial sulfur recovery unit based on Claus straight through process: Comparison with equilibrium model. J Ind Eng Chem 2015;30:50–63.

[7] Rameshni M. Cost effective options to expand SRU capacity using oxygen. Sulfur Recovery Symposium Brimstone Engineering Services, Inc. Banlf. May 2002. Alberta, Calgary.

[8] Norman J, Graville S, Watson R. Oxygen: The solution for sulphur recovery and BTX. Chem Eng Process 2006;45:1.

[9] Selim H, Gupta A, Shoaibi AA. Effect of CO_2 and N_2 concentration in acid gas stream on H_2S combustion. Appl Energy 2012;98:53–8.

[10] Bongartz D, Shanbhogue SJ, Ghoniem AF. Formation and Control of Sulfur Oxides in Sour Gas Oxy-Combustion: Prediction Using a Reactor Network Model. Energy Fuels 2015;29(11):7670–80.

[11] Bongartz D, Ghoniem AF. Impact of sour gas composition on ignition delay and burning velocity in air and oxy-fuel combustion. Combust Flame 2015;162(7):2749–57.

[12] Bongartz D, Ghoniem AF. Chemical kinetics mechanism for oxy-fuel combustion of mixtures of hydrogen sulfide and methane. Combust Flame 2015;162(3):544–53.

[13] Chakroun NW, Ghoniem AF. Techno-economic assessment of sour gas oxy-combustion water cycles for CO_2 capture. Int J Greenhouse Gas Control 2015;36:1–12.

[14] Lu X, Palmer M, Forrest B, McGroddy M. A novel power generation system utilizing un-treated sour gas fuel. Soc Petrol Eng 2018.

[15] Meusinger C, Bluhme AB, Ingemar JL, Feilberg A, Christiansen S, Andersen C, et al. Treatment of reduced sulphur compounds and SO_2 by Gas Phase Advanced Oxidation. Chem Eng J 2017;307:427–34.

[16] Montebello AM, Fernández M, Almenglo F, Ramírez M, Cantero D, Baeza M, Gabriel D. Simultaneous methylmercaptan and hydrogen sulfide removal in the desulfurization of biogas in aerobic and anoxic biotrickling filters. Chem Eng J 2012;200-202:237–46.

[17] San-Valero P, Penya-roja JM, Javier Álvarez-Hornos F, Buitrón G, Gabaldón C, Quijano G. Fully aerobic bioscrubber for the desulfurization of H_2S-rich biogas. Fuel 2019;241:884–91.

[18] Jiang X, Xu W, Liu W, Yue M, Zhu Y, Yang M. Facile preparation of cuprous oxide decorated mesoporous carbon by one-step reductive decomposition for deep desulfurization. Fuel 2019;241:777–85.

[19] Liu C, Zhang R, Wei S, Wang J, Liu Y, Li M, Liu R. Selective removal of H 2 S from biogas using a regenerable hybrid TiO 2 /zeolite composite. Fuel 2015;157:183–90.

[20] Jerzak W, Kuźnia M, Szajding A. Experimental Studies and the Chemical Kinetics Modelling of Oxidation of Hydrogen Sulfide Contained in Biogas. Procedia Eng 2016;157:222–9.

[21] Valera-Medina A, Giles A, Pugh D, Morris S, Pohl M, Ortwein A. Investigation of combustion of emulated biogas in a gas turbine test rig. J. Therm. Sci. 2018;27:331–40.

[22] Awe O, Zhao Y, Nzihou A, Minh D, Lyczko N. A review of biogas utilization, purification and upgrading technologies. Waste Biomass Valorization 2017;8:267–83.

[23] Montoya A, Sendt K, Haynes BS. Gas-phase interaction of H_2S with O_2: A kinetic and quantum chemistry study of the potential energy surface. J Phys Chem A 2005;109:1057–62.

[24] Zhou C, Sendt K, Haynes BS. Theoretical study of hydrogen abstraction and sulfur insertion in the reaction $H_2S + S$. J Phys Chem A 2008;112:3239–47.

[25] Zeng Z, Dlugogorski BZ, Altarawneh M. Flammability of CS_2 and other reduced sulfur species. Fire Saf J 2017;91:226–34.

[26] Zeng Z, Dlugogorski BZ, Oluwoye I, Altarawneh M. Combustion chemistry of carbon disulphide (CS_2). Combust Flame 2019;210:413–25.

[27] Gersen S, van Essen M, Darmeveil H, Hashemi H, Rasmussen CT, Christensen JM, Glarborg P, Levinsky H. Experimental and Modeling Investigation of the Effect of H 2 S Addition to Methane on the Ignition and Oxidation at High Pressures. Energy Fuels 2017;31(3):2175–82.

[28] Zeng Z, Dlugogorski BZ, Oluwoye I, Altarawneh M. Co-oxidation of methane (CH_4) and carbon disulfide (CS_2). Proc Combust Inst 2019;37:677–85.

[29] Zeng Z, Altarawneh M, Oluwoye I, Glarborg P, Dlugogorski BZ. Inhibition and Promotion of Pyrolysis by Hydrogen Sulfide (H_2S) and Sulfanyl Radical (SH). J Phys Chem A 2016;120:8941–8.

[30] Chen M, Yao XY, Ma RC, Song QC, Long YY, He R. Methanethiol generation potential from anaerobic degradation of municipal solid waste in landfills. Env Sci Pollut Res 2017;24:23992–4001.

[31] Alzueta MU, Pernía R, Abián M, Millera Á, Bilbao R. CH_3SH conversion in a tubular flow reactor. Experiments and kinetic modelling. Combust Flame 2019;203:23–30.

[32] Colom-Díaz JM, Abián M, Millera Á, Bilbao R, Alzueta MU. Influence of pressure on H_2S oxidation. Experiments and kinetic modeling. Fuel 2019;258:116145. https://doi.org/10.1016/j.fuel.2019.116145.

[33] Colom-Díaz JM, Abián M, Ballester MY, Millera Á, Bilbao R, Alzueta MU. H_2S conversion in a tubular flow reactor: Experiments and kinetic modeling. Proc Combust Inst 2019;37:727–34.

[34] Zhou CR, Sendt K, Haynes BS. Experimental and kinetic modelling study of H_2S oxidation. Proc Combust Inst 2013;34:625–32.

[35] Y.u. Song H. Hashemi J.M. Christensen C. Zou B.S. Haynes P. Marshall P. Glarborg An Exploratory Flow Reactor Study of H 2 S Oxidation at 30-100 Bar : AN EXPLORATORY FLOW REACTOR STUDY OF H 2 S OXIDATION AT 30-100 BAR Int. J. Chem. Kinet. 49 1 2017 37 52.

[36] Z. Zeng, B.Z. Dlugogorski, I. Oluwoye, M. Altarawneh. Combustion chemistry of COS and occurrence of intersystem crossing. Fuel, paper no 119257, in press.

[37] Salisu I, Abhijeet R. Kinetic simulation of acid gas (H_2S and CO_2) destruction for simultaneous syngas and sulfur recovery. Ind. Eng. Chem. Res. 2016;55:6743–52.

[38] O. Herbinet G. Dayma Jet-Stirred Reactors in Cleaner Combustion. Springer 2013 183 210.

[39] Matras D, Villermaux J. Continuous reactor perfectly agitated by gas jets for kinetic study on rapid chemical reactions. Chem. Eng. Sci 1973;28:129–37.

[40] Freitas GN, Garrido JD, Ballester MY, Nascimiento MAC. Connection between the upper and lower energy regions of the potential energy surface of the ground electronic state of the HSO_2 system. J. Phys. Chem. A 2012;116:7677–85.

[41] Garrido JD, Ballester MY, Orozco-González Y, Canuto S. CASPT2 Study of the potential energy surface of the HSO_2 system. J. Phys. Chem. A 2011;115:1453–61.

[42] X. Zheng E.M. Fisher F.C. Gouldin J.W. Bozzelli Pyrolysis and oxidation of ethyl methyl sulfide in a flow reactor Combustion and Flame 158 6 2011 1049 1058 https://linkinghub.elsevier.com/retrieve/pii/S001021801000307X.

[43] R. Van de Vijver N.M. Vandewiele A.G. Vandeputte K.M. Van Geem M.F. Reyniers W.H. Green et al. Rule-based ab initio kinetic model for alkyl sulfide pyrolysis Chem. Eng. J. 278 2015 385 393.

[44] Colom-Díaz JM, Leciñena M, Peláez A, Abián M, Millera Á, Bilbao R, Alzueta MU. Study of the conversion of CH4/H2S mixtures at different pressures. Fuel 2020;262:116484. https://doi.org/10.1016/j.fuel.2019.116484.

[45] H.e. Bian B. Xu H. Zhang Q. Wang H. Zhang S. Zhang D. Xia Theoretical study on the atmospheric reaction of CH 3 SH with O 2 Int J Quantum Chem 119 5 2019 e25822 10.1002/qua.v119.5 10.1002/qua.25822 http://doi.wiley.com/10.1002/qua.v119.5 http://doi.wiley.com/10.1002/qua.25822.

[46] CHEMKIN-PRO, 15151. Reaction Design San Diego. 2013.

[47] Osborn DL, Taatjes CA. The physical chemistry of Criegee intermediates in the gas phase. Int. Rev. Phys. Chem. 2015;34:309–60.

[48] Mohamed AA, Al-Jifry FA. Substituent effect on the electronic structure of sulfines: molecular orbital treatment. Phosphorus Sulfur Silicon Relat. Elem. 2005;180:2235–53.

[49] Demaison J, Vogt N, Ksenafontov DN. Accuracy of semiexperimental equilibrium structures: sulfine as an example. J. Mol. Struct. 2020;1206:127676.

[50] Maricq MM, Szente JJ, Kaiser EW, Shi J. Reaction of chlorine atoms with methylperoxy and ethylperoxy radicals. J. Phys. Chem. A 1994;98:2083–9.

SUPPLEMENTARY MATERIAL

Oxidation of H_2S and CH_3SH in a jet-stirred reactor: Experiments and kinetic modeling

J. M. Colom-Díaz[1,2,*], M. U. Alzueta[1], Z. Zeng[2], M. Altarawneh[3], B. Z. Dlugogorski[4]

[1] Aragón Institute of Engineering Research (I3A). Department of Chemical and Environmental Engineering, University of Zaragoza, 50018 Zaragoza, Spain.

[2] Murdoch University, College of Science, Health, Engineering and Education, 90 South Street, WA 6150, Australia

[3] United Arab Emirates University, Department of Chemical and Petroleum Engineering, Al-Ain 15551, United Arab Emirates

[4] Charles Darwin University, Energy and Resources Institute, Darwin, NT 0909, Australia

Table of contents:

1) **Comparison of SO_2 concentrations using FTIR and micro-GC equipments**

   Figure S1. Concentrations of H_2S and SO_2 (using FTIR and micro-GC) vs. temperature at the experimental conditions of set 3 in Table 1. Symbols represent experimental concentrations, while lines denote model predictions.

2) **Reaction pathways**

   Figure S2. Reaction pathways for CH_3SH oxidation.

3) **Sensitivity analysis for H_2S**

   Figure S3. Normalized sensitivity analyses for the H_2S oxidation. Set 2 in Table 1, λ = 2.05, 800 K.

4) **Model simulations of CH_3SH experiments from the literature**

   Figure S4. Comparison between experiments and modelling results for λ = 0.99. Set 4 in Table 1 of the work by Alzueta et al. [31].

   Figure S5. Comparison between experiments and model results for λ=5.08. Set 7 in Table 1 of the work by Alzueta et al. [31].

5) **Sensitivity analysis for CH_3SH**

   Figure S6. Normalized sensitivity analyses for the CH_3SH oxidation experiments. Top figure: set 4 in Table 1, λ = 1.01, 775 K. Bottom figure: set 5 in Table 1, λ = 3.55, 750 K.

6) **Simulations of CH_3SH experiments modifying the activation energy of reaction (R3) ($CH_3SH+O_2\rightleftharpoons CH_2SO+H_2O$)**

   Figure S7. Concentrations of CH_3SH, CH_4, CO, H_2S, CO_2 and SO_2 vs. temperature at the experimental conditions of set 4 in Table 1 (λ = 1.01). Symbols represent experimental concentrations, while lines denote model predictions, varying the activation energy of R3. The acronym “pw” in the legend denotes present work and the activation energy of reaction (R3) corresponds to 42 kcal/mol.

   Figure S8. Concentrations of CH_3SH, CH_4, CO, H_2S, CO_2 and SO_2 vs. temperature at the experimental conditions of set 5 in Table 1 (λ = 3.55). Symbols represent experimental concentrations, while lines denote model predictions, varying the activation energy of R3. The acronym “pw” in the legend denotes present work and the activation energy of reaction (R3) is 42 kcal/mol.

7) Simulations of CH_3SH experiments modifying the pre-exponential factor of reaction (R3) ($CH_3SH+O_2\rightleftharpoons CH_2SO+H_2O$)

Figure S9. Concentrations of CH_3SH, CH_4, CO, H_2S, CO_2 and SO_2 vs. temperature at the experimental conditions of set 4 in Table 1 ($\lambda = 1.01$). Symbols represent experimental concentrations, while lines denote model predictions, varying the pre-exponential factor of R3. "The acronym "pw" in the legend denotes present work and the pre-exponential factor of reaction (R3) corresponds to 10^{14}.

Figure S10. Concentrations of CH_3SH, CH_4, CO, H_2S, CO_2 and SO_2 vs. temperature at the experimental conditions of set 5 in Table 1 ($\lambda = 3.55$). Symbols represent experimental concentrations, while lines denote model predictions, varying the pre-exponential factor of R3. The acronym "pw" in the legend denotes present work and the pre-exponential factor of reaction (R3) corresponds to 10^{14}.

1) Comparison of SO_2 concentrations using FTIR and micro-GC equipments

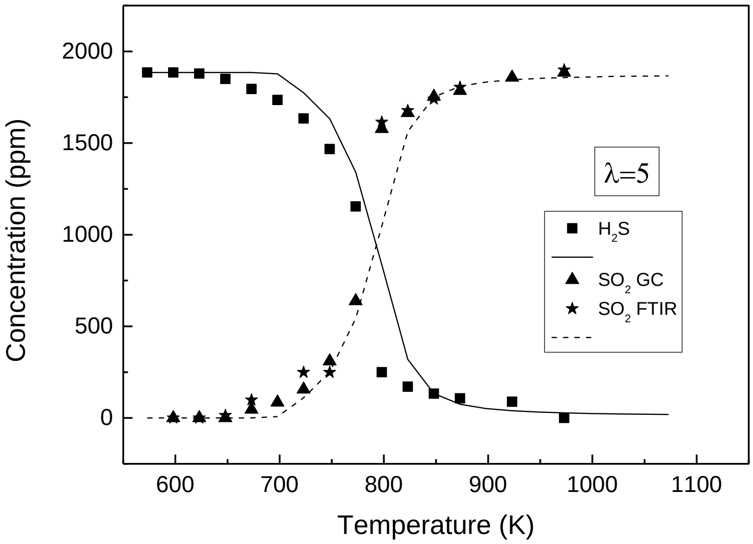

Figure S1. Concentrations of H_2S and SO_2 (using FTIR and micro-GC) vs. temperature at the experimental conditions of set 3 in Table 1. Symbols represent experimental concentrations, while lines denote model predictions.

2) Reaction pathways

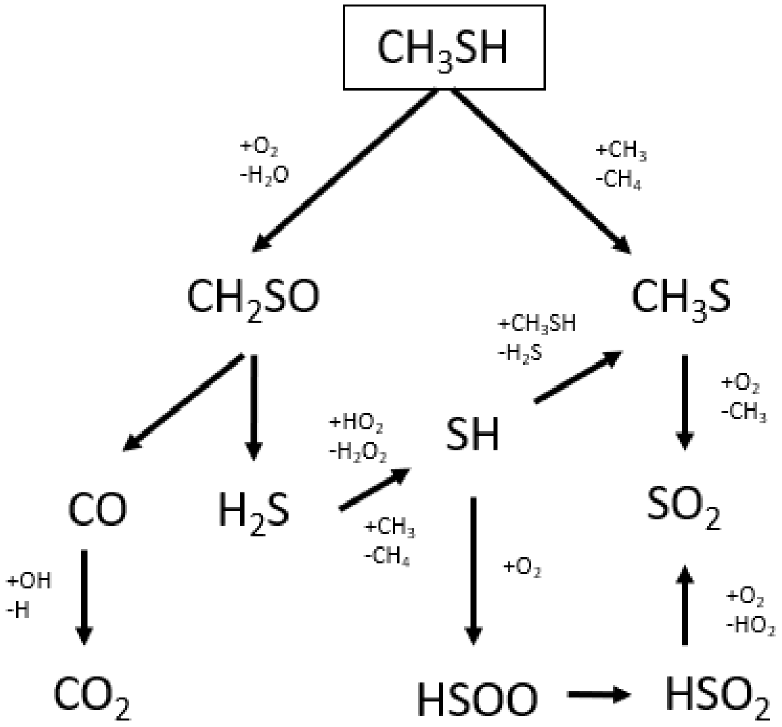
CH3SH
+O2
-H2O
+CH3
-CH4
CH2SO
CH3S
+CH3SH
-H2S
+O2
-CH3
+HO2
-H2O2
SH
CO
H2S
SO2
+CH3
-CH4
+O2
+OH
-H
+O2
-HO2
CO2
HSOO
HSO2

Figure S2. Reaction pathways for CH_3SH oxidation.

3) Sensitivity analysis for H_2S

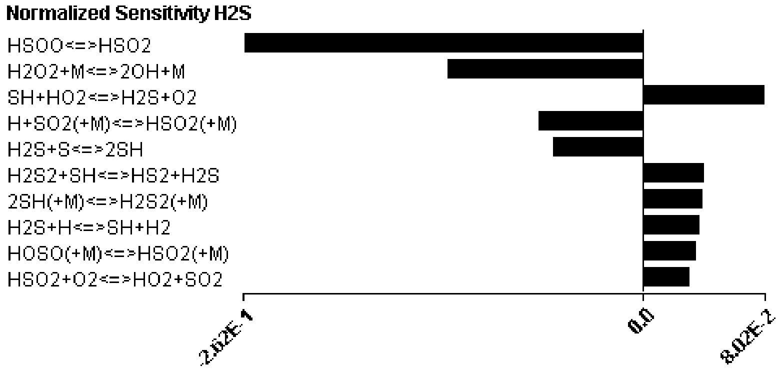

Figure S3. Normalized sensitivity analyses for the H_2S oxidation. Set 2 in Table 1, λ = 2.05, 800 K.

4) Model simulations of CH_3SH experiments from the literature

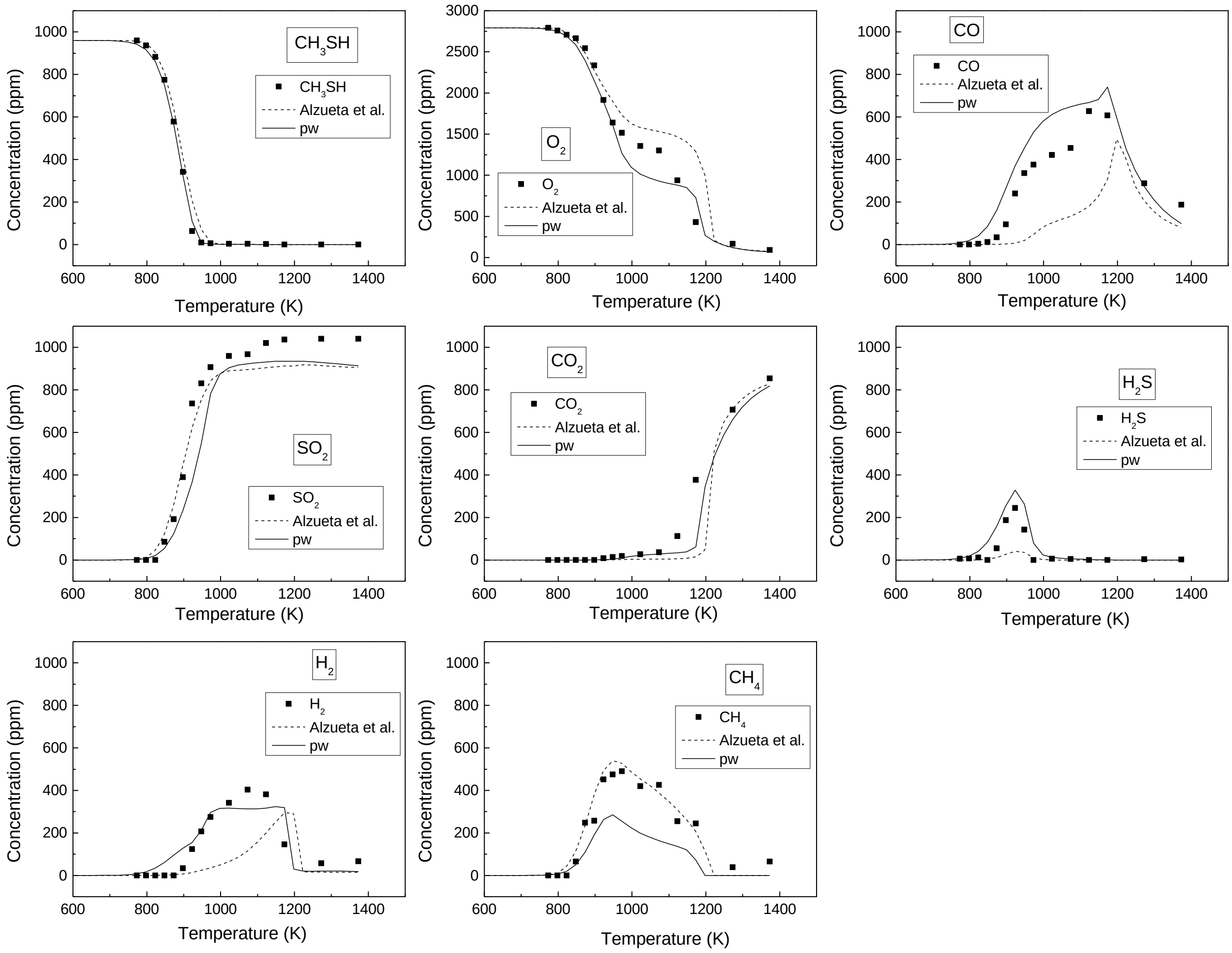

Figure S4. Comparison between experiments and modelling results for *λ* = 0.99. Set 4 in Table 1 of the work by Alzueta et al. [31].

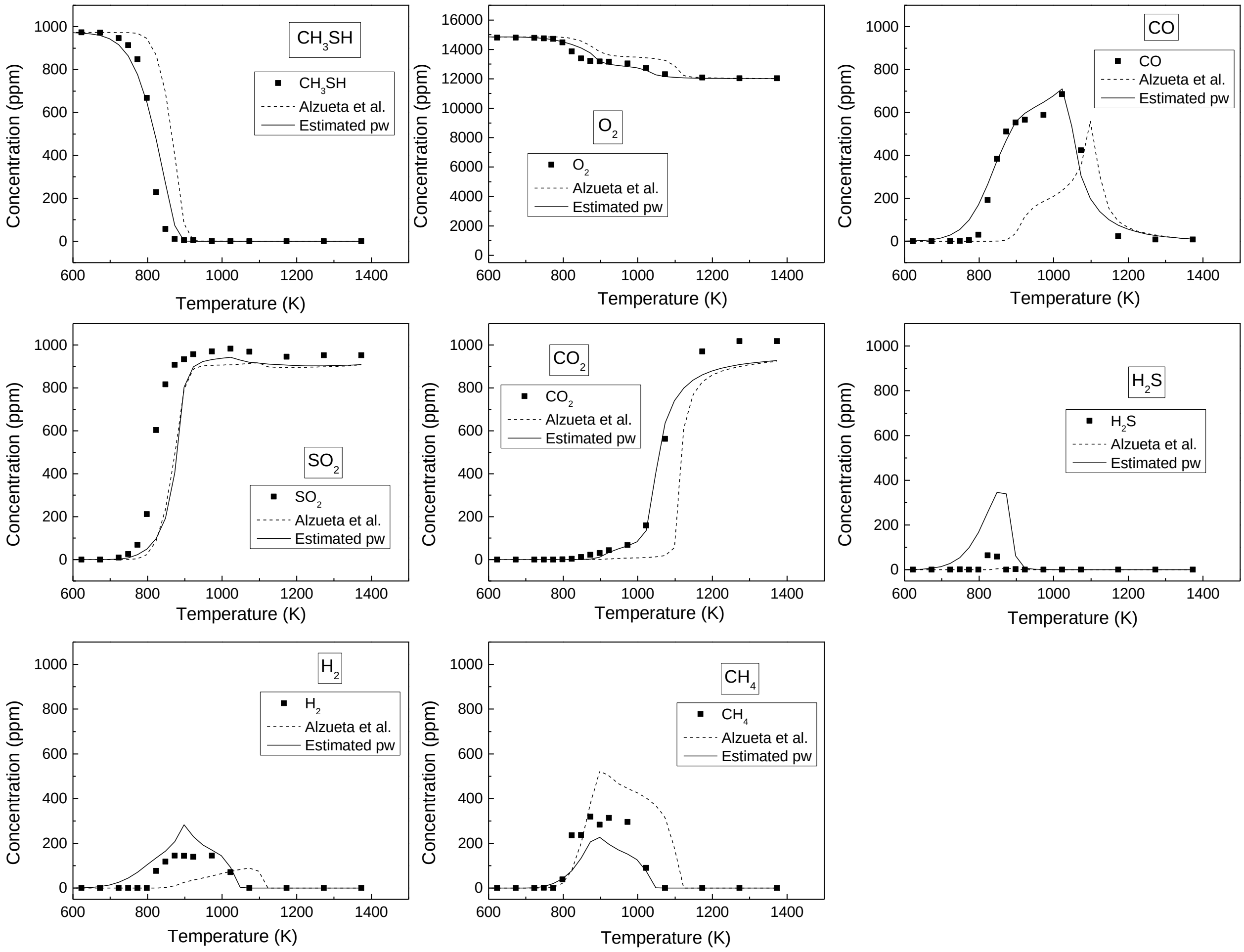

Figure S5. Comparison between experiments and model results for λ=5.08. Set 7 in Table 1 of the work by Alzueta et al. [31].

5) Sensitivity analysis for CH_3SH

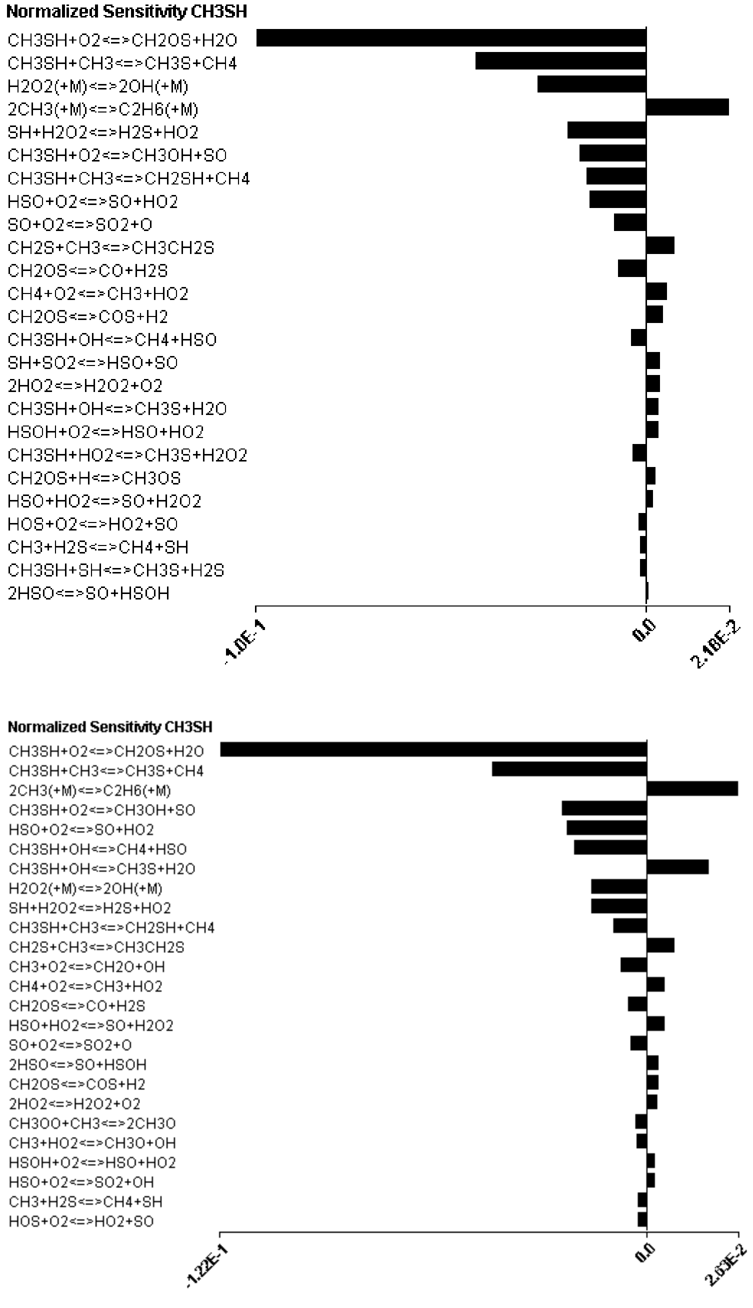

Figure S6. Normalized sensitivity analyses for the CH_3SH oxidation experiments. Top figure: set 4 in Table 1, $\lambda = 1.01$, 775 K. Bottom figure: set 5 in Table 1, $\lambda = 3.55$, 750 K.

6) Simulations of CH_3SH experiments modifying the activation energy of reaction (R3) ($CH_3SH+O_2 \rightleftharpoons CH_2SO+H_2O$)

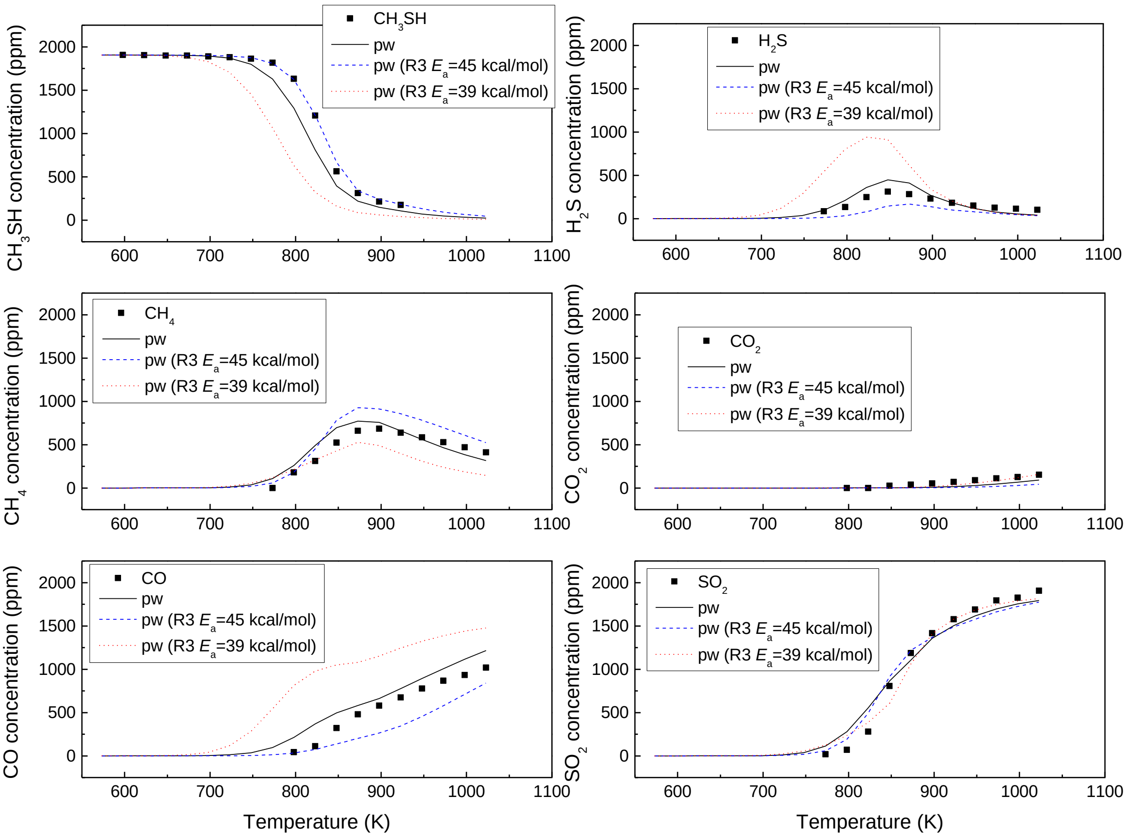

Figure S7. Concentrations of CH_3SH, CH_4, CO, H_2S, CO_2 and SO_2 vs. temperature at the experimental conditions of set 4 in Table 1 (λ = 1.01). Symbols represent experimental concentrations, while lines denote model predictions, varying the activation energy of R3. The acronym “pw” in the legend denotes present work and the activation energy of reaction (R3) corresponds to 42 kcal/mol.

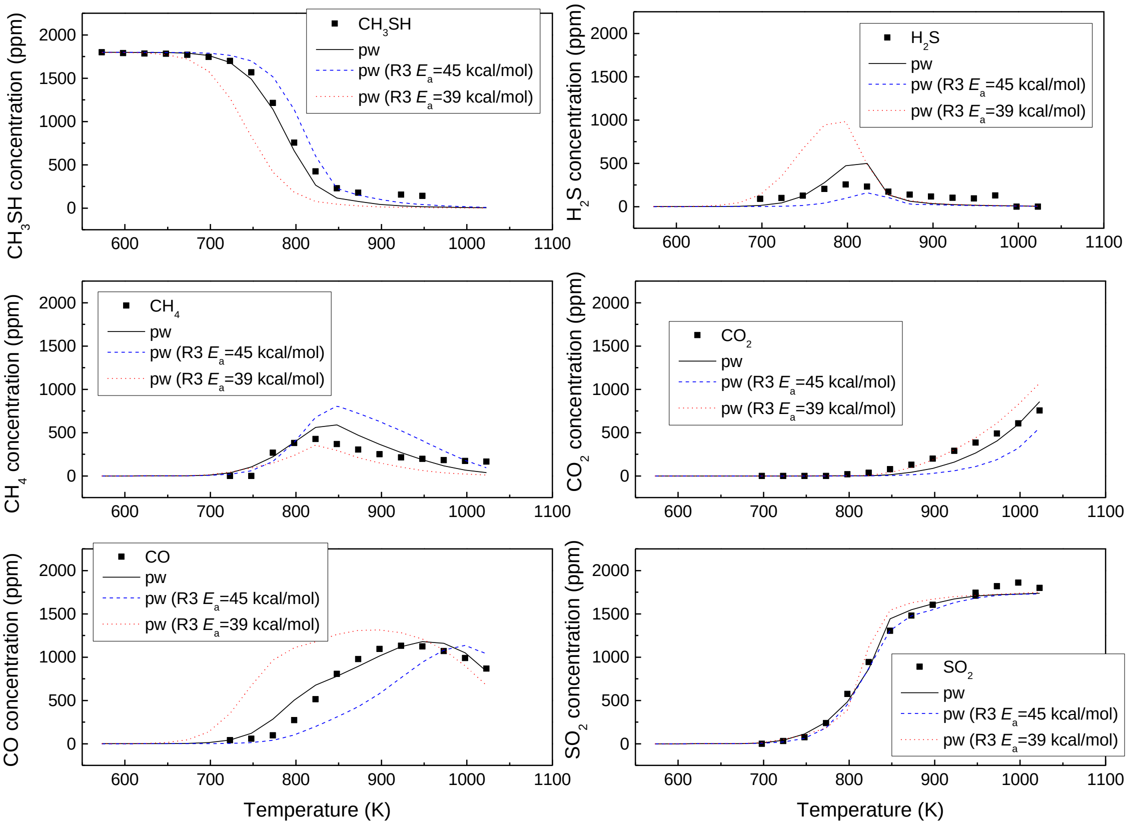

Figure S8. Concentrations of CH_3SH, CH_4, CO, H_2S, CO_2 and SO_2 vs. temperature at the experimental conditions of set 5 in Table 1 (λ = 3.55). Symbols represent experimental concentrations, while lines denote model predictions, varying the activation energy of R3. The acronym “pw” in the legend denotes present work and the activation energy of reaction (R3) is 42 kcal/mol.

7) Simulations of CH_3SH experiments modifying the pre-exponential factor of reaction (R3) ($CH_3SH+O_2 \rightleftharpoons CH_2SO+H_2O$)

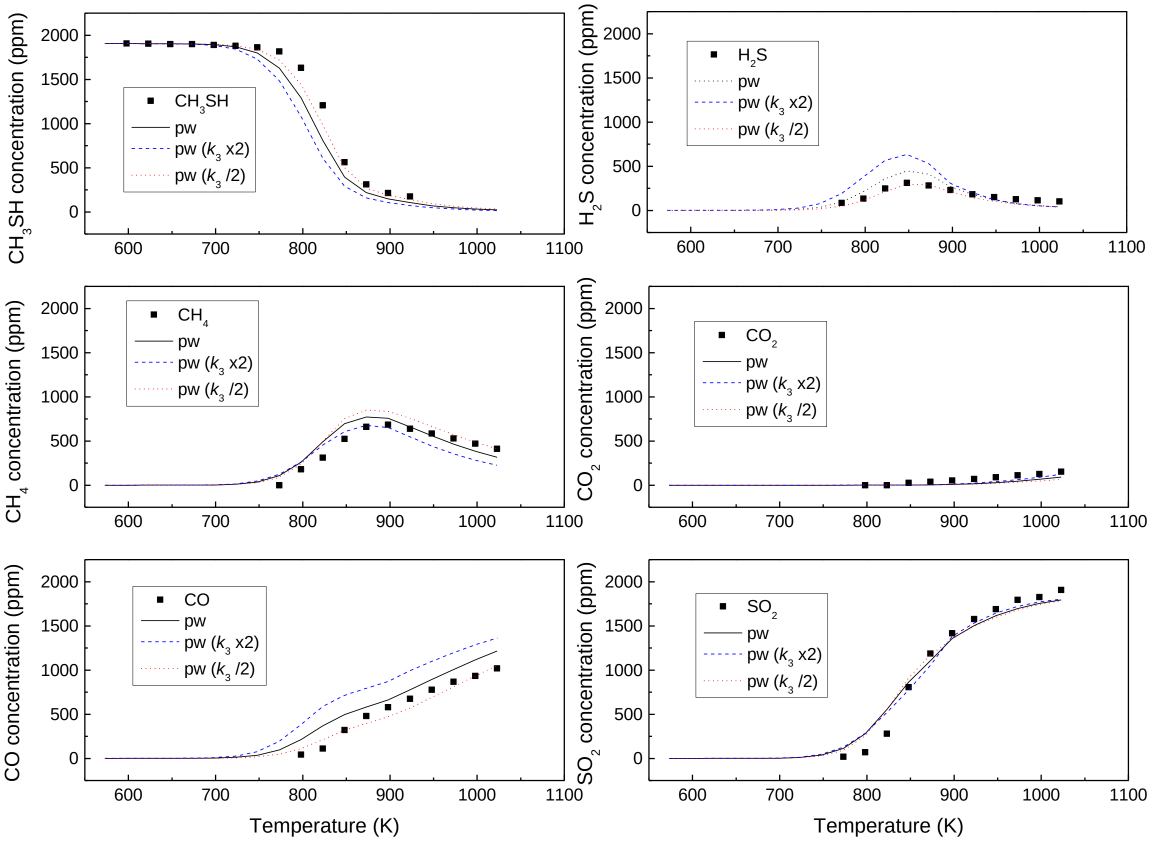

Figure S9. Concentrations of CH_3SH, CH_4, CO, H_2S, CO_2 and SO_2 vs. temperature at the experimental conditions of set 4 in Table 1 (λ = 1.01). Symbols represent experimental concentrations, while lines denote model predictions, varying the pre-exponential factor of R3. “The acronym “pw” in the legend denotes present work and the pre-exponential factor of reaction (R3) corresponds to 10^{14}.

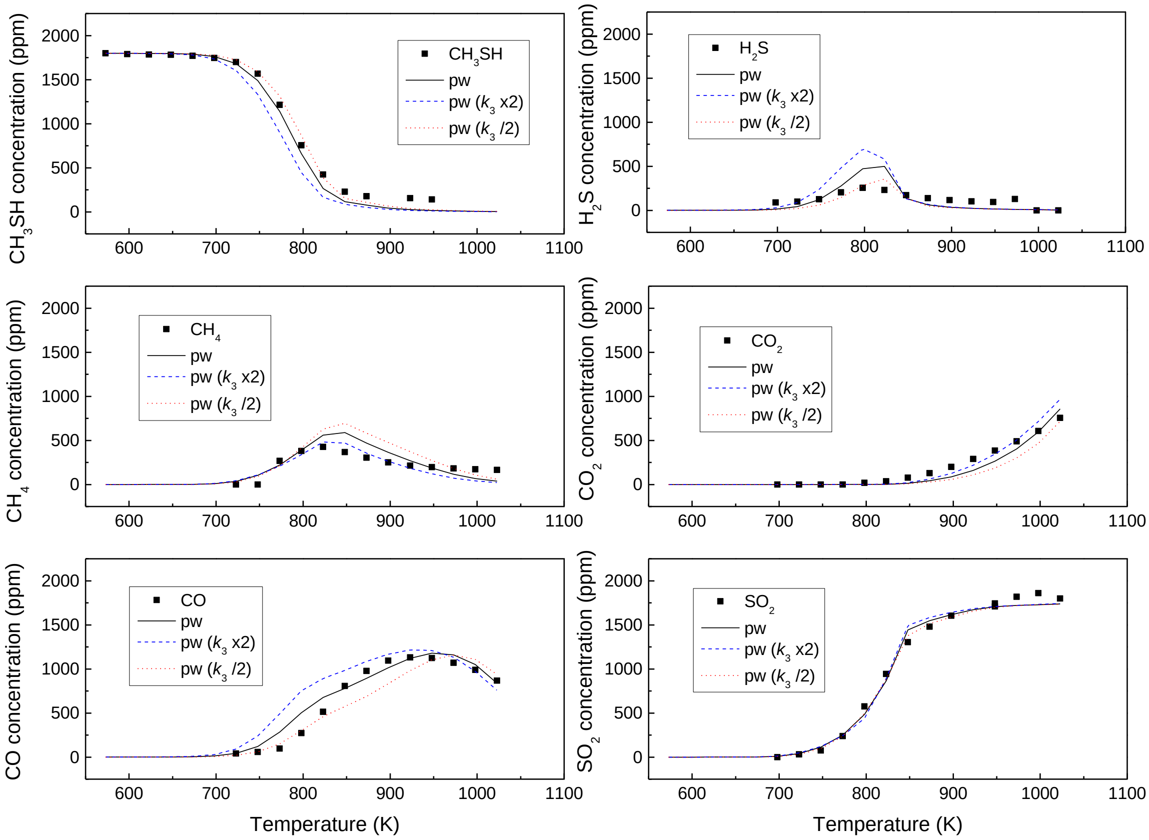

Figure S10. Concentrations of CH_3SH, CH_4, CO, H_2S, CO_2 and SO_2 vs. temperature at the experimental conditions of set 5 in Table 1 (λ = 3.55). Symbols represent experimental concentrations, while lines denote model predictions, varying the pre-exponential factor of R3. The acronym "pw" in the legend denotes present work and the pre-exponential factor of reaction (R3) corresponds to 10^{14}.

References:

[31] Alzueta, M.U.; Pernía, R.; Abián, M.; Millera, Á.; Bilbao, R. (2019). CH_3SH conversion in a tubular flow reactor. Experiments and kinetic modelling. Combustion and Flame 203, 23-30.

FINAL MECHANISM

“This annex contains the final mechanism compiled in the present work”

```
!********************************************************
!
! ***    EXPERIMENTAL AND KINETIC MODELING STUDY OF    ***
! ***                    H2S OXIDATION                          ***
! ***           APPLICATION TO SOUR GAS COMBUSTION          ***
!
! PhD: Colom-Díaz JM; Supervisors: Alzueta MU and Millera A
!
!********************************************************
!
!
ELEMENTS
H O C N S AR HE
END
SPECIES
SNO
HSNO
H2S
CH2SH
SO2
SH
H
OH
O
H2
S2
O3
CO
CO2
COS
CS2
CS
SO
C2H4
C2H2
CH4
HE
CO
CO2
C2H4
CH4
C2H6
C2H2
CH2O
CH
CH2
CH2(S)
CH3
H2O
C2
C2H
C2H3
HCO
```

N2
C2H5
CH2OH
CH3O
O2
CH3OH
HO2
H2O2
C3H2
H2CCCH
C2H2OH
AR
C2O
HCCO
CH2CHCH2
CH3CCH2
CH3CHCH
CH2CO
HCCOH
CH2HCO
C2H5OH
C2H4OH
CH3CH2O
CH3HCO
CH3CO
C2H5CHO
C2H5CO
OCHCHO
HCOO
NO
HCN
C
NO2
NO3
HNO
HONO
H2NO
HNOH
NH3
NH2
NH
N
N2H2
NNH
N2O
CN
NCO
HNCO
HOCN
HCNO
C2N2
NCN
CH3CN

```
CH2CN
H2CN
CH3NO
HONO2
CH3CHOH
CH2OOH
CH3OO
CH3OOH
HNO2
HNO3
HONOc
HONOt
HNO4
N2O4
N2O3
SN
CH3O2
CH2CHCHCH2
CH2CHCHCH
C4H2
HCCHCCH
CH2CHCCH
CH2CHCCH2
H2CCCCH
C4H
H2CCCCCH
HCCCHCCH
C6H2
C5H2
C5H5
H2C4O
SO2
SO2* SO3
SO(S) HSO HOS HOSO HSO2 HOSO2 HOSOH HOSHO H2SO HSOH S HSOO OSSO SSO2 HS2O
HS2 H2S2 HSSO2 H2S3O HSSSOH H2S2O2 VDW1 S4 S5 S6 S7 S8
CH3S CH3SH CH2S CH3CHO CH3SO2 CH3OSO S2O S3 H2SO4 CH3SO HCS
CH3CH2S CH3SCH3 CH2CH2SH CS2OH O2(S) HO3 CHS2 CHS CH4S CH2SO CH3SO
!
END
!
!
THERMO
   300.000  1000.000  5000.000
C2H4              121286C   2H   4          G  0300.00   5000.00  1000.00      1
 0.03528418E+02 0.11485185E-01-0.04418385E-04 0.07844600E-08-0.05266848E-12    2
 0.04428288E+05 0.02230389E+02-0.08614880E+01 0.02796162E+00-0.03388677E-03    3
 0.02785152E-06-0.09737879E-10 0.05573046E+05 0.02421148E+03                   4
CO                121286C   1O   1          G  0300.00   5000.00  1000.00      1
 0.03025078E+02 0.14426885E-02-0.05630827E-05 0.10185813E-09-0.06910951E-13    2
-0.14268350E+05 0.06108217E+02 0.03262451E+02 0.15119409E-02-0.03881755E-04    3
 0.05581944E-07-0.02474951E-10-0.14310539E+05 0.04848897E+02                   4
CO2               121286C   1O   2          G  0300.00   5000.00  1000.00      1
 0.04453623E+02 0.03140168E-01-0.12784105E-05 0.02393996E-08-0.16690333E-13    2
```

```
-0.04896696E+06-0.09553959E+01 0.02275724E+02 0.09922072E-01-0.10409113E-04    3
 0.06866686E-07-0.02117280E-10-0.04837314E+06 0.10188488E+02                   4
CH4               121286C   1H   4          G  0300.00   5000.00  1000.00      1
 0.01683478E+02 0.10237236E-01-0.03875128E-04 0.06785585E-08-0.04503423E-12    2
-0.10080787E+05 0.09623395E+02 0.07787415E+01 0.01747668E+00-0.02783409E-03    3
 0.03049708E-06-0.12239307E-10-0.09825229E+05 0.13722195E+02                   4
CH2O              121286C   1H   2O   1     G  0300.00   5000.00  1000.00      1
 0.02995606E+02 0.06681321E-01-0.02628954E-04 0.04737153E-08-0.03212517E-12    2
-0.15320369E+05 0.06912572E+02 0.16527311E+01 0.12631439E-01-0.01888168E-03    3
 0.02050031E-06-0.08413237E-10-0.14865404E+05 0.13784820E+02                   4
H                 120186H   1               G  0300.00   5000.00  1000.00      1
 0.02500000E+02 0.00000000E+00 0.00000000E+00 0.00000000E+00 0.00000000E+00    2
 0.02547162E+06-0.04601176E+01 0.02500000E+02 0.00000000E+00 0.00000000E+00    3
 0.00000000E+00 0.00000000E+00 0.02547162E+06-0.04601176E+01                   4
H2                121286H   2               G  0300.00   5000.00  1000.00      1
 0.02991423E+02 0.07000644E-02-0.05633828E-06-0.09231578E-10 0.15827519E-14    2
-0.08350340E+04-0.13551101E+01 0.03298124E+02 0.08249441E-02-0.08143015E-05    3
-0.09475434E-09 0.04134872E-11-0.10125209E+04-0.03294094E+02                   4
C                 121086C   1               G  0300.00   5000.00  1000.00      1
 0.02602087E+02-0.01787081E-02 0.09087041E-06-0.11499333E-10 0.03310844E-14    2
 0.08542154E+06 0.04195177E+02 0.02498584E+02 0.08085776E-03-0.02697697E-05    3
 0.03040729E-08-0.11066518E-12 0.08545878E+06 0.04753459E+02                   4
CH                121286C   1H   1          G  0300.00   5000.00  1000.00      1
 0.02196223E+02 0.02340381E-01-0.07058201E-05 0.09007582E-09-0.03855040E-13    2
 0.07086723E+06 0.09178373E+02 0.03200202E+02 0.02072875E-01-0.05134431E-04    3
 0.05733890E-07-0.01955533E-10 0.07045259E+06 0.03331587E+02                   4
CH2(S)            83194H   2C   1    0    0G   300.000  4000.000 1400.00    0 1
 0.40752106E+01 0.15779120E-02-0.10806129E-06-0.84592437E-10 0.14033284E-13    2
 0.50007492E+05-0.15480316E+01 0.35932946E+01 0.13151238E-02 0.30756846E-06    3
 0.42637904E-09-0.34178712E-12 0.50451547E+05 0.17780241E+01                   4
CH2               83194H   2C   1    0    0G   300.000  4000.000 1400.00    0 1
 0.39737520E+01 0.16097502E-02-0.10785119E-06-0.86399922E-10 0.14301196E-13    2
 0.45608973E+05 0.75549729E-01 0.36872995E+01 0.15066403E-02 0.69679857E-07    3
 0.23537297E-09-0.19397147E-12 0.45863672E+05 0.20267601E+01                   4
CH3               121286C   1H   3          G  0300.00   5000.00  1000.00      1
 0.02844051E+02 0.06137974E-01-0.02230345E-04 0.03785161E-08-0.02452159E-12    2
 0.16437809E+05 0.05452697E+02 0.02430442E+02 0.11124099E-01-0.01680220E-03    3
 0.16218288E-07-0.05864952E-10 0.16423781E+05 0.06789794E+02                   4
O                 120186O   1               G  0300.00   5000.00  1000.00      1
 0.02542059E+02-0.02755061E-03-0.03102803E-07 0.04551067E-10-0.04368051E-14    2
 0.02923080E+06 0.04920308E+02 0.02946428E+02-0.16381665E-02 0.02421031E-04    3
-0.16028431E-08 0.03890696E-11 0.02914764E+06 0.02963995E+02                   4
CH4               121286C   1H   4          G  0300.00   5000.00  1000.00      1
 0.01683478E+02 0.10237236E-01-0.03875128E-04 0.06785585E-08-0.04503423E-12    2
-0.10080787E+05 0.09623395E+02 0.07787415E+01 0.01747668E+00-0.02783409E-03    3
 0.03049708E-06-0.12239307E-10-0.09825229E+05 0.13722195E+02                   4
OH                121286O   1H   1          G  0300.00   5000.00  1000.00      1
 0.02882730E+02 0.10139743E-02-0.02276877E-05 0.02174683E-09-0.05126305E-14    2
 0.03886888E+05 0.05595712E+02 0.03637266E+02 0.01850910E-02-0.16761646E-05    3
 0.02387202E-07-0.08431442E-11 0.03606781E+05 0.13588605E+01                   4
H2O               20387H   2O   1           G  0300.00   5000.00  1000.00      1
 0.02672145E+02 0.03056293E-01-0.08730260E-05 0.12009964E-09-0.06391618E-13    2
-0.02989921E+06 0.06862817E+02 0.03386842E+02 0.03474982E-01-0.06354696E-04    3
```

```
 0.06968581E-07-0.02506588E-10-0.03020811E+06 0.02590232E+02                   4
C2                121286C   2               G  0300.00   5000.00  1000.00      1
 0.04135978E+02 0.06531618E-03 0.01837099E-05-0.05295085E-09 0.04712137E-13    2
 0.09967272E+06 0.07472923E+01 0.06996045E+02-0.07400601E-01 0.03234703E-04    3
 0.04802535E-07-0.03295917E-10 0.09897487E+06-0.13862268E+02                   4
C2H               83194H   1C   2    0    0G   300.000  4000.000 1400.00    0 1
 0.52086663E+01 0.12875765E-02-0.10398387E-06-0.67526325E-10 0.11751871E-13    2
 0.64697773E+05-0.53721781E+01 0.39396334E+01 0.32114412E-02-0.39412765E-06    3
-0.74782530E-09 0.27493521E-12 0.65224684E+05 0.17814000E+01                   4
C2H2              121386C   2H   2          G  0300.00   5000.00  1000.00      1
 0.04436770E+02 0.05376039E-01-0.01912816E-04 0.03286379E-08-0.02156709E-12    2
 0.02566766E+06-0.02800338E+02 0.02013562E+02 0.15190446E-01-0.16163189E-04    3
 0.09078992E-07-0.01912746E-10 0.02612444E+06 0.08805378E+02                   4
C2H3              83194H   3C   2    0    0G   300.000  4000.000 1400.00    0 1
 0.71861677E+01 0.34552682E-02-0.29435373E-06-0.20681942E-09 0.36797774E-13    2
 0.32229627E+05-0.15977573E+02 0.24955740E+01 0.10269993E-01-0.10226917E-05    3
-0.27594382E-08 0.96919825E-12 0.34232813E+05 0.10614626E+02                   4
CO                121286C   1O   1          G  0300.00   5000.00  1000.00      1
 0.03025078E+02 0.14426885E-02-0.05630827E-05 0.10185813E-09-0.06910951E-13    2
-0.14268350E+05 0.06108217E+02 0.03262451E+02 0.15119409E-02-0.03881755E-04    3
 0.05581944E-07-0.02474951E-10-0.14310539E+05 0.04848897E+02                   4
C2H4              121286C   2H   4          G  0300.00   5000.00  1000.00      1
 0.03528418E+02 0.11485185E-01-0.04418385E-04 0.07844600E-08-0.05266848E-12    2
 0.04428288E+05 0.02230389E+02-0.08614880E+01 0.02796162E+00-0.03388677E-03    3
 0.02785152E-06-0.09737879E-10 0.05573046E+05 0.02421148E+03                   4
HCO               121286H   1C   1O   1     G  0300.00   5000.00  1000.00      1
 0.03557271E+02 0.03345572E-01-0.13350060E-05 0.02470572E-08-0.01713850E-12    2
 0.03916324E+05 0.05552299E+02 0.02898329E+02 0.06199146E-01-0.09623084E-04    3
 0.10898249E-07-0.04574885E-10 0.04159922E+05 0.08983614E+02                   4
N2                121286N   2               G  0300.00   5000.00  1000.00      1
 0.02926640E+02 0.14879768E-02-0.05684760E-05 0.10097038E-09-0.06753351E-13    2
-0.09227977E+04 0.05980528E+02 0.03298677E+02 0.14082404E-02-0.03963222E-04    3
 0.05641515E-07-0.02444854E-10-0.10208999E+04 0.03950372E+02                   4
C2H5              83194H   5C   2    0    0G   300.000  4000.000 1400.00    0 1
 0.87349157E+01 0.54537677E-02-0.37647177E-06-0.31297920E-09 0.52844000E-13    2
 0.10265269E+05-0.23104086E+02 0.24398923E+01 0.13747212E-01-0.85500653E-06    3
-0.31469924E-08 0.93754355E-12 0.13158588E+05 0.13099146E+02                   4
CH2O              121286C   1H   2O   1     G  0300.00   5000.00  1000.00      1
 0.02995606E+02 0.06681321E-01-0.02628954E-04 0.04737153E-08-0.03212517E-12    2
-0.15320369E+05 0.06912572E+02 0.16527311E+01 0.12631439E-01-0.01888168E-03    3
 0.02050031E-06-0.08413237E-10-0.14865404E+05 0.13784820E+02                   4
C2H6              121686C   2H   6          G  0300.00   4000.00  1000.00      1
 0.04825938E+02 0.13840429E-01-0.04557258E-04 0.06724967E-08-0.03598161E-12    2
-0.12717793E+05-0.05239506E+02 0.14625388E+01 0.15494667E-01 0.05780507E-04    3
-0.12578319E-07 0.04586267E-10-0.11239176E+05 0.14432295E+02                   4
CH2OH             120186H   3C   1O   1     G  0250.00   4000.00  1000.00      1
 0.06327520E+02 0.03608270E-01-0.03201547E-05-0.01938750E-08 0.03509704E-12    2
-0.04474509E+05-0.08329365E+02 0.02862628E+02 0.10015273E-01-0.05285435E-05    3
-0.05138539E-07 0.02246041E-10-0.03349678E+05 0.10397938E+02                   4
CH3O              121686C   1H   3O   1     G  0300.00   3000.00  1000.00      1
 0.03770799E+02 0.07871497E-01-0.02656384E-04 0.03944431E-08-0.02112616E-12    2
 0.12783252E+03 0.02929575E+02 0.02106204E+02 0.07216595E-01 0.05338472E-04    3
-0.07377636E-07 0.02075610E-10 0.09786011E+04 0.13152177E+02                   4
```

```
O2                121386O   2               G  0300.00   5000.00  1000.00      1
 0.03697578E+02 0.06135197E-02-0.12588420E-06 0.01775281E-09-0.11364354E-14    2
-0.12339301E+04 0.03189165E+02 0.03212936E+02 0.11274864E-02-0.05756150E-05    3
 0.13138773E-08-0.08768554E-11-0.10052490E+04 0.06034737E+02                   4
CH3OH             121686C   1H   4O   1     G  0300.00   5000.00  1000.00      1
 0.04029061E+02 0.09376593E-01-0.03050254E-04 0.04358793E-08-0.02224723E-12    2
-0.02615791E+06 0.02378195E+02 0.02660115E+02 0.07341508E-01 0.07170050E-04    3
-0.08793194E-07 0.02390570E-10-0.02535348E+06 0.11232631E+02                   4
HO2               20387H   1O   2         G  0300.00   5000.00  1000.00      1
 0.04072191E+02 0.02131296E-01-0.05308145E-05 0.06112269E-09-0.02841164E-13    2
-0.15797270E+03 0.03476029E+02 0.02979963E+02 0.04996697E-01-0.03790997E-04    3
 0.02354192E-07-0.08089024E-11 0.01762273E+04 0.09222724E+02                   4
H2O2              120186H   2O   2         G  0300.00   5000.00  1000.00      1
 0.04573167E+02 0.04336136E-01-0.14746888E-05 0.02348903E-08-0.14316536E-13    2
-0.01800696E+06 0.05011369E+01 0.03388753E+02 0.06569226E-01-0.14850125E-06    3
-0.04625805E-07 0.02471514E-10-0.01766314E+06 0.06785363E+02                   4
C3H2              102193H   2C   3         G  0150.00   4000.00  1000.00      1
 0.07670981E+02 0.02748749E-01-0.04370942E-05-0.06455599E-09 0.16638874E-13    2
 0.06259722E+06-0.12368903E+02 0.03166713E+02 0.02482571E+00-0.04591637E-03    3
 0.04268019E-06-0.14821524E-10 0.06350421E+06 0.08869446E+02                   4
H2CCCH            032599C   3H   3         G  0300.00   4000.00  1000.00      1
 0.08831047E+02 0.04357194E-01-0.04109066E-05-0.02368723E-08 0.04376520E-12    2
 0.39983875E+05-0.22559194E+02 0.04754199E+02 0.11080277E-01 0.02793323E-05    3
-0.05479212E-07 0.01949629E-10 0.41398515E+05-1.94548824E-01                   4
AR                120186AR  1               G  0300.00   5000.00  1000.00      1
 0.02500000E+02 0.00000000E+00 0.00000000E+00 0.00000000E+00 0.00000000E+00    2
-0.07453750E+04 0.04366000E+02 0.02500000E+02 0.00000000E+00 0.00000000E+00    3
 0.00000000E+00 0.00000000E+00-0.07453750E+04 0.04366000E+02                   4
C2O               121286C   2O   1         G  0300.00   5000.00  1000.00      1
 0.04849809E+02 0.02947585E-01-0.10907286E-05 0.01792562E-08-0.11157585E-13    2
 0.03282055E+06-0.06453225E+01 0.03368850E+02 0.08241803E-01-0.08765145E-04    3
 0.05569262E-07-0.15400086E-11 0.03317081E+06 0.06713314E+02                   4
C3H4              101993H   4C   3         G  0300.00   4000.00  1400.00      1
 0.09776256E+02 0.05302137E-01-0.03701117E-05-0.03026385E-08 0.05089581E-12    2
 0.01954972E+06-0.03077061E+03 0.02539830E+02 0.16334371E-01-0.01764950E-04    3
-0.04647365E-07 0.01729130E-10 0.02251242E+06 0.09935702E+02                   4
C3H4P             101993H   4C   3         G  0300.00   4000.00  1400.00      1
 0.09768102E+02 0.05219151E-01-0.03753140E-05-0.02992191E-08 0.05107878E-12    2
 0.01860277E+06-0.03020678E+03 0.03029730E+02 0.14989613E-01-0.13985000E-05    3
-0.03969619E-07 0.13882165E-11 0.02148408E+06 0.08004594E+02                   4
HCCO              32387H   1C   2O   1     G  0300.00   4000.00  1000.00      1
 0.06758073E+02 0.02000400E-01-0.02027607E-05-0.10411318E-09 0.01965164E-12    2
 0.01901513E+06-0.09071262E+02 0.05047965E+02 0.04453478E-01 0.02268282E-05    3
-0.14820945E-08 0.02250741E-11 0.01965891E+06 0.04818439E+01                   4
CH2CHCH2          82489C   3H   5         G  0300.00   4000.00  1000.00      1
 0.09651539E+02 0.08075596E-01-0.07965424E-05-0.04650696E-08 0.08603281E-12    2
 0.15300955E+05-0.02686773E+03 0.02276486E+02 0.01985564E+00 0.11238421E-05    3
-0.10145757E-07 0.03441342E-10 0.01789496E+06 0.13725151E+02                   4
CH3CCH2           82489C   3H   5         G  0300.00   4000.00  1000.00      1
 0.09101018E+02 0.07964167E-01-0.07884945E-05-0.04562036E-08 0.08529212E-12    2
 0.02670680E+06-0.02150559E+03 0.03385811E+02 0.14045337E-01 0.03204127E-04    3
-0.03824120E-07-0.09053742E-11 0.02909066E+06 0.11266487E+02                   4
CH3CHCH           82489C   3H   5         G  0300.00   4000.00  1000.00      1
```

```
 0.09209764E+02 0.07871412E-01-0.07724522E-05-0.04497357E-08 0.08377272E-12    2
 0.02853967E+06-0.02232369E+03 0.03161863E+02 0.15180997E-01 0.02722659E-04    3
-0.05177112E-07 0.05435286E-12 0.03095547E+06 0.11979733E+02                   4
CH2CO             121686C   2H   2O   1     G  0300.00   5000.00  1000.00      1
 0.06038817E+02 0.05804840E-01-0.01920953E-04 0.02794484E-08-0.14588676E-13    2
-0.08583402E+05-0.07657581E+02 0.02974970E+02 0.12118712E-01-0.02345045E-04    3
-0.06466685E-07 0.03905649E-10-0.07632636E+05 0.08673553E+02                   4
HCCOH              32387H   2C   2O   1     G  0300.00   4000.00  1000.00      1
 0.07328324E+02 0.03336416E-01-0.03024705E-05-0.01781106E-08 0.03245168E-12    2
 0.07598258E+05-0.14012140E+02 0.03899465E+02 0.09701075E-01-0.03119309E-05    3
-0.05537732E-07 0.02465732E-10 0.08701190E+05 0.04491874E+02                   4
C3H6              120186C   3H   6          G  0300.00   5000.00  1000.00      1
 0.06732257E+02 0.14908336E-01-0.04949899E-04 0.07212022E-08-0.03766204E-12    2
-0.09235703E+04-0.13313348E+02 0.14933071E+01 0.02092517E+00 0.04486794E-04    3
-0.16689121E-07 0.07158146E-10 0.10748264E+04 0.16145340E+02                   4
C2H2OH HCCO TRAN  121196H   3C   2O   1    0G   300.000  3000.000 1000.00    0 1
 0.57206843E+01 0.10704185E-01-0.50358494E-05 0.11324499E-08-0.10086621E-12    2
 0.12849424E+05-0.47081776E+01 0.81498282E-01 0.31640644E-01-0.34085361E-04    3
 0.18978838E-07-0.41950165E-11 0.14060783E+05 0.22908977E+02                   4
CH2HCO            110393O   1H   3C   2     G  0300.00   5000.00  1000.00      1
 0.05975670E+02 0.08130591E-01-0.02743624E-04 0.04070304E-08-0.02176017E-12    2
 0.04903218E+04-0.05045251E+02 0.03409062E+02 0.10738574E-01 0.01891492E-04    3
-0.07158583E-07 0.02867385E-10 0.15214766E+04 0.09558290E+02                   4
CH3CO             120186C   2H   3O   1     G  0300.00   5000.00  1000.00      1
 0.05612279E+02 0.08449886E-01-0.02854147E-04 0.04238376E-08-0.02268403E-12    2
-0.05187863E+05-0.03274949E+02 0.03125278E+02 0.09778220E-01 0.04521448E-04    3
-0.09009462E-07 0.03193717E-10-0.04108507E+05 0.11228854E+02                   4
CO2               121286C   1O   2          G  0300.00   5000.00  1000.00      1
 0.04453623E+02 0.03140168E-01-0.12784105E-05 0.02393996E-08-0.16690333E-13    2
-0.04896696E+06-0.09553959E+01 0.02275724E+02 0.09922072E-01-0.10409113E-04    3
 0.06866686E-07-0.02117280E-10-0.04837314E+06 0.10188488E+02                   4
CH3HCO            120186C   2O   1H   4     G  0300.00   5000.00  1000.00      1
 0.05868650E+02 0.10794241E-01-0.03645530E-04 0.05412912E-08-0.02896844E-12    2
-0.02264568E+06-0.06012946E+02 0.02505695E+02 0.13369907E-01 0.04671953E-04    3
-0.11281401E-07 0.04263566E-10-0.02124588E+06 0.13350887E+02                   4
CH3O2             BUR95 H   3C   1O   2    0G   200.000  6000.000  1000.000  0 1
 0.66812963E 01 0.80057271E-02-0.27188507E-05 0.40631365E-09-0.21927725E-13    2
 0.52621851E 03-0.99423847E 01 0.20986490E 01 0.15786357E-01 0.75683261E-07    3
-0.11274587E-07 0.56665133E-11 0.20695879E 04 0.15007068E 02 0.33715510E+04    4
CH3OOH            BUR95 H   4C   1O   2   00G   200.000  6000.000  1000.000    1
 0.61600316E+01 0.10239957E-01-0.36101507E-05 0.57550301E-09-0.34178147E-13    2
-0.17654526E+05-0.61911544E+01 0.49652507E+01 0.92343510E-03 0.34455956E-04    3
-0.44469600E-07 0.17456120E-10-0.16726970E+05 0.29880275E+01-0.14980760E+05    4
C4H               121686C   4H   1          G  0300.00   5000.00  1000.00      1
 0.06242882E+02 0.06193682E-01-0.02085931E-04 0.03082203E-08-0.16364826E-13    2
 0.07568019E+06-0.07210806E+02 0.05023247E+02 0.07092375E-01-0.06073762E-07    3
-0.02275752E-07 0.08086994E-11 0.07623812E+06-0.06942594E+00                   4
C4H2              121686C   4H   2          G  0300.00   5000.00  1000.00      1
 0.09031407E+02 0.06047252E-01-0.01948788E-04 0.02754863E-08-0.13856080E-13    2
 0.05294735E+06-0.02385067E+03 0.04005191E+02 0.01981000E+00-0.09865877E-04    3
-0.06635158E-07 0.06077413E-10 0.05424065E+06 0.01845736E+02                   4
H2CCCCH            82489C   4H   3          G  0300.00   4000.00  1000.00      1
 0.11314095E+02 0.05014414E-01-0.05350444E-05-0.02825309E-08 0.05403279E-12    2
 0.05181211E+06-0.03062434E+03 0.06545799E+02 0.12424768E-01 0.05603226E-05    3
-0.05631141E-07 0.16652183E-11 0.05352502E+06-0.04264082E+02                   4
HCCHCCH           82489C   4H   3          G  0300.00   4000.00  1000.00      1
 0.10752738E+02 0.05381153E-01-0.05549637E-05-0.03052266E-08 0.05761740E-12    2
 0.06121419E+06-0.02973025E+03 0.04153881E+02 0.01726287E+00-0.02389374E-05    3
-0.10187000E-07 0.04340504E-10 0.06338070E+06 0.06036506E+02                   4
CH2CHCCH          82489C   4H   4          G  0300.00   4000.00  1000.00      1
 0.10697773E+02 0.06982014E-01-0.06567747E-05-0.03884517E-08 0.07200946E-12    2
 0.03034803E+06-0.03128430E+03 0.03233893E+02 0.01865634E+00 0.12703205E-05    3
-0.09410096E-07 0.02956110E-10 0.03301097E+06 0.09922676E+02                   4
CH2CHCCH2         82489C   4H   5          G  0300.00   4000.00  1000.00      1
 0.11997762E+02 0.07990580E-01-0.08098172E-05-0.04568733E-08 0.08636911E-12    2
 0.03228493E+06-0.03528494E+03 0.03879443E+02 0.01997663E+00 0.01872777E-04    3
-0.09306953E-07 0.02386116E-10 0.03526859E+06 0.09842152E+02                   4
CH2CHCHCH         82489C   4H   5          G  0300.00   4000.00  1000.00      1
 0.12865971E+02 0.07943369E-01-0.08626466E-05-0.04655635E-08 0.08951131E-12    2
 0.03783552E+06-0.04182502E+03 0.02995240E+02 0.02288456E+00 0.01975471E-04    3
-0.11482454E-07 0.03197823E-10 0.04142218E+06 0.12894539E+02                   4
CH2CHCHCH2       120189C   4H   6          G  0300.00   4000.00  1000.00      1
 0.12544366E+02 0.09596525E-01-0.09187012E-05-0.05429640E-08 0.10053636E-12    2
 0.08597330E+05-0.04217450E+03 0.01931624E+02 0.02479030E+00 0.03018071E-04    3
-0.11546856E-07 0.02586623E-10 0.12554682E+05 0.01701999E+03                   4
OCHCHO           120596H   2C   2O   2    0G   300.000  3000.000 1000.00    0 1
 0.49087462E+01 0.13182673E-01-0.71416730E-05 0.18461316E-08-0.18525858E-12    2
-0.27116386E+05 0.59148768E+00 0.25068862E+01 0.18899139E-01-0.10302623E-04    3
 0.62607508E-09 0.88114253E-12-0.26427374E+05 0.13187043E+02                   4
C5H2              20587C   5H   2          G  0300.00   5000.00  1000.00      1
 0.11329175E+02 0.07424056E-01-0.02628188E-04 0.04082541E-08-0.02301332E-12    2
 0.07878706E+06-0.03617117E+03 0.03062321E+02 0.02709998E+00-0.10091697E-04    3
-0.12727451E-07 0.09167219E-10 0.08114969E+06 0.07071078E+02                   4
H2CCCCCH         101993H   3C   5          G  0300.00   4000.00  1400.00      1
 0.14407361E+02 0.04424058E-01-0.03618244E-05-0.02456408E-08 0.04327859E-12    2
 0.05896103E+06-0.04775144E+03 0.07441420E+02 0.15851654E-01-0.02219895E-04    3
-0.04928037E-07 0.01984559E-10 0.06162266E+06-0.09047891E+02                   4
HCCCHCCH         101993H   3C   5          G  0300.00   4000.00  1400.00      1
 0.14122474E+02 0.04593411E-01-0.03738175E-05-0.02574328E-08 0.04539160E-12    2
 0.06249257E+06-0.04722335E+03 0.06854796E+02 0.01699404E+00-0.02582284E-04    3
-0.05488764E-07 0.02281480E-10 0.06515364E+06-0.07133854E+02                   4
C5H5             101993H   5C   5          G  0300.00   4000.00  1400.00      1
 0.15310937E+02 0.07473806E-01-0.05837457E-05-0.04386651E-08 0.07696839E-12    2
 0.02525889E+06-0.05951593E+03 0.10073161E+01 0.03189880E+00-0.04748189E-04    3
-0.11023903E-07 0.04584680E-10 0.03047390E+06 0.01934167E+03                   4
H2C4O            120189H   2C   4O   1     G  0300.00   4000.00  1000.00      1
 0.10268878E+02 0.04896164E-01-0.04885080E-05-0.02708566E-08 0.05107013E-12    2
 0.02346902E+06-0.02815985E+03 0.04810971E+02 0.13139988E-01 0.09865073E-05    3
-0.06120720E-07 0.16400028E-11 0.02545803E+06 0.02113424E+02                   4
C6H2             121686C   6H   2          G  0300.00   5000.00  1000.00      1
 0.12756519E+02 0.08034381E-01-0.02618215E-04 0.03725060E-08-0.01878850E-12    2
 0.08075469E+06-0.04041262E+03 0.05751085E+02 0.02636719E+00-0.11667596E-04    3
-0.10714498E-07 0.08790297E-10 0.08262012E+06-0.04335532E+02                   4
C6H4             111293H   4C   6          G  0300.00   4000.00  1000.00      1
 0.14016253E+02 0.08242769E-01-0.08099663E-05-0.04654132E-08 0.08748122E-12    2
 0.04410395E+06-0.05139376E+03 0.15200236E+01 0.02876611E+00 0.14177245E-05    3
```

```
-0.16505889E-07 0.05873156E-10 0.04844894E+06 0.01719033E+03                   4
C6H5              82489C   6H   5         G  0300.00   4000.00  1000.00      1
 0.15775887E+02 0.09651109E-01-0.09429416E-05-0.05469111E-08 0.10265216E-12    2
 0.03302698E+06-0.06176280E+03 0.11435567E+00 0.03627324E+00 0.11582856E-05    3
-0.02196964E-06 0.08463556E-10 0.03836054E+06 0.02380117E+03                   4
C6H6              20387C   6H   6         G  0300.00   5000.00  1000.00      1
 0.12910740E+02 0.01723296E+00-0.05024210E-04 0.05893497E-08-0.01947521E-12    2
 0.03664511E+05-0.05002699E+03-0.03138012E+02 0.04723103E+00-0.02962207E-04    3
-0.03262819E-06 0.01718691E-09 0.08890031E+05 0.03657573E+03                   4
CH3CN             111596H   3C   2N   1    0G   300.000  3000.000 1000.00    0 1
 0.23924046E+01 0.15618873E-01-0.79120497E-05 0.19372333E-08-0.18611956E-12    2
 0.84999377E+04 0.11145236E+02 0.25197531E+01 0.13567523E-01-0.25764077E-05    3
-0.30893967E-08 0.14288692E-11 0.85533762E+04 0.10920868E+02                   4
CH2CN             111596H   2C   2N   1    0G   300.000  3000.000 1000.00    0 1
 0.46058146E+01 0.94485160E-02-0.47116329E-05 0.11389957E-08-0.10828942E-12    2
 0.29171486E+05 0.10084415E+01 0.25296724E+01 0.18114138E-01-0.18960575E-04    3
 0.11944583E-07-0.32544142E-11 0.29592293E+05 0.10993441E+02                   4
HNO               pg9601H   1N   1O   1     G  0300.00   5000.00  1000.00      1
 0.03615144E+02 0.03212486E-01-0.01260337E-04 0.02267298E-08-0.01536236E-12    2
 0.11769108E+05 0.04810264E+02 0.02784403E+02 0.06609646E-01-0.09300223E-04    3
 0.09437980E-07-0.03753146E-10 0.12025976E+05 0.09035629E+02                   4
HCN               110193H   1C   1N   1     G  0300.00   4000.00  1000.00      1
 0.03426457E+02 0.03924190E-01-0.01601138E-04 0.03161966E-08-0.02432850E-12    2
 0.01485552E+06 0.03607795E+02 0.02417787E+02 0.09031856E-01-0.01107727E-03    3
 0.07980141E-07-0.02311141E-10 0.01501044E+06 0.08222891E+02                   4
HNCO              110193H   1C   1N   1O   1G  0300.00   4000.00  1400.00      1
 0.06545307E+02 0.01965760E-01-0.01562664E-05-0.01074318E-08 0.01874680E-12    2
-0.01664773E+06-0.01003880E+03 0.03858467E+02 0.06390342E-01-0.09016628E-05    3
-0.01898224E-07 0.07651380E-11-0.01562343E+06 0.04882493E+02                   4
HOCN              110193H   1C   1N   1O   1G  0300.00   4000.00  1400.00      1
 0.06022112E+02 0.01929530E-01-0.01455029E-05-0.01045811E-08 0.01794814E-12    2
-0.04040321E+05-0.05866433E+02 0.03789424E+02 0.05387981E-01-0.06518270E-05    3
-0.01420164E-07 0.05367969E-11-0.03135335E+05 0.06667052E+02                   4
NCO               110193C   1N   1O   1     G  0300.00   4000.00  1400.00      1
 0.06072346E+02 0.09227829E-02-0.09845574E-06-0.04764123E-09 0.09090445E-13    2
 0.01359820E+06-0.08507293E+02 0.03359593E+02 0.05393239E-01-0.08144585E-05    3
-0.01912868E-07 0.07836794E-11 0.01462809E+06 0.06549694E+02                   4
NO*               dummy O   1N   1    0     G  0300.00   4000.00  1400.00      1
 0.06072346E+02 0.09227829E-02-0.09845574E-06-0.04764123E-09 0.09090445E-13    2
 0.01359820E+06-0.08507293E+02 0.03359593E+02 0.05393239E-01-0.08144585E-05    3
-0.01912868E-07 0.07836794E-11 0.01462809E+06 0.06549694E+02                   4
C2H5OH        BUR   8/88C   2H   6O   1     G   200.000  6000.000 1000.00      1
 0.65624365E+01 0.15204222E-01-0.53896795E-05 0.86225011E-09-0.51289787E-13    2
-0.31525621E+05-0.94730202E+01 0.48586957E+01-0.37401726E-02 0.69555378E-04    3
-0.88654796E-07 0.35168835E-10-0.29996132E+05 0.48018545E+01-0.28257829E+05    4
C2H4OH             MARI99C   2H   5O   1    0G   200.000  4000.000 1000.00      1
 0.74564000E+00 0.02930200E-00-2.18510000E-05 8.85746000E-09-1.38170000E-12    2
-0.54736000E+04 0.22235000E+02 0.74564000E+00 0.02930200E-00-2.18510000E-05    3
 8.85746000E-09-1.38170000E-12-0.54736000E+04 0.22235000E+02                   4
C2H5CHO            BURC92C   3H   6O   1    0G   273.150  5000.000 1000.00      1
 0.33137982E+01 0.26619606E-01-0.10475596E-04 0.18815334E-08-0.12761310E-12    2
-0.25459603E+05 0.96608447E+01 0.76044596E+01-0.86403564E-02 0.73930097E-04    3
-0.79687398E-07 0.28004927E-10-0.25489789E+05-0.67643691E+01-0.23097645E+05    4
```

```
C2H5CO           BURC92C   3H   5O   1    0G   298.150  5000.000 1000.00      1
 0.30445698E+01 0.23236429E-01-0.86317936E-05 0.14799550E-08-0.96860829E-13    2
-0.61787211E+04 0.13122302E+02 0.67368294E+01-0.26945299E-02 0.49927017E-04    3
-0.50025808E-07 0.15011503E-10-0.65703366E+04-0.23398732E+01-0.43321855E+04    4
HCOO            BOZELLI C  1H   1O   2    0G   300.000  5000.000 1453.000    01
 6.40920688E+00 3.28189026E-03-1.18710674E-06 1.91323635E-10-1.13932748E-14    2
-2.20542060E+04-1.04575060E+01 1.52482282E+00 1.26249843E-02-6.61406757E-06    3
 7.72750880E-10 2.09088864E-13-2.02040511E+04 1.64205770E+01                   4
CH2SH         BUR   8/88C   1H   3S   1     G   300.000  5000.000 1000.00      1
 0.02560000E+02 0.19780000E-01-0.26780000E-04 2.17600000E-08-0.73490000E-13    2
 0.17539000E+05 1.17400000E+01 0.02560000E+02 0.19780000E-01-0.26780000E-04    3
 2.17600000E-08-0.73490000E-13 0.17539000E+05 1.17400000E+01                   4
SO2             tpis89S  1.O  2.   0.   0.G   200.000  6000.000 1000.        1
 5.38423482E+00 1.67930560E-03-6.32062944E-07 1.08465348E-10-6.66890336E-15    2
-3.76067022E+04-1.83130517E+00 3.67480752E+00 2.28302107E-03 8.46893049E-06    3
-1.36562039E-08 5.76271873E-12-3.69455073E+04 7.96866430E+00-3.56978343E+04    4
SO2*             pg00  S   1O   2         G  0300.00   5000.00  1000.00      1
 0.05254498E+02 0.01978545E-01-0.08204226E-05 0.01576383E-08-0.01120451E-12    2
-0.08300578E+04-0.01146056E+02 0.02911439E+02 0.08103022E-01-0.06906710E-04    3
 0.03329016E-07-0.08777121E-11-0.01400178E+04 0.01111740E+03                   4
SO3             tpis89S  1.O  3.   0.   0.G   200.000  6000.000 1000.        1
 7.29677572E+00 2.73576437E-03-1.06377755E-06 1.80776031E-10-1.12077527E-14    2
-5.03096739E+04-1.24246659E+01 2.37461122E+00 1.59543297E-02-1.26322543E-05    3
 2.81827264E-09 6.23371547E-13-4.89269231E+04 1.31043046E+01-4.76155540E+04    4
SO              tpis89S  1.O  1.   0.   0.G   200.000  6000.000 1000.        1
 3.96894225E+00 3.77296831E-04 7.67102696E-09-1.37544433E-11 1.37139416E-15    2
-7.28571725E+02 3.73493087E+00 3.61859514E+00-2.32173768E-03 1.16462669E-05    3
-1.42092510E-08 5.60765370E-12-4.80621641E+02 6.36504115E+00 5.72529951E+02    4
SO(S)           est09 S   1O   1         G  0300.00   5000.00  1000.00      1
 0.04309940E+02-0.12150870E-02 2.75383045E-06-2.07106108E-09 5.55106589E-13    2
 1.07760928E+04 0.01311757E+02 0.04309940E+02-0.12150870E-02 2.75383045E-06    3
-2.07106108E-09 5.55106589E-13 1.07760928E+04 0.01311757E+02                   4
HSO             T04/07H  1.S  1.O  1.   0.G   200.000  6000.000 1000.        1
 4.34724125E+00 2.53372236E-03-9.51430950E-07 1.58095446E-10-9.65294637E-15    2
-4.20893834E+03 3.15887502E+00 4.13565093E+00-3.69243127E-03 2.05169784E-05    3
-2.40530656E-08 9.17084270E-12-3.82371653E+03 5.88770120E+00-2.61672666E+03    4
HOS             T04/07S  1.O  1.H  1.   0.G   200.000  6000.000 1000.        1
 4.37246017E+00 2.01398865E-03-6.50854476E-07 9.74413078E-11-5.52225169E-15    2
-2.28578181E+03 3.13657231E+00 3.69440567E+00 3.94327613E-04 1.10155102E-05    3
-1.63102588E-08 7.03352877E-12-1.99257018E+03 7.31635620E+00-8.05146665E+02    4
HOSO DAGGLA03 GOUMAR99  H   1O   2S   1    0G   300.000  1500.000 1500.00    0 1
 0.16184697E+01 0.21164061E-01-0.26690482E-04 0.16272216E-07-0.37779005E-11    2
-0.30255641E+05 0.19477260E+02 0.16184697E+01 0.21164061E-01-0.26690482E-04    3
 0.16272216E-07-0.37779005E-11-0.30255641E+05 0.19477260E+02                   4
 DAG/GLA03 GOU/MAR99
HSO2                  H   1O   2S   1    0G    300.00   2000.00 1000.00      1
 0.15627374E+01 0.20691389E-01-0.23112073E-04 0.12670203E-07-0.27274176E-11    2
-0.18214824E+05 0.17556820E+02 0.15627374E+01 0.20691389E-01-0.23112073E-04    3
 0.12670203E-07-0.27274176E-11-0.18214824E+05 0.17556820E+02                   4
 ALZ/GLA01 GOU/MAR99
HOSO2           BOZ/R H   1O   3S   1    0G   300.000  1500.000 1500.00    0 1
 0.24358474E+01 0.29991941E-01-0.40650871E-04 0.26047603E-07-0.62778546E-11    2
-0.48803251E+05 0.14364072E+02 0.24358474E+01 0.29991941E-01-0.40650871E-04    3
```

```
 0.26047603E-07-0.62778546E-11-0.48803251E+05 0.14364072E+02                   4
HOSOH           BOZ/R H   2O   2S   1    0G   300.000  1500.000 1500.00    0 1
 0.17225311E+01 0.25308046E-01-0.30864965E-04 0.18614741E-07-0.42872813E-11    2
-0.39295778E+05 0.16536892E+02 0.17225311E+01 0.25308046E-01-0.30864965E-04    3
 0.18614741E-07-0.42872813E-11-0.39295778E+05 0.16536892E+02                   4
HOSHO           BOZ/R H   2O   2S   1    0G   300.000  1500.000 1500.00    0 1
 0.11903822E+01 0.25644735E-01-0.26622842E-04 0.13479665E-07-0.26474629E-11    2
-0.33744886E+05 0.19095494E+02 0.11903822E+01 0.25644735E-01-0.26622842E-04    3
 0.13479665E-07-0.26474629E-11-0.33744886E+05 0.19095494E+02                   4
H2SO            BOZ/R H   2O   1S   1    0G   300.000  1500.000 1500.00    0 1
 0.19580519E+01 0.97265201E-02 0.68413170E-06-0.62343720E-08 0.24166577E-11    2
-0.66770889E+04 0.14783451E+02 0.19580519E+01 0.97265201E-02 0.68413170E-06    3
-0.62343720E-08 0.24166577E-11-0.66770889E+04 0.14783451E+02                   4
HSOH                  H   2O   1S   1    0G    300.00   5000.00 1388.00      1
 0.25676441E+01 0.11380521E-01-0.58667324E-05-0.59470041E-09 0.87438329E-12    2
-0.15571256E+05 0.11766399E+02 0.25676441E+01 0.11380521E-01-0.58667324E-05    3
-0.59470041E-09 0.87438329E-12-0.15571256E+05 0.11766399E+02                   4
S               J 9/82S  1.   0.   0.   0.G   200.000  6000.000 1000.        1
 2.87936498E+00-5.11050388E-04 2.53806719E-07-4.45455458E-11 2.66717362E-15    2
 3.25013791E+04 3.98140647E+00 2.31725616E+00 4.78018342E-03-1.42082674E-05    3
 1.56569538E-08-5.96588299E-12 3.25068976E+04 6.06242434E+00 3.33128471E+04    4
SH                    H   1S   1    0    0G    300.00   5000.00 1000.00      1
 3.05381000E+00 1.25888400E-03-4.24916900E-07 6.92959100E-11-4.28169100E-15    2
 1.63513273E+04 5.97355100E+00 4.13332700E+00-3.78789300E-04-2.77785400E-06    3
 5.37011200E-09-2.39400600E-12 1.60276973E+04 1.61153500E-01                   4
H2S             g 4/01H  2.S  1.   0.   0.G   200.000  6000.000 1000.        1
 2.97879430E+00 3.59760372E-03-1.22803151E-06 1.96833209E-10-1.16716162E-14    2
-3.51607638E+03 6.77921228E+00 4.12024455E+00-1.87907426E-03 8.21426650E-06    3
-7.06425730E-09 2.14234860E-12-3.68215173E+03 1.53174068E+00-2.47759639E+03    4
HSOO                  H   1O   2S   1    0G    300.00   5000.00 1000.00      1
 5.87948232E+00 4.58580173E-03-2.93621833E-06 1.10178148E-09-1.86219122E-13    2
 1.41706015E+04-1.04622817E+00 3.04640372E+00 1.52114268E-02-1.84762707E-05    3
 1.13862234E-08-2.72421836E-12 1.48073744E+04 1.28748017E+01                   4
S2              tpis89S   2    0    0    0G   200.000  6000.000              1
 3.83249656E+00 8.88970881E-04-2.59080844E-07 3.63847115E-11-1.72606371E-15    2
 1.42836134E+04 5.33000845E+00 2.87736627E+00 5.00301430E-03-6.04370732E-06    3
 3.04738962E-09-3.87017618E-13 1.44342379E+04 9.79873919E+00 1.54669367E+04    4
HS2                   H   1S   2         0G    300.00   2000.00 1000.00      1
 3.59075969E+00 4.98506901E-03-3.43045513E-06 1.19341826E-09-1.67403033E-13    2
 1.17649789E+04 8.92475572E+00 2.81672268E+00 1.03969679E-02-1.55535096E-05    3
 1.24197562E-08-3.90834999E-12 1.18156870E+04 1.21143632E+01                   4
H2S2                  H   2S   2         0G    300.00   2000.00 1000.00      1
 4.69311463E+00 6.01993785E-03-3.01832133E-06 7.52297526E-10-7.91533129E-14    2
 1.72179592E+02 2.47728860E+00 2.07852476E+00 1.94742814E-02-2.93966240E-05    3
 2.37295586E-08-7.52058161E-12 5.96292301E+02 1.44741864E+01                   4
H2S2O2                H   2O   2S   2     G    300.00   5000.00 1000.00      1
 1.16213004E+01 3.43806006E-03-5.74448284E-07-3.13293096E-10 1.00662179E-13    2
-3.91048380E+04-2.90177401E+01 8.28112013E-01 4.74477762E-02-6.95648159E-05    3
 4.87812487E-08-1.32222441E-11-3.69287907E+04 2.29903159E+01                   4
H2S3O                 H   2O   1S   3     G    300.00   5000.00 1000.00      1
 1.18514105E+01 3.33850673E-03-6.86562800E-07-2.02600304E-10 7.47780445E-14    2
-1.28853402E+04-2.85026663E+01 3.67805059E+00 4.07191390E-02-6.67990246E-05    3
 5.28547092E-08-1.60811288E-11-1.13979874E+04 9.98571106E+00                   4
```

```
HSSSOH              H   2O   1S   3     G    300.00    5000.00 1000.00      1
 1.10809208E+01 3.73387762E-03-2.44411342E-07-6.13453741E-10 1.64649581E-13    2
-1.78355780E+04-2.35331548E+01 2.93988478E+00 4.05695638E-02-6.59918573E-05    3
 5.33283075E-08-1.67311298E-11-1.63029028E+04 1.49845285E+01                   4
HSSO2               H   1O   2S   2    0G    300.00    2000.00 1000.00      1
 7.76282262E+00 7.02637234E-03-4.08428794E-06 1.12459784E-09-1.18489230E-13    2
-2.33271862E+04-9.48284274E+00 3.49856646E+00 2.50749289E-02-3.40614452E-05    3
 2.40531480E-08-6.85626593E-12-2.24794312E+04 1.09552126E+01                   4
S4             tpis89S  4.   0.    0.    0.G   200.000  6000.000            1
 9.12781762E+00 9.13784446E-04-3.62719239E-07 6.24637076E-11-3.90794764E-15    2
 1.33309374E+04-1.74976107E+01 1.62124479E+00 3.69694158E-02-6.92243749E-05    3
 6.03240791E-08-1.99529262E-11 1.46879795E+04 1.76312033E+01 1.63127271E+04    4
S5             tpis89S  5.   0.    0.    0.G   200.000  6000.000            1
 1.33325960E+01 2.09782536E-04-3.36431685E-07 8.53311588E-11-6.48294924E-15    2
 1.13787913E+04-3.48611560E+01 3.27621083E+00 4.32967838E-02-8.47662885E-05    3
 8.12574426E-08-2.97793536E-11 1.36965078E+04 1.41196663E+01 1.59953327E+04    4
S6             tpis89S  6.   0.    0.    0.G   200.000  2500.000            1
 1.34043558E+01 3.42127317E-03-1.12816145E-06 1.46420087E-10-6.61286087E-15    2
 8.10860569E+03-3.42545590E+01 2.69715935E+00 6.86818730E-02-1.43788282E-04    3
 1.35427080E-07-4.71805554E-11 9.35349932E+03 1.24775267E+01 1.21853457E+04    4
S7             tpis89S  7.   0.    0.    0.G   200.000  6000.000            1
 1.78534018E+01 1.21114205E-03-4.83082305E-07 8.34576672E-11-5.23294619E-15    2
 7.80776842E+03-5.40618730E+01 2.91732736E+00 8.29649517E-02-1.73743030E-04    3
 1.63959287E-07-5.74388498E-11 1.01380200E+04 1.37221660E+01 1.34572415E+04    4
S8             tpis89S  8.   0.    0.    0.G   200.000  6000.000            1
 2.04307658E+01 5.18092908E-03-2.91895357E-06 5.97574588E-10-4.13758389E-14    2
 5.11843364E+03-6.74373075E+01 4.13158109E+00 9.43298552E-02-2.05775943E-04    3
 2.05747851E-07-7.51844045E-11 8.20318834E+03 7.83537207E+00 1.21807686E+04    4
HS2O                H   1O   1S   2    0G    300.00    2000.00 1000.00      1
 6.11859237E+00 5.59523243E-03-3.70626629E-06 1.22524738E-09-1.62789560E-13    2
-6.05886590E+03-1.97720682E+00 2.70484711E+00 2.32126968E-02-3.77894894E-05    3
 3.04178811E-08-9.47692405E-12-5.52811032E+03 1.36259179E+01                   4
SSO2               O   2S   2        0G    300.00    2000.00 1000.00      1
 6.34280650E+00 6.05027505E-03-4.24571996E-06 1.40852829E-09-1.81318004E-13    2
-2.27684952E+04-3.78737520E+00 2.80168627E+00 1.99919280E-02-2.56401242E-05    3
 1.65559742E-08-4.33620009E-12-2.20225598E+04 1.34189370E+01                   4
VDW1                H   2O   3S   1     G    300.00    5000.00 1000.00      1
 1.01262222E+01 3.57132793E-03-7.13009073E-09-5.82222901E-10 1.37375969E-13    2
-6.93881691E+04-1.74036743E+01 8.13179120E+00 8.32444914E-03-2.04192137E-06    3
-2.95153810E-09 1.78217150E-12-6.88287103E+04-6.98378761E+00                   4
OSSO               O   2S   2        0G    300.00    2000.00 1000.00      1
 8.06932897E+00 2.78600929E-03-1.65788135E-06 4.55717434E-10-4.76687943E-14    2
-1.68597542E+04-1.12637659E+01 4.27684328E+00 1.71764292E-02-2.30032367E-05    3
 1.50850596E-08-3.93335889E-12-1.60275576E+04 7.31095245E+00                   4
HSSO2               H   1O   2S   2    0G    300.00    2000.00 1000.00      1
 7.76282262E+00 7.02637234E-03-4.08428794E-06 1.12459784E-09-1.18489230E-13    2
-2.33271862E+04-9.48284274E+00 3.49856646E+00 2.50749289E-02-3.40614452E-05    3
 2.40531480E-08-6.85626593E-12-2.24794312E+04 1.09552126E+01                   4
CH3NO BUR0302     T12/92C   1H   3N   1O   1G   200.00    6000.00  1000.       1
 0.50677397E+01 0.93871079E-02-0.33958317E-05 0.55076729E-09-0.33095301E-13    2
 0.71852464E+04-0.10709779E+01 0.52463494E+01-0.68175691E-02 0.46713959E-04    3
-0.53482743E-07 0.19916692E-10 0.79241319E+04 0.18687355E+01 0.95017371E+04    4
COS              g5/01C   1O   1S   1    0G   200.000  6000.000  1000.       1
```

```
 5.37456093E+00 2.10411234E-03-7.76417533E-07 1.29745227E-10-7.92407725E-15    2
-1.89178351E+04-3.78473799E+00 1.77198991E+00 1.71486966E-02-2.73082140E-05    3
 2.25553393E-08-7.34373482E-12-1.81328604E+04 1.36810097E+01-1.70424956E+04    4
CS2              g6/95C   1S   2    0    0G   200.000  6000.000  1000.      1
 5.94905043E+00 1.69288150E-03-6.74333823E-07 1.16460519E-10-6.37363519E-15    2
 1.20171256E+04-6.17036834E+00 2.17230835E+00 1.81263444E-02-3.08080090E-05    3
 2.65150564E-08-8.92801520E-12 1.28063739E+04 1.19826948E+01 1.40357038E+04    4
CS               g11/01C   1S   1    0    0G   200.000  6000.000  1000.      1
 3.76959667E+00 7.30980640E-04-2.42920716E-07 2.88070971E-11-5.21956199E-17    2
 3.22498707E+04 3.42022942E+00 3.73124786E+00-3.09803648E-03 1.24828276E-05    3
-1.41633372E-08 5.33370965E-12 3.24420956E+04 4.54855088E+00 3.35016830E+04    4
CS2OH            dummy  C   1H   1S   2O   1G   200.000  6000.000  1000.      1
 5.94905043E+00 1.69288150E-03-6.74333823E-07 1.16460519E-10-6.37363519E-15    2
 1.20171256E+04-6.17036834E+00 2.17230835E+00 1.81263444E-02-3.08080090E-05    3
 2.65150564E-08-8.92801520E-12 1.28063739E+04 1.19826948E+01 1.40357038E+04    4
CH3S             IU3/03H   3C   1S   1    0G   200.000  6000.000  1000.      1
 4.62809340E+00 7.50242892E-03-2.70631691E-06 4.37671177E-10-2.61526827E-14    2
 1.30328459E+04 4.15868210E-02 2.56437070E+00 1.15796385E-02-4.50119584E-06    3
-5.02342418E-10 6.95252997E-13 1.37469790E+04 1.12504946E+01 1.49857923E+04    4
CH3SH            T12/08C   1H   4S   1    0G   200.000  6000.000  1000.      1
 4.50369870E+00 9.49866516E-03-3.34303841E-06 5.31967412E-10-3.15164389E-14    2
-4.46153406E+03 1.51156041E+00 3.78634471E+00 3.77026048E-03 1.96468694E-05    3
-2.65727342E-08 1.05290360E-11-3.87921543E+03 7.09507940E+00-2.45670376E+03    4
CH2S             T11/08C   1H   2S   1    0G   200.000  6000.000  1000.      1
 4.19801901E+00 5.14114256E-03-1.90400104E-06 3.33562196E-10-2.14380834E-14    2
 1.21202116E+04 1.89538934E+00 3.98890625E+00-4.48093468E-03 3.23152583E-05    3
-3.98564197E-08 1.57804745E-11 1.26210562E+04 5.29851918E+00 1.38253747E+04    4
CH3CHO                 C   2H   4O   1    0G   200.000  6000.000  1000.      1
 0.54041108E+01 0.11723059E-01-0.42263137E-05 0.68372451E-09-0.40984863E-13    2
-0.22593122E+05-0.34807917E+01 0.47294595E+01-0.31932858E-02 0.47534921E-04    3
-0.57458611E-07 0.21931112E-10-0.21572878E+05 0.41030159E+01-0.19987949E+05    4
CH3SO2     (ZHU2006)    C   1H   3S   1O   2G   200.00   6000.00  1000.       1
 0.28260000E+01 0.25630000E-01-0.21440000E-04 9.25300000E-09-0.15790000E-13    2
-0.28809000E+05 1.32900000E+01 0.28260000E+01 0.25630000E-01-0.21440000E-04    3
 9.25300000E-09-0.15790000E-13-0.28809000E+05 1.32900000E+01 0.28260000E+01    4
CH3OSO                 C   1H   3S   1O   2G   200.000  6000.000  1000.      1
 0.22960000E+01 0.25080000E-01-0.19940000E-04 8.14500000E-09-0.13260000E-13    2
-0.29221000E+05 1.92800000E+01 0.22960000E+01 0.25080000E-01-0.19940000E-04    3
 8.14500000E-09-0.13260000E-13-0.29221000E+05 1.92800000E+01 0.22960000E+01    4
S2O              tpis89S   2O   1    0    0G   200.000  6000.000  1000.      1
 6.02401811E+00 1.00035579E-03-3.91923038E-07 6.69240060E-11-4.16275707E-15    2
-8.76531218E+03-2.93690271E+00 3.01869800E+00 1.08575811E-02-1.25419070E-05    3
 6.57657832E-09-1.21573834E-12-8.02370855E+03 1.21738889E+01-6.73948254E+03    4
S3                     S   3             G   200.000  6000.000  1000.      1
 6.53302278E+00 4.89117086E-04-1.94120477E-07 3.34257105E-11-2.09106833E-15    2
 1.53186530E+04-4.42378063E+00 2.67426151E+00 1.85725510E-02-3.39241252E-05    3
 2.89518256E-08-9.41515882E-12 1.60320458E+04 1.37269667E+01 1.74079204E+04    4
CH3SCH3                C   2H   6S   1    0G   200.000  6000.000  1000.      1
 6.46633952E+00 1.55897399E-02-5.49135107E-06 8.74455165E-10-5.18380108E-14    2
-7.34925770E+03-8.01940674E+00 5.28055093E+00 2.44703498E-03 4.47525603E-05    3
-5.76668384E-08 2.25740377E-11-6.22993885E+03 2.04977549E+00-4.25469691E+03    4
CH3CH2S                C   2H   5S   1    0G   200.000  6000.000  1000.      1
 6.06146203E+00 1.35096776E-02-4.79809612E-06 7.68421362E-10-4.57369490E-14    2
 8.87147183E+03-5.21760983E+00 4.12080784E+00 6.77995700E-03 2.82399071E-05    3
-3.90230535E-08 1.53781094E-11 1.00274180E+04 7.80653672E+00 1.17370255E+04    4
CH2CH2SH                C   2H   5S   1    0G   200.000  6000.000  1000.       1
 6.32502214E+00 1.54070231E-02-5.45709466E-06 8.72281676E-10-5.18467041E-14    2
-8.26561807E+03-5.41769249E+00 5.40529602E+00 2.42610602E-03 4.12377755E-05    3
-5.18768956E-08 1.99031036E-11-7.22408589E+03 3.16335395E+00-5.23345332E+03    4
H2SO4           T 8/03H   2S   1O   4    0G   200.000  6000.000  1000.       1
 1.13355392E+01 5.60829109E-03-1.94574192E-06 3.07136054E-10-1.81109544E-14    2
-9.21087435E+04-2.96094003E+01 4.53388173E+00 3.10347679E-02-4.10421795E-05    3
 2.95752341E-08-8.81459071E-12-9.05459072E+04 3.93961412E+00-8.81230524E+04    4
CH3SO                   C   1H   3S   1O   1G   200.00   6000.00  1000.        1
 2.49700000E+00 1.79300000E-02-1.24500000E-05 4.60900000E-09-7.05600000E-13    2
-1.09760000E+04 1.51000000E+01 2.49700000E+00 1.79300000E-02-1.24500000E-05    3
 4.60900000E-09-7.05600000E-13-1.09760000E+04 1.51000000E+01 2.49700000E+00    4
HCS                     C   1H   1S   1    0G   200.000  6000.000  1000.       1
 4.24664932E+00 2.35823084E-03-8.25468697E-07 1.30882236E-10-7.73500263E-15    2
 3.24994581E+04 3.27483332E+00 3.79164958E+00-4.94798913E-04 1.27553978E-05    3
-1.73549729E-08 7.20528315E-12 3.27828773E+04 6.50582055E+00 3.39731635E+04    4
HNO4 HOONO2 Perox T 2/16H  1.N  1.O  4.   0.G   200.000  6000.000 1000.        1
 9.75692716E+00 5.63667100E-03-2.05043239E-06 3.34256715E-10-2.01600097E-14    2
-1.05073977E+04-2.26938087E+01 2.44847749E+00 2.85012019E-02-2.93784944E-05    3
 1.50460407E-08-2.95996331E-12-8.61184484E+03 1.44216960E+01-6.84626274E+03    4
H2NO                    H   2N   1O   1     G   298.150  3000.000 1000.00      1
 3.36485636E+00 6.13307432E-03-2.48863886E-06 4.83818467E-10-3.63995936E-14    2
 6.62654717E+03 6.75312730E+00 3.93370869E+00 2.21175605E-03 5.86220201E-06    3
-6.72931776E-09 2.17836171E-12 6.59507215E+03 4.42022091E+00                   4
HCN                     H   1C   1N   1     G   298.150  3000.000 1000.00      1
 2.92308097E+00 4.44713874E-03-2.18020741E-06 5.19245486E-10-4.87687163E-14    2
 1.47106866E+04 6.27783116E+00 2.22381158E+00 8.91348548E-03-1.13836313E-05    3
 8.32413060E-09-2.41730729E-12 1.47670770E+04 9.23408445E+00                   4
HCNN                    H   1C   1N   2     G   298.150  3000.000 1000.00      1
 4.28964676E+00 7.03402383E-03-3.73267471E-06 1.00945822E-09-1.08552184E-13    2
 5.41566507E+04 2.95663204E+00 2.60254129E+00 1.30917550E-02-1.17832354E-05    3
 5.68580799E-09-1.10496695E-12 5.45286063E+04 1.12686134E+01                   4
HCNO                    H   1C   1N   1O   1G   298.150  3000.000 1000.00      1
 4.55025354E+00 7.57617778E-03-4.21171419E-06 1.11675152E-09-1.14509217E-13    2
 1.86270490E+04 4.52782794E-01 3.86648136E+00 1.08161968E-02-9.82913817E-06    3
 5.36663113E-09-1.30321169E-12 1.87385569E+04 3.62535575E+00                   4
HNCO                    H   1C   1N   1O   1G   298.150  3000.000 1000.00      1
 4.16893487E+00 6.17767838E-03-2.35286422E-06 3.24605288E-10-8.03245562E-15    2
-1.59903892E+04 3.07758328E+00 1.86224719E+00 1.72234752E-02-2.16501287E-05    3
 1.50084945E-08-4.13376628E-12-1.56200040E+04 1.37512564E+01                   4
HNC                     H   1C   1N   1     G   298.150  3000.000 1000.00      1
 2.93269187E+00 3.80007742E-03-1.71416245E-06 3.79713171E-10-3.33567957E-14    2
 2.19789829E+04 6.19552896E+00 2.31995135E+00 6.47577653E-03-6.06481667E-06    3
 3.50488635E-09-8.70834349E-13 2.20902942E+04 9.09546350E+00                   4
HNO                     H   1N   1O   1     G   298.150  3000.000 1000.00      1
 2.58819802E+00 4.87708822E-03-2.29243315E-06 5.82214028E-10-5.94811743E-14    2
 1.20213574E+04 1.04315796E+01 4.51988078E+00-5.42507623E-03 1.70239636E-05    3
-1.48708172E-08 4.44763498E-12 1.17637925E+04 1.75618526E+00                   4
HNO2                    H   1N   1O   2     G   298.150  3000.000 1000.00      1
 2.71886798E+00 9.23249468E-03-5.00922160E-06 1.30155189E-09-1.30503734E-13    2
-6.61949139E+03 1.03430537E+01 2.86816457E+00 4.08036347E-03 9.55139253E-06    3
```

```
-1.29604691E-08 4.57373772E-12-6.42160346E+03 1.07615202E+01                   4
HOCN                  H   1C   1N   1O   1G   298.150  3000.000 1000.00      1
 4.26758218E+00 6.14779617E-03-2.91885336E-06 6.92686313E-10-6.47954836E-14    2
-3.34027063E+03 2.82895438E+00 2.77692030E+00 1.20359260E-02-1.16392715E-05    3
 6.43178073E-09-1.48093966E-12-3.03841237E+03 1.00391657E+01                   4
HONO2                 H   1N   1O   3    G   298.150  3000.000 1000.00      1
 5.28851491E+00 1.02507554E-02-6.01108580E-06 1.65260052E-09-1.73502753E-13    2
-1.85463799E+04-1.38461402E+00 1.03437078E+00 2.44807579E-02-2.31762285E-05    3
 1.03094550E-08-1.64107287E-12-1.75562224E+04 1.98358158E+01                   4
HONOc                 H   1N   1O   2    G   298.150  3000.000 1000.00      1
 4.51775109E+00 4.89769814E-03-1.68483435E-06 2.10450542E-10-5.17134670E-15    2
-1.06257968E+04 3.37616097E+00 3.39543853E+00 6.38325409E-03 5.92373117E-07    3
-4.31138204E-09 1.87621036E-12-1.02511495E+04 9.54159386E+00                   4
HONOt                 H   1N   1O   2    G   298.150  3000.000 1000.00      1
 4.19966671E+00 5.94217338E-03-2.95404834E-06 7.19846187E-10-6.74909061E-14    2
-1.08122769E+04 5.08809833E+00 3.49106617E+00 6.81116875E-03-1.30943120E-06    3
-2.34197204E-09 1.18931535E-12-1.05722865E+04 8.99803804E+00                   4
N2H3                  H   3N   2         G   298.150  3000.000 1000.00      1
 3.20302281E+00 7.99162955E-03-3.10892955E-06 5.91433018E-10-4.34549709E-14    2
 2.58689598E+04 8.45902214E+00 3.80271862E+00 5.52764141E-03 6.84860021E-07    3
-2.00296493E-09 6.21445742E-13 2.57522809E+04 5.58213774E+00                   4
N2H4                  H   4N   2         G   298.150  3000.000 1000.00      1
 3.21893892E+00 1.23204128E-02-5.44372150E-06 1.22223350E-09-1.10736520E-13    2
 1.05061274E+04 6.57037382E+00 9.42542945E-01 2.13488271E-02-1.88705886E-05    3
 1.00963087E-08-2.30996292E-12 1.09652651E+04 1.75719609E+01                   4
N2O                   N   2O   1         G   298.150  3000.000 1000.00      1
 3.61316907E+00 5.15970465E-03-2.97227625E-06 8.00505298E-10-8.26331952E-14    2
 8.60075126E+03 4.26880857E+00 2.49126356E+00 9.16224976E-03-8.24847853E-06    3
 3.83289657E-09-7.19461784E-13 8.84938621E+03 9.80262335E+00                   4
N2O3                  N   2O   3         G   298.150  3000.000 1000.00      1
 7.89162265E+00 7.26770322E-03-4.51928602E-06 1.31071704E-09-1.42420748E-13    2
 7.54353970E+03-1.13753920E+01 4.44942395E+00 1.69956247E-02-1.30498583E-05    3
 2.95689187E-09 4.56253878E-13 8.43402311E+03 6.24144529E+00                   4
N2O4                  N   2O   4         G   298.150  3000.000 1000.00      1
 8.07873654E+00 1.21148668E-02-7.75596278E-06 2.25245174E-09-2.44865233E-13    2
-2.24598670E+03-1.36767979E+01 4.01747657E+00 2.19402007E-02-1.28644048E-05    3
-7.61626136E-10 2.11358071E-12-1.11274941E+03 7.52136027E+00                   4
NCCN                  C   2N   2         G   298.150  3000.000 1000.00      1
 4.84080631E+00 6.38810486E-03-3.64903618E-06 9.79067071E-10-1.01200069E-13    2
 3.53620921E+04-7.30725902E-01 3.64573201E+00 1.27413947E-02-1.55384598E-05    3
 1.04783421E-08-2.86926697E-12 3.55224573E+04 4.64156863E+00                   4
NCN                   C   1N   2         G   298.150  3000.000 1000.00      1
 4.47903710E+00 4.18411508E-03-2.63288979E-06 7.49201653E-10-8.04623880E-14    2
 5.30622825E+04 1.83947963E-01 3.15727170E+00 7.25557223E-03-3.91666888E-06    3
-6.10550047E-10 8.13376644E-13 5.34374158E+04 7.11460304E+00                   4
NCO                   C   1N   1O   1    G   298.150  3000.000 1000.00      1
 3.77930605E+00 5.23935486E-03-3.11170901E-06 8.62141939E-10-9.12475403E-14    2
 1.34827126E+04 4.10147682E+00 2.80872271E+00 7.96075832E-03-5.45241934E-06    3
 1.26168560E-09 9.90990185E-14 1.37348757E+04 9.07421285E+00                   4
NH2                   H   2N   1         G   298.150  3000.000 1000.00      1
 2.62839610E+00 3.44379888E-03-1.08606365E-06 1.50714038E-10-4.59423280E-15    2
 2.15909586E+04 7.65372613E+00 3.97883538E+00-5.13888088E-04 2.68436156E-06    3
-9.18832600E-10-9.82251152E-14 2.12486673E+04 7.77619668E-01                   4
```

```
NH3                  H   3N   1         G   298.150  3000.000 1000.00      1
 1.07096958E+00 8.75466951E-03-3.33525419E-06 4.72015791E-10-1.13562571E-14    2
-5.77168689E+03 1.49517392E+01 3.26650510E+00 3.05892867E-03 5.78755223E-07    3
 9.49077412E-10-9.02221969E-13-6.36511405E+03 3.58794921E+00                   4
NH                   H   1N   1         G   298.150  3000.000 1000.00      1
 2.95100955E+00 9.09994439E-04-8.35582439E-08-5.17312027E-11 1.13981436E-14    2
 4.19707045E+04 4.83056694E+00 3.44697209E+00 5.57847818E-04-2.00289360E-06    3
 2.85952922E-09-1.12434284E-12 4.17899268E+04 2.02990852E+00                   4
NNH                  H   1N   2         G   298.150  3000.000 1000.00      1
 2.90981142E+00 4.44718211E-03-1.82919152E-06 3.64004342E-10-3.13273352E-14    2
 2.92696472E+04 9.11653812E+00 4.09254871E+00-2.37173287E-03 1.15311297E-05    3
-1.06308423E-08 3.23937580E-12 2.91374980E+04 3.93250587E+00                   4
NO                   N   1O   1         G   298.150  3000.000 1000.00      1
 2.79462839E+00 2.12260586E-03-1.11936971E-06 2.79521018E-10-2.68625363E-14    2
 1.00019069E+04 8.88322674E+00 4.15036687E+00-4.08890008E-03 9.38071726E-06    3
-7.50908901E-09 2.11742798E-12 9.77018679E+03 2.53971032E+00                   4
NO2                  N   1O   2         G   298.150  3000.000 1000.00      1
 3.65239279E+00 4.71632310E-03-2.74591748E-06 7.45382834E-10-7.63891108E-14    2
 2.57216137E+03 6.52683440E+00 3.39100918E+00 2.62448348E-03 5.09790306E-06    3
-7.62120493E-09 2.79960135E-12 2.78130679E+03 8.57220275E+00                   4
NO3                  N   1O   3         G   298.150  3000.000 1000.00      1
 6.38293838E+00 5.42422503E-03-3.34397780E-06 9.48445417E-10-1.01961714E-13    2
 6.35473962E+03-6.30266486E+00 3.09446759E+00 1.51014573E-02-1.26448498E-05    3
 3.67237581E-09 8.62184172E-14 7.18626632E+03 1.04314685E+01                   4
SN              T 5/12S  1.N  1.   0.   0.G   200.000  6000.000 1000.       1
 3.88274409E+00 6.69209785E-04-2.54355349E-07 4.37689407E-11-2.47821716E-15    2
 3.23072140E+04 4.24200506E+00 4.61308333E+00-6.97041575E-03 2.01423472E-05    3
-2.12369858E-08 7.79086026E-12 3.23593076E+04 1.78352487E+00 3.35645516E+04    4
SNO                  S   1N   1O   1     G   200.000  6000.000 1000.       1
 3.03600000E+00 8.79300000E-03-8.95500000E-06 4.53700000E-09-9.16600000E-13    2
 9.74600000E+03 7.82200000E+00 3.03600000E+00 8.79300000E-03-8.95500000E-06    3
 4.53700000E-09-9.16600000E-13 9.74600000E+03 7.82200000E+00                   4
HSNO            dummy  H   1S   1N   1O   1G   200.000  6000.000  1000.      1
 3.71700000E+00 1.26400000E-02-1.39600000E-05 8.30100000E-09-1.97300000E-12    2
 9.74600000E+03 7.82200000E+00 3.71700000E+00 1.26400000E-02-1.39600000E-05    3
 8.30100000E-09-1.97300000E-12 9.74600000E+03 7.82200000E+00                       4
O2(S)           ATcT06O  2.   0.   0.   0.G   200.000  6000.000 1000.       1
 3.45852381E+00 1.04045351E-03-2.79664041E-07 3.11439672E-11-8.55656058E-16    2
 1.02229063E+04 4.15264119E+00 3.78535371E+00-3.21928540E-03 1.12323443E-05    3
-1.17254068E-08 4.17659585E-12 1.02922572E+04 3.27320239E+00 1.13558105E+04    4
HO3  Equil/trans  T 1/14H  1.O  3.   0.   0.G   200.000  6000.000 1000.       1
 6.36926947E+00 3.02970087E-03-1.04545381E-06 1.64431465E-10-9.67182653E-15    2
 1.11737099E+03-5.67251572E+00 3.58948457E+00 1.08560963E-02-8.05640196E-06    3
 1.50289080E-09 6.16206428E-13 1.86115040E+03 8.60601405E+00 3.34595785E+03    4
CH3OO                 C   1H   3O   2     G   300.000  3000.000 1000.00      1
 2.88425280E+00 1.40067710E-02-6.88363514E-06 1.63789865E-09-1.53129010E-13    2
-2.00432571E+01 1.18152986E+01 2.93065328E+00 8.68504133E-03 8.80315108E-06    3
-1.39560866E-08 5.02939926E-12 2.27483038E+02 1.28754751E+01                   4
CH2OOH                C   1H   3O   2    0G   200.00   2500.00  1000.00      1
 6.98746029E+00 9.00484259E-03-3.24366912E-06 5.24324826E-10-3.13587080E-14    2
 5.01257769E+03-1.02619220E+01 5.83126679E+00-3.51771199E-03 4.54550577E-05    3
-5.66903320E-08 2.21633070E-11 6.06187060E+03-5.79143222E-01                   4
CHS2                 S 2  C 1  H 1      G    3E+02     2E+03    6E+02      1
```

```
 1.78227402E+00 1.84266329E-02-2.01226669E-05 1.05813349E-08-2.03753253E-12    2
 2.58434267E+04 1.76510876E+01 1.78227402E+00 1.84266329E-02-2.01226669E-05    3
CHS                  S 1  C 1  H 1      G     3E+02     2E+03   6E+02      1
 2.96088242E+00 5.92410544E-03-3.72132997E-06 1.85807328E-10 5.69493618E-13    2
 3.31074004E+04 9.20333175E+00 2.96088242E+00 5.92410544E-03-3.72132997E-06    3
 1.85807328E-10 5.69493618E-13 3.31074004E+04 9.20333175E+00                   4
CH4S                 S 1  C 1  H 4      G     3E+02     2E+03   6E+02      1
 4.51293142E+00 5.53073374E-04 2.28501494E-05-2.62285095E-08 9.43823134E-12    2
-4.14338015E+03 4.47095787E+00 4.51293142E+00 5.53073374E-04 2.28501494E-05    3
-2.62285095E-08 9.43823134E-12-4.14338015E+03 4.47095787E+00                   4
CH2SO                H   2C   1O   1S   1g    300.00   5000.00 1000.00      1
 6.32725630E+00 6.12318131E-03-2.34688321E-06 4.14471061E-10-2.76277591E-14    2
-1.06117303E+02-5.96519200E+00 6.63093834E-01 2.57025464E-02-2.85724811E-05    3
 1.63564574E-08-3.67095210E-12 1.24973488E+03 2.22873373E+01                   4
CH3SO                H   3C   1O   1S   1g    300.00   5000.00 1000.00      1
 6.25414196E+00 8.98670280E-03-3.45282520E-06 6.10523587E-10-4.07199592E-14    2
-1.09851534E+04-4.44902766E+00 2.47840898E+00 1.82043780E-02-9.52596218E-06    3
-4.71970539E-10 1.65663633E-12-9.86798339E+03 1.53819174E+01                   4
!
!
!
!
END
!
!
REACTIONS
!
!
  ! ********************************************
  ! *   H2/O2 Subset                           *
  ! ********************************************
  !
 H+O2=O+OH                          1.04E14    0.00    15286 !
 O+H2=H+OH                          3.82E12    0.00     7948 !
  DUP
 O+H2=H+OH                          8.79E14    0.00    19170 !
  DUP
 H2+OH=H2O+H                        2.16E08    1.51     3430 !
 OH+OH=O+H2O                         1.35E07    1.69    -1166 !
  DUP
 OH+OH=O+H2O                        -2.67E10    0.57        0 !
  DUP
 H2+M=H+H+M                         4.58E19   -1.40   104380 !
  H2/2.5/  H2O/12/  CO/1.9/ CO2/3.8/
 O+O+M=O2+M                         6.17E15   -0.50        0 !
  H2/2.5/  H2O/12/  CO/1.9/ CO2/3.8/
 O+H+M=OH+M                         4.71E18   -1.00        0 !
  H2/2.5/  H2O/12/  CO/1.9/ CO2/3.8/ AR/0.75/ !HE/0.75/
 H2O+M=H+OH+M                        6.06E27   -3.32   120790 !
  N2/2.0/  O2/1.5/  CO2/3.8/  !HE/1.1/
  H2O+H2O=H+OH+H2O                  1.01E26   -2.44   120180 !
 H+O2(+M)=HO2(+M)                   4.65E12    0.44        0 !
 LOW /6.37E20 -1.72 525/
 TROE/ 0.5 1E-30 1E30 /
  H2/2.0/  H2O/14/  CO/1.9/ CO2/3.8/ AR/0.67/ O2/0.78/ !HE/0.8/
 HO2+H=H2+O2                    2.75E06    2.09    -1451 !
 HO2+H=OH+OH                    7.08E13    0.00      295 !
 HO2+O=O2+OH                    2.85E10    1.00     -723 !
 HO2+OH=H2O+O2                  1.93E20   -2.49      584 !
  DUP
 HO2+OH=H2O+O2                  1.21E09    1.24    -1310 !
  DUP
 HO2+HO2=H2O2+O2                1.18E09    0.77    -1825 !
  DUP
 HO2+HO2=H2O2+O2                1.25E12    0.30     7397 !
  DUP
 H2O2 (+M)=OH+OH (+M)           2.00E12    0.90    48749 !
  LOW /2.49E24 -2.3 48749/
  TROE/ 0.43 1E-30 1E30 /
  H2/3.7/  H2O/7.5/  CO/2.8/ O2/1.2/ CO2/1.6/ N2/1.5/ H2O2/7.7/ !HE/0.65/
 H2O2+H=H2O+OH                  2.41E13    0.00     3970 !
 H2O2+H=HO2+H2                  1.70E12    0.00     3760 !
 H2O2+O=OH+HO2                  9.55E06    2.00     3970 !
 H2O2+OH=HO2+H2O                1.74E12    0.00      318 !
  DUP
 H2O2+OH=HO2+H2O                7.59E13    0.00     7270 !
  DUP
 H+HO2=O+H2O                    1.19E13    0.00         671 !
 O+OH+M=HO2+M                    1.00E15    0.00       0 !
  H2/2.00/ H2O/12.00/ AR/ .70/ HE/0.7/ CO/1.75/ CO2/3.6/
!*****O3*****
O+O2+M=O3+M                     1.88E21   -2.80        0 !
O+O3=O2+O2                      4.80E12    0.00     4090 !
H+O3=OH+O2                      8.43E13    0.00      950 !
OH+O3=HO2+O2                               1.14E12    0.00     2000 !
HO2+O3=OH+O2+O2                 8.43E09    0.00     1200 !
!
!
! ******************************************************
! ******************************************************
! *****************   NITROGEN subset  ******************
! ******************************************************
! ******************************************************
!
!
! ******************************************************
!    NO subset                                 *
! ******************************************************
!
 NO+H(+M)=HNO(+M)             1.52E15   -0.410      0 !
  LOW /2.357E+14 0.206 -1550/                       !
  TROE /0.82 1E-30 1E+30 1E+30/                     !
  N2/1.6/                                  !
 NO+O(+M)=NO2(+M)             1.30E15   -0.750      0 !
  LOW  /4.72E+24 -2.87 1550/                       ! (Fc=0.95-1E-04*T)
!  TROE /0.780 1E-30 1E+30 1E+30/                    ! (100bar)
!  TROE /0.800 1E-30 1E+30 1E+30/                     ! ( 80bar)
!  TROE /0.820 1E-30 1E+30 1E+30/                     ! ( 50bar)
  TROE /0.850 1E-30 1E+30 1E+30/                     ! ( 20bar)
!  TROE /0.870 1E-30 1E+30 1E+30/                     ! ( 10bar)
!  TROE /0.880 1E+03 1E+04 1E+30/                     ! (  1bar)
   AR/0/                                         !
 NO+O(+AR)=NO2(+AR)           1.30E15   -0.75       0 !
   LOW  /7.56E+19 -1.41 0/                          ! (Fc=0.95-1E-04*T)
!  TROE /0.790 1E-30 1E+30 1E+30/                     ! (100bar)
!  TROE /0.810 1E-30 1E+30 1E+30/                     ! ( 80bar)
!  TROE /0.830 1E-30 1E+30 1E+30/                     ! ( 50bar)
  TROE /0.860 1E-30 1E+30 1E+30/                     ! ( 20bar)
!  TROE /0.955 1E-30 1E+04 1E+30/                     ! ( 10bar)
!  TROE /0.750 1E+03 1E+05 1E+30/                     ! (  1bar)
 NO+OH(+M)=HONO(+M)           1.10E14   -0.300      0 !
   LOW  /3.392E+23 -2.5 0/                          !
   TROE /0.75 1E-30 1E+30 1E+30/                     ! [M=He,T=400K]
 NO+HO2=NO2+OH                2.32E10    0.58     1433 !
!
!
! *******************************************************
!    NO2 subset                                *
! *******************************************************
!
 NO2+H=NO+OH                  8.85E13    0.0        0 !
 NO2+H2=HONO+H                 400       2.76    29770 !
 NO2+H2=HNO2+H                2.39E02    3.15    31100 !
 NO2+O=NO+O2                  1.05E14   -0.52       0 !
 NO2+O(+M)=NO3(+M)            3.52E12    0.24       0 !
   LOW  /2.450E+20 -1.50 0/                          !
   TROE /0.71 1E-30 1700 1E+30/                       !  Fc=0.71*exp(-T/1700)
 NO2+OH(+M)=HONO2(+M)         3.00E13    0.0        0 !
   LOW  /2.938E+25 -3.0 0/                          !
   TROE /0.4 1E-30 1E+30 1E+30/                       !  Fc=0.4
 NO2+HO2=HONO+O2              1.91E00    3.32     3044 !
 NO2+HO2=HNO2+O2              1.85E01    3.26     4983 !
 NO+NO+O2=NO2+NO2             1.20E09    0.00    -1850 !
 NO2+NO2=NO3+NO               9.64E09    0.73    20900 !
 NO2+NO(+M)=N2O3(+M)          1.62E09    1.40       0 !
   LOW  /1.33E+33 -7.7 0/
   TROE /0.6 1E-30 1E+30 1E+30/
 NO2+NO2(+M)=N2O4(+M)         6.020E11   0.00       0 !
   LOW  /1.314E+24 -3.8 0/
   TROE /0.4 1E-30 1E+30 1E+30/
 NO2+OH+M=HNO3+M              5.81E32       -5.40    2186 !
 N2O4+H2O=HONO+HNO3                        2.52E14    0.00       11600 !
!
!
! *******************************************************
!    NO3 subset                                *
! *******************************************************
!
 NO3+H=NO2+OH                 6.0E13     0.0        0 !
 NO3+O=NO2+O2                 1.0E13     0.0         0 !
 NO3+OH=NO2+HO2                1.4E13     0.0         0 !
 NO3+HO2=NO2+O2+OH             1.5E12     0.0         0 !
 NO3+NO2=NO+NO2+O2             5.0E10     0.0      2940 !
!
!
! ********************************************************
!    HNO subset                              *
! ********************************************************
!
 HNO+H=NO+H2                 4.40E11    0.72      650 !
 HNO+O=NO+OH                 2.30E13    0.00        0 !
 HNO+OH=NO+H2O               1.30E07    1.88     -956 !
 HNO+O2=HO2+NO               2.00E13    0.00    16000 !
 HNO+NO2=HONO+NO             4.42E04    2.64     4040 !
 HNO+HNO=N2O+H2O             9.00E08    0.00     3100 !
 HNO+NH2=NH3+NO              3.63E06    1.63    -1252 !
!
!
! ********************************************************
!    HONO subset                              *
! ********************************************************
!
 HONO+O=NO2+OH               1.20E13    0.00     5960 !
 HONO+OH=NO2+H2O             1.70E12    0.00     -520 !
 HONO+NO2=HONO2+NO           2.00E11    0.00    32700 !
 HONO+HONO=NO+NO2+H2O        3.49E-01   3.64    12140 !
!
!
! ********************************************************
!    HNO2 subset                              *
! ********************************************************
!
 HNO2(+M)=HONO(+M)           2.5E14     0.0     32300 !
   LOW  /3.1E+18 0.0 31500/
   TROE /1.149 1E-30 3125 1E+30/
 HNO2+O=NO2+OH               1.7E08     1.5      2000 !
 HNO2+OH=NO2+H2O             4.0E13     0.0         0 !
!
!
! ********************************************************
!    HONO2 subset                              *
! ********************************************************
!
 HONO2+H=H2+NO3              5.56E08    1.5     16400 !
 HONO2+H=H2O+NO2             6.08E01    3.3      6285 !
 HONO2+H=OH+HONO             3.82E05    2.3      6976 !
 HONO2+OH=H2O+NO3            1.03E10    0.0     -1240 !
!
!
! ********************************************************
!    H2NO subset                              *
! ********************************************************
```

```
!
 H2NO+M=HNO+H+M                    2.5E15     0.0     50000 !
   H2O/5/  N2/2/
 H2NO+H=HNO+H2               3.0E07     2.0      2000 !
 H2NO+H=NH2+OH               5.0E13     0.0         0 !
 H2NO+O=HNO+OH               3.0E07     2.0      2000 !
 H2NO+O = NH2+O2             2.0E14     0.0         0 !
 H2NO+OH=HNO+H2O               2.0E07     2.0      1000 !
 H2NO+NO=HNO+HNO               2.0E04     2.0     13000 !
 H2NO+NO2=HNO+HONO               6.0E11     0.0      2000 !
!
!
! *******************************************************
!    NH3 subset                              *
! *******************************************************
!
 NH3+M = NH2+H+M              2.2E16     0.00    93470 !
 NH3+H=NH2+H2                6.4E05     2.39    10171 !
 NH3+O=NH2+OH                9.4E06     1.94     6460 !
 NH3+OH=NH2+H2O              2.0E06     2.04      566 !
 NH3+HO2=NH2+H2O2              3.0E11     0.00    22000 !
!
!
! *******************************************************
!    NH2 subset                              *
! *******************************************************
!
 NH2+H=NH+H2                 4.0E13     0.00     3650 !
 NH2+O=HNO+H                 6.6E14    -0.50        0 !
 NH2+O=NH+OH                 6.8E12     0.00        0 !
 NH2+OH=NH+H2O                 4.0E06     2.00     1000 !
 NH2+HO2=H2NO+OH               5.0E13     0.00        0 !
 NH2+HO2=NH3+O2              1.0E13     0.00        0 !
 NH2+NO=NNH+OH               8.9E12    -0.35        0 !
 NH2+NO=N2+H2O               1.3E16    -1.25        0 !
   DUP
 NH2+NO=N2+H2O              -8.9E12    -0.35        0 !
   DUP
 NH2+NO2=N2O+H2O               3.2E18    -2.20        0 !
 NH2+NO2=H2NO+NO               3.5E12     0.00        0 !
 NH2+H2NO=NH3+HNO               3.0E12     0.00     1000 !
!
!
! *******************************************************
!    NH subset                                    *
! *******************************************************
!
 NH+H=N+H2                   3.0E13     0.00        0 !
 NH+O=NO+H                   9.2E13     0.00        0 !
 NH+OH=HNO+H                   2.0E13     0.00        0 !
 NH+OH=N+H2O                   5.0E11     0.50     2000 !
 NH+O2=HNO+O                   4.6E05     2.00     6500 !
 NH+O2=NO+OH                   1.3E06     1.50      100 !
```

```
NH+NO=N2O+H              2.9E14   -0.40      0 !
  DUP
NH+NO=N2O+H             -2.2E13   -0.23      0 !
  DUP
NH+NO=N2+OH              2.2E13   -0.23      0 !
NH+NO2=N2O+OH              1.0E13    0.00      0 !
NH+NH=N2+H+H              2.5E13    0.00      0 !
NH+N=N2+H               3.0E13    0.00      0 !
HNO+H2=NH+H2O                          7.0E08    0.00      0 !
!
!
! *******************************************************
!   N subset                                      *
! *******************************************************
!
N+OH=NO+H                3.8E13    0.0       0 !
N+O2=NO+O               6.4E09    1.0     6280 !
N+NO=N2+O               3.3E12    0.3       0 !
!
!
! *******************************************************
!   N2H2 subset                             *
! *******************************************************
!
N2H2+M=NNH+H+M             5.0E16    0.0    50000 !
  H2O/15/ O2/2/ N2/2/ H2/2/
N2H2+H=NNH+H2             5.0E13    0.0     1000 !
N2H2+O=NH2+NO             1.0E13    0.0       0 !
N2H2+O=NNH+OH             2.0E13    0.0     1000 !
N2H2+OH=NNH+H2O            1.0E13    0.0     1000 !
N2H2+NO=N2O+NH2            3.0E12    0.0       0 !
N2H2+NH2=NH3+NNH           1.0E13    0.0     1000 !
N2H2+NH=NNH+NH2            1.0E13    0.0     1000 !
!
!
! *******************************************************
!   NNH subset                              *
! *******************************************************
!
NNH=N2+H                1.0E07    0.0       0 !
NNH+H=N2+H2              1.0E14    0.0       0 !
NNH+O=N2+OH              8.0E13    0.0       0 !
NNH+O=N2O+H              1.0E14    0.0       0 !
NNH+O=NH+NO              5.0E13    0.0       0 !
NNH+OH=N2+H2O             5.0E13    0.0       0 !
NNH+O2=N2+HO2             2.0E14    0.0       0 !
NNH+O2=N2+O2+H            5.0E13    0.0       0 !
NNH+NO=N2+HNO             5.0E13    0.0       0 !
NNH+NH2=N2+NH3            5.0E13    0.0       0 !
NNH+NH=N2+NH2             5.0E13    0.0       0 !
!
!
! *******************************************************
!   N2O subset                              *
! ******************************************************
!
 N2O+M=N2+O+M                4.0E14     0.00    56100 !
   N2/1.7/   O2/1.4/ H2O/12/ CO/1.5/  CO2/3/
 N2O+H=N2+OH                 3.3E10     0.00     4729 !
   DUP
 N2O+H=N2+OH                 4.4E14     0.00    19254 !
   DUP
 N2O+O=NO+NO                 6.6E13     0.00    26630 !
 N2O+O=N2+O2                 1.0E14     0.00    28000 !
 N2O+OH=N2+HO2               1.3E-2     4.72    36561 !
 N2O+OH=HNO+NO               1.2E-4     4.33    25081 !
 N2O+NO=NO2+N2               5.3E05     2.23    46281 !
!
!
! ******************************************************
!   ANTIGUAS                                         *
! ******************************************************
!
NO2+SO=SO2+NO                              8.43E12    0.00       0 !
NO2+SO2=SO3+NO           6.31E12    0.00    2.7E4 !
NO2+SH=HSO+NO                                   1.75E13    0.00    -477 !
NH+SO=NO+SH                         3.00E13    0.00       0 !
SH+NH=SN+H2                         1.00E13    0.00       0 !
SN+OH=SH+NO                         1.00E13    0.00       0 !
SO+N=S+NO                           7.00E12    0.00          0 !
SO2+N=SO+NO                         6.40E09    1.00       6280 !
SO2+NH=SO+HNO                                 5.00E12    0.00       20000 !
S+NO(+M)=SNO(+M)                    3.40E13    0.24          0 !
            LOW/2.2E15        0.00       -1870/
            TROE/0.22 7445 1E+30 1E+30/
SH+NO(+M)=HSNO(+M)          1.60E13          0.00          0 !
            LOW/1.4E23        -2.50      0/
            TROE/0.5 1E30 1E-30/
SN+O=S+NO                     3.00E12          0.00          0 !
SNO+H=SH+NO                   1.00E13          0.00          0 !
S+HNO=SH+NO                   1.00E13          0.00          0 !
H2S+NO2=S+NO+H2O                    1.00E08    0.00          0 !
!
!
! *****************************************************
! *   H2S subset                        *
! *****************************************************
!
! *****************************************************
! *   H2S reactions                         *
! *****************************************************
!
H2S+M = S+H2+M                      1.6E24    -2.61    89100 !
   N2/1.5/ SO2/10/ H2O/10/
H2S+S = SH+SH                       7.4E06     2.30     9007 !
DUP
```

```
H2S+S=SH+SH                 1.2E18   -1.69    5970 !
DUP
H2S+H = SH+H2                          3.5E07    1.94     904 !
H2S+O = SH+OH                          7.5E07    1.75    2900 !
H2S+OH = SH+H2O                        8.7E13   -0.70       0 !
DUP
H2S+OH = SH+H2O                        4.1E07    1.77       0 !
DUP
SH+H2O2=H2S+HO2                        5.0E12    0.00       0 !
H2S+HO2=HSO+H2O                        1.0E00    3.29    6224 !
SH+HO2=H2S+O2                          3.8E04    2.78   -1529 !
H2S+O2=HSO+OH                          1.0E11    0.00   49100 !
H2S+O3=SO2+H2O              1.7E03    2.67   11390 !
 DUP
H2S+O3=SO2+H2O              1.3E04    2.19   11607 !
 DUP
H2S+O3=SO2+H2O              5.3E08    1.66   11655 !
 DUP
H2S+O3=HOSO+OH                         1.1E03    2.77   11369 !
H2S+SO(S)=HSO+SH                       1.0E13    0.00   11000 !
H2S+SO=SH+HOS                          1.0E13    0.00   36500 !
H2S+SO2=S2O+H2O                        1.7E06    1.86   37740 !
H2S+S(+M)=H2S2(+M)                     6.4E07    1.28    -478 !
   LOW /2.4E21 -1.612 1670/
   TROE /0.5 726 726/
H2S+SO2=H2S2O2              3.5E18   -2.12   33530 !
H2S+HSO=SH+HSOH             1.0E13    0.00   17300 !
H2S+HOS=SH+HSOH             1.0E13    0.00   12500 !
H2S+S2O=H2S3O                          2.4E19   -2.30   30450 !
H2S+S2O=S3+H2O                                    8.0E07    1.51   34010 !
H2S+S2O=HSSSOH                                    2.9E00    3.64   22681 !
!
! *****************************************************
! *   HS2/H2S2 reactions                            *
! *****************************************************
!
!
HS2+H=H2S+S                            1.5E08    1.55    2259 !
DUP
HS2+H=H2S+S                            4.2E18   -1.56     472 !
DUP
HS2+H=H2+S2                 1.0E08    1.75    -877 !
DUP
HS2+H=H2+S2                 2.9E16   -0.89     -56 !
DUP
HS2+H+M = H2S2+M                       1.0E16    0.00       0 !
HS2+H=SH+SH                            9.7E07    1.62   -1030 !
DUP
HS2+H=SH+SH                            1.6E18   -0.98     261 !
DUP
HS2+O = S2+OH                          1.0E14    0.00       0 !
HS2+OH = S2+H2O                        1.0E14    0.00       0 !
HS2+O2=S2+HO2                          8.4E01    2.95    7071 !
```

```
HS2+SH=S2+H2S                   6.3E03    3.05    -1105 !
HS2+S = S2+SH                   4.2E06    2.20     -600 !
H2S2+H=HS2+H2                   5.0E07    1.93    -1408 !
H2S2+O = HS2+OH                 7.5E07    1.75     2900 !
H2S2+OH = HS2+H2O               1.0E13    0.00        0 !
H2S2+S=HS2+SH                   2.9E06    2.30     1204 !
H2S2+SH=HS2+H2S                           6.4E03    2.98    -1480 !
HS2+O2=HSO+SO                   6.6E03    1.90     7071 !
H2S2+H=H2S+SH                   3.7E08    1.72      477 !
H2S2+O=HSO+SH                   1.0E14    0.00        0 !
H2S2+HO2=HS2+H2O2               1.0E13    0.00        0 !
H2S2+O2=HS2+HO2                           1.0E13    0.00    26000 !
H2S2+SO=HS2+HSO                           1.0E13    0.00    15000 !
H2S2+SO=HS2+HOS                           1.0E13    0.00    19000 !
H2S2+HSO=HS2+HSOH               1.0E13    0.00     2000 !
H2S2+HOS=HS2+HSOH               1.0E13    0.00     2000 !
HS2+O=SH+SO                     1.0E14    0.00        0 !
HS2+HO2=S2+H2O2                           1.0E13    0.00        0 !
HS2+SO=S3+OH                    1.0E13    0.00    14900 !
HS2+SO3=HS2O+SO2                1.0E13    0.00    10000 !
HS2+HSO=HS2O+SH                           1.0E13    0.00     7000 !
HS2+HSO=S2+HSOH                           1.0E13    0.00        0 !
HS2+HOS=S2+HSOH                           1.0E13    0.00        0 !
HS2+HS2=H2S2+S2                           9.6E00    3.37    -1672 !
HS2+O2=HS2O+O                             1.0E13     0.00       26000 !
!
!
! *******************************************************
! *   SH reactions                         *
! *******************************************************
!
SH+O = H+SO                     4.25E11   0.72    -1027 !
SH+O=S+OH                       1.80E12   0.00        0 !
DUP
SH+O=S+OH                       4.3E06    2.10     3583 !
DUP
SH+OH=S+H2O                     1.0E14    0.00           0 !
SH+OH=HOS+H                     1.0E13    0.00     7400 !
SH+HO2=SO+H2O                   3.2E02    2.58    -2071 !
SH+HO2=HSO+OH                   2.5E08    1.48    -2169 !
S+H2O2=SH+HO2                   4.1E06    2.20    12619 !
SH+O2=HSO+O                     2.3E06    1.82    20008 !
SH+O2=S+HO2                     4.7E06    2.02    36913 !
SH+O2=SO+OH                     7.5E04    2.05    16384 !
SH+O2=SO2+H                     1.5E05    2.12    11020 !
SH+O2(+M)=HSOO(+M)              8.7E14   -0.26      298 !
          LOW /3.1E19 -0.201 20/
SH+O3=HSO+O2                    5.7E12    0.00      556 !
SH+H2O2=HSOH+OH                 9.5E03    2.80     9829 !
SH+SH(+M)=H2S2(+M)              9.0E11    0.16    -1432 !
          LOW /2.3E31 -4.94 1998/
          TROE/ 1.0 254 2373 /
SH+S=S2+H                       3.3E12    0.54      -29 !
```

```
SH+SO=HSO+S               1.0E13    0.00    25000 !
SH+SO=HOS+S                         1.0E13    0.00    30000 !
SH+HSO=S+HSOH                                 1.0E11    0.00    11000 !
SH+HSO=S2O+H2                       1.0E14    0.00    14250 !
SH+SO=S2O+H                         1.0E12    0.00     5000 !
SH+SO2=HSO+SO                       1.0E14    0.00    32000 !
SH+SO2=HOS+SO                       1.0E14    0.00    36000 !
SH+SO2=OH+S2O                                 1.0E14    0.00    32000 !
SH+SO2=HSSO2                        1.0E13    0.00    33000 !
SH+H2O2=H2O+HSO                               1.0E12     0.00          0 !
HSO+H2O2=HSO2+H2O                   1.0E12     0.00          0 !
!
!
!
! ******************************************************
! *   S/S2/S3... reactions                             *
! ******************************************************
!
S+H+M=SH+M                          6.2E16    -0.60       0 !
S+H2 = SH+H                         1.4E14    0.00    19300 !
S+OH = H+SO                         1.5E13    0.20    -1361 !
S+HO2=SO+OH                         5.7E13    0.00        0 !
S+O2 = SO+O                         5.4E05    2.10    -1450 !
S+HO2=HOS+O                         1.0E13    0.00        0 !
S+O3=SO+O2                          7.2E12    0.00        0 !
S+H2O2=HOS+OH                                 1.0E12    0.00       0 !
S+S(+M)=S2(+M)            1.4E10    0.00    -825 !
   LOW  /7.2E14 0.0 -408 /
S2+H+M=HS2+M              1.2E25    -2.84    1665 !
   H2S /1.1/ AR /0.88/
S2+O=SO+S                 1.4E11    0.70    -231 !
S2+O+M=S2O+M                        1.9E21    -2.80       0 !
S2+O2=S2O+O                         1.7E04    2.54    34376 !
S2+O2=SO+SO                         2.3E00    2.45    30440 !
S2+S+M=S3+M               1.9E15    0.00    -1788 !
S2+S2+M=S4+M              1.9E15    0.00    -1788 !
S3+H2O=HSSSOH             1.0E14    0.00    25000 !
S3+S2+M=S5+M              1.9E15    0.00    -1788 !
S3+S3+M=S6+M              1.9E15    0.00    -1788 !
S3+S2O=S4+SO              1.0E14    0.00    16000 !
S3+S4+M=S7+M              1.9E15    0.00    -1788 !
S4+S4+M=S8+M              1.9E15    0.00    -1788 !
!
!
! ******************************************************
! *   S2O reactions                            *
! ******************************************************
!
S2O+H2=SH+HOS                       1.0E13    0.00    46000 !
S2O+H+M=HS2O+M            6.4E22    -2.59     287 !
S2O+H=OH+S2               1.0E13    0.00        0 !
S2O+O=SO+SO               9.3E11    0.00        0 !
S2O+OH=S2+HO2             1.0E13    0.00    40000 !
```

```
S2O+S=SO+S2                 1.0E13    0.00       0 !
S2O+SH=HSO+S2               1.0E12    0.00    5000 !
S2O+SH=HS2+SO               1.0E13    0.00    8000 !
S2O+SH=S3+OH                1.0E13    0.00   21450 !
S2O+SO2=S2+SO3              1.0E13    0.00   20000 !
S2O+HSO2=HS2O+SO2                     1.0E13    0.00   32000 !
S2O+S2=S3+SO                1.0E14    0.00   18000 !
S2O+S2O=S3+SO2              1.0E12    0.00    2600 !
!
!
! *****************************************************
! *   SOx reactions                         *
! *****************************************************
!
SO+O+M=SO2+M                4.1E22    -2.17      0 !
 N2/1.5/ SO2/10/ H2O/10/
SO+M = S+O+M                          4.0E14    0.00   107000 !
SO+O2=SO2+O                           7.6E03    2.37     2970 !
SO+HO2=SO2+OH                         1.0E12    0.00        0 !
SO+H+M=HSO+M                          1.9E20    -1.31     662 !
    N2/1.5/ SO2/10/ H2O/10/
SO+O3=SO2+O2                          2.7E12    0.00     2325 !
SO+S+M=S2O+M                                    4.1E22    -2.170      0 !
    N2/1.5/ SO2/10/ H2O/10/
SO+SH=S2+OH                           1.0E12    0.00     4320 !
SO(S)+M=SO+M                          1.0E13    0.00        0 !
SO(S)+O2=SO2+O                        1.0E13    0.00        0 !
SO2+H=SO+OH                           6.7E21    -2.22   30736 !
H+SO+M=HOS+M                3.6E20    -1.92     -29 !
 N2 /0/
H+SO+N2=HOS+N2              2.0E21    -2.09     -72 !
SO2*+M = SO2+M                        1.3E14    0.00     3600 !
SO2*+SO2 = SO3+SO                     2.6E12    0.00     2430 !
SO2+O(+M) = SO3(+M)                   3.7E11    0.00     1689 !
   LOW/2.9E27 -3.58 5206/ !
   TROE/0.43 371 7442/
   SO2/10/ H2O/10/ N2/1/ !CO2/10/
SO2+OH(+M)=HOSO2(+M)                            5.7E12    -0.27      0 !
   LOW/1.7E27 -4.09 0/ !
   TROE/0.10 1E-30 1E+30/
   N2/1.0/ SO2/5/ H2O/5/ !CO2/2.5/
SO2+O3=SO3+O2                                   1.8E12    0.00   14000 !
SO2+S=SO+SO                           6.0E-16   8.21    -9600 !
SO3+H = HOSO+O                        2.5E05    2.92    50300 !
SO3+H = SO2+OH                        8.4E09    1.22     3319 !
SO3+O = SO2+O2                        2.8E04    2.57    29212 !
SO3+OH = SO2+HO2                      4.8E04    2.46    27225 !
SO3+SO=SO2+SO2                        7.6E03    2.37     2980 !
SO3+S=SO+SO2                          1.0E13    0.00        0 !
!
!
! *****************************************************
! *   HSO/HOS reactions                         *
! *****************************************************
!
HSO+O2=SO+HO2                 6.4E05    2.63    19013 !
DUP
HSO+O2=SO+HO2                 2.9E01    3.20    14529 !
DUP
HSO+O2=HSO2+O                 8.4E-7    5.10    11312 !
HSO+O2=SO2+OH                 3.7E01    2.76     6575 !
HSO+O3=SH+O2+O2               1.5E12    0.00     2230 !
HSO+O3=HSO2+O2                1.3E12    0.00     2230 !
HSO+O3=SO+OH+O2               5.0E00    3.60     7191 !
HSO+H = HSOH                  2.5E20   -3.14      920 !
HSO+H = SH+OH                 4.9E19   -1.86     1560 !
HSO+H = S+H2O                 1.6E09    1.37     -340 !
HSO+H = H2SO                  1.8E17   -2.47       50 !
H2S+O=HSO+H                   1.4E09    1.10     5099 !
HSO+H = SO+H2                 1.0E13    0.00        0 !
HSO+O+M = HSO2+M              1.1E19   -1.73      -50 !
HSO+O = SO2+H                 4.5E14   -0.40        0 !
HSO+O+M = HOSO+M              6.9E19   -1.61     1590 !
HSO+O = O+HOS                 4.8E08    1.02     5340 !
HSO+O = OH+SO                 1.4E13    0.15      300 !
HSO+OH = HOSHO                5.2E28   -5.44     3170 !
HSO+OH = HOSO+H               5.3E07    1.57     3750 !
HSO+OH = SO+H2O               1.7E09    1.03      470 !
HSOO(+M)=HSO+O(+M)            2.0E19   -1.07    28374 !
   LOW  /9.3E34 -5.87 30957/
HSO+H=HOS+H                   1.0E14    0.00     4000 !
HSO+OH=H2+SO2                        1.0E11    0.00       0 !
HSO+HO2=SO+H2O2                      1.0E13    0.00       0 !
HSO+HSO=SO+HSOH                      1.0E13    0.00       0 !
HSO+S2=HS2+SO                 1.0E12    0.00     3000 !
HOS+M=HSO+M            5.8E11    0.00   32722 !
   N2 /0/
HOS+N2=HSO+N2          2.9E11    0.00   24601 !
HOS+H=H2+SO                   1.0E13    0.00        0 !
HOS+O=OH+SO                   1.0E14    0.00        0 !
HOS+O=H+SO2                   1.0E14    0.00        0 !
HOS+OH=SO+H2O                        1.0E13    0.00       0 !
HOS+OH=H2+SO2                        1.0E11    0.00       0 !
HOS+O2=HO2+SO                        6.4E05    2.63   19013 !
HOS+O2=SO2+OH                        3.7E01    2.76    6575 !
HOS+HO2=SO+H2O2                      1.0E13    0.00       0 !
HOS+HOS=SO+HSOH                      1.0E13    0.00       0 !
HOS+S2=HS2+SO                 1.0E12    0.00     1000 !
HOS+S2=S3+OH                  1.0E13    0.00    13000 !
HSO+SH=SO+H2S                 1.0E13     0.00         0 !
!
!
! *****************************************************
! *   HSOH reactions                      *
! *****************************************************
!
```

```
HSOH = SH+OH             2.8E39   -8.75   75200 !
HSOH = S+H2O             5.8E29   -5.60   54500 !
HSOH = H2S+O             9.8E16   -3.40   86500 !
HSOH+HO2=HSO+H2O2        1.0E13    0.00       0 !
HSOH+HO2=HOS+H2O2        1.0E13    0.00       0 !
HSOH+O2=HSO+HO2                1.0E13    0.00   26000 !
HSOH+O2=HOS+HO2                1.0E13    0.00   30000 !
HSOH+O=HSO+OH                  1.0E14    0.00       0 !
HSOH+O=HOS+OH                  1.0E14    0.00       0 !
HSOH+H=HSO+H2                  1.0E14    0.00       0 !
HSOH+H=HOS+H2                  1.0E14    0.00       0 !
HSOH+OH=HSO+H2O                1.0E14    0.00       0 !
HSOH+OH=HOS+H2O                1.0E14    0.00       0 !
!
!
! ***************************************************
! *   HOSO reactions                        *
! ***************************************************
!
HOSO(+M)=H+SO2(+M)       1.7E10    0.80   46933 !
   LOW/1.5E31 -4.53 49178/
   TROE/0.30 1E-30 1E30/
   N2/1.0/ SO2/10/ H2O/10/
HOSO(+M) = HSO2(+M)      1.0E09    1.03   50000 !
   LOW/1.7E35 -5.64 55400/
   TROE/0.40 1.E-30 1.E30/
   N2/1.0/ SO2/10/ H2O/10/ !CO2/2.5/
HOSO(+M)=OH+SO(+M)       9.9E21   -2.54   75891 !
   LOW /1.2E46 -9.020 52953/
   TROE/0.95 2989 1.1/
HOSO+M = O+HOS+M         2.5E30   -4.80  119000 !
HOSO+H=SO(S)+H2O         2.4E14    0.00       0 !
HOSO+H=SO2+H2            1.8E07    1.72   -1286 !
HOSO+O=SO2+OH                  1.0E13    0.00       0 !
HOSO+OH=SO2+H2O          6.0E12    0.00       0 !
HOSO+HO2=SO2+H2O2        1.0E13    0.00       0 !
HOSO+O2=SO2+HO2          1.0E12    0.00     500 !
HOSO+SH=SO2+H2S                1.0E13    0.00       0 !
HOSO+S=SO2+SH            1.0E13    0.00       0 !
HOSO+SO=SO2+HSO                1.0E13    0.00       0 !
HOSO+SO=SO2+HOS                1.0E13    0.00       0 !
HOSO+HSO=SO2+HSOH        1.0E13    0.00       0 !
HOSO+HOS=SO2+HSOH        1.0E13    0.00       0 !
HOSO+HS2=SO2+H2S2        1.0E13    0.00       0 !
HOSO+S2=SO2+HS2                1.0E13    0.00       0 !
!
!
! ***************************************************
! *   HSO2 reactions                        *
! ***************************************************
!
H+SO2(+M)=HSO2(+M)       5.31E8    1.59    2472 !
   LOW/1.41E31 -5.19 4513/
```

```
  TROE/0.390 167 2191/
  N2/1.0/ SO2/10/ H2O/10/ !CO2/2.5/
HSO2+H = SO2+H2             5.0E12   0.46    -262 !
HSO2+O2 = HO2+SO2           1.10E3   3.20    -235 !
HSO2+O=SO2+OH                      1.0E13   0.00      0 !
HSO2+OH=SO2+H2O                    1.0E13   0.00      0 !
HSO2+HO2=SO2+H2O2           1.0E13   0.00      0 !
HSO2+O3=SO2+OH+O2           1.0E13   0.00      0 !
HSO2+SH=SO2+H2S                    1.0E13   0.00      0 !
HSO2+S=SO2+SH               1.0E13   0.00      0 !
HSO2+SO=SO2+HSO                    1.0E13   0.00      0 !
HSO2+SO=SO2+HOS                    1.0E13   0.00      0 !
HSO2+HSO=SO2+HSOH           1.0E13   0.00      0 !
HSO2+HS2=SO2+H2S2           1.0E13   0.00      0 !
HSO2+S2=SO2+HS2                    1.0E13   0.00      0 !
HSOO=HSO2                   1.0E17   0.00   21300 !
!
!
! ******************************************************
! *   HS2O reactions                *
! ******************************************************
!
HS2O+H=S2O+H2                      1.0E12   0.00    2600 !
HS2O+H=HS2+OH                      1.0E13   0.00          0 !
HS2O+O=S2O+OH                      1.0E13   0.00      0 !
HS2O+O=SH+SO2                      1.0E13   0.00      0 !
HS2O+OH=S2O+H2O                    1.0E13   0.00      0 !
HS2O+OH=HS2+HO2                    1.0E13   0.00   27000 !
HS2O+HO2=S2O+H2O2           1.0E13   0.00      0 !
HS2O+S=HS2+SO               1.0E13   0.00      0 !
HS2O+S=S2O+SH                      1.0E13   0.00      0 !
HS2O+SH=S2O+H2S                    1.0E13   0.00      0 !
HS2O+HS2=S2O+H2S2           1.0E13   0.00      0 !
HS2O+S2=S2O+HS2                    1.0E13    0.00         0 !
!
!
! ******************************************************
! *   SS2O2 reactions                *
! ******************************************************
!
SO2+S(+M)=SSO2(+M)     3.7E12    0.00    1689 !
  LOW  /2.9E28 -3.58 5206/
  TROE /0.43 371 7442/
  N2/1/ SO2/10/ H2O/10/
SSO2+H=SH+SO2               1.0E13   0.00      0 !
SSO2+O=SO+SO2               1.0E13   0.00         0 !
SSO2+OH=HOS+SO2                    1.0E13   0.00      0 !
SSO2+S=S2+SO2               1.0E13   0.00      0 !
!
!
! ******************************************************
! *   OSSO reactions                *
! ******************************************************
```

```
!
SO+SO+M=OSSO+M                     3.2E32   -5.75       3044 !
OSSO+H=OH+S2O                      1.0E13    0.00          0 !
OSSO+H=SO+HSO                      1.0E13    0.00          0 !
OSSO+H=SO+HOS                      1.0E13    0.00          0 !
OSSO+H=HO2+S2                      1.0E13    0.00   12570 !
OSSO+O=SO+SO2                      1.0E13    0.00      0 !
OSSO+O=O2+S2O                      1.0E13    0.00      0 !
OSSO+OH=HO2+S2O                    1.0E13    0.00   11350 !
OSSO+OH=HOSO+SO                    1.0E12    0.00      0 !
OSSO+SO=SO2+S2O                    1.0E10    0.00      0 !
OSSO+S=S2O+SO              1.0E13   0.00      0 !
OSSO+S=S2+SO2              1.0E13   0.00      0 !
OSSO+SH=HSO+S2O                    1.0E13    0.00      0 !
OSSO+S2=S2O+S2O                    1.0E12    0.00      0 !
!
!
! *******************************************************
! *   HOSO2/HOSHO reactions                    *
! ********************************************************
!
HOSO2+S=SH+SO3                     1.0E13    0.00      0 !
HOSO2 = HOSO+O             5.4E18   -2.34   106300 !
HOSO2 = SO3+H              1.4E18   -2.91    54900 !
HOSO2+H = SO2+H2O          1.0E12    0.00        0 !
HOSO2+O = SO3+OH           5.0E12    0.00        0 !
HOSO2+OH = SO3+H2O         1.0E12    0.00        0 !
HOSO2+O2 = HO2+SO3         7.8E11    0.00      656 !
HOSHO = HOSO+H             6.4E30   -5.89    73800 !
HOSHO = SO+H2O             1.2E24   -3.59    59500 !
HOSHO+H = HOSO+H2          1.0E12    0.00        0 !
HOSHO+O = HOSO+OH          5.0E12    0.00        0 !
HOSHO+OH = HOSO+H2O                1.0E12    0.00      0 !
!
!
! *******************************************************
! *   OTHERS                  *
! *******************************************************
!
H2SO = H2S+O               4.9E28   -6.66    71700 !
HSSO2+M=SH+SO2+M           1.0E17    0.00     3000 !
HSSO2=S2O+OH               1.0E13    0.00    33700 !
H2S2O2+H2O=H2S+VDW1                3.9E05    1.66    3740 !
H2S2O2+H2O=2H2O+S2O        3.6E05    1.56    14290 !
H2S2O2+SH=H2S2+HOSO        1.0E13    0.00     8000 !
SO2+CO=SO+CO2              1.9E13    0.00    65900 !
CO+SO=CO2+S                5.1E13    0.00    53400 !
O+CS2=CS+SO                3.6E13     0.00       1696 !
O+CS=CO+S                  3.2E13     0.00          0 !
O+CS2=CO+S2                1.7E12     0.00       1194 !
O+CS2=COS+S                7.1E12     0.00       2102 !
S+CS2=CS+S2                1.0E14     0.00       4060 !
CS2+O2=CS+SO2              1.0E12     0.00      31050 !
```

```
CS+O2=COS+O                    6.1E12     0.00      16500 !
CS+O2=CO+SO                    6.1E12     0.00      16500 !
CS2+OH=COS+SH                  5.79E8     0.00    -1174 !
COS+OH=CO2+SH                  2.4E10    0.00       0 !
CS2+OH=>CS2OH                  1.0E10     0.00       1743 !
CS2OH+O2=>COS+HSO2             1.6E10     0.00          0 !
CS2+H2O=H2S+COS                        2.1E13     0.00      41497 !
COS+H2O=H2S+CO2                        1.5E13     0.00      35299 !
CS2+SO=COS+S2                  6.9E-5    0.00   -6339 !
CO+SH=COS+H                    2.5E10     0.00      15200 !
COS+O=CO+SO                    4.7E13     0.00       5200 !
 DUP
COS+O=CO+SO               -2.0E13         0.00       7385 !
 DUP
COS+O=CO2+S                    2.0E13    0.00        7385 !
COS+S=CO+S2                    4.0E04    2.57        2345 !
COS+M=CO+S+M            2.5E14    0.00   61400 !
CS+S(+M)=CS2(+M)        1.9E26    -4.30      0 !
            LOW  / 6.2E23 -2.42 0 /
CS+SH=CS2+H             1.2E13    0.00      0 !
!
!
! *****************************************************
! *   C/H reactions                   *
! *****************************************************
!
C2H3+O2=C2H2+HO2               1.34E06    1.61   -383.5 !
C2H4+O2=CH2HCO+OH              2.00E08    1.50    39000 !
C2H4+O2=C2H3+HO2               4.20E13    0.00    57630 !
C2H2+O=HCCO+H           1.40E07    2.00    1900 !
H+C2H2(+M)=C2H3(+M)            3.60E10    1.09     2640 !
            LOW/2.254E40  -7.269 6577./
            TROE/0.5 675. 675./
            H2/2/ CO/2/ CO2/3/ H2O/5/
!#!  H2O/8.59/ H2/2/ CO/2/ CO2/3/
CH3+CH3(+M)=C2H6(+M)           3.6E13     0.00       0 !
            LOW /1.27E41 -7.0 2760/
            TROE /0.62 73 1180 1E30/
CH3+H(+M)=CH4(+M)              2.1E14     0.00       0 !
  LOW  /6.467E23 -1.8 0/
  TROE /0.6376 1E-30 3230 1E30/
  CH4/1.9/ C2H6/4.8/
CH4+O2=CH3+HO2                         2.03E05    2.75    51714 !
CH4+H=CH3+H2            1.30E04    3.00    8040 !
CH4+OH=CH3+H2O          0.20E07    2.10    2460 !
CH4+O=CH3+OH            1.02E09    1.50    8604 !
CH4+HO2=CH3+H2O2               0.18E12    0.00    18700 !
CH3+HO2=CH3O+OH                1.00E12    0.27        688 !
CH3+O=CH2O+H            8.00E13    0.00       0 !
CH3+O2=CH3O+O           2.87E13    0.00   30481 !
CH3+O2=CH2O+OH                         6.38E11    0.00       13514 !
CH2OH+H=CH3+OH          0.10E15    0.00       0 !
CH3O+H=CH3+OH           0.10E15    0.00       0 !
```

```
CH3+OH=CH2+H2O          0.75E07   2.00    5000 !
CH3+HCO=CH4+CO          1.20E14   0.00       0 !
CH3+H=CH2+H2            0.90E14   0.00   15100 !
CH3+OH(+M)=CH3OH(+M)            6.30E13   0.00      0 !
  LOW/1.89E38  -6.3   3100/
  TROE/0.2105 83.5 5398 8370/
  N2/1.43/ H2O/8.58/ CO2/3/ CO/2/ H2/2/
!#!  H2O/8.58/ CO2/3/ CO/2/ H2/2/
CH3OH+O=CH2OH+OH                3.88E05   2.50    3080 !
CH2O+H(+M)=CH3O(+M)             5.40E11   0.45    2600 !
  LOW/1.54E30  -4.8  5560 /
  TROE/ 0.758 94 1555 4200/
   N2/1.43/  H2O/8.58/ CO/2/ H2/2/ CO2/3/
!#!  H2O/8.58/ CO/2/ H2/2/ CO2/3/
H+CH2O(+M)=CH2OH(+M)            5.40E11   0.45    3600 !
    LOW/.91E32 -4.82 6530/
    TROE/0.7187 103 1291 4160/
   N2/1.43/ H2O/8.58/ CO/2/ CO2/3/ H2/2/
!#!  H2O/8.58/ CO/2/ CO2/3/ H2/2/
CH3O+H=CH2O+H2          0.20E14   0.00      0 !
CH3O+OH=CH2O+H2O                0.10E14   0.00      0 !
CH2OH+OH=CH2O+H2O               0.10E14   0.00      0 !
CH3O+O=CH2O+OH                  0.10E14   0.00      0 !
CH3O+O2=CH2O+HO2                0.63E11   0.00    2600 !
CH2OH+O2=CH2O+HO2            1.57E15  -1.00      0 !
 DUP
CH2OH+O2=CH2O+HO2            7.23E13   0.00    3577 !
 DUP
CH2+H=CH+H2              0.10E19  -1.56      0 !
CH2+OH=CH+H2O              0.11E08   2.00    3000 !
CH2+OH=CH2O+H              0.25E14   0.00      0 !
CH+O2=HCO+O              0.33E14   0.00      0 !
CH+O=CO+H              0.57E14   0.00      0 !
CH+OH=HCO+H              0.30E14   0.00      0 !
CH+CO2=HCO+CO              0.34E13   0.00     690 !
CH+H2O=CH2O+H              5.72E12   0.00    -751 !
CH+CH2O=CH2CO+H              0.95E14   0.00    -515 !
CH+C2H2=C3H2+H              0.10E15   0.00      0 !
CH+CH2=C2H2+H              0.40E14   0.00      0 !
CH+CH3=C2H3+H              0.30E14   0.00      0 !
CH+CH4=C2H4+H              0.60E14   0.00      0 !
CH2+CO2=CH2O+CO              0.11E12   0.00    1000 !
CH2+O=CO+H+H              0.50E14   0.00      0 !
CH2+O=CO+H2              0.30E14   0.00      0 !
CH2+O2=CO+H2O                   2.20E22  -3.30    2867 !
CH2+O2=CO2+H+H                  3.29E21  -3.30    2867 !
CH2+O2=CH2O+O                   3.29E21  -3.30    2867 !
CH2+O2=CO2+H2                   2.63E21  -3.30    2867 !
CH2+O2=CO+OH+H                  1.64E21  -3.30    2867 !
CH2+CH2=C2H2+H+H              0.40E14   0.00      0 !
CH2+HCCO=C2H3+CO              0.30E14   0.00      0 !
CH2+C2H2=H2CCCH+H              0.12E14   0.00    6600 !
CH2+CH4=CH3+CH3              4.30E12   0.00   10030 !
```

```
CH2O+OH=HCO+H2O               0.34E10    1.18     -447 !
CH2O+H=HCO+H2                1.30E08    1.62     2166 !
CH2O+M=HCO+H+M               0.33E17    0.00    81000 !
    H2/2/ CO/2/ CO2/3/  H2O/5/
CH2O+O=HCO+OH                0.18E14    0.00     3080 !
CH2O+CH3=HCO+CH4              3.20E01    3.36     4310 !
CH2O+HO2=HCO+H2O2              3.00E12    0.00   13000  !
CH2O+O2=HCO+HO2               6.00E13    0.00    40660 !
HCO+OH=H2O+CO                0.10E15    0.00        0 !
HCO+M=H+CO+M                 3.48E17   -1.00    17010 !
   CO/1.87/   H2/1.87/  CH4/2.81/ CO2/3./ H2O/5./
HCO+H=CO+H2                 0.12E14    0.25        0 !
HCO+O=CO+OH                  0.30E14    0.00        0 !
HCO+O=CO2+H                 0.30E14    0.00        0 !
HCO+O2=HO2+CO                7.58E12    0.00      406 !
CO+O+M=CO2+M                 0.62E15    0.00     3000 !
    H2/2/ CO/2/ CO2/3/  H2O/16/
CO+OH=CO2+H                 1.51E07    1.30     -758 !
CO+O2=CO2+O                 2.53E12    0.00    47688 !
HO2+CO=CO2+OH                1.57E05    2.18    17900 !
C2H4+H=C2H3+H2               5.42E14    0.00    14902 !
C2H4+O=CH3+HCO               8.10E06    1.88      180 !
C2H4+O=CH2CO+H2               6.80E05    1.88      180  !
C2H4+OH=C2H3+H2O              0.20E14    0.00     5955 !
C2H4+CH3=C2H3+CH4             5.00E11    0.00    15000 !
CH2+CH3=C2H4+H               0.40E14    0.00        0 !
C2H4+H(+M)=C2H5(+M)            1.08E12    0.45     1822 !
  LOW/1.112E34  -5.0   4448.0/
 TROE/0.5 95.0  95.0    200./
   H2/2/ CO/2/ CO2/3/ H2O/5/
C2H3+H=C2H2+H2               0.40E14    0.00        0 !
C2H3+O=CH2CO+H               0.30E14    0.00        0 !
C2H3+O2=CH2O+HCO              4.58E16   -1.39     1015 !
C2H3+OH=C2H2+H2O              2.00E13    0.00        0 !
C2H3+C2H=C2H2+C2H2             0.30E14    0.00        0 !
C2H3+CH3=C2H2+CH4             2.10E13    0.00        0 !
C2H3+CH2O=C2H4+HCO             5.40E03    2.81     5860 !
C2H3+HCO=C2H4+CO              9.00E13    0.00        0 !
C2H3+C2H3=H2CCCH+CH3            1.80E13    0.00        0 !
C2H3+C2H3=C2H4+C2H2            6.30E13    0.00        0 !
C2H3+CH=CH2+C2H2              0.50E14    0.00        0 !
OH+C2H2=C2H+H2O               3.37E07    2.00    14000 !
OH+C2H2=HCCOH+H               5.04E05    2.30    13500 !
OH+C2H2=CH2CO+H               2.18E-4    4.50    -1000 !
OH+C2H2=CH3+CO               4.83E-4    4.00    -2000 !
HCCOH+H=HCCO +H2              3.00E07    2.00     1000 !
HCCOH+OH=HCCO+H2O              1.00E07    2.00     1000 !
HCCOH+O=HCCO+OH               2.00E07    3.00     1900 !
C2H2+O=C2H+OH                0.32E16   -0.60    15000 !
C2H2OH+O=OCHCHO+H              5.00E13    0.00        0 !
C2H2OH+O2=OCHCHO+OH            1.00E12    0.00     5000 !
OCHCHO+M=HCO+HCO+M             1.00E17    0.00    25000 !
OCHCHO+H=CH2O+HCO              3.00E13    0.00        0 !
```

```
CH2CO+O=CO2+CH2               0.18E13    0.00     1350 !
CH2CO+H=CH3+CO               5.93E06    2.00     1300 !
CH2CO+H=HCCO+H2               3.00E07    2.00    10000 !
CH2CO+O=HCCO+OH               2.00E07    2.00    10000 !
CH2CO+OH=HCCO+H2O              1.00E07    2.00     3000 !
CH2CO+OH=CH2OH+CO              7.20E12    0.00        0 !
CH2CO+OH=CH3+CO2              3.00E12    0.00        0 !
CH2+CO(+M)=CH2CO(+M)           8.10E11    0.50     4510 !
  LOW/ 1.88E33 -5.11 7095./
  TROE/ 0.5907 275 1226 5185/
    H2/2/ CO/2/ CO2/3/  H2O/8.58/  N2/1.43/
C2H+O2=CO+CO+H           2.52E13    0.00       0 !
C2H+CH4=CH3+C2H2              7.23E12    0.00      976 !
CH+CO(+M)=HCCO(+M)            5.00E13    0.00       0 !
  LOW/ 1.88E28  -3.74 1936 /
  TROE/ 0.5757 237  1652 5069 /
   N2/1.43/ H2O/8.58/ CO/2/ CO2/3/ H2/2/
!#!  H2O/8.58/ CO/2/ CO2/3/ H2/2/
HCCO+C2H2=H2CCCH+CO           1.00E11    0.00     3000 !
H+HCCO=CH2(S)+CO              0.10E15    0.00       0 !
O+HCCO=H+CO+CO                0.10E15    0.00       0 !
HCCO+O2=CO2+CO+H              1.40E07    1.70     1000 !
HCCO+O2=CO +CO +OH            2.88E07    1.70     1000 !
CH+HCCO=C2H2+CO               0.50E14    0.00       0 !
HCCO+HCCO=C2H2+CO+CO           0.10E14    0.00       0 !
HCCO+OH=C2O+H2O               6.00E13    0.00       0 !
C2O+H=CH+CO                  1.00E13    0.00       0 !
C2O+O=CO+CO                  5.00E13    0.00       0 !
C2O+OH=CO+CO+H               2.00E13    0.00       0 !
C2O+O2=CO+CO+O               2.00E13    0.00       0 !
C2H+O=CH+CO                  0.50E14    0.00       0 !
C2H+OH=HCCO+H                0.20E14    0.00       0 !
C2H+OH=C2+H2O                4.00E07    2.00     8000 !
C2+H2=C2H+H                  4.00E05    2.40     1000 !
C2+O2=CO+CO                  5.00E13    0.00       0 !
C2+OH=C2O+H                  5.00E13    0.00       0 !
C2H2+O2=HCO+HCO               0.20E09    1.50    30100 !
C2H2+M=C2H+H+M                9.10E30   -3.70   127138 !
    H2/2/ CO/2/ CO2/3/  H2O/5/
C2H4+M=C2H2+H2+M              3.50E16    0.00    71500 !
     N2/1.5/  H2O/10/
!#!     H2O/10/
C2H3+H(+M)=C2H4(+M)           6.10E12    0.30      280 !
     LOW /0.98E30 -3.86 3320./
     TROE /0.7820 207.50 2663.00 6095.00/
  H2/2.85/ CO/2.1/ CO2/2.85/  H2O/7.14/ CH4/2.85/ C2H6/4.29/  N2/1.43/
!
!
! *******************************************
! *   CH4/CH3/CH2/CH/C Subset              *
! *******************************************
!
CH2(S)+H2=CH3+H               7.2E13     0.0        0 !
```

```
CH2(S)+H2O=CH3+OH              3.0E15    -0.6        0 !
CH2(S)+N2=CH2+N2               1.3E13     0.0      430 !
CH2(S)+AR=CH2+AR               1.5E13     0.0      884 !
CH2(S)+H=CH2+H                 2.0E14     0.0        0 !
CH2(S)+H2O=CH2+H2O             3.0E13     0.0        0 !
CH2(S)+H=CH+H2                 3.0E13     0.0        0 !
CH2(S)+O=CO+H+H                3.0E13     0.0        0 !
CH2(S)+OH=CH2O+H               3.0E13     0.0        0 !
CH2(S)+O2=CO+OH+H              7.0E13     0.0        0 !
CH2(S)+CO2=CH2O+CO             3.0E12     0.0        0 !
CH2(S)+CH4=CH3+CH3             4.3E13     0.0        0 !
CH2(S)+CH3=C2H4+H              2.0E13     0.0        0 !
CH2(S)+CH2CO=C2H4+CO           1.6E14     0.0        0 !
CH2(S)+C2H6=CH3+C2H5           1.2E14     0.0        0 !
CH+H=C+H2                      1.5E14     0.0        0 !
CH+OH=C+H2O                    4.0E07     2.0     3000 !
C+OH=CO+H                      5.0E13     0.0        0 !
C+O2=CO+O                      2.0E13     0.0        0 !
C+CH3=C2H2+H                   5.0E13     0.0        0 !
C+CH2=C2H+H                    5.0E13     0.0        0 !
!
!
! ********************************************
! *   CH3OH/CH2OH/CH2O subset                *
! ********************************************
!
CH2OH+O2=CH2O+HO2              1.6E15    -1.0        0 !
 DUP
CH2OH+O2=CH2O+HO2              7.2E13     0.0     3577 !
 DUP
!
!
! ********************************************
! *   C2H6/C2H5/C2H4/C2H3/C2H2/C2H/C2 subset *
! ********************************************
!
C2H6+H=C2H5+H2                      5.4E02    3.50     5210 !
C2H6+O=C2H5+OH                      3.0E07    2.00     5115 !
C2H6+OH=C2H5+H2O                    7.2E06    2.00      864 !
C2H6+HO2 = C2H5+H2O2                1.3E13    0.00    20460 !
C2H6+O2=C2H5+HO2                    5.0E13    0.00    55000 !
C2H6+CH3=C2H5+CH4                   5.5E-1    4.00     8300 !
C2H5+H(+M) = C2H6(+M)          5.2E17    -0.99     1580 !
  LOW  /  2.0E41 -7.08 6685/
  TROE/  0.8422 125 2219 6882 /
  N2/1.0/ H2O/6/  AR/0.7/
C2H5+H=CH3+CH3                 4.9E12     0.35       0 !
C2H5+O = CH3+CH2O                   4.2E13    0.00        0 !
C2H5+O = CH3HCO+H                   5.3E13    0.00        0 !
C2H5+O = C2H4+OH                    3.0E13    0.00        0 !
C2H5+OH = C2H4+H2O                  2.4E13    0.00        0 !
C2H5+O2 = C2H4+HO2                  1.0E10    0.00    -2190 !
C2H5+CH2O = C2H6+HCO                5.5E03    2.81     5860 !
```

```
C2H5+HCO = C2H6+CO                  1.2E14    0.00       0 !
C2H5+CH3 = C2H4+CH4                 1.1E12    0.00       0 !
C2H5+C2H5 = C2H6+C2H4               1.5E12    0.00       0 !
C2H4+O = CH2HCO+H             4.7E06    1.88     180 !
C2H4+HO2=CH3HCO+OH            2.2E12    0.00    17200 !
C2H3+O2 = CH2HCO+O            3.0E11   -0.29    10.73 !
H2+C2H=C2H2+H               4.1E05    2.39     864 !
C2H2+O=CH2+CO               6.1E06    2.00    1900 !
OH+C2H2(+M)=C2H2OH(+M)        1.5E08    1.70    1000 !
   LOW/1.81E23  -2.0   0.0 /                    !
  H2/2/  CO/2/   CO2/3/   H2O/5/
!
!
! ****************************************************
! *   CH3HCO/CH2HCO/CH3CO/CH2CO/HCCOH/HCCO/C2O subset *
! ****************************************************
!
CH3HCO = CH3+HCO              7.1E15    0.00    81280 !
CH3HCO+H = CH3CO+H2           4.1E09    1.16    2400 !
CH3HCO+O = CH3CO+OH           5.8E12    0.00    1800 !
CH3HCO+OH=CH3CO+H2O           2.3E10    0.73    -1110 !
CH3HCO+HO2 = CH3CO+H2O2        3.0E12    0.00    12000 !
CH3HCO+O2 = CH3CO+HO2         3.0E13    0.00    39000 !
CH3HCO+CH3=CH3CO+CH4          2.0E-6    5.60    2464 !
CH2HCO=CH3+CO               1.0E13    0.00    42000 !
CH2HCO+H=CH3+HCO             1.0E14    0.00       0 !
CH2HCO+H=CH3CO+H             3.0E13    0.00       0 !
CH2HCO+O=CH2O + HCO           5.0E13    0.00       0 !
CH2HCO+OH=CH2CO+H2O           2.0E13    0.00       0 !
CH2HCO+OH=CH2OH+HCO           1.0E13    0.00       0 !
CH2HCO+O2 = CH2O+CO+OH         2.2E11    0.00    1500 !
CH2HCO+CH3=C2H5CHO            5.0E13    0.00       0 !
CH2HCO+CH2=C2H4+HCO           5.0E13    0.00       0 !
CH2HCO+CH =C2H3+HCO           1.0E14    0.00       0 !
C2H5+HCO = C2H5CHO            1.8E13    0.00       0 !
C2H5CHO+H = C2H5CO+H2         8.0E13    0.00       0 !
C2H5CHO+O = C2H5CO+OH         7.8E12    0.00    1730 !
C2H5CHO+OH = C2H5CO+H2O        1.2E13    0.00       0 !
C2H5+CO = C2H5CO             1.5E11    0.00    4800 !
C2H2OH+H=CH2HCO+H             5.0E13    0.00       0 !
CH3CO(+M)=CH3+CO(+M)          2.8E13    0.00    17100 !
  LOW/2.1E15  0.0  14000./
  TROE/ 0.5 1.0E-30 1.0E30 /
    H2/2/ CO/2/ CO2/3/  H2O/5/
CH3CO+H = CH3+HCO             2.1E13    0.00       0 !
CH3CO+H = CH2CO+H2            1.2E13    0.00       0 !
CH3CO+O = CH3+CO2             1.5E14    0.00       0 !
CH3CO+O = CH2CO+OH            4.0E13    0.00       0 !
CH3CO+OH = CH2CO+H2O          1.2E13    0.00       0 !
!
!
! *****************************************************
! *   C2H6OH subset                          *
! *******************************************************
!
C2H5OH(+M) = CH2OH+CH3(+M)      5.9E23    -1.68    91163 !
  LOW /2.9E85 -18.9 109914/
  TROE/ 0.5 200 890 4600 /
  H2O/5.0/ H2/2/ CO/2/ CO2/3/
C2H5OH(+M) = C2H5+OH(+M)        1.2E23    -1.54    96005 !
  LOW /3.2E85 -18.8 114930/
  TROE/ 0.5 300 900 5000 /
  H2O/5.0/ H2/2/ CO/2/ CO2/3/
C2H5OH(+M) = C2H4+H2O(+M)       2.8E13     0.09    66136 !
  LOW /2.6E83 -18.8 86452/
  TROE/ 0.7 350 800 3800 /
  H2O/5.0/
C2H5OH(+M) = CH3HCO+H2(+M)      7.2E11     0.09    91007 !
  LOW /4.5E87 -19.4 115586/
  TROE/ 0.9 900 1100 3500 /
  H2O/5.0/
C2H5OH+OH = C2H4OH+H2O          1.7E11     0.27      600 !
C2H5OH+OH = CH3CH2O+H2O         7.5E11     0.30     1634 !
C2H5OH+H = C2H4OH+H2            1.2E07     1.80     5098 !
C2H5OH+H = CH3CH2O+H2           1.5E07     1.60     3038 !
C2H5OH+O = C2H4OH+OH            9.4E07     1.70     5459 !
C2H5OH+O = CH3CH2O+OH           1.6E07     2.00     4448 !
C2H5OH+CH3 = C2H4OH+CH4         2.2E02     3.18     9622 !
C2H5OH+CH3 = CH3CH2O+CH4        1.4E02     2.99     7649 !
C2H5OH+HO2 = C2H4OH+H2O2        1.2E04     2.55    15750 !
C2H4OH+O2 = CH2O+CH2O+OH        6.0E10     0.00    24500 !
C2H5OH+HO2 = CH3CH2O+H2O2       2.5E12     0.00    24000 !
CH3CH2O+M = CH3HCO+H+M          1.2E35    -5.89    25274 !
CH3CH2O+M = CH3+CH2O+M          1.3E38    -6.96    23800 !
CH3CH2O+CO = C2H5+CO2           4.7E02     3.16     5380 !
CH3CH2O+O2 = CH3HCO+HO2         4.0E10     0.00     1100 !
CH3CH2O+H = CH3+CH2OH           3.0E13     0.00        0 !
CH3CH2O+H = C2H4+H2O            3.0E13     0.00        0 !
CH3CH2O+OH = CH3HCO+H2O         1.0E13     0.00        0 !
!
!
!*******************************************************
! *   CH2O/HCO Subset *
!*******************************************************
!
HCO+HCO=CO+CH2O                 3.0E13     0.0         0 !
!
!
!*******************************************************
! * CH3OH/CH2OH/CH2O Subset *
!*******************************************************
!
CH3OH(+M)=CH2OH+H(+M)           2.7E16    -0.1     98940 !
  LOW/2.34E40  -6.33 103100/
  TROE/0.773 693 5333/
CH3OH+H=CH2OH+H2                1.7E07     2.1      4868 !
```

```
CH3OH+H=CH3O+H2                  4.2E06    2.1     4868 !
CH3OH+OH=CH2OH+H2O               1.4E06    2.0    -3510 !
CH3OH+OH=CH3O+H2O                6.3E06    2.0     6300 !
CH3OH+HO2=CH2OH+H2O2             1.0E12    0.0    10040 !
CH3OH+O2=CH2OH+HO2               2.1E13    0.0    44900 !
CH3OH+CH3=CH2OH+CH4              3.2E01    3.2     7170 !
CH3OH+CH3=CH3O+CH4               1.5E01    3.1     6940 !
CH3O+HO2=CH2O+H2O2               3.0E11    0.0        0 !
CH3O+CO=CH3+CO2                  1.6E13    0.0    11800 !
CH3O+CH3=CH2O+CH4                2.4E13    0.0        0 !
CH3O+CH2O=CH3OH+HCO              1.0E11    0.0     3000 !
CH3O+HCO=CH3OH+CO                9.0E13    0.0        0 !
CH3O+CH3OH=CH3OH+CH2OH                   3.0E11    0.0     4100 !
CH3O+CH3O=CH3OH+CH2O             6.0E13    0.0        0 !
CH2OH+H=CH2O+H2                  4.8E13    0.0        0 !
CH2OH+O=CH2O+OH                  6.5E13    0.0     -700 !
CH2OH+O2=CH2O+HO2                1.6E15   -1.0        0 !
 DUP
CH2OH+O2=CH2O+HO2                7.2E13    0.0     3577 !
 DUP
CH2OH+HO2=CH2O+H2O2              3.6E13    0.0        0 !
CH2OH+HCO=CH3OH+CO               1.2E14    0.0        0 !
CH2OH+HCO=CH2O+CH2O              1.8E14    0.0        0 !
CH2OH+CH2O=CH3OH+HCO             5.5E03    2.8     5860 !
CH2OH+CH2OH=CH3OH+CH2O                   5.0E12    0.0        0 !
CH2OH+CH3O=CH3OH+CH2O                    2.4E12    0.0        0 !
!
!
!*******************************************************
! *   CxHy-SO2 Subset *
!*******************************************************
!
C2+H2S=C2H+SH                    5.36E12    0.00          0 !
C2 + SO2 =C2O+SO                 1.40E12    0.00          0 !
CO+CH3S=COS+CH3                  6.62E07    1.57       6675 !
CH3S+O2=CH2S+HO2                 4.74E24   -4.70       8300 !
CH3S+O2=CH3+SO2                  9.47E25   -3.80      12300 !
CH3+SO2=CH3OSO                   1.55E12    0.00       1291 !
CH3SO2=CH3OSO                    1.20E11    0.75      46300 !
CH3OSO=CH3O+SO                   4.00E08    0.00      57300 !
CH3OSO=CH2O+HSO                  2.44E06    1.82      53000 !
CH3O2+SO2=CH3O+SO3               3.01E07    0.00          0 !
CH2S+CH3=CH3CH2S                 3.98E11    0.00       2007 !
CH3SCH3+H=CH3SH+CH3                      1.80E08    1.70     2152 !
CH3CH2S=CH2CH2SH                 2.00E13    0.00      32000 !
CH2CH2SH=C2H4+SH                 1.58E13    0.00      11000 !
CH3SCH3+O=CH3+CH3SO                      7.83E12    0.00     -813 !
CH3S+O2=O+CH3SO                  5.24E13   -1.50    1.69E04 !
CH3SCH3+OH=CH3OH+CH3S                    0.04       0.00        0 !
CH3SCH3=CH3+CH3S                 6.10E15    0.00      75800 !
CH4+S=CH3+SH                     4.64E14    0.00      20096 !
C2H+C2H=C2H2+C2                          1.81E12    0.00          0 !
CH3SH=CH4+S                      1.00E13    0.00      73000 !
```

```
CH3SH(+M)=CH2SH+H(+M)            2.70E16   -0.08    98940 !
  LOW/2.34E40  -6.33 103100/
  TROE/0.773 693 5333/
CH3SH+OH=CH3S+H2O            1.31E07    1.77   -1689  !
CH3SH+OH=CH2SH+H2O               1.90E05    2.22         718 !
CH3SH+OH=CH3+H2SO                1.00E13    0.00       0 !
CH3SH+OH=CH4+HSO                 1.00E13    0.00       0 !
CH3SH+O=CH3+HSO                  1.78E10    0.00          0 !
CH3SH+O=CH3SO+H                  1.07E10    0.00          0 !
CH3SH+O=CH3O+SH                           1.78E10    0.00          0 !

CH3SH+H=CH3+H2S                  7.17E10    0.77        3225 !
CH3SH+H=CH2SH+H2                 4161        2.92        4747 !
CH3SH+H=CH3S+H2                  1.39E08    1.73         986 !
CH3SH+H=CH4+SH                            6.99E06    1.98      1.65E4 !
CH3SH+O2=CH2SH+HO2               2.10E13    0.00    44900 !
CH2SH+O2=CH2S+HO2                1.60E15   -1.00       0 !
 DUP
CH2SH+O2=CH2S+HO2                7.20E13    0.00     3577 !
 DUP
CH2SH+H=CH2S+H2                  4.80E13    0.00       0 !
CH2SH+O=CH2S+OH                  6.50E13    0.00     -700 !
CH3+H2S=CH4+SH                            1.29E2     3.15          813 !
CH3+SH=CH3SH                     7.3E12     0.23     -139 !
CH3OO+SH=CH3O+HSO                2.5E07     1.48    -2169 !
CH3OOH+SH=CH3OO+H2S                       5.6E03     2.82     8668 !
CH3SH+O=CH3S+OH                  4.2E07     1.82       80 !
CH3SH+O=CH2SH+OH                 3.3E03     2.86         1224 !
CH3SH+HO2=CH3S+H2O2                       9.1E12     0.00        14300 !
CH3SH+HO2=CH2SH+H2O2                      2.0E11     0.00        14500 !
CH3S+HO2=CH3SH+O2                1.7E-15    7.49       -12060 !
CH3SH+CH3=CH3S+CH4               8.1E5      1.90         1700 !
CH3SH+CH3=CH2SH+CH4              1.5E12     0.00         6500 !
CH3SH+SH=CH3S+H2S                1.2E14     0.00         5920 !
CH3S=CH2S+H                      2.50E38   -7.80       62053 !
SO+C2H2=COS+CH2                           1.00E11    0.00          0 !
SO+C2H4=COS+CH4                           1.00E11    0.00          0 !
SO+CH2=COS+H2                    1.00E11    0.00          0 !
SO+CH=COS+H                      1.00E11    0.00          0 !
SO+HCO=COS+OH                             1.00E11    0.00          0 !
SO+CH2O=COS+H2O                           1.00E11    0.00          0 !
SO+C2H2=CS+CH2O                           1.00E11    0.00          0 !
SO+C2H4=CS+CH3OH                 1.00E11    0.00          0 !
SO+CH2=CS+H2O                    1.00E11    0.00          0 !
SO+CH=CS+OH                      1.00E11    0.00          0 !
SO2+CH=CS+HO2                    1.00E11    0.00          0 !
SO2+CH=COS+OH                             1.00E11    0.00          0 !
SO2+CH2=COS+H2O                           1.00E11    0.00          0 !
SO2+CH2=CS+H2O2                           1.00E11    0.00          0 !
SO2+C2H=CS+HCOO                           1.00E11    0.00          0 !
S2+C2H2=CS2+CH2                           1.00E11    0.00          0 !
S2+CH2=CS2+H2                    1.00E11    0.00          0 !
S2+CH=CS2+H                      1.00E11    0.00          0 !
```

```
SH+C2H=CS+CH2                      1.00E11    0.00          0 !
SH+C2H2=CS+CH3                               1.00E09    0.00          0 !
SH+C2H3=CS+CH4                               1.00E11    0.00          0 !
H2S+C2H2=CS+CH4                              5.00E09    0.00          0 !
CS+H2S=CS2+H2                      1.00E11    0.00          0 !
!
!
!*****************************************************
! *   CH3OOH Subset *
!*****************************************************
!
CH3OOH(+M)=CH3O+OH(+M)         4.1E19    -1.15    44226 !
 LOW /3.9E42  -7.502   46730/
 TROE /0.8375  36562  498.8  9990/
CH3OOH+H=CH2OOH+H2           5.4E10     0.00     1860 !
CH3OOH+H=CH3OO+H2            5.4E10     0.00     1860 !
CH3OOH+H=CH3O+H2O            1.2E10     0.00     1860 !
CH3OOH+O=CH2OOH+OH           1.6E13     0.00     4750 !
CH3OOH+O=CH3OO+OH            8.7E12     0.00     4750 !
CH3OOH+OH=CH3OO+H2O          1.1E12     0.00     -437 !
CH3OOH+OH=CH2OOH+H2O         7.2E11     0.00     -258 !
CH3OOH+HO2=CH3OO+H2O2        4.1E04     2.50    10206 !
!
!
!*****************************************************
! *   CH3OO Subset *
!*****************************************************
!
CH3OO+H=CH3O+OH              1.00E14    0.000      0 !
CH3OO+O=CH3O+O2              2.85E10    1.000    -724 !
CH3OO+OH=CH3OH+O2                1.70E14    0.000      0 !
CH3OO+HO2=CH3OOH+O2          2.50E11    0.000   -1490 !
CH3OO+CH3=CH3O+CH3O          5.10E12    0.000   -1411 !
CH3OO+CH4=CH3OOH+CH3                    4.45E-3    4.691   19868 !
CH3OO+CH2OH=CH2O+CH3OOH        1.20E13    0.000      0 !
CH3OO+HCO=CH3O+H+CO2           3.00E13    0.000      0 !
CH3OO+CO=CH3O+CO2            1.60E05    2.180   17940 !
CH3OO+CH2O=CH3OOH+HCO                   1.98E09    1.110   12500 !
CH3OO+CH2O=CH3OOH+H+CO         2.45E14    0.027   30133 !
CH3OO+CH3O=CH2O+CH3OOH         3.00E11    0.000      0 !
CH3OO+CH3OH=CH3OOH+CH2OH       4.00E13    0.000   19400 !
CH3OO+CH3OO=CH3O+CH3O+O2       1.10E18   -2.400    1800 !
  DUP
CH3OO+CH3OO=CH3O+CH3O+O2       7.00E10    0.000     800 !
  DUP
CH3OO+CH3OO=CH3OH+CH2O+O2      2.00E11   -0.550   -1600 !
CH2OOH=CH2O+OH               2.40E12   -0.925    1567 !
 PLOG/ 0.04               9.60E10   -0.925    1567/
 PLOG/ 1.0                2.40E12   -0.925    1567/
 PLOG/ 10.                2.50E13   -0.927    1579/
 PLOG/ 100.               7.00E14   -1.064    1744/
CH3+O2=CH3OO                  5.00E22   -3.850    2000/
  PLOG/ 1.0                      5.00E22   -3.850    2000/
  PLOG/10.0                     3.35E21   -3.200    2300/
  PLOG/20.0                     3.25E29   -5.600    6850/
  PLOG/50.0                 2.83E18   -2.200    1400/
  PLOG/100.0                1.05E19   -2.300    1800/
 DUP
CH3+O2=CH3OO             5.00E22   -3.850    2000 !
  PLOG/20.0                     4.10E20   -2.940    1900/
  PLOG/50.0                 5.60E28   -5.250    6850/
  PLOG/100.0                    4.10E30   -5.700    8750/
 DUP
CH4+S2=CH3+HS2                      8.40E13    0.000   52153 !
CH4+SO=CH3+HSO                      3.50E13    0.000   50718 !
C2H6+SH=C2H5+H2S                2.63E02    3.410   10086 !
!
!
!******************************************************
! *   CHS Subset *
!******************************************************
!
CH2S+H=CHS+H2            2.80E07    2.02     7760 !
CH2S+O=CHS+OH            2.10E13    0.00     3000 !
CH2S+OH=CHS+H2O            5.20E12    0.00      500 !
CH2S+CH3=CHS+CH4           2.30E04    2.37    12280 !
CHS+H2S=CH2S+SH                 7.30E12    0.00     6425 !
CHS+S=CS2+H            2.00E13    0.00        0 !
CHS+H2S2=CH2S+HS2          1.10E13    0.00     3900 !
CHS+S2=CS2+SH           3.00E11    0.00     4000 !
CHS+C2H6=CH2S+C2H5         2.00E14    0.00    24360 !
CH3+CH4S=CH4+CH2SH              7.06E12    0.00    15200 !
CH3+CH4S=CH4+CH3S               9.78E12    0.00        6119 !
CH3S+H2S2=CH4S+HS2              1.51E12    0.00        3274 !
CH3S+H2S=CH4S+SH                2.27E12    0.00     7624 !
CHS+CH4S=CH2S+CH3S              4.89E12    0.00        6119 !
CH4S+H=CH3S+H2                          1.75E04    3.06        -143 !
SH+CH3=CH4S                     7.34E12    0.23        -143 !
CH3SH+O2=CH2SO+H2O              1.00E14    1.40       42000 !
CH2SO=CO+H2S                    1.00E11    0.00           0 !
CH2SO+H=CH3SO                           1.00E11    0.00           0 !
CH3SO=CH3+SO                    1.00E11    0.00           0 !
CH2SO=COS+H2                    1.00E11    0.00           0 !
CH2SO=CS+H2O                    1.00E11    0.00           0 !
CH3SH+O2=CH3OH+SO               1.00E14    0.00       40000 !
!
!
END
```